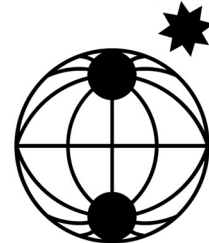


Berichte

zur Polar-
und Meeresforschung

579
2008

Reports
on Polar and Marine Research



The Expedition of the Research Vessel "Polarstern"
to the Arctic in 2007 (ARK-XXII/2)

Edited by
Ursula Schauer
with contributions of the participants



ALFRED-WEGENER-INSTITUT FÜR
POLAR- UND MEERESFORSCHUNG
In der Helmholtz-Gemeinschaft
D-27570 BREMERHAVEN
Bundesrepublik Deutschland

ISSN 1866-3192

Hinweis

Die Berichte zur Polar- und Meeresforschung werden vom Alfred-Wegener-Institut für Polar- und Meeresforschung in Bremerhaven* in unregelmäßiger Abfolge herausgegeben.

Sie enthalten Beschreibungen und Ergebnisse der vom Institut (AWI) oder mit seiner Unterstützung durchgeführten Forschungsarbeiten in den Polargebieten und in den Meeren.

Es werden veröffentlicht:

- Expeditionsberichte (inkl. Stationslisten und Routenkarten)
- Expeditionsergebnisse (inkl. Dissertationen)
- wissenschaftliche Ergebnisse der Antarktis-Stationen und anderer Forschungs-Stationen des AWI
- Berichte wissenschaftlicher Tagungen

Die Beiträge geben nicht notwendigerweise die Auffassung des Instituts wieder.

Notice

The Reports on Polar and Marine Research are issued by the Alfred Wegener Institute for Polar and Marine Research in Bremerhaven*, Federal Republic of Germany. They appear in irregular intervals.

They contain descriptions and results of investigations in polar regions and in the seas either conducted by the Institute (AWI) or with its support.

The following items are published:

- expedition reports (incl. station lists and route maps)
- expedition results (incl. Ph.D. theses)
- scientific results of the Antarctic stations and of other AWI research stations
- reports on scientific meetings

The papers contained in the Reports do not necessarily reflect the opinion of the Institute.

The „Berichte zur Polar- und Meeresforschung“
continue the former „Berichte zur Polarforschung“

* Anschrift / Address

Alfred-Wegener-Institut
Für Polar- und Meeresforschung
D-27570 Bremerhaven
Germany
www.awi.de

Editor in charge:
Dr. Horst Bornemann

Assistant editor:
Birgit Chiaventone

Die "Berichte zur Polar- und Meeresforschung" (ISSN 1866-3192) werden ab 2008 ausschließlich als Open-Access-Publikation herausgegeben (URL: <http://epic.awi.de>).

Since 2008 the "Reports on Polar and Marine Research" (ISSN 1866-3192) are only available as web based open-access-publications (URL: <http://epic.awi.de>)

The Expedition of the Research Vessel "Polarstern" to the Arctic in 2007 (ARK-XXII/2)

**Edited by
Ursula Schauer
with contributions of the participants**

**Please cite or link this item using the identifier
hdl: 10013/epic.30947 or <http://hdl.handle.net/10013/epic.30947>
ISSN 1866-3192**

ARK-XXII/2

29 July 2007 - 7 October 2007

Tromsø - Bremerhaven

Fahrtleiter / Chief Scientist:

Ursula Schauer

Koordinator / Coordinator:

Eberhard Fahrbach

CONTENTS

1.	Expedition ARK-XXII/2: Fahrtverlauf und Zusammenfassung	3
	Summary and itinerary	8
2.	Weather conditions	11
3.	Sea ice properties	14
	3.1 Sea ice thickness measurements	14
	3.2 Sea ice radar backscatter measurements for improved melt-pond and thin-ice cover analysis	31
	3.3 Routine sea ice observations	56
	3.4 Buoy deployments	62
	3.5 Sea ice biology	65
4.	Oceanography	76
	4.1 Physical oceanography	76
	4.2 XCTD observation	92
	4.3 Deployment of ice-tethered buoys	98
5.	GEOTRACES	104
	5.1 A- trace elements	110
	5.2 B- natural and anthropogenic radionuclides	124
	5.3 C- related parameters	142
	5.4 Coupling of methane and DMSP cycles in the marginal ice zone and on polar shelves	144

6.	Marine biology	146
	6.1 Zooplankton investigations	146
	6.2 Biodiversity of polar deep-sea eukaryotic microbiota - molecular versus morphological approach	158
7.	Marine geology	163
	7.1 Parasound sediment echosounding	164
	7.2 Bathymetry	166
	7.3 Geological sampling	166
	7.4 Physical properties	168
	APPENDIX	179
A.1	Participating institutions	181
A.2	Cruise participants	184
A.3	Ship's crew	186
A.4	Station list	187
A.5	Annex coring positions	219
A.6	Sediment core descriptions	227

1. EXPEDITION ARK-XXII/2: FAHRTVERLAUF UND ZUSAMMENFASSUNG

Ursula Schauer
Alfred-Wegener-Institut
für Polar- und Meeresforschung

Der zweite Abschnitt der 22. Arktisexpedition des Forschungsschiffes *Polarstern*, ARK-XXII/2, war ein zentraler Beitrag zum Internationalen Polarjahr 2007/08 (IPY 2007/08). Er trug insbesondere zu zwei im IPY-Wissenschaftsplan aufgeführten Zielen bei:



- “1. Status: to determine the present environmental status of the polar regions”
und*
- “2. Change: to quantify, and understand, past and present natural environmental and social change in the polar regions; and to improve projections of future change” (The Scope of Science for the International Polar Year;
<http://www.ipy.org>)*

Zurzeit finden in der Arktis drastische Veränderungen statt: Das Meereis verringert sich, die oberen Wasserschichten werden wärmer und Strömungen verschieben sich. Daraus sind Auswirkungen auf den Austausch und den Transport von Stoffen und auf Ozean- und Eisorganismen zu erwarten. Für das Verständnis dieser Veränderungen ist eine umfassende Gesamtaufnahme als Ausgangspunkt für Langzeitbeobachtungen notwendig. Gemeinsam mit anderen arktischen Expeditionen im IPY 2007¹ diente ARK-XXII/2 diesem Ziel und übernahm dabei insbesondere die Erfassung der eurasischen und der zentralen Arktis. Gleichzeitig galt die Reise der Untersuchung von biogeochemischen Stoffkreisläufen und der Analyse von Ökosystemen in Eis und Ozean, sowie der quartären Vereisungsgeschichte des östlichen und zentralen Nordpolarmeers.

ARK-XXII/2 war eingebunden in die IPY-Projekte SPACE (Synoptic Pan-Arctic Climate and Environment Study, IPY-EoI #18), GEOTRACES: Spurenstoffe in der Arktis (IPY-EoI #45) und iAOOS (Integrated Arctic Ocean Observing System, IPY-EoI #80) (siehe <http://www.ipy.org/development/eoi/index.htm>), und lieferte einen Beitrag

¹ NABOS (RV Victor Bujnitzky); LOMROG (IB Oden); AGAVE (IB Oden); Drift des französischen Schiffes TARA und der russischen Eisstation NP 35; AARI-Expedition (Academic Fedorov); Beaufortwirbel (IB Louis St.Laurent); Transdrift XII (RV Ivan Petrov)

zu dem deutsch-russischen Projekt VERITAS (Variability and Export of Riverine Matter into the Arctic Ocean and late (Paleo-) Environmental Significance). Gleichzeitig ist ein Großteil der Arbeiten Bestandteil des durch die EU geförderten *Integrated Programmes* DAMOCLES (Developing Arctic Modelling and Observing Capabilities for Long-term Environment Studies).

Um dekadische Veränderungen zu erfassen, wurden hydrographische Schnitte, Zooplanktonbeprobungen und Eisdickenbeobachtungen früherer Expeditionen, wie *Oden* 1991, *Polarstern* 1993, *Polarstern* 1995 und *Polarstern* 1996 wiederholt. Auf diese Weise können räumliche und zeitliche Variabilität unterschieden und damit die Entwicklung ozeanographischer, eisphysikalischer und biologischer Parameter über eine Dekade erfasst werden. Zusätzlich leistete ARK-XXII/2 einen Beitrag zu einem internationalen Langzeitbeobachtungsprogramm von Ozean und Meereis durch Eisbojen, die in diesem Jahr auf verschiedenen Expeditionen erstmalig in großem Umfang arktisweit ausgebracht wurden.

Ein wesentlicher Bestandteil der Reise war ein großes Chemieprogramm im Rahmen von GEOTRACES. Dabei kam erstmalig ein Ultra-clean-System zum Einsatz, mit dem in großem Umfang effektiv Wasserproben für Spurenmetalluntersuchungen genommen werden können. Parallel dazu wurde ein großes Spektrum von natürlichen Radioisotopen für Partikelflussuntersuchungen beprobt.

Die ursprüngliche Planung sah vor, dass ARK-XXII/2 vorwiegend den eurasischen Sektor der Arktis abdeckt. Die unerwartet niedrige Eisbedeckung des Sommers 2007 erlaubte jedoch, die Schnitte bis weit ins amerasische (kanadische) Becken hinein auszudehnen. Auf der anderen Seite zwang die weit nach Norden zurückgezogene Eisgrenze dazu die Bojen sehr viel weiter im Nordwesten auszulegen als eigentlich vorgesehen war.

Die Schnitte erstreckten sich von den Schelfgebieten der Barents-, der Kara- und der Laptewsee über das Nansen-, das Amundsen- und das Makarowbecken bis über den Alpha-Mendelejewrücken in das Kanadabecken. Auf allen Schnitten wurden in engem Stationsabstand CTD-Profile (Temperatur, Salzgehalt, Sauerstoffgehalt und Fluoreszenz) aufgenommen und eine Kombination von Standardproben genommen. In unregelmäßigen Abständen wurden zusätzlich Messungen und Beprobungen zur Dicke und zu Radar-Rückstreuungseigenschaften, sowie zu Organismen des Meereises, zur Verteilung von natürlichen Spurenstoffen und Radioisotopen im Ozean und im Eis und zur Verbreitung und der Anpassung von Zooplankton und zur Biodiversität polarer Tiefsee-Eukaryoten durchgeführt. Die physikalischen Eisuntersuchungen wurden vorwiegend als umfangreiche Fernerkundungsmessungen vom Hubschrauber aus durchgeführt und durch Arbeiten direkt auf dem Meereis ergänzt. In allen Becken, auf den Rücken und auf dem Karaseeschelf wurden Sedimentproben zur Bestimmung der spätquartären Veränderlichkeit des Flusswasserausstroms und der Vereisungsgeschichte der Arktis genommen.

Polarstern lief planmäßig am 28. Juli 2007 aus Tromsø aus. 54 Wissenschaftler aus 19 Instituten in 10 Ländern befanden sich an Bord. Am 29. Juli begannen wir auf der Zentralbank in der Barentssee den ersten Transekt, der entlang 34° E nach Norden ins Nansenbecken führte. Bei etwa 81° 30'N trafen wir auf die Eisgrenze und bei

84° 30'N war das Packeis so dicht, dass ein Fortkommen nahezu unmöglich war. Wir brachen daraufhin am 6. August den Schnitt ab, um nach Osten zum zweiten Schnitt entlang dem 61sten östlichen Längengrad zu gelangen. Auf dem Weg dorthin wurde die Eisbedeckung lockerer. Am 10. August begannen wir den zweiten Schnitt von 84° 40'N aus nach Süden in Richtung Franz-Joseph-Land. Nach den vorliegenden topographischen Daten, die sich oft als fehlerhaft erwiesen, sowie nach Parasound- und Hydrosweepsurveys wurden Positionen für Sedimentproben im tiefen Nansenbecken, am Hang und auf dem Schelf bestimmt und geologische Kerne gezogen. An den Kernpositionen und dazwischen wurden wieder hydrographische Stationen und Netze für Zooplanktonproben gefahren. Um Zeit für die Stationen in der zentralen Arktis zu sparen, entschlossen wir uns zu relativ großen Stationsabständen und füllten die Zwischenräume mit XCTD-(Expendable CTD) Messungen, um die kleinräumigen Wassermassenstrukturen auflösen zu können.

Die Überfahrt auf den dritten Schnitt nordwestlich von Sewernaja Semlja führte durch sehr lockeres Eis in Sichtweite der Eiskante. Am 19. August begannen wir im östlichen Voronintrog unseren dritten Schnitt, der zunächst entlang ca. 86° E wieder nach Norden führte. Wir durchquerten das Nansenbecken, den Gakkelrücken und das Amundsenbecken bis zum Lomonossowrücken. Auf dem Rücken machten wir einen Abstecher nach Norden, um den Tiefenwasseraustausch an der Schwelle zwischen Amundsen- und Makarowbecken zu untersuchen, der durch das so genannte Intrabecken führt. Hier erreichten wir am 31. August bei 88° 38'N die nördlichste Position unserer Fahrt. Die ungestörte Sedimentablagerung im Intrabecken wurde für geologische Kernprobennahmen genutzt. Anschließend setzten wir den ursprünglichen Schnitt bei etwa 88°N nach Osten ins Makarowbecken fort.

Informationen über die immer weiter zurückgehende Eisbedeckung in der eurasischen Arktis bewogen uns, den ursprünglichen Plan für die Auslegung von Eisbojen zu ändern und wir brachten am 2. September bei 87° 51'N 170°W die erste ozeanographische und eine meteorologische Eisboje aus. Gleichzeitig beschlossen wir, das zügige Fortkommen in der lockeren Eisbedeckung zu nutzen und das Makarowbecken bis zum Alpharücken bei 85° 42'N 135°W zu durchqueren. Eine weitere Verlängerung des Schnittes brachte uns bis zur Südflanke des Alpharückens bei 84° 30'N 138° 25'W und damit an den Rand des Kanadabeckens. Hier schlossen wir den Schnitt endgültig mit einer ausführlichen Beprobung von Meereis, physikalischen und chemischen Parametern der Wassersäule, Zooplanktonfängen und Sedimentkernnahmen ab. Sowohl am östlichsten als auch am südlichsten Punkt im arerischen (kanadischen) Becken wurde der CTD-Schnitt durch XCTD-Abwürfe vom Helikopter aus um jeweils weitere 70 nm nach Osten bzw. nach Süden verlängert. Vom südlichen Alpharücken führte ein kurzer Schnitt über einen der Durchlässe zwischen Makarowbecken und Kanadabecken zum östlichen Ende des Mendelejewrückens.

Auf dem Weg zurück nach Westen stand im Vordergrund unserer Arbeit, geeignete Eisschollen für wenigstens zwei weitere Bojenarrangements zu finden. Um im halbwegs dichten Eis zu bleiben, konnte der Schnitt nur etwa 100 nm südlich vom vorigen Schnitt verlaufen, weshalb wir recht große Stationsabstände wählten. Die zweite ozeanographische Boje wurde am 10. September im Makarowbecken bei 86°38'N 177° 33'E ausgebracht. Ein abschließender Test zeigte aber, dass die Boje

nicht funktionierte. So wurde sie wieder aufgenommen und durch eine andere ersetzt und durch eine meteorologische Boje ergänzt. Nach einem weitgehend aus XCTDs bestehenden Schnitt über den Lomonossowrücken wurde am 13. September im Amundsenbecken eine weitere Bojengruppe ausgebracht, diesmal bestehend aus einer CTD-Boje, einer Strömungsmesserboje, einer Boje zur Turbulenzmessung unter dem Eis, einer Eismassenbilanzboje und einer Webcam. Im Abstand von etwa 50 nm um die ozeanographischen Bojen herum wurden per Hubschrauber 6 meteorologische Bojen ausgebracht.

Der Schnitt führte dann mit weiten Stationsabständen zurück zum Gakkelrücken. Beim ersten Kreuzen des Gakkelrückens im August bei 90°E hatten wir Anomalien der Temperatur und verschiedener chemischer Parameter gefunden, die eine hydrothermale Quelle vermuten ließen. Aufgrund der zeitlichen Verzögerung dieser Entdeckung durch die Dauer der Laboranalysen konnten wir die erste Fundstelle jedoch nicht ausgiebiger beproben. Deshalb fuhren wir ab dem 16. September einen Schnitt von 84°41'N nach Süden den Gakkelrücken entlang, um bei einem weiteren Anzeichen einer Anomalie eine umfangreiche chemische Beprobung vorzunehmen. Jegliche weitere Anzeichen solcher Anomalien waren jedoch nur sehr schwach. Am 19. September erreichten wir bei 82°12'N die Eisgrenze und kurz darauf das südliche Ende des Gakkelrückens. Unser Schnitt führte nun über den Kontinentalhang in die Laptewsee, wo das Stationsprogramm am 24. September bei 75°12'N, 121° endete und die Rückreise durch die Nordostpassage angetreten wurde. Am 30. September haben sich bei etwa 72°N 44 Täuflinge der Polartaufe unterzogen. Am 7. Oktober 2007 lief *Polarstern* um 13 Uhr in Bremerhaven ein.



Abb. 1: Fahrtroute ARK-XXII/2

Fig. 1: Cruise track ARK-XXII/2

SUMMARY AND ITINERARY

The expedition ARK-XXII/2 was a central contribution to the International Polar Year 2007/08 (IPY 2007/08). In particular it served two objectives formulated in the IPY science plan:

*"1. Status: To determine the present environmental status of the polar regions"
and*

"2. Change: To quantify, and understand, past and present natural environmental and social change in the polar regions; and to improve projections of future change" (The Scope of Science for the International Polar Year; <http://www.ipy.org>)

Currently enormous changes take place in the Arctic Ocean: the sea ice is shrinking, the upper water layers become warmer and ocean currents are shifting. This will have consequences for ocean-atmosphere fluxes, for the oceanic and ice-related transport of substances, and for marine and ice-related organisms. Ultimately it will feed back to sub-polar climate. To understand these changes a comprehensive pan-Arctic survey is necessary as a benchmark for long-term observations and as a constraint for climate models.

ARK-XXII/2 aimed at meeting its objectives in co-operation with other IPY expeditions¹ thereby focussing on the Eurasian and central Arctic Ocean. Besides the physical system ARK-XXII/2 addressed biogeochemical tracer studies, the ecosystems in ice and ocean as well as the history of quaternary glaciations of the Siberian Arctic.

ARK-XXII/2 contributed to the IPY projects SPACE (Synoptic Pan-Arctic Climate and Environment Study, IPY-EoI #18), GEOTRACES: Geotraces in the Arctic (IPY-EoI #45), iAOOS (Integrated Arctic Ocean Observing System, IPY-EoI #80) (see <http://www.ipy.org/development/eoi/index.htm>), as well as to the German-Russian project VERITAS (Variability and Export of Riverine Matter into the Arctic Ocean and late (Paleo-) Environmental Significance) which is listed on governmental level in the bilateral research programme. Part of the work was funded through the EU Integrated Programme DAMOCLES (Developing Arctic Modelling and Observing Capabilities for Long-term Environment Studies).

In the context of the IPY programmes, ARK-XXII/2 took its share in covering part of the Eurasian sector of the Arctic. To identify decadal change one has to distinguish spatial and temporal variations of hydrography, sea ice, as well as biological and biogeochemical parameters. Therefore the expedition was designed to repeat large-scale sections that were made in the nineties of the last century, such as *Oden* 1991,

¹ NABOS (RV Victor Bujnitzky); LOMROG (IB Oden); AGAVE (IB Oden); Drift des französischen Schiffes TARA und der russischen Eisstation NP 35; AARI-Expedition (Academic Fedorov); Beaufortwirbel (IB Louis St.Laurent); Transdrift XII (RV Ivan Petrov)

Polarstern 1993, 1995 and 1996. To ensure year-round observations of ice and upper ocean a number of ice-tethered buoys were deployed.

A large part of the programme was dedicated to GEOTRACES. In this context for the first time an Ultra Clean System was employed that enabled a systematic survey of trace metals in the Arctic. GEOTRACES also included sampling of a large spectrum of natural radio isotopes for particle flux studies.

ARK-XXII/2 was originally planned to survey the Eurasian part of the Arctic. However, the extremely low ice cover in 2007 enabled us to extend the sections far into the Canadian Basin. On the other hand the unusual low ice cover constricted the deployment of the ice-tethered buoys and forced us to deploy the buoys much further downstream in the Transpolar Drift than it was intended.

The sections reached from the shelves of the Barents, Kara and Laptev Seas across the Nansen, Amundsen and Makarov Basins beyond the Alpha Ridge into the Canada Basin. On all sections CTD/water sampler casts (temperature, salinity, oxygen, fluorescence electronically and samples of nutrients and $\delta^{18}\text{O}$ contents) were conducted in narrow station distances. In larger intervals stations were devoted to investigate thickness and back-scatter characteristics of sea ice, natural trace elements and radioisotopes, chemical composition of dissolved organic matter and their role as markers of water masses, and the distribution of organisms in and below the sea ice and in the water column and the eukaryotic diversity in the deep-sea sediments. North of the Kara Sea as well as along a cross basin section sediment cores were taken for the determination of the Late Quaternary variation of river runoff and of the Eurasian Arctic glaciation history. Helicopter- and ship-borne XCTD-casts were used to extend temperature and salinity sections in the Canadian Basin or to increase the spatial resolution across topographical features.

The cruise began on 28 July 2007 in Tromsø. 54 scientists from 19 institutes in 10 countries were onboard. On 29 July we started station work on the Central Bank in the Barents Sea and run a section along 34°E into the Nansen Basin. At 81°30'N we crossed the ice edge and at 84°30'N the pack ice was so dense that *Polarstern* made hardly any progress. We therefore broke off the section on 6 August and turned eastward heading for our second section at 61°E. En-route the ice cover became significantly less. On 10 August we started at 84°40'N the section in southern direction towards Franz Josef Land. Guided by available bathymetry data - which turned out to be erroneous in large parts – and following Parasound and Hydrosweep surveys positions were determined for sediment coring in the deep Nansen Basin, at the continental slope and on the shelf. At and between the coring positions hydrographic and net stations were conducted.

The transit to the third section which started northwest of Severnaya Zemlya went through very loose ice in the vicinity of the ice edge. On 19 August we started the section in the eastern Voronin Trough and sailed northwards along 86°E. We crossed the Nansen Basin, the Gakkel Ridge and the Amundsen Basin and reached the Lomonosov Ridge on 30 August. During the previous two weeks the light ice conditions had afforded fast progress so that we found time for a detour to the north to investigate the exchange of deep water across the sill of the Lomonosov Ridge between the Makarov and the Amundsen Basins. Here we reached with 88°38'N our

northernmost position. At the sill a small basin (Intra Basin) is located where undisturbed sedimentation was used for geological coring. The section was then continued into the Makarov Basin at about 88°N.

Information about the ongoing seasonal retreat of the ice-cover in the Eurasian Basin induced us to modify our planned cruise track. Because of the light ice we were able to extend our cross-basin section but we also had to modify our plan for deployment of ice-tethered buoys. Instead of deployment on the upstream end of the Siberian branch of the transpolar drift we deployed the first oceanographic and meteorological buoy at 87°51'N 170°W. Then we proceeded to the Alpha Ridge at 85°42'N 135°W and extended the section further up to 85°23'N 136°17'W. At the easternmost as well as at the southernmost corners of the cruise track in the Canadian Basin, our sections were extended by XCTD casts. A last prolongation on September 7 brought us to the rim of the Canada Basin at 84°30'N 138°25'W where we took an extensive station to probe all parameters in ice, water and sediment. Then we turned west to cross one of the deep passages between the Makarov and the Canada Basin and reached the eastern edge of the Mendeleev Ridge on 9 September.

During our return to the Siberian Arctic we focussed on searching suitable floes for at least two out of three more planned buoy arrays. The still retreating ice cover forced us to sail not more than 100 nm south of the previous section in order to meet thick and large enough ice floes. The second oceanographic buoy was deployed on 10 September in the Makarov Basin at 86°38'N 177°W. The final performance test revealed a malfunction of the buoy so that we recovered and replaced it (because of the reduction to three arrays we had a spare buoy). We crossed the Lomonosov Ridge conducting XCTD casts and deployed the last array, consisting of buoys that carry a CTD, a current meter, a turbulence meter and ice and snow mass sensors respectively and a Webcam. In about 50 nm distance from all oceanographic buoy arrays, 6 meteorological buoys were brought out by helicopter.

The section was continued to the Gakkel Ridge. At the first crossing of the Gakkel Ridge in August at about 90°E, anomalies of temperature and of various chemical properties were detected that might have originated from a hydrothermal vent. Because of the delay of this discovery caused by the time needed for lab analyses this location had not been investigated in more detail. Therefore we surveyed the Gakkel Ridge from 84°41'N on southwards with CTD casts in order to detect any further anomalies in temperature or light transmission which then would have been sampled in detail. However, only very weak anomalies were observed. On 19 September we passed the ice edge at 82°12'N and soon after reached the southern end of the Gakkel Ridge. The section was continued up the continental slope to the Laptev Sea where the station work finished on September 24 at 75°12'N 121°E. We turned northwest and passed the Northern Sea Route to the western Barents Sea. On September 30 at about 72°N 44 candidates underwent the polar baptism. RV *Polarstern* returned to Bremerhaven on 7 October 2007.

2. WEATHER CONDITIONS

Manfred Gebauer and Hartmut Sonnabend
Deutscher Wetterdienst

When *Polarstern* left Tromsø on 28 July there was a low pressure system just over the middle of Norway. At the beginning the weather was rather smooth, later the ship was affected by strong easterly winds and wave heights up to 3 m. Finally the weather grew calm under influence of a high over the Barents Sea.

While operating along 34°E, *Polarstern* was accompanied by fresh southerly winds from 4 to 5 Bft. The high was now stationary north of Franz Josef Land. Despite the high pressure the weather was changeable, prevailing conditions were fog or low stratiform clouds with occasional drizzle and sometimes danger of icing of the helicopters.

When 85°N was reached, the high near Franz Josef Land got weaker. Temperatures were mostly near -2 °C, because low pressure systems that arrived from the Barents Sea often brought mild and moist air into the northern Arctic Ocean (Fig. 2.1). A new strong low arrived between Franz Josef Land and Severnaya Zemlya. The wind blew with 7 Bft from northwest, but due to the ice cover there was no heavy sea.

From then on the flight conditions were difficult due to bad visibility and ceiling during most of the scientific work (Figs. 2.2, 2.3). The distribution of air pressure with high pressure over western longitudes and low pressure systems over eastern longitudes of the Arctic Ocean lasted until the end of August. Winds were moderate with forces 3 to 5 Bft, visibility and clouds continued to be difficult, sometimes accompanied by freezing rain or danger of icing. Some small polar lows occurred.

During September the pressure distribution changed. The area around the North Pole was more and more influenced by high pressure, but still there were some small polar lows with intermediately stronger winds and dense snowfall. Temperatures were partly less than -5° C, the wind continued to blow mostly from southerly to southeasterly directions with 2 and 5 Bft (Figs. 2.4, 2.5).

At mid of September the ridge of high pressure above *Polarstern* was reduced by new weather fronts, accompanied again by fog. When arriving in the south of the Laptev Sea, a storm reached us from the Barents Sea. The air temperature rose and on the rear of this low was a strong storm blowing from northwest.

The journey through the Kara and the Barents Sea and along the Norwegian coast was partly laborious due to several stormy lows. Later the weather was fine up to the port of Bremerhaven.

Fig. 2.1: Time series of air temperature

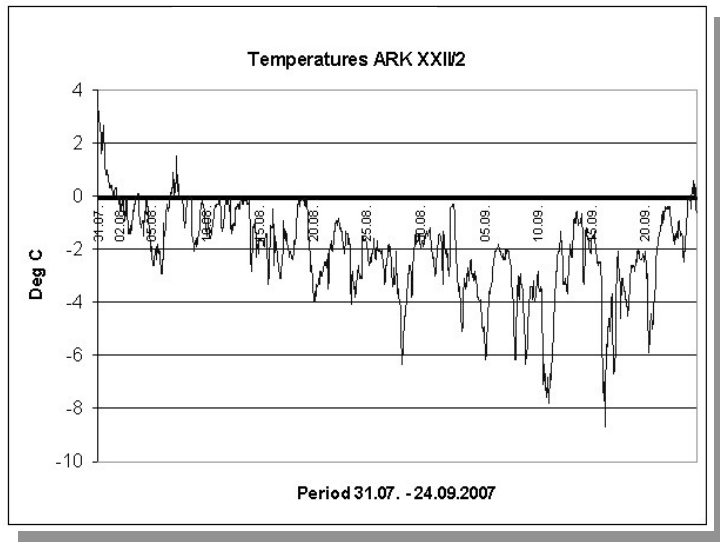


Fig. 2.2: Distribution of Visibility

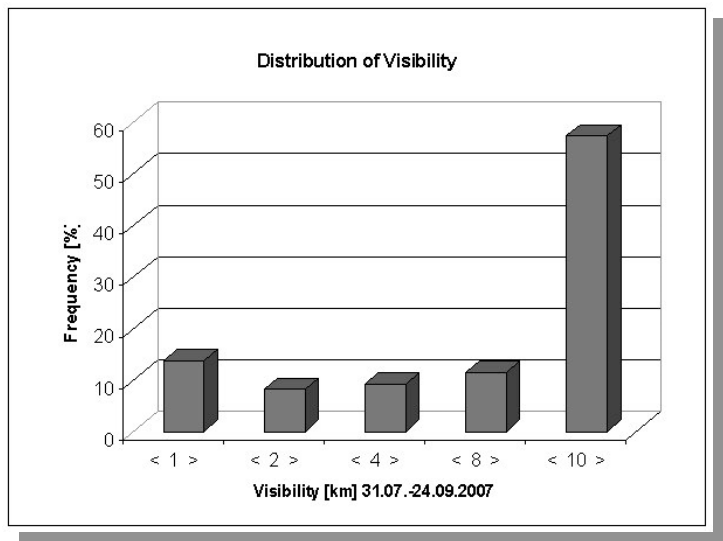


Fig. 2.3: Distribution of Ceiling

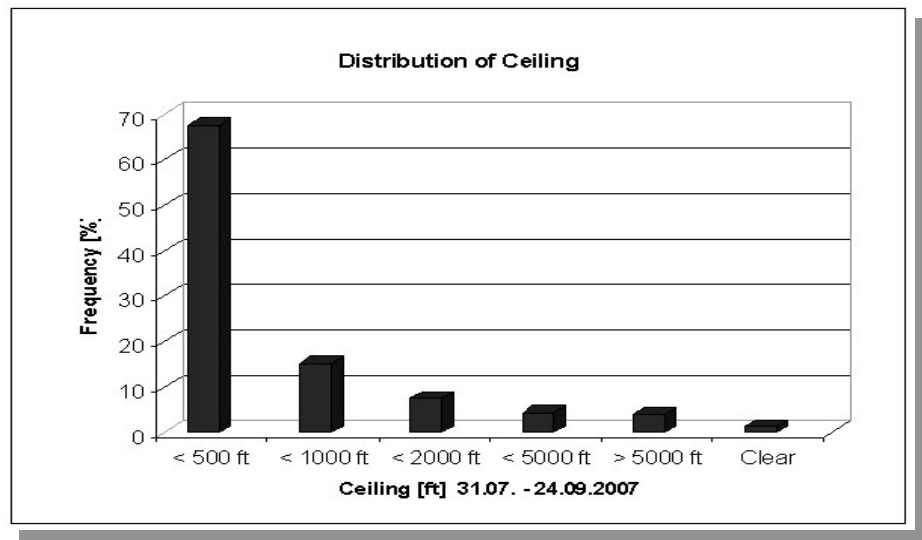


Fig. 2.4:
Distribution of
Wind Direction
31.07. - 24.09.07

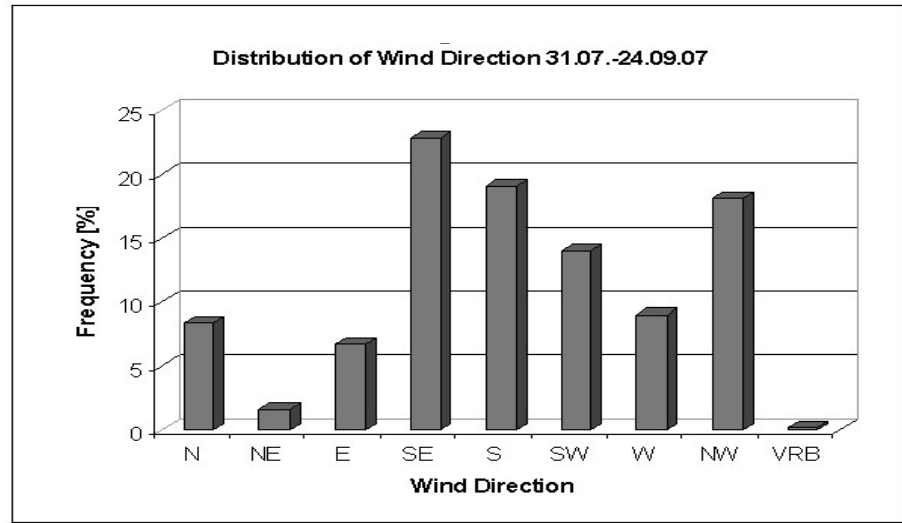
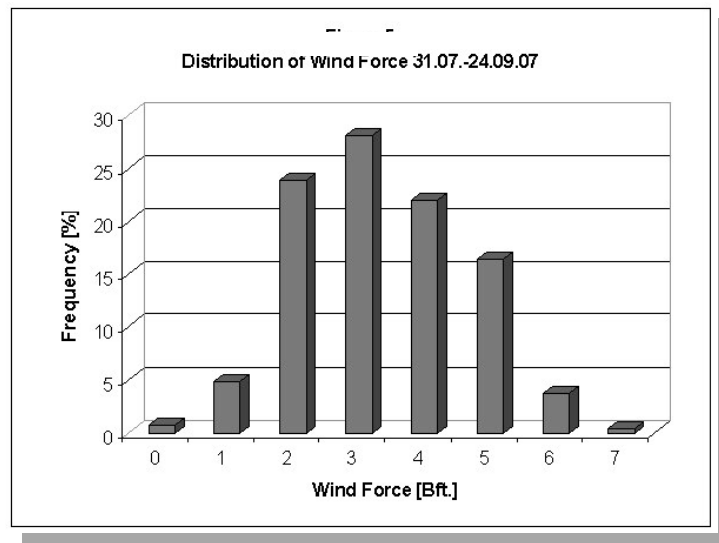


Fig. 2.5:
Distribution of
Wind Force
31.07. - 24.09.07



3. SEA ICE PROPERTIES

Stefan Hendricks¹⁾, Stefan Kern²⁾,
Volker Leinweber¹⁾ Lasse
Rabenstein¹⁾, Gunnar Spreen²⁾,
Andreas Winderlich²⁾

¹⁾Alfred-Wegener-Institut

²⁾Institute of Oceanography IfM HH

INTRODUCTION

The Arctic sea ice cover has been suggested to be one key indicator of the amplification of global warming in the high northern latitudes. One important goal of the *Polarstern* expedition ARK-XXII/2 as part of the International Polar Year (IPY, 03/2007-03/2009) was to assess, together with other scientific expeditions within the IPY, the current status (area, thickness, type, structure) of the Arctic sea ice cover. Our contribution to this international effort comprised sea ice thickness measurements using various techniques: drilling, ground- and airborne electromagnetic sounding, laser profiling, deployment of one ice mass balance buoy and eight sea ice drift buoys (section 3.1). It comprises further airborne multi-frequency sea ice radar backscatter measurements, partly as satellite sensor underflights, aiming at the development of methods to obtain melt pond and thin-ice area fraction and the thin-ice thickness. This suite of remote sensing data is accompanied with *in-situ* investigations of sea ice properties (temperature, salinity, density profiles, roughness) (section 3.2) Finally, hourly / bihourly day-round routine sea ice cover observations from the ships' bridge were conducted (section 3.3).

This report is organized as follows. First, the sea ice thickness measurements will be presented together with buoy deployment activities. Then the sea ice radar backscatter measurements will be described together with a quantitative analysis of sea ice properties that are relevant to interpret the radar data. The work and results described in these two chapters are based on measurements that have been carried out outside the Russian exclusive economic zone (REEZ) in the periods 28 July – 11 August and 24 August – 20 September. The final chapter summarizes routine sea ice observations that were performed during the entire cruise like observations from the ship's bridge, digital photography, and results from routine drilling activities to support the work of the sea ice biology group and the oceanography group.

3.1 Sea ice thickness measurements

Lasse Rabenstein, Stefan Hendricks, Volker Leinweber
Alfred-Wegener-Institut

Objectives

The ultimate goal of sea ice thickness measurements during ARK-XXII/2 was to determine the sea ice thickness distribution within the Trans Polar Drift (TPD). These measurements are a continuation of a series of measurements in the TPD which

have been conducted in irregular intervals by AWI since 1991. Former observations show a thinning of the TPD ice of 20 % within 10 years. The last Arctic summer sea ice campaign took place in 2004. 2005 and 2006 were years with a minimum in sea ice extent. Also the year 2007 shows a new record minimum in sea ice extent. Therefore it is of high interest how the sea ice thickness distribution has developed since 2004 and how its actual status is in 2007.

The instrument of choice is a helicopter based airborne electromagnetic (AEM) induction sounder, the so called "EM-Bird". Furthermore two ground based EM devices, an EM31 and a SLINGRAM instrument, were used during 15 ice stations. Finally an electric driller was used for high accuracy point measurements.

The AWI sea ice physics group used AEM and EM31 instruments during previous campaigns. These methods are well established and a lot of validation measurements were done. It was found that EM methods underestimate thickness over deformed ice. To deepen the understanding of the induction process in deformed ice the SLINGRAM method was used for the first time on sea ice. The advantage of SLINGRAM is a variable frequency and coil separation, in comparison to AEM and EM31, where these parameters are fixed.

Airborne Electromagnetics (AEM) Introduction

Airborne measurements are a very useful way to obtain statistically robust probability distribution functions of sea ice thickness because of two advantages. First, every ice thickness can be sampled and second, the measurements can cover a regional scale of a few hundred kilometres. For this purpose, the Alfred Wegener Institute maintains a helicopter based system that can be operated with every helicopter, which is certified for carrying an external sling load. The so called EM-Bird consists of a cylindrical instrument and a towing cable with a length of 20 meter. The instrument itself is operated in an altitude of 10 to 15 meters above the sea ice. A dragskirt is mounted on the rear for stability during the flight with a typical speed of 80 knots. The system has a weight of 100 kg and a total length of 3.4 meter and is therefore small enough for takeoff and landing operations directly from the helicopter deck.



Fig. 3.1.1: EM-Bird on the helicopter deck of Polarstern. A special cart was used for transport, takeoff and landing operations.

The instrument consists of a pair of rectangular coils, one for generation and one for the reception of low frequency electromagnetic fields. The transmitter coil emits a harmonic signal, the so called primary field, which is the source of induction processes in all conductive mediums in close vicinity to the coil, mainly the ocean water. The induced eddy currents are the source of a secondary electromagnetic field which is detected together with the primary field at the receiver coil of the EM-Bird. From the complex ratio of secondary to primary field the distance between the instrument and the sea water interface can be computed. The EM-Bird used during ARK-XXII/2 has a frequency of 4.06 kHz and a coil spacing of 2.77 meters, with a horizontal coplanar coil configuration. Samples are taken at a rate of 10 Hz, yielding a point spacing of 3 to 4 meters at average flight speeds. Other parts of the EM-Bird are a near infrared laser altimeter system and a GPS receiver. All data are processed fully digitally within the EM-Bird and sent by a wireless data link to the helicopter where it is recorded by a standard laptop PC. All data can be observed by the operator in real time and the laser height of the system is additionally displayed to the pilot by a standard avionic altimeter.

Sea ice thickness can be computed by taking the difference between the distance to the sea water derived by the EM system and the readings of the laser altimeter. Because the return signal of laser always reflects the uppermost reflecting surface, the result of the measurements are the ice plus snow or total thickness if a snow layer is present on the summer sea ice in the Arctic.

Work at sea

Data Acquisition

Measurements were performed with a wide regional coverage of the sea ice of the Transpolar Drift. In total more than 4,000 km of sea ice was profiled during 23 measurement flights. In summer Arctic airborne operations are always hampered by hazards like in-flight icing of the helicopter and poor visibility due to fog patches. Therefore some flights had to be aborted during measurement operations since the weather showed continuously poor conditions during the cruise.

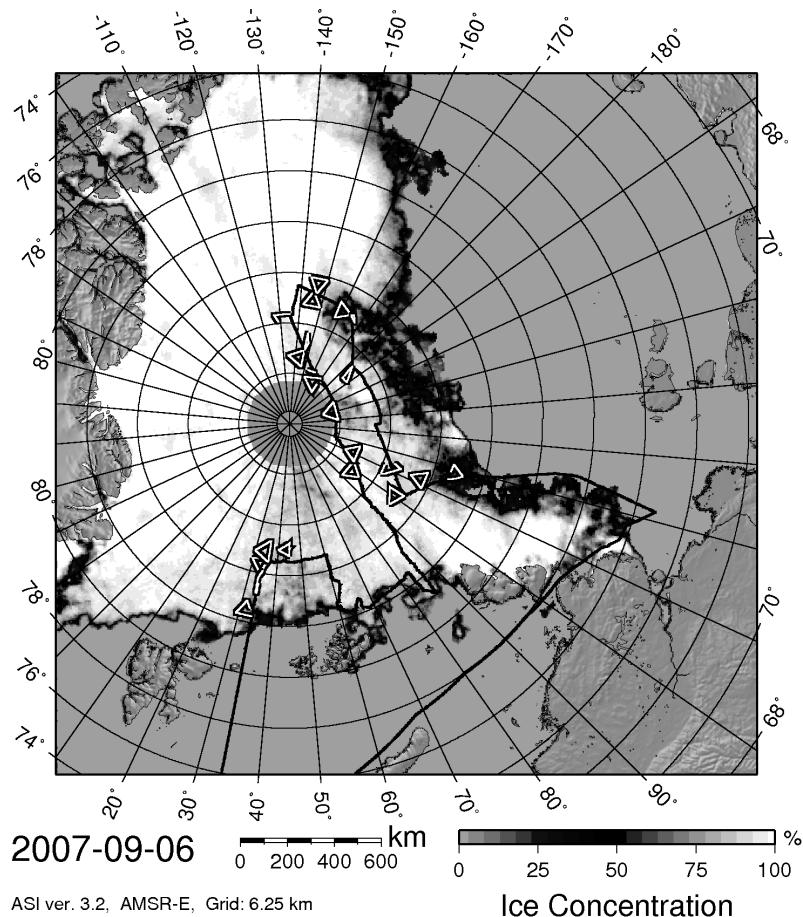


Fig. 3.1.2: Map of EM-Bird flight tracks(triangles)

In general, the flight tracks followed triangles with equally sized sides with a length of 40 nautical miles. On the corners and in the middle of the sides the helicopter ascended to an altitude of roughly 500 feet for system calibration of the EM-Bird and radio contact to the bridge of *Polarstern*. The ascents divided the whole flight in profiles with a length of 15 to 20 minutes. In addition to the EM ice thickness measurements observations of the sea ice surface with a digital camera were conducted by a second person in the front of the helicopter. The images were taken roughly every 5 minutes and geo-located with a waypoint of a handheld GPS. For a more detailed analysis of the surface properties like melt pond coverage of the sea

ice a nadir pointing video camera was also mounted on the helicopter (see section 3.3: Sea ice observations).

Data Processing

The low temperatures of the Arctic play an important role for the performance of electronic components of the EM-Bird. In addition problems with static charges can arise during takeoff procedures, hence the bird has to be disconnected from the power source and cannot be heated at this time. Therefore some electronic components showed significant temperature driven drift behaviour especially in the beginning of the flight. A drift correction is applied by taking zero level measurements in an altitude of more than 300 feet at the beginning and the end of one profile where no signal of the sea water can be received.

Furthermore sites with open water can be used to calibrate the system during the flight. Over open water the EM derived distance and the readings of the laser altimeter are identical. Therefore any larger leads were flagged by the operator manually in the data stream for later identification of suitable calibration points in the data processing.

The conductivity of the ocean water is necessary for the calculation of sea ice thickness. The value is taken from the keel salinometer of *Polarstern*. It is assumed that the conductivity is regionally stable in all areas of the measurements. Errors in the final data product may arise due to local fresh water concentrations caused by stronger melting in the loose ice pack. If possible the conductivity was checked over large leads by measuring the response of open water at different heights of the EM-Bird. In general a good agreement was found and the possible error is assumed to be in the order of 10 cm, which has been found in the variability of the ice thickness result over open water sites. For data processing convenience an average conductivity during the flight is calculated with the *Polarstern* data and sampled into 50 mS/m steps. The conductivity of the surface sea water varied significantly between 2200 mS/m and 2700 mS/m during the cruise depending on the occurrence of melting and the geographical location.

The conductivity value is used to generate an analytical relation between EM readings and distance to the sea water. The relation can be approximated with a series of two exponential functions. The inverse of this function is then used to calculate the distance of the EM-Bird to the sea water. From this distance the laser range is subtracted to get total thickness. As a final step the ice thickness data is geo-located with the onboard GPS antenna.

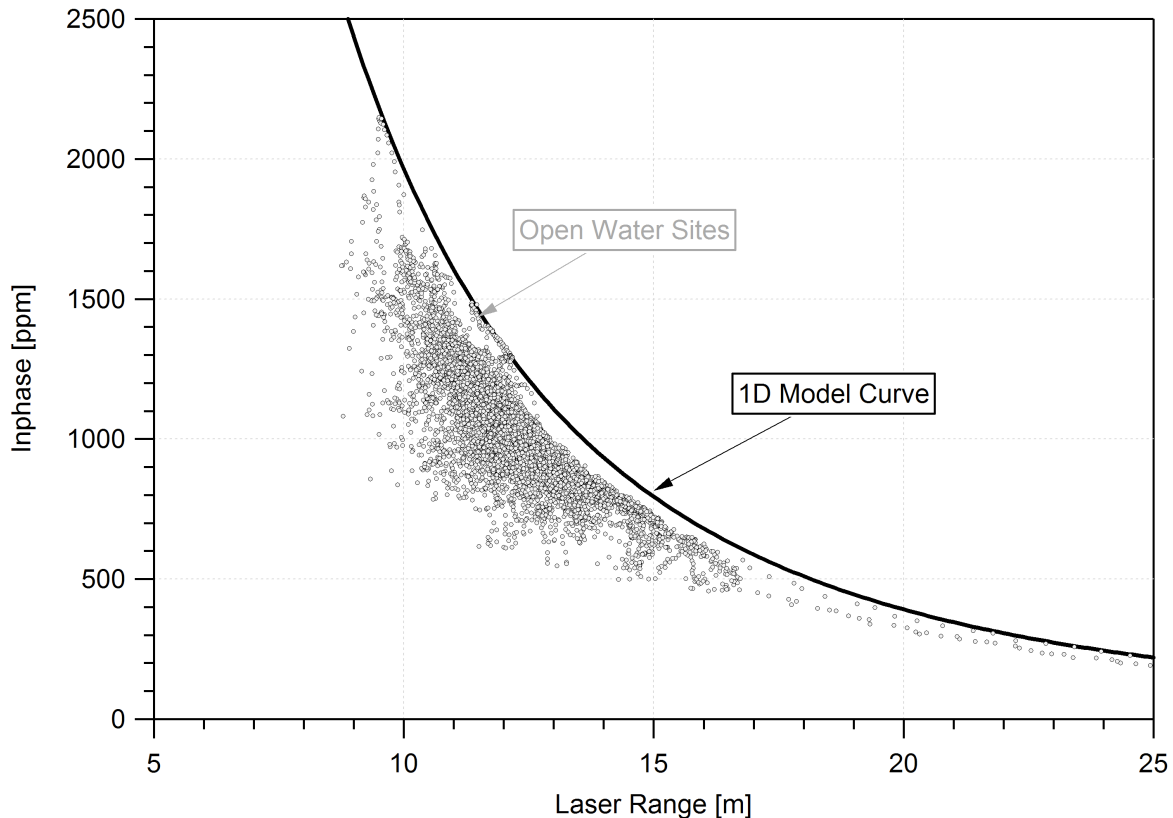


Fig. 3.1.3: EM data taken in different altitude. Displayed distance of the EM Bird to the ice surface is the inphase component (real part of the complex ratio of secondary to primary field) versus the laser range. The black line gives the theoretical values for open water. At a given laser height sea ice causes a reduction of the inphase component, while measurements over open water coincide with the theoretical curve.

Preliminary Results

All flights show a most frequent ice thickness of equal or less than 1 meter (see Table 3.1). No clear thick multiyear ice class could be identified in the individual thickness distribution functions. There are only very weak indications for a modal thickness of 2.3 meters in the second flight on 8 September. This finding coincides with visual observations of thick deformed ice which also carried a lot of sediments. For all other flights it can be assumed that the same ice type was surveyed during the complete cruise.

The measurements can be roughly divided into two zones: The Eurasian and the central Arctic. Both are divided by a time of two weeks, where *Polarstern* was within the REEZ and no EM ice thickness measurement could be carried out. Most of the flights were conducted in the central Arctic and only 5 surveys were done before entering the REEZ.

The results of the preliminary data processing shows that the ice was slightly thicker in the Eurasian zone (20 cm in average ice thickness) than in the later phase of the cruise in the central Arctic. It has to be mentioned that melting was still going on in the mid of September. For later interpretation therefore spatial and temporal effects on the ice thickness distribution have to be decoupled. All ice thickness statistics for

3.1 Sea ice measurements

both zones and all measurements are given in Table 3.2. The last flights of the cruise were dedicated to survey the ice thickness at the very northern ice edge. These flights included a lot of open water which is reflected by the much higher open water fraction.

The open water fraction is defined of the part of the thickness profile which is thinner than 10 cm. This value reflects the accuracy of the system over level ice.

The probability density function (pdf) of both zones are displayed in figure 3.1.4. Additionally to the open water, the fraction of thin ice is also raised compared to the beginning of the cruise where all leads were completely ice free.

Tab. 3.1.1: Results of the individual EM-Bird profiles. The conductivity value represents the value used for the processing.

Date	Flight	Conductivity [mS/m]	Length [km]	Modal Thickness [m]	Mean Thickness [m]	Standard Deviation [m]	Median Thickness [m]
2007/08/03	#1	2650	166,6	1,00	1,32	0,78	1,16
2007/08/06	#1	2650	226,0	1,00	1,40	0,73	1,22
2007/08/06	#2	2650	133,5	0,80	1,30	0,71	1,09
2007/08/07	#1	2700	255,2	0,90	1,31	0,64	1,14
2007/08/10	#1	2650	150,1	0,80	1,40	0,88	1,19
2007/08/28	#1	2550	224,9	1,00	1,34	0,87	1,16
2007/08/28	#2	2500	219,1	1,00	1,30	0,81	1,13
2007/09/01	#1	2400	215,9	0,70	1,13	0,81	0,94
2007/09/03	#1	2350	182,7	0,80	1,22	0,73	1,02
2007/09/03	#2	2350	37,1	0,80	1,36	0,76	1,16
2007/09/04	#1	2300	221,4	0,90	1,43	0,73	1,27
2007/09/04	#2	2300	110,7	0,70	1,16	0,63	1,00
2007/09/06	#1	2300	111,4	0,90	1,34	0,68	1,18
2007/09/08	#1	2250	211,3	0,70	1,18	0,70	0,99
2007/09/08	#2	2250	218,6	1,00	1,48	0,85	1,26
2007/09/09	#1	2200	216,5	0,40	0,88	1,00	0,60
2007/09/09	#2	2200	48,3	0,80	1,24	0,87	1,02
2007/09/10	#1	2400	147,2	0,80	1,30	0,80	1,10
2007/09/15	#1	2550	149,7	0,60	1,01	0,76	0,86
2007/09/16	#1	2550	221,7	0,90	1,14	0,71	1,01
2007/09/17	#1	2550	225,4	0,50	0,81	0,78	0,64
2007/09/18	#1	2500	138,9	0,00	0,46	0,56	0,26

Both zones combined give the summer sea ice thickness distribution of the Transpolar Drift in 2007 (Fig. 3.1.5). The most prominent ice thickness is 90 cm which is significantly lower than measurement in previous years. For example measurements in the Laptev Sea in 1994 showed a modal ice thickness of 2 meter in the Transpolar Drift.

Therefore it can be concluded that in general the sea ice thickness measurements during ARK-XXII/2 support other findings of a decreasing ice thickness and a shrinking of the multiyear ice zone, especially in the Russian Arctic.

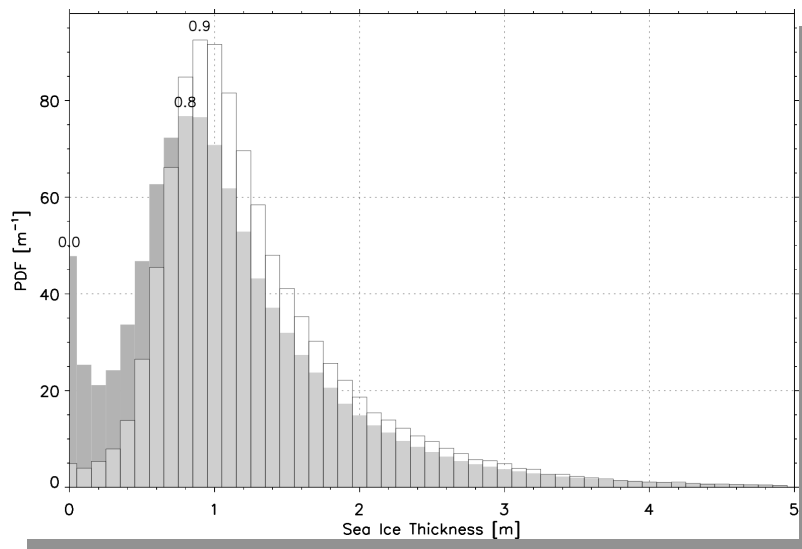


Fig. 3.1.4: Probability Density Functions (pdf) of ice thickness measurements in the Russian (grey) and in the Eurasian Arctic (line)

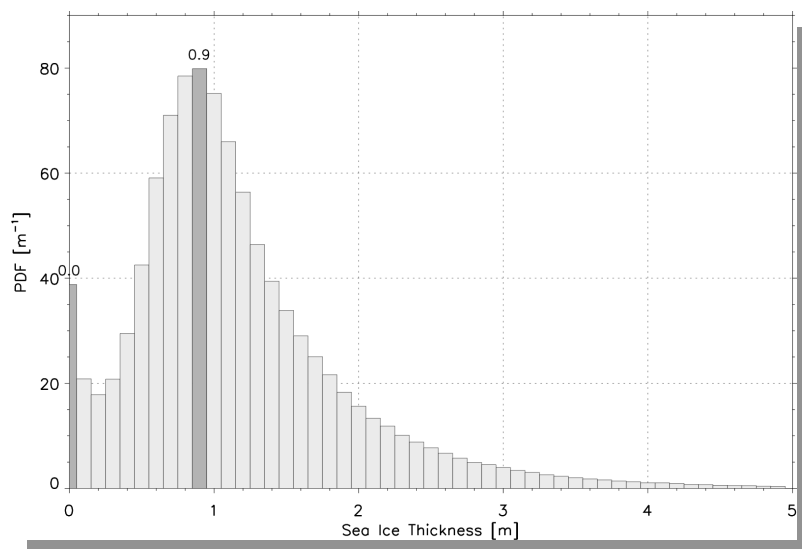


Fig. 3.1.5: Probability Density Function (pdf) assembled with all measurements in the Transpolar Drift in late summer 2007. Marked are the local maxima of the pdf, which give the fraction of open water and the modal thickness of the profiled sea ice.

Tab. 3.1.2: Statistics of the sea ice thickness distribution measured in different zones

Zone	Modal Thickness [m]	Mean Thickness [m]	Standard Deviation [m]	Median Thickness [m]	Open Water Fraction [%]
Eurasian Arctic	0,90	1,34	0,74	1,17	0,7
Russian Arctic	0,80	1,15	0,81	1,01	5,7
Both Zones	0,90	1,20	0,80	1,04	4,7

EM31 ground-based EM measurements

Introduction

Measurements of sea ice thickness in the Transpolar Drift utilizing electromagnetic induction devices have been carried out at Arctic *Polarstern* cruises from 1993 to 2003. This time series has been continued using a Geonics EM31 device during all ice stations. The spatial coverage of the 12 stations ranges from the European basin and the Russian Arctic to the Makarov Basin. Besides obtaining the sea ice thickness distribution surveys were conducted for retrieving supplement data for airborne scatterometer data (section 3.2) and mapping of possible buoy deployment sites (section 3.4).



Fig. 3.1.6: EM31 placed in a kayak and towed over the sea ice

The instrument operates at a frequency of 9.8 kHz and a coil spacing of 3.66 meters. For better signal to noise ratio a horizontal coplanar coil configuration was chosen. The EM readings are recorded by an autonomous data logger at frequency of 0.5 Hz together with geographical positions by an external handheld GPS device. All devices are mounted to a kayak for easy access to every type of ice including melt ponds and even open water. To shelter the EM31 from the external conditions the instrument is placed inside the kayak, while data logger and GPS are mounted outside allowing a quick inspection of the data acquisition process at all time.

The selection of floes for ice stations was mostly restricted by the possibility to access the floe from the ship and therefore mainly by the parameters size, degree of ridging and thickness. In general thick multiyear ice floes were selected for ice stations which will result in a bias of the obtained total ice thickness distribution. The

area of the survey on the ice was normally limited by floe edges and the occasional poor visibility yielding in an average profile length of more than 2 km and a total length of roughly 30 km of ground EM data.

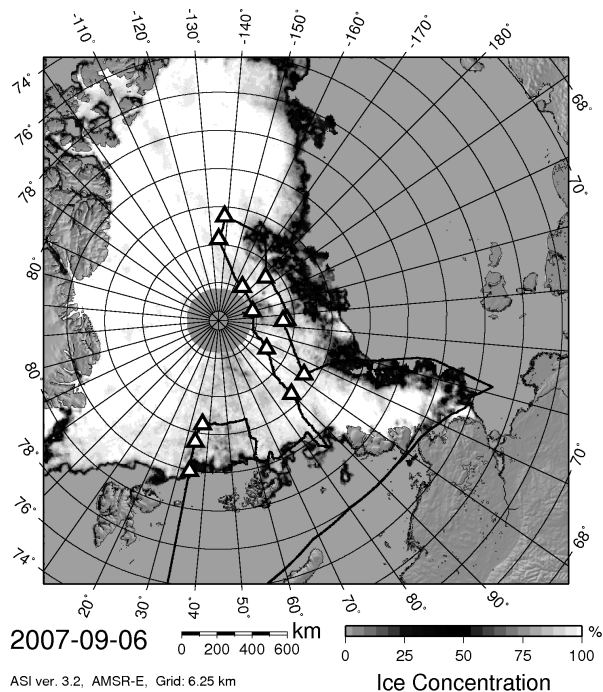


Fig. 3.1.7: Map of ice stations (triangles) with EM31 ground based EM measurements of sea ice thickness

Calibration

Calibration procedures of the EM31 instrument were carried out during several ice stations along the cruise. These were necessary since the instrument showed an offset from the analytical relation of EM readings and distance to the sea water – ice interface. In addition the Inphase reading was always in saturation. This problem could not be solved onboard and was not considered to be critical since the ice thickness is calculated with the apparent conductivity only which showed besides the offset a reasonable behaviour.

For calibration, values of the apparent conductivity are taken with a known distance of the EM31 to the sea water interface. This is equal to ice thickness for an instrument directly placed on the ice. A good location of level ice was investigated by ice drilling to retrieve the ice thickness on an area of roughly 5 m x 5 m. Then an average of thickness values of the different holes is used as reference distance. As a second step, the kayak was lifted to different heights above the sea ice. The distance between ice surface and bottom of the kayak was measured with a ruler tape and the value for the apparent conductivity was recorded. Four different heights were realized: 1) on the ice, 2) hip-height, 3) shoulder height and 4) height above the head. At some ice stations the kayak floated freely in the sea water to get calibration points for very small distances to the conductive medium. To all heights a value of 18 cm was added which was the distance between the centre of the coils and the bottom of the kayak.

3.1 Sea ice measurements

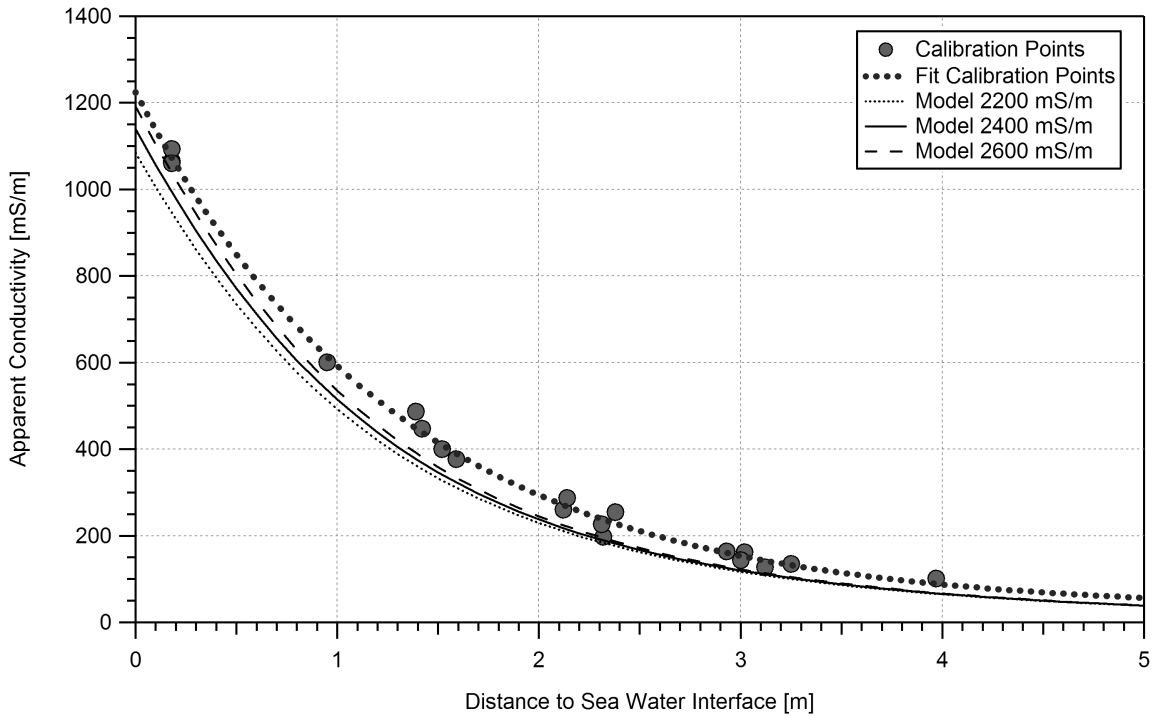


Fig. 3.1.8: Result of EM31 calibration procedure. Marker are calibration point represented by exponential relation (dotted curve). Lower three curves are numerical solution for 2,200, 2,400 and 2,600 mS/m as conductivity of sea water.

From analytical calculation it is known that the retrieved ice thickness depends only weakly on the conductivity of the sea ice. For all the ice stations it is assumed that the conductivity of the sea ice plays no role despite the fact that a lot of brine channels were present during the cruise. Therefore all calibration results of different ice station were used to construct one relation between apparent conductivity and ice thickness which was used for all ice stations (see Fig. 3.1.8). The relation has the following form:

$$z = - 1/a_2 \cdot \ln ((s_a - a_0) / a_1) - h_0$$

(where: z = ice thickness, s_a = apparent conductivity, h_0 = instrument offset of EM31 in kayak, a_i = calibration coefficients). The calibration coefficients were obtained by a fit of an exponential function to the calibration points taken on the ice stations and are listed in Table 3.3.

Tab. 3.1.3: Calibration coefficients obtained during several ice stations

a_0	28.8821
a_1	1196.07
a_2	0.75357

The average error made by the fit compared to the actual data points can be estimated with roughly 10 cm, which lies well within the instrument error.

Processing

With the relation between apparent conductivity and ice thickness obtained by calibration procedure a conversion of the retrieved EM readings in ice thickness is a simple process. In general the files from the data logger are used as an input for a computer programme in the IDL language. The data is already synchronized with the GPS position by the data logger. Since pure GPS positions are of limited use on a drifting ice floe a correction is applied utilizing the GPS position and gyro heading of *Polarstern*. With both information a *Polarstern* Reference Frame (PRF) is established. For the reference frame a cartesian coordinate system in meters is used with the *Polarstern* Trimble1 GPS antenna as origin a northwards pointing y-axis. The GPS antenna of *Polarstern* is used to correct for ice drift, while the change of the gyro heading can be taken to correct for floe rotation. Case studies have shown that a good agreement in PRF-positions can be achieved for repetitions of validation lines with a spacing of a few hours.

From the ice thickness data a probability density function (PDF) can be calculated. But this pdf can be biased since the kayak is never pulled at a constant speed over different types of ice and sometimes measurements were continued while the kayak remained at the same spot for a certain time. To get a statistical correct pdf the profile is re-sampled to constant point spacing. Since the ice drift correction is not perfect a few data points are removed which show only a short variation in position and no change in ice thickness. All points with invalid GPS positions are also not regarded for the final ice thickness distribution.

Preliminary Results

All data has been taken into account for preparing the final ice thickness results except data which has been taken during surveys of buoy deployment sites. During these surveys the profiles were focused to a few areas yielding no representative mapping of the floe.

Tab. 3.1.4: Statistics of the sea ice thickness distribution measured by the EM31

Station	Date	Mean Thickness [m]	Standard Deviation [m]	Median Thickness [m]	Profile length [km]
01	2007/08/02	2.27	0.80	2.46	1.72
02	2007/08/05	1.85	0.80	1.60	1.49
03	2007/08/07	1.60	0.36	1.51	1.39
07	2007/08/24	2.07	0.93	1.73	1.79
08	2007/08/28	1.49	0.80	1.14	4.08
09	2007/08/31	1.69	0.77	1.43	2.46
10	2007/09/02	2.15	0.87	2.01	2.64
11	2007/09/05	2.42	1.39	1.95	2.54

Station	Date	Mean Thickness [m]	Standard Deviation [m]	Median Thickness [m]	Profile length [km]
12	2007/09/07	2.03	0.80	1.78	2.52
13	2007/09/10	1.83	1.30	1.60	4.06
14	2007/09/14	1.64	1.00	1.48	2.11
15	2007/09/16	1.60	0.89	1.32	3.17

Values for ice thickness are higher compared to airborne EM measurements which reflect the selective choice for the ice stations. The average ice thickness is also raised by the fact that no very thin ice was profiled, because it was not accessible for measurements in general. In the pdf (Fig. 3.1.9) a modal thickness of 1.3 meter of the most dominant ice type can be observed, while there is weak indication for a multiyear ice mode of 2.3 meters. But since there were always ice deformation features at almost every ice station this secondary mode of the pdf can also be explained by the thickness of younger ridged or possible rafted sea ice.

Taken all ice station into account the mean ice thickness amounts to 1.86 meter with a standard deviation of 1.01 meter. The median of the distribution gives a slightly lower value of 1.6 meter.

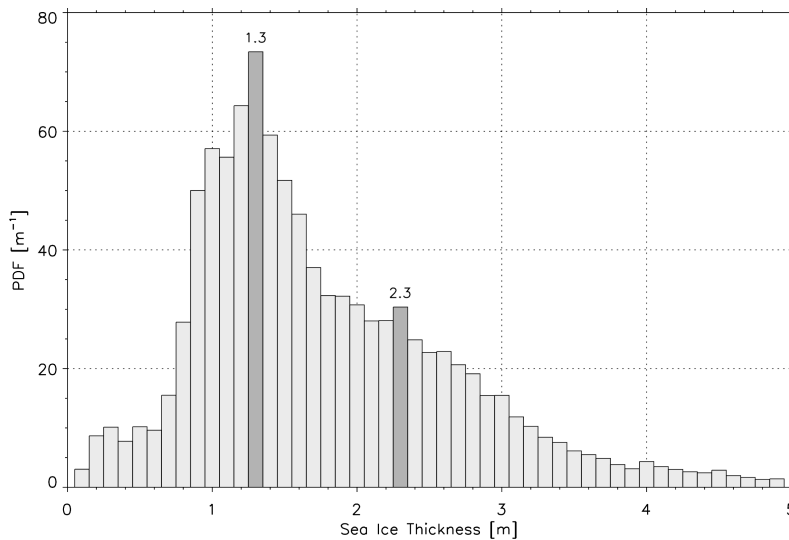


Fig. 3.1.9: Probability density function (pdf) of sea ice thickness obtained with ground-based EM measurements with data of all ice stations

**Slingram ground-based EM measurements
Work at Sea**

The SLINGRAM instrument was tested during one ice station, two times on level ice and one time to profile an ice ridge. To operate the instrument three persons are necessary. One person carries the transmitter coil, one person the receiver coil and the third person writes the data to a protocol. The measurements were performed using a horizontal coplanar loop mode. Therefore it was necessary to hold both, transmitter and receiver, in a horizontal position, which could be achieved with a

level. The whole procedure is time consuming. Nevertheless all measurements were done during one ice station. They include two ridge profiles of 50 meter length with a point spacing of two meters and measurements over level ice. The instrument works with the same principle as the EM31 or the EM-Bird. The transmitter produces a primary magnetic field and the oceans inductive response is measured at the receiver coil. Eight frequencies were used: 440, 880, 1,760, 3,520, 7,000, 14,000, 25,000 and 56,000 Hz. Furthermore three different coil spacings have been used: 5 m, 10 m and 20 m.

The measurements over level ice were done to compare the results of the Slingram instrument with 1D model results. Therefore the level ice thickness at the measurement site was determined by drilling.

The overview about the Slingram Ridge profiling is given in figure 3.1.10. The ridge profiling was done using a coil spacing of 10 and 20 m only. Each profiling started with the receiver on the first point and it ended when the transmitter reached the last point. Therefore profiling with a separation of 10 meters included 21 data points and the profiling with a 20 meter separation included 16 measurements. On every point all eight frequencies were measured. Both profiles were orientated in an angle of $\sim 45^\circ$ to the orientation of the ice ridge, and with an angle of approximately 90° to each other. For every data point the height over sea surface was determined using a levelling laser. Furthermore ice thickness was measured on both profiles using an EM31.

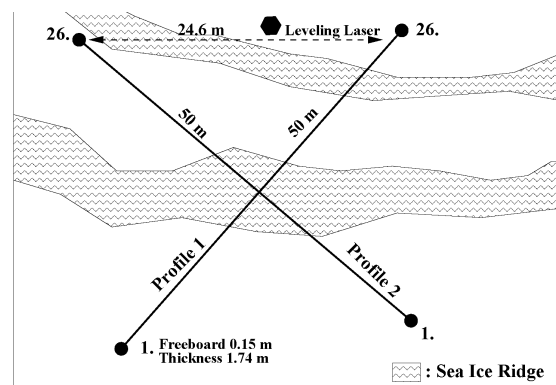


Fig. 3.1.10: Overview about the two Slingram profiles over an ice ridge. On each profile 26 points were measured

Preliminary Results

Figure 3.1.11 shows the results of Slingram measurements over level ice for a coil separation of 10 m and 20 m. The midpoint between receiver and transmitter was fixed. The ice thickness was known by an initial drilling survey. Therefore a 1D forward model could be calculated to compare the model results with the measurements. The graph in figure 3.1.11 shows the ratio of primary to secondary field in percentage for all frequencies. The results for the 10 and 20 meter mode are in good agreement with the model. Only for the higher frequencies the results differ quantitatively from the model. In the 5 m mode the results were in no agreement with the model and are not shown in the graph. The results over level ice show that the Slingram method can be used for sea ice applications.

Results of the ridge profiling are shown in figure 3.1.12. Combined levelling, snow thickness and EM31 measurements provided data of ice and snow thickness, including freeboard and draft. The solid lines show the Slingram results for a coil separation of 10 m in percentage of the primary field. The dark lines are the inphase and the bright ones the quadrature. The data are not yet corrected for the elevation difference between receiver and transmitter. The raw data show no significant correlation to the structure of the ridge, as it is determined with the EM31. A reason

3.1 Sea ice measurements

for this is most probably the 3D nature of the thickness problem in deformed ice and the missing height correction.

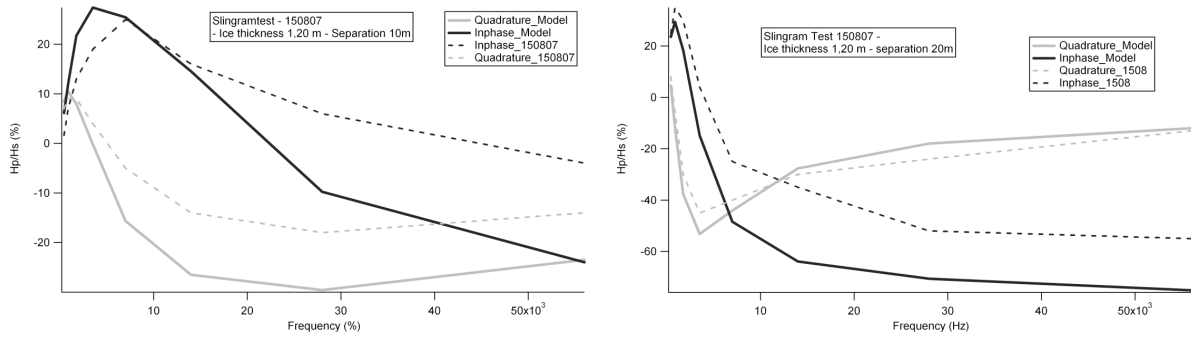


Fig. 3.1.11: Slingram results over level ice. Shown is the ratio of primary to secondary field versus frequency. The left graph shows the results for a coil separation of 10 m and the right graph for a separation of 20 m.

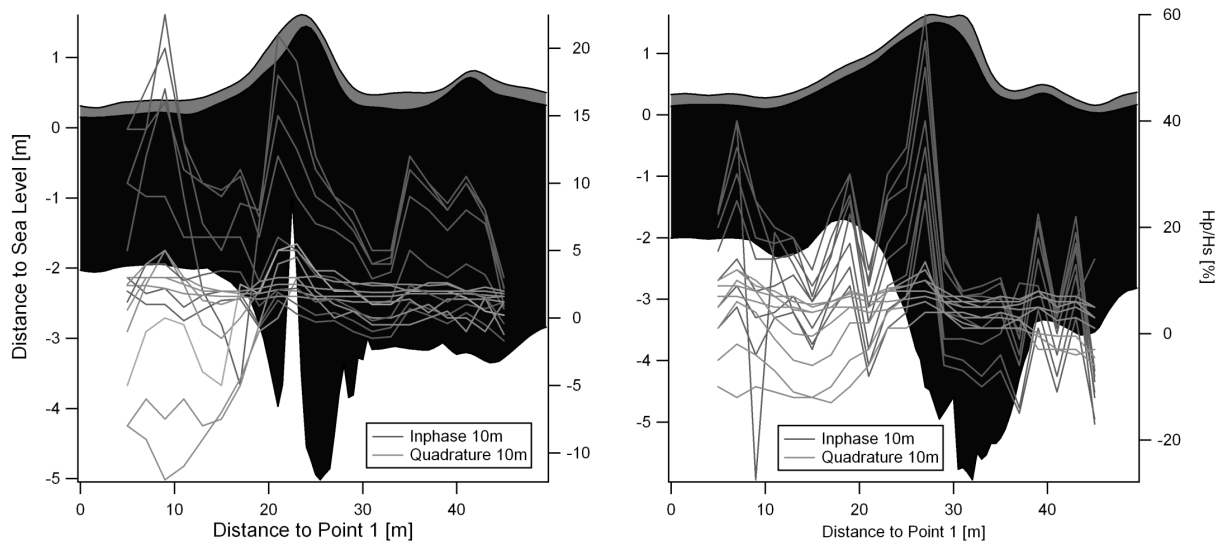


Fig. 3.1.12: The left graph shows profile 1 and the right graph profile 2. The EM31 ice thickness is shown in black, including freeboard and draft, and the snow thickness in grey. The solid lines are the Slingram results.

Video recordings of sea ice surface parameters

In addition to the EM-Bird measurements the ice situation was recorded during parts of the flights with a nadir-looking digital video camera. The camera was mounted inside a metal box to the landing gear of the helicopter. The box was isolated and equipped with a heating element to shelter the camera of the harsh condition during the flight. The system consisted of a Sony Digital Video Camera Recorder with the following technical specifications:

Tab. 3.1.5: Technical specifications of the Camcorder

	F1.6-2.4
focal length	6-72 mm
diameter of objective	58 mm
Opening angle horizontal	ca. 42°
Opening angle vertical	ca. 33°
Effective number of pixels on CCD	400000

The flights were recorded using 4:3 format to Sony Mini-DV tapes by “Single Play”, so the maximum length of one recording was 60 min. Table 3.1.6 shows the recorded movies with their respective date, time, coordinates and length. Figure 3.1.13 shows all coincident data of ice thickness and video recording.

In total, 08:19:23 hours of video data were recorded. Assuming a flight height of 35 m, the area covered by one frame of the movie is around 27 x 21 m or 570 m².

In addition to the visual documentation of the ice situation, the videos can be used to estimate the coverage of the observed area by melt ponds, sea ice and open water. To achieve this, a Matlab algorithm has been developed during the cruise. This algorithm classifies the pixels of single frames of the movie by their brightness and identifies them after calibration as sea ice, melt pond or open water. In a second step, the areas identified as melt ponds, which are connected to open water, are classified as frozen open water.

The software gives reasonable results, but there are still some difficulties to overcome concerning the automatic brightness adaptations of the camera during the flight and masking the shape of the bird and the dirt on the protecting glass window.

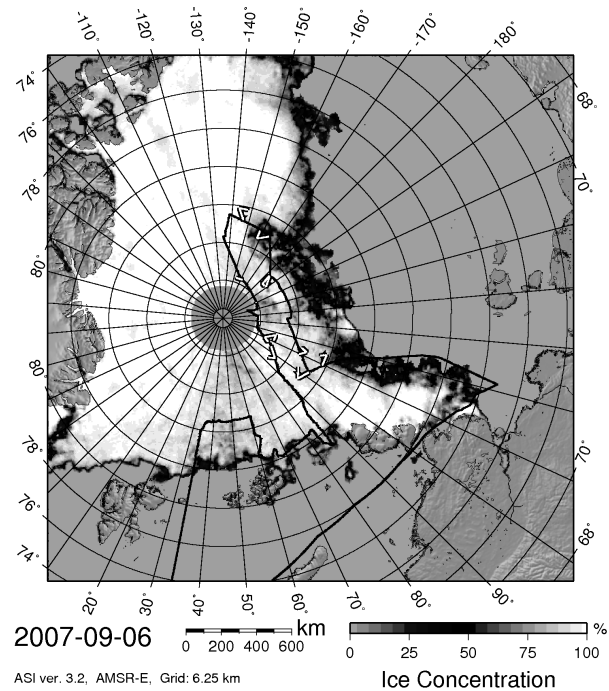
Tab. 3.1.6: List of all video recording taken during EM-Bird measurement flight

Date	Start			End			Length
	Time	Latitude	Longitude	Time	Latitude	Longitude	
03.08.2007	16:00:14	82°17.7161 N	029°16.4692 E	16:12:39	82°32.6989 N	030°16.2661 E	00:12:25
	16:15:49	82°36.5872 N	030°32.5874 E	16:27:18	82°50.3459 N	031°33.2801 E	00:11:29
	16:31:16	82°49.6020 N	031°35.0619 E	16:47:03	82°32.9973 N	032°49.9767 E	00:15:47
	16:51:26	82°28.2229 N	033°10.2398 E	17:02:45	82°16.4028 N	033°58.2857 E	00:11:19
28.08.2007	10:39:42	87°02.9614 N	104°22.6998 E	10:53:20	86°48.6182 N	100°44.1192 E	00:13:38
	10:56:01	86°47.8792 N	100°33.7163 E	11:09:40	86°32.4456 N	097°22.4393 E	00:13:39
	11:12:35	86°33.7119 N	097°06.9774 E	11:26:06	86°50.3290 N	094°13.3823 E	00:13:31
	11:28:51	86°51.4749 N	094°01.0910 E	11:40:12	87°05.8347 N	090°52.7294 E	00:11:21
28.08.2007	15:17:08	87°04.9881 N	111°40.9976 E	15:31:47	87°04.0039 N	117°19.1139 E	00:14:39
	15:35:29	87°05.1920 N	117°09.4166 E	15:46:08	87°18.6246 N	114°30.7017 E	00:10:39
	15:49:45	87°19.3542 N	114°20.3927 E	16:02:21	87°35.1218 N	110°28.6849 E	00:12:36
	16:06:26	87°34.4330 N	110°23.4044 E	16:19:38	87°19.2644 N	107°11.2551 E	00:13:12

3.1 Sea ice measurements

Date	Start			End			Length
	Time	Latitude	Longitude	Time	Latitude	Longitude	
01.09.2007	14:11:39	88°04.1836 N	160°35.8495 E	14:13:17	88°04.2544 N	160°18.0482 E	00:01:48
03.09.2007	14:52:15	87°43.9869 N	161°49.0833 W	15:06:42	87°45.3999 N	153°31.4537 W	00:14:27
04.09.2007	09:17:05	87°10.6261 N	146°27.3298 W	09:17:36	87°11.2502 N	146°28.2624 W	00:00:31
08.09.2007	11:29:10	84°43.4537 N	146°44.6277 W	11:45:41	84°26.1937 N	145°02.7110 W	00:16:31
	11:48:10	84°25.6635 N	144°59.8908 W	12:04:07	84°08.4448 N	143°30.3685 W	00:15:57
	12:07:12	84°08.4686 N	143°35.0653 W	12:22:09	84°08.9914 N	146°44.7200 W	00:15:57
09.09.2007	09:01:31	85°04.1669 N	164°24.0936 W	09:16:06	85°15.4743 N	161°25.4462 W	00:14:35
	09:19:07	85°16.1741 N	161°13.8356 W	09:32:44	85°26.6185 N	158°00.6745 W	00:13:27
	09:35:41	85°25.9655 N	158°01.5749 W	09:53:17	85°05.5649 N	158°01.1665 W	00:17:36
	09:56:15	85°05.3293 N	158°02.0116 W	09:59:31	85°01.6687 N	158°01.2747 W	00:03:16
09.09.2007	12:03:45	85°04.9239 N	164°41.1488 W	12:17:12	85°14.7524 N	167°45.5123 W	00:13:27
	12:19:53	85°16.0452 N	167°55.9689 W	12:30:31	85°23.4635 N	170°30.8678 W	00:10:38
	12:33:45	85°21.4176 N	170°53.9415 W	12:36:10	85°18.3962 N	170°55.5130 W	00:02:25
	12:39:30	85°14.2562 N	170°58.2847 W	12:41:28	85°11.6770 N	171°00.1395 W	00:01:58
	12:55:57	85°05.7821 N	168°00.2283 W	13:05:48	84°52.8497 N	168°00.1506 W	00:09:51
10.09.2007	15:31:15	86°43.4185 N	176°40.9585 E	15:42:03	86°55.8795 N	174°27.9449 E	00:10:48
	15:44:43	86°56.3252 N	174°23.0767 E	15:58:59	87°12.1632 N	170°59.5621 E	00:14:16
	16:04:33	87°13.8627 N	173°18.3394 E	16:13:21	87°10.0143 N	176°10.2976 E	00:08:48
	16:15:27	87°06.9015 N	176°19.9155 E	16:33:48	86°41.8685 N	177°23.4377 E	00:18:21
15.09.2007	13:33:18	85°52.7721 N	116°06.2881 E	13:49:22	85°34.2055 N	114°20.3608' E	00:16:04
	13:52:00	85°33.4614 N	114°16.8876 E	14:07:00	85°15.5707 N	112°49.3017 E	00:15:00
	14:09:28	85°16.0807 N	112°45.1936 E	14:24:09	85°31.2466 N	110°09.4184 E	00:14:41
	14:26:47	85°31.9861 N	110°01.6030 E	14:28:11	85°33.3822 N	109°45.6701 E	00:01:24
16.09.2007	12:16:14	84°39.7946 N	102°31.2567 E	12:30:16	84°48.1923 N	099°30.4372 E	00:14:02
	12:32:31	84°48.3591 N	099°27.3379 E	12:47:03	84°56.2509 N	096°05.6496 E	00:14:32
	12:50:16	84°56.2889 N	096°07.6495 E	13:04:58	85°08.4233 N	099°21.3631 E	00:14:42
	13:07:47	85°09.0479 N	099°31.9153 E	13:18:49	85°17.3151 N	102°05.9464 E	00:11:02
17.09.2007	10:35:50	84°12.6845 N	109°37.6441 E	10:46:50	84°13.0596 N	112°10.9981 E	00:11:00
	10:49:43	84°13.0531 N	112°10.3871 E	11:04:01	84°12.4891 N	115°27.6639 E	00:14:18
	11:07:48	84°13.1707 N	115°23.7404 E	11:21:34	84°30.9297 N	113°52.1853 E	00:13:46
						Total time:	08:19:23

Fig. 3.1.13: Map of coincident EM-Bird ice thickness measurements and video recording of sea ice surface properties (symbols)



3.2 Sea ice radar backscatter measurements for improved melt-pond and thin-ice cover analysis

Stefan Kern, Gunnar Spreen, Andreas Winderlich
Institute of Oceanography (IfM HH)

Background and objectives

Melt Ponds form regularly on summer Arctic sea ice. They are on average 10 m² in size, between a half and one meter deep, and can cover up to 50 % or more of the sea ice area. Coverage and depth varies with the sea ice type and its degree of deformation, as well as the snow thickness at the beginning of the melt period. During freeze-up melt ponds are the first open water areas to re-freeze because of the comparably low surface salinity (even when melted through because of the strong vertical stratification of the ponds' water column). In a physical sense, melt ponds are simply areas of open water. This means, that due to the low albedo of open water (0.06) compared to that of sea ice (melting: 0.62; snow covered: 0.82), substantially more solar radiation is absorbed, further enhancing the melt process. Depending on the depth of the melt pond and upon the thickness and the type of the ice underneath, melt ponds show albedo values between 0.15 and 0.3.

Sea ice concentration retrieval algorithms based on satellite passive microwave observations tend to underestimate the ice concentration under the presence of melt ponds. In this case, no differentiation can be made between the open water of a melt pond and the open water of the leads or breaks between the ice floes. Therefore, quantitative estimation of the melt pond cover fraction on sea ice on a regular basis would support a more accurate retrieval and verification of the sea ice concentration during summer. It would further support numerical modelling of the sea ice decay during summer by providing a more accurate estimate of the summer-time sea ice albedo.

Thin ice (with a thickness below about 30 cm) develops in large areas during freeze-up and in leads, breaks and polynyas during winter. Thin ice areas are sites of enhanced sea ice formation during winter. The associated brine rejection into the ocean can trigger oceanic deep convection and water mass modification. Thin ice areas are sites of enhanced winter-time ocean-atmosphere heat exchange as compared to thick ice. As thin ice can be deformed easily, continuous thin ice formation and deformation under the action of tidal and inertial ocean surface motion can add a substantial amount of ice to the total annual sea ice mass balance. Finally, frost flowers developing on thin ice have been suggested lately to play a significant role in the halogen chemistry in the lower troposphere.

The observed accelerated retreat of the summer Arctic sea ice cover leaves larger open water areas to re-freeze during fall freeze up. Thus, regular observations of the thin ice area and a quantitative estimation of its thickness will become increasingly important in the near future and will allow us to better quantify the salt input into the ocean during sea ice formation.

First attempts to get information about the melt pond cover fraction are either based on high-resolution visible frequency satellite observations (Landsat-TM), or data obtained from active microwave instruments at 5.3 GHz (C-Band) (RADARSAT-1 Synthetic Aperture Radar (SAR)) or 13.4 GHz (Ku-Band) (SeaWinds Quikscat Scatterometer), the latter two instruments having the advantage that they are independent of daylight and cloud cover. One result of these attempts is, that the combination of lower frequency (C-Band or below) with higher frequency (10 GHz (= X-Band) or above) could improve the quality of such observations.

Several methods exist that allow us to identify thin ice and to estimate its thickness using satellite data in the infrared (IR) (clear sky only) and/or microwave (MW) frequency range (independent of clouds). Using data acquired in the IR frequency range requires detailed additional information about the net surface heat and radiation fluxes. Such data are difficult to obtain in the remote polar regions and thus have often to be taken from a numerical model with a grid-cell size, that is much larger than the thin ice areas, typically resulting in an under-estimation of the flux values. Airborne active MW data acquired at co-polarization (see below) have been used to obtain information about the thickness of thin ice. Results are quite diverse, with maximum thin-ice thickness values to be obtained between 10 and 100 cm, depending on the used frequency (1.0 (L-Band) to 10.0 GHz (X-Band)). As mentioned for the melt ponds, a combination of different frequencies (and polarizations) has been suggested to yield an improvement in thin-ice identification and retrieval of its thickness.

Aims

- to find the most appropriate frequency / polarization / incidence angle combination to unambiguously identify melt ponds with active MW radiometry, and to obtain an estimate of the melt-pond cover fraction

- to find the most appropriate frequency / polarization / incidence angle combination to unambiguously identify thin ice with active MW radiometry, and to improve existing methods to estimate the thickness of thin ice

In order to achieve these aims we combined helicopter-borne radar backscatter measurements of sea ice with *in-situ* measurements of relevant sea ice parameters. Measurements of the *in-situ* ice properties are needed to interpret the Multi³Scat radar backscatter signal. The backscattering of the radar electromagnetic waves can be divided in the main processes surface and volume scattering. While the surface scattering is mainly a function of the surface roughness and the near surface conductivity, the volume scattering is influenced by the porosity and conductivity of the scattering medium. Porosity and conductivity can be described by the ice density, salinity, and the amount of liquid water (relevant in case of snow), and determine also the penetration depth of the electromagnetic radiation into the scattering medium. This depth determines at which layer the main scattering processes take place. It is not just a function of density and conductivity of the scattering medium but also of the used frequency. For the frequencies used by the Multi³Scat sensor (see section Work at sea – The Multi³Scat sensor) the maximum penetration depth into sea ice should be below 50 cm. To obtain this information the following quantities are measured on the ice:

- 1) surface properties
 - snow thickness DS
 - snow surface temperature TS
 - snow-ice interface temperature TI
 - air temperature TA
 - photography of snow and ice surface in front of a scale to get e.g. the snow grain size
- 2) volume properties (profiles of only the uppermost meter of the sea ice)
 - temperature
 - salinity
 - density

Additional ice cores were drilled and stored in one piece at -20° C. They are available for the preparation of thick- and thin-sections for analysis of ice grain, air bubble and brine pocket size and distribution at home. It is important to mention, that the salinities and densities measured here, are the pure ice values with most of the brine removed. Especially the warm porous summer ice sampled on this cruise loses most of its brine through the large, opened brine channels when the ice core is removed from the borehole. Only small parts of the brine in closed brine pockets remain in the ice. In the upper few centimetres, which are most important for our later analysis, above the water level this problem might not be severe, but in the lower part of the ice core this effect is definitely not negligible.

Work at Sea

The Multi³Scat Sensor

We used the multi-frequency, multi-polarization mono-static homodyne low-IF Doppler-Scatterometer (Multi³Scat) of the University of Hamburg to obtain measurements of the radar backscattering characteristics of sea ice. Figure 3.2.1 a) shows the components of the Multi³Scat schematically. Table 3.2.1 gives an

overview upon its technical specifications. In this table the polarization combination HH means, that the Multi³Scat transmits and receives electromagnetic radiation at horizontal polarization; VV means the same for vertical polarization. These are the co-polarized channels. HV and VH are the so-called cross-polarized channels, meaning that the radiation is transmitted at either horizontal or vertical polarization and received at the not transmitted polarization, respectively. Thus, the Multi³Scat allows to measure quasi-simultaneously at five different frequencies and four different polarization combinations.

The radar signal is generated in five modules separately for each frequency band by two phased-locked oscillators with external reference frequency input by a Direct Digital Synthesizer (DDS), offset against each other by a frequency in the kHz range (about 700 Hz at L- and about 10 000 Hz at Ku-Band). Microwave switches in the transmit and receive path, which are triggered via the steering unit with another reference signal from the DDS, allow to switch between transmission and reception of the radar signal. For each frequency band the signal is transmitted via a circulator into a multiplexer, where the signals of all bands are combined and subsequently fed into the parabolic dish antenna via a dual-polarization broad-band feed after decomposition into H- and V-polarization. The received signal is first decomposed into the five frequencies, fed into the corresponding module via the circulator and then mixed with the signal of the receive path. The resulting kHz signal is subsequently amplified and filtered before it is digitized and streamed on a hard disc (Fig. 3.2.1).

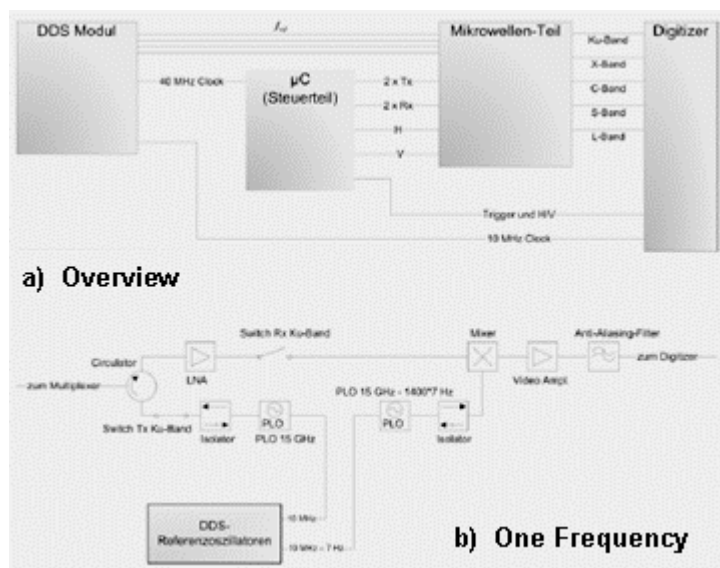


Fig. 3.2.1: a) Schematic overview of the components of the Multi³Scat with, from left to right, the DDS, the steering unit, the MW unit, and the digitizer; b) Schematic overview of one frequency band.

Tab. 3.2.1: Technical specifications of the Multi³Scat

Scatterometer Typ	Homodyne low-IF Doppler-Scatterometer				
Antenna	Parabolic Dish, Ø 96 cm				
Polarization	VV, HH, HV, VH				
Nominal Flight altitude [m]	30-300				
Speed above ground [m/s]	30-50				
Incidence angle θ [°]	20 to 70 (can be altered during flight)				
Pulse repetition [Hz]	81920 (typical)				
Frequency-Bands	L	S	C	X	K _u
Frequency [GHz]	1.0	2.4	5.3	10.0	15.0
Wavelength [cm]	30.0		5.7	3.0	2.0
Emitted Power [mW]	150	100	40	10	10
Antenna Beamwidth (2-Way; 3dB) [°]	13.6	5.6	2.5	1.4	0.9
Footprint: $\theta = 23^\circ$ [m × m]	20.7 × 22.6	8.5 × 9.2	3.8 × 4.1	2.2 × 2.3	1.4 × 1.5
$\theta = 53^\circ$ [m × m]	31.7 × 54.0	13.0 ×	5.8 × 7.9	3.3 × 5.4	2.1 × 3.5

The Multi³Scat is mounted in an aluminium frame, which is designed to be used with a MBB BO-105 helicopter. A lever at the end of this frame carries the antenna and can be steered during flight to allow incidence angles between 20° and 65°. This lever also carries a high-resolution video camera (704 x 584 pixels) and a medium resolution IR camera (384 x 288 pixels, 0.08 K temperature resolution), both looking at the radars' footprint and allowing to monitor the ice situation (type) and to obtain the IR (surface) temperature distribution within the radar's footprint along track at the same incidence angle as the radar (Fig. 3.2.2). A gyro measures continuously the helicopters' pitch- and roll-angle, which is streamed to the hard disc together with data of the helicopters' altimeter and the radar data. Two GPS receivers complete the system, one feeding the position into the data stream of the IR camera, while the position of the other one is acquired together with the radar data.



Fig. 3.2.2: Picture of the radar antenna looking out of the helicopter together with the IR camera (to the left above the antenna) and the Video camera (to the right above the antenna)

Observations

Our work at sea can be divided into two parts: the helicopter-borne (Multi³Scat-) measurements and the sea ice property measurements at so-called ice stations, which will be separately described now in detail.

In-situ Measurements

In total sea ice was sampled at 22 positions. Details can be found in Tab. 3.2.2 and figure 3.2.3. The ice sampling work can be divided in three types. The main type are 13 ice stations beside *Polarstern*, hereafter called ice stations, where always several ice cores were drilled and additional data from other groups are available. These ice stations lasted 3 hours at minimum. The two ice stations in the Russian exclusive economic zone (EEZ) (stations number 5 and 6 in Table 3.2.2 and white circles near Franz-Joseph-Land in Fig. 3.2.3) differ from the other stations, as here due to Russian regulations no sea ice remote sensing work was allowed. Therefore only plain salinity and temperature ice core profiles were taken to complement the sea ice biology data sets (Chapter Sea ice Biology). The second type of ice stations is done by helicopter flights on a floe. The sampling is the same as for the normal *Polarstern* ice stations but time is limited; therefore fewer samples could be taken. But it is advantageous that helicopter Multi³Scat over-flights are secured for these stations and that they can be performed parallel to all other ship station work without using up ship time. Three such helicopter stations were performed. Towards the end of the cruise young ice was sampled at six positions from on board *Polarstern* using the ship's mummy chair.

Tab. 3.2.2: Overview of ice work done during the cruise. Ice samples were either taken at ice stations beside *Polarstern*, on floes visited by helicopter, or by ice fishing from the mummy chair on board *Polarstern*.

Overview of Multi³Scat ice stations during ARK-XXII/2

Nr.	Date	Polarstern, heli-copter or ice fishing station	Multi ³ Scat overflight	Number of ice cores	Number of lead samples	Number of melt pond samples	Number of core for structure analysis
1	2007-08-02	Polarstern	no	8	0	0	1
2	2007-08-07	Polarstern	no	6	0	0	0
3	2007-08-10	helicopter	yes	2	0	0	0
4	2007-08-11	helicopter	yes	2	0	0	0
5	2007-08-12	Polarstern	no	3	0	0	0
6	2007-08-15	Polarstern	no	4	0	0	0
7	2007-08-24	Polarstern	yes	5	0	1	2
8	2007-08-28	Polarstern	yes	3	2	0	1
9	2007-08-31	Polarstern	no	3	0	1	0
10	2007-09-02	Polarstern	yes	3	1	4	1
11	2007-09-04	helicopter	yes	1	0	1	0
12	2007-09-05	Polarstern	yes	3	0	3	1
13	2007-09-07	Polarstern	yes	3	1	2	0
14	2007-09-10	Polarstern	yes	3	2	2	1
15	2007-09-13	Polarstern	yes	4	2	1	0
16	2007-09-16	Polarstern	yes	3	3	1	0
17–22	2007-09-17 to 2007-09-19	six ice fishing stations	no	0	9	0	1
Total		13 Polarstern, 3 helicopter, 6 ice fishing stations	11/16	56	20	16	8

The positions of all 22 ice stations are shown in figure 3.2.3, circles denote ice stations beside *Polarstern*, triangles helicopter ice stations, and diamonds ice fishing from on board *Polarstern*. For 11 out of the 16 normal and helicopter ice stations a

simultaneous Multi³Scat over-flight could be accomplished. In figure 3.2.3 crosses mark all Multi³Scat measurements (see Table 3.2.3 for an overview of Multi³Scat measurements).

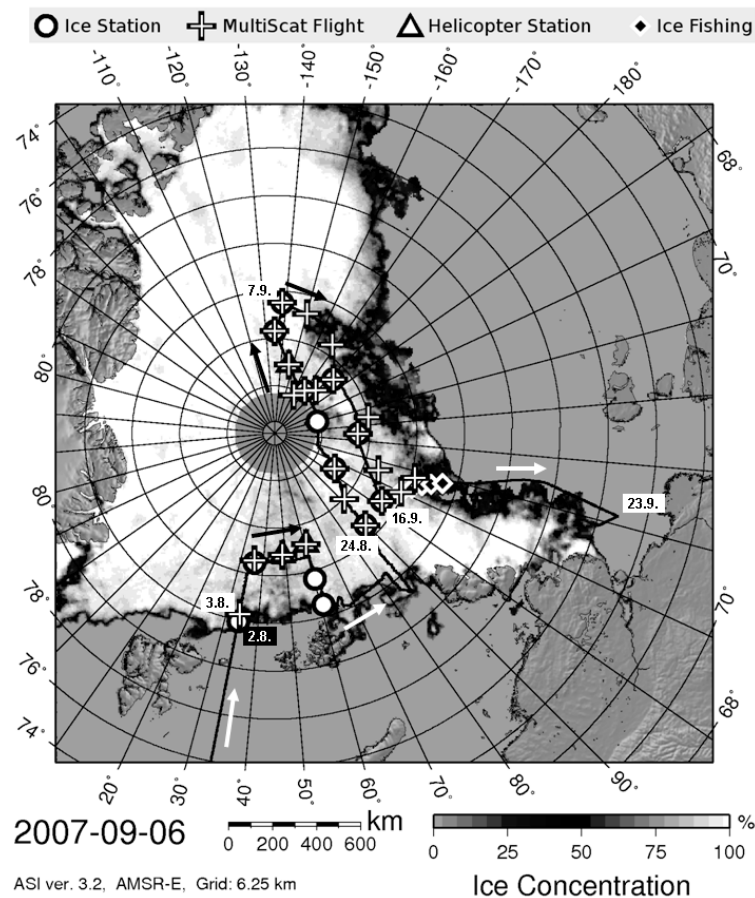


Fig. 3.2.3: Overview of data taken at sea. Circles denote positions of ice stations beside Polarstern, and triangles ice stations accessed via helicopter. Crosses give the rough position of Multi³Scat helicopter flights. Diamonds mark the locations where ice fishing of thin ice from on board Polarstern was performed. The black line together with black and white arrows marks the track of Polarstern. A few key dates are given for better orientation. Underlain are ice concentrations from 6 September 2007 derived from AMSR-E 89 GHz data.

A typical ice station consists of the following steps

1. mark a track on the ice.
2. helicopter Multi³Scat over-flight above this track.
3. taking samples at at least three positions along the track.

The track length was typically between 300 and 600 m. The direction of the track was chosen due to the following requirements: a) If simultaneously or within a time range of a few hours the acquisition of satellite SAR (synthetic aperture radar) data was scheduled, the track was aligned along the SAR look direction. b) If new ice areas were accessible within walking distance of the ship, these were made part of the track. c) Positions of sampling stations of the other groups on the ice were avoided in

order to keep the surface as undisturbed as possible for the Multi³Scat measurements. d) The track has to be easily accessible from the ship and for the helicopter pilots. As example the set up of the last ice station on 16 September 2007 with the accordant Multi³Scat tracks is shown in figure 3.2.4.

The track was marked with blue plastic bags filled with snow, which were distributed in distances of around 100 m along the track. In most cases this was sufficient but in future large flags or larger bags with different colour should be used for better visibility. To not further disturb the surface and get out of the Multi³Scat measurement the people having laid out the track now left the ice.

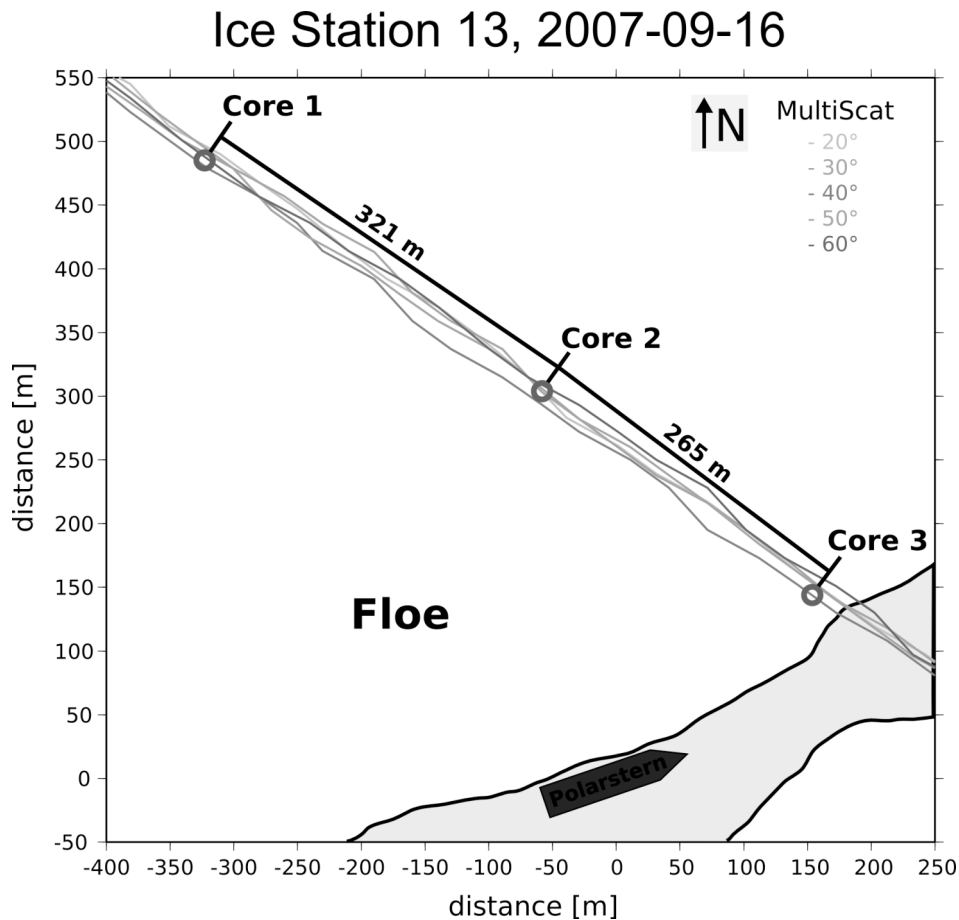
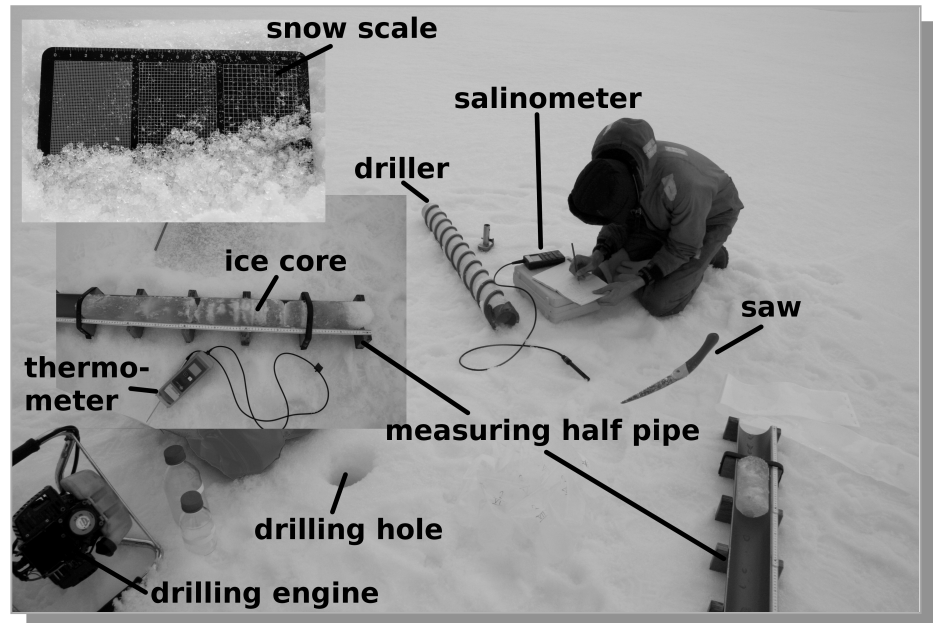


Fig. 3.2.4: Set up of the ice station track on 16 September 2007. Circles mark the positions of the ice cores taken. Grey lines mark the helicopter flight tracks of the over-flights with different angles of the Multi³Scat. All positions were referenced to the Polarstern GPS position to correct for linear drift during the ice station time.

After the Multi³Scat over-flights (see section Work at sea: Multi³Scat Measurements) the actual ice work started. A sledge was used to transport the equipment to the measurement points. Figure 3.2.5 gives an overview of a typical ice station together with the measurement equipment used on the ice.

Fig. 3.2.5: Picture of a typical ice station with the on the ice used measurement equipment



The main part at every measurement point was the drilling of at least one ice core of 1 m length. After drilling the ice core was put in a half pipe for analysis and sawing (Fig. 3.2.5). At first the ice core was photographed (entire core + every 20 cm segment). Then the temperature profile was measured in 5 cm steps with a rod thermometer (Fig. 3.2.5). This thermometer was also used to measure the air temperature, the snow surface temperature and the snow-ice interface temperature. For the salinity and density analysis the ice core was sawed in slices afterwards. As for the Multi³Scat backscatter comparison only the upper part of the ice is important, the upper 55 cm of the ice cores were sampled in 5 cm slices. From the rest of the core only two to three additional 5 cm slices were taken to have some continuation of the profiles. The ice slices were put in plastic bags. Slices with an undisturbed shape and thus could be used for density analysis were marked. At the end of the ice station the ice core slices were transported back on board and in frozen state the weight of the marked slices was measured. By knowing the diameter (9 cm) and the length (5 cm) of the core slice the ice density can be calculated from the weight. At the following day after melting of the ice the salinity and the initial values conductivity and temperature were measured with a handheld salinometer „Cond 3151“ (Fig. 3.2.5). The same salinometer was used on the ice to measure the salinity and temperature in the borehole, in melt ponds, and leads. Some ice cores were continued beyond the first 1 m all through the ice to get the ice thickness and some deeper samples of temperature, salinity and density. But this was not done systematically. With a ruler stick the snow thickness and ice freeboard was obtained. The ice freeboard was always measured, even when the core was not drilled all through the ice. The borehole always filled up with water after a while. If this water level then represents the sea surface level is unsure. Likewise the snow and ice surface as well as the snow grain size was photographed in front of a snow scale (Fig. 3.2.5). Additional ice core and water samples from melt ponds and more important leads were taken after the refreezing had started (i.e. basically after 24 August). If possible the lead and melt pond ice was also analyzed in slices like the

ice cores. If slush was present at the thin ice surface it was sampled and investigated separately. To get further insight in the crystal structure of the sea ice at interesting measurement sights additional ice cores were drilled and stored at -20° C temperature on board *Polarstern*. They will be analyzed by thin cut sections after the cruise. See Table 3.3.2 for an overview what samples had been taken on what dates. If Multi³Scat over-flights were performed the position of every ice core was determined with a GPS connected to a notebook or with a handheld GPS. To bring the ice core positions in accordance with the Multi³Scat measurements sometimes taken hours before, they had to be referenced to the *Polarstern* position at that time. By this procedure linear drift is corrected for and all measurements can be related to each other, as can be seen by the good match in figure 3.2.4.

Multi³Scat Measurements

The Multi³Scat measurements can be divided into two groups:

- measurements at ice stations (group a)
- measurements carried out along long profiles in order to obtain a sample data set representative for a larger region or to obtain a sample data set as coincident as possible with a satellite sensor over-flight (group b).

Table 3.2.3 gives an overview about all measurement flights. The intention behind the measurements of group a) is to repeat Multi³Scat measurements at different incidence angles over sea ice with properties, which are investigated by carrying out *in-situ* measurements as has been described in section Work at sea: *In-situ* Measurements.

Once the profile was laid out, we carried out Multi³Scat measurements at five different incidence angles (20, 30, 40, 50, and 60°) by flying along the profile from always the same direction with constant speed and at constant altitude. In case of a potential satellite sensor overpass the look direction of the Multi³Scat was chosen to be similar to that of the satellite sensor. The length of each flight leg was chosen such that the part over the profile on the floe was situated close to the middle of the leg in order to ensure almost identical tracks. The length of these flight legs varied depending on limitation by time, weather, and daylight between one and five miles.

Flights of group b) that were under-flights of satellite sensor overpasses were carried out such, that at least during one flight leg look direction and incidence angle of the Multi³Scat and the satellite sensor were similar. Different flight pattern were used. However, due to i) the limited chance of obtaining satellite images within the range of *Polarstern* and/or the helicopter, ii) the deviation from the originally planned cruise track to the north and east, and iii) the fact, that, e.g. Envisat ASAR images have to be ordered two weeks in advance, the total number of potential satellite image under-flights is small: 6 out of 24 (see Table 3.2.3).

Flights of group b) that were not under-flights of satellite sensor overpasses were carried out mostly at two different incidence angles (35 and 50°) over approximately the same track, also at constant speed and altitude. The intention here was to cover a larger region and by this to obtain radar backscatter data resembling a larger variety of surface properties than was possible with the ice floe over-flights (group a). The data acquired along these long-distance flights will be used as test and

application data sets for the methods to be developed in the future. Those Multi³Scat data acquired as satellite sensor under-flights will be used as training and validation data sets.

Unfortunately, we lost the L-Band due to the failure of more than one microwave component so that after 11 August Multi³Scat measurements were carried out with only four frequencies (S- to Ku-Band, see Table 3.2.1). Moreover, some problems in the streaming of the data to hard disc caused loss of data and/or a decreased signal to noise ratio in some cases (see Table 3.2.3, x (co) and x (-)).

Table 3.2.3: Overview of all Multi³Scat flights. Given are (from top to bottom) the date, the purpose indicated by an “X” (floe: ice-station floe over-flight (compare Table 3.2.2), SAR: satellite synthetic aperture radar under-flight, other: neither floe nor SAR), the approximate total distance along which data have been acquired, the number of incidence angles used, and the five frequency bands. For meaning of “x”, “x (co)” etc. see legend in right part of lowermost table. The flight of 30 September was an open water flight for control purposes.

Date	03.08.	07.08.	10.08.	11.08.	24.08.	24.08	27.08.	28.08.	02.09.	02.09.
Floe			X	X		X		X		X
SAR					X		X			
other	X	X					X		X	
Length [miles]	15	20	10	5	40	10	100 (-)	10 (-)	60 (-)	10
angles	1	5	5	5	1	5	1 (+)	5	2	5
L	co	co	co	co	-	-	-	-	-	-
S	x	x	x	x	x	x	x (co)	x (co)	x (co)	x
C	-	-	-	-	x	x	x (co)	x (co)	x (co)	x
X	x	x	x	x	x	x	x	x	x	x
Ku	x	x	x	x	x	x	x (-)	x (-)	x (-)	x (-)

Date	03.09.	04.09.	05.09.	07.09.	08.09.	09.09	10.09.	12.09.	13.09.	15.09.
Floe			X	X			X		X	
SAR								X		X
other	X	X			X	X				
Length [miles]	120	60	10	20	10	120	10	70	10	80
angles	2	2	5	5	1	2	5	1	5	1
L	-	-	-	-	-	-	-	-	-	-
S	x (co)	x	-	x	x (co)	x	x	x	x	x
C	-	-	-	-	x	x	x	x	x	x
X	x	x	x	x	x	x	x	x	x	x
Ku	x (-)	x	-	x	x (co)	x	x	x	x	x

Date	16.09.	17.09.	18.09.	30.09.	Legend
Floe	X				L, S, C, X, and Ku: The frequency bands
SAR		X	X		Length (-): Data of some bands missing
other				X	Angles (+): More than one angle used but not along same the track
Length [miles]	10	45	90	20	
angles	5	2	1 (+)	2	At the frequency bands:
L	-	-	-	-	-: no data acquired / signal too weak / too noisy
S	x	x	x	x	co: only co-polarized data fine
C	x	x	x	x	x: all data fine
X	x	x	x	x	x (-): first all data fine, then none fine
Ku	x	x	x	x	x (co): first all data fine, then only co-pol. fine

Some remarks to the ice conditions

The aims of the Multi³Scat measurements were twofold, targeting both, melt pond and thin ice identification. Ice and weather conditions limited observations of open melt ponds to the first four flights (see Table 3.2.3). The lacking permission to carry out Multi³Scat measurements in the Russian EEZ and the growing distance between the ship's position and the nearest point outside the Russian EEZ restricted flights to the period between 11 August and 24 August. At that time, however, most melt ponds were already covered almost completely with a thin ice layer. In the following period until we left the sea ice covered area on 19 September almost continuous northward advection of mild air masses inhibited the expected cooling and considerably limited new ice formation in breaks and leads. Therefore, Multi³Scat measurements targeting our thin ice work were restrained to thin ice with thickness values below about 10 cm.

Preliminary Results

In the following we will first summarize results from the *in-situ* measurements carried out during the ice stations listed in Table 3.2.2 (except of ice stations 5 and 6, which are situated within the Russian EEZ and where only routine ice observations were carried out to support the work of the sea ice biologists and the oceanography group). After that we give an example of Multi³Scat measurements carried out during ice station 7 of August 24, 2007, together with the obtained *in-situ* measurements.

Summary of *in-situ* measurements

Ice Core Temperature

The temperature of the upper part of the sea ice is mainly depending on the surface air temperature also on short time scales. For the summer conditions of this cruise the temperature below 50 cm depth stays fairly constant at between -0.7° C and -1.5° C. Therefore the ice core temperature profiles can be separated into three classes:

a) Stations with relatively high air temperature. In our case these were the nine stations with number 1, 2, 3, 4, 5, 6, 7, 9, and 15 given in Table 3.2.3. These are mainly stations from the beginning of the cruise but also the second last station number 15 at 2007-09-13 had with -0.6° C a relatively high air temperature. The air temperature of these stations varied between -1.1° C and 1.2° C. The mean

temperature profile of the upper first meter of all ice cores from these stations is shown in figure 3.2.6a. Until 30 cm depth the temperature stays fairly constant at -0.2°C . Below the temperature is steadily decreasing until it reaches a minimum of -1.0°C at 92.5 cm depth. With 9 out of 16 stations this profile is typical for the majority of ice cores taken during this cruise. This is also reflected in the number of available measurements for each ice depth shown in the right graph of figure 3.2.6a. In total 56 ice cores were taken. Until a depth of 90 cm the number of measurements stays around 35. As not all ice cores could be recovered completely and thus had a shorter length than 1 m the number of measurements drops thereafter.

b) Stations with relatively low air temperature. These were six stations with numbers 8, 10, 11, 13, 14, and 16 (see Table 3.2.2) towards the end of the cruise. The air temperature here was between -7.2°C and -3.0°C . The mean temperature profile of the cores of these stations is shown in figure 3.2.6b. Starting with a cold surface layer the temperatures stay below -1.5°C until 30 cm depth. Below this depth the temperatures stay at about -1.2°C . The variability of the temperature values is much larger here than for the “high” air temperature case in figure 3.2.6a, as can be seen from the error bars, which denote plus-minus one standard deviation. This may also result from the smaller amount (about 15) of available measurements, shown in the right part of figure 3.2.6b.

c) A profile with depth homogeneous temperature. On this cruise this case could only be observed for the ice station on 5 September 2007. The air temperature was -1.5°C and the temperature profile of the three ice cores stays up to 1 m depth with some variations at around -1°C . Figure 3.2.6c shows the mean temperature profile of this station.

3.2 Sea ice radar backscatter measurements for improved melt-pond and thin-ice cover analysis

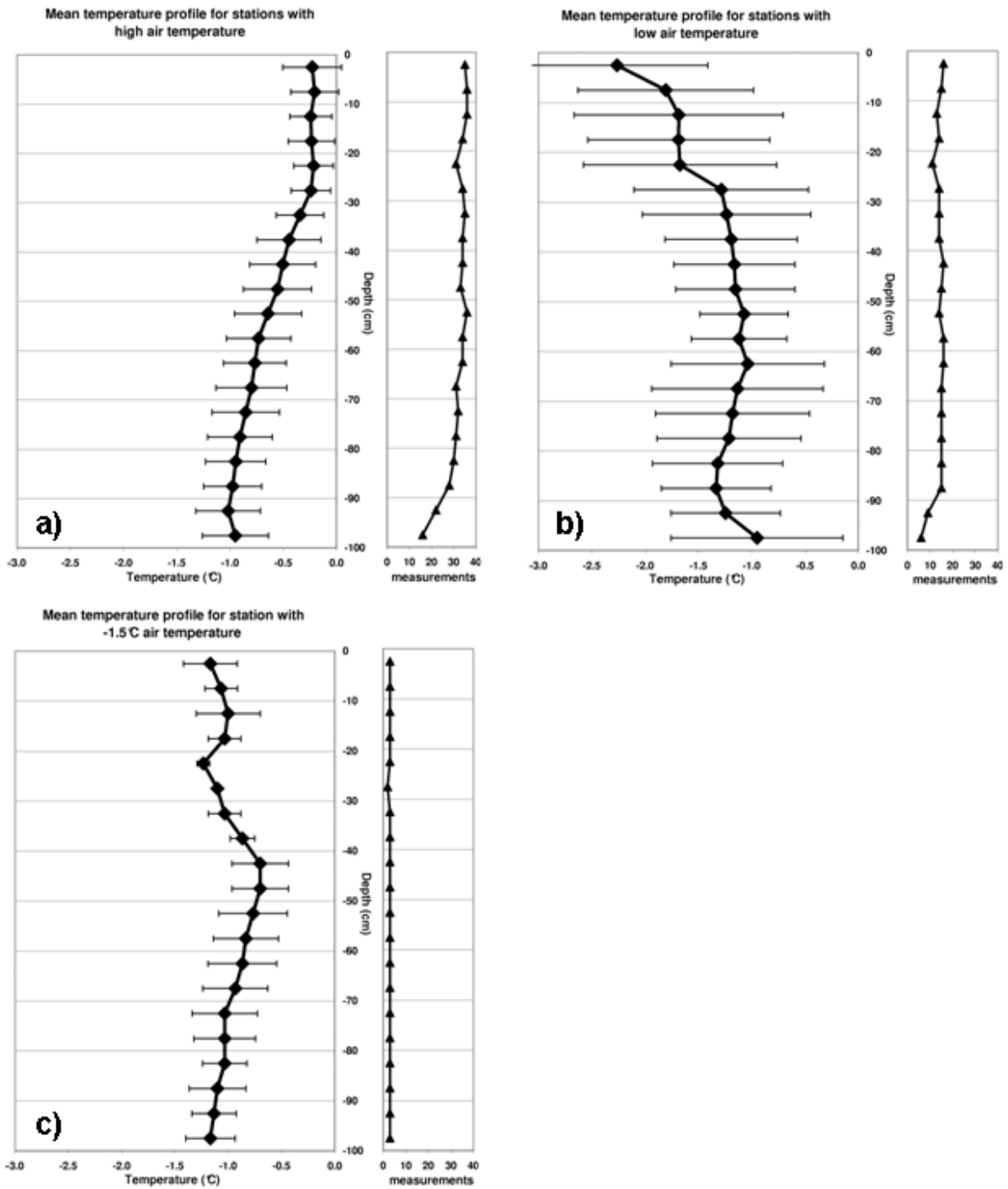


Fig. 3.2.6: Mean temperature profiles of the first meter from ice cores of ice stations with a) relatively high (-1.2 to 1.2 ° C) air temperature, b) relatively low (-7.2 to -3.0° C) air temperatures, and c) for the ice station at 2007-09-05 with -1.5° C air temperature. The right graph of each plot shows the number of used measurements for every depth. Error bars denote the plus-minus one standard deviation interval.

Ice Core Salinity

For the ice core salinity profiles no different classes could be identified clearly. Figure 3.2.7 shows the mean salinity profiles of all 56 ice cores taken. The most distinct feature is the raise of salinity between 25 cm and 50 cm from about 0.2 psu to 2.0 psu. Most individual ice cores show a sharp rise of salinity in this depth range but the increase for an individual ice core in general is much steeper than expressed in the mean salinity profile in figure 3.2.7. This is also reflected by the large standard deviations in the 25 to 50 cm range (error bars in figure 3.2.7). Below 55 cm depth the standard deviations stay high and the profile looks not as smooth anymore. This is due to the reduced number of available measurements (right graph in figure 3.2.7) for this part of the ice cores. Only the first 55 cm of all ice cores were regularly sampled for salinity and density. In the lower part of each core only two to three slices were taken at different depths for every core and thus not every core incorporates in the mean value in the lower part. The number of measurements plot at the right side of figure 3.2.7 shows a sharp drop from about 55 measurements for the first 55 cm to 14 measurements for the rest of the first meter. For the depths 57.5 cm and 62.5 cm only 0 and 2 measurements were available, respectively. They are therefore excluded for the mean value calculation.

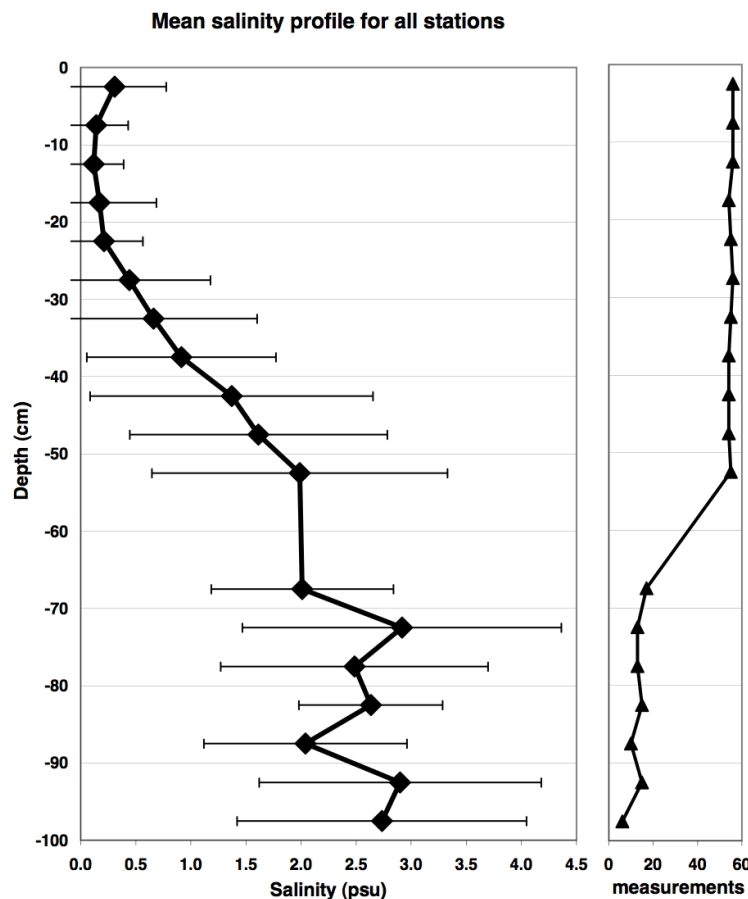


Fig. 3.2.7: Mean salinity profile of the upper meter of all ice cores from all stations. The right part of the graph gives the number of measurements for every depth.

Ice Core Density

The ice density only can be obtained for sawed ice core slices which cylindrical shape is not disturbed. As we only measure the weight of each core slice the volume has to be known to calculate the density. Unfortunately this is only given for a small part of the collected ice core slices. Very often the ice was broken or so porous that no clear volume was defined. Figure 3.2.8 shows the mean density profile of all obtained density samples. Even for the first, always completely sampled 55 cm of the ice cores the number of measurement graph at the right side of figure 3.2.8 only gives values of about 19 measurements out of the 56 available cores. That the lower, sparsely sampled part of the cores is not even worse represented, is based on the free position choice for these samples, where undisturbed core parts were favoured. Nevertheless, the density profile shows the expected shape with lower densities in the upper part of the cores and homogeneous densities below 30 cm. The mean density of the first meter of all cores is 833 kg/m^3 , the mean density for the homogeneous part 25 to 100 cm is 873 kg/m^3 .

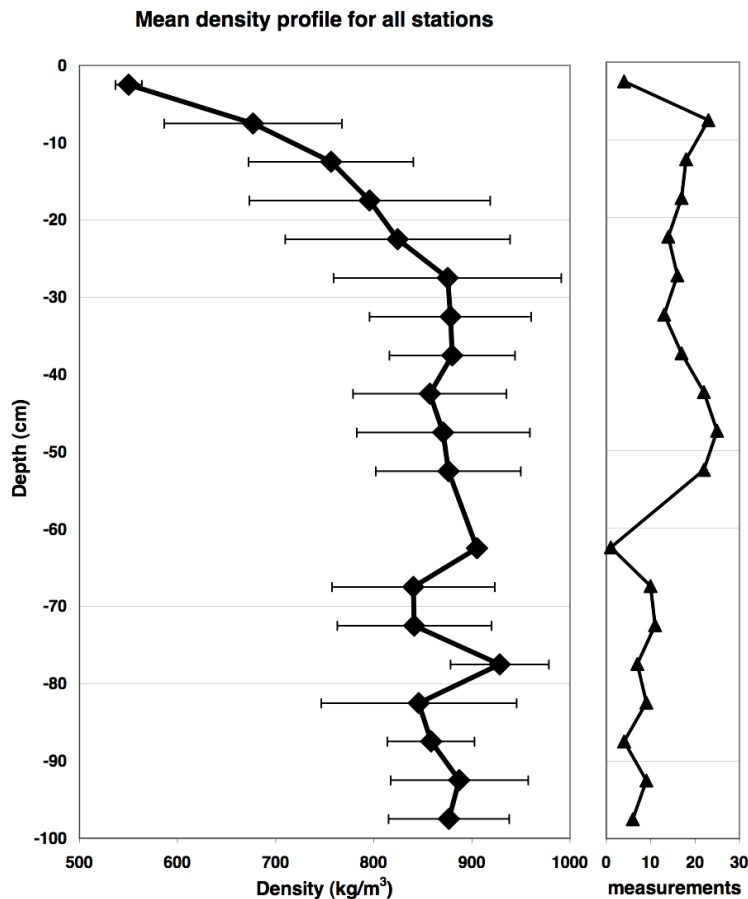


Fig. 3.2.8: Mean density profile of the upper one meter of all ice cores from all stations. The right part of the graph gives the used number of measurements for every depth.

Other Samples

During ice stations and ice fishing stations 20 samples of thin ice were taken with ice thicknesses between 2 and 12 cm. The mean bulk ice salinity of these samples

without an eventually present slush layer is 9.5 ± 3.5 psu. If there was slush on top of the ice its salinity was measured separately. The mean slush salinity amounts to 20 ± 7 psu. There was only one case (ice fishing on 18 September 2007) where the thin ice surface was dry and the salinity of the small snow patches on top was only 0.2 psu. Without this case the mean slush salinity rises to 21 ± 5 psu. During the ice station on 16 September 2007 frost flowers were found on the thin ice. They had a salinity of 28 psu. The air temperature was with -4.3°C still quite high for frost flower growth.

The 16 melt pond samples can be divided into samples from fresh melt ponds and those melted through the ice. All melt ponds with a water salinity below 15 psu are declared fresh, even if some of these might have had some connection to sea water. The often strong vertical stratification of the water of the melt ponds keeps the salinity close to the surface low. The mean water salinity of the fresh melt ponds comes then up to 8 ± 4 psu. The mean fresh melt pond ice salinity amounts to 1.2 ± 0.9 and if slush salinity could be measured it has a mean salinity of 7 ± 4 psu. The same values for the melted through melt ponds amount to 28 ± 4 psu for the pond water, 6 ± 3 psu for the ice, and 17 ± 6 psu for the slush.

So in summary we have gathered a quite complete data set to better interpret the Multi³Scat data acquired of the ice station floes. Not shown here is the archive of digital photographs of each ice core, taken when it was lying in the half pipe which has a scale on one side. There is also an archive of digital photographs of the snow grain size (if possible close to the snow surface but also at the snow-ice interface), the snow surface roughness, the surface roughness of the new ice in leads or melt ponds (often determined by the slush layer), and finally of melt pond freeboard heights, i.e. the height distance between the new thin ice on the melt pond and the surrounding thick ice.

The Ice Station of 24 August 2007 within an acquired Envisat ASAR image

In the following data from 24 August 2007 are shown and discussed. Figure 3.2.9 shows the location of the Multi³Scat flights carried out on that day. That day was unique because this has in fact been the only day (as we know so far at least), when an ice station took place within an acquired Envisat ASAR image. So first a profile was marked on the ice floe as described in section Work at sea: *In-situ* Measurements and as is shown in figure 3.2.9 b); the profile was marked parallel to the look direction of Envisat ASAR, which flew over the floe at 11:54 UTC on that day.

3.2 Sea ice radar backscatter measurements for improved melt-pond and thin-ice cover analysis

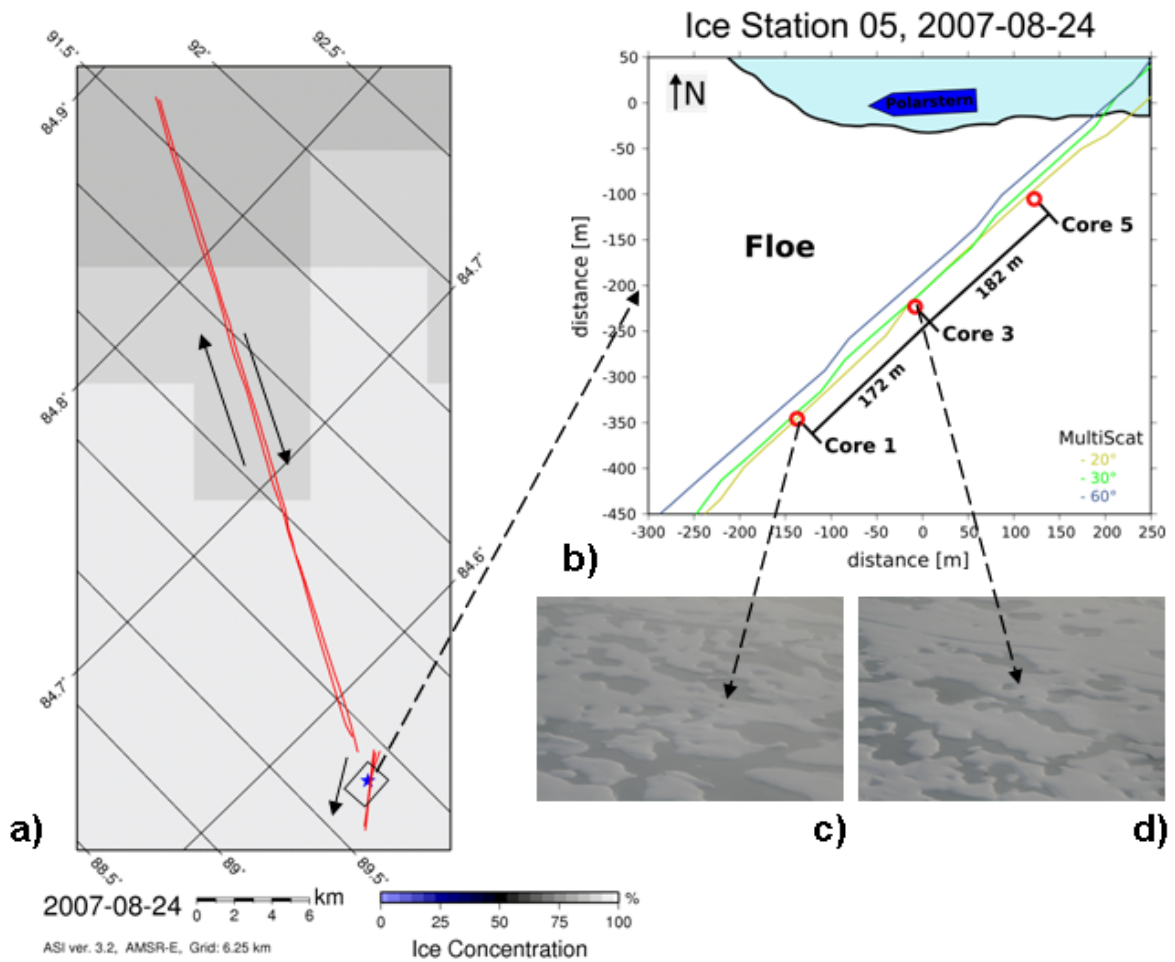


Fig. 3.2.9: a) Flight tracks of the Multi³Scat on August 24, 2007, overlaid upon the sea ice concentration obtained from 89 GHz AMSR-E data. The short legs close to the star, which marks the position of the Polarstern, are floe over-flights. Solid arrows denote the direction of the Multi³Scat flights. The black box indicates the approximate location of the map given in image (b). b) Map showing the location of the profile and the places where three of the five ice cores were drilled (circles) relative to the Polarstern together with the flight tracks of the Multi³Scat (grey lines from upper right to lower left). Photographs in (c) and (d) show the scenery at core 1 and 3, respectively.

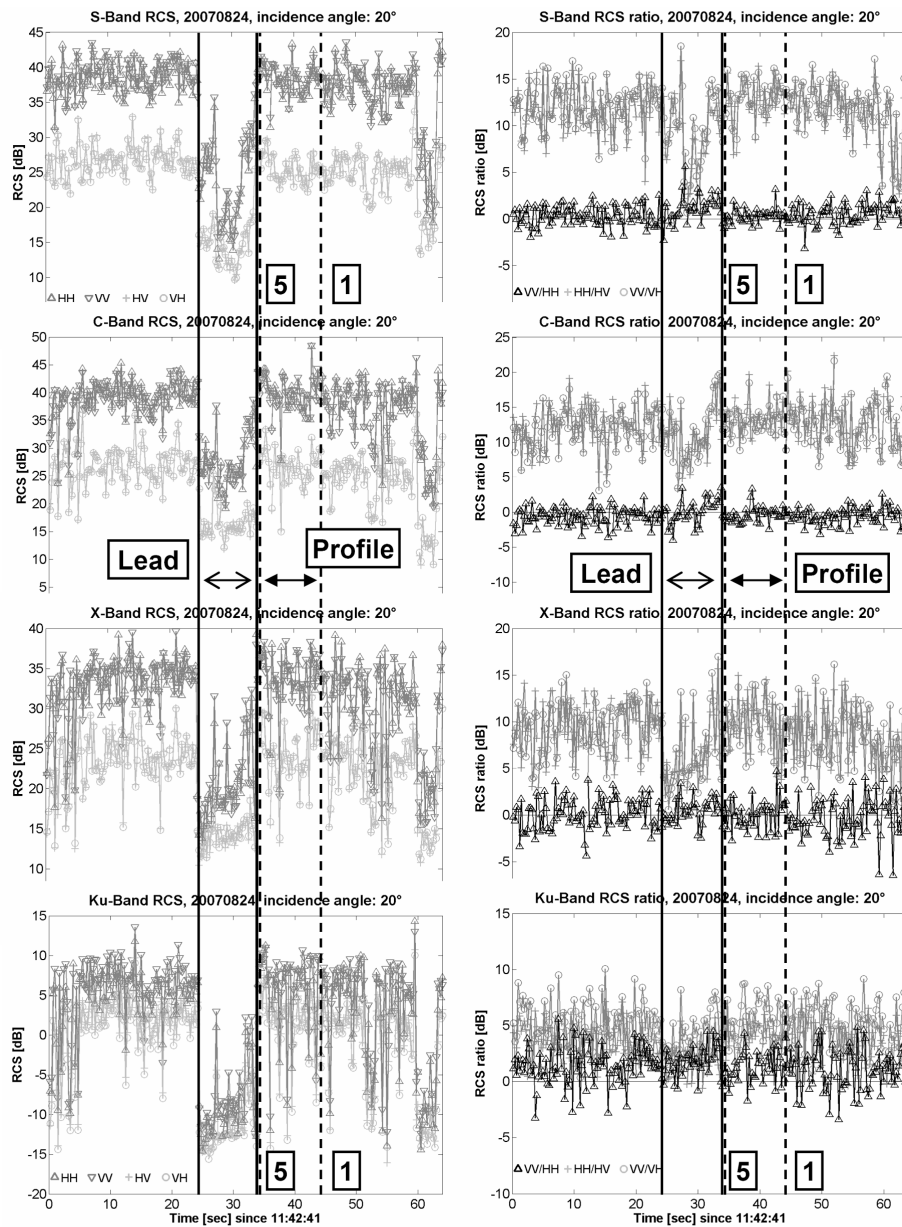


Fig. 3.2.10: Left: Relative radar cross section (RCS) as obtained with the Multi³Scat over the ice station floe (see Fig. 3.2.9) from an altitude of 200 feet at a speed of 80 knots with an incidence angle of 20° at (from top to bottom) S-, C-, X-, and Ku-Band on Aug. 24, 2007. Right: RCS ratios calculated from the RCS values shown left. The lead where the Polarstern was anchored at the ice floe is marked by two solid vertical lines and the normal arrow. The ice station floe follows to the right. Locations where ice cores number 1 and 5 were taken are marked by the two dashed vertical lines and the numbers. The bold arrow indicates the profile marked on the ice floe.

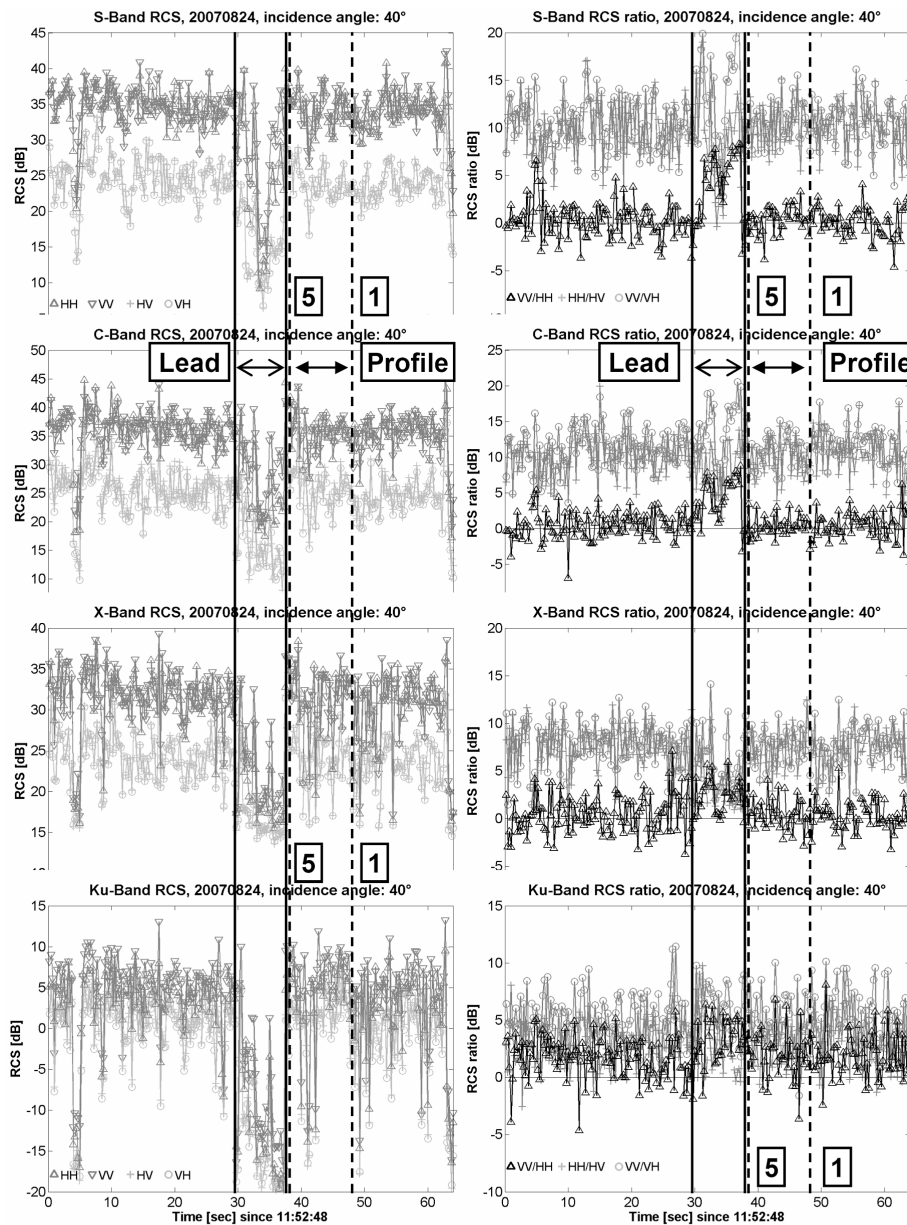


Fig. 3.2.11: As figure 3.2.10 but for an incidence angle of 40°

After the profile was marked we carried out Multi³Scat flights. First we flew two 20 miles long profiles with an incidence angle of 40°, 200 feet altitude, 80 knots speed, starting at around 11:15 UTC; during the first leg we looked against, during the second leg in the look direction of the Envisat ASAR (Fig. 3.2.9 a). After completion of these flights we carried out Multi³Scat measurements over the ice floe along the profile as described in section Work at sea: *Multi³Scat Measurements* using five different incidence angles, approaching the floe from the top right, i.e. northeast (see Fig. 3.2.9 a), lines close to the star, and b)). Almost exactly during the Envisat ASAR

over-flight the Multi³Scat measurement at 40° incidence angle was carried out. Unfortunately, the ice floe started to rotate due to the ice drift so that at the time of our Multi³Scat over-flights the orientation of the profile on the floe was not parallel to the look direction of Envisat ASAR anymore but off that direction by about 30° (Fig. 3.2.9 a).

The figures 3.2.10 and 3.2.11 show the results of the Multi³Scat measurements carried out along the profile at incidence angles of 20 and 40°, respectively. Given are the Radar Cross Section (RCS) derived from the Multi³Scat measurements (left panels) and the RCS ratios as calculated from these RCS values (right panels), for (from top to bottom) S-, C-, X-, and Ku-Band and all available polarization combinations for the first 64 seconds of the flight. These RCS values are obtained by calculating the spectral power density for each frequency band and each polarization combination. In the resulting spectra the backscattered signal can be located as a Doppler peak shifted towards lower frequencies relative to the IF (intermediate frequency) peak. The magnitude of this Doppler peak is a measure for the amount of the backscattered energy. By integrating over the topmost 6 dB of this Doppler peak the RCS value is calculated with an along-track spatial resolution of approximately 10 meters. Note that these RCS values (all RCS values shown in this report) are relative ones, i.e. they have not been calibrated so far. First flights over calibration targets have been carried out already before the cruise, however, allowing a proper calibration of the RCS values at home.

What can we learn from figures 3.2.10 and 3.2.11? First of all, all shown frequency bands show a reasonable separation of the co- (HH- and VV-polarization) from the cross- (HV- and VH polarization) polarized data, except perhaps Ku-Band. All frequency bands pick up nicely the change from thick melt-pond covered sea ice to thin sea ice (mainly dark nilas) in the lead where the *Polarstern* was located, and back to the thick melt-pond covered ice of the ice station floe by showing a pronounced decrease of the RCS values at the beginning of the lead and an increase of the RCS values at the end of the lead. The change in the RCS values amounts between 15 and 25 dB. The solid black vertical lines given in figures 3.2.10 and 3.2.11 mark the mentioned transition between thin and thick sea ice. This change is more abrupt at an incidence angle of 20° than at 40° (compare Figs. 3.2.10 and 3.2.11), because the footprint is smaller at 20° than at 40° incidence angle, shadowing effects by floe margins and ridges are smaller at a steeper incidence angle, and the radar backscatter of thin ice (as was present on the lead) is more influenced by the underlying water at steep than at shallow incidence angles. Within the lead the RCS values are varying quite a lot, particularly at the beginning (left) and more pronounced at 40° than at 20° incidence angle. This is caused by varying ice conditions as will be shown later.

The RCS values over the thick ice tend to be quite smooth at S-Band, while they are extremely variable with a number of pronounced dips at X- and Ku-Band; this applies to both incidence angles shown. Since the ice station floe exhibited rather homogeneous surface properties except that it was covered with melt ponds and since these melt ponds were covered with thin level ice, it seems likely that the observed dips in the RCS values are caused by the melt ponds.

It is known, that the VV/HH RCS-ratio at lower frequencies, say C-Band and below (see Table 3.2.1), takes values well above 0 dB over open water and thin ice. In particular, this RCS-ratio tends to decrease from a high open water value (L-Band: 10 dB) to values close to 0 dB with increasing ice thickness - up to about 30 - 50 cm. This effect increases with increasing incidence angles. Therefore we would expect that the VV/HH RCS-ratio is larger than zero decibel over any open water or thin ice area encountered during Multi³Scat flights carried out with shallow incidence angles. In fact, the VV/HH RCS-ratio obtained at an incidence angle of 40° takes values of up to 8 dB and 6 dB at S-band and C-Band, respectively, over the lead. At X- and Ku-Band there is also an indication for elevated VV/HH RCS-ratios, however less pronounced than at C- and S-Band. Corresponding RCS-ratio values remain close to 0 dB at an incidence angle of 20° (Fig. 3.2.10). At shallower incidence angles, i.e. 50° and 60°, we observed VV/HH RCS-values of up to 12 dB and 16 dB, respectively, at S-Band over the lead at this ice station (not shown). From figures 3.2.10 and 3.2.11 there seems to be no indication, however, that elevated VV/HH RCS –values can be observed over melt ponds as well.

What else can we take from these two figures? At 20° incidence angle the VV/VH and HH/HV RCS ratios change to lower values over the lead than over the thick melt-pond covered sea ice, with the largest (smallest) change at S-Band (Ku-Band). In contrast, these ratios tend to increase, also over the lead, at 40° incidence angle – but only at S- and C-Band. This might deserve future investigations.

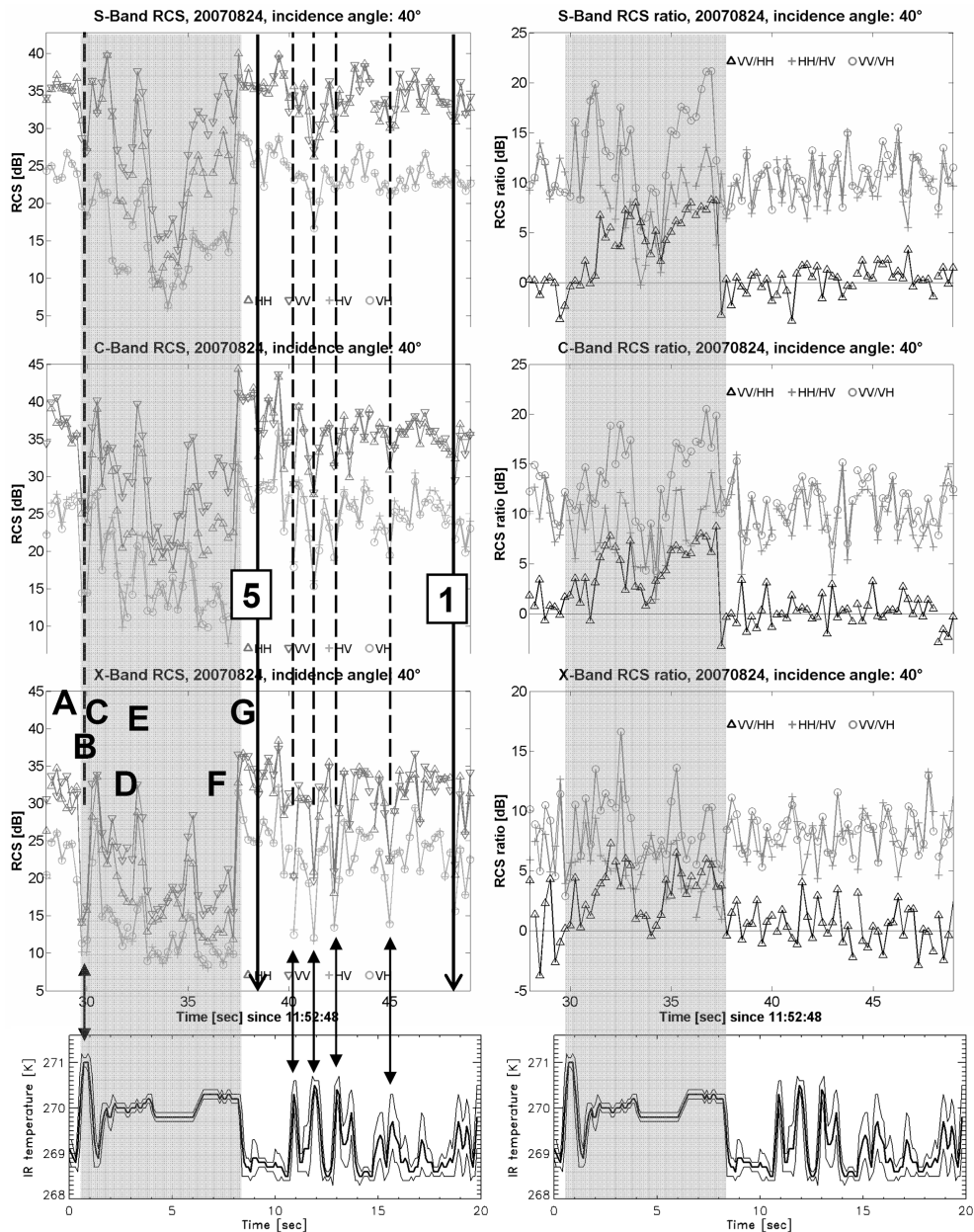


Fig. 3.2.12: Zoom of seconds 28 to 48 of RCS (left) and RCS-ratio (right) of figure 3.2.11 for (from top to bottom) S-, C-, and X-Band together with the mean infrared (IR) temperature and its standard deviation (thick and thin solid lines in lowermost panels) as obtained simultaneously with the IR-camera. Letters A to G refer to surface types shown in figure 3.2.13. Grey areas mark the approximate position of the lead. Double arrows mark examples where RCS dips coincide with elevated IR temperature values; the dashed lines above these arrows intend to show this coincidence at the other frequency bands as well. The location of core stations one and five are marked by the normal arrows.

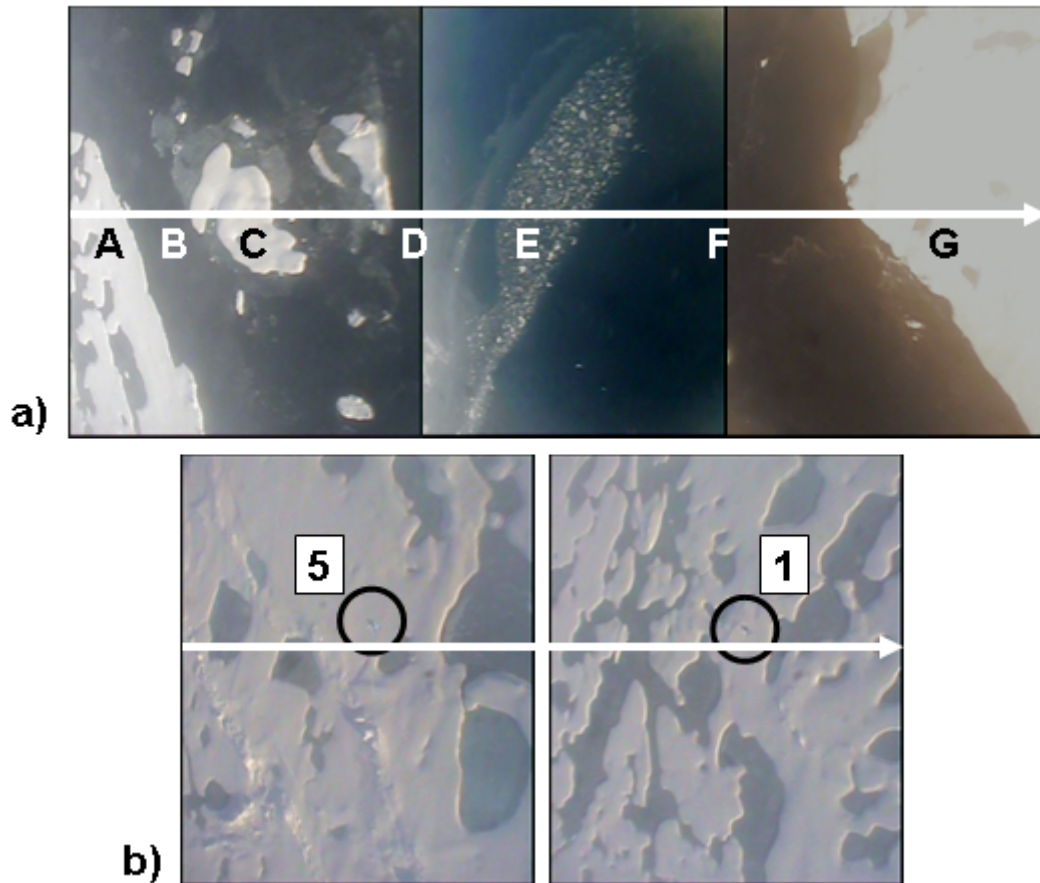


Fig. 3.2.13: a) Different ice types encountered during the lead over-flight (compare Fig. 3.2.12); A to G show: thick ice with melt ponds, light nilas, thick ice, dark nilas, brashed thin ice, dark nilas, thick ice with melt ponds, respectively. b) The ice floe as it looked around core stations one and five viewed by the helicopter video camera. White arrows indicate the flight direction. Black circles mark the location of the plastic bags.

Figure 3.2.12 shows a 20 s (approximately 800 m) long blow-up of figure 3.2.11 together with our coincident helicopter-borne IR temperature measurements. These are basically a measure of the surface temperature. Data from Ku-Band have been omitted here. An elliptical region resembling the footprint size of the Multi³Scat at C-Band was used to calculate the mean IR-temperature and its standard deviation inside this region. Note that consecutive ellipses overlap so that abrupt temperature changes are smoothed a bit. Note also, that these IR-temperature values have not yet been calibrated so that any interpretation should be based on the relative IR-temperature changes rather than the absolute values. The air-temperature during that day hovered around -1°C and did not change too much the days before. Therefore, differences in the IR temperature are expectedly small; the maximum difference amounts to 2 K.

Our *in-situ* measurements revealed an ice surface temperature of the thick ice of about -1.0°C (see also Fig. 3.2.14), while the melt pond surface temperature was around 0.0°C . This would make a difference of 1 K which is smaller than the observed one. However, since there might be small differences in the infrared emissivity between the coarse grained rotten surface of the thick ice and the

relatively smooth surface of the new ice we cannot simply use one emissivity value to directly translate the IR-temperature measurements into surface temperatures. A difference in this emissivity value (typically around 0.98) of 0.01 can already cause a change in the calculated surface temperature of almost 3 K. So we cannot interpret the observed IR-temperatures without knowing exactly the typical infrared emissivity of the involved surface types.

Nevertheless, two different regimes of surface temperatures can be discriminated: IR temperature values around 269 K and IR temperatures at or above 270 K. The former regime can be associated with the thick sea ice as is bordering the lead (see Fig. 3.2.13 a). Temperatures of the latter regime occurred in two ways, either as a quite homogeneous distribution as observed over the lead ice, or as distinct peaks as observed over the ice station floe. It is likely that these peaks show the melt ponds, which can be expected to be a bit warmer than the surrounding thick ice. So melt ponds and the surrounding thick ice can be clearly discriminated from each other. Double arrows in figure 3.2.13 indicate where melt ponds were located along the Multi³Scat measurement profile, which coincide with dips in the observed RCS values at X-Band, all polarization combinations. There is also clear evidence that also at C-Band, and to a smaller degree even at S-Band, melt ponds, which are covered with a thin ice layer, cause a decrease of the RCS values relative to those observed over the surrounding sea ice. The fact that these dips seem to be quite smoothed at S-Band can be explained by the footprint size at this frequency (see Table 3.2.1), which is larger than most of the melt ponds encountered along the profile.

At this station ice cores were drilled at five locations, at two of which additional ice cores for structure analysis were taken. Figure 3.2.9 c) and d) showed examples of the ice surface at core stations one and three. A quite high coverage of melt ponds (30 - 40 %) can be identified. Figure 3.2.14 illustrates the vertical temperature (a) and salinity (b) profiles obtained for the upper meter of the five ice cores.

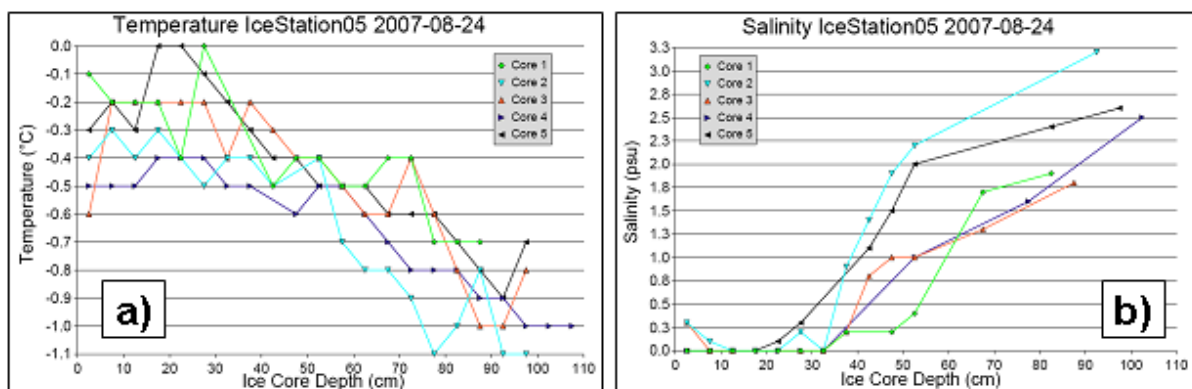


Fig. 3.2.14: a) Vertical temperature profiles as measured in-situ in the ice cores drilled at the ice station on August 24, 2007. b) Vertical salinity profiles as obtained from these cores as has been described in section *Work at sea: in-situ Measurements*.

The temperature profiles show an almost iso-thermal upper layer of about 40 cm thickness with temperatures around -0.3°C , and then a gradual decrease to temperatures around -0.9°C at a depth of 90 cm. Two of the five cores exhibited one

to two values at the melting point. The salinity profiles indicate a fresh upper layer of about 30 - 40 cm thickness with a bulk salinity below 0.5 psu, and then an increase to salinity values between 2 and 3 psu at a depth of about 100 cm - as can be called typically for multiyear sea ice. The density profiles (not shown) revealed a less dense upper layer (750 kg/m^3) and an increase in density (on average) at approximately 40 cm depth, i.e. that depth where the temperature and salinity profiles start or have their largest changes, to values around 925 kg/m^3 . Digital photography of the ice cores (not shown) reveals a quite coarse grained upper layer, which is followed by relatively clear ice containing quite a number of air bubbles.

In summary, this ice floe seems to reveal properties that are typical for multi-year ice, which should be resembled in accordingly high values of the radar backscatter intensity. This will be checked after calibration of the obtained RCS values (Figs. 3.2.10 to 3.2.12) and remains a future task to do, as is the investigation of the structure of the two ice cores drilled in addition for thick and thin section analysis (see Table 3.2.2)

3.3 Routine sea ice observations

Stefan Hendricks¹⁾, Stefan Kern²⁾,
Rainer Kiko³⁾, Takashi Kikuchi⁶⁾,
Maike Kramer³⁾, Volker Leinweber¹⁾,
Sebastian Mechler⁴⁾, Sabine
Mertineit¹⁾, Lasse Rabenstein¹⁾, Alice
Schneider³⁾, Peter Semenov⁵⁾, Stefan
Siebert³⁾, Gunnar Spreen²⁾, Andreas
Winderlich²⁾

¹⁾Alfred-Wegener-Institut

²⁾Institute of Oceanography IfM HH

³⁾Institut für Polarökologie

⁴⁾Optimare

⁵⁾VNIIO All-Russia Research Institute for
Geology and Mineral Resources of the
World Ocean

⁶⁾Japan Agency for Marine Earth Science
and Technology

Visual Observations from the Bridge Introduction

To obtain a continuous record of the sea ice state, standardized visual observations were performed from the ship's bridge every hour during day time. During night observations were conducted more sparsely depending on the observers' working shifts.

Visual observations are the only possibility to regularly obtain a broad range of sea ice parameters extended with photographs and comments about distinctive features. Starting with explorers and whalers visual observations from ships represent the longest time series about the Arctic sea ice state. Today still all ice going research vessels are asked to carry out such standardized observations to enlarge the existing database. Besides being a valuable dataset on its own, these observations can be used as *in-situ* comparison to otherwise obtained measurements like remote sensing data. Nevertheless, it has to be taken into account that all observations strongly depend on the personal view and estimation of each individual observer and such the absolute accuracy is low. Additionally *Polarstern* favours open water and thin ice areas for steaming, which may bias ice thickness observations.

Work at Sea

The bridge observations were executed following the ASPeCt (Antarctic Sea Ice Processes and Climate) observation protocol conceived for Antarctic sea ice, as to our knowledge no special standardized protocol exists for the Arctic. All observations were directly entered in a computer. The appropriate programme and a tutorial to train the sea ice observers were used from Worby, A. P., 1999: *Observing Antarctic sea ice: A practical guide for conducting sea ice observations from vessels operating in the Antarctic pack ice*. A CD-ROM was produced for the Antarctic Sea Ice Processes and Climate (ASPeCt) programme of the Scientific Committee for Antarctic Research (SCAR) Global Change and the Antarctic (GLOCHANT) programme, Hobart, Australia. The following parameters are recorded in the protocol: date, time, latitude, longitude, total ice concentration in tenth part, open water classification (e.g. narrow breaks 50 - 200 m), melt pond coverage, comments. Up to three different ice types are described in more detail starting with the primary, the most thickest, type. For every particular class the following parameters are recorded: ice concentration, ice type e.g. first year 0.7 - 1.2 m, ice thickness estimated from tilted floes with a ruler stick, which was attached to the ship's starboard side, floe size class e.g. medium floes 100 - 500 m, topography class e.g. ridges, new snow covered, ridge area and height, snow type e.g. old melting snow, snow thickness. At last also meteorological data is recorded: air temperature, sea temperature, wind speed, wind direction, cloud octas, visibility and weather code. Additionally, photos showing the views to port side, ahead and starboard side were taken to have a visual impression of the ice situation afterwards. An example of 2007-08-03, 06:00 UTC is shown in figure 3.3.1.



Fig. 3.3.1: Pictures taken during routine sea ice observation at 2007-08-03, 06:00 UTC. Left: view to port side, middle: view ahead, right: view to starboard side

Preliminary Results

The ship entered ice covered waters northeast of Svalbard on 1 August 2007. Even though the ice thickness was mainly below 2 m, the ship could only sail slowly and had to do a lot of ice ramming for the first ten days due to convergent ice drift and thus a very closed ice cover. During the rest of the cruise very favourable ice conditions for ship operation were encountered. Open leads allowed fast steaming and only few ice ramming was needed. *Polarstern* left the ice cover on 19 September 2007 in the Laptev Sea. Later another band of sea ice was encountered in front of Vilkitsky Strait. On 25 September the last sea ice was observed.

3.3 Routine sea ice observations

In total 525 observations on 54 days were carried out, resulting in 9.7 observations per day. Taking into account that for many hours several ship stations took place during these days, this represents good observation coverage in time. During long stations with unchanging sea ice conditions, less observations were needed.

The mean ice concentration during the cruise amounts to 81 %. A plot of the observed ice concentration during the cruise is shown in figure 3.3.2. The main observed ice concentrations are 8 to 10/10. The high number of 10/10 ice concentration observations starting in September is due to the onset of refreezing of the open water areas. After the main part of Arctic sea ice was left on 19 September ice concentrations got very scattered until the last observation on 25 September 2007.

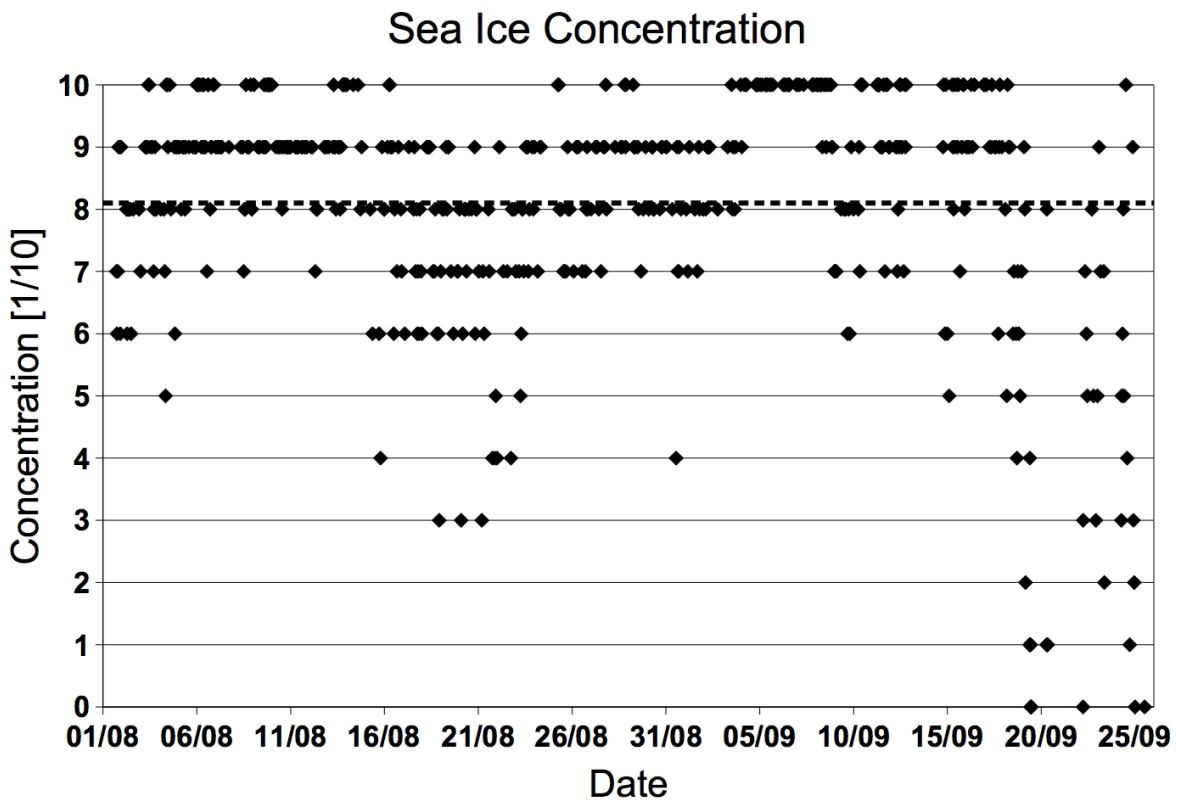


Fig. 3.3.2: Total sea ice concentration observed in tenth part from the bridge of Polarstern between 2007-08-01 and 2007-09-25. The dashed line denotes the mean sea ice concentration of 81 %.

The average level ice thickness of the ice area excluding open water is 95 cm, which matches well with the average ice measured by the helicopter-borne EM-bird (see Section 3.1). Figure 3.3.3 shows the observed ice thickness of the primary and thus thickest ice class during the cruise. For the primary ice class the average ice thickness amounts to 121 ± 46 cm. During the first part of the cruise the thickest ice was observed with a significant part of observations around 2 m. Afterwards the majority of observations lay between 75 cm and 150 cm.

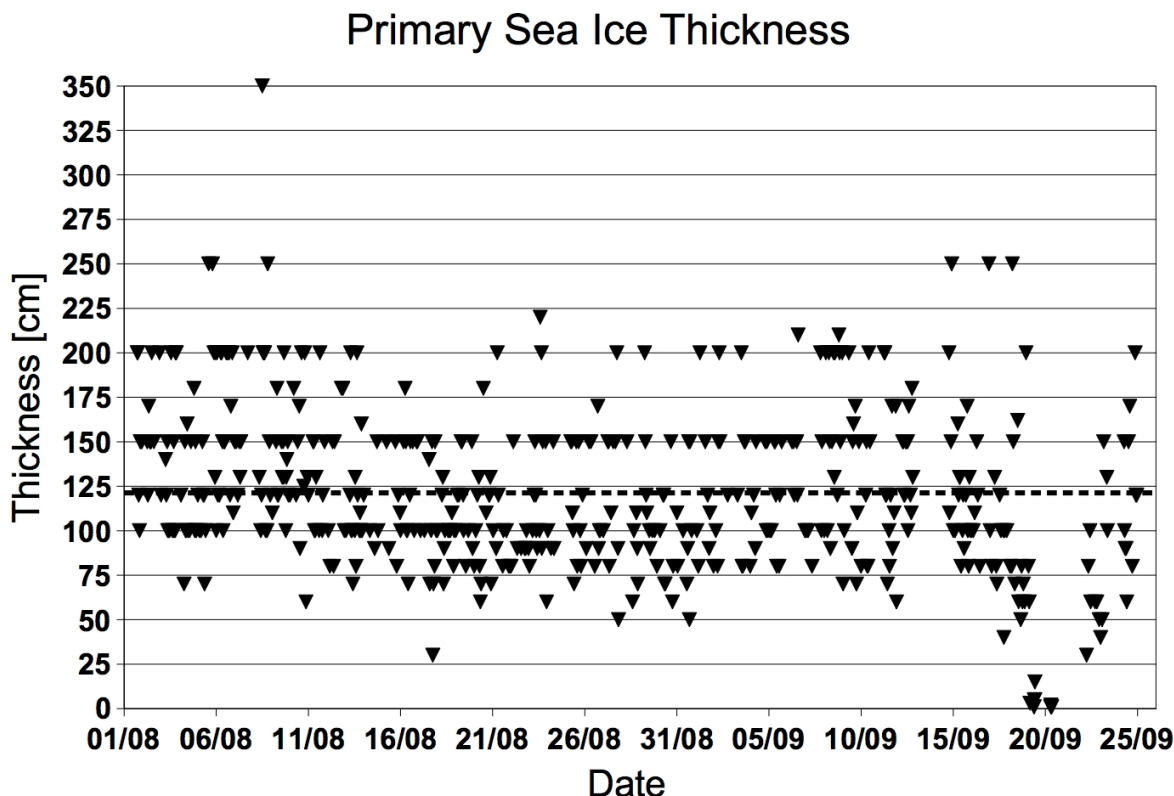


Fig. 3.3.3: Sea ice thickness of the primary ice class observed from the bridge of Polarstern between 2007-08-01 and 2007-09-25. The dashed line denotes the mean primary sea ice thickness of 121 cm.

5 % of the sea ice area consisted of ridges with an average ridged ice thickness of 116 cm. The mean snow depth on sea ice for this cruise is 7 cm, only regarding the snow covered ice the snow depth increases to 9 cm. 74 % of the ice was snow covered and 29 % of the ice was covered with melt ponds. Figure 3.3.4 shows the melt pond coverage in tenth part during the cruise. The average value of 3/10 was also the most common coverage observed. The majority of observations lay between 2 and 4/10 melt pond coverage.

3.3.1 Sea ice thickness around biological stations determined by drilling

Lasse Rabenstein, Stefan Hendricks, Volker Leinweber
Alfred-Wegener-Institut

Background

At some positions, assistance was given to investigations of the sea ice ecosystem by determining ice thickness distribution.

Work at Sea

To determine the thickness distribution of larger areas around sea ice biology stations we flew along randomly chosen straight profiles within approximately 50 x 50 nautical miles. Along these lines we drilled single holes with a spacing of at least the correlation length of the thickness distribution. Since we did not know the correlation

length of the area of interest we used a correlation length of a sea ice thickness distribution from the Beaufort Sea in 1980 which was determined by Rothrock et al (Rothrock, 1986). Therefore the separation of the drill holes was chosen to be two nautical miles to guarantee the statistical independence of the samples. In order to minimize a bias in the statistic by the choice of a proper helicopter landing site we always drilled 50 m on the right of the helicopter. In total 75 holes were drilled on four different profiles (see Fig. 3.3.4). Based on the Rothrock article this leads to a standard deviation of mean ice thickness of approximately 0.3 m. This is only valid as long as the thickness distribution is isotropic and stationary.

During two ice stations drilling profiles with 95 and 50 holes respectively were done with a point spacing of 5 m. On each point ice and snow thickness, freeboard and melt pond depth was measured.

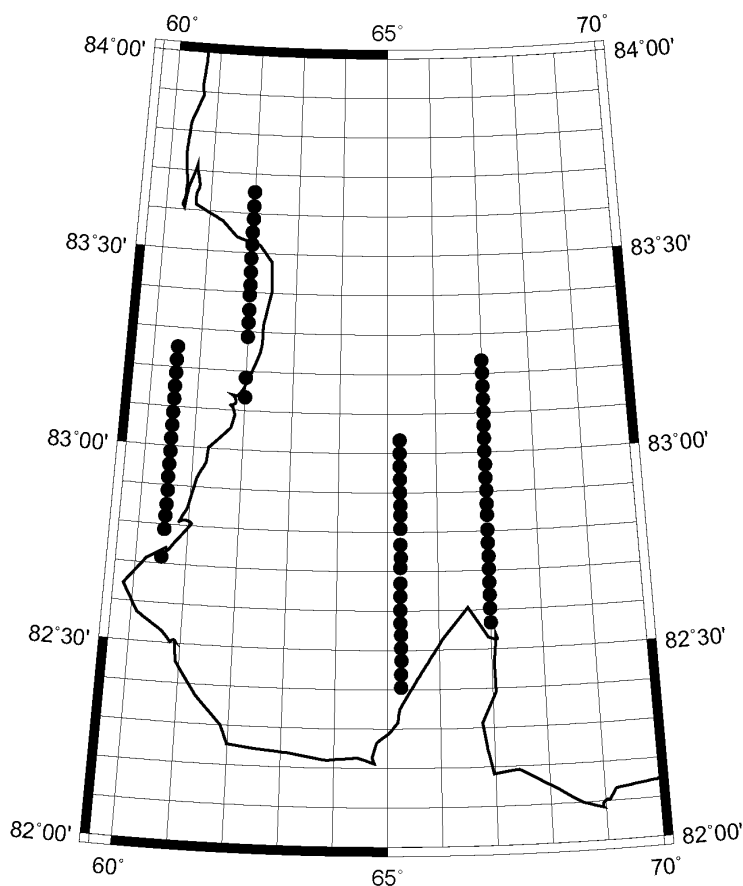


Fig. 3.3.4: Drill hole sites along the four helicopter flights. The solid line is the cruise track of Polarstern.

Preliminary Results

Figure 3.3.5 shows the results of the ice thickness drilling along the four helicopter profiles. The maximum of the Probability Density Function (PDF) can be found at 1.2 meters. As mentioned above the error is approximately +/- 0.3 m. Within the error margins this agrees to the results obtained with the EM Bird in other parts of the Trans Polar Drift.

Figure 3.3.6 shows the result of the drilling along a profile of 250 m length. The ice thickness, including freeboard and draft, the melt pond depth and the snow thickness is displayed. The thinnest ice can be found underneath the melt ponds. The thinning can be explained mostly by surface melting since no draft anomalies under the melt ponds can be observed.

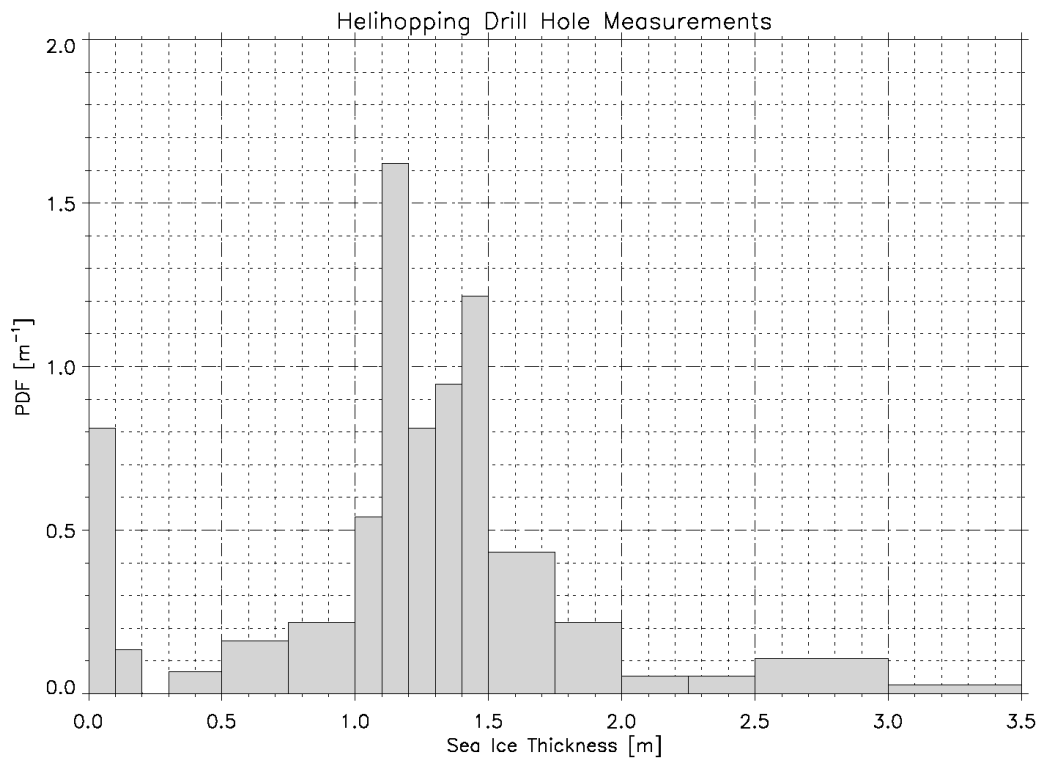


Fig. 3.3.5: Probability Density Function of the sea ice thickness along the four helicopter based drilling profiles

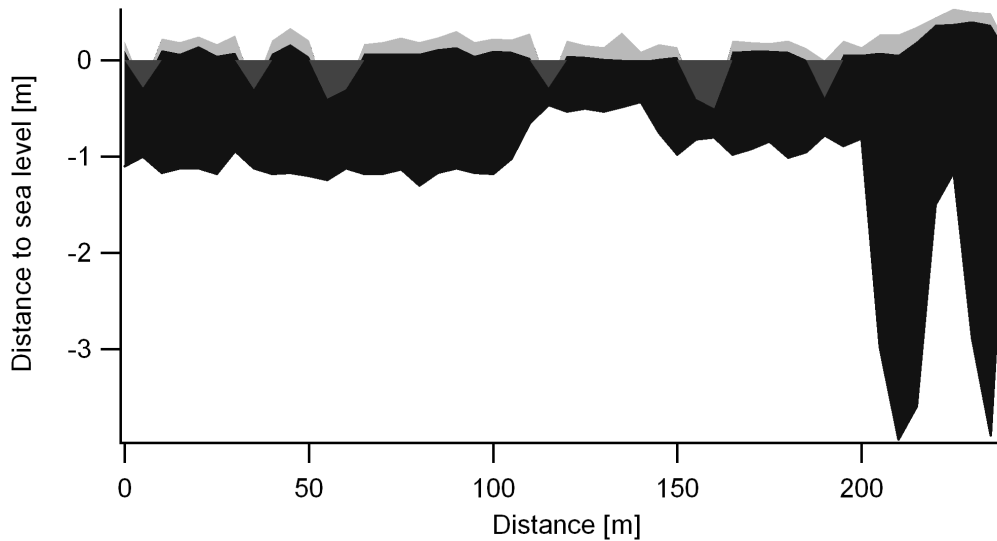


Fig. 3.3.6: A profile consisting of 49 drillholes with measurements of snow thickness, sea ice draft, freeboard and melt pond depth

Reference

Rothrock, 1986, Ice Thickness Distribution - Measurement and Theory, in Geophysics of Sea Ice, Ed. N. Untersteiner, p551-576, Plenum Press.

3.4 Buoy deployments

Background

As a contribution to the International Buoy Program (IABP) eight meteorological buoys and one Ice Mass Balance buoy (IMB) were deployed on several sites in the TPD. At the same time more buoys were deployed by other science vessels all over the Arctic Ocean.

Work at Sea

In total nine drifting buoys were deployed. Four of them were especially designed for meteorological measurements on sea ice. They include a cylindrical shaped main part, with the computer and batteries inside and a pole with an ARGOS antenna, a GPS receiver and a temperature and barometric pressure sensor on its top. The high position of the sensors at the top of the mast guarantees reasonable measurements even after heavy snow fall. The buoy is fastened to the sea ice either inside a 50 cm deep drill hole or by three ice screws. Three of the four buoys are "Ice Beacons" constructed by METOCEAN. The fourth meteorological buoy is an ICEB-CAN16-103, also constructed by METOCEAN.

Four buoys are Surface Velocity Profiler (SVP). They consist of a GPS receiver, a temperature sensor, a barometric pressure sensor and an ARGOS or an IRIDIUM antenna respectively. All sensors are mounted directly to the main plastic body. SVP's are designed for usage in open water but can also be used for deployment on

sea ice. If the buoys are covered by snow, the meteorological data may be wrong. To avoid these we deployed the SVPs at the top of consolidated ice ridges.

One buoy is an Ice Mass Balance Buoy (IMB). It measures air temperature, barometric pressure, GPS position, ice thickness, snow thickness and ice temperature. The IMB was part of the “super buoy station”, which includes in addition to the IMB some oceanography buoys and a webcam (see physical oceanography chapter). The IMB consists of the following components (see Fig. 3.4.1):

- 1) A main part similar to those of the four meteorological buoys.
- 2) A thermistor string of 3.5 meters in length installed in a hole with 5 cm in diameter. It measures a vertical temperature profile with thermistors every 10 cm.
- 3) A vertical pole with an above ice and under ice acoustical sensor to measure ice and snow thickness. For installation a hole with 10 cm in diameter was drilled.

Ideally an IMB is deployed on 2 meters thick level ice. Since no 2 meters thick level ice could be found, the IMB was deployed in a broad zone of approximately 2.5 meters thick heavily weathered but deformed multi year ice. The deployment sites of buoys are shown in Fig. 3.4.2.

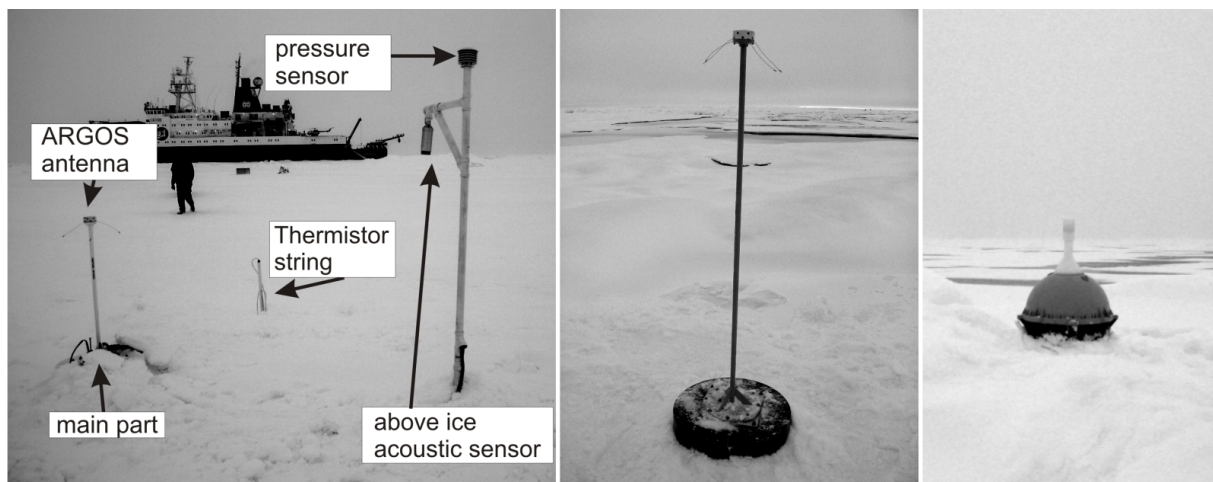


Fig. 3.4.1: Buoy types deployed during ARK-XXII/2. Left: Ice Mass Balance Buoy (IMB) Middle: Meteorological buoy (Ice Beacon) Right: Surface velocity profiler (SVP)

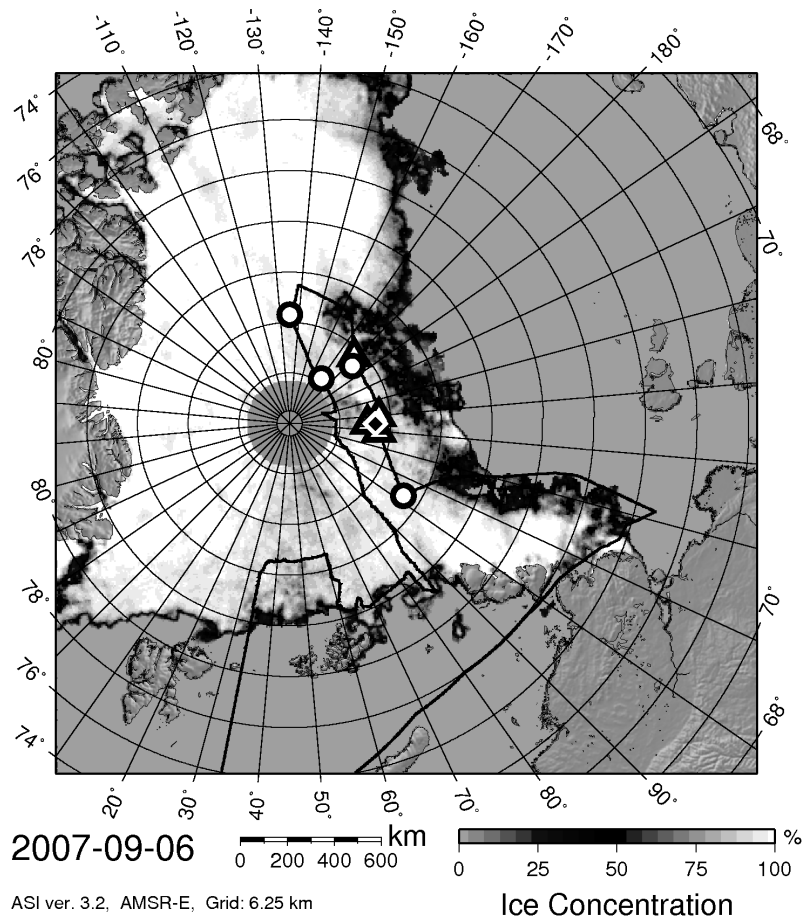


Fig. 3.4.2: Map of all buoy deployment sites. Circles mark ice beacons, triangles the surface velocity profilers and the diamond the ice mass balance buoy

Preliminary Results

All buoy data are sent in regular intervals to the database of the international Arctic buoy programme (IABP). This information is freely distributed to the scientific community. Download information can be found on the IABP homepage.

Acknowledgements

We thank the crew of the *Polarstern*, the team of FIELAX, and the team of Heli-Service International for their excellent collaboration. We thank Ursel Schauer for her kind way of guiding us through thick and thin ice. Finally, all of you who helped us physically, mentally, or with some extra equipment on the ice, in the helicopter, and on the vessel: Thanks a million!

3.5 Sea ice biology

Rainer Kiko¹⁾, Maike Kramer¹⁾,
Stefan Siebert²⁾, Alice Schneider¹⁾,
Karel Bakker³⁾, Liliith Kuckero⁴⁾

¹⁾ Institut für Polarökologie, Kiel

²⁾ Institut für Zoologie, Kiel

³⁾ Royal Netherlands Institute for Sea
Research, Texel

⁴⁾ Alfred-Wegener-Institut für Polar- und
Meeresforschung, Bremerhaven

Background and objectives

Sea ice covers large areas of the polar oceans: in the Arctic, approx. 7 million km² are covered with ice in summer time, 14 million km² in winter time. This ice cover plays a crucial role not only for geophysical processes, but also for the biology in the polar regions. Sea ice is not a solid block, but a matrix permeated with brine channels, which vary in diameter from micrometers to centimetres. These brine channels make up one habitat for a special community, the sympagic (ice-associated) community. It comprises viruses, bacteria, fungi, microalgae, protozoans and small metazoans. With temperatures between approx. 0° C and -22° C, the brine channels represent one of the coldest environments on earth. Salinity in the brine channels is coupled to the environmental temperature and rises when temperatures drop below the freezing point, as only water and not the contained solutes crystallize. The brine salinity can vary between approx. S = 220 at -22° C ice temperature and S = 2 - 3 during meltwater flushing in summer near 0° C.

Our studies focused on sea ice metazoans (also called sympagic meiofauna), multicellular animals in the size range of about 20 µm to 2 mm, as well as on under-ice amphipods. The meiofauna, which has been found in Arctic sea ice so far, comprises mainly of copepods, rotifers, turbellarians and nematodes. While sea ice algae received considerable attention since the beginning of biological sea ice studies, sympagic meiofauna has been studied only recently. Community composition in the Arctic pack ice and the factors influencing it are still not fully understood, especially as seasonality is concerned. Virtually nothing is known about the feeding ecology of sympagic meiofauna. These animals are however expected to play an important role in the sympagic ecosystem and in cryo-pelagic coupling, being a potential mediator of biomass and energy from algae, bacteria and protozoans to higher trophical levels.

The predicted loss of perennial sea ice in the Arctic Ocean will lead to major changes, if not destruction of an ecosystem, which is nearly as large as Australia (7 million km²) (Intergovernmental Panel on Climate Change, 2007). Species dependent on perennial Arctic sea ice will probably be extinguished at the end of the current century. Therefore, studies on all topics of sea ice biology are urgently needed, in especially the identification of endangered species, description of their life cycles and physiology and the collection of genetic information (even complete genomes), as well as the observation and modelling of changes in the whole ecosystem, which might occur due to a change from perennial to seasonal sea ice cover.

Work at sea

Quantitative sampling

Ice properties

The sympagic meiofauna community was analysed qualitatively and quantitatively, and the sea ice habitat characterized in terms of several environmental parameters. For this, several ice cores, cut in sections for vertical resolution, and pump samples of under-ice water were taken at eleven standard stations (Fig. 3.5.1, Table 3.5.1). At most stations eleven ice cores were drilled with a motor-powered KOVACS ice corer (internal diameter: 9 cm) in areas of non-deformed ice (Table 3.5.2). The lowermost part of completely sectioned cores was cut into five segments of 1 cm length, the next segment was 5 cm thick, then a segment of variable thickness followed and the remaining parts of the cores were cut into segments of 20 cm. One core was taken to analyse *in-situ* temperature directly on the floe. Two cores were retrieved and stored at -20° C, one core for texture analysis (AG Sea ice physics, AWI), another one to search for the presence of carbonate crystals within sea ice (AG Sea ice biology, AWI). Another core was retrieved, sectioned and melted directly at 4° C in the dark for determination of bulk salinity, chlorophyll a (chl a) and phaeopigment (phaeo) content, as well as nutrient concentrations (phosphate, silicate, nitrate and nitrite). Furthermore aliquots from this core were preserved in formalin/hexamine for counting of algae. For determination of chl a and phaeo a determined volume was filtered onto Whatman GF/F filters, extracted with 90 % acetone, homogenized and measured fluorometrically. The fifth core taken during each standard station was cut into sections, melted directly in the dark at 4° C and a determined volume was filtered onto precombusted GF/F filters. These were stored at -80° C and will be used for the determination of stable carbon and nitrogen isotopes of the particulate matter. Ice-core sections for meiofauna analyses were generally melted with an excess of 0.2 µm filtered seawater (FSW, 200 ml per 1 cm of ice core) and enriched over a 20 µm gauze. One meiofauna core from each standard station was sectioned completely, worked up as described above and then fixed with 2 % borax buffered formaline. These samples will be analysed for species composition, abundance and biomass in the home laboratory. For each of the eleven standard stations, meiofauna from three ice-core bottom sections (lowermost 5 cm of the cores) was sorted and counted alive onboard the vessel. One bottom section (lowermost 10 cm) was fixed with ethanole and stored at 4° C for determination of unidentifiable objects (e.g. eggs) with DNA sequencing techniques. Two bottom sections (lowermost 2 cm) were immediately flushed with 50 ml FSW, the resulting liquid filtered over a 20 µm gauze, the samples fixed in glutaraldehyde or picric acid formaldehyde (PAF) and stored at 4° C. These samples will be used for gut content analyses in the home laboratory using transmission and scanning electron microscopy. Another 10 cm bottom section was also melted in an excess of FSW, and approx. 200 ml of the resulting sample was thereafter filtered onto a 0.02 µm filter and the filter stored at -80° C. These samples will be used for analysis of hidden diversity within sea ice also using DNA sequencing techniques.

Sub-ice layer

At each standard station, temperature and salinity profiles in the sub-ice water layer (0 - 6 m below the ice underside) were measured *in-situ* with a conductivity meter lowered through a core hole. Discrete water samples for analysis of algal pigments

were collected from 0 m and 5 m depth below the ice with a polyethylene tube with a valve at one end. The unequipped end of the tube was lowered into the water through a core hole with the valve closed. At the sampling depth, the valve was opened and closed again and the tube with the enclosed water sample was hoisted to the surface. An integrated sample from 0 - 10 m water depth under the ice was taken, leaving the valve open while lowering the tube, and closing it at the sampling depth. For determination of chl a and phaeo concentration, samples were treated as described above. Also subsamples for determination of nutrient concentration and algal composition were taken. Organisms from the under-ice water (0 m and 5 m depth below the ice) were quantitatively sampled with an under-ice pumping system equipped with a standardized water meter and inserts of plankton gauze (mesh size 55 μm) to concentrate the organisms. Samples were fixed with 2 % borax buffered formaline. Enumeration of species and stages from the sub-ice layer will be done in the home laboratory. At some of the stations, also some specimens from non-quantitative pump samples (0 m) were fixed in glutaraldehyde and PAF for gut content analyses. Abundances of under-ice amphipods will be estimated from under-ice video images taken during ten standard stations.

Other ice habitats

Samples for analysis described above (except for live counting and gut content analysis) were also retrieved from several melt pools and from newly formed ice in melt pools and leads (Fig. 3.5.1, Tab. 3.5.1).

Qualitative sampling

Meio- and macrofauna was also collected for various experiments and analyses concerning feeding ecology. Individuals were isolated alive from bottom sections of ice cores, from ice pieces collected by ice fishing (through a hole in the bottom of a mummid chair), from newly formed ice in melt pools and from under-ice water and zooplankton net samples. Part of the experiments were already conducted onboard. For further experiments in our home laboratory, cultures of sympagic meiofauna and sympagic algae were established during the cruise.

For morphological studies with light or electron microscopy in the home laboratory, single organisms isolated from qualitative samples were fixed in 2 - 4 % borax buffered formalin, glutaraldehyde or PAF.

In order to gain information about the role of sympagic meiofauna for the sympagic food web, we conduct feeding experiments with dominant sympagic meiofauna species as predators or grazers and different sympagic meiofauna, protozoans or ice algae as food. In basic predator-prey experiments, only one prey taxon is offered to the predators and the influence of predator and prey density on the predation rate (functional response, concurrence) are studied. Additionally, in food-choice experiments, different food is offered to the meiofauna at the same time, and preference for particular food sources is studied. Grazing experiments on ice algae are conducted not only in suspensions of algae but also on surfaces, in order to simulate *in-situ* conditions.

For the biochemical analyses of fatty acids as well as stable carbon and nitrogen isotopes, ice and sub-ice fauna was sorted alive onboard, and stored deep-frozen

(−80 ° C) until analysis in the laboratory. Several fatty acids are not produced by the animals themselves, but are taken up with their food. Fatty acids can thus present information about the diet consumed *in-situ*. The stable isotope ratios of carbon ($\delta^{13}\text{C}$) and nitrogen ($\delta^{15}\text{N}$) provide a time-integrated measure of the trophic position in a certain food web, and can also provide information on the major carbon source of an organism.

Also the above-mentioned gut-content analyses will give information about *in-situ* diets of sympagic meiofauna and sub-ice fauna.

Preliminary results

In total, samples were collected on 31 stations (Fig 3.5.1). On eleven stations, so called standard stations, the above described complete sampling programme of the ice proper and the sub-ice layer was performed. On eleven stations, newly formed ice on melt ponds or in leads was quantitatively sampled for meiofauna abundance, chl a and phaeo concentration, POC/PON, nutrients, algal composition and bulk salinity. During all 31 stations qualitative samples were taken, in order to gather material for experiments, and for lipid and isotope analyses

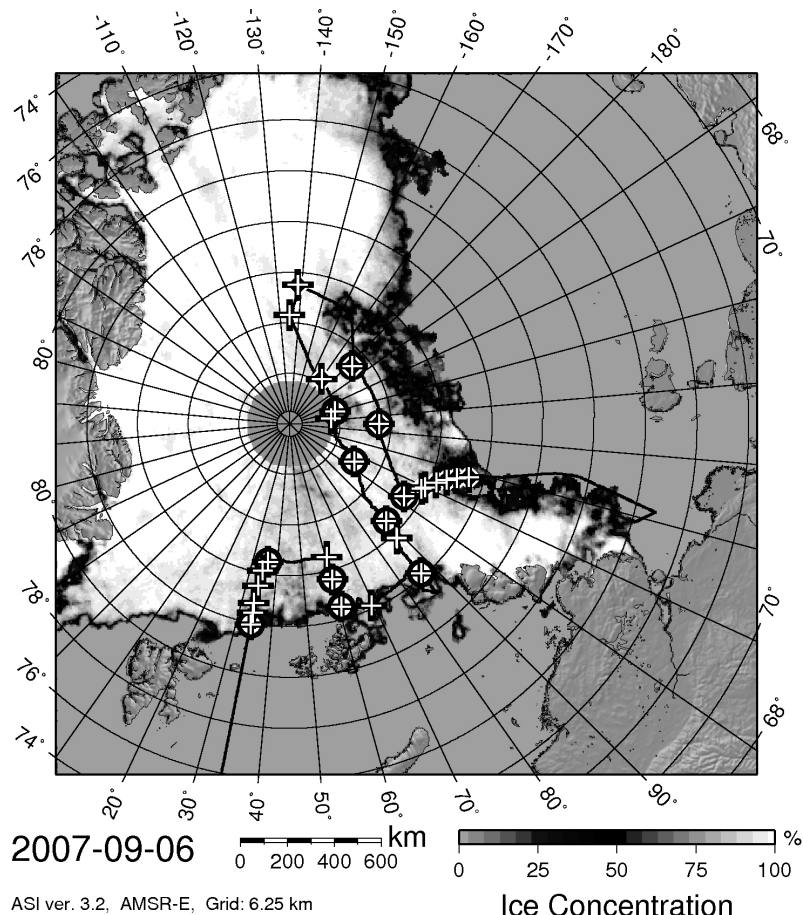


Fig. 3.5.1: Sampling stations plotted together with the cruise track and ice concentrations derived by satellite imagery for the 6 Sept. crosses: qualitative sampling; circles: standard stations; diamonds: thin ice sampling. (Map provided by Gunnar Spreen, IFM Hamburg)

Tab. 3.5.1: Date, time, position and kind of programme performed

Date (yymmdd)	Time (UTC)	Lat	Lon	Programme
070802	13:30-21:00	81°57'N	34°02'E	standard
070803	18:00	82°24'N	34°02'E	ice fishing qualitative
070804	10:55-12:20	82°48'N	33°45'E	qualitative (Heli)
070805	10:00-15:00	83°30'N	33°57'E	qualitative
070806	16:00	84°07'N	34°41'E	ice fishing qualitative
070807	9:30-17:00	84°29'N	36°08'E	standard
070811	16:15	84°32'N	60°37'E	ice fishing qualitative
070812	12:00-18:00	83°38'N	60°23'E	standard
070815	13:00-18:00	82°30'N	60°48'E	standard
070817	12:30-12:50	82°08'N	69°12'E	ice fishing qualitative
070820	13:30-19:00	82°09'N	86°20'E	standard
070823	14:10	83°49'N	88°06'E	qualitative
070823	15:10	83°51'N	88°16'E	Qualitative
070823	16:00	83°52'N	88°22'E	qualitative
070824	9:30-17:30	84°35'N	89°50'E	standard
070827	21:50-4:00	87°03'N	104°48'E	standard
070830	18:35	88°21'N	142°51'E	ice fishing qualitative
070831	18:30	88°08'N	150°05'E	standard, meltpond qualitative
070902	14:00-18:00	87°49'N	170°36'W	Meltpond quantitative
070905	18:30-23:15	85°42'N	135°02'W	qualitative
070907	9:30-12:00	84°30'N	138°22'W	Meltpond quantitative
070907	19:30-19:50	84°30'N	138°26'W	ice fishing qualitative
070910	13:30-18:00	86°38'N	177°33'E	standard, meltpond quantitative
070912-070914	22:15-10:00	86°24'N	135°49'E	standard, meltpond quantitative
070916	12:30-20:00	84°39'N	102°44'E	standard, meltpond quantitative
070917	10:00	84°11'N	108°56'E	ice fishing qualitative, thin ice quantitative
070917	16:45	84°06'N	109°57'E	ice fishing qualitative, thin ice quantitative
070918	1:00	83°46'N	113°08'E	ice fishing thin ice quantitative

Date (yymmdd)	Time (UTC)	Lat	Lon	Programme
070918	6:45-7:25	83°25'N	115°25'E	ice fishing thin ice quantitative
070918	14:20-15:40	83°04'N	116°56'E	ice fishing thin ice quantitative
070919	0:20-1:10	82°37'N	118°24'E	ice fishing qualitative, brash ice quantitative

Tab. 3.5.2: Parameters and samples gathered during standard ice stations

parameter	ice cores	sub-ice water
temperature	complete	0-6 m
(bulk) salinity	complete	0-6 m
brine salinity	complete	--
relative brine volume	complete	--
POC, PON, $\delta^{13}\text{C}$, $\delta^{15}\text{N}$	complete	0 m, 5 m, 0-10 m
NO_2^- , NO_3^- , PO_4^{3-} , SiO_4	complete	0 m, 5 m, 0-10 m
chlorophyll a, phaeopigment a	complete	0 m, 5 m, 0-10 m
algae	complete	0 m, 5 m, 0-10 m
fauna abundance, diversity (alive)	5 cm bottom sections	--
fauna abundance, diversity (formaldehyde fixed)	> 20 μm	0 m, 5 m
fauna diversity (ethanole)	complete	> 55 μm
fauna gut content (PAF, glutaraldehyde fixed)	> 20 μm	--
fauna diversity, taxonomy, morphology (PAF, glutaraldehyde, formaldehyde fixed, deep frozen)	10 cm bottom sections	0 m
fauna fatty acids / alcohols	> 20 μm	> 55 μm
fauna $\delta^{13}\text{C}$, $\delta^{15}\text{N}$	2 cm bottom sections	--
hidden diversity	> 20 μm	0 m

Standard stations

In order to describe the typical environmental parameters found within the ice and in the sub-ice layer data from the stations on the 7 August and 13 September are presented and discussed in the following.

Ice thickness on 7 August was 150 cm with a positive freebord of 8 cm, on the 13 September an ice thickness of 101 cm with a positive freebord of 9 cm was found. On 7 August temperature at the surface of the ice was higher at about -0.1°C and decreased monotonously to -1.1°C at the bottom (Fig. 3.5.2). On 13 September temperature at the surface was lower at -1.5°C , increased then to -0.8°C at 22.5 cm depth and then decreased again to -1.5°C at the bottom. Hence freezing in the upper parts of the ice occurred, due to low atmospheric temperatures, but heat loss from the ocean did not take place through the ice proper as otherwise a monotonous profile could be expected. Temperatures in the sub-ice layer during the station on 7 August showed a typical summer profile with higher temperatures of -1.5°C at 0 cm and 10 cm, -1.6°C at 20 cm and 30 cm directly under the ice and thereafter a temperature of -1.7°C until 600 cm below the ice. This indicates bottom melting of the ice, which is supported by the salinity data. These show a freshened layer of 20 cm thickness ($S = 30.1 - 31.5$) directly under the ice, thereafter salinity rose to 33.5 and stayed almost constant down to 600 cm depth. In contrast on 13 September salinity and temperature were homogenous in the first 600 cm under the ice. Temperature was at -1.7°C and salinity at 31.2, which indicates that bottom melting stopped and heat was transferred to the atmosphere from the ocean through leads and melted through melt pools.

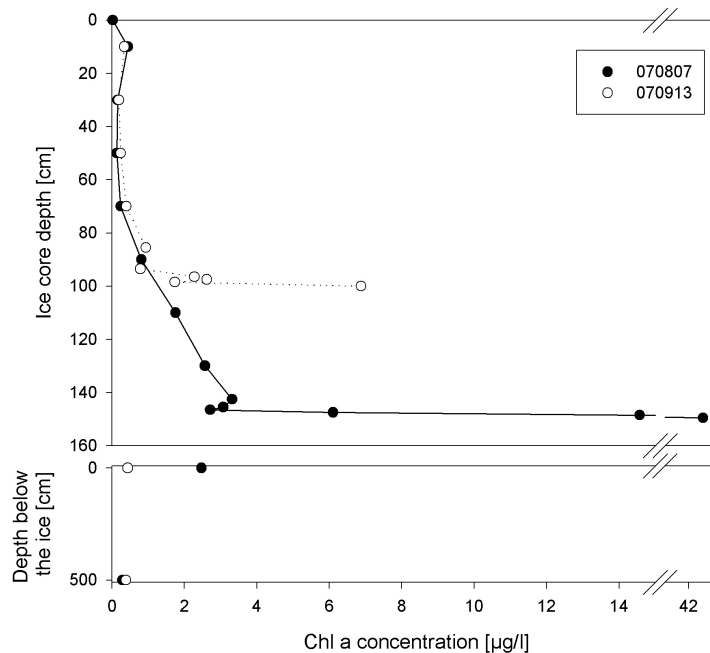


Fig. 3.5.2: Temperature and bulk salinity as measured within the ice on 7 August and 13 September

3.5. Sea ice biology

Chl a profiles from both stations show a typical L-shaped profile (Fig 3.5.3), with lower chl a concentrations around 1 $\mu\text{g/l}$ in the upper part of the core, rising to high chl a concentrations in the bottom layer, with 46.0 $\mu\text{g/l}$ on 7 August and 6.9 $\mu\text{g/l}$ on 13 September. Low chl a concentrations in the upper part were probably due to nutrient limitation (data not shown). Chl a concentration in the water column on 7 August at 0 cm depth below the ice was 3.7 $\mu\text{g/l}$, at 500 cm depth it was 0.4 $\mu\text{g/l}$. Higher concentrations directly under the ice are probably due to a release of algae from the ice through bottom melting. On 13 September chl a concentrations directly under the ice were lower with 0.44 $\mu\text{g/l}$ at 0 cm depth. At 500 cm depth the same concentration as on 7 August of 0.4 $\mu\text{g/l}$ was found. The lower chl a concentration directly under the ice coincides with the end of bottom melting and release of ice algae to the water column.

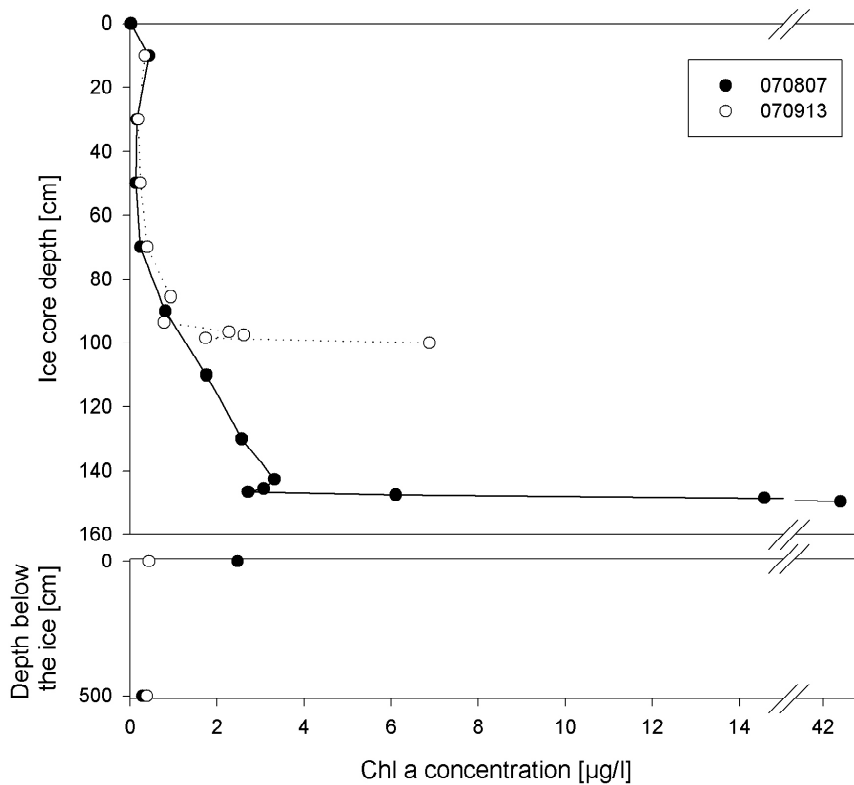


Fig. 3.5.3: Chlorophyll a concentrations in the ice (melted sample; upper panel) and sub-ice layer (lower panel) on 7 August and 13 September

The described environmental parameters will help to interpret the meiofauna abundances throughout the ice and in the water column. These will be the result of sorting, identification and counting of the species to be found in the formalin fixed samples in the home laboratory.

Sea ice meiofauna

Bulk abundances of metazoans in ice-core bottom sections (alive counts on 3 replicates for each of the 11 standard stations) ranged between 9 Ind L⁻¹ and 375 Ind L⁻¹ (in melted ice); abundances of protozoans were an order of magnitude higher (Fig. 3.5.4). The sea ice metazoans were dominated by rotifers, red acoel platyhelminthes, nematodes, the harpacticoid copepods *Halectinosoma sp.* and *Tisbe sp.*, and different cyclopoid copepods in live counts of bottom sections of the 11 standard stations. Also white acoel platyhelminthes with similar shape as the red ones were found, but only in low numbers. Among protozoans, ciliates were dominant, but also the foraminifer *Neogloboquadrina pachyderma* occurred in high numbers. These findings are in accordance with results from former cruises. High abundances of eggs were found in the ice especially during the second half of the cruise, when also egg-carrying females of the copepod *Halectinosoma sp.* were observed.

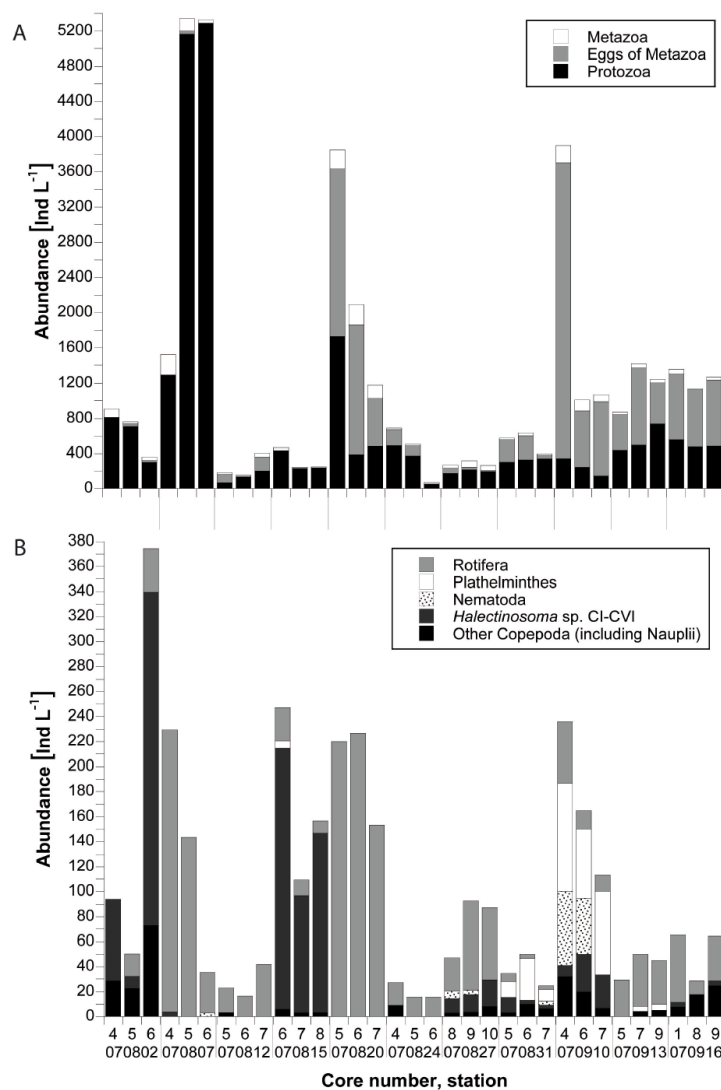


Fig. 3.5.4: Bulk abundances of sea ice meiofauna in ice core bottom sections from 3 replicates for each of the 11 standard stations. a: protozoa, metazoan eggs and metazoa, b: only metazoa

All 11 stations differed significantly in terms of sympagic meiofauna communities (global ANOSIM based on Bray-Curtis similarities, calculated from fourth-root transformed abundances of metazoans in bottom sections counted alive; significance level 5 %), i.e. variability between stations was generally considerably higher than variability between replicate cores. Pair wise comparison of stations (pair wise ANOSIM), as well as multidimensional scaling and hierarchical agglomerative clustering, revealed no distinct areal pattern and showed that at some stations patchiness was high.

In addition, mainly in qualitative samples, we found some taxa, which have not been described for the Arctic sea ice as yet. Elongated white acoel plathyelminthes as well as elongated white plathyelminthes with eye spots (probably rhabditophores) were found at some stations, usually in low numbers. Adults and copepodides of an unidentified calanoid copepod (probably *Limnocalanus* sp.) were found in the ice at two stations. Most interestingly, we also found cnidarians, in the ice, which is the first record of sympagic cnidarians for this area, and the second record of sympagic cnidarians for the Arctic.

The newly formed thin ice on melt ponds, which could be found during the second half of the cruise, was often inhabited exclusively by ciliates, which were always the dominant heterotrophs, and rotifers. Sometimes also red acoel plathyelminthes and few individuals of other meiofauna taxa were found.

Sub-ice fauna

The sub-ice fauna was dominated by *Oithona* spp., different copepod nauplii, *Calanus finmarchicus*, *C. glacialis*, and an unidentified calanoid copepod (probably *Limnocalanus* sp.). Also the foraminifer *N. pachyderma* was frequent in the sub-ice layer. In addition, some other calanoid copepods (*Acartia* sp., *Metridia longa*), few rotifers and single individuals of the pteropod *Limacina* sp. were found. Amphipods found associated with the ice were *Gammarus wilkitzkii*, *Apherusa glacialis* and *Onisimus* spp. Preliminary analysis of the under-ice videos revealed also the presence of ctenophores and the polar cod *Boreogadus saida* in the sub-ice layer. Abundances and diversity of the amphipods seem to be higher in the vicinity of Svalbard, Franz Josef Land and Severnaya Zemlya than in the Central Arctic.

Food web studies

For gut content analyses with the electron microscope, altogether 40 samples (20 each for transmission and scanning electron microscopy) were collected at 13 stations. 32 of these samples are from different ice habitats (level ice and newly formed ice on melt ponds), eight samples are from the sub-ice habitat.

For analyses of fatty acids and alcohols, or of stable carbon and nitrogen isotopes, 139 samples were collected, comprising samples for ten different ice taxa (67 samples) and six different sub-ice taxa (72 samples). For most taxa, replicate samples could be taken. Most of the samples comprised animals from only one station, so that possible regional differences can be detected. Samples from different

types of habitats (sub-ice, first-year ice, multiyear ice, thin ice on melt ponds) taken for several taxa will give insight into the influence of the habitat on feeding.

The data from the gut content and biochemical analyses will give a comprehensive picture of the *in-situ* feeding habits of all dominant sympagic metazoans.

Predation experiments were conducted onboard the vessel using

- cnidarians as predators and rotifers as prey, with varying predator and prey densities
- cnidarians as predators and copepod nauplii as prey
- the copepod *Halectinosoma* sp. as predator and sympagic ciliates as prey, with varying predator densities
- red and white acoel plathyelminthes as predators and ciliates as prey.

The experiments revealed that the cnidarians prey on rotifers as well as on copepod nauplii, being able to ingest prey individuals of their own body size. *Halectinosoma* sp. preys on sympagic ciliates, with predation rates depending on predator densities. Predation of turbellarians on ciliates was not observed. Further predation experiments, as well as grazing experiments and food-choice experiments, will be conducted at the home laboratory. For this purpose, cultures of all dominant sympagic meiofauna species and of ice algae have been successfully established.

The data from the feeding experiments conducted during the cruise, and from further experiments will give predation rates and information about concurrence / functional response of the sympagic organisms. Furthermore, viewed in conjunction with abundances of sympagic metazoans, ciliates, and algae, it will be possible to estimate the predation and grazing impact of sympagic metazoans, and hence their overall role within the ecosystem.

4. OCEANOGRAPHY

4.1 Physical oceanography

Takashi Kikuchi³⁾, Sebastian Mechler⁴⁾, Sergey Pisarev⁵⁾, Benjamin Rabe¹⁾, Bert Rudels²⁾, Ursula Schauer¹⁾, Andreas Wisotzki¹⁾

¹⁾Alfred-Wegener-Institut

²⁾Finnish Institute of Marine Research

³⁾Japan Agency for Marine Earth Science and Technology

⁴⁾Optimare

⁵⁾P.P. Shirshov Institute of Oceanology

Objectives

The circulation and water mass properties of the Arctic Ocean have been changing considerably during the past decades. The aim of the oceanographic part of this cruise was devoted to the IPY theme of quantifying the ocean changes by documenting the present state of the water mass distribution in the Eurasian basins and shelf seas. Due to the light ice conditions we could even include the northern Canada Basin.

Water advected from the North Atlantic has become warmer since the early nineties and the question is still open whether the additional oceanic heat has contributed to the decrease of the sea ice. The Atlantic inflow has also become more saline, but at the same time the hydrological cycle has increased and with that the fresh water supply to the Arctic. Less sea ice might in turn have affected the interaction between ocean and atmosphere and altered the modification of the water on the Eurasian shelves and even in the central Arctic Ocean. Furthermore, changing atmospheric patterns (Arctic Oscillation) influence the input, storage and circulation of the fresh water which is supplied to the Arctic Ocean through continental runoff, precipitation, and Pacific water inflow and which shields the warm Atlantic water from the surface.

Specific questions are: Has the warmer inflow to the Barents Sea lost all its additional heat before entering the central Arctic? To what extent is the Fram Strait branch water exposed to the surface while flowing along the continental slopes and ridges and where is it isolated from the surface by the fresh water layer of the Siberian river run-off? Is Atlantic water upwelling at the shelf edge so that its heat can be released? Where do Fram Strait and Barents Sea branches mix and which fractions recirculate at which time scales towards Fram Strait within the various basins? What is the current position and direction of the Transpolar Drift of fresh waters from the Pacific and from the Siberian rivers? Can we identify individual pulses of warm saline inflow and speculate about the timing of their outflow to the subarctic Atlantic?

To address these questions hydrographic sections were repeated that were taken in the Eurasian Basin during the cruises *Oden* 1991 and 2005 as well as *Polarstern* 1993, 1995 and 1996.

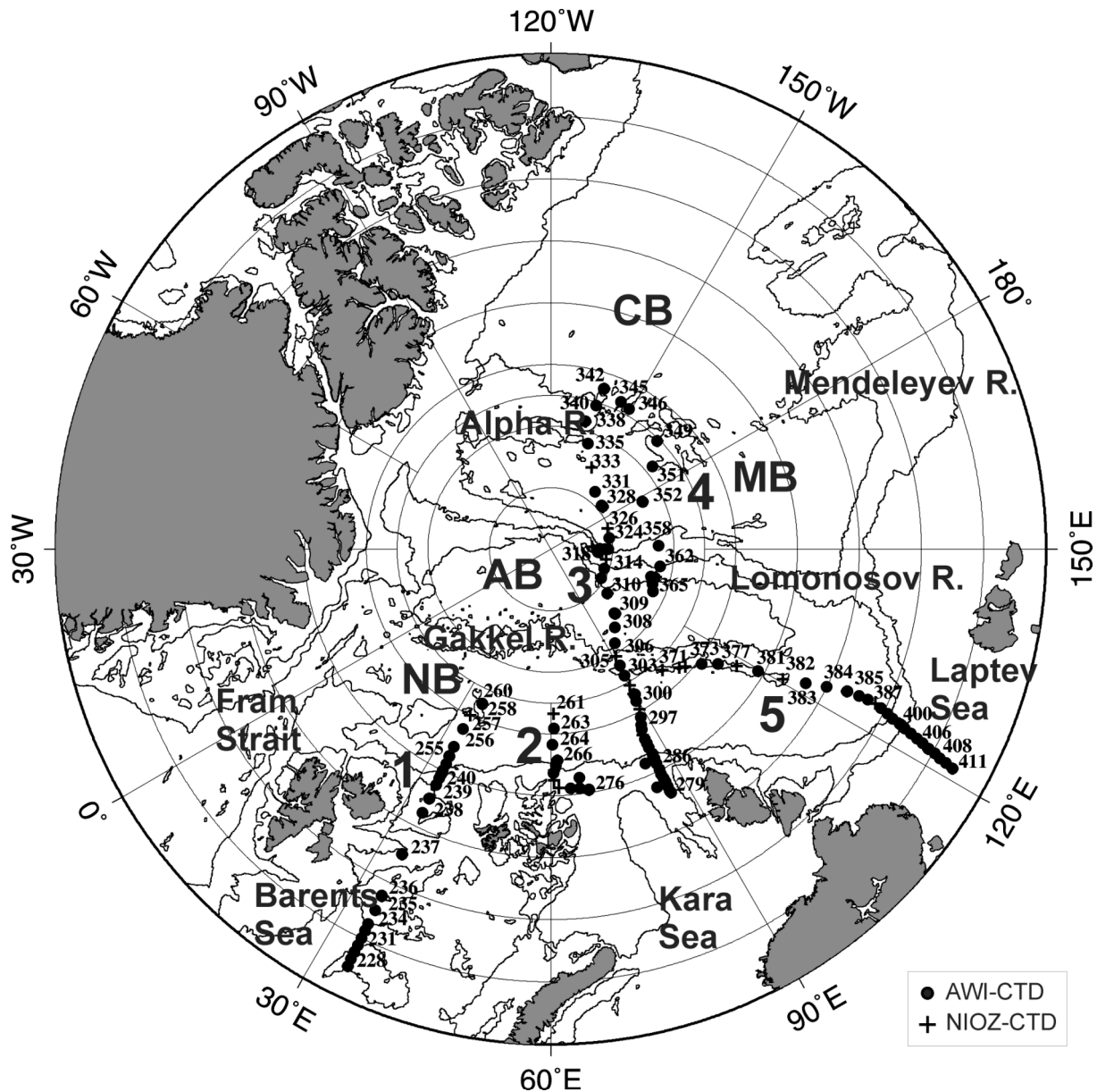


Fig. 4.1.1: Location of CTD stations. Numbers denote sections. AB: Amundsen Basin, NB: Nansen Basin, MB: Makarov Basin, CB: Canadian Basin

Work at sea

Ship-borne measurements

Along the five sections (Fig. 4.1.1), altogether 191 CTD profiles were taken at 127 stations and water samples were collected. 142 casts were carried out with a standard CTD/rosette water sampler (described below) and 49 casts were taken with the ultra-clean system of the GEOTRACES programme (described in chapter 5). Both systems had Seabird CTD components (SBE 911+) with double temperature and conductivity sensors. The standard CTD system, SN 485, from Sea-Bird Electronics Inc SBE911+ was equipped with duplicate temperature and conductivity

sensors (temperature sensors SBE3, SN 2423 and 2460, conductivity sensors SBE4, SN 2078 and 2054 and pressure sensor Digiquartz 410K-105 SN 68997). The CTD was connected to a SBE32 Carousel Water Sampler, SN 202, with 24 12-liter bottles. Additionally, a Benthos Altimeter PSA-916, SN 1228, a Wetlabs C-Star Transmissometer, SN 946, and a SBE 43 dissolved oxygen sensor, SN 743, was mounted on the carousel. The SBE 43 contains a membrane polarographic oxygen detector. The algorithm to compute oxygen concentration requires also measurements of temperature, salinity and pressure which are provided by the CTD system. To calibrate the oxygen profiles 279 water samples at 30 CTD casts were collected and measured onboard with Winkler titration. Continuous profiles of the DOM concentration were obtained with two fluorometers, a Wetlabs ECO-CDOM, SN 742, and a Dr. Haardt Back Scat Model 1184.6, SN 12030. Salinity of 245 water samples was measured using a Guildline salinometer with Standard Water Batch P148 for calibration of the salinity sensor. At 15 stations, 60 water samples at 5 l were collected for Technetium measurements.

In areas with heavy ice, the sections were extended by helicopter-borne XCTD casts. XCTDs were also launched between CTD casts to increase the horizontal resolution in frontal zones. Underway measurements with a vessel-mounted narrow-band 150 kHz ADCP from RD Instruments and two Sea-Bird SBE45 thermosalinographs were conducted to supply temperature, salinity and current data. The thermosalinographs are installed in 6 m depth in the bow thruster tunnel and in 11 m depth in the keel. The salinity of both instruments was controlled by taking water samples. Unfortunately, already at the first section, on 4 August, the ADCP failed and no current measurements were taken thereafter.

In order to provide year-round measurements of temperature, salinity, velocity and under-ice turbulence, ice-tethered platforms (ITPs) with various instrumentation were deployed. These platforms contribute to an “International Arctic Ocean Observation System” (iAOOS) that aims at a persistent observation network.

The oceanographic work of the cruise was part of the EU-funded Integrated Project “DAMOCLES” (Developing Arctic Modelling and Observing Capabilities for Long-term Environment Studies) and the BMBF-funded Project “North-Atlantic”.

First results of the CTD observations

The oceanography work started on Sunday, 29 July 2007, with a station at 72°35'N and 26°0'E to test the two CTD systems, the AWI standard CTD/rosette and the NIOZ ultra-clean (UC) Titan CTD system. All bottles were closed to test for leaking and rosette malfunctions. All sensors and bottles were found to work properly. During the cruise there were, however, constant problems with position 4 on the AWI rosette and in the end it was considered unreliable, leaving 23 working bottles on the AWI rosette.

The sampling of the first real section, taken along the 34°E meridian commenced at 75°N on Monday 30 July at 10 am with station 228 using the UC CTD. The AWI rosette was, however, considered the main instrument and was used at most stations. On several stations both CTD systems were used, sometimes with multiple casts to supply the required water volumes. Only at a few stations just the UC CTD

was used to save time. On the sections prepared and shown here the stations with only UC CTD have been merged with the AWI CTD casts. Especially the AWI CTD was found to well reproduce the numerous intrusions observed in the water column, while the UC CTD data will need extensive post cruise editing to remove spikes and instabilities in the profiles. The conductivity sensors on both CTDs have been preliminary calibrated against salinity samples measured onboard during the cruise and the values shown on the sections are reliable.

Section 1 (Fig. 4.1.2) started in the Barents Sea over the Central Bank and ran northward across the Grand Bank and the continental slope into the Nansen Basin, almost extending to the Gakkel Ridge. Because of heavy ice and slow progress the section was terminated with station 260 at 84°30'N and 36°09'E before the Gakkel Ridge was reached. The section captured the Atlantic water entering through the Barents Sea Opening between Norway and Bear Island, which this year also covered the Central Bank. The salinity was high, >35.1, and the temperature of the upper layer were above 6° C. The polar front was located at the southern edge of the Grand Bank and above the bank the upper salinity was lower, partly due to ice melt, partly due to the presence of less saline Arctic water. A temperature minimum, $T < -1.6^{\circ}$ C, with salinity 34.5 - 34.6 was located between 50 and 100 m, indicating the depth and characteristics of the winter homogenised upper layer. The deeper layers above the bank and in the northern depressions were occupied by Atlantic water, less saline and less warm than farther to the south.

The Fram Strait Atlantic water core was located above the continental slope, close to the shelf break and close to the sea surface, with its thermocline less than 100 m deep. The surface heating and mixing as well as the mixing of heat from below increased the temperature at the shelf break and thus has obviously separated the winter mixed layer in the Barents Sea from the less saline, but colder winter mixed layer of the Nansen Basin. The Atlantic water at the slope was warm, occasionally above 3° C and saline, above 35. Below the Atlantic core, the weak salinity minimum of the Arctic Intermediate Water (AIW) at about 1,000 m and the Nordic Sea Deep Water (NDW), both less saline than the Eurasian Basin Deep Water (EBDW), could be recognised.

Farther offshore the temperature and salinity of the Atlantic water decreased and intrusions were observed. Below the Atlantic core a salinity minimum was present, slightly less dense and located higher in the water column than the AIW at the slope. The salinity minimum was also distinguished by many small-scale intrusions. This minimum, being colder than the upper layer, stems from the Barents Sea while the upper water is one loop of the Fram Strait inflow branch that recirculates within the Nansen Basin along the Gakkel Ridge.

The second section (Fig. 4.1.3) ran from 84°39'N, 60°57'E southward to the Barents Sea shelf northwest of Franz Josef Land. Only on the northernmost station were the characteristics of the Barents Sea branch water and the return circulation of Fram Strait water to be seen. Further south, the warmer, more saline, newly entered water from the west dominated. The southern part of the Atlantic core was even closer to the sea surface, at ~50 m depth, than it was at the 34°E section and here the temperature minimum from the winter homogenisation of the upper layer was absent.

This suggests that Atlantic water is entrained into the upper mixed layer and may influence and reduce the ice formation. Close to the slope less saline and colder water was present, as a detached eddy in the upper 300 - 600 m on one station and at the slope as intrusions around 300 - 500 m, close to the bottom. This indicates an outflow of water from the Barents Sea, presumably flowing northward along the Victoria Channel.

After section 2 was finished on 17 August with station 271 *Polarstern* sailed eastward along the shelf and slope, occupying stations north of Franz Josef Land and in the western part of St. Anna Trough. North of Franz Josef Land similar cold, low salinity intrusions into and below the Atlantic water were observed as at 60°E, showing the persistence of the outflow from the northern Barents Sea. In the St. Anna Trough a colder layer, denser than the outflow from the Victoria Channel, was present. This would then be a part of the main inflow of the Barents Sea branch water to the Arctic Ocean.

In the northern Voronin Trough, some oceanography stations were then occupied in connection with geology work. The main section (Fig. 4.1.4) extended from the Kara Sea shelf west of Severnaya Zemlya at 81°34'N, 86°11'E across the Nansen Basin and the Amundsen Basin and then across the Lomonosov Ridge into the Makarov Basin. It repeated a long section taken by *Polarstern* in 1996 as the section along 34°E was a repeat of the *Polarstern* section taken in 1987 and the section along 60°E towards Franz Josef Land was roughly similar to a *Polarstern* section taken north of Franz Josef Land in 1993. The new section would therefore, in addition to the extended spatial coverage also bring a temporal dimension to the observations.

The scattered stations on the Kara Sea shelf as well as the southernmost stations on the section along 86°E showed cold, low salinity water below a warmer, more saline Atlantic core. The Atlantic water was, however, colder and less saline than that observed at the slope farther to the west, indicating that the northern Kara Sea shelf was dominated by water from the Barents Sea inflow branch. The water was colder and denser than the Barents Sea outflow from the Victoria Channel and also colder and denser than that observed in the western St. Anna Trough. This confirms earlier findings that the Barents Sea branch enters the Arctic Ocean along the eastern flank of the St. Anna Trough and then turns eastward, following the Kara Sea continental slope and also makes a turn into the Voronin Trough west of Severnaya Zemlya.

On the shelf and above the upper continental slope the temperature minimum layer, located at about 50 m depth, was more saline than that found in the interior Nansen Basin, 34.5 as compared to 34.2, indicating different sources for the upper layers in the northern Kara Sea and the interior of the Nansen Basin. The higher salinity of the temperature minimum and the lower temperature in the Atlantic layer below suggest that the upper layer observed here initially has formed through the interaction between sea ice and the cooler Barents Sea branch, while the upper layer in the Nansen Basin is derived from the interaction between sea ice and the Fram Strait inflow branch north of Svalbard.

These two temperature minima were separated from each other by a narrow strip without a temperature minimum, located where the Atlantic water core rose close to

the sea surface (50 m). This situation indicates the possibility of Atlantic water here being entrained into the mixed layer, providing heat to the atmosphere and to ice melt.

The denser part of the Barents Sea branch was present as a wedge above the continental slope, extending down to 1,200 - 1,500 m. Strong intrusions and interleaving between the waters of the Barents Sea branch and the Fram Strait branch were observed in the Atlantic layer as well as in the intermediate water below. The intrusions were seen on the slope at the front between the two branches. Beyond the front a narrow band of Fram Strait branch water contained almost no intrusions. On the other side of this Fram Strait branch the intrusions again increased in prominence. However, the structure of the intrusions on either side of the Fram Strait branch was similar. The largest intrusions were found in the upper part between the temperature maximum and the salinity maximum, where the water column is stably stratified in both components. Below the salinity maximum one or two larger intrusions with several smaller features were observed, and below the salinity minimum, where again both components were stably stratified, several smaller intrusions were encountered. Such intrusions were observed both at the basin side and the shelf side of the Fram Strait branch and coincided with the coldest part of the dense Barents Sea branch inflow. Since the intrusions appear to be created by interaction between the two inflow branches the water column must recirculate somewhere farther to the east and bring the Barents Sea branch water and the intrusions to the offshore side of the Fram Strait branch, forming a narrow recirculation loop.

Beyond the warm ($>3^{\circ}\text{C}$) and saline (>35) Fram Strait branch the core temperature and core salinity decrease to slightly above 2°C and 34.93 respectively and stayed around these values almost up to the Gakkel Ridge. At the Gakkel Ridge a front appeared to be present and the temperature decreased to a little above 1°C and the salinity was reduced to below 34.9. Also the intermediate low salinity layer from the Barents Sea branch decreased in salinity to 34.86 - 34.87. These properties then held from the Gakkel Ridge over the entire Amundsen Basin to the Lomonosov Ridge, where the temperature and salinity again increased. The differences in the return flows in the Nansen and the Amundsen Basins could be explained by a larger prominence of Barents Sea branch water in the Amundsen Basin. Such explanation would not hold for the higher temperatures and salinities encountered on the Amundsen Basin side of the Lomonosov Ridge. One possibility is that different vintages of the inflow branches are observed. The warmer, more saline water at the Lomonosov Ridge would then represent a more recent and warmer Fram Strait inflow than the more sluggish Amundsen Basin circulation carrying colder water that has entered a few years earlier.

Because of the light ice conditions we found the time to make a detour to investigate a small intra-basin in the ridge, where a through-flow of deep water from the Makarov Basin to the Amundsen Basin had been observed by *Oden* in 2005. The intention was to determine if this flow was a permanent feature or if the flow direction of the densest water at the sill could change over time, to study the water mass structure in the intra-basin and to determine the characteristics of the densest water at the sill to the Makarov Basin. It has previously been suggested that to explain the

characteristics of the Makarov Basin bottom water an inflow of Amundsen Basin deep water across the Lomonosov Ridge was necessary, and the sill at the intra-basin could provide a path for such an inflow. In 2005 such a flow was not detected and also now the densest water encountered at the bottom of the sill derived from the Makarov Basin. Therefore any deep flow from the Amundsen Basin to the Makarov Basin must either be very intermittent or perhaps the deep water circulation and exchanges have changed and the flow from Amundsen Basin to the Makarov Basin has been disrupted for a longer period, possibly as a response to warmer conditions in the Arctic. One station in the intra-basin was special. A thin, almost 2° C warm Atlantic layer was overlaying a 1,000 m thick low salinity intermediate layer, resembling an eddy of almost pure Barents Sea branch water. Similar characteristics were not observed elsewhere on the cruise.

The stations at the Makarov Basin side of the Lomonosov Ridge showed low salinity in the intermediate layers, indicating that the denser water of the Barents Sea inflow, was entering the Makarov Basin from the Amundsen Basin through the intra-basin and flowed along the Lomonosov Ridge back towards Siberia. The Atlantic core was cooler, <1° C, on the Makarov side than on the Amundsen Basin side (1.2 - 1.3° C). The water column below the Atlantic layer was characterised by decreasing temperature and increasing salinity with depth, making the water column stable in both properties. This intermediate layer was more saline and warmer in the Makarov Basin than in the Amundsen Basin and the curves in the θ -S diagrams were almost straight with little tendency toward lower temperatures and salinities. Closer to the Alpha Ridge the intermediate water again became cooler and less saline at mid-depth suggesting the presence of a second inflow of less saline Barents Sea branch intermediate water.

As *Polarstern* crossed the Alpha Ridge into the Canada Basin large changes in water mass properties were observed. The temperature maximum of the Atlantic water dropped to 0.5° C and inside the Canada Basin the last station (342) on the section displayed very smooth θ -S characteristics and a temperature maximum of just 0.4° C. This was one of the few stations taken on the cruise where no intrusions were present in the Atlantic water core. This was the common situation in the southern Canada Basin 10 to 15 years ago, and the presence of such a water column in the northern Canada Basin close to the Alpha Ridge indicates that the Atlantic water is circulating around the Canada Basin, some leaking out along the continental slope to the Makarov Basin and partly continuing to the Eurasian Basin and Fram Strait, some re-enter the Canada Basin at the Alpha Ridge.

The intermediate water appeared to follow a similar circulation. The water below the coldest Atlantic water was warmer and more saline than that in the central Makarov Basin, suggesting that it contained not only contributions from the Barents Sea inflow but also from shelf-slope convection and the corresponding entrainment occurring within the Canada Basin.

The long section 3 extending from the Kara Sea to the Canada Basin was finished at 84°30'N, 138°25'W on 7 September, the 1991 North Pole day for *Oden* and *Polarstern*. The upper layers of the section showed the different freshwater contributions to the Arctic Ocean. In the Nansen Basin the low salinity upper layer

was dominated by the seasonal melting. Below this thin melt water layer lies a slightly more saline mixed layer that was formed through ice melting on top of warm Atlantic water north of Svalbard in winter. In the Amundsen Basin a freshwater input from the Siberian shelf seas could be distinguished. This low salinity shelf water is formed through mixing between the river runoff and the Barents Sea inflow branch and is advected into the deep Arctic Ocean basins mainly across the shelf break in the eastern Laptev Sea and western East Siberian Sea. Because it is much less saline, the shelf water flows above the winter mixed layer that is advected in the boundary current from the Nansen Basin. The latter then appears as a halocline between shelf water and the Atlantic layer. Over the Lomonosov Ridge and in the Makarov Basin the input from the shelves was more pronounced, but the vertical structure was similar as in the Amundsen Basin. Closer to the Alpha Ridge and in the Canada Basin different contributions of the Pacific inflow were encountered and the freshwater content in the upper layer increased dramatically, as it became thicker and less saline.

Section 4 (Fig. 4.1.5) extended from the Canada Basin across the Mendeleev Ridge and the Makarov Basin and across the Lomonosov Ridge into the Amundsen Basin. The Pacific water then gradually disappeared and the Makarov Basin was here mostly influenced by the Siberian shelf outflow. This makes sense, having a stronger signal of Pacific water closer to the North American continent, as it moves towards the Canadian Arctic Archipelago and Fram Strait, while the influence of the Siberian shelves remains closer to the Eurasian continent.

The Atlantic water temperature and salinity on section 4 closer to Siberia were similar to those observed on section 3. However, the intermediate water at the Mendeleev Ridge was somewhat colder and less saline than that in the central Makarov Basin suggesting an inflow of Barents Sea branch water that first had crossed the Lomonosov Ridge close to the continental slope and then been injected into the Makarov Basin at the Mendeleev Ridge. This inflow seemed to cross over to the Alpha Ridge providing the less saline, colder intermediate water observed there on section 3 (see above). At the Lomonosov Ridge the salinity and temperature of the intermediate water was even lower and had a similar shape as the intermediate water in the Amundsen Basin. The deep water, however, was warmer and more saline throughout the Makarov Basin up to the Lomonosov Ridge. On this second crossing of the Lomonosov Ridge the difference in temperature between the two cores of Atlantic water was equal to that observed on section 3. This indicates that the water flows in different directions on the two sides of the ridge, towards Greenland on the Amundsen Basin side and towards Siberia on the Makarov Basin side and that little interaction between the two streams takes place across the ridge. By contrast the intermediate water of the Barents Sea branch at the Amundsen Basin side of the ridge appeared to cross the ridge at several locations and return towards Siberia.

Section 5 (Fig. 4.1.6) started at the Gakkel Ridge and led southward onto the Laptev Sea shelf. Little change in properties of the water masses occurred on the first and central part of the section. The water column was characterised by a cooled and diluted Atlantic layer with temperature slightly above 1° C and salinity below 34.9. A depression in the Gakkel Ridge, reaching below 5,000 m was sampled but nothing

spectacular was observed there in the deep and bottom layers. At the continental slope the Atlantic water was above 2° C and more saline, 34.93 - 34.94, but the Atlantic core never reached the high temperatures and salinities observed on sections 1, 2 and 3. The Atlantic core displayed several intrusions and no undisturbed Fram Strait branch Atlantic water mass was seen.

The salinity of the Barents Sea branch intermediate water was at minimum over the central Gakkel Ridge and increased closer to the continental slope as the Atlantic water characteristics became more influenced by the Fram Strait inflow branch. Closer to the slope, where the temperature and salinity of the Atlantic layer again decreased the salinity minimum below the Atlantic core again became stronger, although not as prominent as farther into the basin. Between 1,000 and 2,000 m at the slope a warmer, more saline water mass was encountered. Such water mass was not present on section 3 and does not appear to originate from the Barents Sea branch, at least not without diapycnal mixing with some other water masses. At the deeper part of the slope, close to the bottom the salinity and at stations deeper than 2,500 m also the temperature increased towards the bottom. This could indicate shelf-slope convection with entrainment of intermediate water.

On the upper part of the slope the salinity increased from north to south in the upper layers showing that the Fram Strait branch winter mixed layer was replaced by the winter mixed layer from the Kara Sea associated with the Barents Sea branch. The temperature has increased as compared to section 3 indicating interaction with the underlying Atlantic water, probably due to enhanced mechanical mixing at the continental slope.

On the shallow Laptev Sea the bottom water retained a fairly high salinity, 33 - 34, and at the southernmost station at 46 m water depth, the salinity at the bottom was still close to 33. The upper 10 - 20 m, however, were characterised by low salinity, either due to ice melt or due to river runoff or a combination of both. On all stations except the last the bottom water was cold, below -1.5° C, while the upper low salinity surface layer had temperatures close to or above 0° C. The sampling of the last station, 411, was finished at 3 am on the 24 September at 75°12'N, 121°22'E.

Summary

The extremely light ice conditions allowed for the study of a much larger part of the Arctic Ocean than was initially planned. However, in the ice-covered area the ice melt of about 1.5 m was not extraordinarily large but in the ice-free part a substantially higher melting was observed.

The Barents Sea branch was characterised by a strong salinity minimum in the intermediate layer below the Atlantic water. However, the salinity changed strongly in space suggesting that the inflow was very variable in time and that the salinity of the Barents Sea inflow might have decreased in recent years.

The Atlantic water of the Fram Strait branch became much cooler and fresher between section 3 and section 5, i.e. between the eastern Kara Sea slope and the western Laptev Sea slope. This transformation might partly be due to mixing between the two branches, partly be due to a recirculation of the branches in the Nansen

Basin. This is consistent with the intrusions and interleaving seen in the colder, less saline Atlantic layer offshore of the Fram Strait branch on sections 1, 2 and 3.

The salinity of the winter mixed layer in the Nansen Basin was low, 34.1 - 34.2 as compared with the more commonly encountered 34.3-34.4. This could be due to the fact that the Atlantic water that entered through Fram Strait has become warmer in recent years. By contrast the Barents Sea and the Kara Sea winter mixed layer had salinities around or above 34.5.

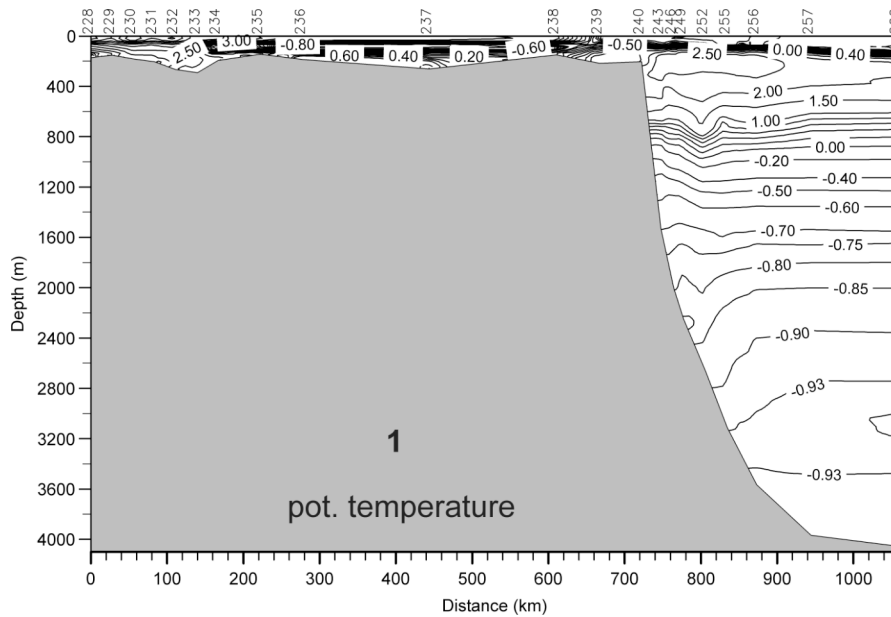


Fig. 4.1.2a: Distribution of potential temperature (degC) along section 1 (see Fig. 4.1.1 for location)

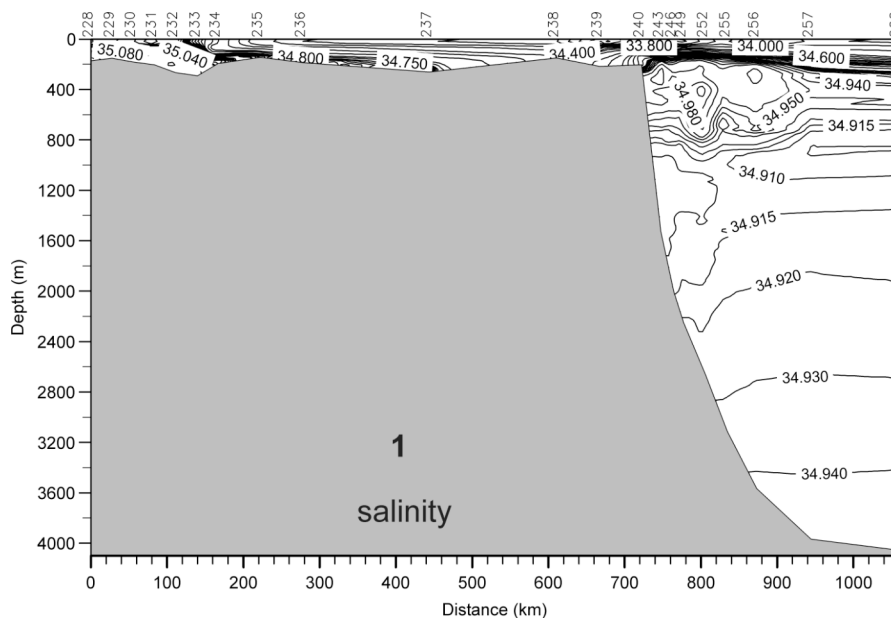


Fig. 4.1.2b: Distribution of salinity (psu) along section 1 (see Fig. 4.1.1 for location)

4.1 Physical oceanography

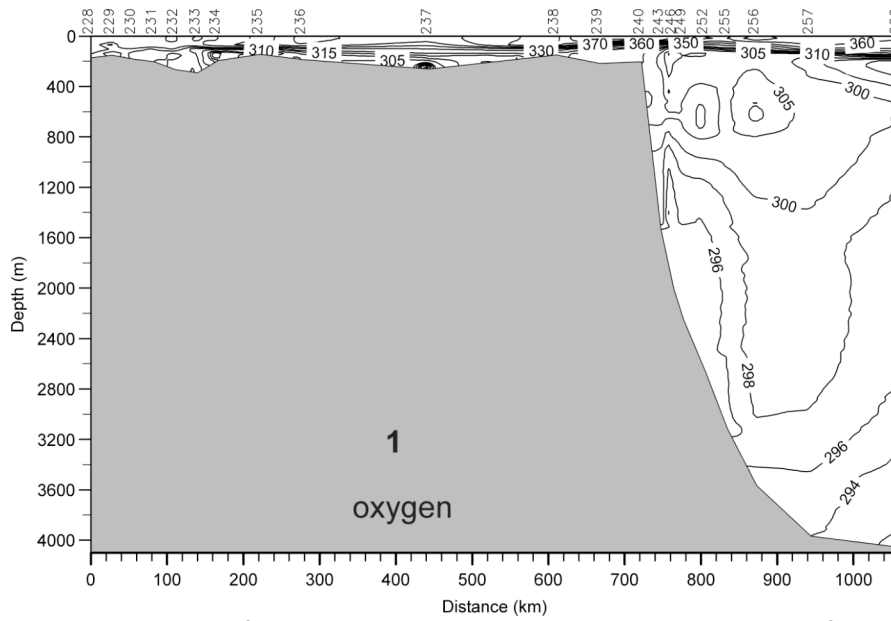


Fig. 4.1.2c: Distribution of oxygen ($\mu\text{mol/kg}$) along section 1 (see Fig. 4.1.1 for location)

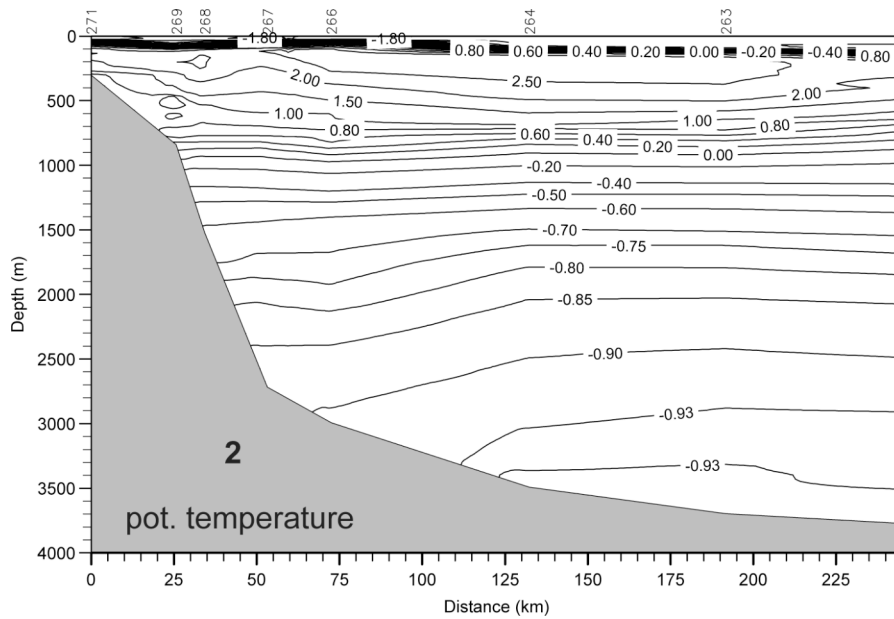


Fig. 4.1.3a: Distribution of potential temperature (degC) along section 2 (see Fig. 4.1.1 for location)

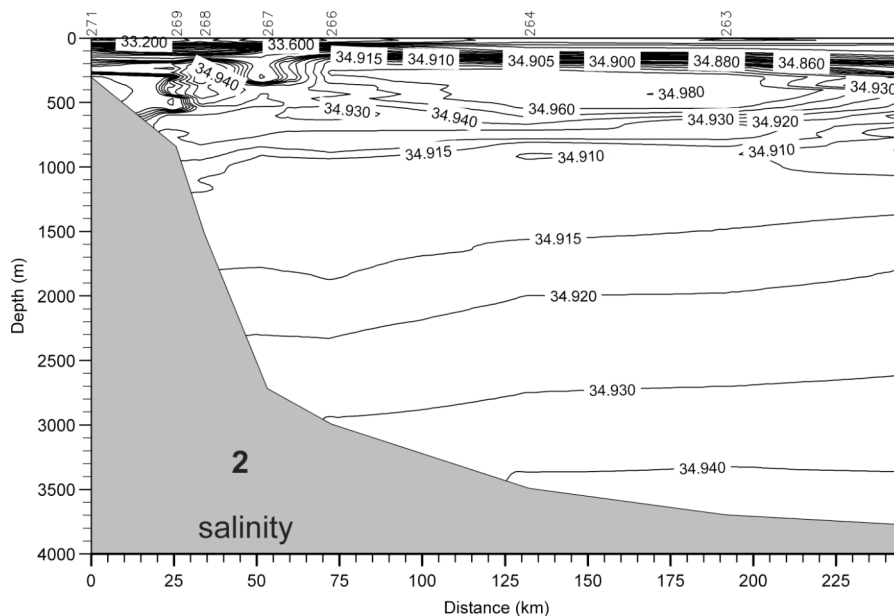


Fig. 4.1.3b: Distribution of salinity (psu) along section 2 (see Fig. 4.1.1 for location)

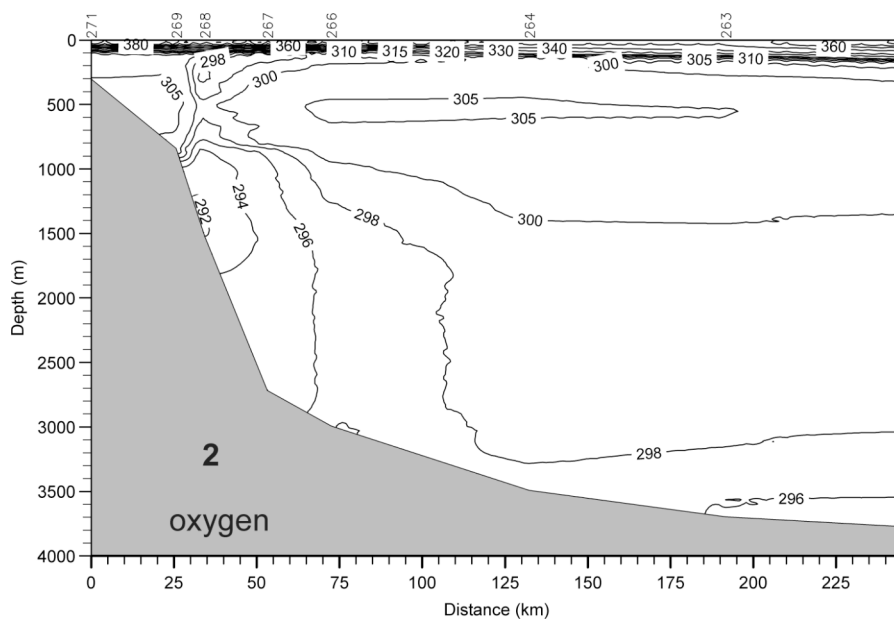


Fig. 4.1.3c: Distribution of oxygen ($\mu\text{mol/kg}$) along section 2 (see Fig. 4.1.1 for location)

4.1 Physical oceanography

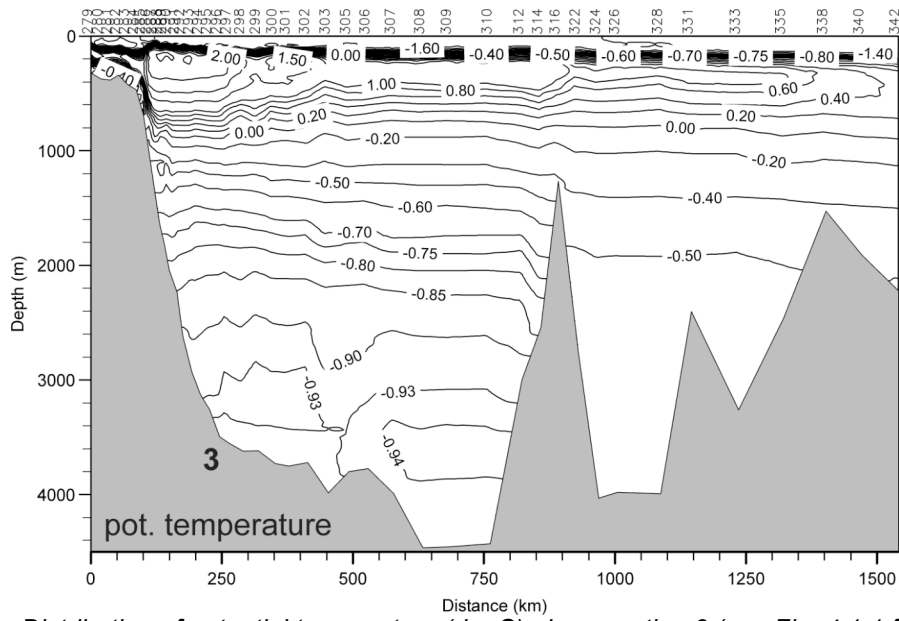


Fig. 4.1.4a: Distribution of potential temperature (degC) along section 3 (see Fig. 4.1.1 for location)

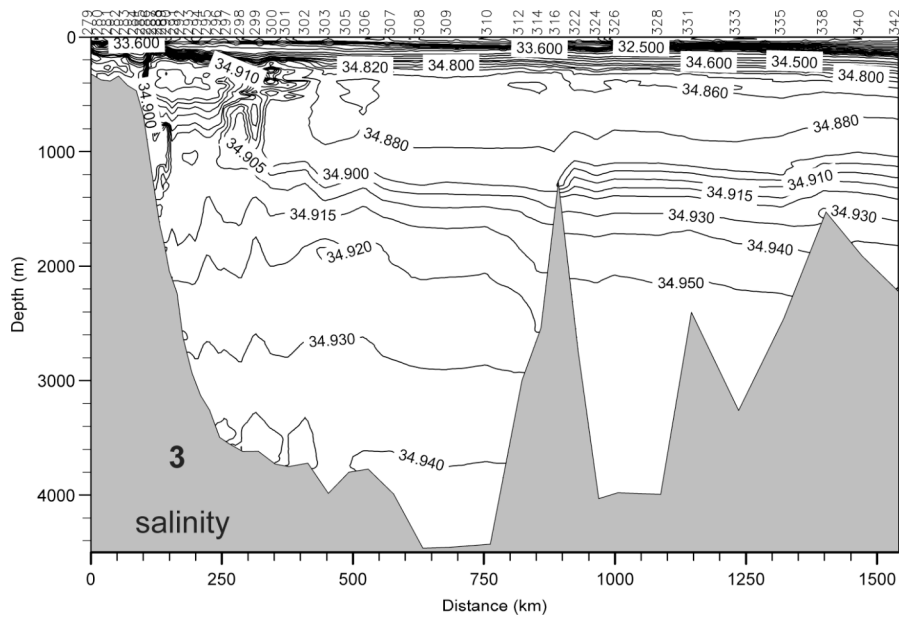


Fig. 4.1.4b: : Distribution of salinity (psu) along section 3 (see Fig. 4.1.1 for location)

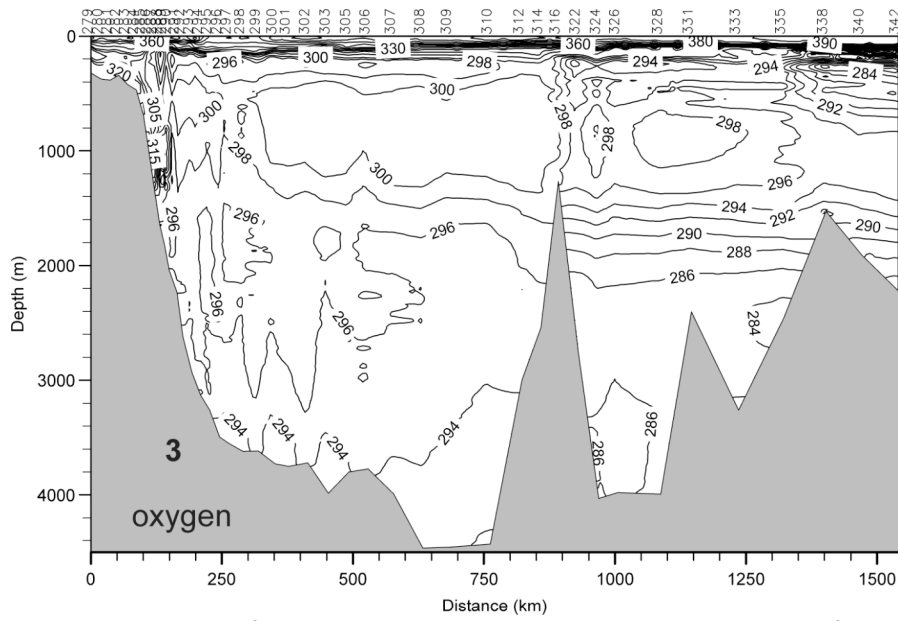


Fig. 4.1.4c: : Distribution of oxygen ($\mu\text{mol/kg}$) along section 3 (see Fig. 4.1.1 for location)

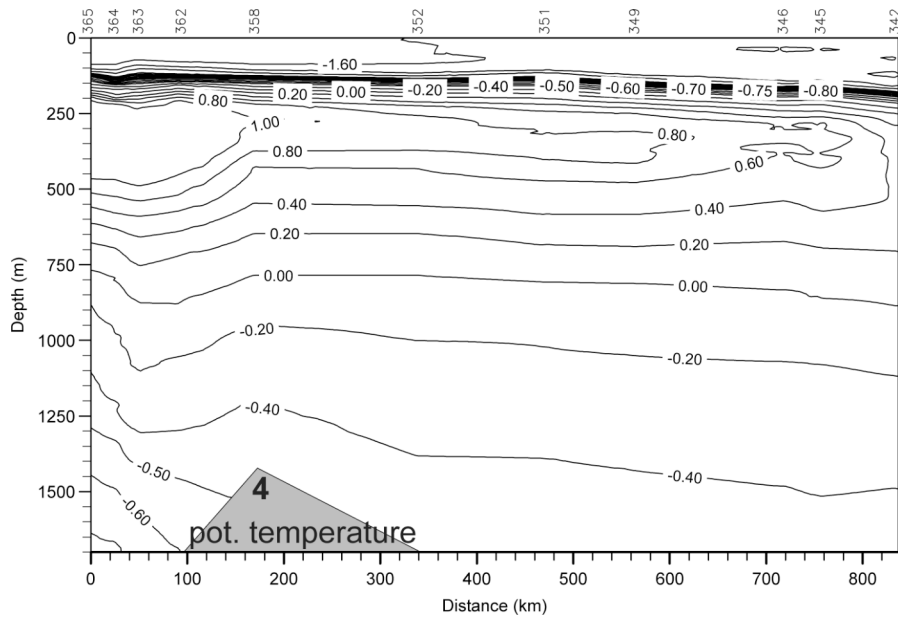


Fig. 4.1.5a: : Distribution of potential temperature (degC) along section 4 (see Fig. 4.1.1 for location)

4.1 Physical oceanography

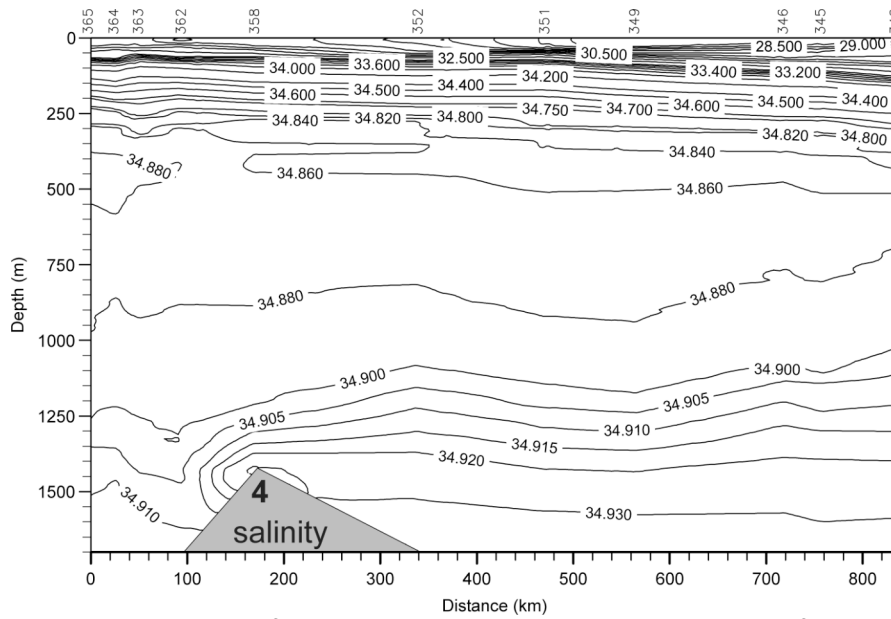


Fig. 4.1.5b: Distribution of salinity (psu) along section 4 (see Fig. 4.1.1 for location)

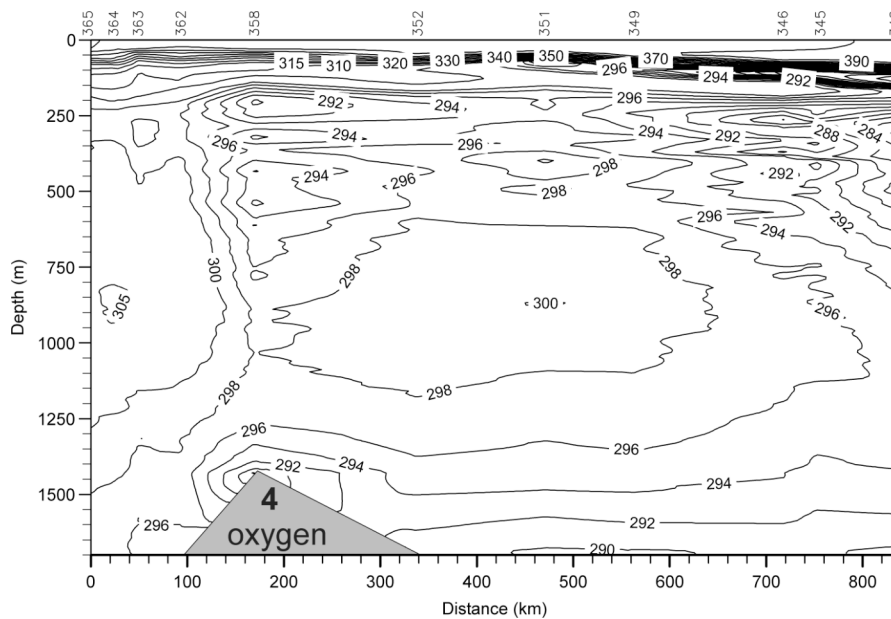


Fig. 4.1.5c: Distribution of oxygen ($\mu\text{mol/kg}$) along section 4 (see Fig. 4.1.1 for location)

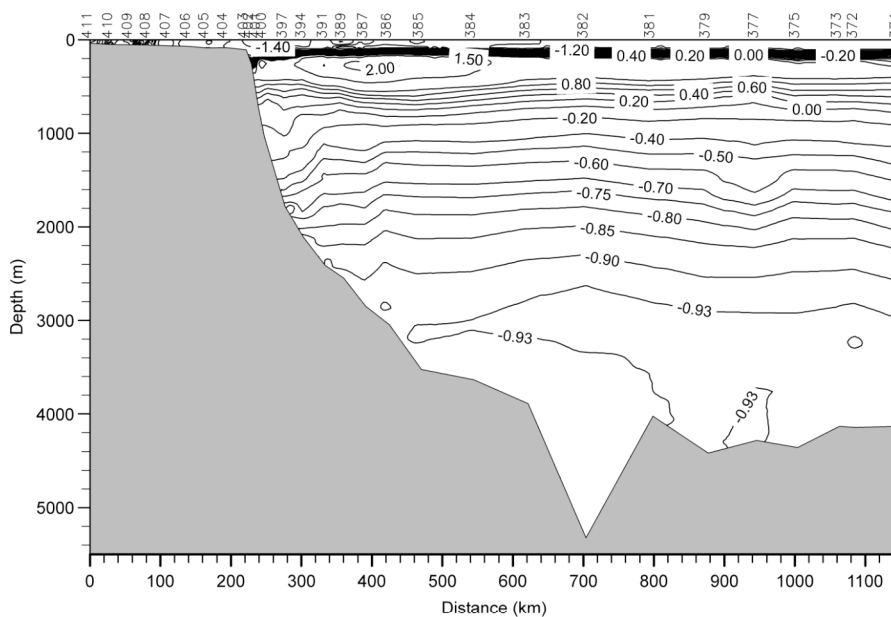


Fig. 4.1.6a: : Distribution of potential temperature (degC) along section 5 (see Fig. 4.1.1 for location)

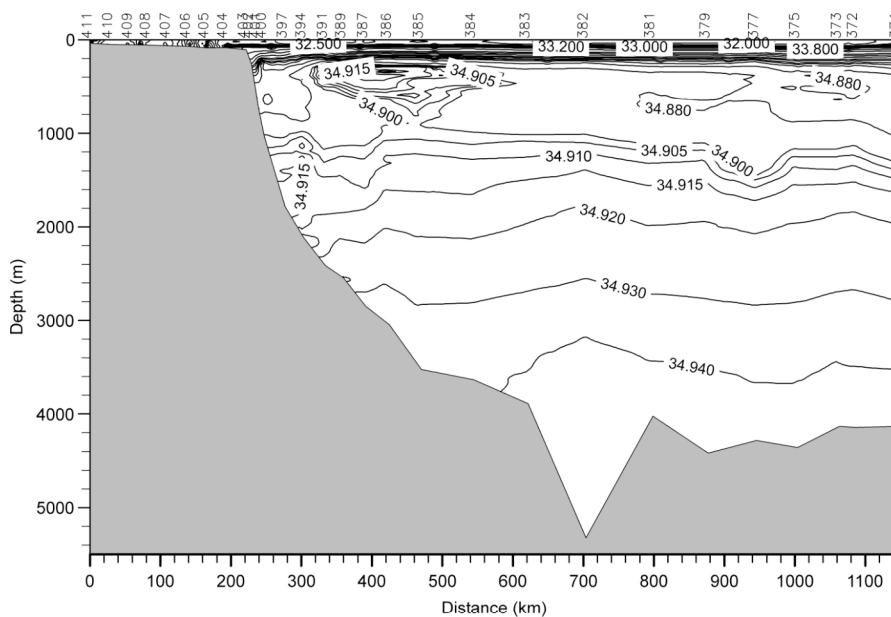


Fig. 4.1.6b: : Distribution of salinity (psu) along section 5 (see Fig. 4.1.1 for location)

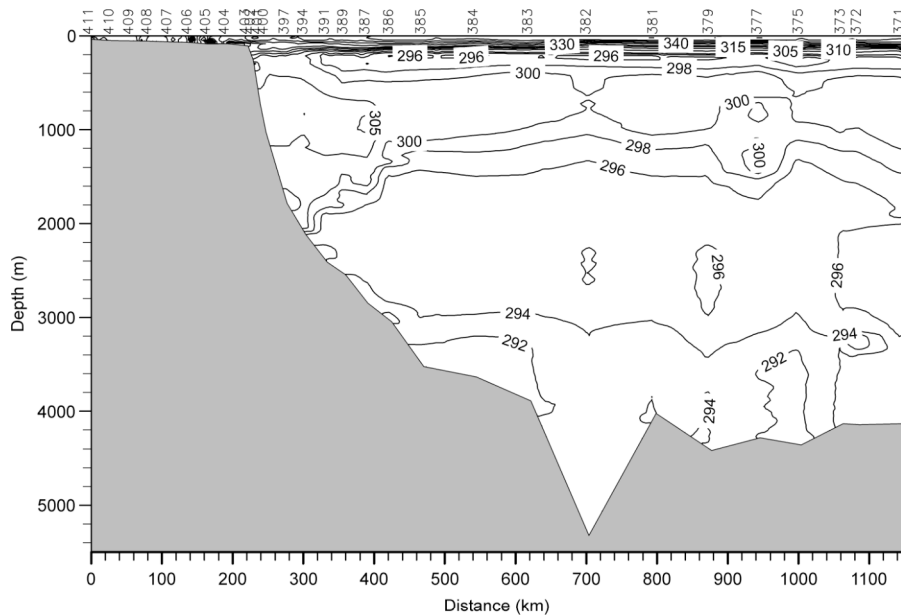


Fig. 4.1.6c: : Distribution of oxygen ($\mu\text{mol/kg}$) along section 5 (see Fig. 4.1.1 for location)

4.2 XCTD observation

Takashi Kikuchi

Japan Agency for Marine-Earth Science and Technology

Background

Boundary currents along the continental slope and the ridges of the Arctic Ocean carry the changing signals advected from the Atlantic and they form part of the origins of the North Atlantic Deep Water. They are very narrow and therefore need hydrographic observations with high resolution which - in accordance with an economic use of ship time - can be achieved with expendable CTDs.

The eXpendable Conductivity, Temperature, and Depth data acquisition and processing equipment (XCTD) can measure temperature and conductivity (i.e., salinity) from sea surface to 1,100 m depth in only five minutes. The XCTD system is manufactured by The Tsurumi-Seiki Co., LTD, Japan. It mainly consists of XCTD probe, launcher, digital converter and personal computer for data processing. The XCTD probe can be launched from the ship or on the ice into water and sinks down with constant velocity measuring temperature and conductivity. Accuracy of XCTD temperature should be better than 0.01°C . However, please note that XCTD salinity has large error rates of more than 0.03 before calibration. By using closest or interpolated CTD data the XCTD salinity data should be calibrated if possible.

XCTD operation has some advantages compared with CTD observation although the accuracies in temperature and salinity is not better than CTD observation. One is that

we can save ship time for the observation. XCTD observation down to 1,100 meter takes only 5 minutes. Another big advantage is that it is portable. The XCTD system with battery pack is less than 10 kg in weight. This allowed us to operate from helicopter. Hence, we used XCTDs between CTD stations to increase the spatial resolution and we extended some of the CTD sections by a line of helicopter-borne XCTDs.

Work at sea

89 XCTD casts at 84 stations were collected during this cruise (Table 4.2.1). Some XCTD stopped data sampling before reaching the bottom or full measurement depth (1,100 m) due to sea ice, software trouble, and so on. 24 of 89 XCTDs were conducted by helicopter operation (Fig. 4.2.1), and others were launched from the ship (Fig. 4.2.2). Figure 4.2.3 shows map of the XCTD observation sites during this cruise as well as CTD observation sites. The map shows that we did XCTD observations mainly focused on across the European continental slope regions and major ridges of the Arctic Ocean with high resolution of 5~10 nm in space. Helicopter XCTD operations were conducted along 65°E across the Eurasian continental slope on 16 and 17 August, 85.7N over the Alpha Ridge on 5 September, and 140W toward the Canadian Basin on 7 September.

After the observation, salinity calibrations of each XCTD data were carried out by using closest or spatially-interpolated CTD data. I used the closest or interpolated CTD data to check salinity values at the Atlantic water depth and at 1,000 meter depth. As results, the calibrated XCTD salinity data had conservative accuracies better than 0.01 psu. Figure 4.2.4 shows temperature-salinity diagram and temperature profiles of all of calibrated XCTD data which was submitted as the final version.

Preliminary results

Figure 4.2.5 shows some results of XCTD observations over Alpha Ridge and in the Canadian Basin (XCTD no. 46~62). The XCTDs were conducted by helicopter operation as extension lines of the section 3. Pacific water (PW) which is defined as temperature maximum around 32.7~33.0 psu in salinity can be found especially in the northern Canadian Basin. We can see the same signal over the Alpha Ridge but weak. In the Makarov Basin such PW signal are much smaller or not found. On the other hand, the lowest Atlantic water temperature observed during this cruise was found here (~0.38° C).

Tab. 4.2.1: Summary of XCTD data sampling date and location

Sta. No.	XCTD No.	Date	Time	Latitude			Longitude				Bottom Depth	Measurement depth
PS70/240	1	2007/8/1	21:00	81	30	44.1	33	59	89.7	E	192	192
PS70/241	2	2007/8/1	22:02	81	34	58.6	34	0	4.9	E	230	230
PS70/242	3	2007/8/1	23:09	81	39	58.9	34	0	14.1	E	713	349
	4	2007/8/1	23:22	81	40	6.1	34	0	27.4	E	713	713
PS70/244	5	2007/8/2	6:18	81	44	54.7	33	59	33.3	E	1650	1100

4.2 XCTD observation

Sta. No.	XCTD No.	Date	Time	Latitude			Longitude				Bottom Depth	Measurement depth
PS70/245	6	2007/8/2	7:30	81	49	52.9	34	0	13.6	E	2000	1100
PS70/247	7	2007/8/2	12:03	81	55	18.4	33	59	0.0	E	2100	1100
PS70/249	8	2007/8/2	23:48	81	59	56.1	33	58	13.2	E	2240	1100
PS70/250	9	2007/8/3	6:38	82	4	56.8	34	0	22.2	E	2300	1100
PS70/251	10	2007/8/3	7:48	82	9	55.8	33	59	51.8	E	2530	1100
PS70/252	11	2007/8/3	12:20	82	15	18.0	34	1	38.2	E	2687	1100
PS70/253	12	2007/8/3	16:28	82	19	54.9	34	0	21.4	E	2800	1100
PS70/254	13	2007/8/3	18:10	82	25	2.0	34	2	28.1	E	3052	1100
PS70/255	14	2007/8/4	4:17	82	31	0.5	33	53	50.2	E	3083	1100
PS70/266	15	2007/8/14	8:36	83	6	46.6	61	41	42.8	E	2769	1100
PS70/268	16	2007/8/14	22:30	82	48	43.0	60	51	13.5	E	1668	1100
by Heli.	17	2007/8/16	18:02	82	40	23.3	65	38	1.6	E	1426	1100
by Heli.	18	2007/8/16	18:21	82	50	19.4	65	35	23.7	E	2024	1100
by Heli.	19	2007/8/16	18:39	83	0	6.0	65	29	10.2	E	2415	1100
by Heli.	20	2007/8/16	18:57	83	10	29.3	65	22	48.9	E	2656	1100
by Heli.	21	2007/8/16	19:17	83	20	6.1	65	16	35.4	E	2889	1100
by Heli.	22	2007/8/17	12:30	81	59	53.7	65	58	19.1	E	538	538
by Heli.	23	2007/8/17	12:56	82	9	55.7	65	55	37.1	E	560	560
by Heli.	24	2007/8/17	13:11	82	19	44.4	65	49	42.6	E	691	691
by Heli.	25	2007/8/17	13:29	82	30	13.3	65	45	34.7	E	1102	1100
PS70/304	26	2007/8/25	21:23	85	18	31.9	90	14	45.1	E	3655	1100
PS70/309	27	2007/8/28	12:25	87	4	10.3	104	37	51.0	E	4269	1100
PS70/311	28	2007/8/29	6:23	87	49	21.7	113	12	56.0	E	4339	588
	29	2007/8/29	6:33	87	49	21.7	113	12	56.0	E	4339	1100
PS70/312	30	2007/8/29	20:55	88	10	13.0	119	46	3.3	E	3442	1100
PS70/313	31	2007/8/29	22:45	88	9	9.8	124	49	21.5	E	2892	1100
PS70/315	32	2007/8/30	7:25	88	11	3.0	135	1	14.7	E	1325	628
PS70/316	33	2007/8/30	10:38	88	11	6.6	139	33	35.8	E	1257	1100
PS70/323	34	2007/9/1	2:28	88	6	2.3	154	39	7.3	E	3496	484
	35	2007/9/1	2:33	88	5	59.3	154	41	54.2	E	3496	1100
PS70/325	36	2007/9/1	16:22	88	2	54.4	165	6	49.5	E	3901	1100
PS70/326	37	2007/9/1	21:29	88	2	16.3	169	59	0.5	E	3851	1100
PS70/327	38	2007/9/2	5:45	87	57	7.2	179	59	1.2	E	3484	1100
by Heli.	39	2007/9/2	16:25	86	19	47.5	178	57	47.2	W	3813	1100
PS70/329	40	2007/9/3	13:15	87	44	36.6	162	37	58.4	W	2898	1100
PS70/332	41	2007/9/4	2:05	87	18	37.4	150	8	52.0	W	3081	1100
PS70/334	42	2007/9/4	22:46	86	42	21.1	142	23	14.1	W	2786	227
	43	2007/9/4	22:55	86	42	19.6	142	22	43.1	W	2786	1100
PS70/336	44	2007/9/5	9:04	86	8	22.5	137	29	44.1	W	2172	1100
PS70/337	45	2007/9/5	12:08	85	56	33.5	136	22	16.2	W	1933	1100
by Heli.	46	2007/9/5	13:19	85	42	47.9	132	26	42.5	W	1486	1100
by Heli.	47	2007/9/5	13:38	85	41	29.5	129	57	39.0	W	1414	1100
by Heli.	48	2007/9/5	13:56	85	42	0.0	127	30	11.2	W	1356	1100

Sta. No.	XCTD No.	Date	Time	Latitude			Longitude				Bottom Depth	Measurement depth
by Heli.	49	2007/9/5	14:18	85	42	28.0	125	5	49.1	W	1624	1100
by Heli.	50	2007/9/5	14:39	85	42	13.0	122	35	9.5	W	1401	1100
by Heli.	51	2007/9/5	14:57	85	41	46.0	120	2	34.8	W	1209	1100
by Heli.	52	2007/9/5	15:17	85	41	52.4	117	35	10.6	W	1642	1100
PS70/339	53	2007/9/6	13:37	85	23	19.5	136	17	2.1	W	1858	121
	54	2007/9/6	13:41	85	23	19.5	136	17	2.1	W	1858	563
PS70/341	55	2007/9/7	0:03	84	47	0.1	137	59	14.1	W	1881	1100
by Heli.	56	2007/9/7	13:24	84	17	39.1	139	59	42.0	W	2268	1100
by Heli.	57	2007/9/7	13:45	84	4	57.0	139	55	46.1	W	2375	1100
by Heli.	58	2007/9/7	14:06	83	52	29.8	140	1	6.2	W	2414	1100
by Heli.	59	2007/9/7	14:25	83	40	53.2	139	59	51.8	W	2587	1100
by Heli.	60	2007/9/7	14:46	83	27	41.8	139	59	8.4	W	2779	1100
by Heli.	61	2007/9/7	15:09	83	15	5.5	139	59	24.6	W	2907	1100
by Heli.	62	2007/9/7	15:40	83	3	19.9	139	57	6.1	W	2996	1100
PS70/344	63	2007/9/8	2:16	84	36	36.9	141	40	53.7	W	1991	917
PS70/347	64	2007/9/8	20:35	84	52	32.6	154	8	33.8	W	2216	1100
PS70/348	65	2007/9/9	0:39	84	58	44.4	158	42	12.6	W	1997	1100
PS70/350	66	2007/9/9	15:40	85	22	26.3	167	12	6.7	W	1900	1100
PS70/353	67	2007/9/11	15:06	86	35	43.9	162	12	47.7	E	3848	1100
PS70/354	68	2007/9/11	17:19	86	33	51.2	159	43	5.5	E	3758	1100
PS70/355	69	2007/9/11	19:10	86	31	39.6	157	17	5.8	E	2762	1100
PS70/356	70	2007/9/11	20:28	86	31	18.2	155	30	1.4	E	1622	833
PS70/357	71	2007/9/11	21:38	86	30	45.0	153	44	55.1	E	1288	1100
PS70/359	72	2007/9/12	9:09	86	28	15.8	149	17	44.7	E	1184	1100
PS70/360	73	2007/9/12	10:55	86	26	18.6	146	47	47.8	E	1101	1100
PS70/361	74	2007/9/12	12:43	86	25	36.2	144	4	25.0	E	871	871
PS70/366	75	2007/9/15	9:50	86	3	31.5	119	18	28.0	E	4245	1100
PS70/367	76	2007/9/15	17:10	85	39	50.0	112	21	32.1	E	4060	1100
PS70/368	77	2007/9/16	1:09	85	10	59.0	106	59	36.8	E	3953	1100
PS70/369	78	2007/9/16	3:36	85	0	59.0	105	26	5.7	E	3985	1100
PS70/370	79	2007/9/16	8:15	84	50	36.3	103	59	30.9	E	3901	772
PS70/387	80	2007/9/21	5:21	78	38	13.1	124	35	51.2	E	2731	871
PS70/388	81	2007/9/21	6:19	78	29	58.0	124	35	31.4	E	2570	1100
PS70/390	82	2007/9/21	15:15	78	14	19.1	124	22	31.8	E	2339	1100
PS70/392	83	2007/9/21	18:28	78	1	46.8	124	6	52.3	E	2143	517
PS70/393	84	2007/9/21	19:08	77	56	36.3	124	1	37.0	E	2079	1100
PS70/395	85	2007/9/21	21:46	77	46	30.1	123	47	51.6	E	1871	1100
PS70/396	86	2007/9/21	22:10	77	42	35.0	123	42	21.1	E	1801	1100
PS70/398	87	2007/9/22	4:53	77	33	17.2	123	34	52.2	E	1516	1100
PS70/399	88	2007/9/22	5:28	77	28	48.3	123	29	36.8	E	1335	1100
PS70/400	89	2007/9/22	12:19	77	22	14.6	123	25	13.7	E	1034	1034



Fig. 4.2.1: XCTD observation on the ice by helicopter operation at XCTD no. 18 on August 17



Fig. 4.2.2: XCTD observation from the Polarstern at PS70/268 (XCTD no. 16) on August 14

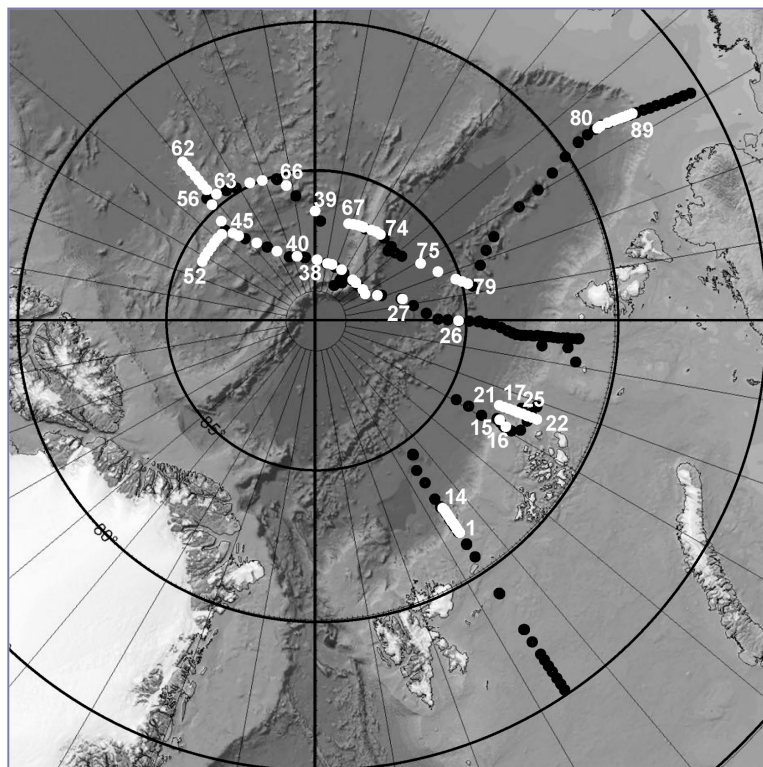


Fig. 4.2.3: Map of XCTD observation site (white) with CTD location (black) on the IBCAO chart

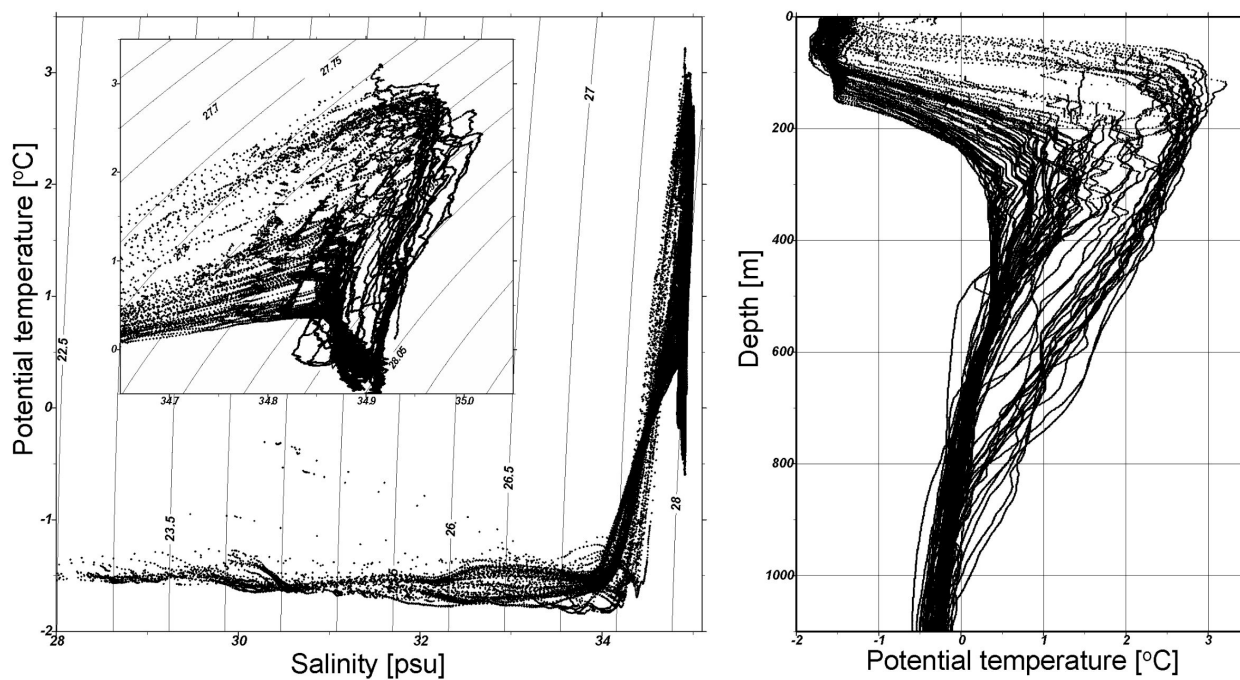


Fig. 4.2.4: (Left) Potential temperature-salinity diagram and (Right) potential temperature profiles of all 89 XCTD data

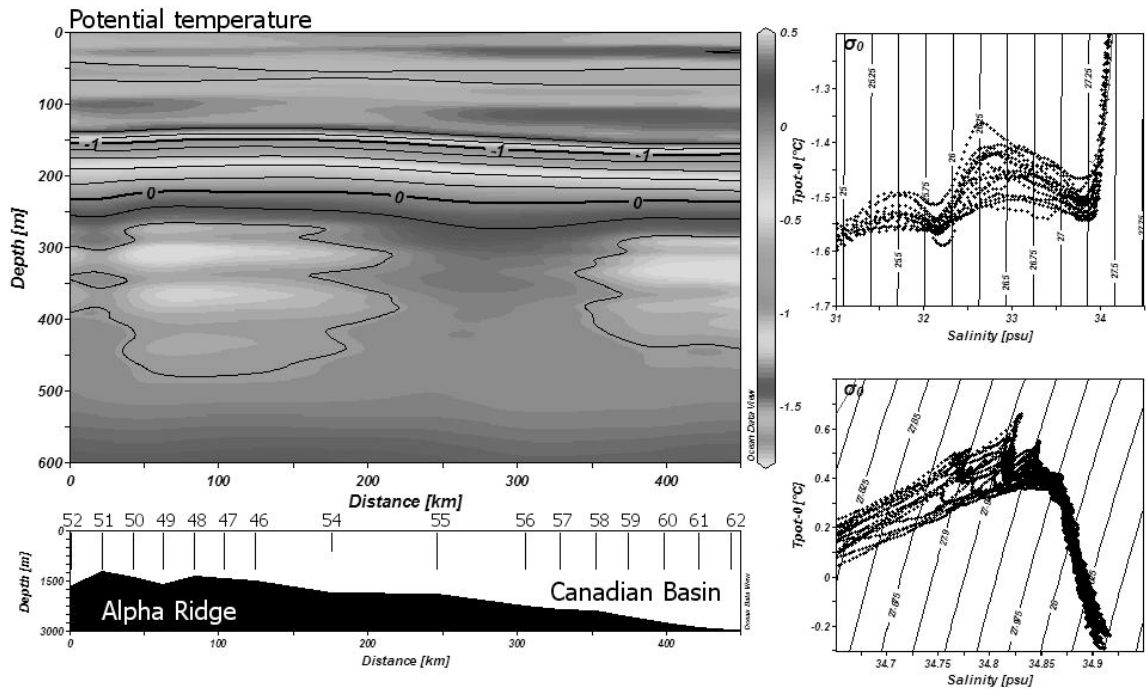


Fig. 4.2.5: Results of XCTD no. 46 to 62 which were conducted by helicopter operation. (Left, top) Potential temperature section. (Left, bottom) Bottom topography over the XCTD station. (Right, top) Potential temperature-salinity diagram between 31 and 34.5 psu in salinity range. (Right, bottom) Potential temperature-salinity diagram between 34.65 and 34.95 psu in salinity range.

4.3 Deployment of ice-tethered buoys

Takashi Kikuchi²⁾, Sebastian Mechler³⁾, Sergey Pisarev⁴⁾, Benjamin Rabe¹⁾

¹⁾Alfred-Wegener-Institut

²⁾Japan Agency for Marine Earth Science and Technology

³⁾Optimare

⁴⁾P.P. Shirshov Institute of Oceanology

In order to obtain year-round measurements of temperature, salinity, velocity and under-ice turbulence, ice-tethered platforms (ITPs) with various instrumentation were deployed. They consist of a sub-ice sensor system that is connected by a cable to a surface unit that transmits the data to shore via satellite. Since they drift with the host ice floe they have the potential to provide observations over a substantial region of the Arctic Ocean.

- 3 ITPs (Ice-Tethered Profilers) equipped with Seabird CTDs that will sample temperature and salinity profiles once per day between the surface and 800 m water depth,
- 1 ITAC (Ice-tethered Acoustic Current profiler) consisting of a RDI ADCP (75 kHz, Long Ranger) that measures the velocity profile of the upper 500 m once per day,
- 1 OFB (Ocean Flux Buoy, from Tim Stanton, Naval Postgraduate School) that measures turbulent fluxes of heat and salt immediately below the ice.

These platforms contribute to the “International Arctic Ocean Observation System” (iAOOS) that aims at a persistent observation network.

In total, seven different types of ice buoy systems were deployed. Here we report on the ocean measurement systems and refer to chapter 3 for ice-related measurements.

Three Ice Tethered Profilers (ITP) measure thrice daily temperature/salinity/depth profiles with 1 m vertical resolution between 8 and 760 m using a profiling CTD unit (Seabird Electronics, Inc. model 41CP) on a wire tether and an inductive modem to communicate the data to a surface unit (SU). The ITP SU records GPS position and relays all data via an Iridium satellite modem connection to a server at Woods Hole Oceanographic Institution (WHOI) in Woods Hole (Massachusetts, USA). The ITPs are manufactured by WHOI with a profiler from McLane Research Laboratories (Falmouth, Massachusetts, USA).

A system similar to the ITP, a Polar Ocean Profiling System (POPS) manufactured by MetOcean Data Systems (Dartmouth, Nova Scotia, Canada) financed by the Japan Agency for Marine-Earth Science and Technology (JAMSTEC, Tokyo, Japan) was deployed, but unfortunately had to be recovered after on-site tests failed.

One Arctic Ocean Flux Buoy (AOFB) from Tim Stanton at the Naval Postgraduate School in Monterey (California, USA), equipped with one set of temperature, salinity and depth sensors and an FSI current meter, measures small scale fluctuations in the surface layer a few meters below the ice. In addition, a RDI 300 kHz Acoustic Doppler Current Profiler measures velocity profiles of the top 80 m of the water column. Similar to the ITP, an SU relays the information to the Naval Postgraduate School via Iridium. A wind generator provides additional power to extend the operating life of the buoy beyond the capacity of the buoy batteries.

The prototype of a buoy newly developed by Optimare Sensorsysteme AG (Bremerhaven, Germany) in collaboration with the Alfred Wegener Institute in Bremerhaven (Germany) was deployed for the first time: An Ice Tethered Acoustic Current profiler (ITAC), measuring ocean current velocity profiles from 2 m under the ice to a depth of around 500 m, incorporates an ADCP mounted (initially) 50 cm under the ice floe. The ADCP is rigidly connected via a stainless steel pole with a wooden beam on the surface. A cable provides the electrical connection to a SU with a GPS receiver and an Iridium modem. To allow the recording of the ADCP orientation even in regions of low horizontal magnetic field strength, a 2nd GPS is positioned about 98 m away in line with the wooden beam and the ITAC SU. Data are relayed daily via the Iridium Short Burst Data (SBD) message service to an e-mail address at Optimare; all ITAC SU data, which also include temperature and horizontal tilt measurements, are also relayed via the ARGOS system once a week. The communication is bi-directional and also allows setting of data sampling parameters via SBD messages, both for the ADCP and the ITAC SU (e.g. GPS sampling rate).

4.3 Deployment of ice-tethered buoys

The buoys were deployed in different combinations along the cruise track (Fig. 4.3.1). The weak and thin sea ice cover posed a severe challenge to find suitable ice floes. Generally, if an appropriate floe could not be easily found from the bridge of *Polarstern*, one or more survey flights were conducted by helicopter, landing on potentially usable floes and drilling a few holes with a 2' electrically powered ice auger to test ice thickness. Once a floe was identified, an initial survey of the ice thickness was carried out by the sea ice physics group to provide guidance in finding a suitable deployment site. The survey was performed with the EM31 canoe in conjunction with 2' drilling and visual observation of ice surface features, such as melt-ponds and ridges. For the deployments, ice holes were drilled, and the system was lowered using tripods with chain hoists. Since the ITAC required a hole of 60 cm the mechanical drilling required considerable effort and time. For future deployments, a hot-water system, similar to that employed by WHOI, should be used. Maps of three different buoy deployment sites, where ITPs were deployed, show the distribution of sea ice thickness in relation to the buoy locations (Fig. 4.3.2). In particular the large 'Super Station' presented a compromise between availability of suitable ice floes as well as sufficiently thick but uniform areas and the large number of buoys that needed to be deployed with certain minimum spacing. The required thickness of around 2 to 2.5 m and expected long-term stability of the ice could only be found in areas close to some old ridge systems as the remainder of the floe was largely covered by refrozen melt-ponds.

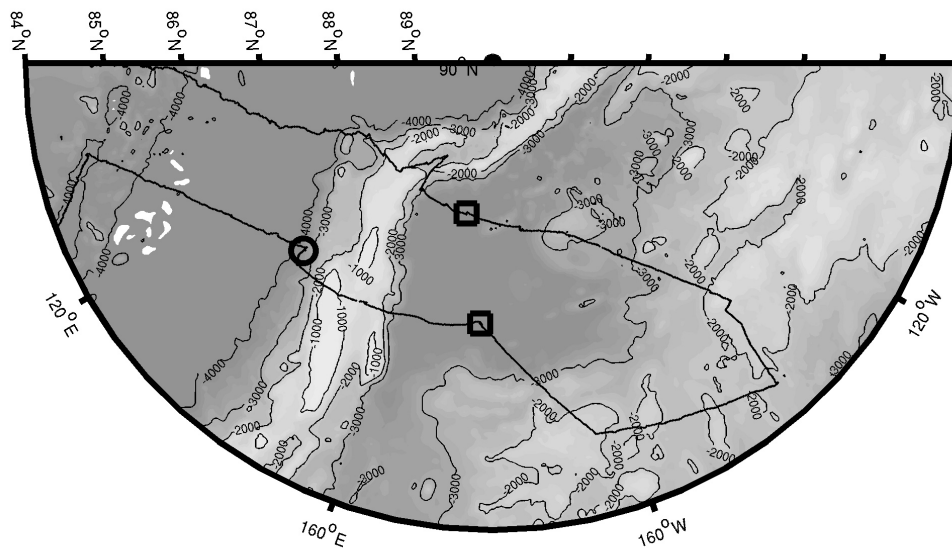
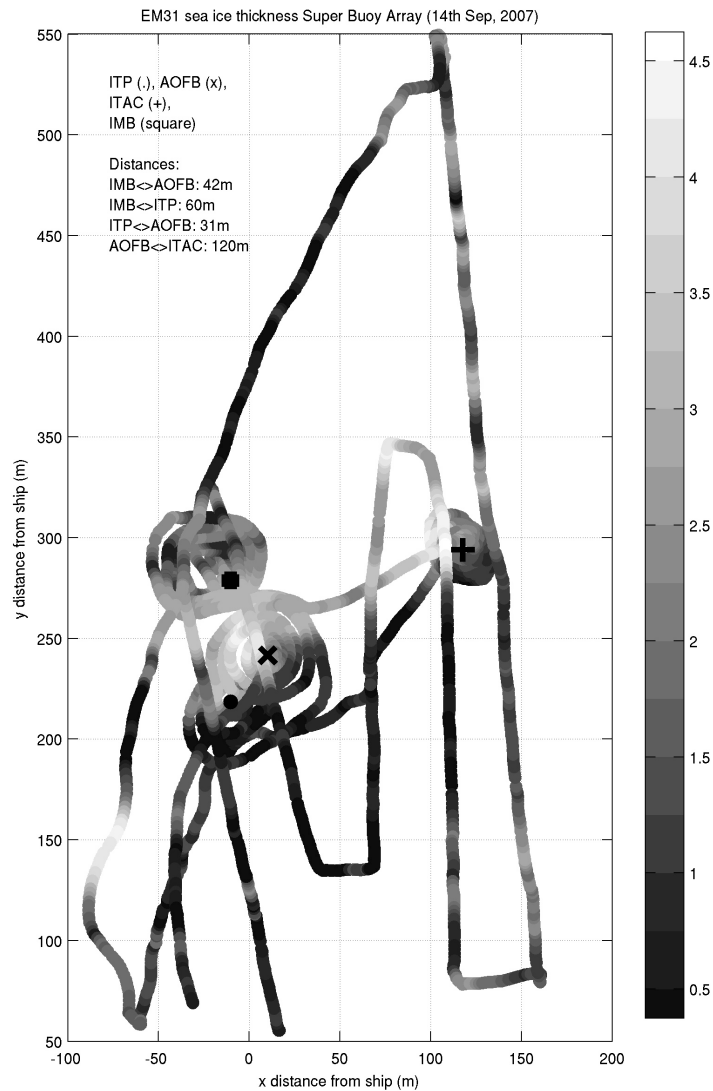


Fig. 4.3.1: Cruise track with ocean ice-buoy deployment locations: The squares represent ITP#16 and ITP#15, each deployed with a surface meteorological buoy; the circle marks the 'Super Buoy Station', including ITP#12, ITAC, AOFB and an Ice-Mass-balance Buoy (IMB) and a webcam. Contours represent ocean bottom topography from the IBCAO dataset (in m).

Fig. 4.3.2: Ice-floe survey map of 'Super Station' with buoy locations. Shades represent EM31 sea ice thickness in m (courtesy of the AWI Sea ice Physics group).



Due to the real-time transmission and processing of the buoy data we can present first results of the some of the deployed systems. The ITP#12 surveyed, as part of the 'Super Buoy Station', around the Lomonosov Ridge between 86° 40' to 87° 24' N (see Fig. 4.3.3), on the edge between the Amundsen and Makarov Basins. The temperature section against time (Fig. 4.3.4) shows occasional drops in the maximum in the Atlantic water layer, around 300 dbar. This is representative of the margin between the two basins and is in agreement with previous findings that the Atlantic water layer is generally colder in the Makarov Basin than in the Amundsen Basin, e.g. during the Oden 91 expedition (Anderson et al., 1994). These intrusions are also evident around 300 dbar in both the salinity profiles (Fig. 4.3.5) and the temperature profiles (Fig. 4.3.6).

References

Anderson, L.G., Björk, G., Holby, O., Jones, E.P., Kattner, G., Koltermann, K.-P., Liljeblad, B., Lindegren, R., Rudels, B. and Swift, J.H. 1994. Water masses and circulation in the Eurasian Basin: Results from the Oden 91 Expedition, J. Geophys. Res., 99, p. 3273-3283.

4.3 Deployment of ice-tethered buoys

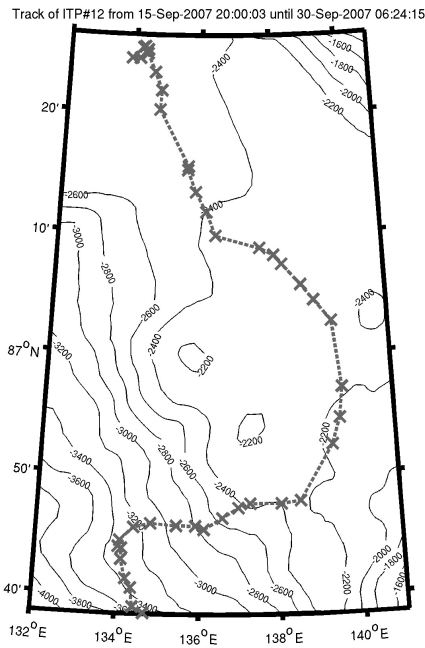


Fig. 4.3.3: Drift track of ITP#12 ('Super Station' ice floe) during September 2007

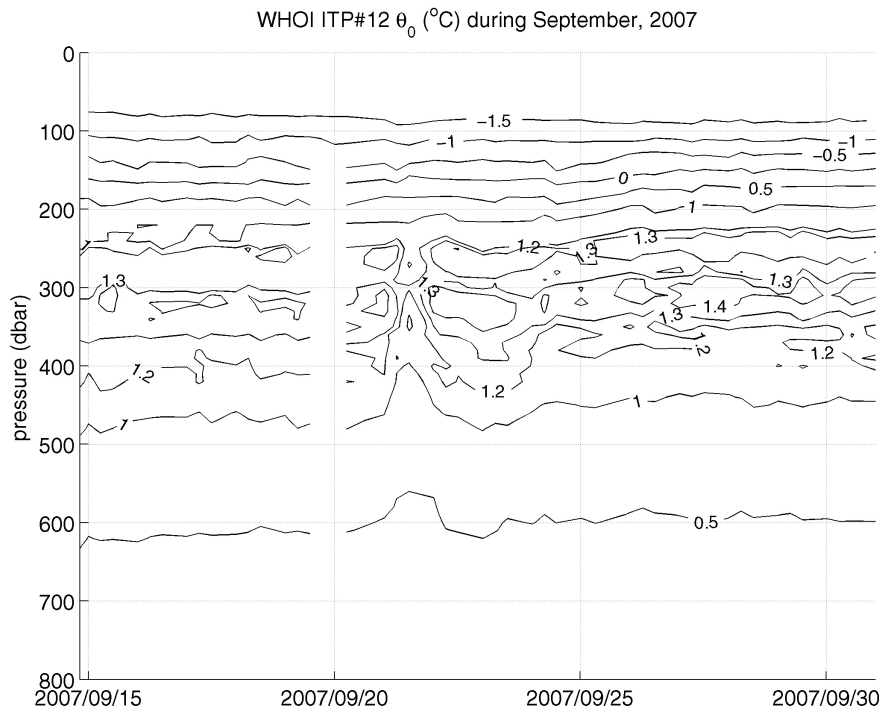


Fig. 4.3.4: ITP#12 potential temperature, referenced to θ dbar vs. pressure and time for the drift track shown in figure 4.3.3

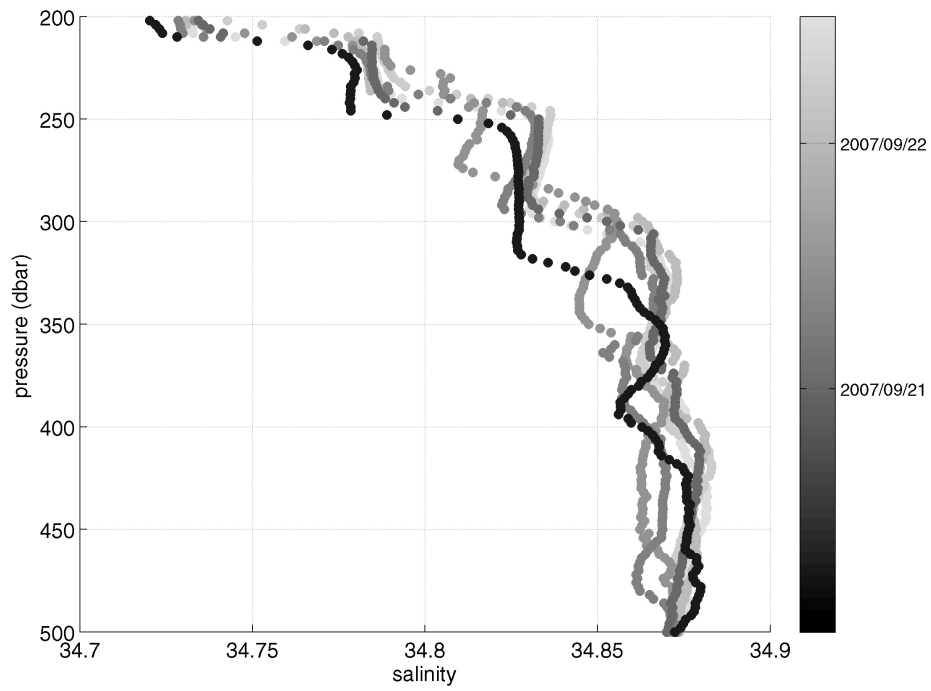


Fig. 4.3.5: Selected profiles of ITP#12 in the vicinity of the Lomonosov Ridge: Salinity.

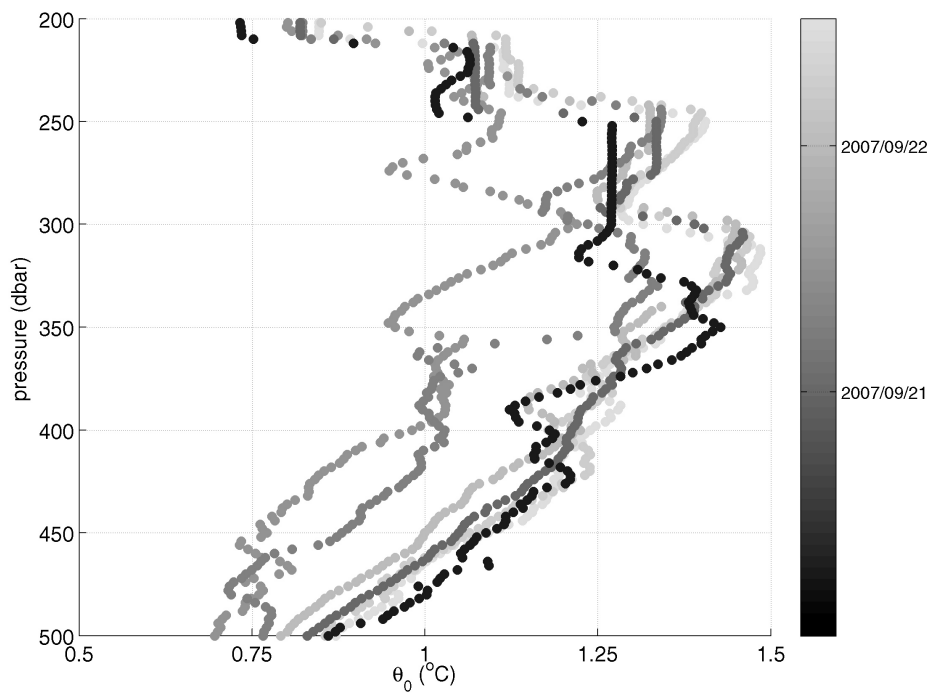


Fig. 4.3.6: Selected profiles of ITP#12 in the vicinity of the Lomonosov Ridge: Potential temperature, referenced to θ dbar

5. GEOTRACES

Background and general objectives

The availability of trace elements and isotopes (TEI) in the ocean controls and limits marine productivity, their present distributions reflect ocean circulation and they can be used to identify the sources and sinks of metals and other matter. TEI records in sediments allow the reconstruction of past climatic conditions and of past changes in ocean circulation. Our knowledge of tracer distribution is still strongly based on the successful GEOSECS expeditions in the 1970s. Since then, there have been major improvements in sampling, analytical, and modelling techniques. The international programme GEOTRACES has been initiated to make use of these developments and make major advances in our understanding of TEI cycling in the coming decade. One major aim of international GEOTRACES (<http://www.geotraces.org>) is:

"To determine global ocean distributions of selected trace elements and isotopes, including their concentration, chemical speciation, and physical form, and to evaluate the sources, sinks, and internal cycling of these species to characterise more completely the physical, chemical and biological processes regulating their distributions".

The International Polar Year (IPY) is an excellent opportunity to study Trace Elements and Isotopes in the Arctic and Antarctic Oceans. An international suite of vertical sections in the polar oceans is integrated in the IPY project No. 35 (<http://www.ipy.org/development/eoi/proposal-details.php?id=35>) entitled: "International Polar Year GEOTRACES: An international study of the biogeochemical cycles of Trace Elements and Isotopes in the Arctic and Southern Oceans". ARK-XXII/2 was the first expedition carried out in the context of this IPY-GEOTRACES. A second *Polarstern* expedition is scheduled in the Southern Ocean (ANT-XXIV/3; 2008).

The present expedition allowed the parallel sampling of a wide spectrum of tracers. Most of the key parameters mentioned in the GEOTRACES science plan are covered at least at some large stations. Sampling included tracers for river and shelf inputs, plankton production and particle rain, anthropogenic inputs and water mass circulation.

Intercomparison/Intercalibration

Intercalibration activities are ongoing for trace metals (SAFe) and nutrients (see report below). Special GEOTRACES intercalibration expeditions devoted to other parameters are scheduled for the summer of 2008. In order to allow a proper intercomparison of data acquired during our expedition with data produced after these intercalibration expeditions, we have collected sets of samples for some groups of tracers to be distributed among participating laboratories. Details of the sampling for Th/Pa, REE and Barium are given in the respective subprojects.

Data Management

All data of Isotopes and Trace Metals will be reported into the worldwide database of the GEOTRACES programme.

Work at sea

It was our objective to make parallel analyses of a wide spectrum of tracers at the same stations. This strategy is essential if we want to interpret the signals of the various tracers in a common context. Backbone of the tracer studies was the sampling with the new ultra clean CTD/Rosette of NIOZ (see below), with additional casts of the conventional rosette for less contamination-prone parameters. While some tracers could be determined at all sampled stations and depths, others could only be analysed at selected stations because of the large water volumes required or analytical constraints. The resulting sampling programme is presented in Table 5.1.

Tab. 5.1 GEOTRACES: Sampling list of trace elements, isotopes and supporting parameters

Station	trace metals 1)	DC/Alk	Nu- trients 2)	CH ₄ DMSP 2,3)	δ ¹⁸ O 2)	δ ¹³ C DIC 2)	Ba	REE	εNd/Be	²³⁴ Th	ISP	Pa/Th	²¹⁰ Po/ ²¹⁰ Pb ²⁰⁶ Pb	²²⁶ Ra 7)	²²⁸ Ra 8)	²²⁶ Ra 9)	²²⁸ Ra ²³⁰ Th ²²⁸ Ac ²²⁸ Ac 10)	DOC DON 11)	lignin δ ¹⁵ N- NO ₃	POC/ BSi	Chlora	TEP	
PS70228	X	X	X	X	X		X	X		X								X					
PS70229			X																				
PS70232			X																				
PS70236	X	X	X	X	X		X	X		X		PD	X	S	S			X			X	X	X
PS70237	X	X	X	X	X		X	X		X		PD	X	S	S			X			X	X	X
PS70239	X	X	X	X	X		X	X		X			X	S	S			X			X	X	X
PS70240			X																				
PS70241			X																				
PS70243			X			X	X			X													
PS70246	X	X	X	X	X		X	X		X													
PS70248			X																				
PS70255	X	X	X	X	X		X	X		X		T	X	S	S			X			S	X	S
PS70257	X	X	X	X	X		X	X		X			S	S	S			X	B		S	X	S
PS70258	X	X	X	X	X		X	X		X			S	S	S			X			S	X	S
PS70260	X	X	X	X	X		X	X		X		PD	X	S	S			X			X	X	X
PS70261	X	X	X	X	X		X	X		X			S	S	S			X			S	X	S
PS70263			X			X				X			S	S	S			X			S	X	S
PS70264			X							X			S	S	S			X			S	X	S
PS70265			X							X			S	S	S			X			S	X	S
PS70266	X	X	X	X	X		X	X		X		T	X	S	S			X			X	X	X
PS70267			X		X	X				X			S	S	S			X			S	X	S
PS70268	X	X	X	X	X		S	S		X			S	S	S			X			S	X	S
PS70271			X		X		S	S		X			S	S	S			X			S	X	S
PS70272	X	X	X	X	X		S	S		X			S	S	S			X			S	X	S
PS70273			X		X					X			S	S	S			X			S	X	S
PS70274			X		X					X			S	S	S			X			S	X	S
PS70276	X	X	X	X	X		X	X		X		PD	X	S	S			X			S	X	X
PS70277			X		X					X			X	S	S			X			S	X	X
PS70279	X	X	X	X	X		X	X		X		PD	X	S	S			X			X	X	X

Tab. 5.1 GEOTRACES: Sampling list of trace elements, isotopes and supporting parameters

Station	trace metals 1)	DC/Alk	Nu- trients 2)	CH ₄ DMSP 2,3)	δ ¹⁸ O 2)	δ ¹³ C DIC 2)	Ba	REE	εNd/Be	²³⁴ Th	ISP	Pa/Th	²¹⁰ Po/ ²¹⁰ Pb 0)	²²⁶ Ra 7)	²²⁸ Ra 8)	²²⁶ Ra 9)	²²⁸ Ra 10)	²³⁵ U/ ²³⁸ U 11)	DOC DON	lignin δ ¹⁵ N- NO ₃	POC/ BSi	Chlora	TEP		
PS70280			X	X	X													X							
PS70283			X	X	X	X													X						
PS70284			X	X	X	X													X						
PS70285	X	X	X	X	X	X	S	S		X			S	S				X	F		S		S		
PS70286			X	X	X	X																			
PS70288			X	X	X	X																			
PS70289			X	X	X	X																			
PS70290			X	X	X	X		S					S	S				X			S		S		
PS70291	X	X	X	X	X	X	S	S					S	S				X							
PS70292			X	X	X	X													X						
PS70294			X	X	X	X													X						
PS70295	X	X	X	X	X	X				X			S	S				X	F		S		S		
PS70298	X	X	X	X	X	X		X					S	S				X	F		S		S		
PS70299	X	X	X	X	X	X	X	X					S	S				X	F		S		S		
PS70301	X	X	X	X	X	X	S	S		X	X	T	X	S				X	F		X	X	X		
PS70302	X	X	X	X	X	X							S	S				X	F		S		S		
PS70303			X	X	X	X																			
PS70305			X	X	X	X		S					S	S				X	F		S		S		
PS70306	X	X	X	X	X	X				X			S	S				X	F		S		S		
PS70307			X	X	X	X																			
PS70308			X	X	X	X													X	F					
PS70309	X	X	X	X	X	X	X	X		X	X	PD	X	S				X	FB		X	X	X		
PS70310	X	X	X	X	X	X							S	S				X	F		S		S		
PS70312			X	X	X	X																			
PS70314			X	X	X	X				X															
PS70316	X	X	X	X	X	X	X	X																	
PS70319	X	X	X	X	X	X																			
PS70320			X	X	X	X							S												
PS70321			X	X	X	X													X	F		S		S	

Tab. 5.1 GEOTRACES: Sampling list of trace elements, isotopes and supporting parameters

Station	trace metals	DC/Alk	Nu- trients	CH ₄ DMSP	δ ¹⁸ O	δ ¹³ C DIC	Ba	REE	εNd/Be	²³⁴ Th	ISP	Pa/Th	²¹⁰ Po/ ²¹⁰ Pb	²²⁶ Ra	²²⁸ Ra	²²⁸ Ra	²²⁶ Ra	²³⁰ Th	²³² Th	²²⁶ Ra	²²⁸ Ra	²²⁸ Ra	²²⁶ Ra	²³⁰ Th	Pu/Cs ¹² 9	⁹⁹ Tc	DOC DON	lignin δ ¹⁵ N-NO ₃	POC/ BSi	Chlora	TEP	
	1)		2)	2,3)	2)	2)				4)	5)	6)	7)	8)	9)									10)	11)							
PS70322			X		X					S				S										X	F							
PS70324			X							S				S										X	F							
PS70326	X	X	X	X						S				S										X	F							
PS70328	X	X	X	X	X	X	X	X	X	S	X	PD I	X	X	S	X	X	X	X	X	X	X	X	X	FB	X	X	X	X	X	X	
PS70331			X		X	X				S			S											X	F							
PS70333			X		X	X				S			S											X	F							
PS70335			X		X	X				S			S											X	F							
PS70338	X	X	X	X	X	X	X	X	X	S	X		X	X	S	X	X	X	X	X	X	X	X	X	FB	X	X	X	X	X	X	
PS70340			X		X	X				S			S											X	F							
PS70342	X	X	X	X	X	X	X	X	X	S	X	T	X	S										X	FB	X	X	X	X	X	X	
PS70345			X		X	X				S			S											X	F							
PS70346			X		X	X				S			S											X	FB							
PS70349	X	X	X	X	X	X	X	X	X	S			S											X	FB							
PS70351			X		X	X				S			S											X	FB							
PS70352	X	X	X	X	X	X	I			S			S											X	F							
PS70358			X	X	X	X				S	X		S	X										X	F	X	X	X	X	X	X	X
PS70362			X	X	X	X				S			S											X	F							
PS70363	X	X	X	X	X	X				S			S											X	FB							
PS70365			X		X	X				S			S											X	FB							
PS70371	X	X	X	X	X	X	X	X	X	S			S											X	F							
PS70372	X	X	X	X	X	X				S			S											X	F							
PS70373	X	X	X	X	X	X				S			S											X	F							
PS70375			X		X	X				S			S											X	F							
PS70377			X		X	X				S			S											X	F							
PS70379	X	X	X	X	X	X				S			S											X	F							
PS70381			X		X	X				S			S											X	F							
PS70382	X	X	X	X	X	X	X	X	X	S			S											X	F							
PS70383			X		X	X				S			S											X	F							
PS70384			X		X	X				S			S											X	F							

Tab. 5.1 GEOTRACES: Sampling list of trace elements, isotopes and supporting parameters

Station	trace metals	DC/Alk	Nu-trients	CH ₄ DMSP	δ ¹⁸ O	δ ¹³ C DIC	Ba	REE	εNd/Be	²³⁴ Th	ISP	Pa/Th	²¹⁰ Po/ ²¹⁰ Pb	²²⁶ Ra	²²⁸ Ra	²²⁶ Ra	²²⁸ Ra	²²⁶ Ra	²²⁸ Ra	Pu/Cs ¹² / ₉	⁹⁹ Tc	DOC DON	lignin δ ¹⁵ N-NO ₃	POC/BSi	Chlora	TEP
	1)		2)	2,3)	2)	2)				4)	5)	6)	7)	8)	9)						10)	11)				
PS70385	X	X	X		X		X	X		X		T	X	X	S					S		X	B	X	X	X
PS70387			X		X							S	S							S	X	X	F	S		S
PS70389	X	X	X		X		X	X												S						
PS70391			X		X							S								S	X	X	F	S		S
PS70394			X		X															S	X	X				
PS70397			X		X															S	X	X				
PS70400	X	X	X		X		X	X		X	X	PD	X	X	X					X	X	X	F	X	X	X
PS70401			X		X															S	X	X				
PS70403			X	X	X					X										S		X				S
PS70404			X		X								S							S		X				
PS70405			X	X	X															S		X	F			
PS70407	X	X	X	X	X		X	X		X	X		X	X	S					S	S	X	F	X	X	X
PS70409			X	X	X							S	S	X						S	S	X	B	S	S	S
PS70411	X	X	X	X	X		X	X		X	X	PD	X	X	X					X	X	X	FB	X	X	X

- 1) for details see table GEOTRACES-2
- 2) more stations were sampled in-between
- 3) upper 200 m of water column
- 4) samples were collected from 0, 25, 50, 75, 100, 150 and 200 m.
- 5) ISP: *in-situ* pumps for Radium and size-fractionated POC/²³⁴Th down to 1,000 m water depth
- 6) PD particulate and dissolved ²³⁰Th and ²³¹Pa
- 7) T total ²³⁰Th and ²³¹Pa
- 8) short-lived Ra isotopes with RaDeCC technique
- 9) adsorption on MnO₂ cartridges
- 10) BaSO₄ precipitation
- 11) Sampling in the Atlantic Layer including optics/fluorescence spectra
- 12) Pu surface sample; Cs and ¹²⁹I profile

- X depth profile
- S surface water only
- B bottom sample
- F fluorescence maximum
- I Inter-calibration

5.1 A- trace elements

Karel Bakker, Lorendz Boom, Maarten Klunder, Rob Middag, Sven Ober, Charles-Edouard Thuroczy and Patrick Laan
Royal Netherlands Institute of Sea Research

Objectives

The distribution and biological availability of Fe is strongly controlled by its physical-chemical speciation within seawater, where colloids and Fe-organic complexes are dominant actors. The external sources of Fe into the oceans are either from above (dust) or from below (sediments) and will be constrained by Al and Mn for aeolian dust input and sedimentary redox cycling sources, respectively. The Fe enhances phytoplankton growth, which in turn strongly controls the biological pump for uptake of CO₂ from the atmosphere into polar oceans. The increasing CO₂ in polar ocean waters may affect phytoplankton ecophysiology, with key link of metal Fe in the overall photosynthetic apparatus.

Work at Sea

The Ultra Clean CTD system (UCC)
Sven Ober, Patrick Laan, Lorendz Boom
Royal Netherlands Institute of Sea Research

During the cruise a special CTD-system was used to sample for trace-elements and isotopes. This CTD-system consists of 3 major modules: a winch with a superaramide CTD-cable, a box-shaped titanium CTD-frame and a clean air container that is designed to hold the CTD-frame in order to enable subsampling and filtration under clean air conditions. The CTD-frame is made of pure titanium and was equipped with a Seabird SBE9+ CTD underwater unit, a SBE3 thermometer, a SBE4 conductivity-sensor, a SBE5 underwater pump, a SBE43 DO-sensor, a Chelsea MK-III fluorometer, a Seapoint OBS and a special sampling-system. This sampling-system consists of a Multivalve hydraulic multiplexer and 24 GoFlo sampling bottles each with its own hydraulic release unit. (De Baar et al., 2007; Ober et al., 2002).

In addition to the above mentioned sensors a Dr. Haardt fluorometer type BackScat 1 for detecting yellow substance was mounted from station 266, cast 1. From station 371, cast 2 the Aquatracka fluorometer was dismantled and a WetLabs C-Star transmissometer was mounted instead.

Tab. 5.2: Deployment list of Ultra-Clean CTD with sampling list of trace metals

Station	Position Lat	Position Lon	Sample depth [m]	DFe	DAI	DMn	Lib rary	DIC/ Alk	Fe liga nds	Nu trients	Silver
PS70/228-1	75° 0.03' N	34° 0.00' E	100	yes	yes	yes	yes	yes		yes	
PS70/236-1	77° 30.05' N	33° 59.20' E	150	yes	yes	yes	yes	yes		yes	
PS70/237-1	78° 59.83' N	33° 59.39' E	225	yes	yes	yes	yes	yes		yes	
PS70/239-1	80° 59.68' N	33° 59.80' E	175	yes	yes	yes	yes	yes		yes	
PS70/246-1	81° 52.27' N	34° 0.68' E	1750	yes	yes	yes	yes	yes		yes	
PS70/255-1	82° 30.25' N	33° 57.01' E	2950	yes	yes	yes	yes	yes		yes	
PS70/258-1	83° 59.94' N	33° 59.81' E	3990	yes	yes	yes	yes	yes		yes	

Station	Position Lat	Position Lon	Sample depth [m]	DFe	DAI	DMn	Lib rary	DIC/ Alk	Fe liga nds	Nu trients	Silver
PS70/260-2	84° 29.38' N	36° 8.29' E	3935	yes	yes	yes	yes	yes		yes	
PS70/260-4	84° 29.51' N	36° 6.15' E	3935	yes	yes	yes			yes	yes	Charly cast
PS70/261-1	84° 38.27' N	60° 55.24' E	3700	yes	yes	yes	yes	yes		yes	
PS70/266-1	83° 8.09' N	61° 46.17' E	2950	yes	yes	yes	yes	yes		yes	
PS70/268-1	82° 48.48' N	60° 48.35' E	1500	yes	yes	yes	yes	yes		yes	
PS70/272-1	82° 15.15' N	61° 59.67' E	210	yes	yes	yes	yes	yes		yes	
PS70/276-1	82° 5.05' N	68° 57.50' E	650	yes	yes	yes	yes	yes		yes	
PS70/279-2	81° 14.68' N	86° 12.49' E	315	yes	yes	yes	yes	yes		yes	
PS70/279-6	81° 12.20' N	86° 18.47' E	300	yes	yes	yes	yes	yes		yes	
PS70/285-2	82° 8.47' N	86° 20.20' E	680	yes	yes	yes	yes	yes		yes	
PS70/291-1	82° 42.71' N	86° 16.33' E	2200	yes	yes	yes	yes	yes		yes	
PS70/295-1	83° 16.14' N	86° 18.04' E	3200	yes	yes	yes	yes	yes		yes	
PS70/299-1	84° 3.02' N	89° 3.42' E	3550	yes	yes	yes	yes	yes		yes	
PS70/301-2	84° 34.30' N	89° 50.89' E	3650	yes	yes	yes	yes	yes	yes	yes	
PS70/302-1	84° 53.23' N	90° 5.94' E	3650	yes	yes	yes	yes	yes		yes	
PS70/306-1	85° 55.42' N	91° 10.79' E	3700	yes	yes	yes	yes	yes		yes	
PS70/309-2	87° 2.71' N	104° 50.31' E	1500	yes	yes	yes	yes	yes	yes	yes	combi cast
PS70/309-4	87° 1.94' N	104° 51.24' E	4325	yes	yes	yes	yes	yes		yes	
PS70/310-1	87° 39.81' N	111° 57.18' E	4250	yes	yes	yes	yes	yes		yes	
PS70/316-1	88° 10.75' N	139° 36.22' E	1250	yes	yes	yes	yes	yes		yes	
PS70/319-1	88° 40.05' N	153° 42.58' E	2650	yes	yes	yes	yes	yes		yes	
PS70/326-1	88° 1.85' N	169° 59.63' E	3900	yes	yes	yes	yes	yes		yes	
PS70/328-2	87° 49.60' N	170° 24.44' W	3900	yes	yes	yes	yes	yes		yes	
PS70/328-4	87° 49.50' N	170° 21.17' W	2000	yes	yes	yes	yes	yes		yes	
PS70/333-1	87° 1.64' N	146° 23.42' W	3200	yes	yes	yes	yes	yes		yes	
PS70/338-2	85° 42.20' N	135° 2.09' W	1475	yes	yes	yes	yes	yes		yes	
PS70/342-1	84° 29.97' N	138° 24.75' W	2200	yes	yes	yes	yes	yes		yes	
PS70/349-1	85° 3.92' N	164° 29.82' W	1950	yes	yes	yes	yes	yes		yes	
PS70/352-2	86° 38.52' N	177° 32.69' E	3900	yes	yes	yes	yes	yes		yes	
PS70/363-5	86° 27.95' N	134° 55.46' E	3850	yes	yes	yes	yes	yes		yes	
PS70/371-2	84° 39.32' N	102° 43.99' E	4050	yes	yes	yes	yes	yes		yes	
PS70/372-1	84° 19.84' N	107° 22.44' E	4060	yes	yes	yes	yes	yes		yes	
PS70/373-2	84° 11.79' N	108° 56.93' E	4050	yes	yes	yes	yes	yes		yes	
PS70/379-1	82° 51.57' N	117° 51.13' E	4352	yes	yes	yes	yes	yes		yes	
PS70/382-1	81° 21.45' N	120° 43.15' E	5200	yes	yes	yes	yes	yes		yes	
PS70/385-1	79° 20.88' N	124° 20.83' E	3425	yes	yes	yes	yes	yes		yes	yes
PS70/389-1	78° 21.30' N	124° 31.30' E	2500	yes	yes	yes	yes	yes		yes	
PS70/400-1	77° 22.94' N	123° 24.80' E	1091	yes	yes	yes	yes	yes		yes	
PS70/407-1	76° 10.83' N	122° 7.86' E	55	yes	yes	yes	yes	yes	yes	yes	
PS70/411-1	75° 12.03' N	121° 21.61' E	35	yes	yes	yes	yes	yes		yes	

In total 49 casts were carried out with the UCC-system including 2 test casts (Table 5.2).

Throughout the whole cruise the system worked very reliably, although some small technical problems occurred. The conductivity-sensor had to be exchanged for a spare because it appeared to have a slightly shifted calibration (although it was

calibrated recently) and the OBS had to be exchanged, because this sensor apparently did not survive the pressure during the deepest cast of the cruise (5,220 m) although this sensor was rated up to 6,000 m. The Dissolved Oxygen-sensor showed erratic values at depths over about 2,000 m. This problem was solved by exchanging the cable between the sensor and the underwater unit. At steep gradients some salinity-spiking was observed. Possible cause is the changed duct of the CTD. The longer tubes slow down the flow of the water and therefore the standard timing of the sensors is not optimal. This will become clear during postprocessing of the data in the near future. In case the retuning of timing of the sensors will not solve the spiking the most probable cause is a disturbed flow near the sensors. Another, more free-flow, location for the sensors in the frame must be considered.

The hydraulic bottle control system worked perfectly (100 %) and the GOFLO-samplers worked almost perfectly (99 % based on nutrient data). Prior to the cruise the edges of the holes in the top and bottom closing spheres of each Go-FLO sampler were made less sharp and prior to each cast all the spheres were sprayed with Teflon spray. These efforts clearly paid off.

Highest priority was given to the sampling of complete vertical profiles throughout the complete (4 - 5 km depth) water column at deep water stations in the different central Arctic Ocean basins. The sampling depth differed from 33 meter as the shallowest station, in the Laptev Sea, up to 5,220 meter for the deepest station at the south of the Gakkel Ridge. From these 49 casts 27 were deeper than 2,000 meter.

References

- De Baar, H.J.W., K.R. Timmermans, P. Laan, H.H. De Porto, S. Ober, J.J. Blom, M.C. Bakker, J. Schilling, G. Sarthou, M.G. Smit and M. Klunder (2008) Titan: A new facility for ultraclean sampling of trace elements and isotopes in the deep oceans in the international Geotraces programme, *Marine Chemistry*, in press.
- Ober, S., Groenewegen, R.L., Boekel, H.J., Keijzer, E.J.H., Derksen, J.D.J., Laan, M., 2002. A new way of oceanographic watersampling. Abstract of presentation at Inmartech, 8 October 2002, Yokosuka, Japan. <http://www.jamstec.go.jp/jamstec-e/whatsnew/inmartech2002/programme.pdf>.

Results

After recovery the complete frame with its 24 samplers was placed inside its home laboratory. This is the ultraclean laboratory container NIOZ-7 placed on the aft-deck (Arbeitsdeck). The seawater was processed and either filtered, over filtration cartridges by pressurizing each sampler with nitrogen gas from cylinders, or unfiltered and collected in pre-cleaned bottles for the analyses of dissolved Fe, Al, Mn and alkalinity and dissolved inorganic carbon and brought to the different analysts for analysis.

Besides this, the sampling for a variety of the GEOTRACES community was done like Rare Earth Elements, Ba, Uranium and Thorium. Also an extra litre bottle was sampled for analyses of various trace elements like Fe, Co, Ni, Cu, Zn, Ag, Cd and Pb on ICPMS in the home laboratory.

Titan proved to be extremely robust and easy to handle. The possibility to sample 24 depths in combination with the direct CTD data was extremely convenient and improved the trace metal data quality compared to the traditional way of trace metal sampling. With this system we are able to sample every small anomaly present. For the trace metals extreme caution in sample handling was done. All sample bottles were rinsed 5 times with a small amount of the sample. For the determination of the dissolved fractions the seawater was filtered using a Sartobran 300 cellulose acetate filter from Sartorius. This filter contains a 0.45 μm front filter and a 0.2 μm end filter. For this filtering we used pressurized N_2 gas from a bottle. An overpressure of less than 1 bar was sufficient.

After sampling the samples were double bagged to avoid any air borne contamination and transported to another clean room container where the samples were acidified to pH 1.8 with Seastar 12M baseline grade hydrochloric acid. An overall success rate of 99 % was achieved for the GoFlo (General Oceanics) bottles based on the nutrient data.

Three deep stations were sampled for ID ICPMS for Fe for inter-calibration purposes of the at sea method.

Subproject A1: Dissolved iron

Maarten Klunder

Royal Netherlands Institute of Sea Research

Dissolved iron was measured directly on board by Flow Injection Analysis (FIA) after De Jong et al. 1998 in a cleanroom container. In a continuous FIA system the acidified pH 1.8, filtered (0.2 μm) seawater is buffered to pH 4.0. The iron is concentrated on a column which contains the column material aminodiacetic acid (IDA). This material binds only transition metals and not the interfering salts. After washing off the column with ultra pure water (MQ) the column is eluted with diluted acid. After mixing with luminol, peroxide and ammonium the oxidation of luminol with peroxide is catalysed by iron and a blue light is produced and detected with a photon counter. The amount of iron is calculated using a standard calibration line, where a known amount of iron is added to low iron containing seawater. Using this calibration line a number of counts per nM iron is obtained.

All 47 stations and corresponding depths have been analyzed on board. The values of DFe measured varied from 0.18 nM to 10.4 nM. The standard deviation varied between 0 % and 7 % (exceptional), but was generally lower than 5 %. The standard deviation of the values is determined of a duplicate measurement of the same sample bottle. To correct for contamination during the process or in the sample bottle a duplicate sample was taken of every station depth. The daily consistency of the system was verified using a drift standard. Regularly a certified SAFe standard for the long term consistency and absolute accuracy was measured. Our average value of the certified SAFe (D2) standard was 0.93 (+/- 0.07) nM (n=24), well within range of the 0.91 (+/- 0.17) nM certified value (Johnson et al., 2007).

Next to the 47 stations also the amount of dissolved iron in the 1,000 kDa filtered fraction was measured for five casts. The corresponding 0.2 μm filtered fraction of the same cast was also measured. The 1,000 kDa filtered fraction generally contained a lower amount of dissolved iron.

Preliminary results

The preliminary data shows that the values for dissolved iron in the Nansen basin are according to the ranges found for the North Atlantic Deep Waters, 0.6 - 0.7 nM. (Martin et al, 1993). In the Amundsen and Makarov Basins the values appear to decrease to ranges of 0.4 - 0.6 nM. The stations west of the Gakkel Ridge appear to have the common Fe-distribution in the surface waters, with a minimum value at the chlorophyll maximum depth (varying from 100 to 25 meter). After passing the Gakkel Ridge an increase in the surface waters (0 - 100 m) was found, of up to 3 nM at maximum. This is expected to be caused by river input. On the northernmost station of the Gakkel Ridge an increase of dissolved iron was found at around a depth of 2,500 - 3,000 metres, of which a trace was to be seen into the Amundsen Basin.

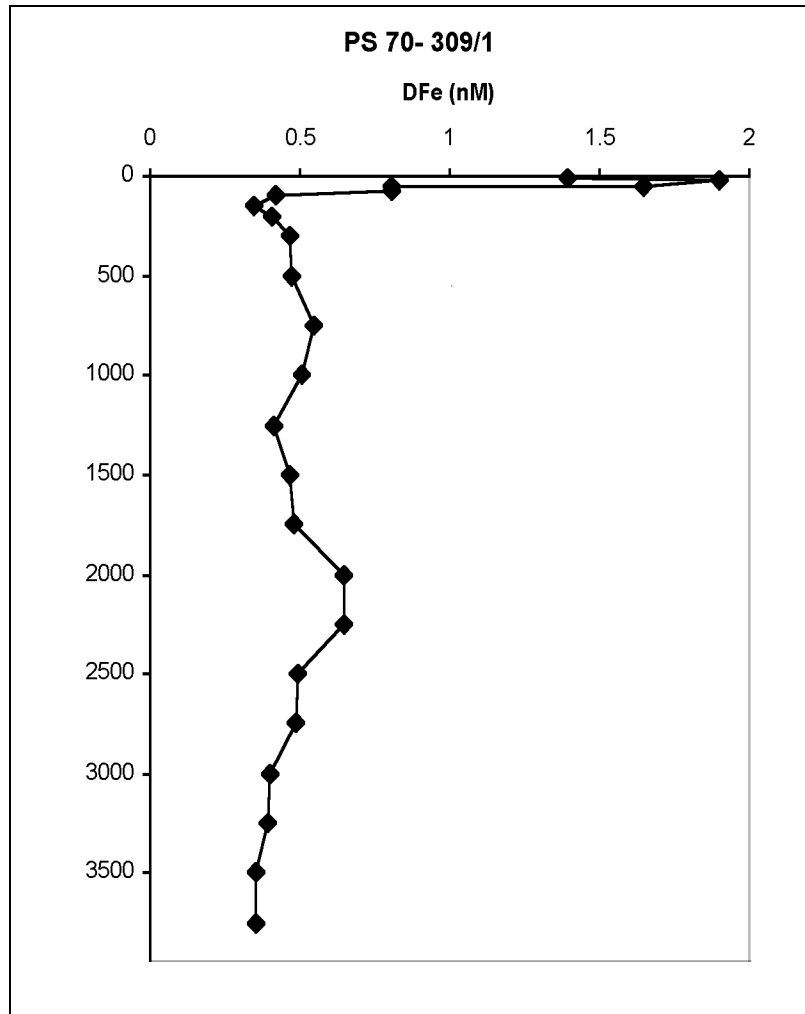


Fig. 5.1: Depth profile of dissolved iron in the Amundsen Basin

References

- Johnson et al., 2007. Developing standards for dissolved iron in Seawater. *Eos*, Vol 88, n. 11.
- Martin J.H., Fitzwater, S.E., Gordon, R.M., Hunter, C.N., and Tanner, S.J. (1993), Iron, primary production, and carbon- nitrogen flux studies during the JGOFS North Atlantic Bloom Experiment. *Deep sea Research II*. 40, 115-134.
- De Jong, J.T.M, den Das, J., Bathmann, U., Stoll, M. H.C., Kattner, G., Nolting, R.F., and de Baar, H.J.W. (1998). Dissolved iron at subnanomolar levels in the Southern Ocean as determined by shipboard analysis. *Analytica Chimica Acta*, 377, 113-124.

Subproject A2: Physical and chemical speciation of dissolved iron

Charles-Edouard Thuroczy

Royal Netherlands Institute of Sea Research

To understand the distribution of the iron in the seawater the concentration of natural ligands binding iron and their strength (conditional stability constant) are measured after a size fractionation of the seawater: 3 classes of size are studied here: unfiltered water, 0.2 μm filtrated water and < 1,000 kDa ultra-filtrated water.

Four deep stations have been sampled in order to characterize and show any difference between 3 basins in the Arctic Ocean: Nansen basins (2,950 m and 3,935 m), Amundsen Basin (4,500 m) and Makarov Basin (3,900 m). 3 shallow stations have also been sampled to show the influence of the river inputs on these basins: Barents Sea (175 m), Kara Sea (310 m) and Laptev Sea (55 m). Four of these stations will be used later on to study the kinetic exchange between the different forms of iron.

In a clean-room container the filtered seawater is ultra-filtrated as to isolate the colloids size class of dissolved iron (< 1,000 kDa). The ultrafiltrate comprising the 'truly dissolved' fraction, as well as the dissolved organic complexed fraction were analysed for Fe, Mn and Al.

The natural ligand concentration is measured by doing a complexing ligand titration with addition of iron (between 0 to 8 nM of Fe added). The competing ligand 'TAC' is used (2-(2-Thiazolylazo)-p-cresol) and the complex $(\text{TAC})_2\text{-Fe}$ is directly measured by cathodic stripping voltammetry (CSV). The electrical signal recorded with this method (nA) is converted as a concentration (nM), then the ligand concentration is calculated by knowing the dissolved iron concentration:

$$[\text{Fe-L}] = [\text{Fe}_{\text{added}}] + [\text{dFe}] - [(\text{TAC})_2\text{-Fe}].$$

Subproject A3: Dissolved Al and Mn as source tracers for iron

Rob Middag

Royal Netherlands Institute of Sea Research

Dissolved Al and dissolved Mn were measured directly using shipboard FIA measurements. In a continuous FIA system, the acidified pH 1.8, filtered (0.2 µm) seawater is buffered to pH 4.8 and 8.5 for Al and Mn, respectively. The metals are concentrated on a column which contains the column material aminodiacetic acid (IDA). This material binds only transition metals and not the interfering salts. After washing off the column with ultra pure water (MQ) the column is eluted with diluted acid.

The Al is determined using lumogallion after Resing et al. 1994. Lumogallion is a fluorometric agent and reacts with aluminium. The change in the fluorescence detected by a fluorometer is used as a measure for the dissolved Al concentration.

In order to verify the consistency of the analysis, every day a sample was measured from a 25 litre tank that was filled in the beginning of the cruise. The average value was 4.98 nM with a standard deviation of 3.16 % (0.157 nM). Also a duplicate sample was taken every cast and this sample was analysed with the samples of the next cast to further check for inter daily variation. Since the sample was from a different station every time one cannot calculate a standard deviation like for the samples from the 25 litre tank. However, one can calculate the percentage deviation for every duplicate and calculate the average from the absolute deviation percentages. This was 3.57 %.

The Mn is detected using the chemoluminescence method of Doi et al. 2004. The oxidation of luminol by hydrogen peroxide produces a blue light. This oxidation reaction is catalyzed by manganese and the increase in the production of blue light is detected by a photon counter and used as a measure for the dissolved Mn concentration.

Also for Mn similar consistency checks as for Al have been performed. The average value for the 25 litre tank was 0.998 nM with a standard deviation of 2.19 % (0.022 nM). The average absolute deviation percentage between the duplicates was 2.84 %. Furthermore seawater was analysed that was collected on a NIOZ cruise at two depths in the Atlantic Ocean. One depth per day was analysed, so a specific depth was analysed every other day. There was some variability between the different bottles of the same depth, but the deviation within a bottle was similar to that of the 25 litre tank.

All 47 stations and corresponding depths have been analyzed on board. The daily consistency of the system was verified using a so-called drift standard and regularly a certified SAFe standard was run for long term consistency and absolute accuracy.

Preliminary results

The preliminary data shows that the values in the surface for dissolved aluminium in all the basins are extremely low and increasing with depth. This indicates that no dust input occurred throughout the entire cruise.

For dissolved manganese the surface values were relatively high most likely caused by input from the shelf and/or by rivers. The values in the deep waters were much lower than expected.

On the northern most station of the Gakkel Ridge an increase of dissolved manganese was found at around a depth of 2,500 - 3,000 m, of which a trace was to be seen into the Amundsen Basin. For dissolved aluminium no increase was found at these depths.

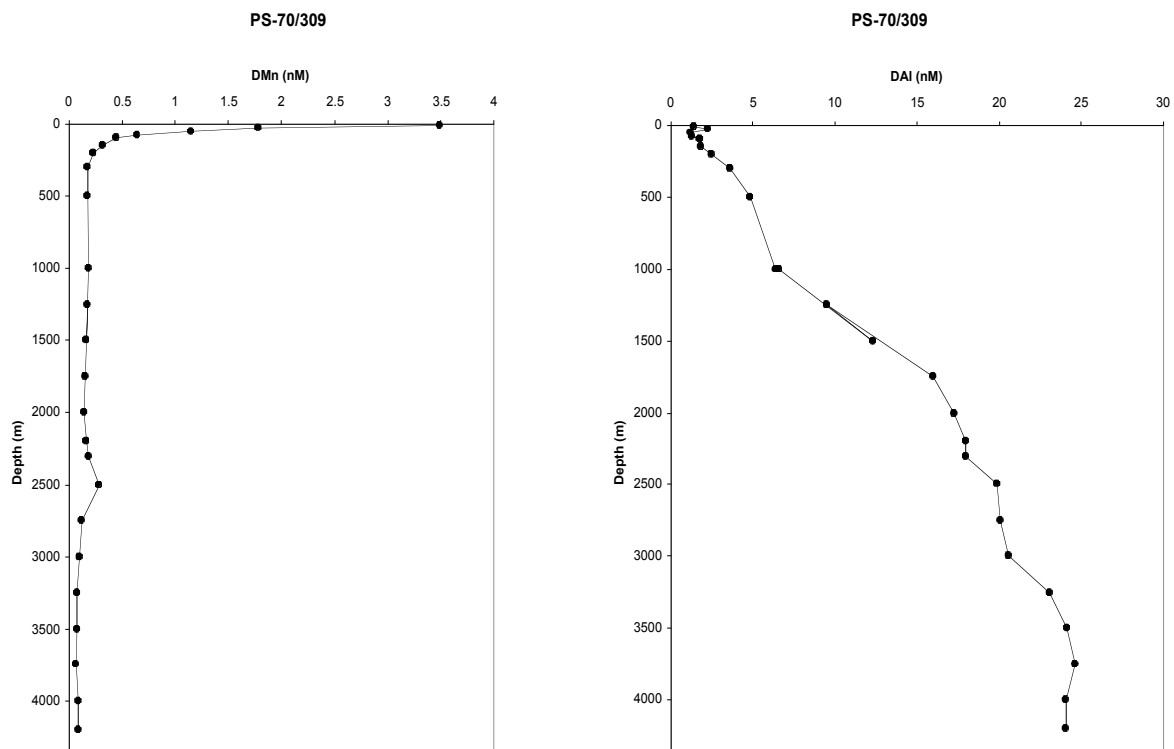


Fig. 5.2: Depth profiles of dissolved manganese and aluminium in the Amundsen Basin

References

- Doi, T., Obata, H., Maruo, M., 2004. Shipboard analysis of picomolar levels of manganese in seawater by chelating resin concentration and chemiluminescence detection. *Anal Bioanal Chem* 37, 1288-1293.
- Resing, J., Measures, C.I., 1994. Fluorimetric determination of Al in seawater by FIA with in-line preconcentration. *Anal. Chem.* 66, 4105–4111.

Subproject A4: Alkalinity and Dissolved Inorganic Carbon

Sven Ober

Royal Netherlands Institute of Sea Research

For unravelling the geochemical cycles of the ocean it is necessary to measure the CO₂-system. Therefore high-precision measurements were made of the total

dissolved inorganic carbon (DIC) content and total alkalinity (TA). Alk/DIC-samples were drawn from the GoFlo-samplers of the UCC-system prior to the sub-sampling for the other parameters.

Analysis of DIC was performed using the "coulometric method" (Johnson, 1993; Dickson, 1993). The Total Alkalinity (TA) analysis was performed with the 'standard' titration, using curve fits along modified Gran plots (Gran, 1952; Bradshaw 1981; Dickson, 1993). Both analyses were performed using a single integrated system: the VINDTA system (Versatile Instrument for Determination of Titration Alkalinity, MARIANDA: Marine Analytics and Data, Kiel, Germany), which also controlled the coulometer. Analyses accuracy was assured through the use of certified reference material (CRM, supplied by Dr. A. Dickson, Scripps Institute of Oceanography).

For the coulometric determination of DIC (a slight adaptation of the method described by Johnson 1993), an accurately known amount of sample (~20 ml) is dispensed with an automated, thermostated pipette into a stripper vessel. The sample is acidified here, converting all carbonate and bicarbonate species into CO₂(aq). The evolving CO₂ is rapidly removed from the sample by using N₂ as a carrier gas. The CO₂-enriched N₂ stream is led through the solution in the coulometric cell, which absorbs the CO₂ and becomes more transparent. The coulometer subsequently electrically titrates the solution back to its original opacity. The required amount of charge is a direct and linear measure of the amount of CO₂ absorbed. With knowledge of the sample's volume and density, the concentration of DIC (the sum of CO₂-species in the sample) is easily calculated. Total alkalinity is mathematically derived from a fourth-order curve fit along a modified Gran plot of electrode potential versus volume of acid added to an accurately known amount of sample (~100 ml), dispensed with an automated thermostated pipette. Titration is performed in a thermostated cell. Samples are brought to the calibration temperature of the pipettes.

Before samples were analyzed the VINDTA was stabilized by running 4 to 6 dummy samples. As soon as the VINDTA was stable a CRM was applied (in duplicate). After a batch of samples was measured a second CRM was applied to check for drift of the VINDTA. In cases the batch was big an extra CRM was applied after about half of the batch in order to obtain an extra reference point. In most cases the VINDTA did not drift significantly. A final estimation of the data quality has to be done after a careful re-evaluation of all the measurements at NIOZ.

References

- Bradshaw, Alvin L.; Brewer, Peter G.; Shafer, Deborah K.; Williams, Robert T.; 1981; Measurements of total carbon dioxide and alkalinity by potentiometric titration in the GEOSECS programme; Earth and Planetary Science Letters, Volume 55, Issue 1, p. 99-115.
- DOE (1994) Handbook of methods for the analysis of the various parameters of the carbon dioxide system in sea water. Version 2, A. G. Dickson & C. Goyet, eds. ORNL/CDIAC-74.
- Gran, G. (1952) Determination of the equivalence point in potentiometric titrations, Analyst, 77, 661.

Johnson K. M. (1); Wills K. D. (1); Butler D. B.; Johnson W. K. ; Wong C. S. (1993)
Coulometric total carbon dioxide analysis for marine studies: maximizing the performance of an automated gas extraction system and coulometric detector
Marine Chemistry, 44, 167-187.

Subproject A5: Nutrients

Karel Bakker

Royal Netherlands Institute of Sea Research

Equipment and methods

Nutrients were analysed in a thermostated laboratory container with a Technicon TRAACS 800, continuous flow auto-analyser. The sample rate was set at 60 samples per hour, measuring about 4,500 samples during the cruise. Measurements were made simultaneously on four channels: phosphate, silicate, nitrate and nitrite together, and nitrite separately. All measurements were calibrated with standards diluted in low nutrient seawater LNSW, and LNSW was used as wash water between the samples.

The colorimetric methods used are as follows

Phosphate: Ortho-phosphate is measured by formation of a blue reduced Molybdophosphate-complex at pH 0.9-1.1. Potassium Antimonytartrate used as the catalyst and ascorbic acid as a reducing agent. The absorbency is measured at 880 nm. (Murphy, J. & Riley, 1962).

Silicate: Measured as a blue reduced Silicomolybdenium-complex at 800 nm. Ascorbic acid is used as reducing agent and oxalic acid is used to prevent interference of phosphate. (Strickland and Parsons, 1972).

Nitrite: Diazotation of nitrite with sulfanylamide and N-(1-naphtyl)-ethylene diammonium dichloride to form a pink dye measured at 550 nm.

Nitrate and Nitrite (here called Nox): Nitrate is first reduced in a copperized cadmium-coil using imidazole as buffer and is then measured as nitrite at 550 nm. (K. Grasshoff et al, 1983).

Sample handling

The samples were collected in 100 ml high-density polyethylene sample bottles, after first being rinsed three times with a small amount of the sample, taken directly from the CTD-rosette bottles. The samples were kept cool and dark, stored in a refrigerator and analysed normally within 10 hours and within 16 hours as a maximum. Analyses were carried out using high-density polyethylene "pony-vials" with a volume of 6 ml, they were rinsed three times before filling with the samples. For duplicate analysis purposes between runs, the deepest sample at every station was capped in a pony-vial to be measured for a second time during the next run. To avoid evaporation during the runs, all vials including the calibration standards used were sealed with "parafilm" under tension, so that a sharpened sample needle easily penetrated through leaving a small hole in the film.

Calibration and Standards

Nutrient primary stock standards were prepared at the home laboratory, NIOZ.
Phosphate: by weighing Potassium dihydrogen phosphate in a calibrated volumetric PP flask set to 1mM PO₄.

Silicate: for silicate a certified standard (Merck) was diluted until 1.78 mM Si (stored at room temperature in an 100 % humidified box).

Nitrate: weighing in Potassium nitrate set to 10mM NO₃.

Nitrite: weighing in Sodium nitrite set to 1mM NO₂.

The calibration standards were prepared daily by diluting the separate stock standards, using three electronic pipettes, into four volumetric 100 ml PP flasks (calibrated at the lab) filled with low nutrient sea water LNSW. The blank values of the LNSW were measured on board and added to the calibration values to get the absolute nutrient values.

Cocktail standard

This standard acts as a lab reference and its use is described under "quality control". It is made in the laboratory containing phosphate, silicate and nitrate in a solution containing 40 mg Hg₂Cl₂ per litre as a preservative. Every time it was used it was diluted 250 times with the same pipette, and the same volumetric flask.

Quality Control

Our standards have already been proven by inter calibration exercises like ICES and Quasimeme, and last year the RMNS exercise organised from Michio Aoyama MRI/Japan, to be within the best obtainable limits to the mean of the better laboratories. To gain some accuracy the Cocktail standard is monitored now since 1997, showing between run reproducibility better than 1.5 %, but typically 0.7 % of its average value.

	average value	S.D	N
PO ₄	086 µM	0.008µM	74
SiO ₂	13.5 µM	0.054µM	74
NO ₃	13.9 µM	0.091µM	52

The advantage of a cocktail standard is like using a reference standard with three nutrients mixed into one bulk, giving for each run a quite good overview of how the instrument is performing. It also provides a methodology to correct data from run to run for producing better isoline-plots from station to station along horizontal surfaces within the ocean.

In preceding cruises, especially in an area like the Weddell Sea, where nutrient gradients in deep water are very small, back-correction (implying a factor in each run to multiply with, for gaining the average cocktail value after the whole transect in each run) with use of the cocktail is absolutely necessary to be able to discern the small true differences between samples.

Others have reported the use of a real reference standard supplied from deep water (2,000 m) but this turns out to be not stable over a period longer than three weeks. However during the second transect of the current cruise, the cocktail-based data produced was well within expected performance, so back-correcting afterwards is not necessary.

During the cruise, a graph was made for all the runs with a listing of the cocktail values. So bad runs were easily recognised if a value was not within the alarm-settings of $\pm 1.5\%$ (this was typically better than $\pm 1\%$). Deviations beyond the $\pm 1.5\%$ verification setting, did upon further verification, usually show up as irregularities of the analyser instrument (as noisy peaks, or gain calculation problems etc.), upon which the given samples were then re-analysed.

Statistics

For most of the nutrient parameters in this area it was not interesting to calculate the mean detection limit MDL. The exception was NO_2 , which showed a few small detectable peaks at the surface layer, and for the rest of the profile values around or below detection limits smaller than $0.01\ \mu\text{M}$. In the same statistical run the MDL was calculated as well as the standard deviation on standards at two levels.

Mean Detection Limits (calculated as $6 \times \text{S.D.}$ of the sampled baseline water)

	μM	Used measuring ranges μM
PO_4	0.01	1.50 *
SiO_2	0.01	18.0 *
NO_3+NO_2	0.03	21.0
NO_2	0.007	1.00

* for SiO_2 the preset range of the instrument was raised in the most Eastern part of the cruise region, to higher range of $31\ \mu\text{M}$, and similarly for PO_4 to higher range of $2\ \mu\text{M}$. This was necessary because of the highly nutrient-enriched waters derived from the Pacific Ocean at a depth around 70 - 125 m.

Reproducibility: of 5 sample bottles at two levels given with coefficient of variation %

	level I	Std dev.	Cv %	level II	Std dev.	Cv %
PO_4	0.193 μM	0.002	0.85	0.96 μM	0.002	0.17
SiO_2	2.504 μM	0.001	0.39	8.772 μM	0.021	0.24
NO_3+NO_2	0.312 μM	0.004	1.43	13.648 μM	0.029	0.22
NO_2 *	0.010 μM	0.001	0.11*	0.41 μM	0.002	0.20*

* For NO_2 the % listed is the percentage of the full scale value due to the low natural concentration in the seawater being only lower than 40 % of full range!

In order to obtain better values, an attempt was made to scale in the range for the nutrients to be measured such that the maximum was always at a level of 60 - 90 % of full scale.

Cross-runs statistics

In order to obtain cross-run statistical values, analyses were carried out twice on the same sample from the bottle closed at the bottom layer in the first run, and in the consecutive run. This provides the possibility to estimate the precision from station to station in a horizontal way. It is well known that the reproducibility within one calibrated run for an auto analyser is much better than measurements made across several runs, with each run having its own calibration settings. Analysis of these (cross runs) duplicate samples shows that the absolute differences are for

PO ₄	to be s.d.0.015µM	(avg. level 0.9µM PO ₄ n=23)
SiO ₂	to be s.d.0.131µM	(avg. level 8.17µM SiO ₂ n=23)
NO ₃ +NO ₂	to be s.d.0.175µM	(avg. level 12.70µM NO ₃ +NO ₂ n=23)

In the raw data set of the first transect, due to the improvement in temperature stability during following transects those values will improve especially for PO₄ to better than 0.01 µM.

Nevertheless, for our cocktail standard measured in every run, the resulting values remained stable for all nutrients during the cruise. In the future it would be highly advisable to produce and distribute a certified nutrient reference material, like the standard seawater for salinity, DIC, DOC. Such approach is now being pursued in the international community, and very likely would greatly improve the true accuracy, hence much improved compatibility of data better comparison between various laboratories and cruises.

Problems

Temperature stability

Temperature stability of the laboratory container in the first week, using an air-conditioning unit just diagonal opposite the analyser, gave a data offset been seen in recording the cocktail standard in a plot of +/- 0.02 µM PO₄. Just by placing a kind of sieve curtain between the air-conditioner and the analyser to lead the cold air not massively, but gently towards the other half of the container where the analyser is placed, largely solved this problem. This curtain improved the temperature stability within 1° C instead of 2° C, and reduced the cross-run offset in the cocktail for PO₄ to +/-0.01 µM on a value of 0.86 µM PO₄.

Evaporation during analysis

After the first two transects, I noticed that evaporation of sample water in the sampler-tubes can effect the data depending on the length of the run and the volume in the tube; evaporation was about 1.6 % per day, so 0.1 % within a run from start to end (measured relative humidity in the lab-container was around 23 %!!). It was clear that all sample tubes in the sampler should be covered with parafilm, although there is routinely made a gain-drift control assuming that the drift for all samples tubes is linear.

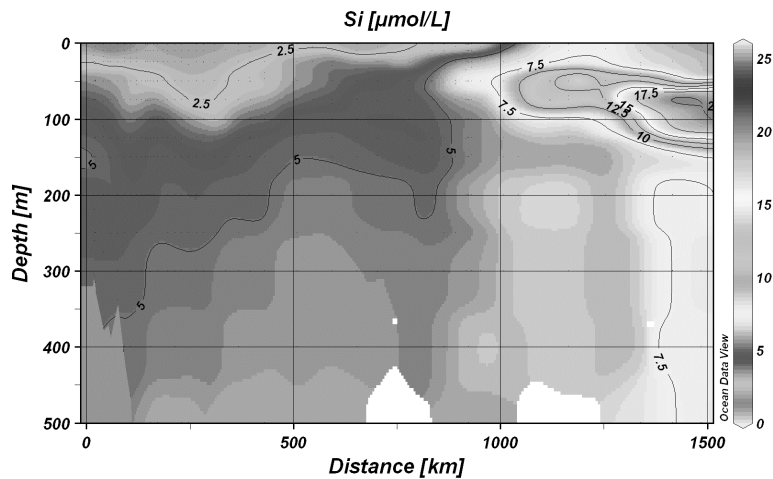


Fig. 5.3: Dissolved silicate values obtained during the third transect

References

- Murphy, J. & Riley, J.P., 1962. A modified single solution method for the determination of phosphate in natural waters. *Analytica chim. Acta* 27, 31-36
- Strickland and Parsons, 1972: A practical handbook of sea water analysis, J. Fish. Res. Bd. Canada. 167: 311 pp.
- Grasshoff K. et al, 1983: Methods of seawater analysis. Verlag Chemie GmbH, Weinheim. 419 pp.

Subproject A6: Involvement of Co, Ni, Cu, Zn, Ag, Cd in biological cycles

Sample bottles of one litre each were filled with filtered seawater for measurements afterwards in the home laboratory of Co, Ni, Cu, Zn, Cd as well as dissolved Fe. Latter dissolved Fe as a duplication hence confirmation/verification of the direct shipboard detection. The home laboratory measurement of this suite of trace metals will be done by High-Resolution Inductively Coupled Plasma Mass Spectrometry (HR-ICP-MS) with preceding in-line column pre-concentration of the metal elements from seawater. Another set of small 60 ml bottles was collected and stored for measurements afterwards of dissolved silver Ag in the laboratory of collaborator Dr. Eric Achterberg, National Oceanography Centre, Southampton, UK.

5.2 B- natural and anthropogenic radionuclides

Subproject B1: ^{234}Th as tracer of export production of POC

Michiel Rutgers van der Loeff¹⁾, Ingrid Voege¹⁾, Pinghe Cai²⁾, Kate Lepore³⁾
¹⁾Alfred-Wegener-Institut
²⁾Xiamen University, China
³⁾University College of Dublin

Objectives

- 1) To acquire accurate estimates of upper ocean POC export fluxes in the Arctic Ocean;
- 2) to infer the export fluxes of some particle-reactive elements/compounds (i.e., Fe, Al, Mn, Cu, Cd, Ni, Zn, and Ag) that will be measured by other researchers in the same regions (see section on trace metals above; and
- 3) to carry out the intercomparison of POC export studies between $^{234}\text{Th}/^{238}\text{U}$ and $^{210}\text{Po}/^{210}\text{Pb}$ methods.

Work at sea

1. A total of 38 depth profiles of total ^{234}Th in 4-l water samples were collected with the CTD.
2. *In-situ* pumps were deployed at 14 stations (see Table GEOTRACES-5.1) down to 1,000 m depth. The pumps at 50, 100, 150, and 300 m depth were equipped with multiple filter heads enabling the successive filtration over 100 μm , 53 μm screens and a 1 μ precombusted QMA filter in order to determine the POC/ ^{234}Th ratio in those size fractions. MnO_2 cartridges mounted behind these filters and in two more pumps deployed at 500 and 1,000 m depth will be used for the analysis of the $^{228}\text{Ra}/^{226}\text{Ra}$ ratio (see subproject 4).
3. The AWI-Isitec developed automated ^{234}Th analyser “Nick” was used throughout the expedition. The performance of the system and the yield of the automated MnO_2 precipitation was judged using deep-water samples and by comparison with the 4-l technique.

Preliminary results

The depth profiles of total ^{234}Th show that the ^{234}Th deficit is only confined over the shelf and in the upper 25 m of the deep basin of the Arctic Ocean (see Fig. 5.4 below). This indicates that little export of POC has occurred over the time scale of ^{234}Th in all areas aside from the shelf region.

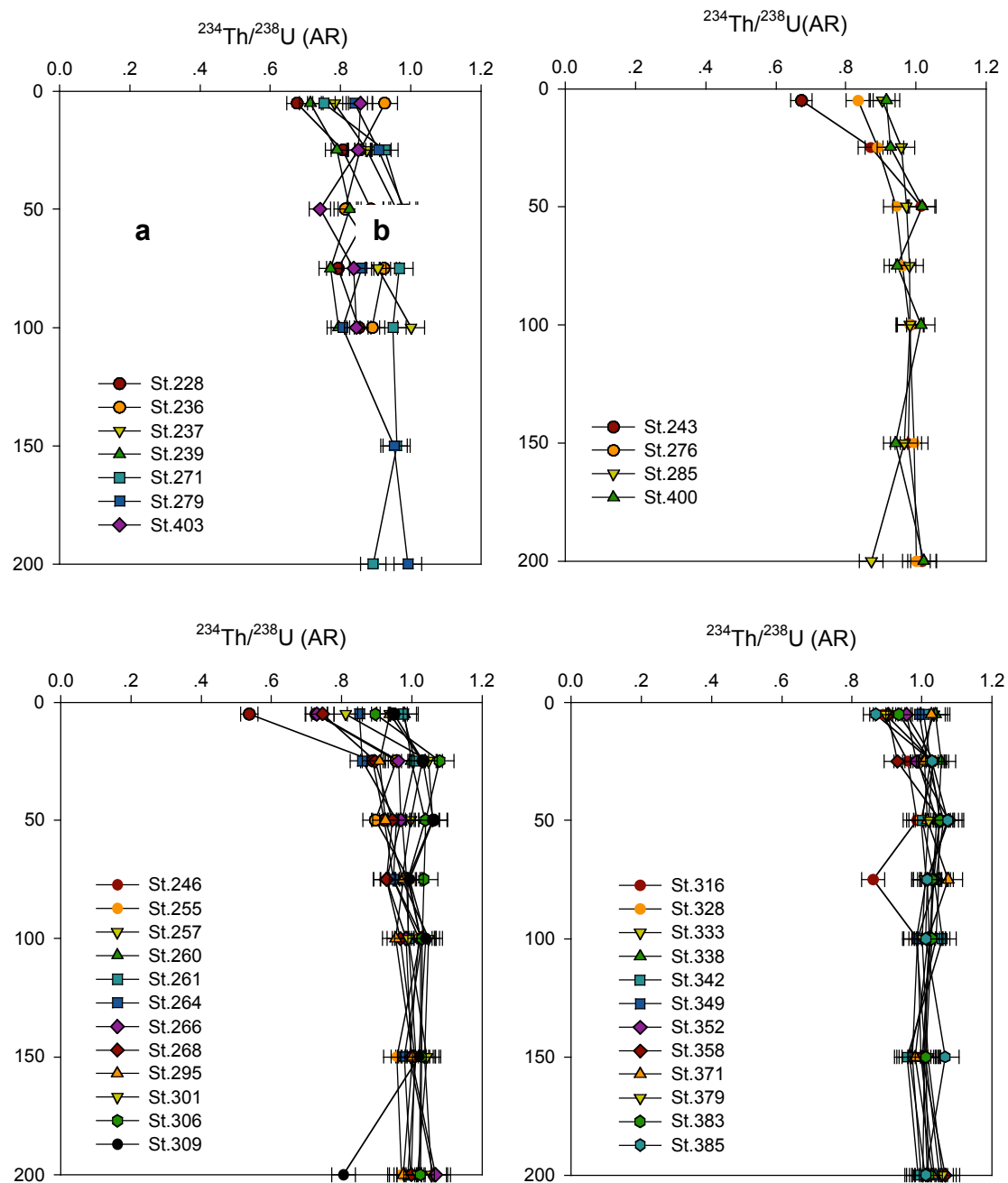


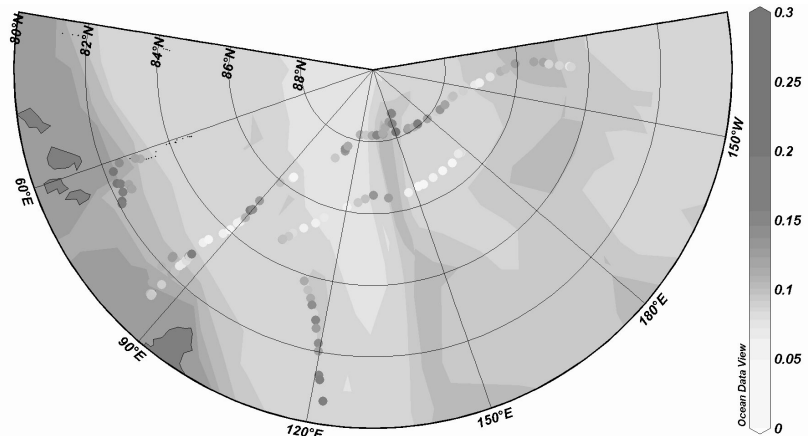
Fig. 5.4: Depth profiles of total ^{234}Th over the shelf (a), slope (b) and deep basin (c, d) of the Arctic Ocean. Note that the recovery for ^{234}Th is yet to be determined.

The automated ^{234}Th analyser (“Nick”) yielded a semi-continuous series of samples of suspended matter. Beta counting yielded the surface distribution of particulate ^{234}Th (Fig. 5.5) which is closely related to the suspended load. Suspended load was very low in the Nansen Basin and in the eastern and southern Makarov Basin. Higher loads were observed in shelf regions but also over the Lomonosov and Alpha Ridge.

5.3 C-related parameters

Samples obtained in this way could in principle also be used to obtain a distribution of e.g. POC or chlorophyll-a.

Fig. 5.5: Map of the distribution of particulate ^{234}Th (expressed as $^{234}\text{Th}/^{238}\text{U}$ ratio) in surface water over the entire cruise



The performance of the automated precipitation was improved by adjusting the addition of chemicals and the time allowed for the formation of the MnO_2 precipitate. The recovery remained somewhat lower than for the usual small-volume technique, but sufficiently reproducible to allow the monitoring of the ^{234}Th depletion in the surface water (Fig. 5.6). Final results can only be given after the yield determinations of the 4-l technique through the recovery of the added ^{230}Th spike.

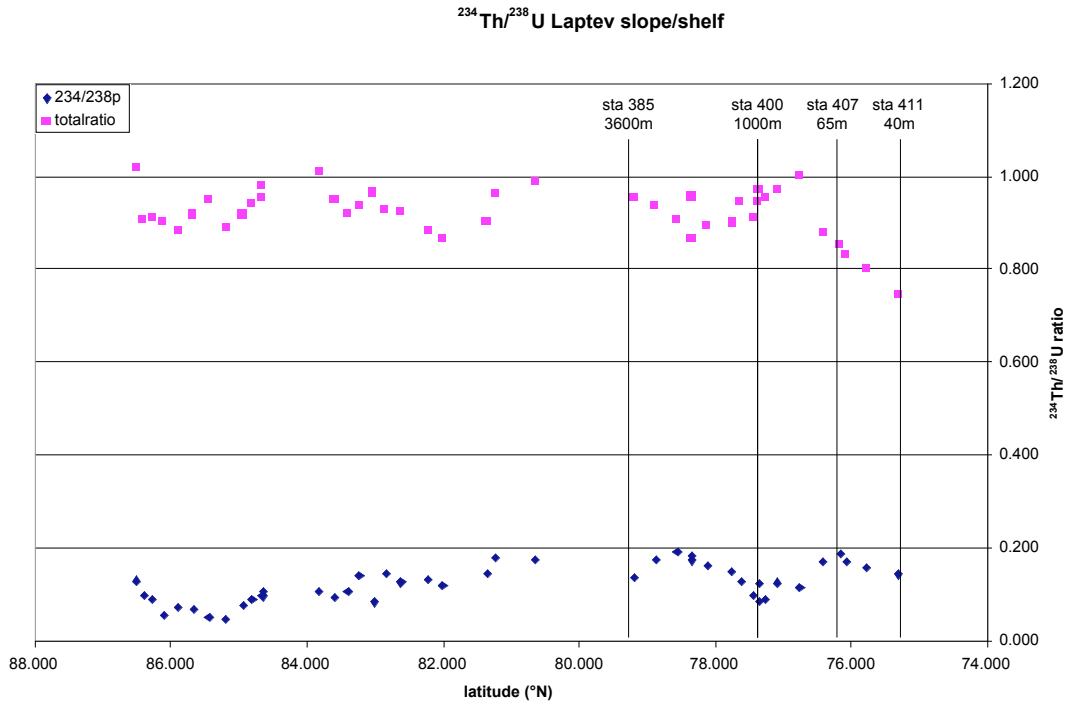


Fig. 5.6: The distribution of particulate and total $^{234}\text{Th}/^{238}\text{U}$ ratio in surface waters on the last transect along the Gakkel Ridge towards the Laptev shelf, as measured with the automated Th analyser. Particulate Th, related to overall particulate load in the surface water, goes through a minimum in the deep Amundsen Basin. Whereas there is some minor depletion of total ^{234}Th in the deep basin, a consistent and large depletion signifying an export of particles to the seafloor is only found on the shelf, south of 77°N .

Subproject B2: Tracing flux of particulate organic matter with Polonium-210 and Lead-210

Oliver Lechtenfeld

Alfred-Wegener-Institut

Background

Polonium-210 (^{210}Po , 138 days half life) and Lead-210 (^{210}Pb , 22.3 years half life) are produced by stepwise radioactive decay of Uranium-238 in seawater. These particle-reactive radionuclides ^{210}Po and ^{210}Pb are present in seawater in dissolved form and adsorbed onto particles. Following adsorption onto particle surfaces, ^{210}Po especially is transported into the interior of cells where it binds to proteins. In this way, ^{210}Po also accumulates in the food chain. ^{210}Po is therefore considered to be a good tracer for POC, and traces particle export over a timescale of months. ^{210}Pb adsorbs preferably onto structural components of cells, biogenic silica and lithogenic particles, and is therefore a better tracer for more rapidly sinking matter. In combination with Thorium-234 the ^{210}Po - ^{234}Th tracer pair can be used to distinguish POC and silica flux. This work is coordinated by Jana Friedrich, AWI.

Objectives

Our goals were (1) to get a better insight into Po binding sites in organic matter and (2) to trace pathways of particulate and dissolved matter leaving the Siberian Shelf.

- (1) We investigate to which extent TEP can play a role in extending ^{210}Po as a proxy for POC and whether TEP and $^{210}\text{Po}/^{210}\text{Pb}$ data can be related. This work is done in collaboration with Maya Robert and Uta Passow (AWI). We further look into the distribution of ^{210}Po on POC and in different plankton assemblages.
- (2) The pathways of particulate and dissolved matter were followed by the combined use of ^{210}Po and ^{234}Th as a tracer pair (and perhaps ^{210}Pb) for particle flux (collaboration with Pinghe Cai). This information gathered from water column will be complemented with the results of the ^{210}Po - ^{210}Pb study in sea ice (subproject 5, Patricia Camara) to provide a more thorough picture of particle transport from the shelf to the open sea and from surface to depth.

Work at sea

Depth profiles of $^{210}\text{Po}/^{210}\text{Pb}$ were sampled at 17 stations (see Table 5.1). In the upper approximately 500 m of the water column the particulate matter was collected separately by filtration; below this depth total activities were determined. At the same stations samples were taken for the analysis of POC and TEP. At a further 34 stations (Table 5.1) these same parameters were sampled in the surface water from the ship's seawater line.

Expected results

The study of ^{234}Th (subproject 1) showed that very little export had occurred on the time scale of ^{234}Th decay in all areas apart from the continental shelf. All the more interesting will it be to see whether any vertical particle transport can be observed on the somewhat longer time scales reflected by the isotopes ^{210}Po and ^{210}Pb .

Subproject B3: Pan-Arctic Investigation of Modern and Past Changes in Boundary Scavenging using ^{231}Pa and ^{230}Th

Kate Lepore

University College of Dublin

Background

The distributions of ^{231}Pa and ^{230}Th in the Arctic Ocean are primarily determined by patterns in particle flux and boundary scavenging. The activities of these radionuclides in marine sediments can be used to investigate past changes in the magnitude and spatial distribution of particle flux. In addition, changes in the water column distribution of these isotopes are indicative of changes in the rate of water mass ventilation as well as particle flux.

In this study, water samples were collected for the analysis of total, dissolved, and particulate ^{231}Pa and ^{230}Th activities. In addition, sediment cores were sampled for the analysis of surface sediment and down-core activity ratios of ^{231}Pa and ^{230}Th . As part of the GEOTRACES programme, intercalibration samples were collected at one

station in the Makarov Basin for the analysis of total ^{231}Pa and ^{230}Th at participating laboratories.

Work at sea

Water samples were collected along all transects (Fig. 5.4). Depth profiles of samples for analysis of total ^{231}Pa and ^{230}Th were collected at 6 stations, and samples for particulate and dissolved ^{231}Pa and ^{230}Th were collected at 9 stations. These stations were distributed across the basins and margins visited during ARK-XXII/2.

Sediment samples were collected everywhere samples were taken for dissolved and particulate ^{231}Pa and ^{230}Th . In addition, subsections of the box cores were taken throughout the shelf and slope of the Kara Sea, and the Nansen, Amundsen, and Makarov Basins (Fig. 5.5).

Water samples were collected at 2,000 m in the Makarov Basin (station 328) for the intercalibration of total ^{231}Pa and ^{230}Th measurements. 1 l, 2 l, and 10 l samples were collected and acidified with ultra clean nitric acid for independent analyses at ten oceanographic institutes.

Preliminary Results;

^{231}Pa and ^{230}Th analyses are performed in an ultra clean laboratory using mass spectrometry techniques. Therefore, no analyses were performed at sea.

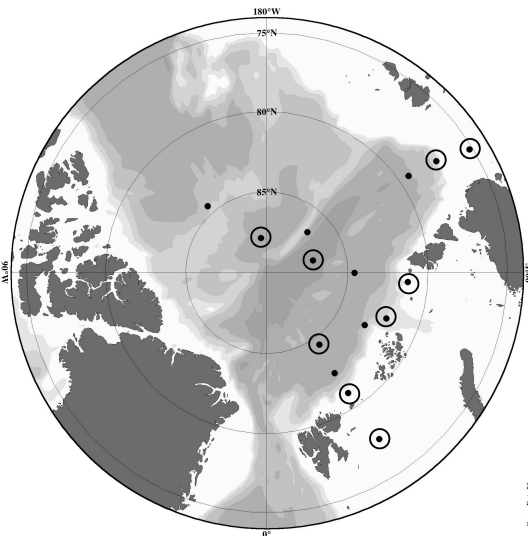


Fig 5.7. Map of water column ^{231}Pa and ^{230}Th samples. Circled stations are those where dissolved and particulate samples were collected.

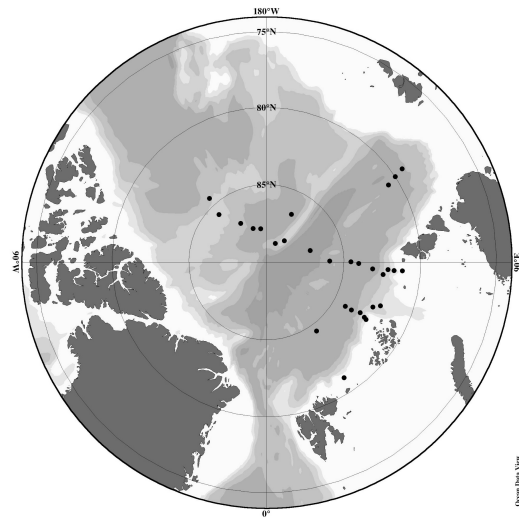


Fig 5.8. Map of sediment samples collected for ^{231}Pa and ^{230}Th analysis.

Subproject B4: Radium isotopes and ^{227}Ac

Michiel Rutgers van der Loeff, Lars Gremlowski
Alfred-Wegener-Institut

Background

Four radium isotopes are supplied to the ocean by contact with the continent or (deep-sea)-sediments: ^{223}Ra , (half-life 11.4 d); ^{224}Ra (3.7 d), ^{226}Ra (1620 y) and ^{228}Ra (5.8 y). The distribution of these isotopes in seawater has been shown to be most helpful to evaluate shelf-basin exchange and water residence times. The distribution of ^{228}Ra can add information on circulation time to that obtained of the other tracers of fresh water and continental inputs (like $\delta^{18}\text{O}$, fluorescence, Ba, nutrients). Like Ra isotopes, ^{227}Ac is released from sea sediments, but its main source is in deep-sea sediments. This tracer is therefore especially useful to study deep water mixing and ventilation.

Cooperation partners: Claudia Hanfland (AWI), Brad Moran (URI).

Work at sea

^{222}Rn was monitored semi-continuously by gas-water exchange in the ship's seawater supply using a RAD7 system.

Large volume surface water samples were collected for radium isotopes using the *Polarstern's* seawater intake, filtered through a 1 μm cartridge filter. For $^{228}\text{Ra}/^{226}\text{Ra}$, 1 - 2 m^3 of filtrate were passed over MnO_2 -coated polypropylene cartridges. The isotope ratio will be quantified in the home laboratory by Soxhlet leaching and subsequent gamma spectroscopy. For the quantification of ^{226}Ra Radium was coprecipitated on BaSO_4 from 20-l samples (19 surface water samples and 2 depth profiles; see Table 5.1). ^{226}Ra in other samples will be interpolated from a relationship we expect to derive between ^{226}Ra and dissolved silicate (determined in the same samples by Karel Bakker, NIOZ).

For short-lived radium isotopes, the filtrate was transferred to 300-l tanks, positioned in the fish lab of *Polarstern*. Each sample was pumped at <1 l/min using an electric *in-situ* aquarium pump (in each drum) through MnO_2 -impregnated acrylic fiber to scavenge radium isotopes. Occasionally subsurface samples of 50 - 150 l were obtained with the regular CTD (stations 272, 277, 342, 407, 409, 411; Table 5.1 GEOTRACES). Fibers were partially dried using compressed air, and short-lived ^{223}Ra and ^{224}Ra measured using RaDeCC detectors. Longer-lived ^{228}Ra will be measured on the fibers by gamma counting $^{228}\text{Ra}/^{226}\text{Ra}$ ratio in the shore-based lab and/or by recounting the ^{224}Ra activity after ingrowth of ^{228}Th .

Further subsurface samples were obtained with *in-situ* pumps. Whenever these were deployed (subproject 1; 14 stations, see Table 5.1 GEOTRACES) 1 or 2 MnO_2 -coated cartridges were fitted behind the filtration unit to absorb Ra and Th isotopes. These pump casts will provide ^{228}Ra activities at 50, 100, 150, 300, 500 and 1,000 m depth.

In all major basins ^{227}Ac profiles were sampled. At stations 260, 266, 301 (Nansen Basin), 309, 363 (Amundsen Basin), and 328 (Makarov Basin) 50-l samples were collected at 3 - 5 depths in parallel with sampling of ^{231}Pa (subproject 3, Kate

Lepore), an essential parameter to determine which part of the ^{227}Ac activity is supported by its parent ^{231}Pa . The Ac was coprecipitated on MnO_2 , the filters will be analysed in Bremerhaven.

Preliminary Results

Radium isotopes

The activity of ^{224}Ra in surface water, as measured with the RaDeCC system, showed a dramatic increase from the Nansen Basin towards the Alpha Ridge. It is to be expected that ^{224}Ra reflects the distribution of ^{228}Ra . Although the intermediate nuclide ^{228}Th is highly particle reactive, the Th export from the surface water is so low (subproject 1) that it is not to be expected that ^{228}Th becomes strongly depleted relative to ^{228}Ra , and the short lived daughter of ^{228}Th must then be in near-equilibrium with ^{228}Ra . We therefore consider the distribution measured on board as representing ^{228}Ra . The salient results are

- 1- Even at the easternmost station in the Canada Basin there was no indication yet of a decline of ^{228}Ra , so we may not even have reached the maximum ^{228}Ra activity. The maximum ^{228}Ra is much further east than found in 1991, more like the situation from 1994 as described by Smith et al., 2003.
- 2- The activity found in the easternmost station is far higher than the activities found on the Laptev shelf. Contrary to our expectations, the Laptev shelf cannot be the source of the high ^{228}Ra activities in the central Arctic. The source of those activities must be found in the Bering Strait/Chukchi Sea area.
- 3- recent external inputs of ^{224}Ra can be expected from shelf sediments. The usual procedure to determine excess ^{224}Ra (not supported by ^{228}Ra and ^{228}Th) is to recount the samples after several weeks (^{224}Ra half life is 3.5 days). According to this procedure, there would be excess ^{224}Ra throughout the surface Arctic, because part of the supporting ^{228}Th is removed by filtration.

^{222}Rn

We had expected that this isotope might be measurable if there had been sufficient release from the seafloor and exchange with surface waters on the shallow shelf, but even in the shallow Laptev Sea stations ^{222}Rn did not reach the detection limit of the RAD7 system (order of $4 \text{ Bq}\cdot\text{m}^{-3}$).

Subproject B5: Radionuclides as tracers of the role of sea ice in the transport, dispersion and accumulation of particulate matter and associated species in the Arctic Ocean

Patricia Cámara Mor

Universitat Autònoma de Barcelona

Background and objectives

The Arctic Ocean is covered by sea ice, perennial or seasonal. The sea ice plays an important role in the global and regional climate system and also in the oceanic circulation. It controls and influences in the surface heat, momentum and salt balance, energy balance between ocean-atmosphere through the albedo, light penetration important for biological productivity. There is a link between ocean-ice-atmosphere, the sea ice being an indicator of climatic change.

Sea ice is formed during winter mainly on the shallow continental shelves (<50 m depth), especially the Laptev, Kara and Barents Seas (Aagaard et al., 1981; Colony and Thorndike, 1985; Reimnitz et al., 1992; Dethleff et al., 1998; 2005; Eicken et al., 2005). The sea ice drifts mainly with the Transpolar Drift (TPD) over the Euroasian Basin and the anticyclonic Beaufort Gyre in the Canadian Basin (Barrie et al., 1998).

The origin, drifting patterns and fate of sea ice drive the transport of sea ice sediments (SIS) in the Arctic Ocean. The entrainment and enrichment of sediments or particles take place during sea ice formation and by deposition during the transit (Kempema et al., 1989; Barner et al., 1989; Reimnitz et al., 1992; Rigor and Colony, 1997). The sediments entrained in sea ice are transported for long distances across the Arctic Ocean and they are released during transit across the Arctic Ocean and in ablation areas, namely the Fram Strait, the Greenland shelves and the Barents Sea (Pfirman et al., 1990; Hebbeln and Wefer, 1991; Parlov and Pfirman, 1995), linking the marginal seas (especially Laptev and Kara Seas) to the deep basins and the central Arctic to the lower latitudes. Indeed, the sediment discharge significantly increases the sedimentation rate in the ablation areas, and even in the open Arctic Ocean (Nürnberg et al., 1994; Hebbeln, 2000; Dethleff, 2005).

Sea ice also transports many chemical species. Since the 1990s, a number of studies have pointed out that sea ice plays a major role in the transport and redistribution of SIS and associated chemical species, including radionuclides (Pfirman et al., 1995; Meese et al., 1997; Landa et al., 1998; Cooper et al., 1998, 2000; Masqué et al., 2003, 2007). Understanding the processes involved in the incorporation, transport, accumulation and redistribution of radionuclides from different sources is essential to assess their fate.

Radionuclides tend to be absorbed and/or associated in sediments, especially in the fine-grained particles. Once incorporated, radionuclides can be transported and redistributed across the Arctic Ocean associated with sea ice-sediments. The radionuclide content in SIS depends on a number of parameters; mineralogy, sediment size, chemistry properties, conditions of sea ice formation and there are many theories trying to explain the radionuclide activity in SIS.

Some processes during sea ice transit may enhance the concentrations of both sediments and radionuclides: sea ice tends to redistribute the sediments on the surface through freezing/melting cycles. During transit the formation of cryoconite holes takes place. Some effects of its formation are the aggregation of sediment particles and potential enhanced scavenging of particle reactive species present in sea ice (Nürnberg et al., 1994). Furthermore, chemical species and particles may be incorporated through deposition of aerosols from Arctic haze, snow, rain and dry deposition. Another source of radionuclides is the scavenging by SIS from the ocean surface.

The fact that sea ice is an important agent for the transport and dispersion of sediments and dissolved or particulate chemical species in the Arctic Ocean has several implications: i) its relative importance in the global ocean in terms of fluxes in the Arctic and export to the Atlantic Ocean; ii) the basic mechanisms that regulate the incorporation of tracer element and isotopes (TEIs) species to ice and, particularly, to

entrained sediments; and iii) the final fate of sediments and TEIs by release during transit and, especially, in main ablation areas such as the Fram Strait. These processes are modulated by the mechanisms that regulate the TEIs-sediments-ice-water interactions, within a frame of changing conditions in the Arctic Ocean. Radionuclides, both of natural and artificial origin are a group of relevant TEIs in the GEOTRACES programme, as potential chronometers of environmental processes and because of the knowledge of their source terms.

Our objectives are focused on the study of the role of sea ice in the transport of radionuclides (namely ^{210}Pb , ^{210}Po , ^7Be , ^{230}Th , ^{231}Pa , ^{234}Th , ^{239}Pu , ^{240}Pu , ^{137}Cs , Ra , ^{129}I) in the Arctic, with special emphasis on those associated to sea ice sediments, with the aim of using them as tracers of several processes. This includes: i) investigating what is the actual importance of the interaction with sea water in respect to scavenging of particle reactive radionuclides from sea water by sea ice sediments in comparison to atmospheric inputs during transit and concentrations in sediments in sea ice formation areas. ii) Potential use of some of the radionuclides as tracers of transit times of sea ice. iii) Estimate the actual balance of these isotopes in the Arctic, and in particular in respect to understanding the importance of release of sea ice sediments and associated radionuclides.

Work at sea

During this cruise samples of sea ice, atmosphere and sediments were taken (Table 5.3). Further sampling and analysis of water samples is described in subproject 8 (anthropogenic radionuclides). With respect to sea ice, we obtained samples of sea ice (20), sub-ice water (11), whole ice cores (14), melt ponds (10), sea ice sediments (9) and ice cores sliced every 10 cm (11). Atmosphere samples consisted of aerosol filters (18) and precipitation (wet, dry and weekly, 18). Samples will be further processed at the home laboratory by ion column chemistry and prepared for isotope and activity determinations. The measurement of ^7Be and $^{210}\text{Pb}/^{210}\text{Po}$ from sea ice, water sub ice and whole core will be analysed via gamma and alpha detectors respectively in the University Autonomous of Barcelona (UAB).

In addition, 29 sediment cores were taken at selected sites for the analysis of the distribution of man-made radionuclides in the sediment.

Sea ice samples

Sea ice samples consist in sea ice, sub-ice water, whole cores and melt points. In order to obtain 100 l of water once sea ice or sea ice cores were melted, we collected up to 6 30 l-barrels or drilled from 6 to 10 sea ice core depending on the thickness of the ice in the case of sea ice samples and whole core, respectively. Once on board, the samples were transferred into 120 l barrels and left to melt completely. Further processing was identical to the procedure described for water samples, although in this case ^{209}Po spike and stable Pb as chemical carrier were added.

In addition, sea ice cores were drilled and sliced every 10 cm in order to analyse ^{210}Pb and ^{210}Po . Each section was transferred to a plastic container until melting, subsequently the salinity was measured and the sample was filtered. The filtrate was acidified with 32 % HCl. ^{209}Po and stable Pb as chemical yield tracers and an iron carrier solution (FeCl_3)₂ were added under constant stirring. After waiting 12 hours to

reach chemical equilibrium, the pH was then raised to 9 with NaOH in order to precipitate the iron as $\text{Fe}(\text{OH})_3$. This scavenges the polonium and lead isotopes onto the precipitate. After that the precipitate was stored in small plastic bottles for further processing at the laboratory.

Sea ice sediments were sampled when dirty ice was detected from the vessel bridge and flights on helicopter. Once “dirty ice” was observed, approximately 20 kg of dirty ice were collected from the upper surface ice floes and from ridges by using stainless steel shovels or/and ice-hammer in order to obtain blocs of turbid sea ice. Onboard, sea ice samples were thawed and sea ice sediments were isolated from the supernatant liquid by careful decantation. Afterwards, sea ice sediments were kept frozen (-20°C) in plastic bags until their analysis in the laboratory.

Sediment cores

29 sediment cores were collected with the multicorer or boxcorer, depending on the station. The top first 5 cm were cut in slices every 0,5 cm, sections from 5 to 21 cm were cut every 2 cm and the bottom part every 5 cm. Samples were stored in the freezer at -20°C .

Atmosphere samples

Atmosphere samples consist in aerosols and precipitation (wet and dry). 18 aerosol filters were collected by using an aerosol pump placed on top of the vessel (Peildeck). Filters for aerosols were changed every 24 hours during transit sections. Precipitation samples comprise 7 total (wet and dry), 8 wet and 6 weekly. Ad-hoc precipitation collectors were placed on the top of the *Polarstern* (Peildeck). For wet precipitation, the collector was opened upon start of rain or snow and closed at its end; for wet plus dry precipitation, the collector was constantly opened and the sample was changed once the wet event ended; the weekly samples remained opened for a week. Precipitation samples were transferred to plastic bottles and were acidified with 32 % HCl. ^{209}Po , stable Pb and Be spikes as chemical yield tracers and an iron carrier solution (FeCl_3)₂ were added under constant stirring. After waiting 12 hours in order to get a chemical equilibrium, the pH was then raised to 9 with NaOH in order to precipitate the iron as $\text{Fe}(\text{OH})_3$. The precipitate was transferred to small bottles and stored for further processing at home.

Absorption/desorption experiment

In order to investigate the role that sea ice sediments play in the transport of ^{230}Th and ^{231}Pa and the implications it may have on the use of the Pa/Th proxy in the Arctic, an absorption/desorption experiment was carried out on board. It was replayed three times. The experiment consisted in adding into plastic bottles with filtered sea water some grams of sea ice sediments. These were kept in suspension using a motor which stirred the water. After different times (1 h, 2 h, 4 h, 6 h, 12 h, 24 h, 48 h, 72 h, 96 and 120 h), a bottle was filtered to isolate the sediments from the water. Water was acidified with 32 % HCl and sediment filters were kept frozen (20°C) in plastic bags until their analysis at home.

References

- Aagaard K., 1981. On the deep circulation of the Arctic Ocean. *Deep-Sea Research*, 82: 251-268.
- Barnes P., Reimnitz E., Fox D.H., 1982. Ice rafting of fine grained sediment, a sorting and transport mechanism, Beaufort Sea., Alaska. *Journal of Sedimentary Petrology*, 52 (2), 493-501.
- Barrie L., Falck E., Gregor D., Iverson T., Loeng H., Macdonald R., 1998. The influence of physical and chemistry processes on contraminant transport into and within the Arctic. In: Gregor D., Barrie L., Loeng H., editors. *The AMAP assessment*, 1998, 25-116 pp.
- Colony R., Thorndike A.S., 1985. Sea ice motion as a drunkard's walk. *Journal of Geophysical Research*, 90, 965-974.
- Cooper L.W., Kelley J.M., Bond L.A., Orlandini K.A., Grebmeier J.M., 2000. Sources of the transuranic elements plutonium and neptunium in Arctic marine sediments. *Marine Chemistry*, 69, 253-276.
- Cooper L.W., Larsen, I.L., Beasley, T.M., Dolvin, S.S., Grebmeier, J.M., Kelley, J.M., Scott, M. and Johnson-Pyrtle, A., 1998. The distribution of radiocesium and plutonium in Sea Ice-entrained Arctic sediments in relation to potential Sources and sinks. *Journal of Environmental Radioactivity*, 39 (3), 279-303.
- Dethleff D., 2005. Entrainment and export of Laptev Sea ice sediments, Siberian Arctic. *Journal of Geophysical Research*, 110, C07009, doi:10.1029/2004JC002740.
- Dethleff D., Loewe P., Kleine E., 1998. The Laptev Sea flaw lead - Detailed investigation on ice formation and export during 1991/92 winter season. *Cold Region. Science Technology*, 27 (3), 225-243.
- Eicken H., Gradinger, R., Gaylord, A., Mahoney, A., Rigor, I., Melling, H., 2005. Sediment transport by sea ice in the Chukchi and Beaufort Seas: Increasing importance due to changing ice conditions?. *Deep-Sea Research II*, 52, 3281-3302.
- Hebbeln D., 2000. Flux of ice-rafted detritus from sea ice in the Fram Strait. *Deep-Sea Research II*, 47, 1773-1790.
- Hebbeln D., Wefer G., 1991. Effects of ice coverage and ice-rafted material on sedimentation in the Fram Strait. *Nature*, 350, 409-411.
- Kempema E.W., Reimnitz E., Barnes P.W., 1989. Sea ice sediment entrainment and rafting in the Arctic. *Journal of Sedimentary Petrology*, 59, 308-317.
- Landa E., Reimnitz E., Beals D., Pochkowski J., Rigor I., 1998. Transport of ^{137}Cs and $^{239,240}\text{Pu}$ with ice-rafted debris in the Arctic Ocean. *Arctic*, 51, 27-39.
- Masqué P., Cochran J.K., Hebbeln D., Hirschberg D.J., Dethleff D., Winkler A., 2003. The role of sea ice in the fate of contaminants in the Arctic Ocean: Plutonium atom ratios in the Fram Strait. *Environmental Science and Technology*, 37, 4848-4864.
- Masqué P., Cochran J.K., Hirschberg D.J., Dethleff D., Hebbeln D., Winkler A. and Pfirman S., 2007. Radionuclides in Arctic sea ice: tracers of sources, fates and ice transit time scales. *Deep-Sea Research I*, doi:10.1016/j.dsr.2007.04.016

- Meese D.A., Reimnitz E., Tucker W.B.III, Gow A.J., Bischof J., Darby D., 1997. Evidence for radionuclide transport by sea ice. *Science of Total Environment*, 202-267.
- Nürnberg D., Wollenburg I., Dethleff D., Eicken H., Kassens H., Letzig T., Reimnitz E., Thiede J., 1994. Sediments in Arctic Sea ice: implications for entrainment, transport and release. *Marine Geology*, 119, 185 -214.
- Pavlov V., Pfirman S., 1995. Hydrographic structure and variability of Kara Sea: implications for pollutant distribution. *Deep-Sea Research II*, 42 (6), 1369-1390.
- Pfirman S., Lange M.A., Wollenburg I., Schlosser P., 1990. Sea ice characteristics and the role of sediment inclusions in deep-sea deposition: Arctic-Antarctic comparisons. In: U. Bleil and J. Thiede (eds.), *Geological History of the Polar Oceans: Arctic versus Antarctic*. Kluwer Academic Publishers, pp. 187-211.
- Pfirman S.L., Eicken H., Bauch D., Weeks W.F., 1995. The potential transport of pollutants by Arctic Sea ice. *Science of the Total Environment*, 159, 129-146.
- Reimnitz E., Marinovich L., McCormick M., Briggs W., 1992. Suspension freezing of bottom sediment and biota in the Northwest Passage and implications for Arctic Ocean sedimentation. *Canadian Journal of Earth Science*, 29, 693-703.
- Rigor I., Colony R., 1997. Sea ice production and transport of pollutants in Laptev Sea, 1979-1993. *The Science of the Total Environment*, 202, 89-110.
- Smith, J.N., Moran, S.B., Macdonald, Robie W., 2003. Shelf-basin interactions in the Arctic Ocean based on ²¹⁰Pb and Ra isotope tracer distributions. *Deep-Sea Research, Part 1*, 50(3): 397-416.

Tab. 5. 3: Summary of sea ice and sediment samples

Station	sea ice sample	whole core	section core	melt ponds	water sub ice	sea ice sediments	sediment core
PS70/239							X
PS70/348	X	X	X	X	X		
PS70/255							
PS70/357	X	X	X				
PS70/259							
PS70/260	X	X	X	X	X		X
PS70/363							X
PS70/264	X	X	X	X	X		
PS70/365							X
PS70/266							X
PS70/369							X
PS70/370							X
PS70/271	X	X	X	X	X		
PS70/374							X
PS70/276							X
PS70/377							X
PS70/279							X
PS70/382							X
PS70/285	X	X	X		X		X
PS70/394							X
PS70/399							X

Station	sea ice sample	whole core	section core	melt ponds	water sub ice	sea ice sediments	sediment core
PS70/301	X	X	X	X	X		X
PS70/306							X
PS70/308							
PS70/309	X	X	X	X	X		X
PS70/316							X
PS70/319							X
PS70/322	X	X		X	X		
PS70/328	X	X		X			X
PS70/333							X
PS70/338	X	X	X	X			X
PS70/342	X			X		X	X
PS70/352	X	X		X	X		
PS70/358							X
PS70/363	X	X	X		X		
PS70/365							
PS70/371	X	X	X		X		
PS70/383							X
PS70/384							X
PS70/385							X
Helistation 82°47,50N-33° 58,37E	X						
Helistation 83° 59,58N-34° 23,12E						X	
Helistation 83° 59,61N-34° 01,58E						X	
Helistation 82°30,13N-65° 45,35E	X						
Helistation 83° 36,269N-60° 23,930E	X					X	
Helistation 83° 25,52N-61° 59,16E						X	
Helistation 85° 08,7N-60° 48,9E						X	
Helistation 83° 17,75N-86° 11,32E	X						
Helistation 85°33,88N-90° 26,36E	X						
Helistation 87°29,89N-109°33,33E	X						
Helistation 84°27,01N-148°25,70W						X	
Helistation 84°15,65N-108°44,76E						X	
Helistation 82°12,91N-108° 54,95E						X	

Subproject B6: Rare Earth Elements, ^{10}Be and the isotopic composition of Nd (ϵ_{Nd})

Sabine Mertineit, Michiel Rutgers van der Loeff
Alfred-Wegener-Institut

Objectives

Rare Earth Elements (REE) and the isotopic composition of Nd are important water mass tracers. The varying REE-pattern and isotopic signature of Nd is transferred to the ocean via processes such as riverine inputs, dust inputs, or leaching of shelf sediments and ice drifted sediments. In addition to selective weathering, elemental fractionation may also occur during aqueous transport, where natural particles and colloids are of great importance. The REE concentrations coupled with the Nd isotopic ratios are powerful tracers to investigate scavenging processes and to predict the fate of elements brought from the continent. The REE's residence times on the order of 1,000 years make them ideal tracers for water masses as it allows for long distance transport while preventing complete homogenisation. Especially Nd isotopes are useful in paleoceanography, as their isotopic signature is preserved in ferromanganese nodules, foraminifera, and Fe-Mn oxide coatings of sediments.

Beryllium isotopes (cosmogenic ^{10}Be and lithogenic ^9Be) give additional information on inputs and water mass sources. Cooperation partners: Per Andersson (National Museum of Natural History, Stockholm, Sweden) and Martin Frank (IFM-GEOMAR, Kiel).

Work at sea

Samples have been collected for REE in dissolved and particulate form and in sea ice sediments.

For dissolved REE, 1-l seawater samples were collected using the ultra-clean CTD-Rosette. The samples passed an in-line 0.2μ cellulose acetate filter (see trace metals UCC procedure). They were acidified with 1 ml of distilled nitric acid (HNO_3).

For the purpose of intercalibration/intercomparison with other laboratories, 20 filtered samples were taken from the ultra-clean CTD as well as from the AWI CTD-Rosette at 2,000 m in the Makarov Basin (sta 328). These samples were acidified in the same way and will be distributed to other laboratories.

Particulate REE in surface waters was collected by the ship's seawater membrane pump (Klaus pump with inlet at 11 m depth) and a continuous flow centrifuge. 2,000 - 6,800 l of seawater were centrifuged at a rate of about 500 - 1,000 l per hour at 16,000 g.

Sea ice sediments were sampled by coring. Cores were sliced in 10 cm pieces and melted aboard in parallel with similar experiments on radionuclides (subproject 5). It was important to prevent contamination thus the ice cores were drilled by hand and the location for drilling on the floe was always chosen upwind so that the fumes of other working groups with motor drills or from the ship were blown in the counter

direction. Furthermore all the working tools and containers for the ice slices were cleaned thoroughly before every sampling. Because of the different interests of all the groups on the ice it was not possible to start coring as the very first one without any other people on the floe. But at one ice station (sta. 352) it was examined if and how much the fumes of motor drills and helicopters could contaminate the ice cores. Therefore at the very beginning of the ice station one ice core was drilled by hand where no other group was working on the ice and some time later a second core was drilled by hand under the usual conditions as described above.

Tab. 5.4: Time and location of ice core stations where samples were collected for REE studies

number	stations	date	time	coordinates	
1	PS 70/248	02.08.07	13:13	81° 56.71' N	34° 2.16' E
2	PS70/260	07.08.07	09:27	84° 29.37' N	36° 8.29' E
3	PS70/264	12.08.07	11:07	83° 39.16' N	60° 25.59' E
4	PS70/271/1	15.08.07	12:58	82° 30.18' N	60° 47.67' E
5	PS70/285/1	20.08.07	12:54	82° 8.59' N	86° 19.08' E
6	PS70/301/1	24.08.07	09:25	84° 34.77' N	89° 50.26' E
7	PS70/309/1	27.08.07	21:49	87° 2.74' N	104° 47.78' E
8	PS70/328	02.09.07	12:00	87° 49.79' N	170° 33.37' W
9	PS70/352/1	10.09.07	12:07	86° 38.27' N	177° 33.49' E

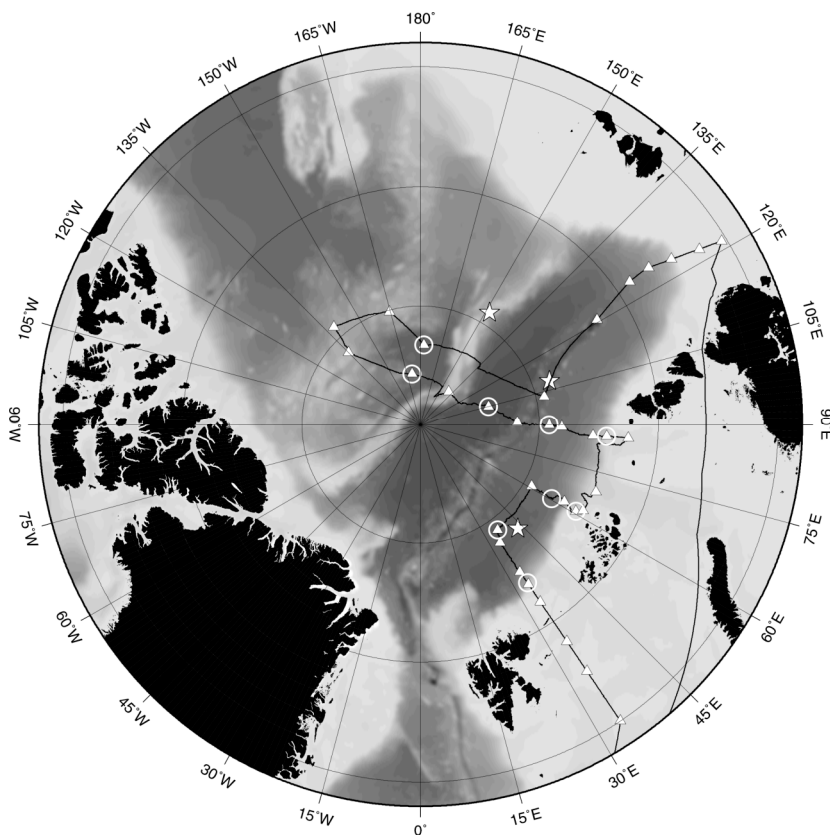


Fig. 5.9: Location of REE water column sampling (triangles), Ice stations (circles) and locations where dirty ice was sampled by helicopter (stars)

After melting, subsamples were taken for $\delta^{18}\text{O}$ and Ba. The remainder was filtered and the particulate matter was stored at -20°C for later analysis of REE.

When sea ice sediments come into contact with seawater, desorption and dissolution of REE may cause changes in the REE pattern and isotopic composition of Nd in the seawater. This process was investigated experimentally. Dirty ice was sampled on three stations visited by helicopter:

#	date	coordinates
1	06 Aug 07	83°59.61' N, 43°01.58' E
2	08 Sep 07	84°27.01' N, 148°25.70' W
3	17 Sep 07	84°15.65' N, 108° 44.76' E

The interaction of REE between these ice-rafted sediments and filtered seawater was studied by one exchange experiment (with sample #1) on board. After melting a large (approx 80-l) dirty-ice sample, the water was separated by decantation and centrifugation and about 1 g of the remaining sediments was added to freshly filtered sea water. 24 hours later it was filtered. In parallel, 10-l of dirty ice was melted, filtered and the filtrate was collected. All filtrate samples were acidified with 8 ml of distilled nitric acid (HNO_3).

The REE composition will be compared to that of the same water with no dirty ice added to test the contribution of sea ice sediments to the isotopic signature of Nd and the REE-pattern. Further experiments with ice-rafted and centrifuged sediments will be carried out at AWI.

Fifteen 10-litre samples of seawater were collected from surface water and CTD/Rosette casts in the Russian shelf region for ϵNd and Be analyses (Table 5.1). These samples were filtered and acidified for Neodymium isotopic analysis in Stockholm. A parallel 1-l aliquot of these filtered samples was acidified for ^{10}Be and ^9Be analysis in Kiel (IFM-GEOMAR).

Subproject B7: Barium as river water tracer

Sabine Mertineit, Michiel Rutgers van der Loeff
Alfred-Wegener-Institut

Objectives

Barium has been shown to be a powerful tracer to distinguish river water masses from Eurasian and American origin (Taylor et al., 2003). In combination with other tracers of fresh water components (salinity, $\delta^{18}\text{O}$, fluorescence, ^{228}Ra , nutrients) it will be possible to obtain an overview of the distribution of the various fresh water sources during our expedition as a contribution to the EU programme DAMOCLES.

Work at sea

15 ml unfiltered seawater samples for Ba analyses were collected throughout the expedition from the ultra-clean CTD (Table 5.1). The samples were acidified with 30 μl distilled HCl and will be analysed with isotope dilution ICPMS at AWI. In order to determine whether ultra clean sampling is necessary for this element, parallel

samples were taken on the entire depth profile using the conventional AWI Rosette at station 266.

For the purpose of intercalibration/intercomparison with other laboratories, 20 samples were taken from a single bottle of the ultra-clean CTD as well as from the AWI CTD at 2,000 m in the Makarov Basin (sta 352). These samples will be distributed to other laboratories.

Reference

Taylor J. R., Falkner K. K., Schauer U., and Meredith M. (2003) Quantitative considerations of dissolved barium as a tracer in the Arctic Ocean. *J. Geophys. Res.* 108(C12), 3374, doi:10.1029/2002JC001635.

Subproject B8: Anthropogenic radionuclides ^{129}I , ^{99}Tc , ^{137}Cs and Pu

Andreas Wisotzki¹, Patricia Camara²,
Kate Lepore³

¹Alfred-Wegener-Institut

²Universitat Autònoma de Barcelona

³University College of Dublin

Objectives

The main source of ^{129}I and ^{99}Tc is their release by reprocessing plants of nuclear fuel. The sources (Sellafield, La Hague) are well known. ^{137}Cs and Pu isotopes have also been released by fallout, and the isotopic composition of Pu differs among the various sources. The distribution of these tracers is used to model the Arctic circulation and especially the relative contributions of Atlantic and Pacific water masses. Cooperation partners: Michael Karcher (AWI/OASYS), Claudia Hanfland (AWI), Pere Masque (UAB), Brad Moran (URI), John Smith (BIO).

Work at sea

Plutonium isotopes and Cesium-137 are present at ultra trace levels, which complicates their measurement and forces us to collect large volume samples. Large volume (100 l) sea water samples were collected by using Niskin bottles mounted on the CTD rosette, comprising 56 surface water samples and 11 water profiles of 6 - 8 depths (Table 5.1). The 100-l water samples were transferred into a plastic barrel and acidified with 32 % HCl. ^{242}Pu and stable Be spikes as chemical yield tracers, and an iron carrier solution (FeCl_3)₂ were added under constant stirring. After waiting 12 hours in order to get a chemical equilibrium, the pH was then made 9 with NaOH in order to precipitate the iron as $\text{Fe}(\text{OH})_3$. This scavenges beryllium and plutonium onto the precipitate while cesium stays in solution. After that the supernatant was transferred into a second barrel while the precipitate was stored in small plastic bottles for further processing in the home laboratory. By addition of 65 % HNO_3 , the pH was lowered again and subsequently stable Cs was added as a chemical yield tracer. Then, a pre-weighed sample of ammonium molybdophosphate was added while stirring thoroughly. This produced a yellow precipitate that scavenges Cs. The precipitate was left to settle and then transferred into smaller bottles. The isotopic composition of Pu will be determined by AMS at the University of Sevilla, Spain, and ^{137}Cs activities will be analyzed via gamma-counting at UAB. In one case (station 352) ^{137}Cs was collected with KCFC resin (to be analysed at BIO).

^{129}I was sampled along with ^{137}Cs and Pu isotopes (Table GEOTRACES-1). 1-l samples for ^{129}I were collected from the CTD-rosette and stored with no special requirements (e.g., at room-temperature) until shore-based analysis. ^{99}Tc was sampled especially in the Atlantic layer (Table 5.1). For ^{99}Tc , 5-l samples were collected from the CTD-rosette and stored in plastic canisters with no special requirements.

5.3 C- related parameters

Subproject C1: Dissolved organic matter (DOM) in the Arctic Ocean

Sally Walker

Texas A&M University at Galveston

Recently a project was funded by the NSF (USA) to investigate the formation of the Arctic Halocline by using organic tracers and *in-situ* fluorescence. We found elevated levels of terrestrial DOM and associated fluorescence in halocline waters which is very intriguing and suggests the involvement of river water in halocline formation. Unfortunately, we also found that the fluorescence signal can not be attributed to the terrestrial source alone, rather there seem to be several sources involved. The *in-situ* probe is very general and does not allow any further distinction of the fluorescence signal. With the samples we hope to unravel some of these different sources by using a new method combining high resolution spectrofluorometry and parallel factor analysis. With this new method we will be in a much better position to determine source waters involved in halocline formation which is critical for our understanding of climate change the Arctic Ocean system.

Work at sea

With a fluorescence sensor mounted on the CTD unit, a full water depth profile of fluorescence was obtained at every station. This gave us real time information on the horizontal and vertical distribution of fluorescence which is caused by certain organic compounds dissolved in seawater. Based on the fluorescence signal we selected our sampling location and depth and collected between 1 and 20 l of seawater at several depth levels. We collected samples from 70 stations throughout the cruise as seen in figure 5.10. Each sample was split into subsamples to determine the following parameters: dissolved organic carbon (DOC), dissolved organic nitrogen (DON), optical properties (absorbance and fluorescence), carbohydrates, lignin phenols, and nitrogen isotopes (nitrate). Water samples were immediately filtered, frozen and will be transported to the home laboratory for further analyses which will take 1 to 2 years to complete.

Preliminary Results

Depth distribution of *in-situ* fluorescence in the Arctic Ocean reveals a subsurface maximum of fluorescence throughout most of the basin, most likely dominated by river CDOM. The maximum fluorescence in the Canadian Basin appears to be associated with halocline waters while the maximum fluorescence in the Eurasian Basin appears to be associated with the transpolar drift surface waters. To confirm a common origin of fluorescence in these two basins, we will pair them with molecular level analyses, 3-dimensional fluorescence coupled with parallel factor analysis.

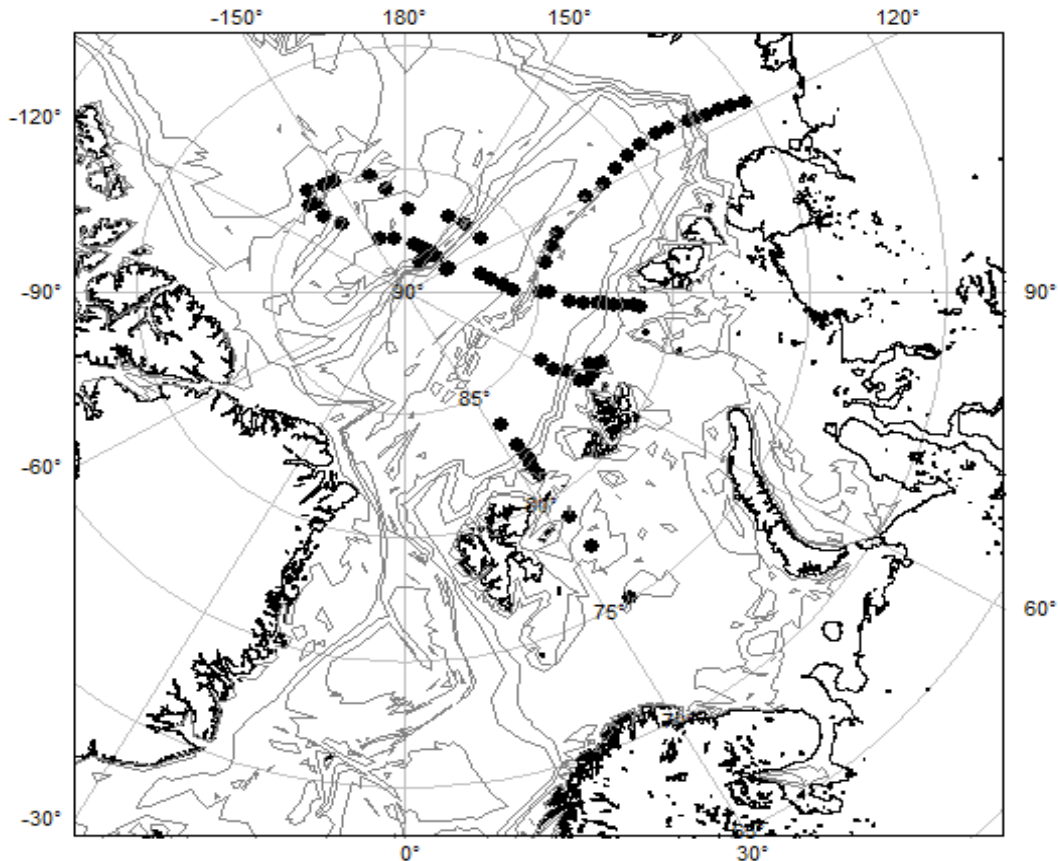


Fig 5.10: Map of stations collected during ARK-XXII/2 for DOM analyses.

Subproject C2: Phyto- and Protozooplankton ecology in the water column

Lilith Kuckero

Alfred-Wegener-Institut

Objectives

Since the 1990s phyto- and protozooplankton ecological investigations on biomass, productivity and related biochemical parameters as chlorophyll a, particulate organic carbon/ nitrogen (POC/PON), carbonate, and biogenic silica have been carried out in Arctic waters mainly in the Fram Strait area. During the years 1993-1996 sampling was also conducted in the Amundsen and Nansen Basins. During the present cruise, about 10-15 years later, the same investigations will be done for comparison with the old data to understand eventual changes due to a changing environment. Specific questions addressed: Are there regional differences in the seasonal distribution patterns of phytoplankton and protozooplankton, POC/PON, carbonate and biogenic silica in the ice-covered Arctic ocean? What is the influence of the respective abiotic factors? Which are the most remarkable processes within it for the pelagic food web? What changes can we measure?

Work at sea

Water was sampled with the CTD-Rosette at different depths from surface to bottom for filtration and measurements of Chlorophyll a, POC/PON and biogenic silica at home. Also water samples from surface down to 100 m depth have been taken (from the CTD) for species abundances on several station during the cruise. These samples were fixed with buffered formaldehyde. Additionally water was sampled by Apstein-net (a hand-operated net) at several stations to obtain an overview of the biodiversity.

Expected results

A quantitative and qualitative analysis of the fixed samples will give an overview of the regional and seasonal distribution of the phyto- and protozooplankton species and their abundances. At station PS70/411 a high abundance of several Chaetoceros species was observed in contrast to the species abundance observed at other stations.

5.4 Coupling of methane and DMSP cycles in the marginal ice zone and on polar shelves

Ellen Damm, Ingrid Voege
Alfred-Wegener-Institut

Background

Recent change in the Arctic may have profound effect on natural biogeochemical cycles in seawater. Especial feedback effects to pathways of climatically relevant biogases like methane and DMS will loom large in the equation of change. The recent marine methane cycle is influenced by microbial induced in situ production, which creates a methane surplus relative to the atmospheric equilibrium concentration in ocean surface water. However the potential of the upper ocean methane cycle remains underestimated because in situ production is masked by a simultaneous and nearly equals in situ oxidation. Hence the carbon isotopic ratio of methane will be used to trace the in situ production and the subsequent consumption processes, which provides insights into the recent methane cycle.

A principal pathway by which methane is readily formed is the methylotrophic methanogenesis. However, direct evidence of this role of methylated substrates in aerobic seawater is still lacking. An abundant methylated substrate in the surface ocean is dimethylsulfoniopropionate (DMSP). Large amounts are produced annually by marine phytoplankton and its turnover plays a significant role in carbon and sulfur cycling in the surface ocean. Cleavage of DMSP leads to formation of dimethylsulfide (DMS). DMS partly escapes to the atmosphere while bacteria will oxidize large amounts of DMS in the water column before it can be released to the atmosphere. Anaerobic metabolism of DMS may result in the production of methane. Here we focus on the coupling of methane production/consumption cycle with DMSP turnover in polar water during phytoplankton bloom especially in the marginal ice zone.

Work at sea

Methane concentrations were measured at 50 stations in the Barents Sea, Kara Sea, Laptev Sea and in the central Arctic Ocean. Water samples were collected in Niskin bottles mounted on a rosette sampler from 200 m depths up to the surface. The dissolved gases were immediately extracted from the water and were analysed for methane by gas chromatograph equipped with a flame ionization detector (FID) on board ship. Gas samples were stored for investigations of the $\delta^{13}\text{C}_{\text{CH}_4}$ values in the home laboratory. Furthermore at each station samples for the analyses of DMSP (p), DMSP (d), were taken, which will be analyzed in the home lab.

Preliminary results

Methane in situ production occurs during the summer phytoplankton bloom in surface water indicated by increased methane concentrations. The highest methane concentration is detected at the marginal ice zone shown along a transect running from an open water region up to under the ice figure 5.11.

In the shallow shelf area of the Laptev Sea unusually extended methane anomaly is indicated by methane concentrations up to 300 nM, which exceeds the equilibrium concentration with the atmosphere up to hundredfold. Here the strong water stratification and freshwater inflows primarily restrict the sea to air flux of methane during summer and consequently favour the accumulation of methane in the water column. Conspicuous is the missing methane oxidation, which should be under consideration for deeper understanding of the recently marine methane cycle.

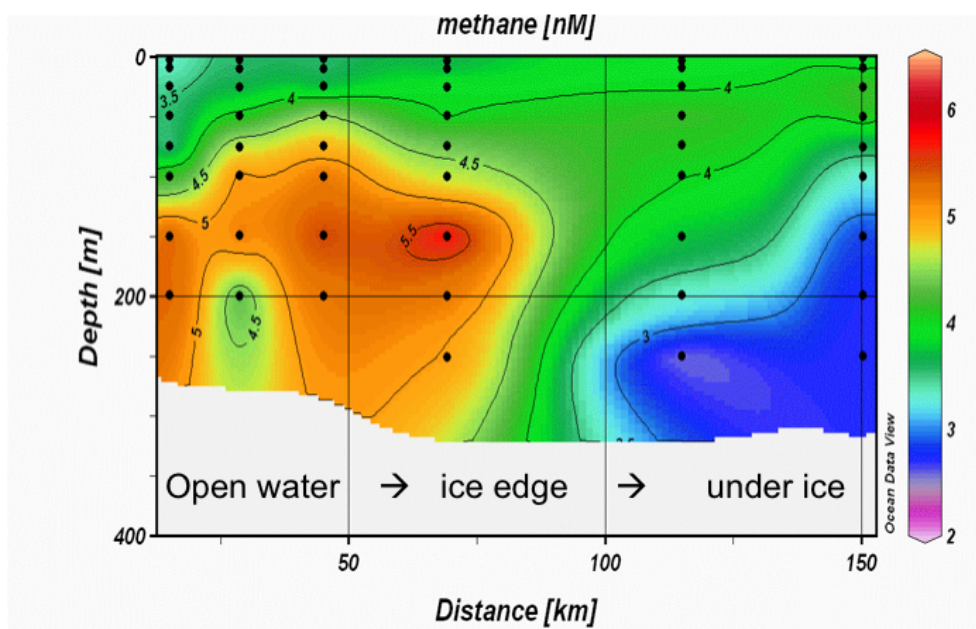


Fig. 5.11: Methane concentration in polar surface water

6. MARINE BIOLOGY

6.1 Zooplankton investigations

Kristina Barz¹, Adrian Basilico¹,
Ksenia Kosobokova², Antoine
Nowaczyk³

¹Alfred-Wegener-Institut

²Shirshov institute of Oceanology

³Laboratoire d'Océanographie et de
Biogéochimie

Background and objectives

Biological investigations in the Greenland Sea and Eurasian Basin in the 1990s demonstrated that the composition and distribution of pelagic fauna in the Arctic Ocean is strongly affected by the inflow of Atlantic water (Hirche & Mumm, 1992, Mumm, 1993; Kosobokova, Hirche, 2000). This inflow advects North-Atlantic zooplankton populations from the Greenland Sea via the Fram Strait and from the Barents Sea shelf into the Eurasian Basin (Hirche & Mumm, 1992; Kosobokova & Hirche, 2000). The conditions to which these populations are physiologically adapted are quite different from the conditions in the Arctic Ocean, so that their survival in the Arctic largely depends on their tolerance to Arctic conditions. While many species die off shortly after entering the Arctic Ocean, others survive due to their starvation potential or even continue their development for some time. Consequently, the Arctic Ocean is a large sink for organic carbon produced in the North Atlantic, with the region of sedimentation dependent on transport velocity and survival time.

During the 1990s, various observations indicated that the circulation of Atlantic-derived water in the Arctic Ocean had changed considerably. In the Eurasian Basin the Atlantic layer had become warmer and saltier (Schauer et al., 2004) and the boundary between the Atlantic and Pacific waters moved into the Canada Basin to an extent not previously observed (McLaughlin et al., 2002). These changes may have strong consequences for the pelagic ecosystems and hence sequestration of carbon and biogeochemical cycles in the Arctic Ocean. An increase of advection of Atlantic populations may significantly increase the sedimentation of advected biogenic material. Further warming could favour the survival of the highly productive Atlantic communities, which finally could replace the Arctic fauna characterized by low biomass and low production (Hirche & Mumm, 1992; Kosobokova & Hirche, 2000).

In order to understand the processes and factors regulating advection of Atlantic zooplankton in the western Arctic and trophodynamic processes in the Arctic pelagic communities, the zooplankton work focused on the following aspects:

- composition and spatial distribution of zooplankton on transects perpendicular to the continental slope and across the ridges in relation to the Atlantic water inflow

- starvation potential of *C. finmarchicus* as an estimate of the tolerance of this Atlantic copepod to the Arctic conditions - low temperature and poor food availability
- analyses of organic carbon content, C/N ratio, stable isotopes ratio, dry mass, and lipid composition to understand the life strategies and trophodynamic relationships in the Arctic pelagic food web
- reproductive biology and life strategies of mesopelagic copepods to understand adaptations of the deep-water plankters to short pulsed flux of organic matter down to the Arctic deep sea
- role of small plankton animals (1 - 2 mm) in the Arctic food web and their adaptations to the environment

References

- Hirche, HJ & Mumm, N (1992). Distribution of dominant copepods in the Nansen Basin, Arctic Ocean, in summer. *Deep-Sea Res.* 39 Suppl. 2: S485-S505.
- Kosobokova, KN & Hirche, HJ. (2000). Zooplankton distribution across the Lomonosov Ridge, Arctic Ocean: species inventory, biomass and vertical structure. *Deep-Sea Res I* 47: 2029-2060.
- McLaughlin, F., Carmack, E., MacDonald, R.W., Weaver, A.J. & Smith, J. (2002). The Canada Basin 1989–1995: Upstream events and farfield effects of the Barents Sea, *J. Geophys. Res.* 107, doi:10.1029/2001JC000904.
- Mumm, N. (1993). Composition and distribution of mesozooplankton in the Nansen Basin, Arctic Ocean, during summer. *Polar Biol.* 13: 451-461.
- Schauer, U., E. Fahrbach, S. Osterhus, and G. Rohardt (2004), Arctic warming through the Fram Strait: Oceanic heat transport from 3 years of measurements, *Journal of Geophysical Research*, 109(C06026), 10.1029/2003JC001823.

6.1.2 Zooplankton sampling

Kristina Barz¹, Adrian Basilico¹, Ksenia
Kosobokova², Antoine Nowaczyk³

¹Alfred-Wegener-Institut

²Shirshov institute of Oceanology

³Laboratoire d'Océanographie et de
Biogéochimie

For the investigation of the species composition and distribution, zooplankton were collected by a multiple closing net (XXL multi-net, 0.5 µm² mouth opening, 150 µm mesh size, Hydrobios, Kiel), which provided stratified sampling of the entire water column from the surface to the bottom. Multi-net sampling was carried out on five transects. Three of them extended seaward from the outer continental shelf over the continental slope into the deep Nansen and Makarov Basins north of the Barents, western Kara and Laptev Seas (Transects A, B, E). Transect C extended from the north-eastern continental slope of the Kara Sea into the deep Nansen Basin, crossed the Nansen-Gakkel Ridge, deep Amundsen Basin, the Lomonosov Ridge at latitude 88°N, and then extended into the deep Makarov Basin up to the Alfa-Mendelejev Ridge. Transect D extended from the deep Makarov Basin across the Lomonosov Ridge to the Nansen-Gakkel Ridge along 85 - 86°N. Between three and five multi-net stations were taken on transects A, B, D, and E, and fifteen stations along transect C.

6.1 Zooplankton investigations

From four to eight layers were sampled in the shelf region, and nine depth layers at all stations off the shelf.

In total, 30 multi-net stations were taken: four in the shelf region, seven in the slope region and 19 in the deep basins (eleven of them in the area deeper than 3,000 m, and two deeper than 4,000 m, Fig. 6.1). The samples were preserved in 4 % borax-buffered formaldehyde for further processing.

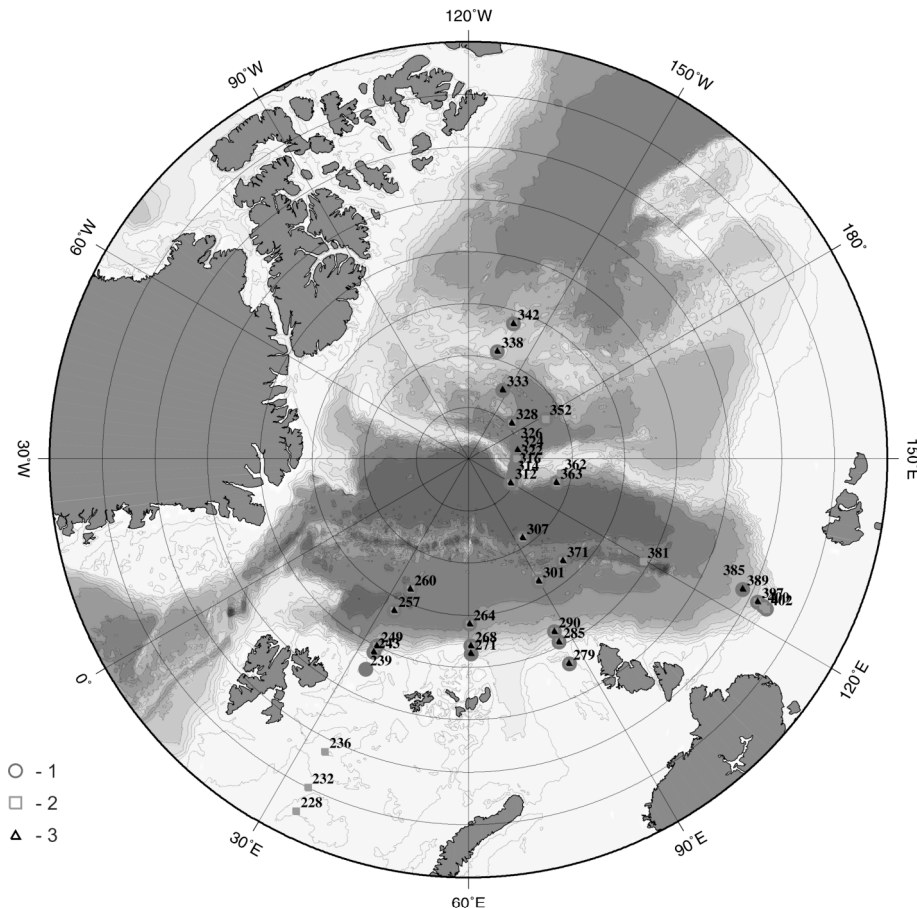


Fig. 6.1.1: Zooplankton station locations. 1 – Multi-net; 2 – Bongo net, 100 μm and 300 μm mesh size; 3 – Bongo net, 300 μm and 500 μm mesh size

For the study of life strategies and trophodynamics of the Arctic pelagic food web, zooplankton were collected by Bongo nets towed vertically from the upper 100 m and 1,500 m. The catches of the 100 and 300 μm mesh size nets were used for experiments with live small plankton organisms (grazing, excretion, gut evacuation rate, oxygen consumption). The catches of 300 and 500 μm mesh size nets were used to collect larger animals, e.g., *Calanus finmarchicus*, for starvation experiments, and *C. finmarchicus* and other copepods for analyses of carbon, C/N ratio, lipid composition, stable isotope ratios, dry weight, and egg production experiments. In total, Bongo nets were taken at 54 stations (Fig. 6.1).

6.1.2 Starvation experiments

Kristina Barz¹⁾, Adrian Basilico¹⁾,
Ksenia Kosobokova²⁾,

¹⁾Alfred-Wegener-Institut
²⁾Shirshov institute of Oceanology

Starvation experiments were carried out with *Calanus finmarchicus* adult females and copepodite stage V (CV). Three experiments were set up: (1) with animals collected on the shelf of the Barents Sea (st. 232), (2) with animals from the northern slope of the Barents Sea influenced by the Atlantic water inflow (st. 243), and (3) with animals collected west of the crest of the Lomonosov Ridge at 88° N in the back flow of Atlantic water (st. 312). *C. finmarchicus* were sorted out of the Bongo net catches immediately after capture. Five replicates of CVs were set up in the first experiment, 3 of adult females and 2 of CVs in the second, and 2 replicates of adult females and 2 of CVs in the third experiment. Each replicate contained 50 specimens. Animals were placed in five 2,000 ml Plexiglas insets with 300 - 500 µm mesh false bottoms suspended in 3,000 ml TPX jars. The jars were filled with filtered sea water and kept at dim light at temperatures between -1.0 and +0.5° C. The condition of animals was checked every second day, dead specimens were removed, counted and preserved in 4 % formaldehyde. The water was exchanged on the third day after set up of each experiment, and every second week thereafter.

After 30 days of starvation, 10 CV specimens were removed from the first experiment at random and stored for Corg content analysis. From the second and third experiments, 8 females and 8 CV specimens were removed after 30 days for the same purpose. After 60 days of starvation the same amount of animals were again removed for Corg analyses from each pool of experimental animals.

Preliminary results

The first two experiments were set up on 2 and 3 August, and thus lasted for nearly two months until the end of the cruise, while the third experiment was set up at the very end of August and lasted 5 weeks. In all experiments, the number of animals decreased by the end of observational period, although the patterns of decrease differed between the experiments and between stages within the same experiment.

In Exp.1 with CVs from the northern Barents Sea there was no mortality within the first 9 days after setup (Fig. 6.1.2 a.). During the following two months abundance was decreasing at a rate of ca. 4 ind day⁻¹. After 2 months only ca. 10 % of the animals survived (Fig. 6.1.2). Some of them moulted to adult females, which might have caused high mortality.

In Exp.2 with animals collected north of Svalbard, the first dead females were observed on day 9, and the first dead CVs on day 17 (Fig. 6.1.3 a, b). The mortality rates were lower than in Exp.1. In CVs a rate of ca. 0.6 ind day⁻¹ was observed, while in females it was ca. 1.3 ind day⁻¹. By the end of the observational period, ca. 70 % of CVs and 45 % of females had survived.

In Exp.3 during the first 12 days a few CVs and females died (Fig. 6.1.4 a, b), however, mortality rate was quite low. Within the next 25 days of observations the mortality rate in CVs averaged 0.7, and in females 1.6 ind day⁻¹. The mortality rates

were higher in adult females compared to CVs in both Exp.1 and Exp.2. The experiments will be continued at AWI.

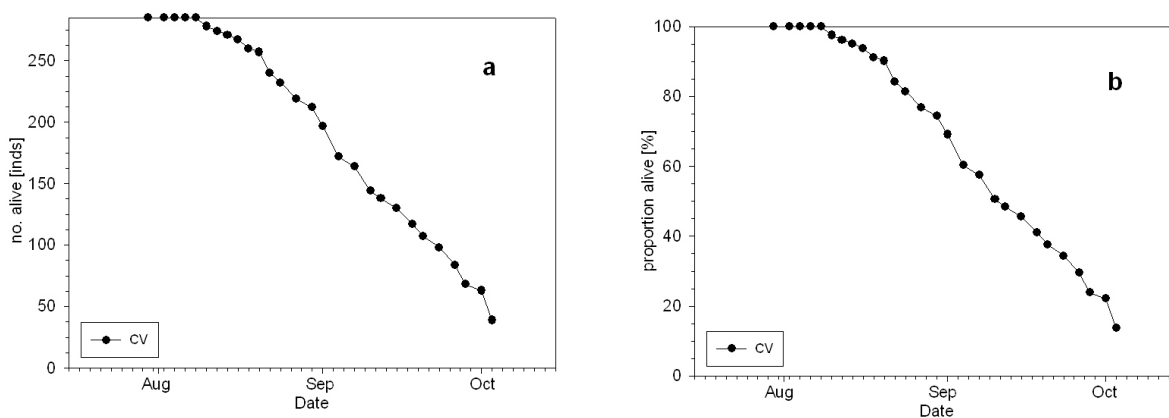


Fig. 6.1.2 a, b: *Calanus finmarchicus*, starvation experiment 1, st. 232. a – number of alive specimens, b – proportion (%) of alive specimens

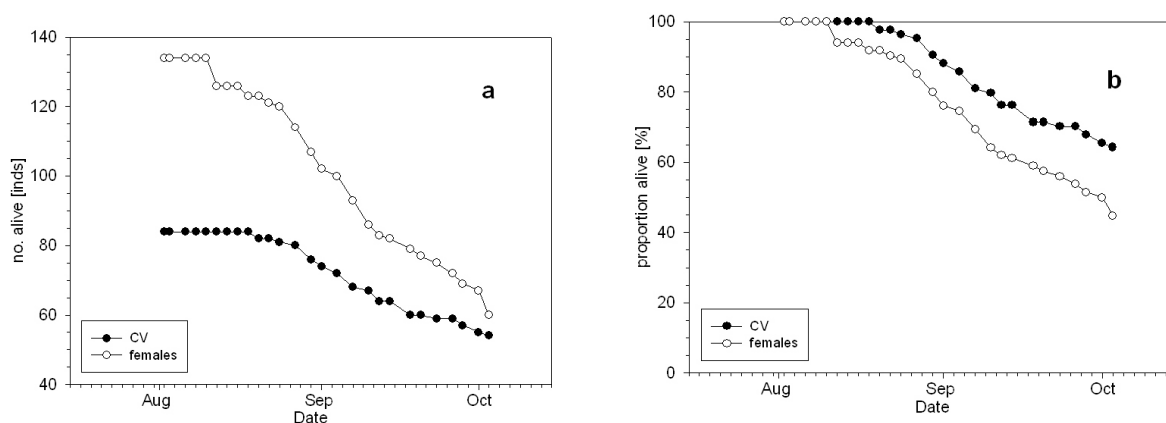


Fig. 6.1.3 a, b: *Calanus finmarchicus*, starvation experiment 2, st. 243. a – number of alive specimens, b – proportion (%) of alive specimens

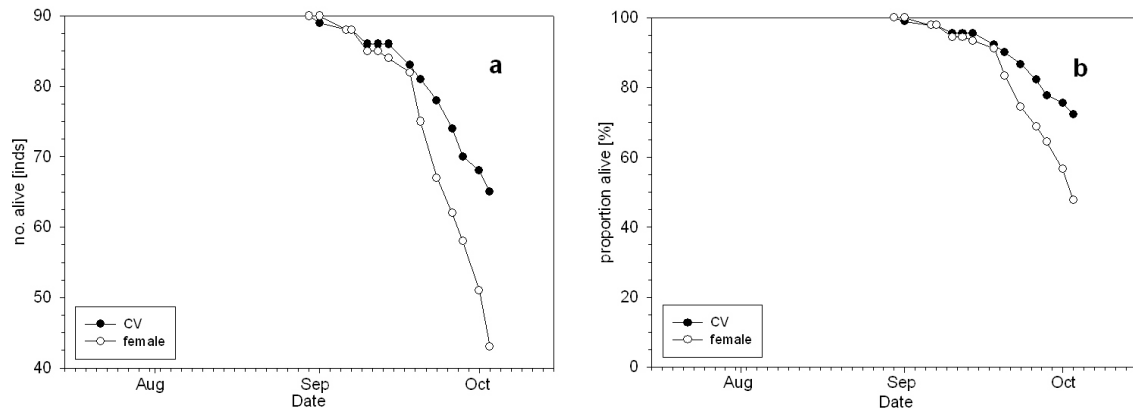


Fig. 6.1.4 a, b: *Calanus finmarchicus*, starvation experiment 3, st. 312. a – number of alive specimens, b – proportion (%) of alive specimens

6.1.3 Organic carbon content, C/N ratio, stable isotope ratios and dry mass measurements

Kristina Barz¹⁾, Ksenia Kosobokova²⁾,

¹⁾Alfred-Wegener-Institut

²⁾Shirshov institute of Oceanology

Adult animals, eggs and copepodite stages II-V of 29 copepod species, and eggs and embryos of a chaetognath *Eukrohnia hamata* were collected for measurements of organic carbon content, C/N ratio, dry mass and lipid composition. Live specimens of target species were sorted from Bongo net catches immediately after collection, pre-sorted to species and stage level and kept in filtered sea water for 24 hours.

For carbon content, C/N ratio, stable isotope ratios and dry mass measurements, 1 to 5 specimens of large animals (5 - 10 mm) and 20 to 100 smaller ones (2 - 5 mm) with empty guts were used for each replicate. The specimens were shortly rinsed in distilled water and placed in tin caps. For dry weight measurements, animals were placed in pre-weighted aluminum caps. Whenever possible, 2 - 3 replicates of each stage of each particular species were prepared for each analysis. The samples were stored at -80° C.

For lipid composition analyses animals were transferred to Dichlormethane-Methanol (2:1) and stored at -20° C.

6.1.4 Reproductive biology of pelagic copepods

Adrian Basilico¹⁾, Ksenia
Kosobokova²⁾

¹⁾Alfred-Wegener-Institut

²⁾Shirshov institute of Oceanology

Egg production experiments were carried out with the interzonal copepod *Calanus finmarchicus*, *C. glacialis*, and the mesopelagic *Paraeuchaeta glacialis*, *Gaetanus tenuispinus*, and *G. brevispinus*. Clutch size was also assessed for the mesopelagic

species *P. barbata*, *P. polaris*, *Chiridius obtusifrons*, *Augaptilus glacialis*, and *Euaugaptilus hyperboreus*.

Calanus finmarchicus and *C. glacialis* used for egg production experiments were sorted from the 0 - 1,500 m Bongo net catches immediately after capture. 25 – 30 single females of each species were placed in cell wells filled with filtered sea-water from the 0 - 100 m water layer. Additionally, 25 - 30 females were pooled in 150 ml Plexiglas insets with a mesh (300 - 500 μm) false bottom to separate eggs from females. These were then suspended in 250 ml TPX jars containing filtered sea water. Egg production during the first 24 hours was used as a measure of the actual rate in the field (*in-situ* egg production rate).

Mature females of mesopelagic species were also sorted immediately after capture for egg production studies. Single females of the free-spawning *Gaetanus tenuispinus*, and *G. brevispinus* were placed in cell wells filled with pre-screened seawater collected from below 300 m. They were incubated at dim light at temperatures between -1.0°C and $+0.5^{\circ}\text{C}$. The females were checked every 12 h for egg production. Eggs were counted and removed; subsequently, egg size was measured and egg morphology was studied under a stereomicroscope. Females of egg-brooding *Paraeuchaeta barbata*, *P. polaris*, *Chiridius obtusifrons*, *Augaptilus glacialis*, and *Euaugaptilus hyperboreus* were also sorted immediately after capture, and the number of eggs in the egg sacs was counted after preservation in 4 % borax-buffered formaldehyde. The formaldehyde-preserved multi-net catches were additionally used to enumerate and measure eggs in the egg sacs of these egg-brooding species. The clutch size was estimated as the number of eggs produced during one spawning event by a free-spawning or egg-brooding female. Female prosome and total length were measured under a stereomicroscope at 25 x magnification.

Egg-bearing females of *P. glacialis* and females with developing eggs in the ovaries were sorted alive and incubated in 250 ml TPX jars at -1.0°C to $+0.5^{\circ}\text{C}$ to assess the duration of egg development and spawning intervals. Females were checked daily for egg production. Hatching nauplii were counted and removed.

Preliminary results

Egg production experiments with *Calanus glacialis* were carried out at 9 stations. Spawning females were observed on the slope north of Franz Josef Land and on the northern Kara Sea shelf only (sts. 268, 271, 279). Egg production rate (EPR) was generally low and varied from 0.6 to 4.5 eggs $\text{fem}^{-1} \text{d}^{-1}$. The only exception was st. 271, where EPR reached 13.5 eggs $\text{fem}^{-1} \text{d}^{-1}$. Individual clutch size varied from 16 to 19 eggs fem^{-1} . No egg production was observed on the Barents Sea shelf (st. 236) or in the ice-covered deep basins (st. 257, 260, 264, 338, 371).

Egg production experiments with *C. finmarchicus* were carried out at 4 stations (sts. 243, 268, 271, 279). Egg-laying was observed at the only station 271 north of the Franz Josef Land. Average EPR for the pooled 84 females was 1.95 eggs $\text{fem}^{-1} \text{d}^{-1}$, individual clutch size varied from 21 to 31 eggs fem^{-1} .

Observations on egg production of mesopelagic copepods were carried out at 18 stations. In total, successful reproduction was observed in 62 specimens of 8 species.

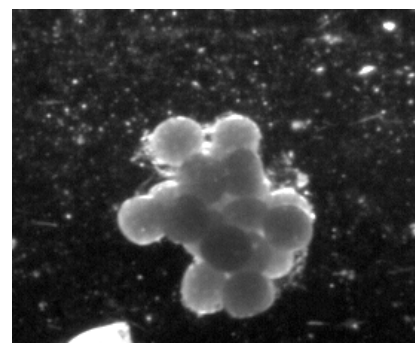
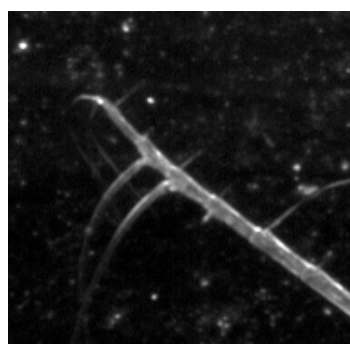
6.1.5 LOKI

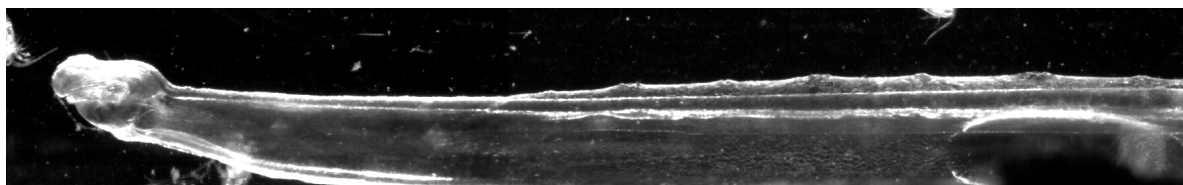
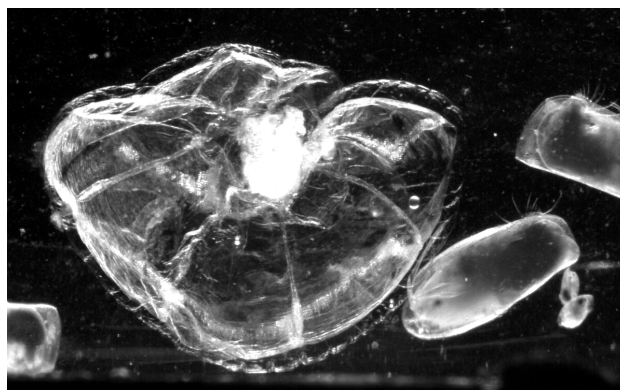
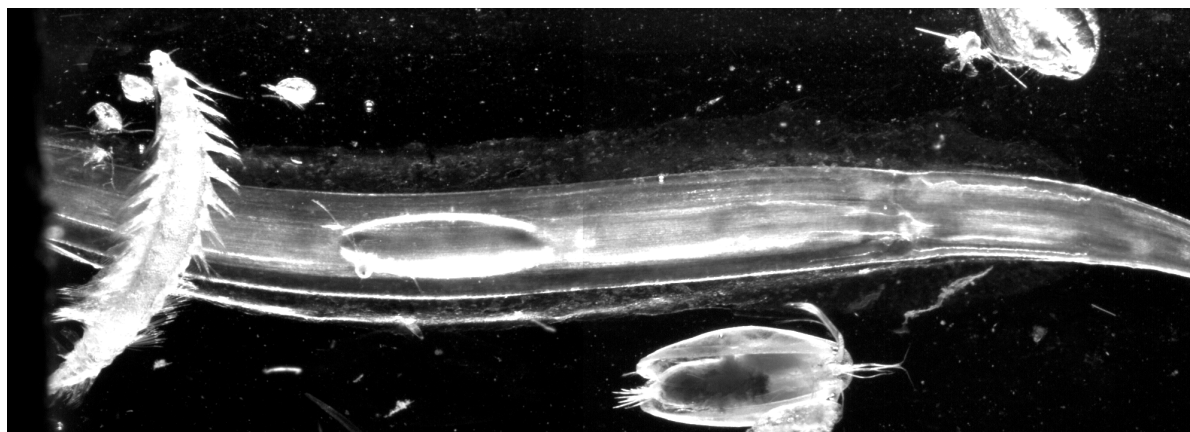
Adrian Basilico
Alfred-Wegener-Institut

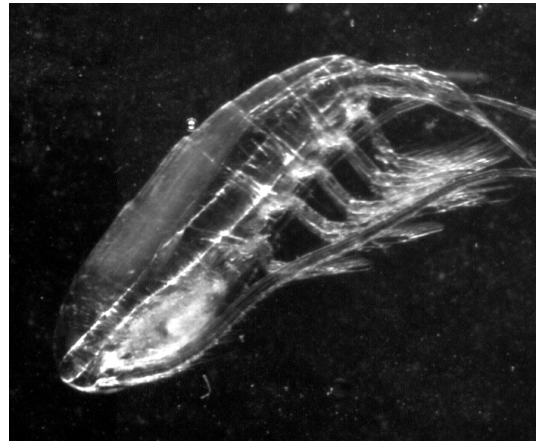
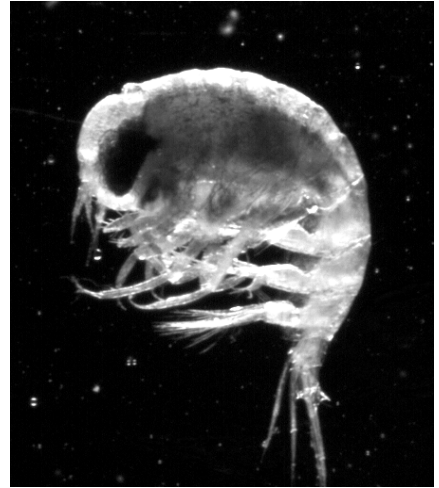
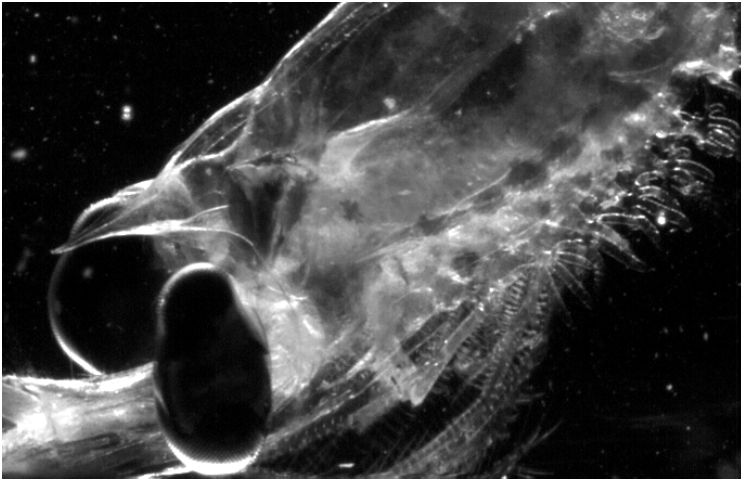
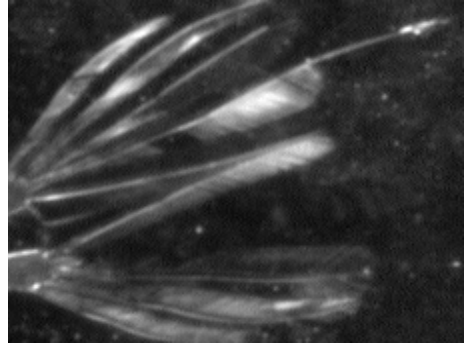
LOKI

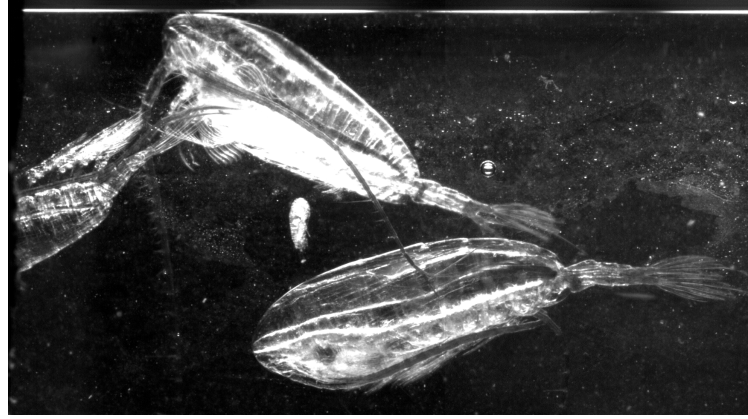
The newly developed system FLOKI (Flowthrough Onsite Key species Investigation) was tested on the cruise for the first time in the field. This system produces high-resolution pictures of objects in the size spectrum between 200 μm and nearly 2 cm. It is the aim of this system to store images of live organisms, which are easier identified than preserved material, and thus to facilitate zooplankton counting. FLOKI consists of a digital camera with 4 megapixels resolution, which acquires pictures at a rate of 15 images/sec from particles passing through a glass cuvette of 2*1*0.4 cm (length, width, height). The sample is pumped through the cuvette at a rate of ca. 100 ml min^{-1} . Each object of a certain light intensity (region of interest) is cut out and stored separately on a hard disk. In the laboratory, the images will be screened and sorted by an image analysis programme.

15 Bongo net (100 μm , 300 μm) samples were processed by FLOKI during the cruise. After initial technical problems the instrument worked well, and more than half a million pictures were taken and sorted (Fig. 6.1.5). The test revealed some technical problems, that will need amendment. Thus, air bubbles in and steam on the cuvette were probably the result of too large temperature differences between sample and working location of FLOKI. The pumping speed will need to be increased for fast swimming large animals as found in the Arctic, cuvette size and correspondent tubing should be customisable to organism size. The results of the FLOKI counts will be compared with manual counts.









6.1.6 Role of small plankton and trophodynamic relationships in the Arctic pelagic food web

Antoine Nowaczyk

Laboratoire d'oceanographie et de Biogeochemie

Among the copepods present in the Arctic Ocean, the cosmopolitan and small *Oithona similis*, the Atlantic *Calanus finmarchicus*, and the Arctic *Calanus glacialis*, *Calanus hyperboreus* and *Metridia longa* are the major objects of the study. *O. similis* is one of the most abundant zooplanktonic organisms in all oceans. The other chosen species strongly dominate the zooplankton biomass in the Arctic Ocean. In order to quantify their grazing impact on lower trophic levels and to study the mechanisms of adaptation of small and large-sized organisms to the conditions in the Arctic pelagic ecosystem, process studies were performed.

From the 100 µm mesh size Bongo net tows (0 - 100 m), samples were collected at 19 stations (Table 6.1), quickly filtered onto GF/F filters, frozen in liquid nitrogen then transferred to the -80° C freezer. Instantaneous measurements of feeding through pigment gut contents, amino and fatty acids will be assessed from these samples at a specific level. Upon return to the lab, pigment gut contents will be performed by fluorimetry according to Dam and Peterson. Amino acids and fatty acids composition will be measured by gas chromatography. The composition of those compounds will also give a good indication of the recent feeding history of the individuals studied (most common species). The data will be used to assess the grazing impact of each species and the daily removal of phytoplankton.

Feeding experiments were run throughout the cruise at 16 stations (Table 6.1). Live individuals (i.e. moving under the dissecting microscope) of *Oithona sp.*, *C. finmarchicus*, *C. glacialis*, *C. hyperboreus* and *M. longa* were transferred to incubation bottles containing water collected at the chlorophyll max. Feeding rates will be assessed through measurements of pigment composition between control and experimental bottles. HPLC analysis will allow the determination of preferential

grazing of taxonomical groups of phytoplankton (CHEMTAX). Water was also preserved (acid lugol) for microscopic analysis.

Excretion experiments were run at 16 stations. In order to measure the ammonium and phosphate excretion of the main species of copepods (same as for the feeding experiments), individuals were incubated in filtered 0.2 μm sea water. At the end of the experiment, samples were frozen at -20°C and will be analyzed upon return to the lab using a technicon autoanalyser and low phosphate method (MAGIC method: Rimmelin, P. & T. Moutin. 2005. Re-examination of the MAGIC method to determine low orthophosphate concentration in seawater. *Analytica Chimica Acta*, 548(1-2), 174-182). To estimate the diurnal variability of excretion rate, a 48h experiment was carried out at station PS 70/379, water sub samples were taken at 2, 5, 9, 13, 17, 21, 24, 36 and 48 hours.

Gut evacuation rates experiments were carried out at 4 stations in order to estimate phytoplankton ingestion rates from gut contents.

Individuals collected at each station as well as those from the experiments were measured under a dissecting microscope and frozen at -80°C for subsequent measurements of dry weight and C/N/P contents.

Table 6.1: Experiments

Stations	Specific Instantaneous rates Gut contents Amino acid Fatty acid C/N/P contents	Excretion experiment	Feeding Experiment	Feeding experiment large volume	Abundance	Gut evacuation rate
70/232	x		X			
70/236	x	x				
70/243	x	x	X	X		
70/257	x	x	X	X		
70/260	x	x	x			
70/264	x	x	x	X		
70/268	x	x	x			
70/279	x	x	x	X		
70/290	x	x	x			
70/301	x	x	x			
70/307	x	x	x			
70/312	x	x	x	X	x	
70/322	x	x			x	
70/328	x	x	x		x	

70/338	x	x	x	X	x	x
70/352	x	x	x		x	
70/362	x					x
70/371	x					x
70/385	x					x
TOTAL	19	15	15	6	5	4

Reference

Rimmelin, P. & T. Moutin. 2005. Re-examination of the MAGIC method to determine low orthophosphate concentration in seawater. *Analytica Chimica Acta*, 548(1-2), 174-182.

6.2 Biodiversity of polar deep-sea eukaryotic microbiota - molecular versus morphological approach

Béatrice Lecroq
University of Geneva Sciences III

Background

Over the past few years, cultivation-independent identification of microbial organisms by PCR amplification and sequencing of ribosomal RNA genes revealed a huge diversity of microbiota in environmental samples. Many new species and higher-level lineages have been discovered. However, the microbial diversity in the polar deep-sea benthos is still largely unexplored. Foraminifera and the closely related large testate (shell-bearing) gromiids, are a significant and often visually conspicuous component of the deep-sea and high-latitude benthic fauna. In addition to the geologically important and well-known calcareous foraminifera, deep-sea and high-latitude assemblages include substantial numbers of soft-shelled, mostly single chambered species, most of which are undescribed. Our previous studies of polar Foraminifera revealed exceptionally high morphological and molecular diversity of some monothalamous (single-chambered) morphospecies, particularly abundant in high-latitude settings (Gooday et al., 1996, Pawlowski et al., 2002, Pawlowski et al., 2005). On the other hand, we found very weak genetic differentiation between some common Arctic and Antarctic deep-sea calcareous species (Pawlowski et al., 2007).

Objectives

The main objective of this project was to examine the diversity of microbial eukaryotes (protists) in deep-sea Arctic sediments by using environmental DNA approach. The project is focus on two important groups of marine protists: Foraminifera and Cercozoa. Both groups belong to the recently established supergroup of Rhizaria (Nikolaev et al., 2004).

Using material collected during this cruise, we aim to

- (1) obtain rDNA sequence data for broad taxon sampling of Arctic Foraminifera and Cercozoa;
- (2) establish their phylogenetic relationships with Antarctic and other deep-sea species;
- (3) describe new species based on their morphological and genetic characteristics.

Methods

The foraminifera were isolated from surface sediment samples (1 - 2 cm) collected by multicorer (usually 1 or 2 cores were examined for each site) and boxcorer (about 100 cm² were collected for each corer). 5 ml of the surface sediment was collected and immediately deep frozen in the liquid nitrogen. These samples will be used for total DNA extraction and study of microbial eukaryote diversity. The rest of sediment was sieved through the sieves of 0.5 mm, 0.125 mm and 0.063 mm. The sieving took place in the cooler container and the samples were stored at 3° C. The samples were examined at dissecting microscopes and all living foraminifera were isolated. The isolated foraminifera were identified, photographed with digital camera mounted on the microscope and later either immediately processed for DNA extraction or frozen in the liquid nitrogen. Some species have been fixed in the formalin for further morphological study.

Preliminary Results

During the course of the expedition a total of 30 stations were sampled, yielding 608 DNA extracts, 30 samples of frozen sediment for total environmental DNA analysis and 31 preserved specimens in formalin (Table 6.2).

A total of 84 morphospecies regrouped under 50 Genera were identified (Fig. 6.2.1). Regarding the stations, samples showed great differences in abundance and composition of living specimens. Further investigations might be able to precise whether the depth could also be involved in those diversities differences. The number of specimens sampled, isolated, extracted and fixed fully satisfy the quantitative objective of this campaign. This will enable a successful comparison of this material with specimens previously sampled in other parts of the world.

Tab. 6.2: Summary of the samples collected in each station

Stations	Frozen sedimental samples	Specimens preserved in Formaline	DNA extractions in Guanidine or AP1 buffer	Genera
239-6	5	0	57	19
260-5	1	0	1	1
263-2	4	14	24	8
265-1	3	0	13	6
265-2	2	1	9	6
266-7	2	0	53	3
271-5	3	0	73	13
276-7	3	0	16	10
277-2	3	0	14	7
279-12	3	0	1	1

6.2 Biodiversity of polar deep-sea eukaryotic microbiota - molecular versus morphological approach

Stations	Frozen sedimental samples	Specimens preserved in Formaline	DNA extractions in Guanidine or AP1 buffer	Genera
282-2	3	1	7	39
285-6	2	0	9	20
285-7	3	0	22	10
294-2	3	8	22	4
294-3	2	0	3	2
299-2	3	0	3	2
301-11	3	0	1	1
306-2	2	1	22	10
309-8	3	6	21	6
316-5	2	0	14	5
316-6	2	0	20	8
319-2	2	0	7	24
330-1	3	0	71	4
333-4	3	0	28	4
338-9	3	0	16	5
342-10	3	0	11	5
352-3	2	0	14	7
358-3	3	0	38	16
384-1	2	0	9	7
385-9	2	0	9	5
Total	80	31	608	50

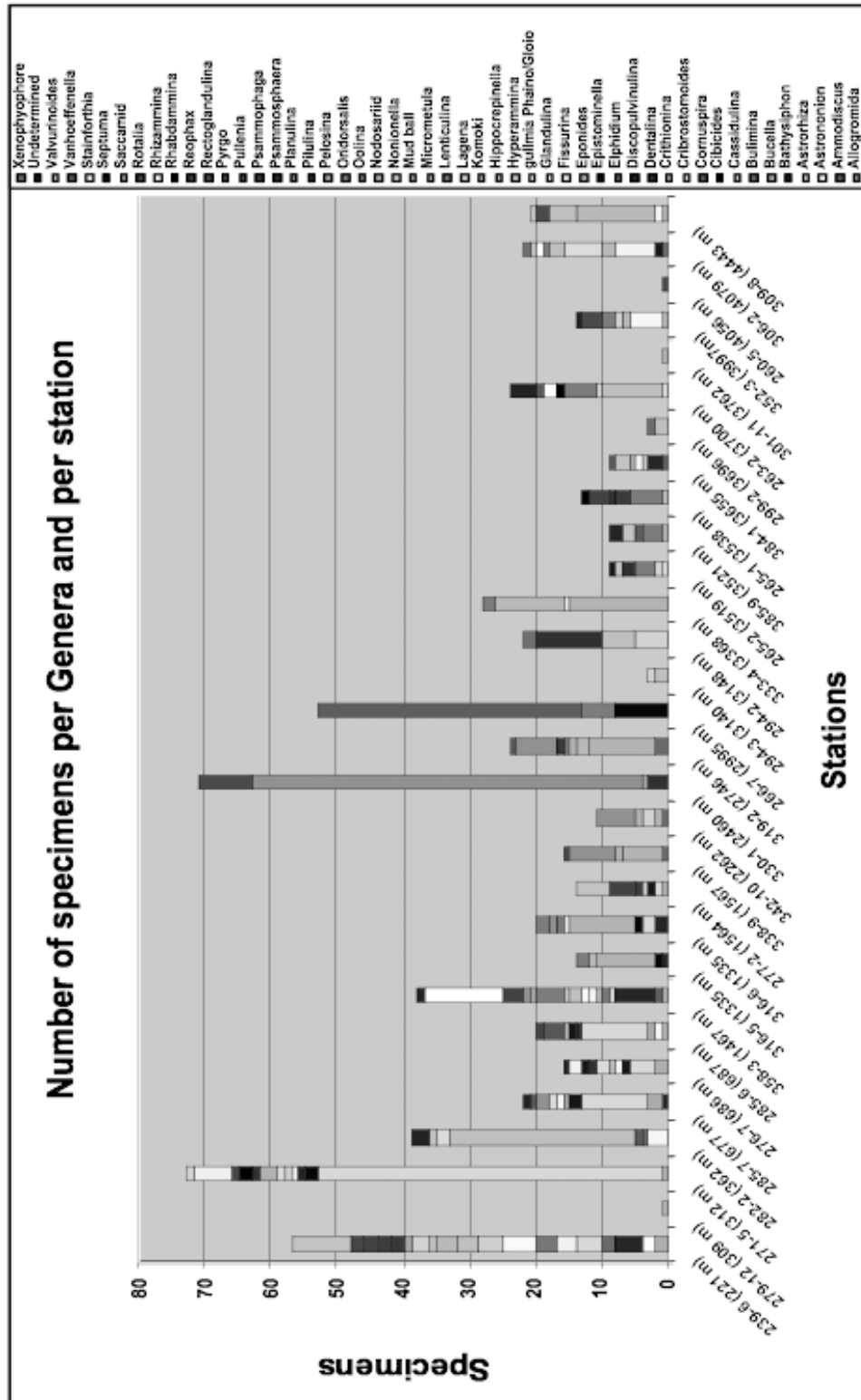


Fig. 6.2.1. Number of specimens per Genera and per station (with depths of the stations)

References

- Gooday, A.J., Bowser, S.S. and Bernhard, J.M., (1996) Benthic foraminiferal assemblages in Explorers Cove, Antarctica: A shallow-water site with deep-sea characteristics. *Prog. Oceanog.* 37: 117-166.
- Nikolaev, S.I., Berney, C., Fahrni, J., Bolivar, I., Polet, S., Mylnikov, A.P., Aleshin, V.V., Petrov, N.B., Pawlowski, J. (2004) The twilight of Heliozoa and rise of Rhizaria: an emerging supergroup of amoeboid eukaryotes. *Proc. Natl. Acad. Sci. USA* 101:8066- 8071.
- Pawlowski, J., Fahrni, J.F., Brykczynska, U., Habura, A., Bowser, S.S. (2002) Molecular data reveal high taxonomic diversity of allogromiid Foraminifera in Explorers Cove (McMurdo Sound, Antarctica). *Polar Biology* 25: 96-105.
- Pawlowski, J., Fahrni, J.F., Guiard, J., Konlan, K., Hardecker, J., Habura, A., Bowser, S.S. (2005) Allogromiid foraminifera and gromiids from under the Ross Ice Shelf: morphological and molecular diversity. *Polar Biology* 28:514-522
- Pawlowski J., Fahrni J., Lecroq B., Longet D., Cornelius N., Excoffier L., Cedhagen T., Gooday A.J. (2007) Bipolar gene flow in deep-sea foraminifera. *Molecular Ecology*. 16 :4089-96.

Acknowledgements

The author would like to thank the captain Stefan Schwarze and his crew for the optimal working conditions they provided at sea. I am also extremely grateful to the Alfred-Wegener-Institut and the members which have supervised this cruise. Finally I wish to say a very special thank to Robert Spielhagen, Anna Schmidt, Kristin Daniel and Norbert Lensch for their great help in corers manipulation and to Antoine Nowaczyk and Charles-Edouard Thuroczy for their rich collaboration in the laboratory.

7. MARINE GEOLOGY

Kristin Daniel¹⁾, Catalina Gebhardt¹⁾,
Norbert Lensch¹⁾, Valery Rusakov³⁾,
Anna Schmidt²⁾, Pjotr Semenov⁴⁾,
Robert Spielhagen²⁾

¹⁾Alfred-Wegener-Institut

²⁾IFM-GEOMAR

³⁾Vernadsky Institut of Geochemistry and
Analytical Chemistry

⁴⁾VNIIO All-Russia Research Institute for
Geology and Mineral Resources of the
World Ocean

Background and goals

Paleoenvironmental changes in and around the Arctic Ocean have been fundamental in the last 1 million years and especially in the last 200,000 years. Terrestrial and marine research has revealed a high variability of ice sheets on the circum-Arctic continents and equally important changes in the ice coverage and Atlantic Water inflow in the Arctic Ocean and the river-runoff. Arctic river run-off is of vital importance for the Arctic low saline surface water outflow and the formation of the Arctic sea ice cover, both a prerequisite for the maintenance of strong oceanographic contrasts in the Nordic Seas and the deepwater renewal, which runs the thermohaline convection (THC), as well as for the sediment and chemical budgets of the Arctic Ocean. While there is some evidence for Holocene variability of river-runoff from earlier studies in the southern Kara Sea (SIRRO Project), knowledge for changes in the deglaciation, the Weichselian, and the last interglacial ("Eemian") are scarce. It was unknown prior to cruise ARK-XXII/2 whether the river run-off across the Kara Sea shelf was blocked by the northern Eurasian ice sheet during part of the last glacial maximum (LGM). For earlier glacial episodes, the exact glacial limits of ice sheets on the Kara Sea are also elusive. The position of the ice front and its variability must have exerted enormous influence on the sediment export to the Arctic Eurasian Basin (debris flows, turbidites etc.). It was one of the goals to retrieve sediment cores from which the glacial history of the northern Kara Sea and its major outlets (the St. Anna and Voronin troughs) can be reconstructed at utmost high time resolution.

In the last two decades a number of sediment cores had been investigated which gave valuable information on the history of the Late Quaternary Arctic Ocean, its water masses, and its ice coverage. Most of these cores stemmed from the eastern Arctic Ocean (15°W-75°E) and the Lomonosov Ridge relatively close to the Pole. Marine geological information from the Siberian sector of the eastern Arctic Ocean and from the area beyond the Lomonosov Ridge was still rather scarce. The second major goal of cruise ARK-XXII/2 was therefore to increase the archive of sediment cores available for paleoenvironmental studies of the central Arctic Ocean with special emphasis of the Amerasian Basin.

7.1 Parasound sediment echosounding

Wiebke Nehmiz
FIELAX

Scientific objectives, technical settings and operation conditions

One of the fixed sensor installations onboard *Polarstern* is the sediment echosounder PARASOUND (Atlas Hydrographics, Bremen). The system provides digital, high resolution information on the sediment coverage and the internal structure of the sediments. This can be used to interpret the sedimentary environments and their changes in space and time. During ARK-XXII/2, the aim of PARASOUND profiling was to select coring locations for gravity cores, box cores, multi corer and kastenlot cores.

In order to obtain bottom and sub-bottom reflection patterns, the echosounder uses the so-called parametric effect: PARASOUND radiates two primary frequencies in the range of 18 to 23.5 kHz that generate a secondary pulse of lower frequency which provides the signal. This parametric frequency is the difference frequency of the two primary waves transmitted. The parametric frequency can be chosen between 2.5 and 5.5 kHz and is adjusted by varying the primary frequencies. During this cruise, the primary low frequency was set to 18 kHz and the primary high frequency was set to 22 kHz, so the signal had a frequency of 4 kHz. Due to its low secondary frequency and a small emitting angle of 2 degrees, PARASOUND achieves high resolution of the sediment structures and penetrating depths of around 70 meters with a possible vertical resolution of ca. 30 cm.

During ARK-XXII/2 only the operation mode Single Pulse was used with the registration of the full trace length including the water column. This mode transmits a beam and waits to send the next one until having stored the reflected signal. The former PAR mode of the DS2-System is now called Pulse Train and was not available on this trip yet. The parametric pulse length was always set to 2. Partly, heavy ice conditions affected the quality of the data negatively causing noisy records with some traces missing.

The PARASOUND system onboard *Polarstern*

The Atlas Parasound is a permanently installed hull mounted system on *Polarstern*. This highest level narrow-beam parametric sub-bottom profiler system for deep sea applications was upgraded to system version P-70 in May 2007. After the sea acceptance test was not passed during the leg ARK-XXII/1a, some parts of the system were not running stable, but nevertheless useful sediment information to take geological samples were acquired.

The hardware and software configuration using two Windows-based PCs for system control and data management, respectively, offers a lot of functions via both Operator and Data Storage PC. Data recording is done by the software ATLAS PARASTORE-3 (Atlas Hydrographics, Bremen). This software provides a user-friendly graphical interface and has been designed to acquire, visualize, process, store, convert, quality control, replay and print data from the profiles of the system. One additional PC is set up in the "Windleitstand" for watch keeping purposes and as a backup system.

During ARK-XXII/2, this was used once for data storage during a break down of the other two PCs.

Additionally to the features that were used on this cruise, the new system and the PARASTORE-3 software offer many more possibilities to adjust parameters and operate in different modes of sounding. Most of these are not used for standard procedures. On this cruise only settings were used that are comparable to the old system to be able to reproduce the standard of former cruises and to be able to compare the data sets acquired with the systems of different age.

Due to problems with the online-print function of the ATLAS PARASTORE-3 software (usually the software is supposed to be able to acquire, store and print the data simultaneously, but until now the online-print function has caused a complete crash of the software if the other two functions are used at the same time), the final visualisation of the PS3 data was done with the software SeNT (Hanno von Lom, Universität Bremen). The graphics were saved in the GIF format and printed out later than the data was acquired.

Data Management

The capabilities of ATLAS PARASTORE-3 in acquiring the PARASOUND data are two-fold: (i) simultaneously as raw data from the parametric channel and the NBS channel for full trace length including the water column, and (ii) selected in specific depth windows, in PS3 and SEG-Y formats. The recorded data of both parametric and NBS signals are stored in a hybrid raw data format (ASD format) in either a ring buffer or into user selected folders on hard disc. Either full soundings of both signals or defined depth windows can be acquired and stored. Optionally, the parametric data can be converted online into standard SEG-Y format for further processing using industrial post-processing software. In addition, the parametric data can be stored in the formerly used PS3 format. This function, however, requires careful watch keeping because only data kept in a selected depth window of commonly 200 m length is stored.

On this cruise, the data was stored as ASDF and PS3 formats for all time periods the system was running and data was stored. In addition, the replay option of PARASTORE-3 gives the opportunity to replay the soundings of parametric data and/or NBS data and record them again as PS3 and/or SEG-Y data.

Because all the data can be produced and stored simultaneously, a well-organized data management is necessary. In order to avoid confusion with the different formats and the status of the data, the data management was carried out by one designated person.

The data storage was organized in such a way that the parametric raw data (.asd files) and the subsequent data set of PS3 data (.ps3) were packed in four hour packages of the UNIX based TAR format (.tar files) and saved to the ships intern server space as well as the visualised graphics (.gif). For backup reasons, all changes to the server the resulting data collection is saved to are simultaneously copied to tape. Finally, LTO-tapes and a set of 30 DVDs with the complete data set of ASD, PS3 and GIF files were sent to AWI directly after the cruise. In addition to

this, meta-files were produced to ease the input of these files into the data base PANGAEA.

7.2 Bathymetry

Precise knowledge of the seafloor morphology is a basic requirement for geological work. Bathymetric data combined with parasound profiles allow a three-dimensional reconstruction of history of the upper sediment layers. Therefore, bathymetric data were recorded along with parasound data in the same areas.

During the ARK-XXII/2 expedition, depth measurements were carried out using ATLAS Hydrosweep DS-2, a deep-sea multibeam echo sounding system installed permanently on *Polarstern*. The hull-mounted Hydrosweep DS-2 system operates at a frequency of 15.5 kHz transmitting sound pulses perpendicular to the ship's long axis. In addition to depth measurements, echo amplitudes can be recorded and converted into multibeam sidescan and angular backscatter data.

Hydrosweep was operated with a swath width of 90°. Accuracy of the depth measurements is mainly dependent on precise sound velocity profiles of the water column. Therefore, CTD measurements carried out by the oceanography group were used for calibration (21 CTD stations in total). Only before the first stations (i.e. Barents Sea), the Hydrosweep system was calibrated by comparison of slant and vertical beams of sweep profiles perpendicular to the ship's long axis with profiles from the ship's longitudinal direction.

The recorded depth and positioning data were stored in 8 hour intervals in a sensor-independent raw data format (SURF). Post-processing such as cleaning of erroneous position and depth data was not carried out onboard *Polarstern*.

7.3 Geological sampling

Geological sampling was performed in two areas on the northern Kara Sea continental margin, along a transect from the Kara Sea across the Gakkel Ridge and the Lomonosov Ridge (at 88°40'N, 140°E) to the Alpha Ridge, and on a shorter transect from the Alpha Ridge transect back to the Lomonosov Ridge at 86°30'N, 152°E (Fig. 7.1). Coring sites were selected based on Parasound results, with emphasis on morphological highs in the central and eastern Arctic Ocean (Lomonosov and Alpha Ridges). In the two working areas on the Kara Sea continental margin, one continuous N-S coring transect was performed in each area, covering water depths from the shelf (ca. 300 m) to the continental foot (ca. 4,000 m).

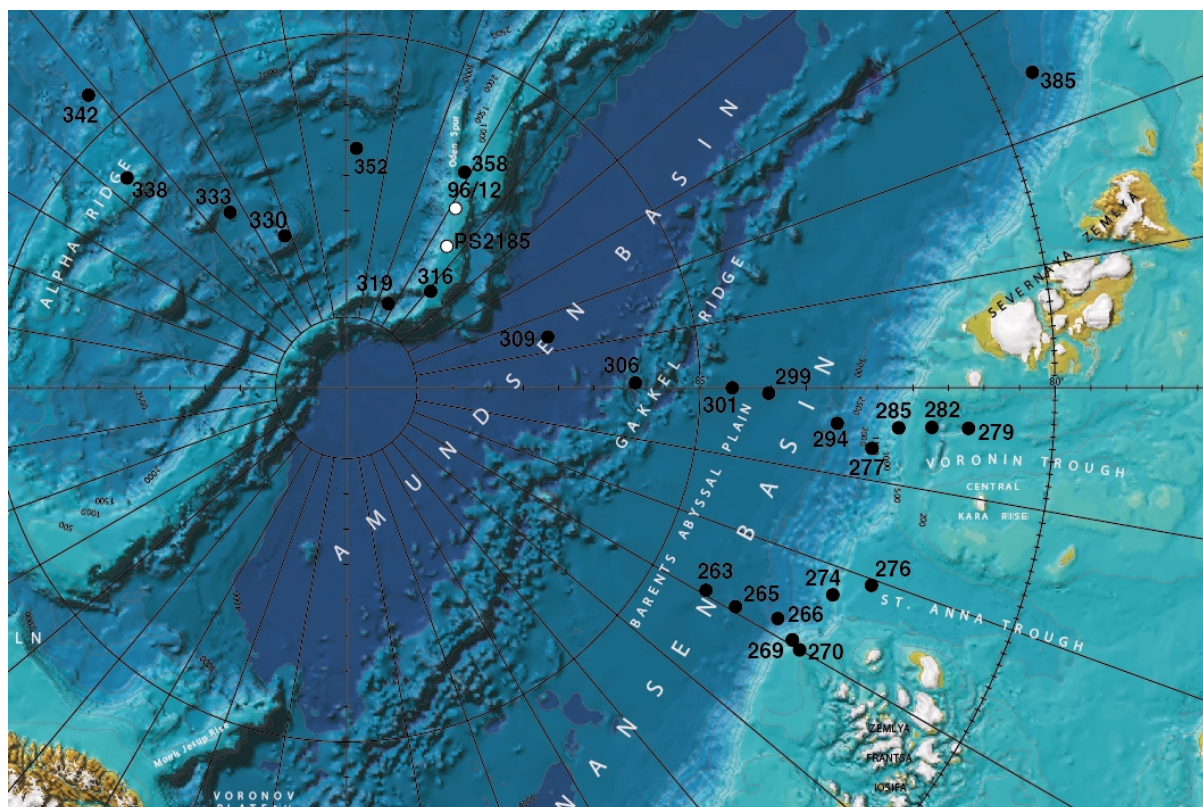


Fig. 7.1: Bathymetric map of the working area. Coring positions are indicated by black dots and the station number (add PS70/ for full number). Referenced sites PS2185 and 96/12 are shown as white dots.

Surface-near sediments were sampled at 24 geological sampling sites with a large volume grab (box corer, 50 cm x 50 cm x 50 cm). Except for the very first station PS70/261, where the technical problems prevented successful coring, the box corer always provided excellent results with recoveries of 0.33 - 0.50 cm of undisturbed surface-near sediments. After opening of the cores they were photographed. A detailed description of the surface and geological profile was followed by sampling for various purposes, including the recovery of 3 archive tubes and 1 - 3 archive boxes which preserved the full sequence of deposits in the corer box. Additional samples were taken downcore for X-ray analyses and dry bulk density determinations. All samples were stored at 4° C.

In addition to the box corer, a multicorer with 12 plastic tubes of 8 cm diameter was used at 7 selected stations to retrieve sediments with an absolutely undisturbed water-sediment interface. The very first and the very last multicorer casts (stations /239 and /385) were performed without other geological sampling tools, mainly for microbiological sampling purposes. Sampling was done as 1 cm-slices. Samples were frozen (-18° C) or stored at 4° C. At station /352 a microcorer (technically similar to a multicorer) with 4 plastic tubes was used, hanging under the CTD/rosette. It recovered 21 cm of sediment which were handled as described above.

To obtain long sediment cores at selected stations, a gravity corer (SL) of 5 or 10 m length and 12 cm diameter with a penetration weight of 1.5 t or a square-barrel kastenlot corer (30 x 30 x 1,200 cm) with a penetration weight of ca. 3 t were used. At station /294 both systems were run. In total, 12 gravity cores (length 0.50 - 5.93 m) and 4 kastenlot cores (length 2.93 - 7.70 m) were recovered (Fig. 7.2). A characteristic lithological boundary in the two cores from station /294 (at 282 and 322 cm core depth in the gravity and kastenlot core, respectively) allows to determine a sediment compression of ca. 15 % in the gravity core at this site, if compared to the kastenlot core.

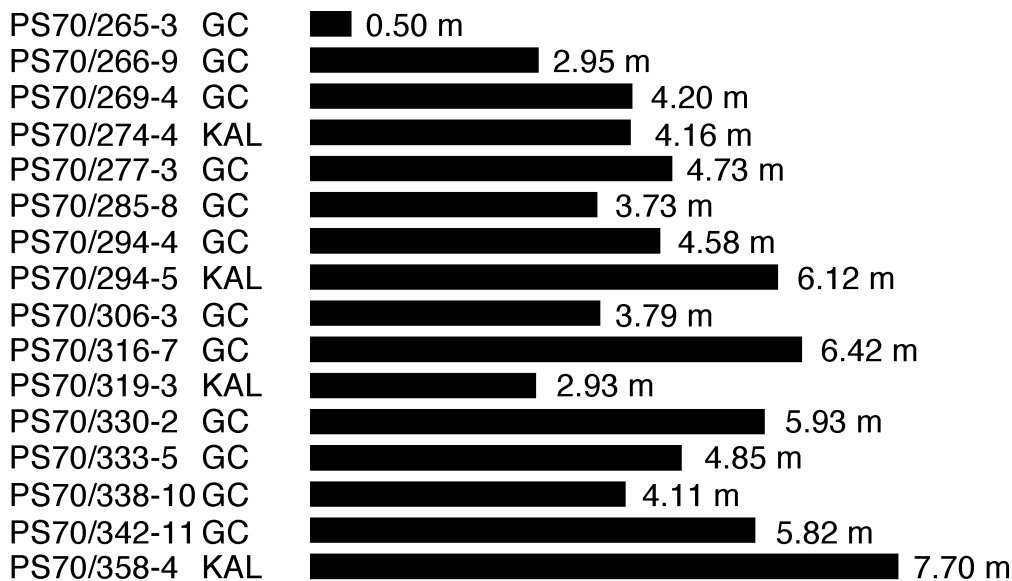


Fig. 7.2: Core recovery of gravity and kastenlot cores.

All cores were opened on board, photographed, visually described, and sampled for X-ray analyses, dry bulk density determinations, and other purposes. Core descriptions are given in the annex. From the kastenlot cores, several 1 m long archive boxes were taken in parallel from along the entire core and frozen or stored at 4° C. In addition to the visual description, the sediment colour was determined at 1 cm intervals using a Minolta CM-2002 spectrophotometer (see next chapter).

All sediment cores were be stored cool on board and transported to the AWI core depository in Bremerhaven from where they will be made available for investigations.

7.4 Physical properties

Multi-Sensor Core Logging

Non-destructive whole-core physical properties provide initial core characterization with a very high vertical resolution and are commonly used for lateral correlation of cores. Physical property measurements were carried out onboard using a Multi-Sensor-Core-Logger (MSCL, GEOTEK Ltd., UK). P-wave travel times, magnetic susceptibility, g-ray-absorption and non-contact electrical resistivity were measured simultaneously including control measurements of core diameter and sediment

temperature. From these data, the physical properties wet bulk density, magnetic susceptibility, fractional porosity, P-wave velocity, and formation factor can be calculated using the MSCL software package. The technical description of the system is given in Table 7.1:

Tab. 7.1: Technical specifications of the GEOTEK MSCL14

P-wave velocity and core diameter	<p>Plate transducer diameter: 4 cm Transmitter pulse frequency: 250 kHz Pulse repetition rate: 1 kHz Received pulse resolution: 50 ns Gate: 5000 Delay: 0 μs</p>
Density	<p>Gamma ray source: Cs-137 (1983) Activity: 356 MBq Energy: 0.662 MeV Collimator diameter: 5.0 mm for gravity and box cores, 2.5 for Kastenlot cores Gamma detector: Gammasearch2, Model SD302D, Ser. Nr. 3043, John Count Scientific Ltd., 10 s counting time</p>
Fractional porosity	<p>Mineral grain density = 2.65, water density = 1.026</p>
Magnetic susceptibility	<p>Loop sensor: BARTINGTON MS-2C, Ser. Nr. 208 Loop sensor diameter: 14 cm Point sensor: BARTINGTON MS-2F, Ser. Nr. 139 Alternating field frequency: 565 Hz, counting time 10 s, precision $0.1 \cdot 10^{-5}$ (SI) Magnetic field intensity: ca. 80 A/m RMS Krel: 1.56 (SL, 12 cm core-\emptyset), 0.60 (KAL, cross section 50.27 cm², = 8 cm core-\emptyset) Loop sensor correction coefficient: 6.391 (SL) and 16.689 (KAL) for 10⁻⁶ (SI), respectively Point sensor: BARTINGTON MS-2F, Ser. No. 139 counting time 10 s</p>

Gravity and box cores were measured in coring liners with 12.5 cm diameter, whereas Kastenlot cores were measured in sub-cores retrieved from the original core using length-wise open transparent plastic boxes of 1,000 mm length and 75 times 75 mm cross section. In order to allow for magnetic-susceptibility sensor correction according to the Bartington correction requirements, the rectangular cross section of the box was equalized to a size-equivalent circular section, of which a fictive core diameter was calculated as input parameter for loop-sensor correction coefficient (Tab. xx). For both core sizes (gravity/box and Kastenlot cores), the density calibration was carried out using a set of defined mixtures of aluminium and distilled water in a gravity liner and Kastenlot sub-sampling box, respectively (Best and Gunn, 1999).

In addition, measurements of magnetic susceptibility using a Bartington point sensor were performed directly on the sediment surface. Gravity cores were measured shortly after splitting. For box core point sensor magnetic susceptibility measurements, a second sub-core was taken in a transparent plastic box with open surface. MSCL and point sensor data of the box cores thus origin of different sub-cores. For Kastenlot cores, the measurements were carried out on the same sub-core as MSCL measurements. For practical reasons, the point sensor was hooked up on the GEOTEK Color-Line-Scan-Logger. The step intervals of the measurements were 1.0 cm.

Spectrophotometer measurements

Quantitative estimates of spectral reflectance and sediment colour were carried out using a handheld Minolta CM-2002 spectrophotometer (Minolta Camera Co., Osaka, Japan). A precise documentation of the camera settings is given in Balsam et al. (1998). The split core surfaces of the archive halves were covered by a standard film to protect the spectrophotometer. Calibration and operation of the spectrophotometer were done according to the Minolta CM-2002 users' manual (Minolta Camera Co., 1991). Measurement spacing was generally set to 1 cm.

Preliminary results

Parasound surveys and data interpretation

The first PARASOUND profile was run continuously from the northern Barents Sea north into the Nansen Basin and then south into the first marine geological working area on the NE Kara Sea continental margin (St. Anna Trough). The system had to be turned off for transit to the second working area and was switched on again at ca. 83°E on the NW Kara sea continental margin (Voronin Trough). From there on the system worked continuously again on the way to the Gakkal, Lomonosov, and Alpha Ridges and back to the Gakkal Ridge. The Parasound survey ended at ca. 79°N in the Laptev Sea. In the following, a short description of the Parasound profiles and the characteristics of the deposits will be given, as imaged from the PARASOUND data.

Barents Sea

The first, more southern part of the northward profile in the Barents Sea is characterized by a smooth topography with a distinct hard reflector at the surface. Only in a few locations, a penetration deeper than 10 m could be recognized. The

northern part, close to the continental margin, displays a rough glacial topography with steep troughs and walls. It is interpreted to reflect the erosional activity of the Barents Sea ice sheet which had covered the area during the last glacial maximum (cf. Svendsen et al., 2004). Data recovery on the steep slope was poor in many depth intervals. Otherwise there is evidence for levee structures and a strong activity of slumps and slides.

The Nansen, Amundsen, and Makarov Basins

Sediments in the basins are generally flat lying. Penetration was 20 - 40 m. During earlier expeditions (ARK-IV/3, ARK-VIII/3) the long sediment cores obtained from the basins revealed the presence of thick turbidite sequences, intercalated with thinner layers from more pelagic sedimentation.

Northern Kara Sea continental margin

Sediments on the lower slope NW of the St. Anna Trough and N of the Voronin Trough up to ca. 2,500 m depth usually show 10 - 20 m of good penetration. The images are characterized either by a single or double layer signature. Below the uppermost, ca. 3 - 4 m layer without a clear internal structure, an acoustically more transparent layer can be observed. Its thickness is sometimes only 1 - 2, but can increase in lense-shaped bodies to more than 20 m. These bodies are interpreted as slides. Below the transparent layer, a second more reflective layer of a few meters in thickness can often be observed. The succession is tentatively interpreted as intercalated slides and layers of pelagic sedimentation.

Northwest of the St. Anna Trough the slope between 2,500 m and 1,200 m is extremely steep and does not allow a characterization from the records. North of the Voronin Trough this depth interval also shows evidence of slides, but especially between 1,800 and 2,800 m the reflective layers are thicker (5 - 15 m) and show a distinct internal layering (Fig. 7.3).

In both areas, profiles up to ca. 650 m showed an undulated morphology and often evidence for large- and small-scale slide structures (Fig. 7.4). Penetration was variable, but often the reflective top layer of 4 - 8 captured most of the energy and it is difficult to analyze the deeper structure.

Above 650 m, a very rough small-scale topography is usually dominating. It partly consists of channels incising 5 - 15 m into the otherwise more undulated surface, but in other areas the entire profile is hummocky and no horizontal layering is visible. The first type is interpreted as the result of erosional effects during times of lower sea level, whereas the second type was probably formed by an overriding ice sheet, followed by severe iceberg ploughing.

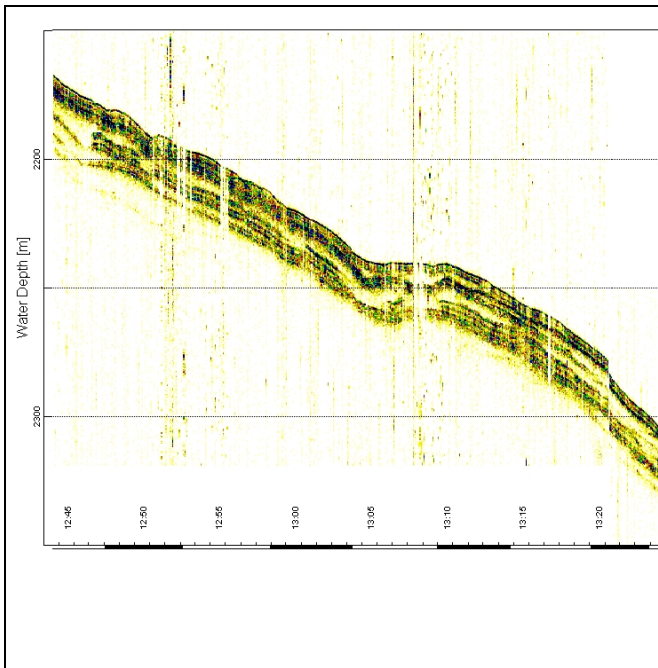


Fig. 7.3: PARASOUND-Profile of sediment layers at the lower slope of the Voronin Trough. Note the layering and the transparent lenses in certain parts of the profile.

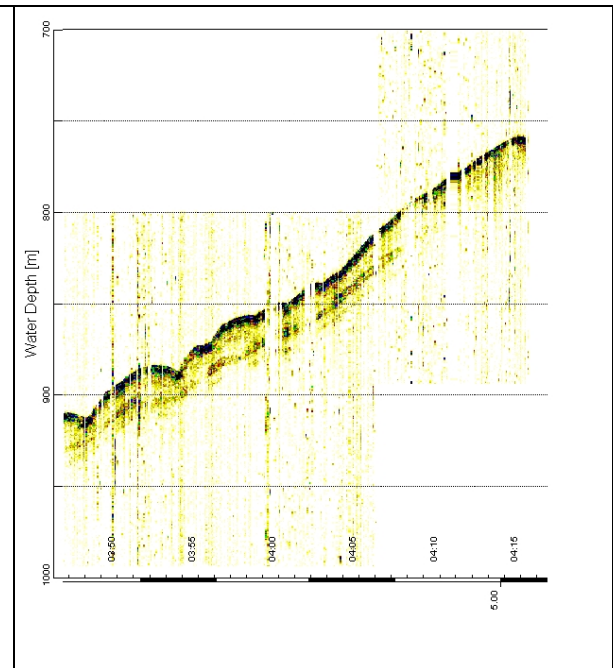


Fig. 7.4: PARASOUND-Profile of sediment layers at the upper slope of the St. Anna Trough. Note the undulating surface of sedimentary layers.

Gakkel Ridge

PARASOUND records from the Gakkel Ridge revealed an extremely rough topography. Only in a few pockets between the volcanoes of this active mid-ocean spreading ridge small subbasins could be found where well-layered sediments have accumulated. In general, the data recovery in the Gakkel Ridge are was very poor.

Lomonosov Ridge

Both transects across the Lomonosov Ridge gave similar results as during earlier crossings (ARK-VIII/3, ARK-XIV/1a). While the steep slopes did only rarely allow an analysis of the underground, the upper slope and the ridge crest showed the well-layered structure of the uppermost part of the sedimentary sequence. A special feature within the ridge is the interior basin at ca. 88°30'-89°N and 140 - 180°E. The cruise track crossed the basin in its southern part and a profile from the ridge crest at ca. 1,300 m into the basin at ca. 2,700 m water depth was recorded. The flanks of the basin were very steep and data quality was poor. However, in the basin, the records reveal horizontally layered sediments. These observations fully confirm the results of Björk et al. (in press).

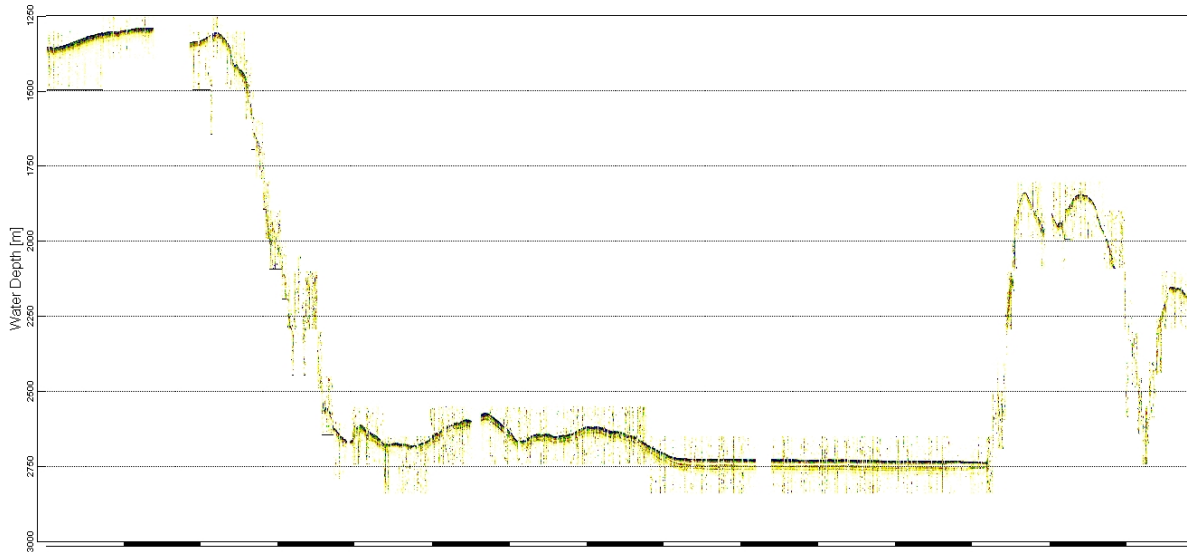


Fig. 7.5: PARASOUND-Profile of sediment layers from the crest of the Lomonosov Ridge into the interior basin of the ridge. Note the distinct horizontal layering in the basin.

Alpha Ridge

Independent of the water depth which reached <1,500 m in the shallowest regions, the topography of the Alpha Ridge was generally rough and the surfaces were undulated (Figs. 7.6 and 7.7). Well-layered sediments of a wider regional or local extent (i.e., a few kilometre) were never observed. Almost all PARASOUND records from the Alpha Ridge show abundant side echoes which prohibited a detailed analysis of the subsurface layers. From these shipboard data it seems difficult to analyze the internal structure of the upper sedimentary layers.

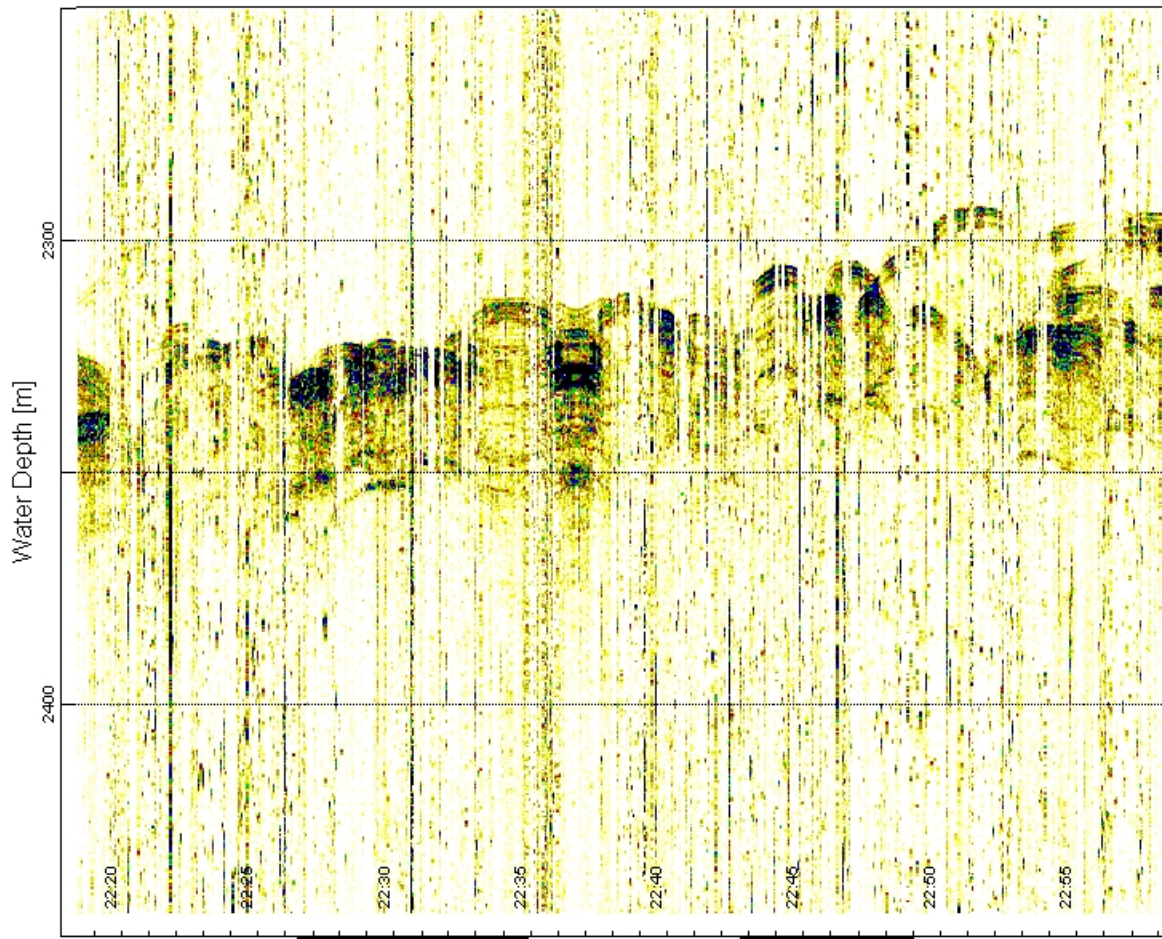


Fig. 7.6: PARASOUND-Profile of sediment layers on the lower Alpha Ridge. Note the irregular surface caused by side echoes.

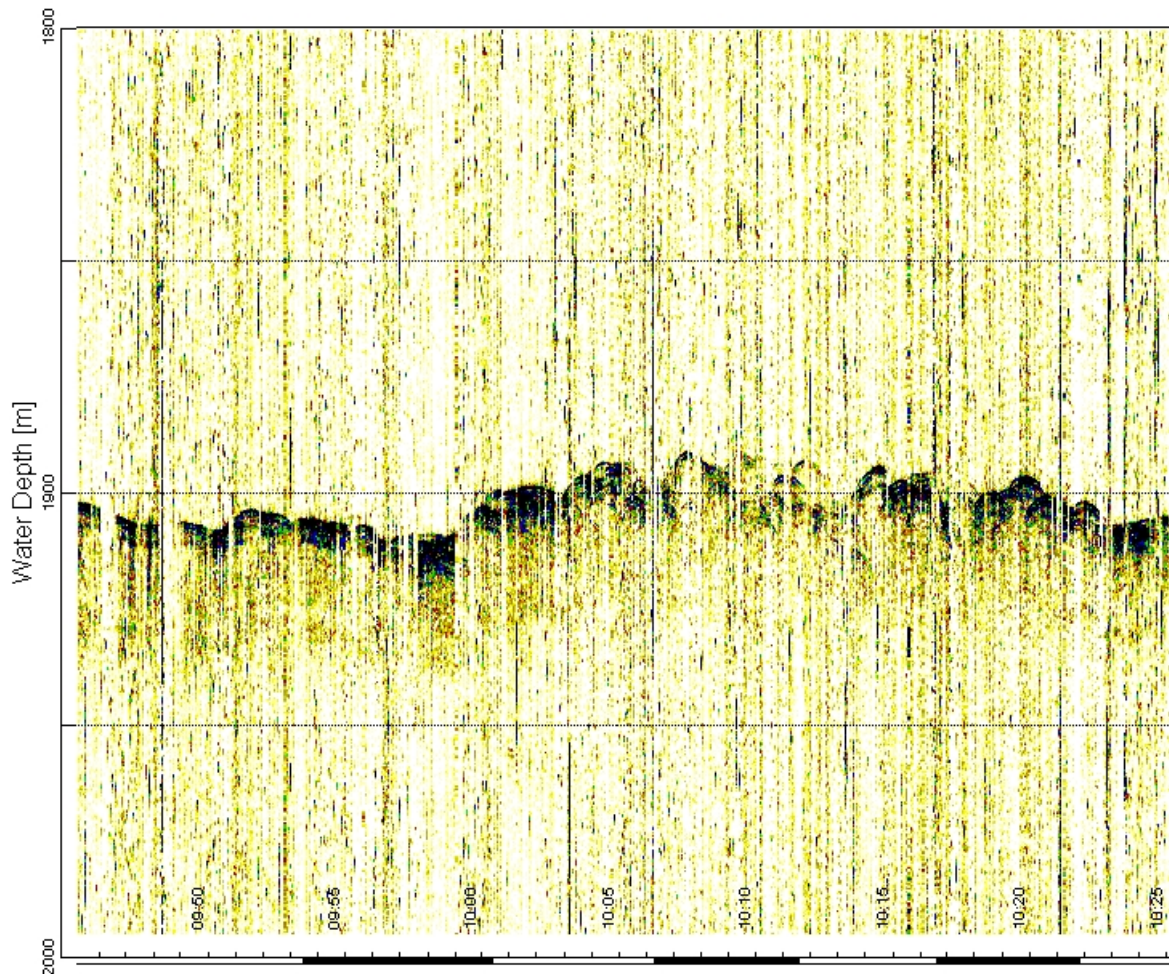


Fig. 7.7: PARASOUND-Profile of sediment layers on the Alpha Ridge. Note the irregular surface caused by side echoes.

Sediment characteristics and paleoenvironmental interpretations

Coring operations during ARK-XXII/2 recovered only soft sediments and there is no obvious evidence for pre-Quaternary deposits. Based on the sediment descriptions and the different lithologies found in the cores, a subdivision of 4 sedimentary provinces seems possible (Kara Sea continental margin, Gakkel Ridge, Lomonosov Ridge, and Alpha Ridge). The box cores from the central Nansen and Amundsen Basins (stations /299, /301, and /309) held sequences of mostly sandy silty clays, as observed earlier during other expeditions (e.g., ARK-VIII/3). Typically, these sequences are underlain by a sandy layer which has been determined to be ca. 50 – 60 ky old (Nørgaard-Pedersen et al., 1998, 2003).

Kara Sea continental margin

12 box cores, 6 gravity cores, and 2 kastenlot cores were obtained from the Kara sea continental margins at water depths between 4,000 and 300 m. The uppermost few decimetres of sediment usually consist of dark yellowish brown silty clays and sandy

silty clays, underlain at sediment depths of 30 - 40 cm by more olive greyish sandy silty clays. The sediment surfaces often contain calcareous micro- and macroorganisms (incl. bivalve fragments and benthic foraminifers) and the sediments are homogenized or strongly mottled from bioturbation, but sporadic sieving tests of subsurface sediments rarely revealed microfossils in the coarse fraction.

Grain sizes in the gravity and kastenlot cores typically range from silty clays to sandy silts. The deposits have mainly greyish olive colours of variable lightness, but dark grey and olive brown layers also occur. Especially the dark gray (colour codes N4 and N3) and dark olive gray (5Y4/1 and 5Y3/1) sediments are characteristic features. In all 6 cores from the Kara Sea margin which were longer than 3 meters, the dark greyish deposits were found in the bottom part of the cores. The maximum recovered thickness of this ubiquitous layer was 290 cm in kastenlot core PS70/294-5, and in none of the cores this layer was fully penetrated. It often contained iceberg-rafted dropstones in variable amounts and in cores from the continental margin off the Voronin Trough also coal particles of up to 5 cm. One or two similar dark grey layers also occur higher up in the cores, but their thickness is in most cores restricted to 10 - 50 cm. In kastenlot core PS70/294-5 the dark grey layer at ca. 150 - 250 cm consists of silty clay with sandy laminae, indicating a redistribution of sand particles by turbidity or contour currents. The dropstone content clearly marks the dark grey layers as of glacial origin. Since the cores stem from the margin of the two major glacial outlets of the Kara Sea, it is tempting to correlate the dark grey layers with the glaciation episodes of northern Eurasia as revealed by terrestrial and marine investigations in the last decade (e.g., Svendsen et al., 2004; Spielhagen et al., 2004). According to this correlation the dark greyish layers in the long cores were deposited at ca. 50 - 60 ka, 80 - 90 ka, and 130 - 180 ka. In most cases the thick dark grey layer at the bottom of the cores would thus stem from the Saalian glaciation which probably had the most extensive ice sheet on the Siberian shelves and in northern Eurasia ever in the Quaternary. Following this interpretation, the more olive and olive brownish to brownish layers in the sediment cores which are often homogeneous or strongly mottled from bioturbation represent the climatically warmer and intermediate periods in the Late Quaternary. Detailed investigations will be performed in the home laboratories to establish a high-resolution age model for the cores and reconstruct the paleoenvironmental history of the Kara Sea continental margin, the adjacent Arctic Ocean, and the hinterland.

Gakkel Ridge

At site PS70/306 (ca. 4,000 m water depth) a box core and a 3.79 m long gravity core were retrieved. With very few exceptions the sediments consisted of sandy silty clay and sandy silt. The sequence of sediments is similar to that from the Kara Sea continental slope. Intercalated among dark brownish and olive deposits it contains three dark grey (N4) layers which probably can be correlated to those in cores from the margin, implying an iceberg transport of shelf-derived sediments to the Gakkel Ridge area during times of continental glaciations. The lowermost dark grey layer is underlain by olive brownish deposits. If the above described correlation holds true, the bottom sediments in PS70/306-2 may be ca. 200 ky old.

Lomonosov Ridge

Three box cores, one gravity core, and two kastenlot cores were retrieved from the eastern sector of the Lomonosov Ridge between 86°30' and 88°40'N. Sites PS70/316 and /319 are only 50 km apart. While site /316 is situated slightly below the ridge crest (1,300 m), site /319 is in a small interior basin within the Lomonosov Ridge (2,700 m deep), which is connected both with the Makarov and Amundsen Basins, allowing a water mass exchange above the 1,900 m depth level (cf. Björk et al., in press). The sediments consist mostly of sandy silty clays which are strongly mottled, indicating a high degree of bioturbation. Lithological correlation seems difficult based on sediment colours and grain sizes, possibly because of winnowing effects on the ridge top. Preliminary investigations of the microfossil content in PS70/319-3 revealed uninterrupted occurrences of planktic foraminifers within the uppermost 75 cm. Since the deposits in nearby core PS2185 from 87°32'N 144°E have a distinct foraminifer-barren interval below 45 cm (50 ka, Spielhagen et al., 2004), it can be concluded that the time resolution in the interior basin sediments is by a factor of 1.5 or more higher than on the top of the ridge, possibly due to trapping effects of sediments winnowed from the crest.

At site PS70/358 the longest core obtained during cruise ARK-XXII/2 was recovered from near the crest of the Lomonosov Ridge at 86°32'E. It holds a sequence of mostly sandy silty clays which are well-known from other sites on the ridge (e.g., 96/12, PS2185). The lithological similarity in this area suggests that the age models of nearby cores can be tentatively transferred to PS70/358-4. This method would give an age of ca. 200 ka at ca 250 cm and a bottom age of the core near 1 My. The strongly mottled or homogeneous colours of the sediment are evidence for a high activity of burrowing organisms. According to Jakobsson et al. (2000) the various colour changes from brown to olive brown reflect a cyclic variability of manganese oxide contents which are thought to be related to changes in intermediate and bottom water ventilation caused by oceanographic and climate changes in the Arctic.

Alpha Ridge

Four box cores and four gravity cores (up to 5.82 m) were retrieved from the morphologically very heterogeneous area of the Alpha Ridge. The water depths of the coring sites lie between 1,500 and 3,300 m. The lithology of the cores was rather monotonous; they consisted almost entirely of sandy silty clays with very little changes in grain size. Sediment colours ranged from dark brown to olive brown. Almost all layers were strongly mottled and sometimes no basic colour could be determined ("sploshy colours"). According to the interpretation of Jakobsson et al. (2000) for similar sediments on the Lomonosov Ridge, the colour variability may be interpreted as evidence of changes in manganese oxide contents, which in turn reflect climate variability.

At site PS70/338 both the box core and the gravity core contained a layer of carbonate-cemented worm tubes a few centimetre below the sediment surface. The layer was hard and ca. 3 - 4 cm thick. Washed pieces were whitish grey in colour and up to 10 cm in size. Two further hard layers at 40 and 75 cm in the gravity core were of similar thickness, but consisted of strongly burrowed, stiff sandy silty clay of the similar colours as the soft sediments above and beneath. The origin of these hardground layers remains yet elusive

References

- Balsam W. L., Deaton B. C., & Damuth J. E., 1998. The effects of water content on diffuse reflectance spectrophotometry studies of deep-sea sediment cores. *Marine Geology* 149, 177-189.
- Best, A. I. and D. E. Gunn, 1999. Calibration of marine sediment core loggers for quantitative acoustic impedance studies. *Marine Geology* 160, 137-146.
- Björk, G., Jakobsson, M., Rudels, B., Swift, J.H., Anderson, L., Darby, D.A., Backman, J., Coakley, B., Winsor, P., Polyak, L., and Edwards, M. (in press). Bathymetry and deep-water exchange across the central Lomonosov Ridge at 88°-89°N. *Deep-Sea Res.*
- Jakobsson, M., Løvlie, R., Al-Hanbali, H., Arnold, E., Backman, J., Mörth, M., 2000. Manganese and colour cycles in the Arctic Ocean sediments constrain Pleistocene chronology. *Geology* 28, 23-26.
- Nørgaard-Pedersen, N., Spielhagen, R. F., Thiede, J., Kassens, R., 1998. Central Arctic surface ocean environment during the past 80,000 years. *Paleoceanography* 13, 193-204.
- Nørgaard-Pedersen, N., Spielhagen, R. F., Erlenkeuser, H., Grootes, P. M., Heinemeier, J., Knies, J., 2003. The Arctic Ocean during the Last Glacial Maximum: Atlantic and Polar domains of surface water mass distribution and ice cover. *Paleoceanography*.
- Spielhagen, R.F., Baumann, K.-H., Erlenkeuser, H., Nowaczyk, N.R., Nørgaard-Pedersen, N., Vogt, C., Weiel, D., 2004. Arctic Ocean deep-sea record of Northern Eurasian ice sheet history. *Quat. Sci. Rev.*, 23 (11-13): 1455-1483.
- Svendsen, J.I., Alexanderson, H., Astakhov, V.I., Demidov, I., Dowdeswell, J.A., Funder, S., Gataullin, V., Henriksen, M., Hjort, C., Houmark-Nielsen, M., Hubberten, H.W., Ingólfsson, Ó., Jakobsson, M., Kjær, K.H., Larsen, E., Lokrantz, H., Lunkka, J.P., Lyså, A., Mangerud, J., Matioushkov, A., Murray, A., Möller, P., Niessen, F., Nikolskaya, O., Polyak, L., Saarnisto, M., Siegert, C., Siegert, M.J., Spielhagen, R.F. and Stein, R., 2004. Late Quaternary ice sheet history of northern Eurasia. *Quat. Sci. Rev.*, 23 (11-13): 1229-1271.

APPENDIX

A.1 PARTICIPATING INSTITUTIONS

A.2 CRUISE PARTICIPANTS

A.3 SHIP'S CREW

A.4 STATION LIST

A.5 ANNEX CORING POSITIONS

A.6 SEDIMENT CORE DESCRIPTIONS

A.1 PARTICIPATING INSTITUTIONS

Adresse /Address

AWI	Alfred-Wegener-Institut für Polar- und Meeresforschung Am Handelshafen 12 27570 Bremerhaven / Germany
DWD	Deutscher Wetterdienst Hamburg Abteilung Seeschifffahrt Bernhard-Nocht Str. 76 20359 Hamburg / Germany
FAZ	Frankfurter Allgemeine Zeitung GmbH Wissenschaftsredaktion Hellerhofstraße 2-4 60 327 Frankfurt / Germany
FIELAX	FIELAX Gesellschaft für wissenschaftliche Datenverarbeitung mbH Schifferstraße 10-14 27568 Bremerhaven Germany
FIMR	Finnish Institut of Marine Research (FIMR), Finland Erik Palménin aukio 1, P. O. Box 2, 00561 Helsinki/ Finland
GEOKHI	Vernadsky Institute of Geochemistry and Analytical Chemistry, Russian Academy of Sciences, 19, Kosygin Str, 117975 Moscow /Russia
Heli Service	Heli Service International GmbH Im Geisbaum 2 63329 Egelsbach Germany

Adresse /Address

IFM-GEOMAR	Leibniz-Institut für Meereswissenschaften IFM-GEOMAR Düsternbrooker Weg 20 24105 Kiel / Germany
IFM HH	Universität Hamburg, Fakultät 6, Fachbereich Geowissenschaften, Institut für Meereskunde Bundesstraße 53, 20146 Hamburg / Germany
IPÖ	Institut für Polarökologie Wischhofstr. 1-3, Geb. 12, 24148 Kiel / Germany
JAMSTEC	Institute of Observational Research for Global Change, Japan Agency for Marine-Earth Science and Technology (JAMSTEC) 2-15, Natsushima-cho, Yokosuka Kanagawa, 237-0061 / Japan
Laeisz	Reederei F. Laeisz (Bremerhaven) GmbH Brückenstrasse 25 27568 Bremerhaven / Germany
LOB	Laboratoire d'Océanographie et de Biogéochimie (LOB) UMR 6535 Centre d'Océanologie de Marseille Campus de Luminy, Case 901 13288 Marseille Cedex 09 / France
NIOZ	Royal Netherlands Institute for Sea Research PO box 59, 1751 AB Den Burg, Texel / The Netherlands
OPTIMARE	OPTIMARE Sensorsysteme AG Am Luneort 15a 27572 Bremerhaven / Germany
SIO	P.P. Shirshov Institute of Oceanology Russian Academy of Science, Russia 36 Nachimovsky prospect, Moscow, 117851 / Russia

Adresse /Address

Texas A&M	Texas A&M University at Galveston 5007 Avenue U, Galveston, Texas 77551 / USA
UAB	Institut de Ciència i Tecnologia Ambientals Universitat Autònoma de Barcelona 08193 Bellaterra / Spain
UCD	School of Physics, University College of Dublin, Belfield, Dublin 4 / Ireland
UG	Molecular Systems Group, Department of Zoology and Animal Biology, Universität von Genf 30, Quai Ernest Ansermet, CH-1211 Genf 4 / Switzerland
VNIIO	VNIIO All-Russia Research Institute for Geology and Mineral Resources of the World Ocean VNII Okeangeologiya 1, Angliysky ave., 190121 St.Petersburg / Russia
XU	XU Research Center for Environmental Science Xiamen University Xiamen 361005 / China

A.2 CRUISE PARTICIPANTS

Name	Vorname/ First Name	Institut/ Institute	Beruf / Profession
Bakker	Karel	NIOZ	Geochemist
Barz	Kristina	AWI	Biologist
Basilico	Adrian	AWI	Biologist
Boom	Lorendz	NIOZ	Technician/Geotraces
Breier	Florian		Journalist
Büchner	Jürgen	Heli Service	Pilot
Cai	Pinghe	XU	Geochemist
Camara	Patricia	UAB	Geochemist
Damm	Ellen	AWI	Geochemist
Daniel	Kristin	AWI	Student/Geology
Gebauer	Manfred	DWD	Meteorologist
Gebhardt	Catalina	AWI	Geologist
Gremlowski	Lars	AWI	Geochemist
Heckmann	Hans H.	Heli Service	Pilot
Heckmann	Markus	Heli Service	Technician
Hendricks	Stefan	AWI	Geophysicist
Kern	Stefan	IfMH	Geophysicist
Kiko	Rainer	IPÖ	Biologist
Kikuchi	Takashi	JAMSTEC	Oceanographer
Klunder	Maarten	NIOZ	Geochemist
Kosobokova	Ksenia	SIO	Biologist
Kramer	Maike	IPÖ	Biologist
Kuckero	Lilith	AWI	Student /Geotraces
Laan	Patrick	NIOZ	Geochemist
Lechtenfeld	Oliver	AWI	Geochemist
Lecroq	Beatrice	UG	Biologist
Leinweber	Volker	AWI	Student/Sea ice phys
Lensch	Norbert	AWI	Technician/Geology
Lepore	Kate	UCD	Geochemist
Mechler	Sebastian	Optimare	Engineer/Oceanogr
Mertineit	Sabine	AWI	Geochemist
Middag	Rob	NIOZ	Geochemist
Nehmiz	Wiebke	FIELAX	Geologist
Nowazyk	Antoine	COM	Biologist
Ober	Sven	NIOZ	Technician/Geotraces

Name	Vorname/ First Name	Institut/ Institute	Beruf / Profession
Pisarev	Sergey	SIO	Oceanographer
Rabe	Benjamin	AWI	Oceanographer
Rabenstein	Lasse	AWI	Geophysicist
Rudels	Bert	FIMR	Oceanographer
Rusakov	Valery	GEOKHI	Geologist
Rutgers v d Loeff	Michiel	AWI	Geochemist
Schauer	Ursula	AWI	Chief Scientist
Schmidt	Anna	IFM-GEOMAR	Geologist
Schneider	Alice	IPÖ	Biologist
Semenov	Pjotr	VNIIO	Geologist
Siebert	Stefan	IPÖ	Biologist
Sonnabend	Hartmut	DWD	Meteorol. Technician
Spielhagen	Robert	IFM-GEOMAR	Geologist
Spreen	Gunnar	IfM HH	Geophysicist
Stimac	Michael	Heli Service	Technician
Thuroczy	Charles-Edouard	NIOZ	Geochemist
Vöge	Ingrid	AWI	Technician/Geochemistry
Walker	Sally	Texas A&M	Student/Biochemistry
Winderlich	Andreas	IfM HH	Geophysicist
Wisotzki	Andreas	AWI	Technician/Oceanogr

A.3 SHIP'S CREW

No.	Name	Rank
01.	Schwarze, Stefan	Master
02.	Spielke, Steffen	1.Offc.
03.	Farysch, Bernd	Ch. Eng.
04.	Fallei, Holger	2.Offc./L.
05.	Wunderlich, Thomas	2.Offc.
06.	Kaufmann, Tino	2.Offc.
07.	Schuhardt	Doctor
08.	Hecht, Andreas	R.Offc.
09.	Minzlaff, Hans-Ulrich	2.Eng.
10.	Schäfer, Marc	3.Eng.
11.	Sümnicht, Stefan	3.Eng.
12.	Scholz, Manfred	Elec Eng.
13.	Nasis, Ilias	Electron.
14.	Verhoeven, Roger	Electron.
15.	Muhle, Helmut	Elec.Tech
16.	Himmel, Frank	Electron.
17.	Loidl, Reiner	Boatsw.
18.	Reise, Lutz	Carpenter
19.	Rhau, Lars-Peter	A.B.
20.	Stutz, Heinz-Werner	A.B.
21.	Winkler, Michael	A.B.
22.	Reichert, Jörg	A.B.
23.	Hagemann, Manfred	A.B.
24.	Schmidt, Uwe	A.B.
25.	Bäcker, Andreas	A.B.
26.	Wende, Uwe	A.B.
27.	Preußner, Jörg	A.B.
28.	Ipsen, Michael	Storek.
29.	Voy, Bernd	Mot-man
30.	Elsner, Klaus	Mot-man
31.	Hartmann, Ernst-Uwe	Mot-man
32.	Pinske, Lutz	Mot-man
33.	Müller-Homburg, R.-D.	Cook
34.	Silinski, Frank	Cooksmate
35.	Martens, Michael	Cooksmate
36.	Jürgens, Monika	Stwdess
37.	Wöckener, Martina	1. Stwdss/Kr
38.	Czyborra, Bärbel	2.Stwdess
39.	Silinski, Carmen	2.Stwdess.
40.	Gaude, Hans-Jürgen	2.Steward
41.	Huang, Wu-Mei	2.Steward
42.	Möller, Wolfgang	2.Stwdard
43.	Yu, Kwok Yuen	Laundrym.

A.4 STATION LIST

Station	Date	Time	Position Lat	Position Lon	Depth [m]	Gear Abbreviation	Action
PS70/227-1	29.07.07	15:04	72° 34.67' N	26° 0.44' E	277.9	CTD/RO	surface
PS70/227-1	29.07.07	15:16	72° 34.83' N	26° 0.54' E	276.4	CTD/RO	at depth
PS70/227-1	29.07.07	15:27	72° 34.99' N	26° 0.74' E	278.8	CTD/RO	on deck
PS70/227-2	29.07.07	15:45	72° 35.22' N	26° 1.07' E	278.2	CTD/UC	into Water
PS70/227-2	29.07.07	15:48	72° 35.25' N	26° 1.15' E	280.1	CTD/UC	on Depth
PS70/227-2	29.07.07	16:05	72° 35.47' N	26° 1.44' E	278.6	CTD/UC	on Deck
PS70/228-1	30.07.07	10:06	75° 0.03' N	33° 59.95' E	178.1	CTD/UC	into Water
PS70/228-1	30.07.07	10:14	75° 0.03' N	34° 0.00' E	178.1	CTD/UC	on Depth
PS70/228-1	30.07.07	10:34	75° 0.05' N	34° 0.08' E	180.7	CTD/UC	on Deck
PS70/228-2	30.07.07	10:44	75° 0.06' N	34° 0.09' E	182.5	CTD/RO	surface
PS70/228-2	30.07.07	10:53	75° 0.06' N	34° 0.14' E	181.2	CTD/RO	at depth
PS70/228-2	30.07.07	11:12	75° 0.07' N	34° 0.21' E	180.1	CTD/RO	on deck
PS70/228-3	30.07.07	11:23	75° 0.08' N	34° 0.26' E	180.3	BONGO	surface
PS70/228-3	30.07.07	11:32	75° 0.13' N	34° 0.22' E	182.4	BONGO	at depth
PS70/228-3	30.07.07	11:40	75° 0.15' N	34° 0.29' E	183.7	BONGO	on deck
PS70/229-1	30.07.07	13:25	75° 15.05' N	34° 0.08' E	158.5	CTD/RO	surface
PS70/229-1	30.07.07	13:33	75° 15.09' N	34° 0.19' E	160.2	CTD/RO	at depth
PS70/229-1	30.07.07	13:45	75° 15.14' N	34° 0.53' E	160.2	CTD/RO	on deck
PS70/230-1	30.07.07	15:26	75° 30.00' N	34° 0.27' E	190.6	CTD/RO	surface
PS70/230-1	30.07.07	15:35	75° 30.05' N	34° 0.43' E	189.0	CTD/RO	at depth
PS70/230-1	30.07.07	15:49	75° 30.04' N	34° 0.27' E	190.7	CTD/RO	on deck
PS70/231-1	30.07.07	17:27	75° 44.92' N	34° 0.01' E	216.9	CTD/RO	surface
PS70/231-1	30.07.07	17:38	75° 44.95' N	33° 59.86' E	216.7	CTD/RO	at depth
PS70/231-1	30.07.07	17:53	75° 44.86' N	33° 59.77' E	214.7	CTD/RO	on deck
PS70/232-1	30.07.07	19:30	76° 0.01' N	33° 59.90' E	283.0	CTD/RO	surface
PS70/232-1	30.07.07	19:44	76° 0.04' N	34° 0.02' E	281.7	CTD/RO	at depth
PS70/232-1	30.07.07	20:05	76° 0.01' N	34° 0.27' E	278.0	CTD/RO	on deck
PS70/232-2	30.07.07	20:12	76° 0.02' N	34° 0.30' E	277.6	BONGO	surface
PS70/232-2	30.07.07	20:26	76° 0.05' N	34° 0.32' E	278.5	BONGO	at depth
PS70/232-2	30.07.07	20:37	76° 0.04' N	34° 0.40' E	277.1	BONGO	on deck
PS70/233-1	30.07.07	22:23	76° 15.69' N	34° 0.08' E	311.1	CTD/RO	surface
PS70/233-1	30.07.07	22:37	76° 15.72' N	34° 0.28' E	310.0	CTD/RO	at depth
PS70/233-1	30.07.07	22:57	76° 15.78' N	34° 0.38' E	307.3	CTD/RO	on deck
PS70/234-1	31.07.07	00:31	76° 30.16' N	34° 0.14' E	206.3	CTD/RO	surface
PS70/234-1	31.07.07	00:41	76° 30.17' N	34° 0.52' E	206.1	CTD/RO	at depth
PS70/234-1	31.07.07	00:57	76° 30.18' N	34° 1.04' E	208.1	CTD/RO	on deck
PS70/235-1	31.07.07	04:01	76° 59.93' N	34° 0.29' E	155.7	CTD/RO	surface
PS70/235-1	31.07.07	04:09	76° 59.94' N	34° 0.30' E	156.8	CTD/RO	at depth
PS70/235-1	31.07.07	04:20	76° 59.88' N	34° 0.15' E	157.6	CTD/RO	on deck
PS70/236-1	31.07.07	07:34	77° 30.04' N	33° 59.79' E	195.0	CTD/UC	into Water
PS70/236-1	31.07.07	07:47	77° 30.05' N	33° 59.20' E	190.3	CTD/UC	on Depth
PS70/236-1	31.07.07	08:03	77° 30.02' N	33° 58.67' E	189.1	CTD/UC	on Deck
PS70/236-2	31.07.07	08:15	77° 30.03' N	33° 58.42' E	189.5	CTD/RO	surface
PS70/236-2	31.07.07	08:25	77° 30.07' N	33° 58.35' E	191.6	CTD/RO	at depth
PS70/236-2	31.07.07	08:38	77° 30.09' N	33° 58.40' E	192.9	CTD/RO	on deck
PS70/236-3	31.07.07	08:43	77° 30.10' N	33° 58.42' E	192.4	BONGO	surface
PS70/236-3	31.07.07	08:50	77° 30.13' N	33° 58.35' E	196.2	BONGO	at depth
PS70/236-3	31.07.07	09:00	77° 30.17' N	33° 58.36' E	197.6	BONGO	on deck
PS70/236-4	31.07.07	09:12	77° 30.21' N	33° 58.50' E	195.6	CTD/RO	surface

Station	Date	Time	Position Lat	Position Lon	Depth [m]	Gear Abbre- viation	Action
PS70/236-4	31.07.07	09:22	77° 30.25' N	33° 58.67' E	195.8	CTD/RO	at depth
PS70/236-4	31.07.07	09:36	77° 30.31' N	33° 58.87' E	196.8	CTD/RO	on deck
PS70/236-5	31.07.07	10:02	77° 30.46' N	33° 59.28' E	197.3	CTD/RO	surface
PS70/236-5	31.07.07	10:11	77° 30.51' N	33° 59.50' E	196.8	CTD/RO	at depth
PS70/236-5	31.07.07	10:27	77° 30.59' N	33° 59.96' E	193.5	CTD/RO	on deck
PS70/237-1	31.07.07	18:26	78° 59.83' N	33° 59.68' E	275.6	CTD/UC	into Water
PS70/237-1	31.07.07	18:35	78° 59.83' N	33° 59.39' E	275.4	CTD/UC	on Depth
PS70/237-1	31.07.07	19:00	78° 59.86' N	33° 58.48' E	273.4	CTD/UC	on Deck
PS70/237-2	31.07.07	19:09	78° 59.80' N	33° 58.32' E	273.8	CTD/RO	surface
PS70/237-2	31.07.07	19:22	78° 59.79' N	33° 58.02' E	272.5	CTD/RO	at depth
PS70/237-2	31.07.07	19:39	78° 59.79' N	33° 57.51' E	271.9	CTD/RO	on deck
PS70/237-3	31.07.07	20:06	78° 59.89' N	33° 56.85' E	269.9	CTD/RO	surface
PS70/237-3	31.07.07	20:19	78° 59.94' N	33° 56.50' E	270.6	CTD/RO	at depth
PS70/237-3	31.07.07	20:41	79° 0.06' N	33° 55.98' E	268.5	CTD/RO	on deck
PS70/238-1	01.08.07	04:31	80° 29.66' N	33° 59.81' E	159.7	CTD/RO	surface
PS70/238-1	01.08.07	04:39	80° 29.63' N	34° 0.13' E	159.3	CTD/RO	at depth
PS70/238-1	01.08.07	04:51	80° 29.58' N	34° 0.85' E	163.9	CTD/RO	on deck
PS70/239-1	01.08.07	08:18	80° 59.69' N	33° 59.76' E	222.3	CTD/UC	into Water
PS70/239-1	01.08.07	08:24	80° 59.68' N	33° 59.80' E	222.1	CTD/UC	on Depth
PS70/239-1	01.08.07	08:46	80° 59.72' N	33° 59.68' E	223.0	CTD/UC	on Deck
PS70/239-2	01.08.07	09:01	80° 59.73' N	33° 59.85' E	221.6	ISP	into water
PS70/239-2	01.08.07	09:17	80° 59.76' N	33° 59.89' E	223.5	ISP	into water
PS70/239-2	01.08.07	09:18	80° 59.76' N	33° 59.89' E	223.5	ISP	pump at depth
PS70/239-2	01.08.07	12:25	81° 0.31' N	34° 3.05' E	229.8	ISP	on deck
PS70/239-3	01.08.07	12:31	81° 0.30' N	34° 3.06' E	229.0	CTD/RO	surface
PS70/239-3	01.08.07	12:42	81° 0.28' N	34° 3.10' E	229.6	CTD/RO	at depth
PS70/239-3	01.08.07	13:00	81° 0.25' N	34° 3.17' E	233.1	CTD/RO	on deck
PS70/239-4	01.08.07	13:34	80° 59.67' N	33° 59.90' E	222.4	MN	surface
PS70/239-4	01.08.07	13:44	80° 59.69' N	33° 59.90' E	223.0	MN	at depth
PS70/239-4	01.08.07	13:45	80° 59.68' N	33° 59.90' E	223.1	MN	Hoisting
PS70/239-4	01.08.07	14:03	80° 59.63' N	33° 59.82' E	222.9	MN	on deck
PS70/239-5	01.08.07	14:39	80° 59.54' N	34° 0.00' E	221.6	CTD/RO	surface
PS70/239-5	01.08.07	14:49	80° 59.50' N	34° 0.07' E	223.8	CTD/RO	at depth
PS70/239-5	01.08.07	15:08	80° 59.43' N	34° 0.12' E	223.0	CTD/RO	on deck
PS70/239-6	01.08.07	15:14	80° 59.40' N	34° 0.13' E	223.0	MUC	surface
PS70/239-6	01.08.07	15:22	80° 59.37' N	34° 0.07' E	221.7	MUC	at sea bottom
PS70/239-6	01.08.07	15:32	80° 59.32' N	33° 59.94' E	220.6	MUC	on deck
PS70/240-1	01.08.07	20:23	81° 29.97' N	34° 0.23' E	210.4	CTD/RO	surface
PS70/240-1	01.08.07	20:33	81° 30.03' N	33° 59.75' E	213.2	CTD/RO	at depth
PS70/240-1	01.08.07	20:50	81° 30.16' N	33° 59.27' E	217.4	CTD/RO	on deck
PS70/240-2	01.08.07	20:54	81° 30.19' N	33° 59.22' E	218.1	XCTD	surface
PS70/241-1	01.08.07	22:01	81° 34.98' N	34° 0.03' E	261.8	XCTD	surface
PS70/242-1	01.08.07	23:10	81° 40.06' N	34° 0.26' E	740.3	XCTD	surface
PS70/242-2	01.08.07	23:14	81° 40.11' N	34° 0.38' E	742.5	XCTD	surface
PS70/243-1	02.08.07	00:15	81° 43.83' N	33° 59.85' E	1456.0	CTD/RO	surface
PS70/243-1	02.08.07	00:49	81° 44.06' N	34° 0.99' E	1568.0	CTD/RO	at depth
PS70/243-1	02.08.07	01:40	81° 44.34' N	34° 3.98' E	1531.0	CTD/RO	on deck
PS70/243-2	02.08.07	01:54	81° 44.40' N	34° 4.73' E	1515.0	MN	surface
PS70/243-2	02.08.07	02:46	81° 44.49' N	34° 7.41' E	1405.0	MN	at depth
PS70/243-2	02.08.07	02:46	81° 44.49' N	34° 7.41' E	1405.0	MN	Hoisting

Station	Date	Time	Position Lat	Position Lon	Depth [m]	Gear Abbre- viation	Action
PS70/243-2	02.08.07	03:37	81° 44.44' N	34° 9.45' E	1418.0	MN	on deck
PS70/243-3	02.08.07	03:45	81° 44.40' N	34° 9.66' E	1386.0	BONGO	surface
PS70/243-3	02.08.07	04:33	81° 44.32' N	34° 10.89' E	1327.0	BONGO	at depth
PS70/243-3	02.08.07	05:20	81° 44.23' N	34° 11.74' E	1325.0	BONGO	on deck
PS70/243-4	02.08.07	05:29	81° 44.23' N	34° 11.79' E	1325.0	BONGO	surface
PS70/243-4	02.08.07	05:33	81° 44.22' N	34° 11.79' E	1324.0	BONGO	at depth
PS70/243-4	02.08.07	05:41	81° 44.21' N	34° 11.82' E	1320.0	BONGO	on deck
PS70/244-1	02.08.07	06:11	81° 44.94' N	33° 59.58' E	1705.0	XCTD	surface
PS70/245-1	02.08.07	07:16	81° 49.90' N	34° 0.12' E	1892.0	XCTD	surface
PS70/246-1	02.08.07	07:59	81° 52.10' N	34° 0.72' E	2005.0	CTD/UC	into Water
PS70/246-1	02.08.07	08:29	81° 52.27' N	34° 0.68' E	2008.0	CTD/UC	on Depth
PS70/246-1	02.08.07	09:32	81° 52.65' N	34° 1.28' E	2020.0	CTD/UC	on Deck
PS70/246-2	02.08.07	09:44	81° 52.72' N	34° 1.37' E	2024.0	CTD/RO	surface
PS70/246-2	02.08.07	10:28	81° 53.04' N	34° 2.42' E	2026.0	CTD/RO	at depth
PS70/246-2	02.08.07	11:20	81° 53.38' N	34° 3.79' E	2023.0	CTD/RO	on deck
PS70/247-1	02.08.07	11:56	81° 55.31' N	33° 58.99' E	2124.0	XCTD	surface
PS70/248-1	02.08.07	13:03	81° 56.67' N	34° 1.84' E	2049.0	ICE	Alongside Floe
PS70/248-1	02.08.07	13:09	81° 56.75' N	34° 1.95' E	2050.0	ICE	Ice Gangway on the ice
PS70/248-1	02.08.07	13:13	81° 56.71' N	34° 2.16' E	2152.0	ICE	Scientists on the ice
PS70/248-1	02.08.07	21:01	81° 57.12' N	34° 4.28' E	2149.0	ICE	Scientists on board
PS70/248-1	02.08.07	21:12	81° 57.18' N	34° 4.14' E	2152.0	ICE	Ice Gangway on board
PS70/248-1	02.08.07	21:12	81° 57.18' N	34° 4.14' E	2152.0	ICE	Departure from floe
PS70/249-1	02.08.07	22:02	81° 59.78' N	33° 59.44' E	2271.0	CTD/RO	surface
PS70/249-1	02.08.07	22:50	81° 59.88' N	33° 58.65' E	2281.0	CTD/RO	at depth
PS70/249-1	02.08.07	23:45	81° 59.95' N	33° 58.12' E	2286.0	CTD/RO	on deck
PS70/249-2	02.08.07	23:48	81° 59.96' N	33° 58.07' E	2285.0	XCTD	surface
PS70/249-3	02.08.07	23:57	81° 59.97' N	33° 57.99' E	2287.0	MN	surface
PS70/249-3	03.08.07	00:59	81° 60.00' N	33° 57.60' E	2292.0	MN	at depth
PS70/249-3	03.08.07	01:00	81° 60.00' N	33° 57.59' E	2292.0	MN	Hoisting
PS70/249-3	03.08.07	02:16	82° 0.12' N	33° 56.70' E	2302.0	MN	on deck
PS70/249-4	03.08.07	02:27	82° 0.10' N	33° 56.84' E	2299.0	BONGO	surface
PS70/249-4	03.08.07	02:32	82° 0.10' N	33° 56.78' E	2295.0	BONGO	at depth
PS70/249-4	03.08.07	02:38	82° 0.10' N	33° 56.74' E	2296.0	BONGO	on deck
PS70/249-5	03.08.07	02:47	82° 0.11' N	33° 56.66' E	2300.0	BONGO	surface
PS70/249-5	03.08.07	04:09	82° 0.15' N	33° 56.04' E	2302.0	BONGO	at depth
PS70/249-5	03.08.07	05:28	82° 0.20' N	33° 55.95' E	2307.0	BONGO	on deck
PS70/250-1	03.08.07	06:39	82° 4.97' N	34° 0.46' E	2412.0	XCTD	surface
PS70/251-1	03.08.07	07:47	82° 9.95' N	33° 59.94' E	2567.0	XCTD	surface
PS70/252-1	03.08.07	10:18	82° 15.04' N	34° 2.22' E	2679.0	CTD/RO	surface
PS70/252-1	03.08.07	11:10	82° 15.17' N	34° 2.04' E	2686.0	CTD/RO	at depth
PS70/252-1	03.08.07	12:14	82° 15.29' N	34° 1.83' E	2691.0	CTD/RO	on deck
PS70/252-2	03.08.07	12:18	82° 15.30' N	34° 1.82' E	2688.0	XCTD	surface
PS70/253-1	03.08.07	16:21	82° 19.90' N	34° 0.39' E	2808.0	XCTD	surface
PS70/254-1	03.08.07	18:09	82° 25.06' N	34° 2.38' E	2959.0	XCTD	surface
PS70/255-1	03.08.07	19:30	82° 30.20' N	33° 57.12' E	3100.0	CTD/UC	into Water

Station	Date	Time	Position Lat	Position Lon	Depth [m]	Gear Abbre- viation	Action
PS70/255-1	03.08.07	20:22	82° 30.25' N	33° 57.01' E	3104.0	CTD/UC	on Depth
PS70/255-1	03.08.07	21:46	82° 30.37' N	33° 56.88' E	3106.0	CTD/UC	on Deck
PS70/255-2	03.08.07	22:11	82° 30.41' N	33° 57.35' E	3104.0	ISP	into water
PS70/255-2	03.08.07	22:15	82° 30.41' N	33° 57.32' E	3109.0	ISP	Information
PS70/255-2	03.08.07	22:31	82° 30.45' N	33° 57.22' E	3108.0	ISP	Information
PS70/255-2	03.08.07	22:39	82° 30.52' N	33° 57.43' E	3107.0	ISP	Information
PS70/255-2	03.08.07	22:43	82° 30.52' N	33° 57.48' E	3109.0	ISP	Information
PS70/255-2	03.08.07	22:48	82° 30.53' N	33° 57.58' E	3109.0	ISP	into water
PS70/255-2	03.08.07	22:52	82° 30.53' N	33° 57.55' E	3109.0	ISP	into water
PS70/255-2	03.08.07	22:53	82° 30.54' N	33° 57.54' E	3110.0	ISP	pump at depth
PS70/255-2	04.08.07	01:06	82° 30.74' N	33° 56.09' E	3120.0	ISP	Information
PS70/255-2	04.08.07	01:39	82° 30.81' N	33° 55.78' E	3124.0	ISP	on deck
PS70/255-3	04.08.07	01:53	82° 30.86' N	33° 55.16' E	3124.0	CTD/RO	surface
PS70/255-3	04.08.07	02:57	82° 30.91' N	33° 54.42' E	3128.0	CTD/RO	at depth
PS70/255-3	04.08.07	04:10	82° 31.03' N	33° 53.78' E	3131.0	CTD/RO	on deck
PS70/255-4	04.08.07	04:17	82° 31.04' N	33° 53.78' E	3132.0	XCTD	surface
PS70/255-5	04.08.07	04:57	82° 31.16' N	33° 53.57' E	3137.0	CTD/RO	surface
PS70/255-5	04.08.07	05:22	82° 31.24' N	33° 53.46' E	3135.0	CTD/RO	at depth
PS70/255-5	04.08.07	05:51	82° 31.34' N	33° 53.38' E	3140.0	CTD/RO	on deck
PS70/255-6	04.08.07	06:20	82° 31.44' N	33° 53.28' E	3142.0	CTD/RO	surface
PS70/255-6	04.08.07	06:31	82° 31.49' N	33° 53.34' E	3143.0	CTD/RO	at depth
PS70/255-6	04.08.07	06:45	82° 31.53' N	33° 53.42' E	3144.0	CTD/RO	on deck
PS70/256-1	04.08.07	14:15	82° 51.48' N	33° 52.48' E	3574.0	CTD/RO	surface
PS70/256-1	04.08.07	15:26	82° 51.75' N	33° 51.40' E	3578.0	CTD/RO	at depth
PS70/256-1	04.08.07	16:42	82° 52.02' N	33° 50.13' E	3581.0	CTD/RO	on deck
PS70/257-1	05.08.07	10:00	83° 29.81' N	34° 2.79' E	3958.0	ICE	Alongside Floe
PS70/257-1	05.08.07	10:06	83° 29.82' N	34° 2.78' E	3957.0	ICE	Ice Gangway on the ice
PS70/257-1	05.08.07	10:13	83° 29.84' N	34° 2.70' E	3962.0	ICE	Scientists on the ice
PS70/257-2	05.08.07	10:21	83° 29.86' N	34° 2.60' E	3959.0	CTD/RO	surface
PS70/257-2	05.08.07	11:36	83° 30.04' N	34° 1.53' E	3963.0	CTD/RO	at depth
PS70/257-2	05.08.07	13:05	83° 30.21' N	33° 59.93' E	3968.0	CTD/RO	on deck
PS70/257-3	05.08.07	13:12	83° 30.23' N	33° 59.80' E	3966.0	BONGO	surface
PS70/257-3	05.08.07	14:10	83° 30.31' N	33° 58.58' E	3963.0	BONGO	at depth
PS70/257-1	05.08.07	14:40	83° 30.34' N	33° 57.92' E	3970.0	ICE	Scientists on board
PS70/257-1	05.08.07	14:49	83° 30.35' N	33° 57.72' E	3972.0	ICE	Ice Gangway on board
PS70/257-1	05.08.07	14:50	83° 30.35' N	33° 57.70' E	3970.0	ICE	Departure from floe
PS70/257-3	05.08.07	15:12	83° 30.38' N	33° 57.22' E	3963.0	BONGO	on deck
PS70/257-4	05.08.07	15:22	83° 30.39' N	33° 57.00' E	3962.0	BONGO	surface
PS70/257-4	05.08.07	15:27	83° 30.39' N	33° 56.89' E	3966.0	BONGO	at depth
PS70/257-4	05.08.07	15:34	83° 30.40' N	33° 56.73' E	3966.0	BONGO	on deck
PS70/257-5	05.08.07	16:06	83° 30.44' N	33° 56.03' E	3963.0	MN	surface
PS70/257-5	05.08.07	17:48	83° 30.54' N	33° 54.00' E	3964.0	MN	at depth
PS70/257-5	05.08.07	20:06	83° 30.67' N	33° 51.85' E	3966.0	MN	on deck
PS70/258-1	06.08.07	10:32	83° 59.93' N	34° 0.62' E	4055.0	CTD/UC	into Water

Station	Date	Time	Position Lat	Position Lon	Depth [m]	Gear Abbreviation	Action
PS70/258-1	06.08.07	11:39	83° 59.94' N	33° 59.81' E	4055.0	CTD/UC	on Depth
PS70/258-1	06.08.07	13:22	83° 59.97' N	33° 58.43' E	4054.0	CTD/UC	on Deck
PS70/259-1	06.08.07	16:16	84° 7.16' N	34° 41.05' E	4056.0	EF	start
PS70/259-1	06.08.07	16:29	84° 7.16' N	34° 40.87' E	4057.0	EF	End
PS70/260-1	07.08.07	08:07	84° 29.35' N	36° 8.32' E	4052.0	ICE	Alongside Floe
PS70/260-1	07.08.07	08:16	84° 29.36' N	36° 8.34' E	4050.0	ICE	Ice Gangway on the ice
PS70/260-2	07.08.07	08:45	84° 29.36' N	36° 8.31' E	4051.0	CTD/UC	into Water
PS70/260-1	07.08.07	09:27	84° 29.37' N	36° 8.29' E	4054.0	ICE	Scientists on the ice
PS70/260-2	07.08.07	09:51	84° 29.38' N	36° 8.29' E	4056.0	CTD/UC	on Depth
PS70/260-2	07.08.07	11:33	84° 29.42' N	36° 8.25' E	4052.0	CTD/UC	on Deck
PS70/260-3	07.08.07	11:46	84° 29.42' N	36° 8.23' E	4053.0	ISP	into water
PS70/260-3	07.08.07	12:17	84° 29.43' N	36° 8.15' E	4055.0	ISP	pump at depth
PS70/260-3	07.08.07	14:47	84° 29.46' N	36° 7.34' E	4052.0	ISP	Information
PS70/260-3	07.08.07	15:17	84° 29.47' N	36° 7.07' E	4054.0	ISP	on deck
PS70/260-4	07.08.07	15:42	84° 29.48' N	36° 6.82' E	4055.0	CTD/UC	into Water
PS70/260-4	07.08.07	16:46	84° 29.51' N	36° 6.15' E	4054.0	CTD/UC	on Depth
PS70/260-1	07.08.07	17:48	84° 29.57' N	36° 5.54' E	4052.0	ICE	Scientists on board
PS70/260-1	07.08.07	17:57	84° 29.58' N	36° 5.45' E	4053.0	ICE	Ice Gangway on board
PS70/260-4	07.08.07	18:23	84° 29.62' N	36° 5.24' E	4054.0	CTD/UC	on Deck
PS70/260-5	07.08.07	18:35	84° 29.63' N	36° 5.15' E	4053.0	MN	surface
PS70/260-5	07.08.07	20:17	84° 29.80' N	36° 4.73' E	4056.0	MN	at depth
PS70/260-5	07.08.07	22:41	84° 30.04' N	36° 4.96' E	4055.0	MN	on deck
PS70/260-6	07.08.07	22:56	84° 30.07' N	36° 4.99' E	4055.0	CTD/RO/M IC	MIC in water
PS70/260-6	07.08.07	23:03	84° 30.08' N	36° 5.01' E	4053.0	CTD/RO/M IC	CTD/RO to water
PS70/260-6	08.08.07	00:22	84° 30.19' N	36° 5.15' E	4053.0	CTD/RO/M IC	MIC at bottom and CTD at depth
PS70/260-6	08.08.07	01:47	84° 30.30' N	36° 5.03' E	4049.0	CTD/RO/M IC	MIC on deck
PS70/260-7	08.08.07	01:57	84° 30.31' N	36° 4.99' E	4055.0	BONGO	surface
PS70/260-7	08.08.07	02:02	84° 30.31' N	36° 4.97' E	4054.0	BONGO	at depth
PS70/260-7	08.08.07	02:06	84° 30.32' N	36° 4.95' E	4054.0	BONGO	on deck
PS70/260-8	08.08.07	02:31	84° 30.35' N	36° 4.81' E	4050.0	CTD/RO	surface
PS70/260-8	08.08.07	02:54	84° 30.38' N	36° 4.65' E	4052.0	CTD/RO	at depth
PS70/260-8	08.08.07	03:23	84° 30.41' N	36° 4.42' E	4056.0	CTD/RO	on deck
PS70/260-9	08.08.07	03:27	84° 30.42' N	36° 4.38' E	4053.0	BONGO	surface
PS70/260-9	08.08.07	04:04	84° 30.47' N	36° 4.04' E	4054.0	BONGO	at depth
PS70/260-9	08.08.07	04:40	84° 30.52' N	36° 3.67' E	4050.0	BONGO	on deck
PS70/260-10	08.08.07	04:52	84° 30.54' N	36° 3.54' E	4049.0	CTD/RO	surface
PS70/260-10	08.08.07	05:02	84° 30.55' N	36° 3.44' E	4052.0	CTD/RO	at depth

Station	Date	Time	Position Lat	Position Lon	Depth [m]	Gear Abbre- viation	Action
PS70/260-10	08.08.07	05:18	84° 30.58' N	36° 3.28' E	4056.0	CTD/RO	on deck
PS70/261-1	11.08.07	09:11	84° 38.72' N	60° 56.02' E	3854.0	CTD/UC	into Water
PS70/261-1	11.08.07	10:15	84° 38.27' N	60° 55.24' E	3846.0	CTD/UC	on Depth
PS70/261-1	11.08.07	11:53	84° 37.51' N	60° 53.37' E	3850.0	CTD/UC	on Deck
PS70/261-2	11.08.07	12:09	84° 37.38' N	60° 52.99' E	3842.0	BC	surface
PS70/261-2	11.08.07	12:58	84° 37.00' N	60° 51.64' E	3843.0	BC	atsea bottom
PS70/261-2	11.08.07	13:46	84° 36.64' N	60° 50.23' E	3841.0	BC	on deck
PS70/262-1	11.08.07	16:14	84° 32.08' N	60° 37.57' E	3831.0	EF	start
PS70/262-1	11.08.07	16:48	84° 31.97' N	60° 35.78' E	3844.0	EF	End
PS70/263-1	11.08.07	22:10	84° 10.35' N	60° 59.92' E	3702.0	CTD/RO	surface
PS70/263-1	11.08.07	23:26	84° 10.02' N	60° 57.55' E	3713.0	CTD/RO	at depth
PS70/263-1	12.08.07	00:56	84° 9.65' N	60° 53.74' E	3707.0	CTD/RO	on deck
PS70/263-2	12.08.07	01:04	84° 9.62' N	60° 53.43' E	3708.0	BC	surface
PS70/263-2	12.08.07	01:49	84° 9.45' N	60° 51.42' E	3700.0	BC	atsea bottom
PS70/263-2	12.08.07	02:37	84° 9.35' N	60° 48.78' E	3702.0	BC	on deck
PS70/264-1	12.08.07	10:47	83° 39.25' N	60° 25.52' E	3512.0	ICE	Alongside Floe
PS70/264-1	12.08.07	11:07	83° 39.16' N	60° 25.59' E	3509.0	ICE	Ice Gangway on the ice
PS70/264-1	12.08.07	12:06	0° 0.00' N	0° 0.00' E	0.0	ICE	Scientists on the ice
PS70/264-1	12.08.07	12:34	83° 38.56' N	60° 25.76' E	3492.6	ICE	Information
PS70/264-2	12.08.07	12:44	83° 38.49' N	60° 25.71' E	3491.7	CTD/RO	surface
PS70/264-2	12.08.07	13:53	83° 37.97' N	60° 25.04' E	3499.0	CTD/RO	at depth
PS70/264-2	12.08.07	15:12	83° 37.44' N	60° 23.92' E	3495.0	CTD/RO	on deck
PS70/264-3	12.08.07	15:24	83° 37.37' N	60° 23.74' E	3495.0	MN	surface
PS70/264-3	12.08.07	16:58	83° 36.99' N	60° 22.61' E	3493.0	MN	at depth
PS70/264-1	12.08.07	18:08	83° 36.80' N	60° 22.20' E	3493.0	ICE	Scientists on board
PS70/264-1	12.08.07	18:12	83° 36.80' N	60° 22.20' E	3496.0	ICE	Ice Gangway on board
PS70/264-3	12.08.07	19:06	83° 36.68' N	60° 22.54' E	3490.0	MN	on deck
PS70/264-4	12.08.07	19:15	83° 36.66' N	60° 22.63' E	3496.0	BONGO	surface
PS70/264-4	12.08.07	19:18	83° 36.66' N	60° 22.66' E	3491.0	BONGO	at depth
PS70/264-4	12.08.07	19:23	83° 36.65' N	60° 22.72' E	3489.0	BONGO	on deck
PS70/264-5	12.08.07	19:28	83° 36.63' N	60° 22.78' E	3491.0	BONGO	surface
PS70/264-5	12.08.07	20:24	83° 36.47' N	60° 23.71' E	3489.0	BONGO	at depth
PS70/264-5	12.08.07	21:17	83° 36.25' N	60° 24.83' E	3490.0	BONGO	on deck
PS70/265-1	12.08.07	23:24	83° 42.58' N	60° 38.27' E	3534.0	BC	surface
PS70/265-1	13.08.07	00:08	83° 42.17' N	60° 39.26' E	3538.0	BC	atsea bottom
PS70/265-1	13.08.07	00:50	83° 41.73' N	60° 40.18' E	3526.0	BC	on deck
PS70/265-2	13.08.07	01:08	83° 41.54' N	60° 40.55' E	3528.0	MUC	surface
PS70/265-2	13.08.07	01:47	83° 41.12' N	60° 41.38' E	3519.0	MUC	atsea bottom
PS70/265-2	13.08.07	02:31	83° 40.59' N	60° 42.29' E	3513.0	MUC	on deck
PS70/265-3	13.08.07	02:56	83° 40.27' N	60° 42.76' E	3512.0	GC	surface

Station	Date	Time	Position Lat	Position Lon	Depth [m]	Gear Abbre- viation	Action
PS70/265-3	13.08.07	03:34	83° 39.78' N	60° 43.27' E	3512.0	GC	atsea bottom
PS70/265-3	13.08.07	03:34	83° 39.78' N	60° 43.27' E	3512.0	GC	offground hoisting
PS70/265-3	13.08.07	04:17	83° 39.24' N	60° 43.52' E	3501.0	GC	on deck
PS70/266-1	13.08.07	23:13	83° 8.27' N	61° 44.46' E	3040.0	CTD/UC	into Water
PS70/266-1	14.08.07	00:05	83° 8.09' N	61° 46.17' E	3030.0	CTD/UC	on Depth
PS70/266-1	14.08.07	01:28	83° 7.69' N	61° 48.35' E	3016.0	CTD/UC	on Deck
PS70/266-2	14.08.07	01:41	83° 7.62' N	61° 48.55' E	3021.0	CTD/RO	surface
PS70/266-2	14.08.07	02:43	83° 7.31' N	61° 48.85' E	3011.0	CTD/RO	at depth
PS70/266-2	14.08.07	03:45	83° 7.05' N	61° 48.13' E	3004.0	CTD/RO	on deck
PS70/266-3	14.08.07	03:54	83° 7.01' N	61° 47.93' E	3004.0	ISP	into water
PS70/266-3	14.08.07	04:35	83° 6.89' N	61° 46.70' E	3001.0	ISP	pump at depth
PS70/266-3	14.08.07	06:57	83° 6.79' N	61° 41.88' E	2999.0	ISP	Information
PS70/266-3	14.08.07	07:30	83° 6.80' N	61° 41.38' E	2998.0	ISP	on deck
PS70/266-4	14.08.07	07:37	83° 6.80' N	61° 41.32' E	2999.0	CTD/RO	surface
PS70/266-4	14.08.07	08:01	83° 6.80' N	61° 41.25' E	2997.0	CTD/RO	at depth
PS70/266-4	14.08.07	08:28	83° 6.80' N	61° 41.41' E	2996.0	CTD/RO	on deck
PS70/266-4	14.08.07	08:35	83° 6.80' N	61° 41.50' E	2996.0	XCTD	surface
PS70/266-4	14.08.07	09:06	83° 6.77' N	61° 42.09' E	2998.0	CTD/RO	surface
PS70/266-4	14.08.07	09:12	83° 6.76' N	61° 42.23' E	3001.0	CTD/RO	at depth
PS70/266-4	14.08.07	09:24	83° 6.74' N	61° 42.53' E	2996.0	CTD/RO	on deck
PS70/266-7	14.08.07	09:36	83° 6.72' N	61° 42.85' E	2996.0	BC	surface
PS70/266-7	14.08.07	10:13	83° 6.62' N	61° 43.92' E	2995.0	BC	atsea bottom
PS70/266-7	14.08.07	10:48	83° 6.48' N	61° 44.95' E	2990.0	BC	on deck
PS70/266-8	14.08.07	11:03	83° 6.40' N	61° 45.35' E	2987.0	MUC	surface
PS70/266-8	14.08.07	11:35	83° 6.22' N	61° 46.17' E	2985.0	MUC	atsea bottom
PS70/266-8	14.08.07	12:10	83° 5.99' N	61° 46.84' E	2979.0	MUC	on deck
PS70/266-9	14.08.07	12:35	83° 5.82' N	61° 47.23' E	2973.0	GC	surface
PS70/266-9	14.08.07	13:05	83° 5.60' N	61° 47.56' E	2965.0	GC	atsea bottom
PS70/266-9	14.08.07	13:06	83° 5.60' N	61° 47.57' E	2967.0	GC	offground hoisting
PS70/266-9	14.08.07	13:41	83° 5.35' N	61° 47.82' E	2957.0	GC	on deck
PS70/267-1	14.08.07	16:28	82° 57.96' N	61° 16.96' E	2751.0	CTD/RO	surface
PS70/267-1	14.08.07	17:22	82° 57.70' N	61° 15.88' E	2747.0	CTD/RO	at depth
PS70/267-1	14.08.07	18:25	82° 57.54' N	61° 15.01' E	2737.0	CTD/RO	on deck
PS70/268-1	14.08.07	21:06	82° 48.37' N	60° 47.82' E	1575.0	CTD/UC	into Water
PS70/268-1	14.08.07	21:33	82° 48.48' N	60° 48.35' E	1609.0	CTD/UC	on Depth
PS70/268-1	14.08.07	22:24	82° 48.68' N	60° 50.28' E	1670.0	CTD/UC	on Deck
PS70/268-2	14.08.07	22:31	82° 48.70' N	60° 50.64' E	1675.0	XCTD	surface
PS70/268-3	14.08.07	22:39	82° 48.72' N	60° 51.06' E	1685.0	BONGO	surface
PS70/268-3	14.08.07	22:42	82° 48.73' N	60° 51.23' E	1686.0	BONGO	at depth
PS70/268-3	14.08.07	22:49	82° 48.75' N	60° 51.63' E	1693.0	BONGO	on deck
PS70/268-4	14.08.07	22:53	82° 48.75' N	60° 51.86' E	1703.0	BONGO	surface
PS70/268-4	14.08.07	23:49	82° 48.79' N	60° 55.32' E	1734.0	BONGO	at depth
PS70/268-4	15.08.07	00:42	82° 48.73' N	60° 58.62' E	1667.0	BONGO	on deck
PS70/268-5	15.08.07	01:03	82° 48.69' N	60° 59.55' E	1643.0	MN	surface
PS70/268-5	15.08.07	01:46	82° 48.55' N	61° 1.33' E	1647.0	MN	at depth
PS70/268-5	15.08.07	01:47	82° 48.55' N	61° 1.37' E	1648.0	MN	Hoisting

Station	Date	Time	Position Lat	Position Lon	Depth [m]	Gear Abbre- viation	Action
PS70/268-5	15.08.07	02:49	82° 48.29' N	61° 4.34' E	1767.0	MN	on deck
PS70/269-1	15.08.07	05:05	82° 43.96' N	60° 36.34' E	862.8	CTD/RO	surface
PS70/269-1	15.08.07	05:26	82° 43.95' N	60° 36.26' E	861.4	CTD/RO	at depth
PS70/269-1	15.08.07	05:57	82° 44.01' N	60° 35.79' E	860.8	CTD/RO	on deck
PS70/269-1	15.08.07	06:06	82° 44.01' N	60° 35.73' E	861.0	BC	surface
PS70/269-1	15.08.07	06:20	82° 44.01' N	60° 35.96' E	864.1	BC	at sea bottom
PS70/269-1	15.08.07	06:35	82° 44.05' N	60° 36.04' E	866.1	BC	on deck
PS70/269-1	15.08.07	06:54	82° 44.19' N	60° 35.46' E	873.4	MUC	surface
PS70/269-1	15.08.07	07:04	82° 44.22' N	60° 35.54' E	876.7	MUC	at sea bottom
PS70/269-1	15.08.07	07:20	82° 44.21' N	60° 35.50' E	876.1	MUC	on deck
PS70/269-4	15.08.07	07:38	82° 44.34' N	60° 35.60' E	887.1	GC	surface
PS70/269-4	15.08.07	07:48	82° 44.37' N	60° 35.50' E	888.8	GC	at sea bottom
PS70/269-4	15.08.07	07:48	82° 44.37' N	60° 35.50' E	888.8	GC	off ground hoisting
PS70/269-4	15.08.07	08:06	82° 44.47' N	60° 34.97' E	897.4	GC	on deck
PS70/270-1	15.08.07	10:56	82° 34.41' N	60° 6.60' E	326.2	BC	surface
PS70/270-1	15.08.07	11:03	82° 34.45' N	60° 6.78' E	324.9	BC	at sea bottom
PS70/270-1	15.08.07	11:12	82° 34.48' N	60° 7.10' E	322.7	BC	on deck
PS70/271-1	15.08.07	12:34	82° 30.03' N	60° 46.99' E	327.4	ICE	Alongside Floe
PS70/271-1	15.08.07	12:39	82° 30.07' N	60° 47.10' E	332.4	ICE	Ice Gangway on the ice
PS70/271-1	15.08.07	12:58	82° 30.18' N	60° 47.67' E	328.5	ICE	Scientists on the ice
PS70/271-2	15.08.07	12:59	82° 30.18' N	60° 47.71' E	326.7	CTD/UC	into Water
PS70/271-2	15.08.07	13:33	82° 30.34' N	60° 48.86' E	319.3	CTD/UC	on Deck
PS70/271-3	15.08.07	13:49	82° 30.39' N	60° 49.45' E	312.6	MN	surface
PS70/271-3	15.08.07	14:02	82° 30.43' N	60° 49.93' E	314.2	MN	at depth
PS70/271-3	15.08.07	14:03	82° 30.43' N	60° 49.97' E	314.5	MN	Hoisting
PS70/271-3	15.08.07	14:22	82° 30.47' N	60° 50.68' E	314.7	MN	on deck
PS70/271-4	15.08.07	14:31	82° 30.48' N	60° 51.01' E	313.8	BONGO	surface
PS70/271-4	15.08.07	14:42	82° 30.49' N	60° 51.41' E	314.1	BONGO	at depth
PS70/271-4	15.08.07	14:54	82° 30.49' N	60° 51.84' E	316.2	BONGO	on deck
PS70/271-5	15.08.07	15:01	82° 30.49' N	60° 52.08' E	315.4	MUC	surface
PS70/271-5	15.08.07	15:10	82° 30.48' N	60° 52.38' E	312.6	MUC	at sea bottom
PS70/271-5	15.08.07	15:18	82° 30.48' N	60° 52.63' E	309.7	MUC	on deck
PS70/271-1	15.08.07	18:20	82° 30.35' N	60° 53.13' E	303.5	ICE	Scientists on board
PS70/271-1	15.08.07	18:23	82° 30.35' N	60° 53.08' E	303.9	ICE	Ice Gangway on board
PS70/271-1	15.08.07	18:25	82° 30.35' N	60° 53.05' E	302.6	ICE	Departure from floe
PS70/272-1	15.08.07	21:43	82° 15.12' N	61° 59.76' E	230.8	CTD/UC	into Water
PS70/272-1	15.08.07	21:55	82° 15.15' N	61° 59.67' E	231.1	CTD/UC	on Depth
PS70/272-1	15.08.07	22:15	82° 15.22' N	61° 59.54' E	230.4	CTD/UC	on Deck
PS70/273-1	16.08.07	03:03	82° 12.74' N	64° 45.24' E	503.8	CTD/RO	surface

Station	Date	Time	Position Lat	Position Lon	Depth [m]	Gear Abbreviation	Action
PS70/273-1	16.08.07	03:18	82° 12.75' N	64° 45.57' E	504.7	CTD/RO	at depth
PS70/273-1	16.08.07	03:42	82° 12.75' N	64° 46.04' E	505.0	CTD/RO	on deck
PS70/274-1	16.08.07	13:24	82° 31.28' N	67° 6.60' E	1174.0	CTD/RO	surface
PS70/274-1	16.08.07	13:51	82° 31.41' N	67° 5.99' E	1176.0	CTD/RO	at depth
PS70/274-1	16.08.07	14:30	82° 31.49' N	67° 5.98' E	1178.0	CTD/RO	on deck
PS70/274-2	16.08.07	14:40	82° 31.45' N	67° 6.83' E	1182.0	MUC	surface
PS70/274-2	16.08.07	14:57	82° 31.50' N	67° 6.63' E	1182.0	MUC	at sea bottom
PS70/274-2	16.08.07	15:14	82° 31.54' N	67° 6.78' E	1188.0	MUC	on deck
PS70/274-3	16.08.07	15:32	82° 31.52' N	67° 7.05' E	1185.0	BC	surface
PS70/274-3	16.08.07	15:48	82° 31.54' N	67° 7.18' E	1187.0	BC	at sea bottom
PS70/274-3	16.08.07	16:03	82° 31.56' N	67° 7.38' E	1189.0	BC	on deck
PS70/274-4	16.08.07	16:35	82° 31.61' N	67° 7.39' E	1188.0	KAL	to the water
PS70/274-4	16.08.07	16:56	82° 31.66' N	67° 7.27' E	1193.0	KAL	on the ground
PS70/274-4	16.08.07	17:25	82° 31.74' N	67° 7.05' E	1194.0	KAL	on deck
PS70/275-1	16.08.07	23:44	82° 11.00' N	66° 57.51' E	640.5	CTD/RO	surface
PS70/275-1	17.08.07	00:02	82° 10.95' N	66° 58.51' E	638.8	CTD/RO	at depth
PS70/275-1	17.08.07	00:28	82° 11.11' N	66° 58.66' E	640.0	CTD/RO	on deck
PS70/276-1	17.08.07	03:48	82° 5.00' N	68° 57.58' E	679.8	CTD/UC	into Water
PS70/276-1	17.08.07	04:05	82° 5.05' N	68° 57.50' E	678.5	CTD/UC	on Depth
PS70/276-1	17.08.07	04:44	82° 5.07' N	68° 57.24' E	680.5	CTD/UC	on Deck
PS70/276-2	17.08.07	04:51	82° 5.09' N	68° 57.18' E	680.2	CTD/RO	surface
PS70/276-2	17.08.07	05:10	82° 5.13' N	68° 57.01' E	679.9	CTD/RO	at depth
PS70/276-2	17.08.07	05:32	82° 5.20' N	68° 57.00' E	680.0	CTD/RO	on deck
PS70/276-3	17.08.07	06:05	82° 5.28' N	68° 56.89' E	679.7	CTD/RO	surface
PS70/276-3	17.08.07	06:24	82° 5.36' N	68° 56.82' E	680.9	CTD/RO	at depth
PS70/276-3	17.08.07	06:48	82° 5.46' N	68° 56.83' E	680.8	CTD/RO	on deck
PS70/276-4	17.08.07	06:58	82° 5.51' N	68° 56.90' E	680.5	ISP	into water
PS70/276-4	17.08.07	07:22	82° 5.62' N	68° 57.14' E	681.0	ISP	pump at depth
PS70/276-5	17.08.07	09:12	82° 6.07' N	68° 59.86' E	680.1	HN	surface
PS70/276-5	17.08.07	09:19	82° 6.08' N	69° 0.09' E	680.8	HN	on deck
PS70/276-4	17.08.07	10:22	82° 6.19' N	69° 2.23' E	684.3	ISP	on deck
PS70/276-6	17.08.07	10:29	82° 6.21' N	69° 2.43' E	686.5	CTD/RO	surface
PS70/276-6	17.08.07	10:45	82° 6.21' N	69° 2.83' E	687.2	CTD/RO	at depth
PS70/276-6	17.08.07	11:06	82° 6.20' N	69° 3.41' E	688.4	CTD/RO	on deck
PS70/276-7	17.08.07	11:12	82° 6.19' N	69° 3.62' E	687.7	BC	surface
PS70/276-7	17.08.07	11:23	82° 6.18' N	69° 4.00' E	686.9	BC	at sea bottom
PS70/276-7	17.08.07	11:34	82° 6.16' N	69° 4.38' E	686.8	BC	on deck
PS70/276-8	17.08.07	12:31	82° 7.99' N	69° 12.07' E	691.8	EF	start
PS70/276-8	17.08.07	12:51	82° 7.91' N	69° 12.37' E	691.4	EF	End
PS70/277-1	18.08.07	13:40	82° 23.52' N	83° 49.93' E	1526.0	CTD/RO	surface
PS70/277-1	18.08.07	14:15	82° 23.92' N	83° 51.48' E	1527.0	CTD/RO	at depth
PS70/277-1	18.08.07	14:59	82° 24.37' N	83° 52.28' E	1550.0	CTD/RO	on deck
PS70/277-2	18.08.07	15:06	82° 24.44' N	83° 52.21' E	1555.0	BC	surface
PS70/277-2	18.08.07	15:26	82° 24.57' N	83° 52.21' E	1564.0	BC	at sea bottom
PS70/277-2	18.08.07	15:46	82° 24.65' N	83° 52.55' E	1568.0	BC	on deck
PS70/277-3	18.08.07	16:08	82° 24.75' N	83° 52.71' E	1574.0	GC	surface

Station	Date	Time	Position Lat	Position Lon	Depth [m]	Gear Abbreviation	Action
PS70/277-3	18.08.07	16:25	82° 24.83' N	83° 52.70' E	1579.0	GC	atsea bottom
PS70/277-3	18.08.07	16:47	82° 24.94' N	83° 52.59' E	1584.0	GC	on deck
PS70/278-1	19.08.07	03:09	81° 31.82' N	84° 3.54' E	384.8	CTD/RO	surface
PS70/278-1	19.08.07	03:24	81° 31.79' N	84° 4.02' E	386.0	CTD/RO	at depth
PS70/278-1	19.08.07	03:44	81° 31.70' N	84° 4.74' E	386.7	CTD/RO	on deck
PS70/279-1	19.08.07	11:15	81° 13.81' N	86° 10.89' E	325.1	CTD/RO	surface
PS70/279-1	19.08.07	11:29	81° 13.79' N	86° 11.24' E	327.6	CTD/RO	at depth
PS70/279-1	19.08.07	11:48	81° 13.77' N	86° 11.60' E	330.7	CTD/RO	on deck
PS70/279-2	19.08.07	12:25	81° 14.71' N	86° 12.13' E	334.7	CTD/UC	into Water
PS70/279-2	19.08.07	12:34	81° 14.68' N	86° 12.49' E	337.2	CTD/UC	on Depth
PS70/279-2	19.08.07	13:02	81° 14.54' N	86° 13.73' E	338.5	CTD/UC	on Deck
PS70/279-3	19.08.07	13:11	81° 14.50' N	86° 13.33' E	335.2	CTD/RO	surface
PS70/279-3	19.08.07	13:25	81° 14.43' N	86° 13.94' E	336.5	CTD/RO	at depth
PS70/279-3	19.08.07	13:40	81° 14.34' N	86° 14.84' E	343.5	CTD/RO	on deck
PS70/279-4	19.08.07	13:46	81° 14.30' N	86° 15.23' E	345.7	ISP	into water
PS70/279-4	19.08.07	14:19	81° 14.06' N	86° 17.28' E	354.5	ISP	pump at depth
PS70/279-5	19.08.07	15:09	81° 13.74' N	86° 17.30' E	350.4	HN	surface
PS70/279-5	19.08.07	15:18	81° 13.67' N	86° 17.31' E	353.4	HN	on deck
PS70/279-4	19.08.07	16:54	81° 12.48' N	86° 18.82' E	321.8	ISP	on deck
PS70/279-6	19.08.07	17:06	81° 12.32' N	86° 18.60' E	321.8	CTD/UC	into Water
PS70/279-6	19.08.07	17:16	81° 12.20' N	86° 18.47' E	317.2	CTD/UC	on Depth
PS70/279-6	19.08.07	17:45	81° 11.92' N	86° 19.46' E	316.6	CTD/UC	on Deck
PS70/279-7	19.08.07	17:54	81° 11.85' N	86° 19.70' E	318.6	CTD/RO	surface
PS70/279-7	19.08.07	18:07	81° 11.73' N	86° 19.67' E	321.5	CTD/RO	at depth
PS70/279-7	19.08.07	18:27	81° 11.58' N	86° 19.88' E	325.1	CTD/RO	on deck
PS70/279-8	19.08.07	18:39	81° 11.47' N	86° 19.69' E	321.6	MN	surface
PS70/279-8	19.08.07	18:47	81° 11.40' N	86° 19.55' E	319.3	MN	at depth
PS70/279-8	19.08.07	19:00	81° 11.26' N	86° 19.44' E	317.9	MN	on deck
PS70/279-9	19.08.07	19:18	81° 11.05' N	86° 19.51' E	318.4	CTD/RO	surface
PS70/279-9	19.08.07	19:24	81° 10.98' N	86° 19.50' E	315.6	CTD/RO	at depth
PS70/279-9	19.08.07	19:36	81° 10.88' N	86° 19.27' E	312.3	CTD/RO	on deck
PS70/279-10	19.08.07	19:41	81° 10.83' N	86° 19.18' E	312.2	BONGO	surface
PS70/279-10	19.08.07	19:45	81° 10.80' N	86° 19.13' E	311.2	BONGO	at depth
PS70/279-10	19.08.07	19:51	81° 10.74' N	86° 19.12' E	312.7	BONGO	on deck
PS70/279-11	19.08.07	19:54	81° 10.71' N	86° 19.10' E	313.3	BONGO	surface
PS70/279-11	19.08.07	20:08	81° 10.58' N	86° 18.99' E	312.2	BONGO	at depth
PS70/279-11	19.08.07	20:20	81° 10.47' N	86° 18.96' E	310.5	BONGO	on deck
PS70/279-12	19.08.07	20:24	81° 10.44' N	86° 18.96' E	309.1	BC	surface
PS70/279-12	19.08.07	20:30	81° 10.38' N	86° 18.98' E	309.4	BC	atsea bottom
PS70/279-12	19.08.07	20:38	81° 10.30' N	86° 19.08' E	309.5	BC	on deck
PS70/280-1	19.08.07	23:08	81° 24.92' N	86° 14.97' E	396.6	CTD/RO	surface
PS70/280-1	19.08.07	23:23	81° 24.91' N	86° 15.37' E	393.5	CTD/RO	at depth

Station	Date	Time	Position Lat	Position Lon	Depth [m]	Gear Abbre- viation	Action
PS70/280-1	19.08.07	23:46	81° 24.80' N	86° 16.62' E	400.7	CTD/RO	on deck
PS70/281-1	20.08.07	01:30	81° 34.53' N	86° 15.40' E	404.1	CTD/RO	surface
PS70/281-1	20.08.07	01:47	81° 34.51' N	86° 15.72' E	404.0	CTD/RO	at depth
PS70/281-1	20.08.07	02:08	81° 34.49' N	86° 15.86' E	404.9	CTD/RO	on deck
PS70/282-1	20.08.07	03:36	81° 42.96' N	86° 12.98' E	358.0	CTD/RO	surface
PS70/282-1	20.08.07	03:51	81° 42.88' N	86° 13.32' E	359.4	CTD/RO	at depth
PS70/282-1	20.08.07	04:10	81° 42.78' N	86° 13.58' E	359.9	CTD/RO	on deck
PS70/282-2	20.08.07	04:15	81° 42.75' N	86° 13.61' E	360.6	BC	surface
PS70/282-2	20.08.07	04:21	81° 42.72' N	86° 13.68' E	361.9	BC	at sea bottom
PS70/282-2	20.08.07	04:31	81° 42.63' N	86° 13.80' E	359.6	BC	on deck
PS70/283-1	20.08.07	07:04	81° 52.16' N	86° 6.73' E	442.6	CTD/RO	surface
PS70/283-1	20.08.07	07:17	81° 52.17' N	86° 6.51' E	444.0	CTD/RO	at depth
PS70/283-1	20.08.07	07:42	81° 52.02' N	86° 6.47' E	439.5	CTD/RO	on deck
PS70/284-1	20.08.07	09:57	82° 1.27' N	86° 12.13' E	487.7	CTD/RO	surface
PS70/284-1	20.08.07	10:13	82° 1.35' N	86° 11.72' E	492.8	CTD/RO	at depth
PS70/284-1	20.08.07	10:38	82° 1.26' N	86° 11.92' E	490.2	CTD/RO	on deck
PS70/285-1	20.08.07	12:35	82° 8.61' N	86° 19.11' E	726.0	ICE	Alongside Floe
PS70/285-1	20.08.07	12:54	82° 8.59' N	86° 19.08' E	725.5	ICE	Ice Gangway on the ice
PS70/285-1	20.08.07	13:31	0° 0.00' N	0° 0.00' E	0.0	ICE	Scientists on the ice
PS70/285-2	20.08.07	13:32	82° 8.51' N	86° 19.75' E	720.5	CTD/UC	into Water
PS70/285-2	20.08.07	13:51	82° 8.47' N	86° 20.20' E	723.6	CTD/UC	on Depth
PS70/285-2	20.08.07	14:33	82° 8.36' N	86° 21.40' E	719.3	CTD/UC	on Deck
PS70/285-3	20.08.07	14:37	82° 8.34' N	86° 21.52' E	718.4	BONGO	surface
PS70/285-3	20.08.07	15:03	82° 8.26' N	86° 22.40' E	712.1	BONGO	at depth
PS70/285-3	20.08.07	15:30	82° 8.15' N	86° 23.34' E	705.1	BONGO	on deck
PS70/285-4	20.08.07	15:33	82° 8.13' N	86° 23.44' E	704.8	BONGO	surface
PS70/285-4	20.08.07	15:38	82° 8.11' N	86° 23.61' E	701.4	BONGO	at depth
PS70/285-4	20.08.07	15:43	82° 8.09' N	86° 23.78' E	702.4	BONGO	on deck
PS70/285-5	20.08.07	15:51	82° 8.05' N	86° 24.04' E	700.6	MN	surface
PS70/285-5	20.08.07	16:11	82° 7.95' N	86° 24.69' E	698.1	MN	at depth
PS70/285-5	20.08.07	16:40	82° 7.80' N	86° 25.61' E	695.6	MN	on deck
PS70/285-6	20.08.07	16:48	82° 7.75' N	86° 25.84' E	689.6	MUC	surface
PS70/285-6	20.08.07	16:56	82° 7.71' N	86° 26.07' E	687.0	MUC	at sea bottom
PS70/285-6	20.08.07	17:08	82° 7.64' N	86° 26.40' E	682.9	MUC	on deck
PS70/285-7	20.08.07	17:24	82° 7.53' N	86° 26.82' E	679.2	BC	surface
PS70/285-7	20.08.07	17:34	82° 7.47' N	86° 27.05' E	677.2	BC	at sea bottom
PS70/285-7	20.08.07	17:47	82° 7.38' N	86° 27.33' E	674.6	BC	on deck
PS70/285-8	20.08.07	17:57	82° 7.32' N	86° 27.53' E	672.1	GC	surface
PS70/285-8	20.08.07	18:07	82° 7.25' N	86° 27.72' E	668.8	GC	at sea bottom
PS70/285-8	20.08.07	18:20	82° 7.16' N	86° 27.93' E	665.2	GC	on deck
PS70/285-1	20.08.07	18:38	82° 7.04' N	86° 28.17' E	660.6	ICE	Scientists on board
PS70/285-1	20.08.07	18:48	82° 6.97' N	86° 28.34' E	658.0	ICE	Departure from floe
PS70/286-1	20.08.07	20:31	82° 14.38' N	86° 15.20' E	1054.0	CTD/RO	surface

Station	Date	Time	Position Lat	Position Lon	Depth [m]	Gear Abbre- viation	Action
PS70/286-1	20.08.07	20:57	82° 14.25' N	86° 15.16' E	1044.0	CTD/RO	at depth
PS70/286-1	20.08.07	21:32	82° 14.14' N	86° 14.66' E	1037.0	CTD/RO	on deck
PS70/287-1	20.08.07	22:53	82° 20.05' N	86° 11.64' E	1387.0	CTD/RO	surface
PS70/287-1	20.08.07	23:23	82° 20.00' N	86° 11.61' E	1383.0	CTD/RO	at depth
PS70/287-1	21.08.07	00:03	82° 19.98' N	86° 11.94' E	1383.0	CTD/RO	on deck
PS70/288-1	21.08.07	01:25	82° 25.19' N	86° 20.04' E	1663.0	CTD/RO	surface
PS70/288-1	21.08.07	02:01	82° 25.27' N	86° 20.41' E	1666.0	CTD/RO	at depth
PS70/288-1	21.08.07	02:51	82° 25.19' N	86° 21.54' E	1667.0	CTD/RO	on deck
PS70/289-1	21.08.07	03:48	82° 30.08' N	86° 15.70' E	1857.0	CTD/RO	surface
PS70/289-1	21.08.07	04:26	82° 30.06' N	86° 16.83' E	1860.0	CTD/RO	at depth
PS70/289-1	21.08.07	05:16	82° 29.97' N	86° 17.99' E	1859.0	CTD/RO	on deck
PS70/290-1	21.08.07	06:34	82° 34.80' N	86° 25.40' E	2078.0	CTD/RO	surface
PS70/290-1	21.08.07	07:18	82° 34.60' N	86° 26.29' E	2071.0	CTD/RO	at depth
PS70/290-1	21.08.07	08:11	82° 34.36' N	86° 26.64' E	2066.0	CTD/RO	on deck
PS70/290-2	21.08.07	08:20	82° 34.29' N	86° 27.17' E	2063.0	MN	surface
PS70/290-2	21.08.07	09:13	82° 34.10' N	86° 27.71' E	2049.0	MN	at depth
PS70/290-2	21.08.07	10:29	82° 33.95' N	86° 28.02' E	2044.0	MN	on deck
PS70/290-3	21.08.07	10:42	82° 33.92' N	86° 28.27' E	2042.0	BONGO	surface
PS70/290-3	21.08.07	11:20	82° 33.91' N	86° 27.96' E	2041.0	BONGO	at depth
PS70/290-3	21.08.07	11:56	82° 33.98' N	86° 27.39' E	2045.0	BONGO	on deck
PS70/290-4	21.08.07	11:57	82° 33.98' N	86° 27.38' E	2046.0	BONGO	surface
PS70/290-4	21.08.07	12:04	82° 34.00' N	86° 27.29' E	2048.0	BONGO	at depth
PS70/290-4	21.08.07	12:11	82° 34.02' N	86° 27.19' E	2046.0	BONGO	on deck
PS70/291-1	21.08.07	13:53	82° 42.61' N	86° 15.92' E	2396.0	CTD/UC	into Water
PS70/291-1	21.08.07	14:33	82° 42.71' N	86° 16.33' E	2400.0	CTD/UC	on Depth
PS70/291-1	21.08.07	15:39	82° 42.88' N	86° 17.66' E	2407.0	CTD/UC	on Deck
PS70/292-1	21.08.07	21:33	82° 48.79' N	86° 16.84' E	2650.0	CTD/RO	surface
PS70/292-1	21.08.07	22:26	82° 48.65' N	86° 16.17' E	2646.0	CTD/RO	at depth
PS70/292-1	21.08.07	23:36	82° 48.56' N	86° 15.36' E	2640.0	CTD/RO	on deck
PS70/293-1	22.08.07	01:54	82° 58.11' N	86° 16.01' E	2950.0	CTD/RO	surface
PS70/293-1	22.08.07	02:52	82° 58.26' N	86° 16.38' E	2955.0	CTD/RO	at depth
PS70/293-1	22.08.07	04:05	82° 58.48' N	86° 17.84' E	2958.0	CTD/RO	on deck
PS70/294-1	22.08.07	06:16	83° 6.88' N	86° 14.72' E	3148.0	CTD/RO	surface
PS70/294-1	22.08.07	07:19	83° 6.86' N	86° 16.54' E	3148.0	CTD/RO	at depth
PS70/294-1	22.08.07	08:39	83° 6.74' N	86° 17.85' E	3148.0	CTD/RO	on deck
PS70/294-2	22.08.07	08:45	83° 6.73' N	86° 17.87' E	3145.0	BC	surface
PS70/294-2	22.08.07	09:23	83° 6.65' N	86° 17.95' E	3148.0	BC	at sea bottom
PS70/294-2	22.08.07	10:02	83° 6.59' N	86° 17.77' E	3140.0	BC	on deck
PS70/294-3	22.08.07	10:09	83° 6.58' N	86° 17.70' E	3143.0	MUC	surface
PS70/294-3	22.08.07	10:41	83° 6.55' N	86° 17.37' E	3140.0	MUC	at sea bottom
PS70/294-3	22.08.07	11:22	83° 6.50' N	86° 17.07' E	3139.0	MUC	on deck
PS70/294-4	22.08.07	11:41	83° 6.49' N	86° 16.87' E	3138.0	GC	surface
PS70/294-4	22.08.07	12:12	83° 6.47' N	86° 16.50' E	3138.0	GC	at sea bottom
PS70/294-4	22.08.07	12:13	83° 6.47' N	86° 16.49' E	3138.0	GC	off ground hoisting
PS70/294-4	22.08.07	12:55	83° 6.47' N	86° 15.95' E	3140.0	GC	on deck
PS70/294-5	22.08.07	14:24	83° 6.58' N	86° 15.06' E	3138.0	KAL	to the water
PS70/294-5	22.08.07	15:14	83° 6.70' N	86° 15.01' E	3145.0	KAL	on the ground

Station	Date	Time	Position Lat	Position Lon	Depth [m]	Gear Abbre- viation	Action
PS70/294-5	22.08.07	16:04	83° 6.85' N	86° 15.17' E	3149.0	KAL	on deck
PS70/295-1	22.08.07	19:26	83° 16.33' N	86° 16.97' E	3359.0	CTD/UC	into Water
PS70/295-1	22.08.07	20:22	83° 16.14' N	86° 18.04' E	3357.0	CTD/UC	on Depth
PS70/295-1	22.08.07	21:55	83° 15.75' N	86° 18.16' E	3349.0	CTD/UC	on Deck
PS70/296-1	23.08.07	00:20	83° 26.11' N	86° 44.66' E	3508.0	CTD/RO	surface
PS70/296-1	23.08.07	01:21	83° 25.91' N	86° 44.42' E	3505.0	CTD/RO	at depth
PS70/296-1	23.08.07	02:36	83° 25.96' N	86° 43.00' E	3506.0	CTD/RO	on deck
PS70/297-1	23.08.07	04:38	83° 35.25' N	87° 14.21' E	3562.0	CTD/RO	surface
PS70/297-1	23.08.07	05:40	83° 35.22' N	87° 15.33' E	3563.0	CTD/RO	at depth
PS70/297-1	23.08.07	06:46	83° 35.06' N	87° 16.49' E	3559.0	CTD/RO	on deck
PS70/298-1	23.08.07	10:00	83° 48.40' N	88° 5.93' E	3631.0	CTD/RO	surface
PS70/298-1	23.08.07	11:03	83° 48.06' N	88° 2.82' E	3632.0	CTD/RO	at depth
PS70/298-1	23.08.07	12:18	83° 47.78' N	87° 58.13' E	3636.0	CTD/RO	on deck
PS70/299-1	23.08.07	17:09	84° 3.06' N	89° 2.53' E	3693.0	CTD/UC	into Water
PS70/299-1	23.08.07	18:10	84° 3.02' N	89° 3.42' E	3694.0	CTD/UC	on Depth
PS70/299-1	23.08.07	19:46	84° 2.63' N	89° 5.56' E	3699.0	CTD/UC	on Deck
PS70/299-2	23.08.07	20:03	84° 2.52' N	89° 5.80' E	3701.0	BC	surface
PS70/299-2	23.08.07	20:48	84° 2.22' N	89° 6.07' E	3696.0	BC	at sea bottom
PS70/299-2	23.08.07	21:35	84° 1.87' N	89° 5.63' E	3693.0	BC	on deck
PS70/300-1	24.08.07	01:30	84° 20.25' N	89° 17.34' E	3737.0	CTD/RO	surface
PS70/300-1	24.08.07	02:42	84° 20.20' N	89° 14.30' E	3738.0	CTD/RO	at depth
PS70/300-1	24.08.07	04:01	84° 20.26' N	89° 13.45' E	3740.0	CTD/RO	on deck
PS70/301-1	24.08.07	09:00	84° 34.97' N	89° 49.17' E	3751.0	ICE	Alongside Floe
PS70/301-1	24.08.07	09:15	84° 34.85' N	89° 50.02' E	3761.0	ICE	Ice Gangway on the ice
PS70/301-2	24.08.07	09:20	84° 34.81' N	89° 50.14' E	3767.0	CTD/UC	into Water
PS70/301-1	24.08.07	09:25	84° 34.77' N	89° 50.26' E	3760.0	ICE	Scientists on the ice
PS70/301-2	24.08.07	10:23	84° 34.30' N	89° 50.89' E	3762.0	CTD/UC	on Depth
PS70/301-2	24.08.07	11:59	84° 33.65' N	89° 48.86' E	3760.0	CTD/UC	on Deck
PS70/301-3	24.08.07	12:08	84° 33.61' N	89° 48.48' E	3755.0	CTD/RO	surface
PS70/301-3	24.08.07	13:13	84° 33.42' N	89° 45.50' E	3758.0	CTD/RO	at depth
PS70/301-3	24.08.07	14:17	84° 33.43' N	89° 43.46' E	3755.0	CTD/RO	on deck
PS70/301-4	24.08.07	14:25	84° 33.44' N	89° 43.30' E	3759.0	ISP	into water
PS70/301-4	24.08.07	15:03	84° 33.51' N	89° 42.88' E	3749.0	ISP	pump at depth
PS70/301-4	24.08.07	18:01	84° 33.86' N	89° 49.67' E	3752.0	ISP	on deck
PS70/301-5	24.08.07	18:07	84° 33.86' N	89° 50.11' E	3756.0	CTD/RO	surface
PS70/301-5	24.08.07	18:29	84° 33.85' N	89° 51.81' E	3755.0	CTD/RO	at depth
PS70/301-5	24.08.07	18:54	84° 33.81' N	89° 53.79' E	3757.0	CTD/RO	on deck
PS70/301-6	24.08.07	19:03	84° 33.79' N	89° 54.50' E	3751.0	BONGO	surface
PS70/301-6	24.08.07	20:01	84° 33.58' N	89° 58.96' E	3761.0	BONGO	at depth
PS70/301-1	24.08.07	20:48	84° 33.33' N	90° 1.90' E	3758.0	ICE	Scientists on board
PS70/301-6	24.08.07	20:56	84° 33.29' N	90° 2.32' E	3761.0	BONGO	on deck
PS70/301-1	24.08.07	20:58	84° 33.27' N	90° 2.43' E	3766.0	ICE	Ice Gangway on board
PS70/301-7	24.08.07	21:05	84° 33.23' N	90° 2.78' E	3757.0	CTD/RO	surface
PS70/301-7	24.08.07	21:16	84° 33.17' N	90° 3.31' E	3765.0	CTD/RO	at depth

Station	Date	Time	Position Lat	Position Lon	Depth [m]	Gear Abbre- viation	Action
PS70/301-7	24.08.07	21:34	84° 33.06' N	90° 4.08' E	3757.0	CTD/RO	on deck
PS70/301-8	24.08.07	21:41	84° 33.01' N	90° 4.34' E	3762.0	BONGO	surface
PS70/301-8	24.08.07	21:53	84° 32.94' N	90° 4.75' E	3754.0	BONGO	at depth
PS70/301-8	24.08.07	22:06	84° 32.85' N	90° 5.12' E	3750.0	BONGO	on deck
PS70/301-9	24.08.07	22:15	84° 32.79' N	90° 5.34' E	3758.0	CTD/RO	surface
PS70/301-9	24.08.07	22:23	84° 32.74' N	90° 5.51' E	3757.0	CTD/RO	at depth
PS70/301-9	24.08.07	22:34	84° 32.67' N	90° 5.70' E	3753.0	CTD/RO	on deck
PS70/301-10	24.08.07	22:42	84° 32.62' N	90° 5.82' E	3754.0	MN	surface
PS70/301-10	25.08.07	00:17	84° 32.16' N	90° 5.81' E	3754.0	MN	at depth
PS70/301-10	25.08.07	00:18	84° 32.16' N	90° 5.80' E	3758.0	MN	Hoisting
PS70/301-10	25.08.07	02:33	84° 32.15' N	90° 5.79' E	3756.0	MN	on deck
PS70/301-11	25.08.07	02:37	84° 32.16' N	90° 5.87' E	3753.0	BC	surface
PS70/301-11	25.08.07	03:24	84° 32.31' N	90° 7.17' E	3762.0	BC	at sea bottom
PS70/301-11	25.08.07	04:11	84° 32.48' N	90° 9.33' E	3761.0	BC	on deck
PS70/302-1	25.08.07	10:38	84° 53.56' N	90° 3.27' E	3776.0	CTD/UC	into Water
PS70/302-1	25.08.07	11:40	84° 53.23' N	90° 5.94' E	3778.0	CTD/UC	on Depth
PS70/302-1	25.08.07	13:18	84° 53.02' N	90° 6.35' E	3778.0	CTD/UC	on Deck
PS70/303-1	25.08.07	17:37	85° 14.58' N	90° 9.69' E	3967.0	CTD/RO	surface
PS70/303-1	25.08.07	18:47	85° 14.78' N	90° 13.86' E	3985.0	CTD/RO	at depth
PS70/303-1	25.08.07	20:01	85° 14.91' N	90° 19.28' E	3996.0	CTD/RO	on deck
PS70/304-1	25.08.07	21:23	85° 18.54' N	90° 14.39' E	4328.0	XCTD	surface
PS70/305-1	26.08.07	01:38	85° 35.79' N	90° 41.53' E	3715.0	CTD/RO	surface
PS70/305-1	26.08.07	02:45	85° 35.63' N	90° 38.74' E	3844.0	CTD/RO	at depth
PS70/305-1	26.08.07	04:02	85° 35.68' N	90° 34.05' E	3868.0	CTD/RO	on deck
PS70/306-1	26.08.07	08:52	85° 55.37' N	91° 7.26' E	4018.0	CTD/UC	into Water
PS70/306-1	26.08.07	09:54	85° 55.42' N	91° 10.79' E	4019.0	CTD/UC	on Depth
PS70/306-1	26.08.07	11:32	85° 55.16' N	91° 14.72' E	4037.0	CTD/UC	on Deck
PS70/306-2	26.08.07	11:54	85° 54.79' N	90° 56.45' E	4084.0	BC	surface
PS70/306-2	26.08.07	12:41	85° 54.71' N	90° 56.13' E	4079.0	BC	at sea bottom
PS70/306-2	26.08.07	13:31	85° 54.48' N	90° 54.68' E	4067.0	BC	on deck
PS70/306-3	26.08.07	13:42	85° 54.49' N	90° 54.35' E	4068.0	GC	surface
PS70/306-3	26.08.07	14:23	85° 54.33' N	90° 51.96' E	4053.0	GC	at sea bottom
PS70/306-3	26.08.07	14:23	85° 54.33' N	90° 51.96' E	4053.0	GC	off ground hoisting
PS70/306-3	26.08.07	15:10	85° 54.21' N	90° 48.66' E	4037.0	GC	on deck
PS70/307-1	26.08.07	20:40	86° 18.19' N	94° 16.95' E	3982.0	CTD/RO	surface
PS70/307-1	26.08.07	21:51	86° 18.06' N	94° 20.94' E	3992.0	CTD/RO	at depth
PS70/307-1	26.08.07	23:11	86° 17.86' N	94° 24.74' E	3973.0	CTD/RO	on deck
PS70/307-2	26.08.07	23:21	86° 17.82' N	94° 25.11' E	3969.0	MN	surface
PS70/307-2	27.08.07	00:59	86° 17.33' N	94° 26.47' E	3988.0	MN	at depth
PS70/307-2	27.08.07	01:00	86° 17.32' N	94° 26.46' E	3983.0	MN	Hoisting
PS70/307-2	27.08.07	03:19	86° 16.66' N	94° 20.51' E	4123.0	MN	on deck
PS70/307-3	27.08.07	03:28	86° 16.63' N	94° 19.89' E	4133.0	BONGO	surface
PS70/307-3	27.08.07	03:32	86° 16.62' N	94° 19.63' E	4135.0	BONGO	at depth

Station	Date	Time	Position Lat	Position Lon	Depth [m]	Gear Abbre- viation	Action
PS70/307-3	27.08.07	03:38	86° 16.60' N	94° 19.27' E	4135.0	BONGO	on deck
PS70/307-4	27.08.07	03:41	86° 16.58' N	94° 19.02' E	4137.0	BONGO	surface
PS70/307-4	27.08.07	04:35	86° 16.48' N	94° 15.57' E	4162.0	BONGO	at depth
PS70/307-4	27.08.07	05:33	86° 16.53' N	94° 12.79' E	4175.0	BONGO	on deck
PS70/308-1	27.08.07	11:47	86° 42.35' N	99° 16.20' E	4454.0	CTD/RO	surface
PS70/308-1	27.08.07	13:06	86° 41.82' N	99° 18.52' E	4453.0	CTD/RO	at depth
PS70/308-1	27.08.07	14:33	86° 41.39' N	99° 17.90' E	4447.0	CTD/RO	on deck
PS70/309-1	27.08.07	21:00	87° 2.77' N	104° 42.84' E	4447.0	ICE	Alongside Floe
PS70/309-1	27.08.07	21:30	87° 2.74' N	104° 45.41' E	4454.0	ICE	Ice Gangway on the ice
PS70/309-2	27.08.07	21:44	87° 2.74' N	104° 47.21' E	4447.0	CTD/UC	into Water
PS70/309-1	27.08.07	21:49	87° 2.74' N	104° 47.78' E	4450.0	ICE	Scientists on the ice
PS70/309-2	27.08.07	22:12	87° 2.71' N	104° 50.31' E	4444.0	CTD/UC	on Depth
PS70/309-2	27.08.07	23:01	87° 2.59' N	104° 54.94' E	4446.0	CTD/UC	on Deck
PS70/309-3	27.08.07	23:10	87° 2.56' N	104° 55.64' E	4445.0	CTD/RO	surface
PS70/309-3	28.08.07	00:27	87° 2.25' N	104° 59.02' E	4449.0	CTD/RO	at depth
PS70/309-3	28.08.07	01:37	87° 2.00' N	104° 57.85' E	4443.0	CTD/RO	on deck
PS70/309-4	28.08.07	01:56	87° 1.95' N	104° 56.85' E	4442.0	CTD/UC	into Water
PS70/309-4	28.08.07	03:08	87° 1.94' N	104° 51.24' E	4449.0	CTD/UC	on Depth
PS70/309-1	28.08.07	04:01	87° 2.10' N	104° 46.19' E	4449.0	ICE	Information
PS70/309-4	28.08.07	04:49	87° 2.35' N	104° 41.91' E	4444.0	CTD/UC	on Deck
PS70/309-5	28.08.07	04:59	87° 2.41' N	104° 41.14' E	4449.0	CTD/RO	surface
PS70/309-5	28.08.07	05:06	87° 2.45' N	104° 40.63' E	4450.0	CTD/RO	at depth
PS70/309-5	28.08.07	05:21	87° 2.54' N	104° 39.62' E	4450.0	CTD/RO	on deck
PS70/309-6	28.08.07	05:43	87° 2.68' N	104° 38.34' E	4450.0	ISP	into water
PS70/309-6	28.08.07	06:21	87° 2.95' N	104° 36.68' E	4448.0	ISP	pump at depth
PS70/309-6	28.08.07	09:11	87° 3.95' N	104° 37.62' E	4444.0	ISP	on deck
PS70/309-7	28.08.07	09:18	87° 3.97' N	104° 37.83' E	4442.0	CTD/RO	surface
PS70/309-1	28.08.07	09:30	87° 4.01' N	104° 38.19' E	4442.0	ICE	Scientists on the ice
PS70/309-7	28.08.07	09:50	87° 4.07' N	104° 38.75' E	4449.0	CTD/RO	at depth
PS70/309-7	28.08.07	10:23	87° 4.13' N	104° 39.47' E	4444.0	CTD/RO	on deck
PS70/309-8	28.08.07	10:30	87° 4.14' N	104° 39.57' E	4447.0	BC	surface
PS70/309-8	28.08.07	11:24	87° 4.18' N	104° 39.56' E	4443.0	BC	at sea bottom
PS70/309-8	28.08.07	12:19	87° 4.17' N	104° 37.65' E	4449.0	BC	on deck
PS70/309-9	28.08.07	12:25	87° 4.17' N	104° 37.33' E	4450.0	XCTD	surface
PS70/309-1	28.08.07	12:52	87° 4.17' N	104° 35.61' E	4447.0	ICE	Scientists on board
PS70/309-1	28.08.07	12:55	87° 4.17' N	104° 35.39' E	4449.0	ICE	Ice Gangway on board
PS70/309-1	28.08.07	12:56	87° 4.17' N	104° 35.31' E	4443.0	ICE	Departure from floe
PS70/310-1	28.08.07	22:07	87° 39.46' N	112° 2.23' E	4414.0	CTD/UC	into Water
PS70/310-1	28.08.07	23:19	87° 39.81' N	111° 57.18' E	4406.0	CTD/UC	on Depth
PS70/310-1	29.08.07	01:01	87° 40.19' N	111° 44.50' E	4412.0	CTD/UC	on Deck
PS70/310-2	29.08.07	01:12	87° 40.23' N	111° 42.95' E	4415.0	CTD/RO	surface
PS70/310-2	29.08.07	02:30	87° 40.56' N	111° 31.23' E	4417.0	CTD/RO	at depth

Station	Date	Time	Position Lat	Position Lon	Depth [m]	Gear Abbre- viation	Action
PS70/310-2	29.08.07	03:44	87° 40.98' N	111° 19.23' E	4415.0	CTD/RO	on deck
PS70/311-1	29.08.07	06:27	87° 49.29' N	113° 14.76' E	4401.0	XCTD	surface
PS70/311-2	29.08.07	06:33	87° 49.34' N	113° 14.02' E	4400.0	XCTD	surface
PS70/312-1	29.08.07	13:23	88° 7.11' N	120° 12.56' E	3046.0	CTD/RO	surface
PS70/312-1	29.08.07	14:19	88° 7.47' N	120° 8.81' E	3009.0	CTD/RO	at depth
PS70/312-1	29.08.07	15:21	88° 7.90' N	120° 3.64' E	3009.0	CTD/RO	on deck
PS70/312-2	29.08.07	15:31	88° 7.95' N	120° 2.70' E	3015.0	MN	surface
PS70/312-2	29.08.07	16:46	88° 8.47' N	119° 58.67' E	2976.0	MN	at depth
PS70/312-2	29.08.07	18:33	88° 9.25' N	119° 52.74' E	2957.0	MN	on deck
PS70/312-3	29.08.07	18:40	88° 9.30' N	119° 52.25' E	2969.0	BONGO	surface
PS70/312-3	29.08.07	18:48	88° 9.35' N	119° 51.99' E	2960.0	BONGO	at depth
PS70/312-3	29.08.07	18:54	88° 9.40' N	119° 51.33' E	2963.0	BONGO	on deck
PS70/312-4	29.08.07	18:57	88° 9.42' N	119° 51.01' E	2960.0	BONGO	surface
PS70/312-4	29.08.07	20:00	88° 9.82' N	119° 48.33' E	2961.0	BONGO	at depth
PS70/312-4	29.08.07	20:55	88° 10.19' N	119° 47.01' E	2979.0	BONGO	on deck
PS70/312-5	29.08.07	21:00	88° 10.24' N	119° 46.15' E	2977.0	XCTD	surface
PS70/313-1	29.08.07	22:48	88° 9.19' N	124° 49.56' E	2998.0	XCTD	surface
PS70/314-1	30.08.07	00:47	88° 9.73' N	130° 6.21' E	2600.0	CTD/RO	surface
PS70/314-1	30.08.07	01:35	88° 9.97' N	130° 3.43' E	2558.0	CTD/RO	at depth
PS70/314-1	30.08.07	02:33	88° 10.24' N	129° 59.41' E	2523.0	CTD/RO	on deck
PS70/314-2	30.08.07	02:46	88° 10.28' N	129° 59.03' E	2514.0	MN	surface
PS70/314-2	30.08.07	03:52	88° 10.62' N	129° 54.55' E	2524.0	MN	at depth
PS70/314-2	30.08.07	05:20	88° 11.07' N	129° 45.50' E	2437.0	MN	on deck
PS70/315-1	30.08.07	07:23	88° 11.05' N	135° 2.94' E	1385.0	XCTD	surface
PS70/316-1	30.08.07	09:18	88° 10.58' N	139° 37.07' E	1299.0	CTD/UC	into Water
PS70/316-1	30.08.07	09:46	88° 10.75' N	139° 36.22' E	1298.0	CTD/UC	on Depth
PS70/316-1	30.08.07	10:34	88° 11.06' N	139° 34.29' E	1306.0	CTD/UC	on Deck
PS70/316-2	30.08.07	10:38	88° 11.08' N	139° 34.16' E	1306.0	XCTD	surface
PS70/316-3	30.08.07	10:48	88° 11.15' N	139° 33.78' E	1305.0	MN	surface
PS70/316-3	30.08.07	11:24	88° 11.37' N	139° 32.49' E	1314.0	MN	at depth
PS70/316-3	30.08.07	12:14	88° 11.68' N	139° 30.86' E	1317.0	MN	on deck
PS70/316-4	30.08.07	12:41	88° 11.84' N	139° 29.97' E	1321.0	MN	surface
PS70/316-4	30.08.07	12:59	88° 11.95' N	139° 29.34' E	1324.0	MN	at depth
PS70/316-4	30.08.07	13:00	88° 11.95' N	139° 29.31' E	1328.0	MN	Hoisting
PS70/316-4	30.08.07	13:23	88° 12.09' N	139° 28.50' E	1331.0	MN	on deck
PS70/316-5	30.08.07	13:30	88° 12.13' N	139° 28.25' E	1330.0	BC	surface
PS70/316-5	30.08.07	13:48	88° 12.24' N	139° 27.58' E	1335.0	BC	at sea bottom
PS70/316-5	30.08.07	14:08	88° 12.36' N	139° 26.80' E	1335.0	BC	on deck
PS70/316-6	30.08.07	14:15	88° 12.40' N	139° 26.51' E	1335.0	MUC	surface
PS70/316-6	30.08.07	14:31	88° 12.50' N	139° 25.86' E	1338.0	MUC	at sea bottom
PS70/316-6	30.08.07	14:49	88° 12.60' N	139° 25.12' E	1339.0	MUC	on deck
PS70/316-7	30.08.07	15:10	88° 12.72' N	139° 24.28' E	1343.0	GC	surface
PS70/316-7	30.08.07	15:25	88° 12.81' N	139° 23.67' E	1346.0	GC	at sea bottom
PS70/316-7	30.08.07	15:26	88° 12.81' N	139° 23.63' E	1345.0	GC	off ground hoisting
PS70/316-7	30.08.07	15:47	88° 12.93' N	139° 22.77' E	1349.0	GC	on deck
PS70/317-1	30.08.07	18:35	88° 21.39' N	142° 51.00' E	2677.0	EF	start
PS70/317-1	30.08.07	18:51	88° 21.48' N	142° 50.52' E	2670.0	EF	End
PS70/318-1	30.08.07	20:30	88° 27.29' N	146° 11.34' E	2612.0	CTD/RO	surface
PS70/318-1	30.08.07	21:18	88° 27.60' N	146° 10.84' E	2601.0	CTD/RO	at depth

Station	Date	Time	Position Lat	Position Lon	Depth [m]	Gear Abbreviation	Action
PS70/318-1	30.08.07	22:12	88° 27.99' N	146° 12.91' E	2590.0	CTD/RO	on deck
PS70/319-1	31.08.07	01:33	88° 39.86' N	153° 39.66' E	2743.0	CTD/UC	into Water
PS70/319-1	31.08.07	02:21	88° 40.05' N	153° 42.58' E	2742.0	CTD/UC	on Depth
PS70/319-1	31.08.07	03:40	88° 40.38' N	153° 43.94' E	2742.0	CTD/UC	on Deck
PS70/319-2	31.08.07	03:57	88° 40.42' N	153° 43.76' E	2744.0	BC	surface
PS70/319-2	31.08.07	04:26	88° 40.51' N	153° 44.06' E	2746.0	BC	atsea bottom
PS70/319-2	31.08.07	05:03	88° 40.58' N	153° 43.46' E	2746.0	BC	on deck
PS70/319-3	31.08.07	05:18	88° 40.62' N	153° 45.53' E	2742.0	KAL	to the water
PS70/319-3	31.08.07	06:06	88° 40.65' N	153° 45.27' E	2742.0	KAL	on the ground
PS70/319-3	31.08.07	06:55	88° 40.79' N	153° 43.18' E	2741.0	KAL	on deck
PS70/320-1	31.08.07	11:05	88° 24.49' N	150° 20.18' E	1975.0	CTD/RO	surface
PS70/320-1	31.08.07	11:42	88° 24.67' N	150° 19.56' E	1952.0	CTD/RO	atdepth
PS70/320-1	31.08.07	12:31	88° 24.87' N	150° 17.92' E	1926.0	CTD/RO	on deck
PS70/321-1	31.08.07	14:11	88° 15.25' N	150° 6.26' E	2241.0	CTD/RO	surface
PS70/321-1	31.08.07	14:56	88° 15.36' N	150° 8.54' E	2249.0	CTD/RO	atdepth
PS70/321-1	31.08.07	15:49	88° 15.51' N	150° 9.03' E	2238.0	CTD/RO	on deck
PS70/322-1	31.08.07	17:50	88° 7.63' N	150° 4.63' E	2773.0	ICE	Alongside Floe
PS70/322-1	31.08.07	17:59	88° 7.68' N	150° 5.78' E	2770.0	ICE	Ice Gangway on the ice
PS70/322-1	31.08.07	18:17	88° 7.76' N	150° 7.04' E	2770.0	ICE	Scientists on the ice
PS70/322-2	31.08.07	18:18	88° 7.76' N	150° 7.11' E	2772.0	CTD/RO	surface
PS70/322-2	31.08.07	19:06	88° 7.92' N	150° 10.63' E	2772.0	CTD/RO	atdepth
PS70/322-2	31.08.07	20:04	88° 8.11' N	150° 15.53' E	2805.0	CTD/RO	on deck
PS70/322-3	31.08.07	20:15	88° 8.15' N	150° 16.48' E	2806.0	MN	surface
PS70/322-3	31.08.07	21:25	88° 8.41' N	150° 23.46' E	2827.0	MN	atdepth
PS70/322-3	31.08.07	23:06	88° 8.85' N	150° 36.58' E	2914.0	MN	on deck
PS70/322-4	31.08.07	23:19	88° 8.91' N	150° 38.70' E	2939.0	BONGO	surface
PS70/322-4	31.08.07	23:30	88° 8.96' N	150° 40.61' E	2954.0	BONGO	atdepth
PS70/322-4	31.08.07	23:42	88° 9.02' N	150° 42.79' E	2972.0	BONGO	on deck
PS70/322-1	31.08.07	23:58	88° 9.09' N	150° 45.81' E	3006.0	ICE	Scientists on board
PS70/322-1	01.09.07	00:04	88° 9.12' N	150° 46.95' E	3016.0	ICE	Ice Gangway on board
PS70/322-1	01.09.07	01:00	88° 9.38' N	150° 58.42' E	3106.0	ICE	Departure from floe
PS70/323-1	01.09.07	02:24	88° 6.03' N	154° 39.32' E	3876.0	XCTD	surface
PS70/323-2	01.09.07	02:29	88° 5.96' N	154° 42.05' E	3882.0	XCTD	surface
PS70/324-1	01.09.07	04:49	88° 4.48' N	160° 37.69' E	4028.0	CTD/RO	surface
PS70/324-1	01.09.07	06:00	88° 4.49' N	160° 48.86' E	4021.0	CTD/RO	atdepth
PS70/324-1	01.09.07	07:19	88° 4.56' N	161° 0.03' E	4022.0	CTD/RO	on deck
PS70/324-2	01.09.07	07:30	88° 4.58' N	161° 1.44' E	4026.0	MN	surface
PS70/324-2	01.09.07	10:30	88° 5.03' N	161° 26.92' E	4022.0	MN	atdepth
PS70/324-2	01.09.07	12:54	88° 5.50' N	161° 45.15' E	4028.0	MN	on deck
PS70/324-3	01.09.07	13:00	88° 5.52' N	161° 45.82' E	4025.0	BONGO	surface
PS70/324-3	01.09.07	13:57	88° 5.66' N	161° 51.34' E	4026.0	BONGO	atdepth
PS70/324-3	01.09.07	14:52	88° 5.74' N	161° 54.51' E	4023.0	BONGO	on deck

Station	Date	Time	Position Lat	Position Lon	Depth [m]	Gear Abbre- viation	Action
PS70/325-1	01.09.07	16:24	88° 2.88' N	165° 7.30' E	4024.0	XCTD	surface
PS70/326-1	01.09.07	18:37	88° 1.71' N	170° 5.23' E	4022.0	CTD/UC	into Water
PS70/326-1	01.09.07	19:44	88° 1.85' N	169° 59.63' E	4022.0	CTD/UC	on Depth
PS70/326-1	01.09.07	21:24	88° 2.21' N	169° 58.93' E	4016.0	CTD/UC	on Deck
PS70/326-2	01.09.07	21:30	88° 2.24' N	169° 59.14' E	4017.0	XCTD	surface
PS70/326-3	01.09.07	21:42	88° 2.29' N	169° 59.68' E	4018.0	MN	surface
PS70/326-3	01.09.07	23:21	88° 2.83' N	170° 7.24' E	4019.0	MN	at depth
PS70/326-3	02.09.07	01:37	88° 3.50' N	170° 23.90' E	4025.0	MN	on deck
PS70/327-1	02.09.07	05:41	87° 57.12' N	179° 57.96' W	3610.0	XCTD	surface
PS70/328-1	02.09.07	11:12	87° 49.96' N	170° 44.46' W	3992.0	ICE	Alongside Floe
PS70/328-1	02.09.07	11:42	87° 49.83' N	170° 36.79' W	4001.0	ICE	Ice Gangway on the ice
PS70/328-2	02.09.07	11:56	87° 49.80' N	170° 34.10' W	3995.0	CTD/UC	into Water
PS70/328-1	02.09.07	12:00	87° 49.79' N	170° 33.37' W	3992.0	ICE	Scientists on the ice
PS70/328-2	02.09.07	13:01	87° 49.60' N	170° 24.44' W	3992.0	CTD/UC	on Depth
PS70/328-2	02.09.07	14:39	87° 49.30' N	170° 18.60' W	3996.0	CTD/UC	on Deck
PS70/328-3	02.09.07	14:50	87° 49.28' N	170° 18.49' W	3997.0	CTD/RO/M IC	MIC in water
PS70/328-3	02.09.07	14:58	87° 49.26' N	170° 18.48' W	3996.0	CTD/RO/M IC	CTD/RO to water
PS70/328-3	02.09.07	16:07	87° 49.24' N	170° 19.57' W	3992.0	CTD/RO/M IC	MIC at bottom and CTD at depth
PS70/328-3	02.09.07	17:27	87° 49.37' N	170° 21.41' W	3997.0	CTD/RO/M IC	CTD/RO on deck
PS70/328-3	02.09.07	17:27	87° 49.37' N	170° 21.41' W	3997.0	CTD/RO/M IC	MIC on deck
PS70/328-4	02.09.07	17:40	87° 49.40' N	170° 21.49' W	3992.0	CTD/UC	into Water
PS70/328-4	02.09.07	18:14	87° 49.50' N	170° 21.17' W	3992.0	CTD/UC	on Depth
PS70/328-4	02.09.07	19:08	87° 49.68' N	170° 18.71' W	3992.0	CTD/UC	on Deck
PS70/328-5	02.09.07	19:24	87° 49.73' N	170° 17.59' W	3991.0	ISP	into water
PS70/328-5	02.09.07	19:58	87° 49.84' N	170° 14.45' W	3992.0	ISP	pump at depth
PS70/328-5	02.09.07	22:24	87° 49.98' N	169° 54.74' W	3996.0	ISP	on deck
PS70/328-5	02.09.07	22:27	87° 49.97' N	169° 54.31' W	4000.0	ISP	on deck
PS70/328-5	02.09.07	22:29	87° 49.97' N	169° 54.01' W	3999.0	ISP	on deck
PS70/328-5	02.09.07	22:34	87° 49.96' N	169° 53.29' W	3998.0	ISP	on deck

Station	Date	Time	Position Lat	Position Lon	Depth [m]	Gear Abbre- viation	Action
PS70/328-5	02.09.07	22:39	87° 49.95' N	169° 52.58' W	3996.0	ISP	on deck
PS70/328-5	02.09.07	22:49	87° 49.94' N	169° 51.17' W	3996.0	ISP	on deck
PS70/328-5	02.09.07	22:51	87° 49.93' N	169° 50.90' W	3997.0	ISP	on deck
PS70/328-6	02.09.07	22:58	87° 49.92' N	169° 49.94' W	3998.0	CTD/RO	surface
PS70/328-6	02.09.07	23:44	87° 49.78' N	169° 44.06' W	3994.0	CTD/RO	at depth
PS70/328-1	02.09.07	23:45	87° 49.78' N	169° 43.95' W	3995.0	ICE	Scientists on board
PS70/328-1	02.09.07	23:57	87° 49.73' N	169° 42.69' W	3992.0	ICE	Ice Gangway on board
PS70/328-6	03.09.07	00:33	87° 49.59' N	169° 39.64' W	3998.0	CTD/RO	on deck
PS70/328-7	03.09.07	01:47	87° 49.28' N	169° 36.53' W	3990.0	CTD/RO	surface
PS70/328-7	03.09.07	02:20	87° 49.17' N	169° 36.61' W	3992.0	CTD/RO	at depth
PS70/328-7	03.09.07	02:52	87° 49.09' N	169° 37.46' W	3996.0	CTD/RO	on deck
PS70/328-8	03.09.07	03:00	87° 49.07' N	169° 37.78' W	3991.0	MN	surface
PS70/328-8	03.09.07	04:43	87° 48.95' N	169° 42.82' W	3992.0	MN	at depth
PS70/328-8	03.09.07	07:02	87° 49.23' N	169° 44.59' W	3994.0	MN	on deck
PS70/328-9	03.09.07	07:13	87° 49.25' N	169° 44.05' W	3994.0	CTD/RO	surface
PS70/328-9	03.09.07	07:23	87° 49.27' N	169° 43.44' W	3992.0	CTD/RO	at depth
PS70/328-9	03.09.07	07:39	87° 49.30' N	169° 42.34' W	3991.0	CTD/RO	on deck
PS70/328-10	03.09.07	07:48	87° 49.31' N	169° 41.66' W	3994.0	BONGO	surface
PS70/328-10	03.09.07	08:46	87° 49.36' N	169° 36.29' W	3991.0	BONGO	at depth
PS70/328-11	03.09.07	09:06	87° 49.36' N	169° 34.13' W	3993.0	ICE	Ice Gangway on the ice
PS70/328-11	03.09.07	09:09	87° 49.36' N	169° 33.80' W	3989.0	ICE	Scientists on the ice
PS70/328-10	03.09.07	09:40	87° 49.33' N	169° 30.39' W	3987.0	BONGO	on deck
PS70/328-12	03.09.07	09:46	87° 49.32' N	169° 29.74' W	3991.0	CTD/RO	surface
PS70/328-12	03.09.07	09:51	87° 49.31' N	169° 29.20' W	3988.0	CTD/RO	at depth
PS70/328-12	03.09.07	10:02	87° 49.29' N	169° 28.06' W	3996.0	CTD/RO	on deck
PS70/328-13	03.09.07	10:07	87° 49.27' N	169° 27.55' W	3996.0	BONGO	surface

Station	Date	Time	Position Lat	Position Lon	Depth [m]	Gear Abbreviation	Action
PS70/328-13	03.09.07	10:11	87° 49.26' N	169° 27.15' W	3989.0	BONGO	atdepth
PS70/328-11	03.09.07	10:12	87° 49.26' N	169° 27.05' W	3994.0	ICE	Scientists on board
PS70/328-11	03.09.07	10:15	87° 49.25' N	169° 26.75' W	3990.0	ICE	Ice Gangway on board
PS70/328-13	03.09.07	10:17	87° 49.25' N	169° 26.56' W	3992.0	BONGO	on deck
PS70/328-11	03.09.07	10:18	87° 49.25' N	169° 26.46' W	3996.0	ICE	Departure from floe
PS70/329-1	03.09.07	13:15	87° 44.61' N	162° 37.47' W	3400.0	XCTD	surface
PS70/330-1	03.09.07	15:39	87° 40.51' N	158° 25.63' W	2464.0	BC	surface
PS70/330-1	03.09.07	16:10	87° 40.49' N	158° 26.95' W	2460.0	BC	atsea bottom
PS70/330-1	03.09.07	16:43	87° 40.50' N	158° 28.19' W	2461.0	BC	on deck
PS70/330-2	03.09.07	16:55	87° 40.52' N	158° 28.69' W	2462.0	GC	surface
PS70/330-2	03.09.07	17:20	87° 40.55' N	158° 29.48' W	2464.0	GC	atsea bottom
PS70/330-2	03.09.07	17:52	87° 40.59' N	158° 29.90' W	2462.0	GC	on deck
PS70/331-1	03.09.07	18:54	87° 39.14' N	157° 36.36' W	2428.0	CTD/RO	surface
PS70/331-1	03.09.07	19:43	87° 39.20' N	157° 35.32' W	2433.0	CTD/RO	atdepth
PS70/331-1	03.09.07	20:36	87° 39.24' N	157° 33.59' W	2441.0	CTD/RO	on deck
PS70/332-1	04.09.07	02:12	87° 18.62' N	150° 8.26' W	3049.0	XCTD	surface
PS70/333-1	04.09.07	07:07	87° 1.68' N	146° 23.98' W	3279.0	CTD/UC	into Water
PS70/333-1	04.09.07	08:00	87° 1.64' N	146° 23.42' W	3285.0	CTD/UC	on Depth
PS70/333-1	04.09.07	09:33	87° 1.51' N	146° 22.14' W	3298.0	CTD/UC	on Deck
PS70/333-2	04.09.07	09:42	87° 1.49' N	146° 22.01' W	3302.0	MN	surface
PS70/333-2	04.09.07	11:10	87° 1.33' N	146° 20.89' W	3328.0	MN	atdepth
PS70/333-2	04.09.07	13:10	87° 1.10' N	146° 19.72' W	3353.0	MN	on deck
PS70/333-3	04.09.07	13:21	87° 1.07' N	146° 19.55' W	3355.0	BONGO	surface
PS70/333-3	04.09.07	14:16	87° 0.98' N	146° 18.83' W	3362.0	BONGO	atdepth
PS70/333-3	04.09.07	15:07	87° 0.89' N	146° 18.14' W	3371.0	BONGO	on deck
PS70/333-4	04.09.07	15:15	87° 0.88' N	146° 18.00' W	3367.0	BC	surface

Station	Date	Time	Position Lat	Position Lon	Depth [m]	Gear Abbre- viation	Action
PS70/333-4	04.09.07	15:56	87° 0.82' N	146° 17.40' W	3368.0	BC	atsea bottom
PS70/333-4	04.09.07	16:36	87° 0.77' N	146° 16.77' W	3372.0	BC	on deck
PS70/333-5	04.09.07	16:45	87° 0.76' N	146° 16.58' W	3374.0	GC	surface
PS70/333-5	04.09.07	17:20	87° 0.71' N	146° 15.94' W	3373.0	GC	atsea bottom
PS70/333-5	04.09.07	18:02	87° 0.66' N	146° 15.05' W	3368.0	GC	on deck
PS70/334-1	04.09.07	22:48	86° 42.31' N	142° 22.77' W	2845.0	XCTD	surface
PS70/335-1	05.09.07	00:00	86° 21.83' N	139° 21.51' W	2499.0	CTD	surface
PS70/335-1	05.09.07	04:39	86° 21.77' N	139° 19.76' W	2492.0	CTD	at depth
PS70/335-1	05.09.07	05:29	86° 21.97' N	139° 18.16' W	2499.0	CTD	on deck
PS70/336-1	05.09.07	09:04	86° 8.34' N	137° 29.57' W	2243.0	XCTD	surface
PS70/337-1	05.09.07	12:08	85° 56.61' N	136° 22.57' W	1791.0	XCTD	surface
PS70/338-1	05.09.07	18:00	85° 42.30' N	135° 2.46' W	1537.0	ICE	Alongside Floe
PS70/338-1	05.09.07	18:20	85° 42.29' N	135° 2.53' W	1537.0	ICE	Ice Gangway on the ice
PS70/338-1	05.09.07	18:37	85° 42.25' N	135° 2.37' W	1540.0	ICE	Scientists on the ice
PS70/338-2	05.09.07	18:40	85° 42.25' N	135° 2.35' W	1537.0	CTD/UC	into Water
PS70/338-2	05.09.07	19:08	85° 42.20' N	135° 2.09' W	1543.0	CTD/UC	on Depth
PS70/338-2	05.09.07	20:03	85° 42.09' N	135° 1.63' W	1558.0	CTD/UC	on Deck
PS70/338-3	05.09.07	20:12	85° 42.08' N	135° 1.54' W	1558.0	CTD	surface
PS70/338-3	05.09.07	20:46	85° 42.01' N	135° 1.20' W	1569.0	CTD	at depth
PS70/338-3	05.09.07	21:22	85° 40.95' N	135° 0.82' W	1570.0	CTD	on deck
PS70/338-4	05.09.07	21:27	85° 41.94' N	135° 0.75' W	1574.0	ISP	into water
PS70/338-4	05.09.07	22:14	85° 41.85' N	135° 0.14' W	1574.0	ISP	pump at depth
PS70/338-1	05.09.07	23:15	85° 41.73' N	134° 59.30' W	1575.0	ICE	Scientists on board
PS70/338-1	05.09.07	23:27	85° 41.71' N	134° 59.13' W	1573.0	ICE	Ice Gangway on board
PS70/338-4	06.09.07	01:01	85° 41.54' N	134° 57.79' W	1569.0	ISP	on deck
PS70/338-5	06.09.07	01:08	85° 41.52' N	134° 57.68' W	1570.0	CTD	surface
PS70/338-5	06.09.07	01:15	85° 41.51' N	134° 57.60' W	1570.0	CTD	at depth
PS70/338-5	06.09.07	01:30	85° 41.78' N	134° 57.34' W	1576.0	CTD	on deck
PS70/338-6	06.09.07	01:41	85° 41.45' N	134° 57.17' W	1580.0	MN	surface

Station	Date	Time	Position Lat	Position Lon	Depth [m]	Gear Abbreviation	Action
PS70/338-6	06.09.07	02:19	85° 41.37' N	134° 56.70' W	1580.0	MN	at depth
PS70/338-6	06.09.07	03:18	85° 41.24' N	134° 56.03' W	1580.0	MN	on deck
PS70/338-7	06.09.07	03:26	85° 41.23' N	134° 55.95' W	1578.0	BONGO	surface
PS70/338-7	06.09.07	04:24	85° 41.10' N	134° 55.44' W	1572.0	BONGO	at depth
PS70/338-7	06.09.07	05:19	85° 41.00' N	134° 55.11' W	1570.0	BONGO	on deck
PS70/338-8	06.09.07	05:21	85° 40.99' N	134° 55.10' W	1568.0	BONGO	surface
PS70/338-8	06.09.07	05:26	85° 40.99' N	134° 55.06' W	1570.0	BONGO	at depth
PS70/338-8	06.09.07	05:32	85° 40.98' N	134° 55.04' W	1569.0	BONGO	on deck
PS70/338-9	06.09.07	05:41	85° 40.96' N	179° 5.02' E	1570.0	BC	surface
PS70/338-9	06.09.07	06:04	85° 40.92' N	134° 54.90' W	1567.0	BC	at sea bottom
PS70/338-9	06.09.07	06:28	85° 40.89' N	134° 54.82' W	1564.0	BC	on deck
PS70/338-10	06.09.07	06:38	85° 40.87' N	134° 54.78' W	1567.0	GC	surface
PS70/338-10	06.09.07	06:54	85° 40.84' N	134° 54.72' W	1567.0	GC	at sea bottom
PS70/338-10	06.09.07	07:17	85° 40.82' N	134° 54.66' W	1565.0	GC	on deck
PS70/339-1	06.09.07	13:37	85° 23.29' N	136° 16.99' W	2043.0	XCTD	surface
PS70/340-1	06.09.07	18:52	85° 6.74' N	137° 24.17' W	1955.0	CTD/RO	surface
PS70/340-1	06.09.07	19:28	85° 6.70' N	137° 24.12' W	1953.0	CTD/RO	at depth
PS70/340-1	06.09.07	20:16	85° 6.65' N	137° 23.97' W	1951.0	CTD/RO	on deck
PS70/341-1	07.09.07	00:03	84° 46.96' N	137° 59.18' W	2069.0	XCTD	surface
PS70/342-1	07.09.07	04:17	84° 30.00' N	138° 25.12' W	2302.0	CTD/UC	into Water
PS70/342-1	07.09.07	04:55	84° 29.97' N	138° 24.75' W	2275.0	CTD/UC	on Depth
PS70/342-1	07.09.07	06:04	84° 29.94' N	138° 24.12' W	2256.0	CTD/UC	on Deck
PS70/342-2	07.09.07	06:12	84° 29.94' N	138° 24.04' W	2245.0	CTD/RO	surface
PS70/342-2	07.09.07	06:54	84° 29.94' N	138° 23.55' W	2232.0	CTD/RO	at depth
PS70/342-2	07.09.07	07:39	84° 29.96' N	138° 22.91' W	2203.0	CTD/RO	on deck
PS70/342-3	07.09.07	08:23	84° 30.08' N	138° 22.14' W	2242.0	ICE	Alongside Floe

Station	Date	Time	Position Lat	Position Lon	Depth [m]	Gear Abbreviation	Action
PS70/342-3	07.09.07	08:54	84° 30.15' N	138° 21.52' W	2264.0	ICE	Ice Gangway on the ice
PS70/342-4	07.09.07	09:06	84° 30.16' N	138° 21.33' W	2267.0	MN	surface
PS70/342-3	07.09.07	09:29	84° 30.18' N	138° 20.96' W	2291.0	ICE	Scientists on the ice
PS70/342-4	07.09.07	10:03	84° 30.22' N	138° 20.37' W	2286.0	MN	at depth
PS70/342-4	07.09.07	11:30	84° 30.28' N	138° 18.66' W	2288.0	MN	on deck
PS70/342-5	07.09.07	11:37	84° 30.29' N	138° 18.51' W	2288.0	CTD/RO	surface
PS70/342-5	07.09.07	11:49	84° 30.29' N	138° 18.24' W	2289.0	CTD/RO	at depth
PS70/342-5	07.09.07	12:00	84° 30.30' N	138° 17.99' W	2287.0	CTD/RO	on deck
PS70/342-6	07.09.07	12:07	84° 30.30' N	138° 17.84' W	2288.0	BONGO	surface
PS70/342-6	07.09.07	13:04	84° 30.32' N	138° 16.50' W	2283.0	BONGO	at depth
PS70/342-6	07.09.07	13:57	84° 30.30' N	138° 15.36' W	2261.0	BONGO	on deck
PS70/342-7	07.09.07	14:04	84° 30.30' N	138° 15.23' W	2260.0	CTD/RO	surface
PS70/342-7	07.09.07	14:17	84° 30.29' N	138° 14.98' W	2257.0	CTD/RO	at depth
PS70/342-3	07.09.07	14:23	84° 30.29' N	138° 14.87' W	2253.0	ICE	Scientists on board
PS70/342-7	07.09.07	14:34	84° 30.30' N	138° 14.60' W	2252.0	CTD/RO	on deck
PS70/342-3	07.09.07	14:36	84° 30.29' N	138° 14.56' W	2253.0	ICE	Ice Gangway on board
PS70/342-3	07.09.07	14:37	84° 30.29' N	138° 14.55' W	2249.0	ICE	Departure from floe
PS70/342-8	07.09.07	14:40	84° 30.29' N	138° 14.49' W	2249.0	BONGO	surface
PS70/342-8	07.09.07	14:44	84° 30.29' N	138° 14.41' W	2255.0	BONGO	at depth
PS70/342-8	07.09.07	14:50	84° 30.29' N	138° 14.29' W	2250.0	BONGO	on deck
PS70/342-9	07.09.07	15:16	84° 30.27' N	138° 13.81' W	2255.0	CTD/RO	surface
PS70/342-9	07.09.07	15:23	84° 30.27' N	138° 13.69' W	2256.0	CTD/RO	at depth
PS70/342-9	07.09.07	15:38	84° 30.26' N	138° 13.43' W	2258.0	CTD/RO	on deck
PS70/342-10	07.09.07	15:46	84° 30.25' N	138° 13.29' W	2259.0	BC	surface
PS70/342-10	07.09.07	16:14	84° 30.24' N	138° 12.84' W	2262.0	BC	at sea bottom
PS70/342-10	07.09.07	16:41	84° 30.22' N	138° 12.44' W	2261.0	BC	on deck

Station	Date	Time	Position Lat	Position Lon	Depth [m]	Gear Abbreviation	Action
PS70/342-11	07.09.07	17:02	84° 30.22' N	138° 12.17' W	2264.0	GC	surface
PS70/342-11	07.09.07	17:23	84° 30.21' N	138° 11.91' W	2260.0	GC	atsea bottom
PS70/342-11	07.09.07	18:03	84° 30.22' N	138° 11.37' W	2262.0	GC	on deck
PS70/343-1	07.09.07	19:33	84° 29.88' N	138° 25.91' W	2298.0	EF	start
PS70/343-1	07.09.07	19:52	84° 29.90' N	138° 25.60' W	2299.0	EF	End
PS70/344-1	08.09.07	02:16	84° 36.63' N	141° 41.40' W	2225.0	XCTD	surface
PS70/345-1	08.09.07	07:27	84° 41.57' N	145° 26.48' W	2355.0	CTD/RO	surface
PS70/345-1	08.09.07	08:12	84° 41.65' N	145° 25.75' W	2356.0	CTD/RO	at depth
PS70/345-1	08.09.07	09:06	84° 41.77' N	145° 25.10' W	2349.0	CTD/RO	on deck
PS70/346-1	08.09.07	13:39	84° 47.63' N	149° 7.22' W	2355.0	CTD/RO	surface
PS70/346-1	08.09.07	14:23	84° 47.76' N	149° 5.19' W	2351.0	CTD/RO	at depth
PS70/346-1	08.09.07	15:18	84° 47.91' N	149° 2.75' W	2335.0	CTD/RO	on deck
PS70/347-1	08.09.07	20:36	84° 52.55' N	154° 8.99' W	2188.0	XCTD	surface
PS70/348-1	09.09.07	00:40	84° 58.73' N	158° 42.03' W	2088.0	XCTD	surface
PS70/349-1	09.09.07	08:19	85° 3.83' N	164° 28.14' W	2020.0	CTD/UC	into Water
PS70/349-1	09.09.07	08:54	85° 3.92' N	164° 29.82' W	2020.0	CTD/UC	on Depth
PS70/349-1	09.09.07	10:06	85° 4.25' N	164° 32.17' W	2013.0	CTD/UC	on Deck
PS70/349-2	09.09.07	10:14	85° 4.29' N	164° 32.37' W	2008.0	CTD/RO	surface
PS70/349-2	09.09.07	10:54	85° 4.48' N	164° 33.05' W	1996.0	CTD/RO	at depth
PS70/349-2	09.09.07	11:39	85° 4.70' N	164° 33.08' W	1994.0	CTD/RO	on deck
PS70/350-1	09.09.07	15:48	85° 22.45' N	167° 12.34' W	1985.0	XCTD	surface
PS70/351-1	09.09.07	20:37	85° 44.73' N	170° 45.90' W	2699.0	CTD/RO	surface
PS70/351-1	09.09.07	21:27	85° 44.90' N	170° 47.28' W	2702.0	CTD/RO	at depth
PS70/351-1	09.09.07	22:24	85° 45.18' N	170° 48.76' W	2705.0	CTD/RO	on deck
PS70/352-1	10.09.07	11:36	86° 37.93' N	177° 35.37' E	4002.0	ICE	Alongside Floe
PS70/352-1	10.09.07	11:53	86° 38.22' N	177° 33.87' E	4002.0	ICE	Ice Gangway on the ice
PS70/352-1	10.09.07	12:07	86° 38.27' N	177° 33.49' E	4001.0	ICE	Scientists on the ice
PS70/352-2	10.09.07	12:12	86° 38.29' N	177° 33.38' E	4005.0	CTD/UC	into Water
PS70/352-2	10.09.07	13:19	86° 38.52' N	177° 32.69' E	4005.0	CTD/UC	on Depth

Station	Date	Time	Position Lat	Position Lon	Depth [m]	Gear Abbreviation	Action
PS70/352-2	10.09.07	15:02	86° 38.69' N	177° 33.60' E	4001.0	CTD/UC	on Deck
PS70/352-3	10.09.07	15:15	86° 38.69' N	177° 33.77' E	4003.0	CTD/RO/MIC	MIC in water
PS70/352-3	10.09.07	15:20	86° 38.69' N	177° 33.81' E	3997.0	CTD/RO/MIC	CTD/RO to water
PS70/352-3	10.09.07	16:30	86° 38.62' N	177° 34.34' E	4001.0	CTD/RO/MIC	MIC at bottom and CTD at depth
PS70/352-3	10.09.07	18:05	86° 38.46' N	177° 33.09' E	4000.0	CTD/RO/MIC	MIC on deck
PS70/352-3	10.09.07	18:06	86° 38.46' N	177° 33.06' E	3996.0	CTD/RO/MIC	CTD/RO on deck
PS70/352-4	10.09.07	21:24	86° 38.50' N	177° 21.84' E	4000.0	BONGO	surface
PS70/352-4	10.09.07	21:30	86° 38.51' N	177° 21.45' E	3992.0	BONGO	at depth
PS70/352-4	10.09.07	21:36	86° 38.53' N	177° 21.06' E	3997.0	BONGO	on deck
PS70/352-5	10.09.07	21:55	86° 38.58' N	177° 19.88' E	3998.0	CTD/RO	surface
PS70/352-5	10.09.07	22:03	86° 38.61' N	177° 19.40' E	3999.0	CTD/RO	at depth
PS70/352-5	10.09.07	22:15	86° 38.65' N	177° 18.71' E	3998.0	CTD/RO	on deck
PS70/352-6	10.09.07	22:24	86° 38.68' N	177° 18.21' E	4001.0	MN	surface
PS70/352-6	11.09.07	00:06	86° 39.10' N	177° 14.06' E	3998.0	MN	at depth
PS70/352-1	11.09.07	00:08	86° 39.11' N	177° 14.01' E	3997.0	ICE	Scientists on board
PS70/352-1	11.09.07	00:43	86° 39.26' N	177° 13.35' E	3995.0	ICE	Scientists on the ice
PS70/352-6	11.09.07	02:21	86° 39.61' N	177° 13.22' E	4000.0	MN	on deck
PS70/352-1	11.09.07	03:36	86° 39.76' N	177° 13.71' E	3998.0	ICE	Scientists on board
PS70/352-1	11.09.07	03:40	86° 39.77' N	177° 13.72' E	3993.0	ICE	Ice Gangway on board
PS70/352-1	11.09.07	03:40	86° 39.77' N	177° 13.72' E	3993.0	ICE	Departure from floe
PS70/353-1	11.09.07	15:05	86° 35.71' N	162° 11.97' E	4015.0	XCTD	surface
PS70/354-1	11.09.07	17:20	86° 33.84' N	159° 42.31' E	3987.0	XCTD	surface
PS70/355-1	11.09.07	19:08	86° 31.64' N	157° 16.54' E	2645.0	XCTD	surface
PS70/356-1	11.09.07	20:28	86° 31.30' N	155° 29.35' E	1522.0	XCTD	surface
PS70/357-1	11.09.07	21:39	86° 30.75' N	153° 44.15' E	1379.0	XCTD	surface
PS70/358-1	11.09.07	23:12	86° 30.24' N	151° 58.53' E	1459.0	CTD/RO	surface
PS70/358-1	11.09.07	23:41	86° 30.38' N	151° 57.78' E	1459.0	CTD/RO	at depth
PS70/358-1	12.09.07	00:22	86° 30.59' N	151° 57.18' E	1459.0	CTD/RO	on deck
PS70/358-2	12.09.07	00:34	86° 30.65' N	151° 57.13' E	1457.0	ISP	into water
PS70/358-2	12.09.07	01:13	86° 30.85' N	151° 57.36' E	1460.0	ISP	pump at depth
PS70/358-2	12.09.07	04:04	86° 31.50' N	152° 4.62' E	1466.0	ISP	on deck
PS70/358-3	12.09.07	04:09	86° 31.51' N	152° 4.90' E	1468.0	BC	surface
PS70/358-3	12.09.07	04:29	86° 31.54' N	152° 5.98' E	1467.0	BC	at sea bottom
PS70/358-3	12.09.07	04:54	86° 31.56' N	152° 7.24' E	1466.0	BC	on deck
PS70/358-4	12.09.07	05:06	86° 31.57' N	152° 7.79' E	1466.0	KAL	to the water
PS70/358-4	12.09.07	05:30	86° 31.58' N	152° 8.77' E	1462.0	KAL	on the ground

Station	Date	Time	Position Lat	Position Lon	Depth [m]	Gear Abbreviation	Action
PS70/358-4	12.09.07	05:58	86° 31.57' N	152° 9.63' E	1464.0	KAL	on deck
PS70/359-1	12.09.07	09:09	86° 28.27' N	149° 17.29' E	1175.0	XCTD	surface
PS70/360-1	12.09.07	10:56	86° 26.28' N	146° 47.51' E	1160.0	XCTD	surface
PS70/361-1	12.09.07	12:44	86° 25.59' N	144° 4.10' E	901.2	XCTD	surface
PS70/362-1	12.09.07	14:52	86° 24.12' N	140° 58.10' E	2222.0	CTD/RO	surface
PS70/362-1	12.09.07	15:32	86° 24.38' N	140° 57.28' E	2199.0	CTD/RO	at depth
PS70/362-1	12.09.07	16:24	86° 24.65' N	140° 56.75' E	2112.0	CTD/RO	on deck
PS70/362-2	12.09.07	16:30	86° 24.67' N	140° 56.95' E	2097.0	BONGO	surface
PS70/362-2	12.09.07	16:34	86° 24.69' N	140° 56.95' E	2079.0	BONGO	at depth
PS70/362-2	12.09.07	16:40	86° 24.74' N	140° 56.97' E	2064.0	BONGO	on deck
PS70/363-1	12.09.07	20:36	86° 23.52' N	135° 50.81' E	3800.0	ICE	Alongside Floe
PS70/363-1	12.09.07	21:06	86° 23.59' N	135° 49.09' E	3802.0	ICE	Ice Gangway on the ice
PS70/363-1	12.09.07	21:12	86° 23.60' N	135° 48.76' E	3802.0	ICE	Scientists on the ice
PS70/363-1	12.09.07	23:24	86° 24.01' N	135° 38.15' E	3833.0	ICE	Scientists on board
PS70/363-2	12.09.07	23:34	86° 24.06' N	135° 37.11' E	3830.0	BONGO	surface
PS70/363-2	13.09.07	00:31	86° 24.41' N	135° 31.18' E	3838.0	BONGO	at depth
PS70/363-2	13.09.07	01:26	86° 24.82' N	135° 25.55' E	3847.0	BONGO	on deck
PS70/363-3	13.09.07	01:30	86° 24.85' N	135° 25.17' E	3847.0	BONGO	surface
PS70/363-3	13.09.07	01:34	86° 24.89' N	135° 24.78' E	3847.0	BONGO	at depth
PS70/363-3	13.09.07	01:39	86° 24.93' N	135° 24.31' E	3846.0	BONGO	on deck
PS70/363-4	13.09.07	01:44	86° 24.97' N	135° 23.86' E	3848.0	MN	surface
PS70/363-4	13.09.07	03:26	86° 25.84' N	135° 16.60' E	3859.0	MN	at depth
PS70/363-4	13.09.07	05:40	86° 26.72' N	135° 10.72' E	3882.0	MN	on deck
PS70/363-1	13.09.07	07:54	86° 27.42' N	135° 2.58' E	3987.0	ICE	Alongside Floe
PS70/363-1	13.09.07	08:00	86° 27.46' N	135° 2.16' E	3994.0	ICE	Ice Gangway on the ice
PS70/363-5	13.09.07	08:12	86° 27.53' N	135° 1.18' E	3987.0	CTD/UC	into Water
PS70/363-1	13.09.07	08:36	86° 27.68' N	134° 59.12' E	3986.0	ICE	Scientists on the ice
PS70/363-5	13.09.07	09:16	86° 27.95' N	134° 55.46' E	3991.0	CTD/UC	on Depth
PS70/363-5	13.09.07	10:58	86° 28.78' N	134° 45.54' E	3989.0	CTD/UC	on Deck
PS70/363-6	13.09.07	11:45	86° 29.23' N	134° 41.41' E	3964.0	CTD/RO	surface
PS70/363-6	13.09.07	12:58	86° 30.02' N	134° 36.75' E	3867.0	CTD/RO	at depth
PS70/363-6	13.09.07	14:16	86° 30.91' N	134° 34.58' E	3822.0	CTD/RO	on deck
PS70/363-7	13.09.07	18:36	86° 33.06' N	134° 39.67' E	3808.0	BONGO	surface
PS70/363-7	13.09.07	19:33	86° 33.34' N	134° 40.51' E	3800.0	BONGO	at depth
PS70/363-7	13.09.07	20:28	86° 33.59' N	134° 40.52' E	3793.0	BONGO	on deck
PS70/363-1	13.09.07	22:44	86° 34.26' N	134° 38.28' E	3782.0	ICE	Scientists on board
PS70/363-1	13.09.07	22:46	86° 34.27' N	134° 38.24' E	3777.0	ICE	Ice Gangway on board
PS70/363-1	14.09.07	08:30	86° 35.85' N	134° 49.34' E	3681.0	ICE	Ice Gangway on the ice

Station	Date	Time	Position Lat	Position Lon	Depth [m]	Gear Abbre- viation	Action
PS70/363-1	14.09.07	08:36	86° 35.85' N	134° 49.06' E	3688.0	ICE	Scientists on the ice
PS70/363-8	14.09.07	16:05	86° 38.06' N	134° 39.18' E	3584.0	CTD/RO	surface
PS70/363-8	14.09.07	16:40	86° 38.18' N	134° 40.13' E	3578.0	CTD/RO	at depth
PS70/363-1	14.09.07	16:51	86° 38.21' N	134° 40.45' E	3585.0	ICE	Scientists on board
PS70/363-1	14.09.07	17:05	86° 38.25' N	134° 40.84' E	3581.0	ICE	Ice Gangway on board
PS70/363-8	14.09.07	17:09	86° 38.25' N	134° 40.95' E	3583.0	CTD/RO	on deck
PS70/363-1	14.09.07	17:11	86° 38.26' N	134° 41.01' E	3585.0	ICE	Departure from floe
PS70/364-1	14.09.07	20:12	86° 30.58' N	130° 59.83' E	4099.0	CTD/RO	surface
PS70/364-1	14.09.07	20:48	86° 30.55' N	130° 58.77' E	4112.0	CTD/RO	at depth
PS70/364-1	14.09.07	21:28	86° 30.57' N	130° 56.93' E	4144.0	CTD/RO	on deck
PS70/365-1	15.09.07	00:46	86° 24.48' N	127° 26.59' E	4386.0	CTD/RO	surface
PS70/365-1	15.09.07	01:20	86° 24.58' N	127° 24.56' E	4388.0	CTD/RO	at depth
PS70/365-1	15.09.07	02:02	86° 24.73' N	127° 24.27' E	4380.0	CTD/RO	on deck
PS70/366-1	15.09.07	09:50	86° 3.54' N	119° 17.79' E	4433.0	XCTD	surface
PS70/367-1	15.09.07	17:04	85° 39.77' N	112° 21.11' E	4442.0	XCTD	surface
PS70/367-2	15.09.07	17:11	85° 39.77' N	112° 21.23' E	4433.0	XCTD	surface
PS70/367-1	15.09.07	17:11	85° 39.77' N	112° 21.23' E	4433.0	XCTD	surface
PS70/367-2	15.09.07	17:11	85° 39.77' N	112° 21.23' E	4433.0	XCTD	surface
PS70/368-1	16.09.07	01:09	85° 10.96' N	106° 59.23' E	3966.0	XCTD	surface
PS70/369-1	16.09.07	03:36	85° 0.95' N	105° 25.73' E	4167.0	XCTD	surface
PS70/370-1	16.09.07	08:16	84° 50.57' N	103° 59.22' E	4053.0	XCTD	surface
PS70/371-1	16.09.07	11:12	84° 39.16' N	102° 43.94' E	4278.0	ICE	Alongside Floe
PS70/371-1	16.09.07	11:24	84° 39.18' N	102° 44.14' E	4274.0	ICE	Ice Gangway on the ice
PS70/371-2	16.09.07	11:37	84° 39.19' N	102° 44.18' E	4274.0	CTD/UC	into Water
PS70/371-1	16.09.07	12:12	84° 39.25' N	102° 44.10' E	4273.0	ICE	Scientists on the ice
PS70/371-2	16.09.07	12:48	84° 39.32' N	102° 43.99' E	4271.0	CTD/UC	on Depth
PS70/371-2	16.09.07	14:35	84° 39.63' N	102° 44.23' E	4266.0	CTD/UC	on Deck
PS70/371-3	16.09.07	14:49	84° 39.68' N	102° 44.37' E	4266.0	MN	surface
PS70/371-3	16.09.07	16:34	84° 40.01' N	102° 46.51' E	4257.0	MN	at depth
PS70/371-3	16.09.07	19:02	84° 40.29' N	102° 51.77' E	4260.0	MN	on deck
PS70/371-4	16.09.07	19:07	84° 40.29' N	102° 51.95' E	4263.0	BONGO	surface
PS70/371-4	16.09.07	19:11	84° 40.29' N	102° 52.10' E	4265.0	BONGO	at depth
PS70/371-4	16.09.07	19:17	84° 40.29' N	102° 52.32' E	4266.0	BONGO	on deck
PS70/371-5	16.09.07	19:20	84° 40.30' N	102° 52.43' E	4266.0	BONGO	surface
PS70/371-5	16.09.07	20:16	84° 40.30' N	102° 54.32' E	4261.0	BONGO	at depth
PS70/371-5	16.09.07	21:07	84° 40.29' N	102° 55.73' E	4263.0	BONGO	on deck
PS70/371-1	16.09.07	21:08	84° 40.29' N	102° 55.76' E	4267.0	ICE	Scientists on board
PS70/371-6	16.09.07	21:12	84° 40.29' N	102° 55.85' E	4261.0	BONGO	surface
PS70/371-6	16.09.07	21:17	84° 40.29' N	102° 55.97' E	4263.0	BONGO	at depth
PS70/371-1	16.09.07	21:22	84° 40.28' N	102° 56.09' E	4263.0	ICE	Ice Gangway on board
PS70/371-6	16.09.07	21:22	84° 40.28' N	102° 56.09' E	4263.0	BONGO	on deck

Station	Date	Time	Position Lat	Position Lon	Depth [m]	Gear Abbreviation	Action
PS70/371-1	16.09.07	21:30	84° 40.28' N	102° 56.22' E	4267.0	ICE	Departure from floe
PS70/372-1	17.09.07	04:22	84° 19.66' N	107° 18.49' E	4262.0	CTD/UC	into Water
PS70/372-1	17.09.07	05:33	84° 19.84' N	107° 22.44' E	4232.0	CTD/UC	on Depth
PS70/372-1	17.09.07	07:30	84° 20.07' N	107° 29.39' E	4271.0	CTD/UC	on Deck
PS70/373-1	17.09.07	09:42	84° 12.65' N	108° 52.35' E	4276.0	EF	start
PS70/373-1	17.09.07	10:07	84° 12.56' N	108° 53.68' E	4275.0	EF	End
PS70/373-2	17.09.07	10:55	84° 11.93' N	108° 56.10' E	4282.0	CTD/UC	into Water
PS70/373-2	17.09.07	12:03	84° 11.79' N	108° 56.93' E	4281.0	CTD/UC	on Depth
PS70/373-2	17.09.07	13:44	84° 11.73' N	108° 57.74' E	4289.0	CTD/UC	on Deck
PS70/374-1	17.09.07	16:54	84° 6.19' N	109° 57.87' E	4303.0	EF	start
PS70/374-1	17.09.07	17:30	84° 6.18' N	110° 0.31' E	4303.0	EF	End
PS70/375-1	17.09.07	21:26	83° 50.31' N	112° 40.65' E	4352.0	CTD/RO	surface
PS70/375-1	17.09.07	22:42	83° 49.98' N	112° 43.42' E	4355.0	CTD/RO	at depth
PS70/375-1	18.09.07	00:20	83° 49.70' N	112° 44.86' E	4357.0	CTD/RO	on deck
PS70/376-1	18.09.07	01:05	83° 46.74' N	113° 8.55' E	4356.0	EF	start
PS70/376-1	18.09.07	02:05	83° 46.66' N	113° 10.31' E	4360.0	EF	End
PS70/377-1	18.09.07	06:43	83° 25.41' N	115° 25.33' E	4292.0	EF	start
PS70/377-1	18.09.07	07:25	83° 25.33' N	115° 27.86' E	4256.0	EF	End
PS70/377-2	18.09.07	07:43	83° 24.93' N	115° 28.63' E	4263.0	CTD/RO	surface
PS70/377-2	18.09.07	08:58	83° 24.76' N	115° 33.06' E	4301.0	CTD/RO	at depth
PS70/377-2	18.09.07	10:33	83° 24.59' N	115° 36.02' E	4347.0	CTD/RO	on deck
PS70/378-1	18.09.07	14:17	83° 4.40' N	116° 55.97' E	4445.0	EF	start
PS70/378-1	18.09.07	15:37	83° 4.66' N	116° 57.67' E	4456.0	EF	End
PS70/379-1	18.09.07	18:22	82° 51.93' N	117° 49.73' E	4415.0	CTD/UC	into Water
PS70/379-1	18.09.07	19:37	82° 51.57' N	117° 51.13' E	4413.0	CTD/UC	on Depth
PS70/379-1	18.09.07	21:28	82° 51.29' N	117° 51.83' E	4401.0	CTD/UC	on Deck
PS70/380-1	19.09.07	00:22	82° 37.77' N	118° 24.22' E	4491.0	EF	start
PS70/380-1	19.09.07	01:08	82° 37.95' N	118° 24.52' E	4493.0	EF	End
PS70/381-1	19.09.07	04:42	82° 11.70' N	119° 33.66' E	4026.0	CTD/RO	surface
PS70/381-1	19.09.07	05:52	82° 11.64' N	119° 34.69' E	4023.0	CTD/RO	at depth
PS70/381-1	19.09.07	07:09	82° 11.51' N	119° 34.14' E	4017.0	CTD/RO	on deck
PS70/381-2	19.09.07	07:14	82° 11.51' N	119° 34.12' E	4022.0	BONGO	surface
PS70/381-2	19.09.07	07:18	82° 11.51' N	119° 34.11' E	4023.0	BONGO	at depth
PS70/381-2	19.09.07	07:23	82° 11.50' N	119° 34.16' E	4025.0	BONGO	on deck
PS70/382-1	19.09.07	11:58	81° 21.45' N	120° 43.12' E	5345.0	CTD/UC	into Water
PS70/382-1	19.09.07	13:27	81° 21.45' N	120° 43.15' E	5343.0	CTD/UC	on Depth
PS70/382-1	19.09.07	15:36	81° 21.39' N	120° 42.91' E	5346.0	CTD/UC	on Deck
PS70/383-1	19.09.07	19:32	80° 39.60' N	122° 13.52' E	3899.0	CTD/RO/M IC	MIC in water
PS70/383-1	19.09.07	19:37	80° 39.57' N	122° 13.42' E	3899.0	CTD/RO/M IC	CTD/RO to water
PS70/383-1	19.09.07	20:47	80° 39.35' N	122° 12.32' E	3902.0	CTD/RO/M IC	MIC at bottom and CTD at depth
PS70/383-1	19.09.07	22:12	80° 39.40' N	122° 12.65' E	3894.0	CTD/RO/M IC	MIC on deck
PS70/383-1	19.09.07	22:13	80° 39.41' N	122° 12.69' E	3901.0	CTD/RO/M IC	CTD/RO on deck
PS70/384-1	20.09.07	02:10	79° 59.77' N	123° 27.00' E	3654.0	CTD/RO/M IC	MIC in water

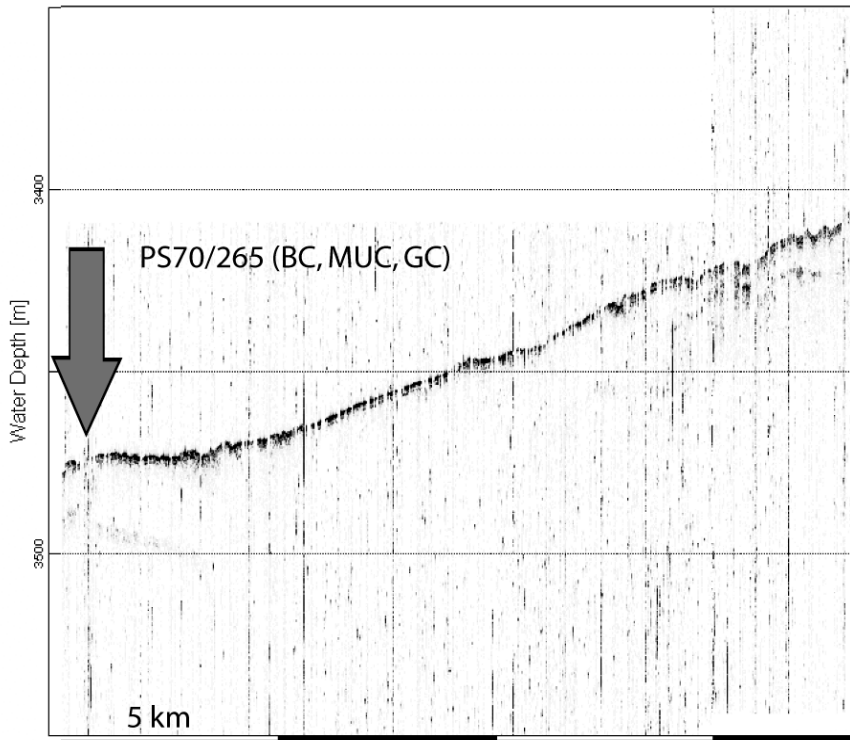
Station	Date	Time	Position Lat	Position Lon	Depth [m]	Gear Abbre- viation	Action
PS70/384-1	20.09.07	02:13	79° 59.78' N	123° 26.94' E	3655.0	CTD/RO/M IC	CTD/RO to water
PS70/384-1	20.09.07	03:21	79° 59.71' N	123° 27.32' E	3653.0	CTD/RO/M IC	MIC at bottom and CTD at depth
PS70/384-1	20.09.07	04:40	79° 59.70' N	123° 26.82' E	3653.0	CTD/RO/M IC	CTD/RO on deck
PS70/384-1	20.09.07	04:42	79° 59.69' N	123° 26.79' E	3654.0	CTD/RO/M IC	MIC on deck
PS70/385-1	20.09.07	08:28	79° 21.14' N	124° 21.63' E	3532.0	CTD/UC	into Water
PS70/385-1	20.09.07	09:32	79° 20.88' N	124° 20.83' E	3529.0	CTD/UC	on Depth
PS70/385-1	20.09.07	11:05	79° 20.78' N	124° 20.74' E	3530.0	CTD/UC	on Deck
PS70/385-2	20.09.07	11:12	79° 20.78' N	124° 20.81' E	3525.0	CTD/RO	surface
PS70/385-3	20.09.07	11:22	79° 20.79' N	124° 20.96' E	3531.0	HN	surface
PS70/385-3	20.09.07	11:28	79° 20.80' N	124° 21.10' E	3530.0	HN	on deck
PS70/385-2	20.09.07	12:16	79° 20.76' N	124° 21.82' E	3525.0	CTD/RO	at depth
PS70/385-2	20.09.07	13:23	79° 20.81' N	124° 22.79' E	3526.0	CTD/RO	on deck
PS70/385-4	20.09.07	13:28	79° 20.79' N	124° 22.80' E	3527.0	BONGO	surface
PS70/385-4	20.09.07	13:33	79° 20.77' N	124° 22.80' E	3528.0	BONGO	at depth
PS70/385-4	20.09.07	13:37	79° 20.75' N	124° 22.80' E	3524.0	BONGO	on deck
PS70/385-5	20.09.07	13:44	79° 20.73' N	124° 22.83' E	3526.0	BONGO	surface
PS70/385-5	20.09.07	14:07	79° 20.70' N	124° 23.03' E	3529.0	BONGO	at depth
PS70/385-5	20.09.07	14:34	79° 20.65' N	124° 23.23' E	3528.0	BONGO	on deck
PS70/385-6	20.09.07	14:42	79° 20.64' N	124° 23.24' E	3528.0	CTD/RO	surface
PS70/385-6	20.09.07	14:53	79° 20.63' N	124° 23.17' E	3527.0	CTD/RO	at depth
PS70/385-6	20.09.07	15:11	79° 20.60' N	124° 23.02' E	3530.0	CTD/RO	on deck
PS70/385-7	20.09.07	15:17	79° 20.59' N	124° 22.98' E	3527.0	ISP	into water
PS70/385-7	20.09.07	15:57	79° 20.54' N	124° 23.22' E	3536.0	ISP	pump at depth
PS70/385-7	20.09.07	18:52	79° 20.37' N	124° 23.67' E	3520.0	ISP	on deck
PS70/385-8	20.09.07	19:00	79° 20.38' N	124° 23.69' E	3519.0	CTD/RO	surface
PS70/385-8	20.09.07	19:05	79° 20.38' N	124° 23.69' E	3520.0	CTD/RO	at depth
PS70/385-8	20.09.07	19:18	79° 20.39' N	124° 23.66' E	3518.0	CTD/RO	on deck
PS70/385-9	20.09.07	19:32	79° 20.41' N	124° 23.57' E	3522.0	MUC	surface
PS70/385-9	20.09.07	20:11	79° 20.46' N	124° 23.38' E	3521.0	MUC	at sea bottom
PS70/385-9	20.09.07	20:55	79° 20.44' N	124° 23.10' E	3523.0	MUC	on deck
PS70/386-1	20.09.07	23:24	78° 56.23' N	124° 32.85' E	3061.0	CTD/RO	surface
PS70/386-1	21.09.07	01:31	78° 56.13' N	124° 33.12' E	3063.0	CTD/RO	on deck
PS70/387-1	21.09.07	03:16	78° 38.27' N	124° 36.75' E	2867.0	CTD/RO	surface
PS70/387-1	21.09.07	04:06	78° 38.22' N	124° 36.68' E	2864.6	CTD/RO	at depth
PS70/387-1	21.09.07	05:12	78° 38.19' N	124° 35.81' E	2865.6	CTD/RO	on deck
PS70/387-2	21.09.07	05:14	78° 38.19' N	124° 35.79' E	2865.6	XCTD	surface
PS70/387-3	21.09.07	05:21	78° 38.19' N	124° 35.68' E	2865.3	XCTD	surface
PS70/388-1	21.09.07	06:18	78° 29.96' N	124° 35.50' E	2703.4	XCTD	surface
PS70/389-1	21.09.07	07:26	78° 21.30' N	124° 30.89' E	2599.6	CTD/UC	into Water
PS70/389-1	21.09.07	08:15	78° 21.30' N	124° 31.30' E	2599.8	CTD/UC	on Depth
PS70/389-1	21.09.07	09:36	78° 21.41' N	124° 32.13' E	2601.0	CTD/UC	on Deck
PS70/389-2	21.09.07	09:48	78° 21.41' N	124° 32.24' E	2600.4	MN	surface
PS70/389-2	21.09.07	10:53	78° 21.34' N	124° 32.69' E	2599.2	MN	at depth
PS70/389-2	21.09.07	12:23	78° 21.29' N	124° 32.93' E	2597.4	MN	on deck
PS70/389-3	21.09.07	12:29	78° 21.27' N	124° 32.91' E	2597.1	BONGO	surface

Station	Date	Time	Position Lat	Position Lon	Depth [m]	Gear Abbre- viation	Action
PS70/389-3	21.09.07	13:27	78° 21.28' N	124° 32.90' E	2597.4	BONGO	at depth
PS70/389-3	21.09.07	14:19	78° 21.25' N	124° 32.78' E	2597.4	BONGO	on deck
PS70/390-1	21.09.07	15:15	78° 14.32' N	124° 22.61' E	2494.5	XCTD	surface
PS70/391-1	21.09.07	16:05	78° 7.79' N	124° 14.53' E	2436.0	CTD/RO	surface
PS70/391-1	21.09.07	16:50	78° 7.78' N	124° 14.54' E	2435.4	CTD/RO	at depth
PS70/391-1	21.09.07	17:42	78° 7.85' N	124° 14.60' E	2436.6	CTD/RO	on deck
PS70/392-1	21.09.07	18:28	78° 1.77' N	124° 6.87' E	2362.8	XCTD	surface
PS70/393-1	21.09.07	19:06	77° 56.64' N	124° 1.38' E	2244.6	XCTD	surface
PS70/394-1	21.09.07	19:48	77° 51.80' N	123° 55.68' E	2144.7	CTD/RO	surface
PS70/394-1	21.09.07	20:29	77° 51.74' N	123° 56.14' E	2141.4	CTD/RO	at depth
PS70/394-1	21.09.07	21:13	77° 51.72' N	123° 57.07' E	2136.9	CTD/RO	on deck
PS70/395-1	21.09.07	21:45	77° 46.87' N	123° 48.26' E	2047.5	XCTD	surface
PS70/396-1	21.09.07	22:10	77° 42.53' N	123° 42.27' E	1941.3	XCTD	surface
PS70/397-1	21.09.07	22:42	77° 38.05' N	123° 36.12' E	1817.1	CTD/RO	surface
PS70/397-1	21.09.07	23:18	77° 38.02' N	123° 36.38' E	1813.5	CTD/RO	at depth
PS70/397-1	21.09.07	23:59	77° 37.92' N	123° 36.73' E	1809.3	CTD/RO	on deck
PS70/397-2	22.09.07	00:09	77° 37.91' N	123° 36.81' E	1807.8	MN	surface
PS70/397-2	22.09.07	00:56	77° 37.87' N	123° 37.28' E	1802.7	MN	at depth
PS70/397-2	22.09.07	02:02	77° 37.78' N	123° 37.42' E	1799.4	MN	on deck
PS70/397-3	22.09.07	02:08	77° 37.76' N	123° 37.46' E	1798.8	BONGO	surface
PS70/397-3	22.09.07	02:13	77° 37.76' N	123° 37.50' E	1798.5	BONGO	at depth
PS70/397-3	22.09.07	02:18	77° 37.75' N	123° 37.54' E	1798.2	BONGO	on deck
PS70/397-4	22.09.07	02:23	77° 37.74' N	123° 37.58' E	1797.9	BONGO	surface
PS70/397-4	22.09.07	03:21	77° 37.62' N	123° 38.58' E	1795.8	BONGO	at depth
PS70/397-4	22.09.07	04:16	77° 37.38' N	123° 39.17' E	1793.1	BONGO	on deck
PS70/398-1	22.09.07	04:51	77° 33.30' N	123° 34.56' E	1588.2	XCTD	surface
PS70/399-1	22.09.07	05:28	77° 28.84' N	123° 29.32' E	1453.2	XCTD	surface
PS70/400-1	22.09.07	06:29	77° 23.29' N	123° 24.02' E	1158.6	CTD/UC	into Water
PS70/400-1	22.09.07	06:57	77° 22.94' N	123° 24.80' E	1123.8	CTD/UC	on Depth
PS70/400-1	22.09.07	07:41	77° 22.36' N	123° 24.64' E	1084.5	CTD/UC	on Deck
PS70/400-2	22.09.07	07:53	77° 22.23' N	123° 24.80' E	1071.0	CTD/RO	surface
PS70/400-2	22.09.07	08:18	77° 21.97' N	123° 25.18' E	1048.8	CTD/RO	at depth
PS70/400-2	22.09.07	08:42	77° 21.72' N	123° 25.76' E	1020.3	CTD/RO	on deck
PS70/400-3	22.09.07	08:47	77° 21.67' N	123° 25.81' E	1017.0	ISP	into water
PS70/400-3	22.09.07	08:52	77° 21.65' N	123° 25.75' E	1015.5	ISP	into water
PS70/400-3	22.09.07	09:24	77° 21.71' N	123° 25.86' E	1018.8	ISP	pump at depth
PS70/400-3	22.09.07	10:45	77° 21.98' N	123° 25.65' E	1041.0	ISP	pump at depth
PS70/400-3	22.09.07	11:45	77° 22.23' N	123° 24.95' E	1069.8	ISP	Information
PS70/400-3	22.09.07	12:16	77° 22.25' N	123° 25.09' E	1070.7	ISP	on deck
PS70/400-3	22.09.07	12:17	77° 22.25' N	123° 25.07' E	1070.1	ISP	on deck
PS70/400-4	22.09.07	12:18	77° 22.25' N	123° 25.07' E	1070.4	XCTD	surface
PS70/400-5	22.09.07	12:31	77° 22.20' N	123° 25.41' E	1067.1	CTD/RO	surface
PS70/400-5	22.09.07	12:43	77° 22.17' N	123° 25.47' E	1063.5	CTD/RO	at depth
PS70/400-5	22.09.07	13:05	77° 22.22' N	123° 25.11' E	1067.1	CTD/RO	on deck
PS70/400-6	22.09.07	13:10	77° 22.23' N	123° 25.10' E	1068.6	BONGO	surface
PS70/400-6	22.09.07	13:30	77° 22.20' N	123° 25.16' E	1065.0	BONGO	at depth
PS70/400-6	22.09.07	13:50	77° 22.14' N	123° 25.16' E	1060.2	BONGO	on deck
PS70/400-7	22.09.07	13:56	77° 22.12' N	123° 25.13' E	1059.3	CTD/RO	surface
PS70/400-7	22.09.07	14:06	77° 22.10' N	123° 25.08' E	1058.4	CTD/RO	at depth
PS70/400-7	22.09.07	14:23	77° 22.03' N	123° 25.16' E	1052.4	CTD/RO	on deck

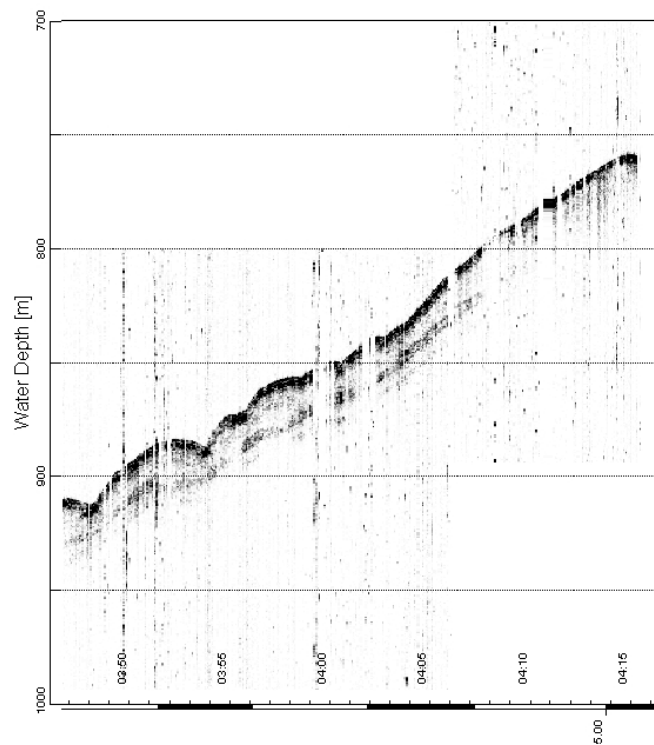
Station	Date	Time	Position Lat	Position Lon	Depth [m]	Gear Abbre- viation	Action
PS70/400-8	22.09.07	14:31	77° 21.99' N	123° 25.26' E	1048.5	MN	surface
PS70/400-8	22.09.07	15:02	77° 21.99' N	123° 25.34' E	1046.1	MN	at depth
PS70/400-8	22.09.07	15:03	77° 21.99' N	123° 25.36' E	1045.5	MN	Hoisting
PS70/400-8	22.09.07	15:42	77° 21.84' N	123° 26.02' E	1025.1	MN	on deck
PS70/400-9	22.09.07	15:48	77° 21.82' N	123° 26.15' E	1023.0	CTD/RO	surface
PS70/400-9	22.09.07	15:54	77° 21.78' N	123° 26.33' E	1018.8	CTD/RO	at depth
PS70/400-9	22.09.07	16:04	77° 21.69' N	123° 26.76' E	1009.2	CTD/RO	on deck
PS70/401-1	22.09.07	16:55	77° 17.92' N	123° 21.05' E	733.5	CTD/RO	surface
PS70/401-1	22.09.07	17:13	77° 17.69' N	123° 21.58' E	735.6	CTD/RO	at depth
PS70/401-1	22.09.07	17:37	77° 17.38' N	123° 22.02' E	710.7	CTD/RO	on deck
PS70/402-1	22.09.07	18:33	77° 12.90' N	123° 11.70' E	284.1	CTD/RO	surface
PS70/402-1	22.09.07	18:42	77° 12.76' N	123° 11.86' E	275.4	CTD/RO	at depth
PS70/402-1	22.09.07	19:00	77° 12.46' N	123° 12.06' E	250.8	CTD/RO	on deck
PS70/402-1	22.09.07	19:09	77° 12.31' N	123° 12.08' E	238.8	MN	surface
PS70/402-1	22.09.07	19:17	77° 12.18' N	123° 12.30' E	226.2	MN	at depth
PS70/402-1	22.09.07	19:34	77° 11.95' N	123° 12.59' E	201.3	MN	on deck
PS70/402-3	22.09.07	19:46	77° 11.81' N	123° 12.77' E	183.6	BONGO	surface
PS70/402-3	22.09.07	19:52	77° 11.74' N	123° 12.85' E	179.1	BONGO	at depth
PS70/402-3	22.09.07	20:00	77° 11.65' N	123° 12.89' E	166.5	BONGO	on deck
PS70/402-4	22.09.07	20:03	77° 11.61' N	123° 12.94' E	161.4	BONGO	surface
PS70/402-4	22.09.07	20:10	77° 11.51' N	123° 13.06' E	150.9	BONGO	at depth
PS70/402-4	22.09.07	20:18	77° 11.36' N	123° 13.28' E	130.8	BONGO	on deck
PS70/403-1	22.09.07	20:54	77° 8.99' N	123° 7.46' E	120.3	CTD/RO	surface
PS70/403-1	22.09.07	21:00	77° 8.91' N	123° 7.48' E	120.3	CTD/RO	at depth
PS70/403-1	22.09.07	21:09	77° 8.84' N	123° 7.48' E	119.4	CTD/RO	on deck
PS70/404-1	23.09.07	00:22	76° 53.88' N	122° 52.30' E	94.2	CTD/RO	surface
PS70/404-1	23.09.07	00:27	76° 53.82' N	122° 52.11' E	94.2	CTD/RO	at depth
PS70/404-1	23.09.07	00:36	76° 53.73' N	122° 52.05' E	93.9	CTD/RO	on deck
PS70/405-1	23.09.07	03:03	76° 39.47' N	122° 38.14' E	182.4	CTD	surface
PS70/405-1	23.09.07	03:09	76° 39.39' N	122° 38.10' E	96.9	CTD	at depth
PS70/405-1	23.09.07	03:20	76° 39.30' N	122° 37.91' E	0.0	CTD	on deck
PS70/406-1	23.09.07	05:43	76° 25.84' N	122° 25.76' E	82.2	CTD/RO	surface
PS70/406-1	23.09.07	05:47	76° 25.82' N	122° 25.85' E	82.2	CTD/RO	at depth
PS70/406-1	23.09.07	05:56	76° 25.78' N	122° 26.19' E	82.2	CTD/RO	on deck
PS70/407-1	23.09.07	08:44	76° 10.83' N	122° 7.72' E	75.3	CTD/UC	into Water
PS70/407-1	23.09.07	08:50	76° 10.83' N	122° 7.86' E	0.0	CTD/UC	on Depth
PS70/407-1	23.09.07	09:09	76° 10.85' N	122° 8.33' E	75.0	CTD/UC	on Deck
PS70/407-2	23.09.07	09:18	76° 10.88' N	122° 8.46' E	75.3	CTD/RO	surface
PS70/407-2	23.09.07	09:23	76° 10.89' N	122° 8.54' E	75.3	CTD/RO	at depth
PS70/407-2	23.09.07	09:33	76° 10.91' N	122° 8.82' E	75.9	CTD/RO	on deck
PS70/407-3	23.09.07	09:36	76° 10.91' N	122° 8.91' E	75.3	ISP	into water
PS70/407-3	23.09.07	09:43	76° 10.90' N	122° 9.22' E	75.3	ISP	into water
PS70/407-3	23.09.07	09:48	76° 10.89' N	122° 9.47' E	75.0	ISP	into water
PS70/407-3	23.09.07	09:52	76° 10.89' N	122° 9.65' E	74.4	ISP	into water
PS70/407-3	23.09.07	09:53	76° 10.89' N	122° 9.70' E	74.4	ISP	pump at depth
PS70/407-3	23.09.07	12:07	76° 10.72' N	122° 9.88' E	73.5	ISP	Information
PS70/407-3	23.09.07	12:15	76° 10.80' N	122° 9.90' E	74.1	ISP	on deck
PS70/407-4	23.09.07	12:20	76° 10.87' N	122° 9.92' E	74.1	CTD	surface
PS70/407-4	23.09.07	12:25	76° 10.91' N	122° 9.95' E	74.1	CTD	at depth
PS70/407-4	23.09.07	12:39	76° 10.97' N	122° 10.31' E	73.5	CTD	on deck
PS70/408-1	23.09.07	15:36	75° 55.82' N	121° 57.24' E	65.7	CTD	surface

Station	Date	Time	Position Lat	Position Lon	Depth [m]	Gear Abbre- viation	Action
PS70/408-1	23.09.07	15:40	75° 55.82' N	121° 57.16' E	65.7	CTD	at depth
PS70/408-1	23.09.07	15:50	75° 55.83' N	121° 57.24' E	65.7	CTD	on deck
PS70/409-1	23.09.07	18:51	75° 42.32' N	121° 46.14' E	65.4	CTD/RO	surface
PS70/409-1	23.09.07	18:55	75° 42.35' N	121° 46.19' E	65.4	CTD/RO	at depth
PS70/409-1	23.09.07	19:11	75° 42.46' N	121° 46.25' E	65.1	CTD/RO	on deck
PS70/410-1	23.09.07	20:48	75° 27.53' N	121° 34.76' E	60.6	CTD/RO	surface
PS70/410-1	23.09.07	20:54	75° 27.59' N	121° 34.82' E	60.3	CTD/RO	at depth
PS70/410-1	23.09.07	21:00	75° 27.64' N	121° 34.92' E	60.3	CTD/RO	on deck
PS70/411-1	23.09.07	22:37	75° 12.00' N	121° 21.45' E	48.3	CTD/UC	into Water
PS70/411-1	23.09.07	22:42	75° 12.03' N	121° 21.61' E	48.3	CTD/UC	on Depth
PS70/411-1	23.09.07	22:58	75° 12.06' N	121° 21.77' E	48.6	CTD/UC	on Deck
PS70/411-2	23.09.07	23:06	75° 12.06' N	121° 21.80' E	48.3	CTD/RO	surface
PS70/411-2	23.09.07	23:11	75° 12.06' N	121° 21.82' E	48.3	CTD/RO	at depth
PS70/411-2	23.09.07	23:19	75° 12.05' N	121° 21.85' E	48.3	CTD/RO	on deck
PS70/411-3	23.09.07	23:56	75° 12.05' N	121° 21.91' E	48.3	CTD/RO	surface
PS70/411-3	24.09.07	00:01	75° 12.05' N	121° 21.92' E	48.6	CTD/RO	at depth
PS70/411-3	24.09.07	00:10	75° 12.05' N	121° 21.93' E	48.6	CTD/RO	on deck
PS70/411-4	24.09.07	00:15	75° 12.06' N	121° 21.98' E	48.3	ISP	into water
PS70/411-4	24.09.07	00:26	75° 12.06' N	121° 21.97' E	48.3	ISP	pump at depth
PS70/411-4	24.09.07	02:38	75° 11.89' N	121° 21.58' E	48.3	ISP	Information
PS70/411-4	24.09.07	02:46	75° 11.87' N	121° 21.53' E	48.3	ISP	on deck
PS70/411-4	24.09.07	02:51	75° 11.86' N	121° 21.55' E	48.3	CTD/RO	surface
PS70/411-4	24.09.07	02:55	75° 11.86' N	121° 21.57' E	48.3	CTD/RO	at depth
PS70/411-4	24.09.07	03:00	75° 11.85' N	121° 21.63' E	48.3	CTD/RO	on deck

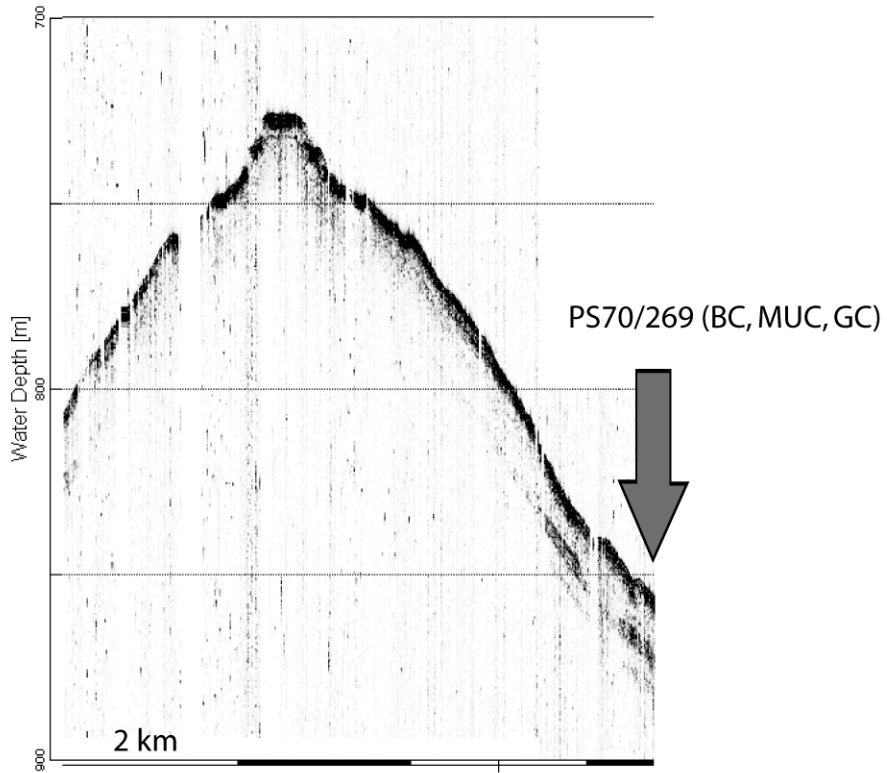
A.5 CORING POSITIONS



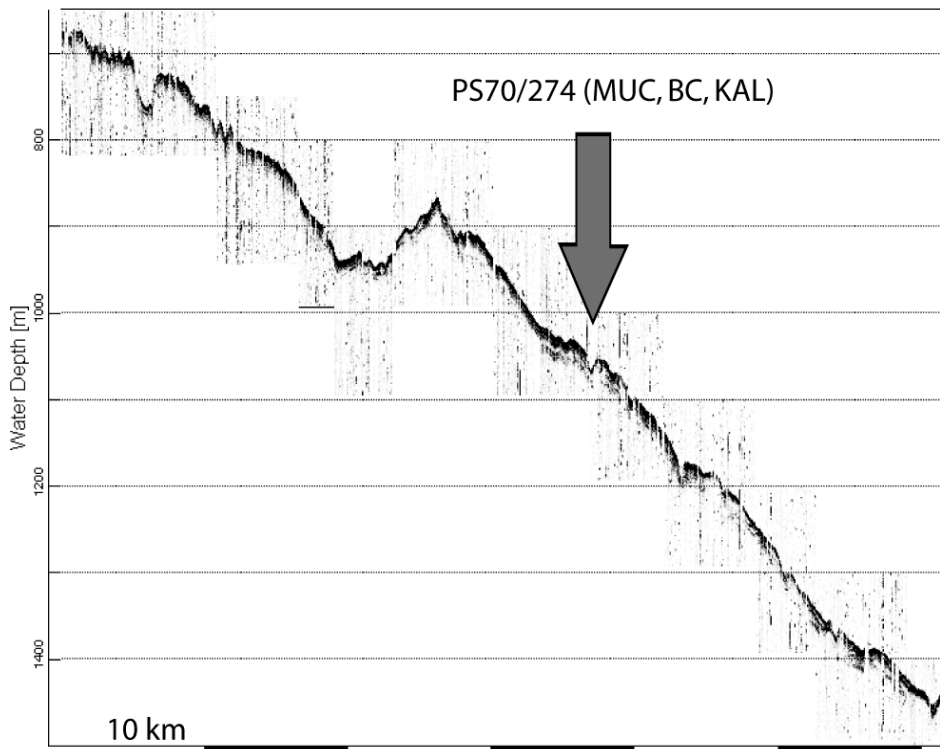
Parasound profile at location PS70/265



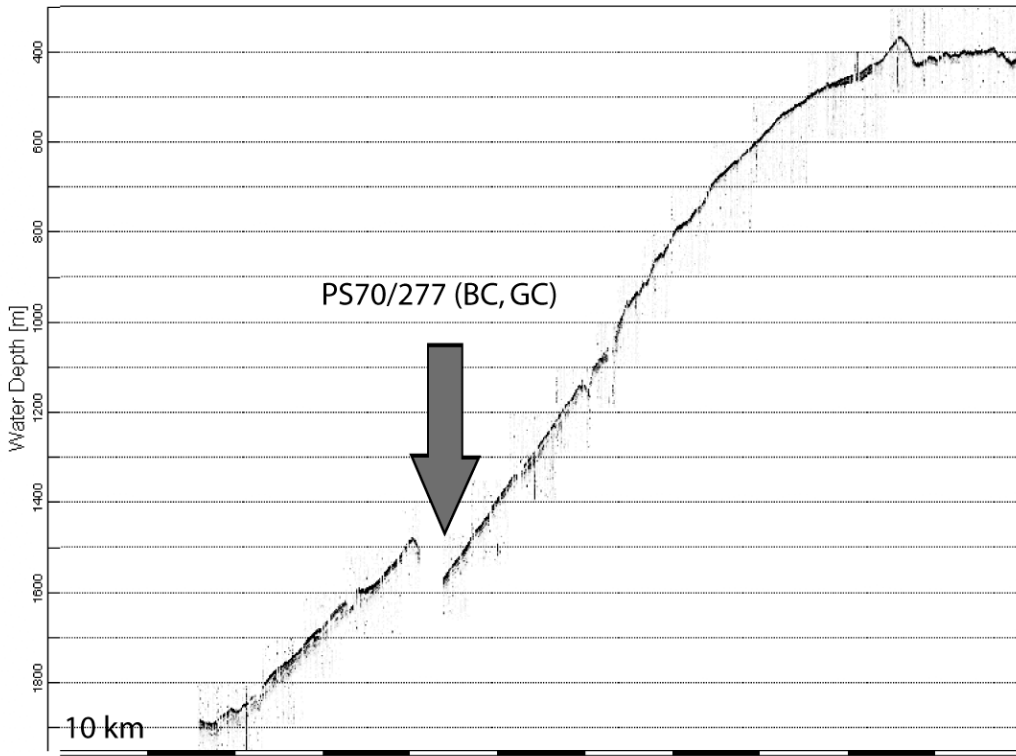
Parasound profile at location PS70/266



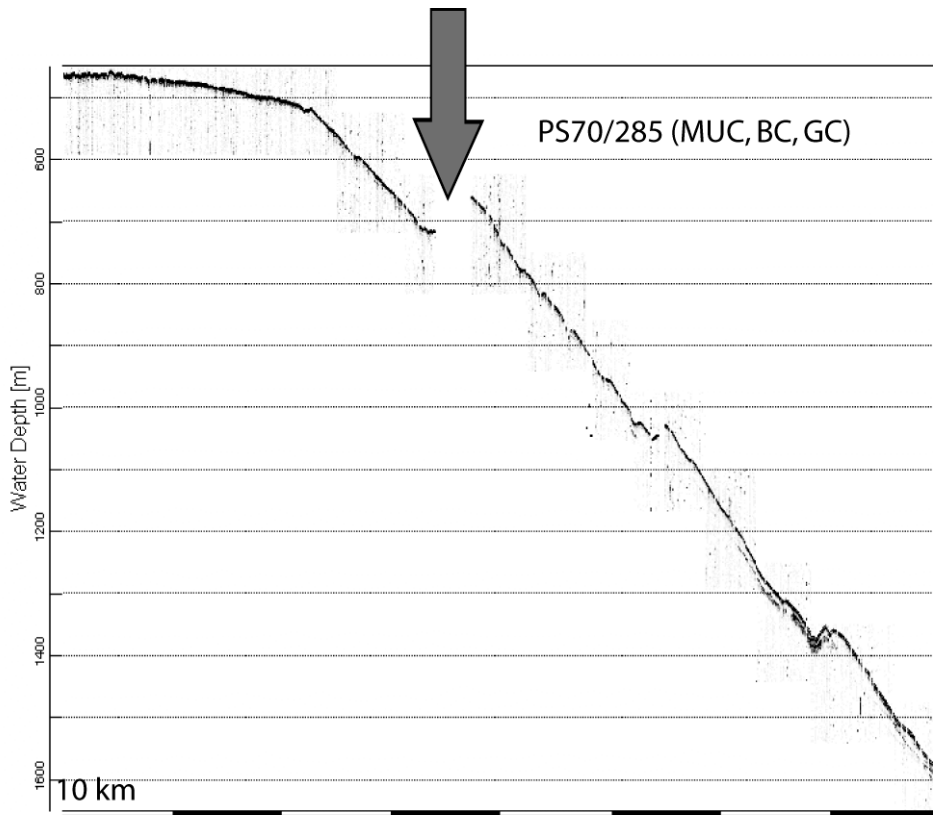
Parasound profile at location PS70/269



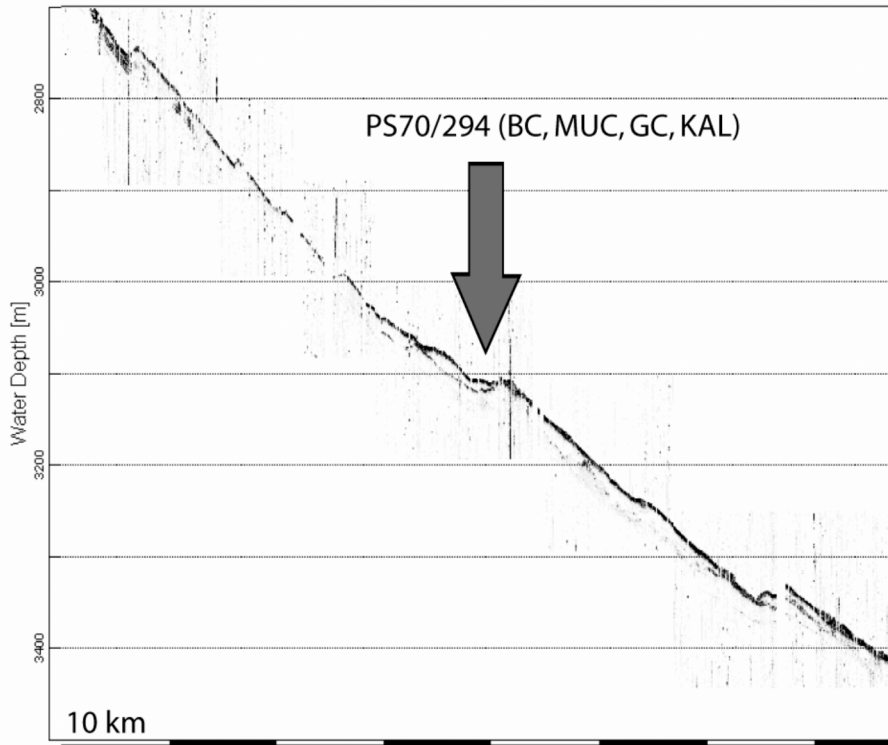
Parasound profile at location PS70/274



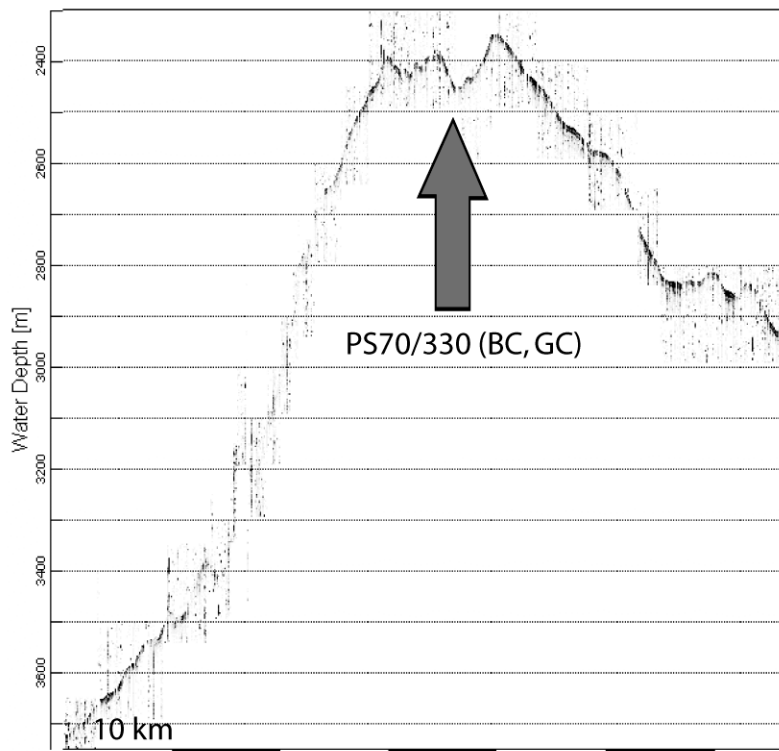
Parasound profile at location PS70/277



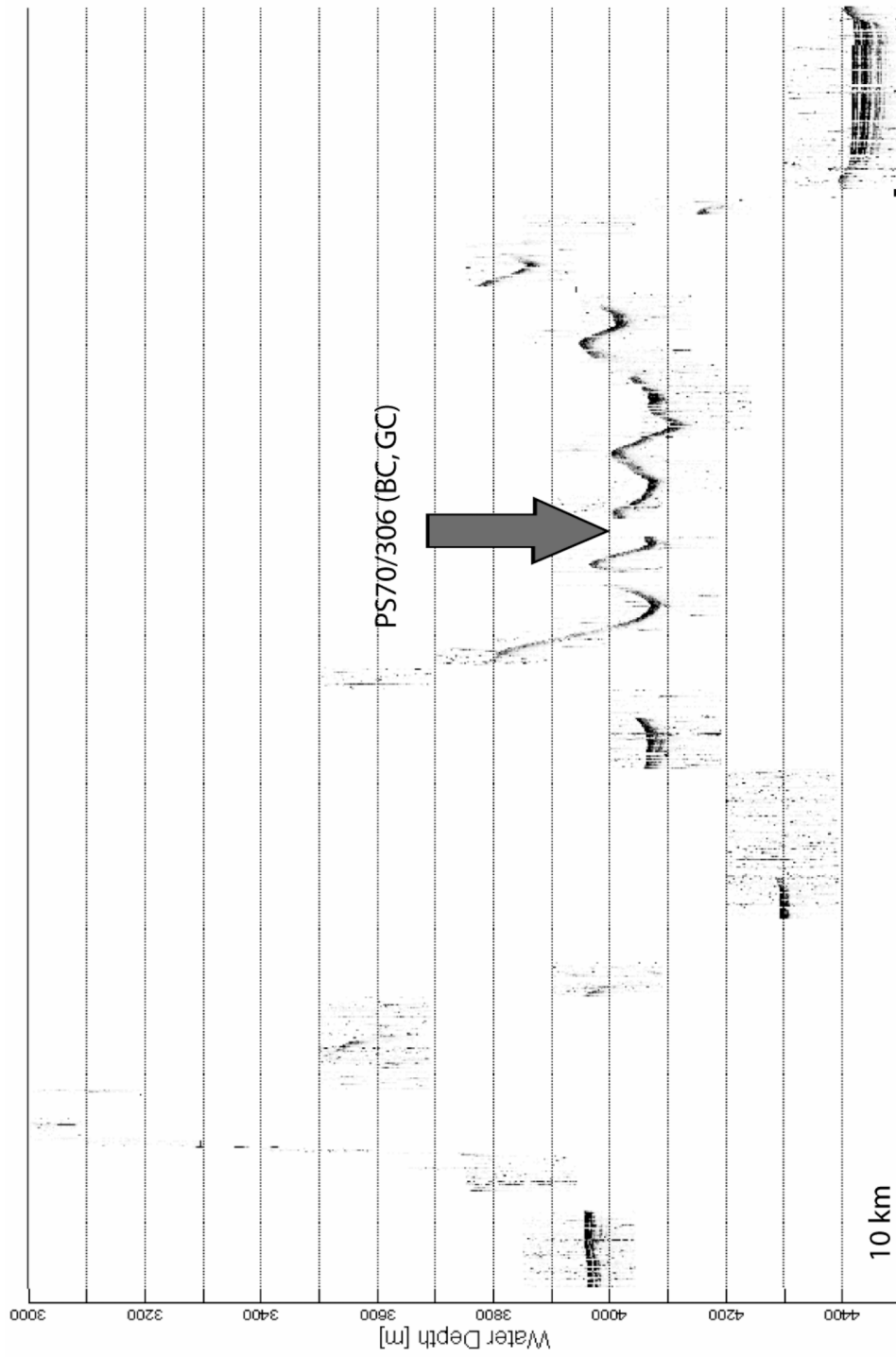
Parasound profile at location PS70/285



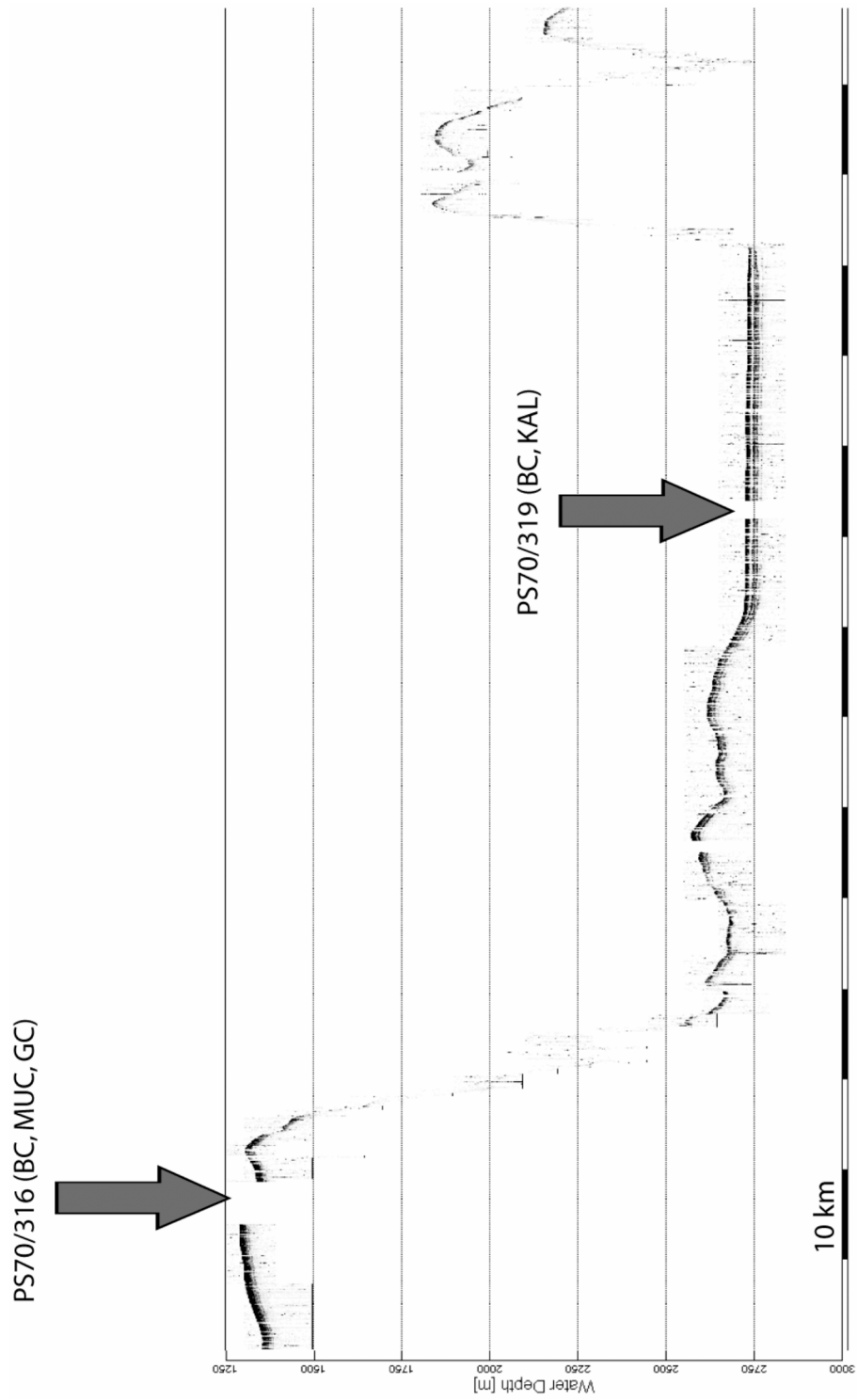
Parasound profile at location PS70/294



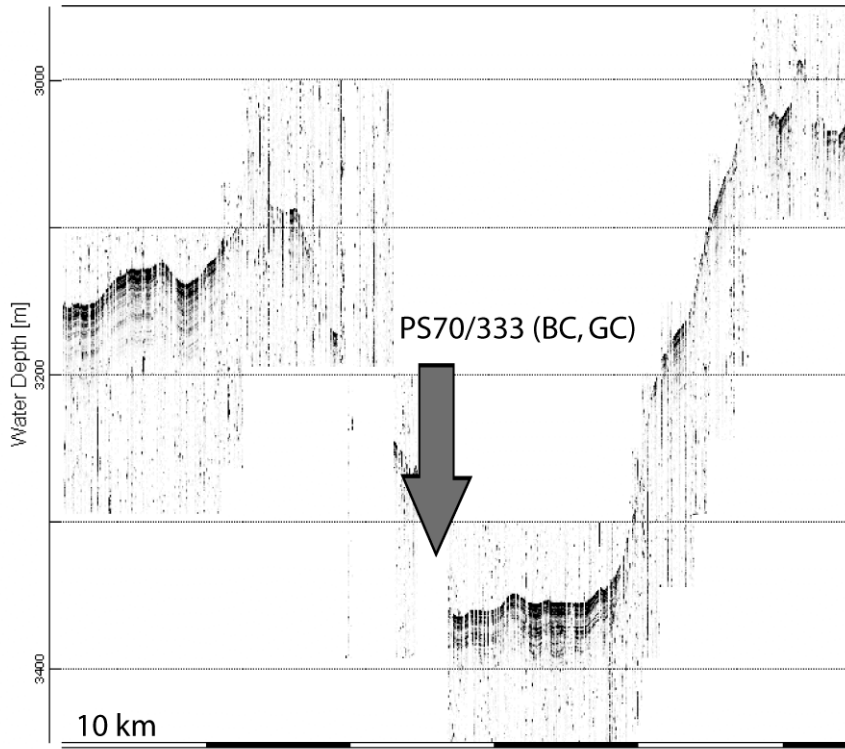
Parasound profile at location PS70/330



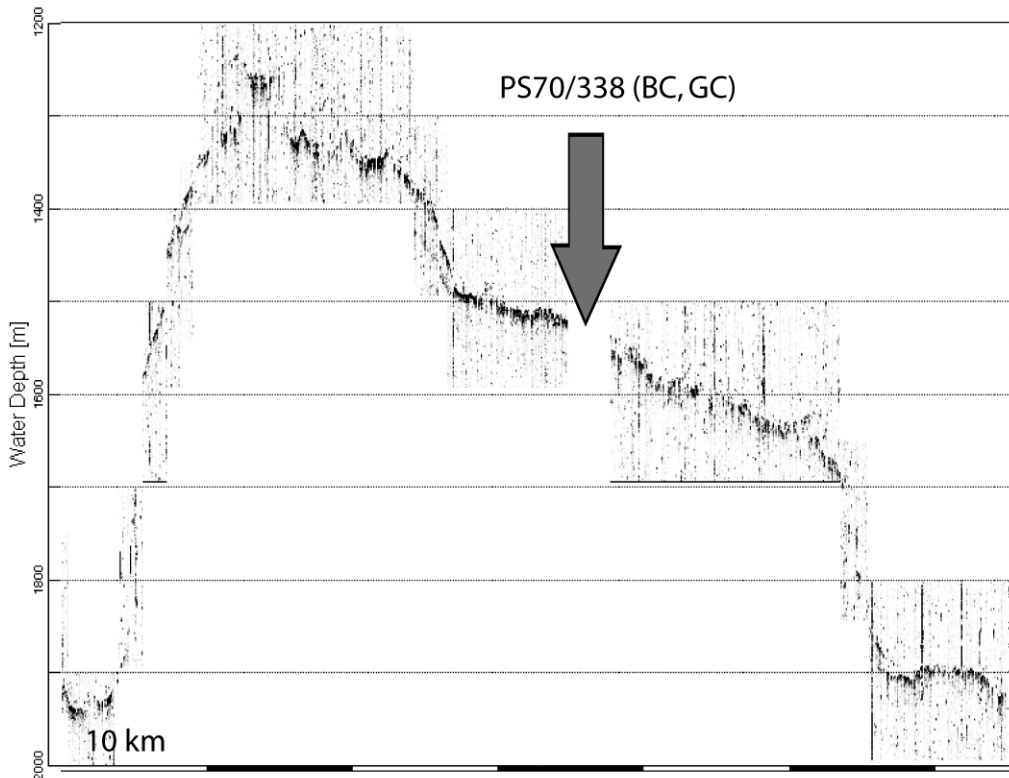
Parasound profile at location PS70/306



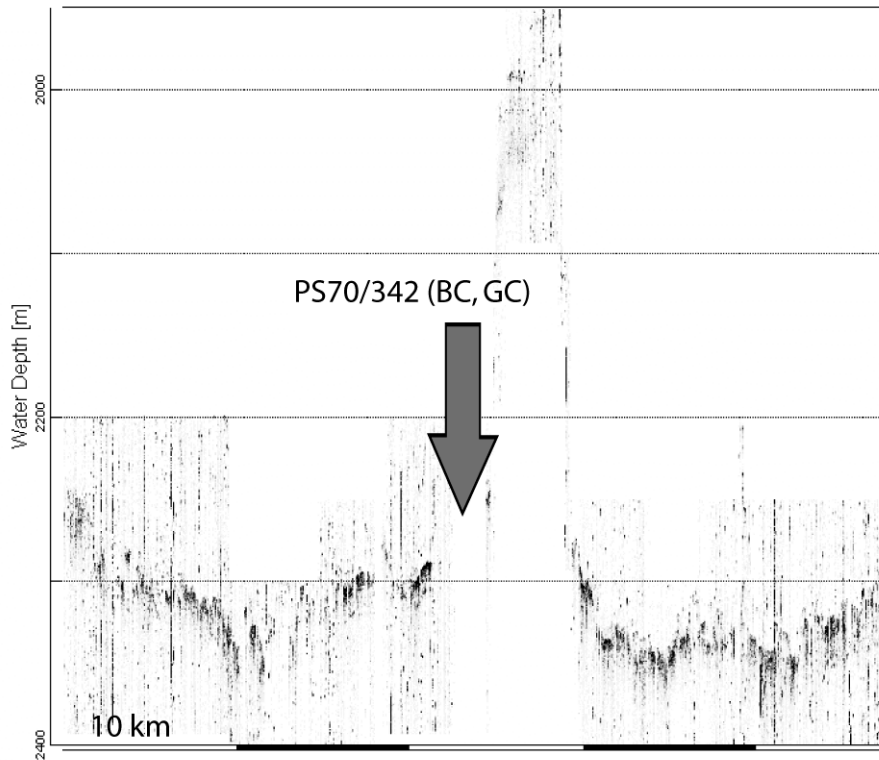
Parasound profile at locations PS70/316 and 319



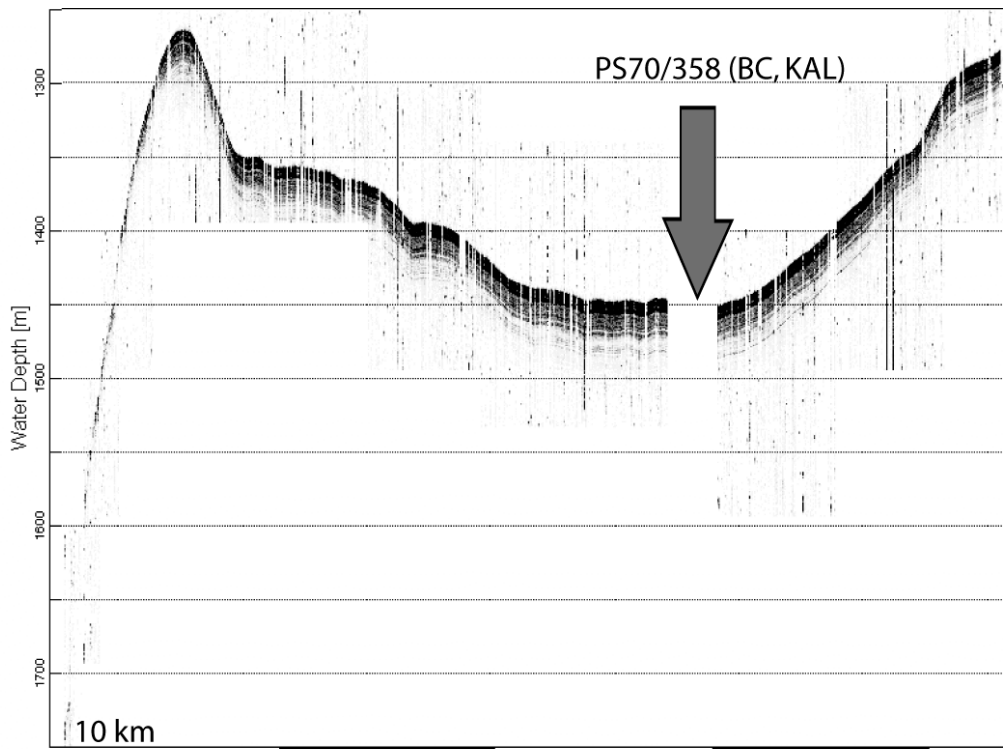
Parasound profile at location PS70/333



Parasound profile at location PS70/338

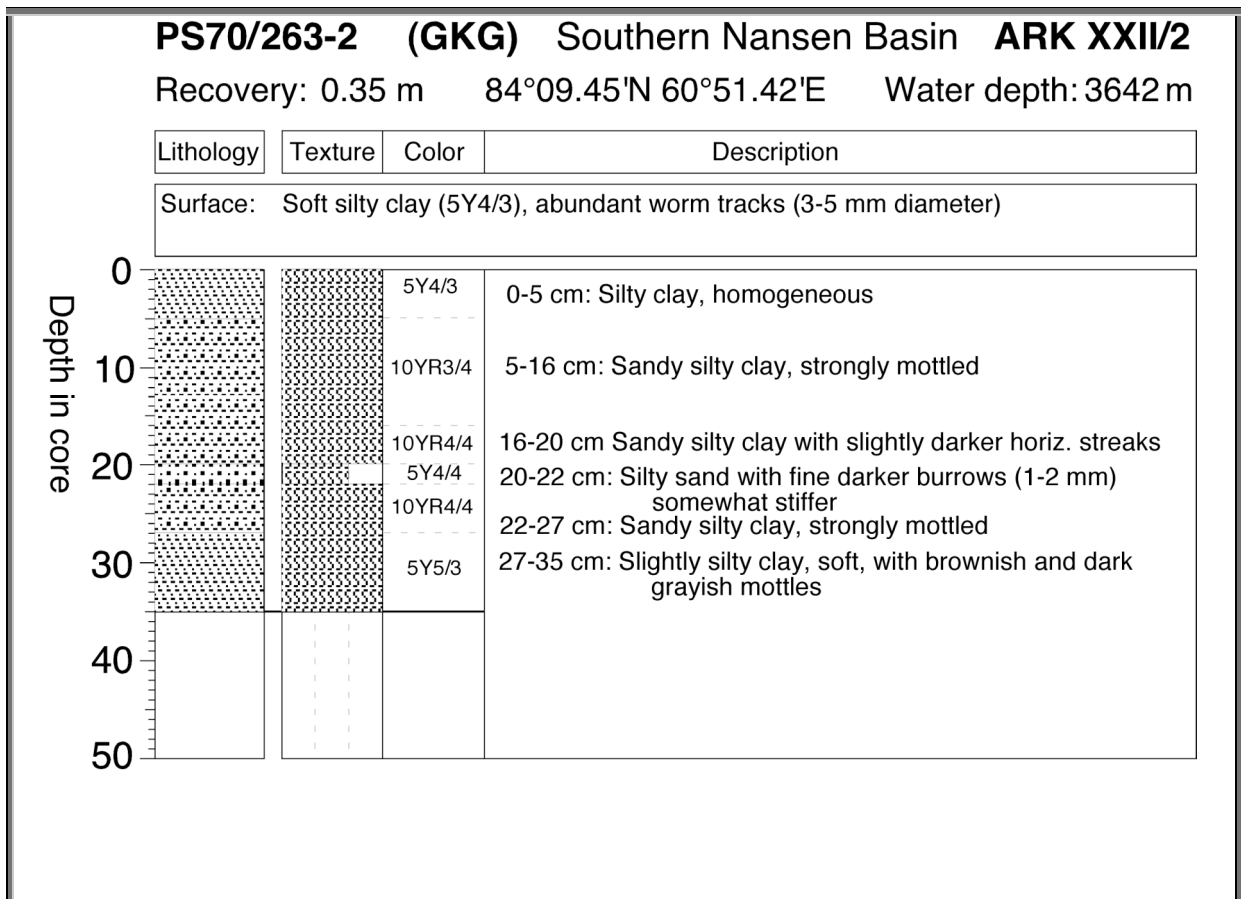
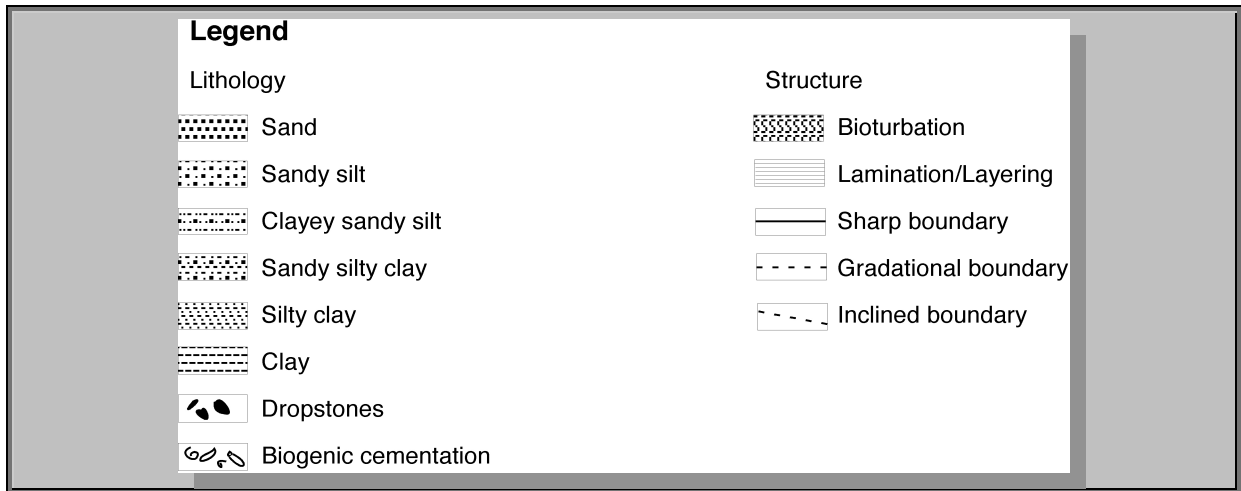


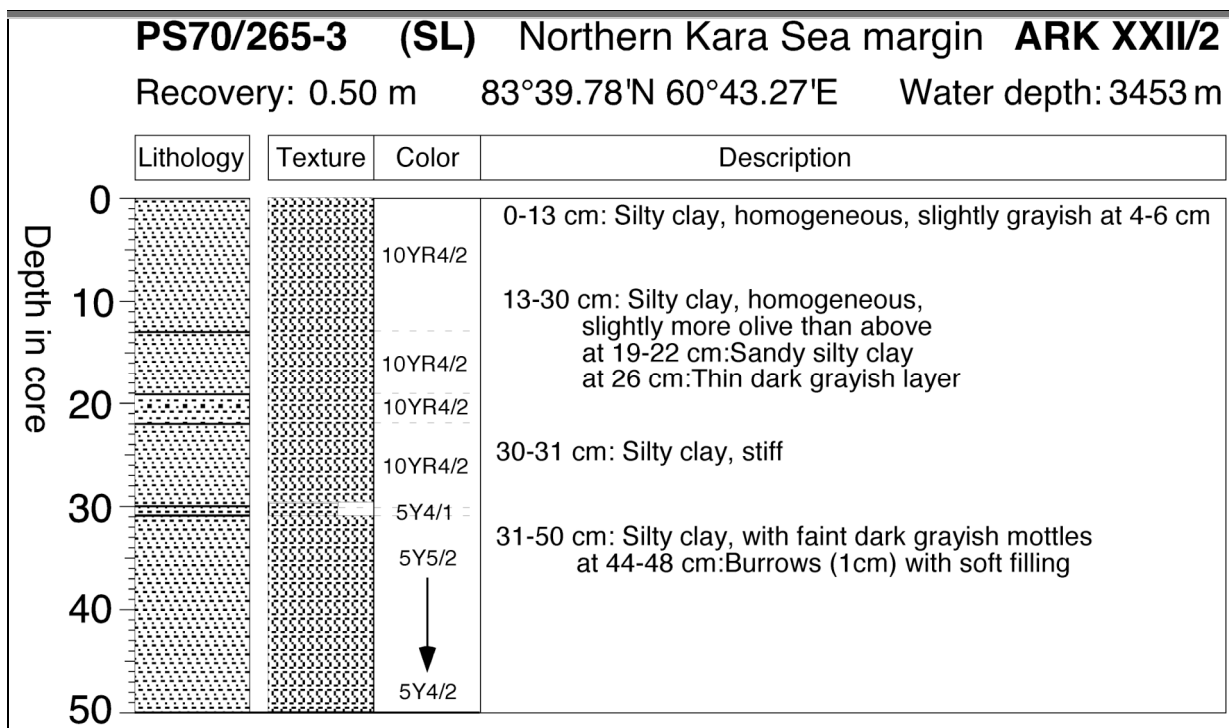
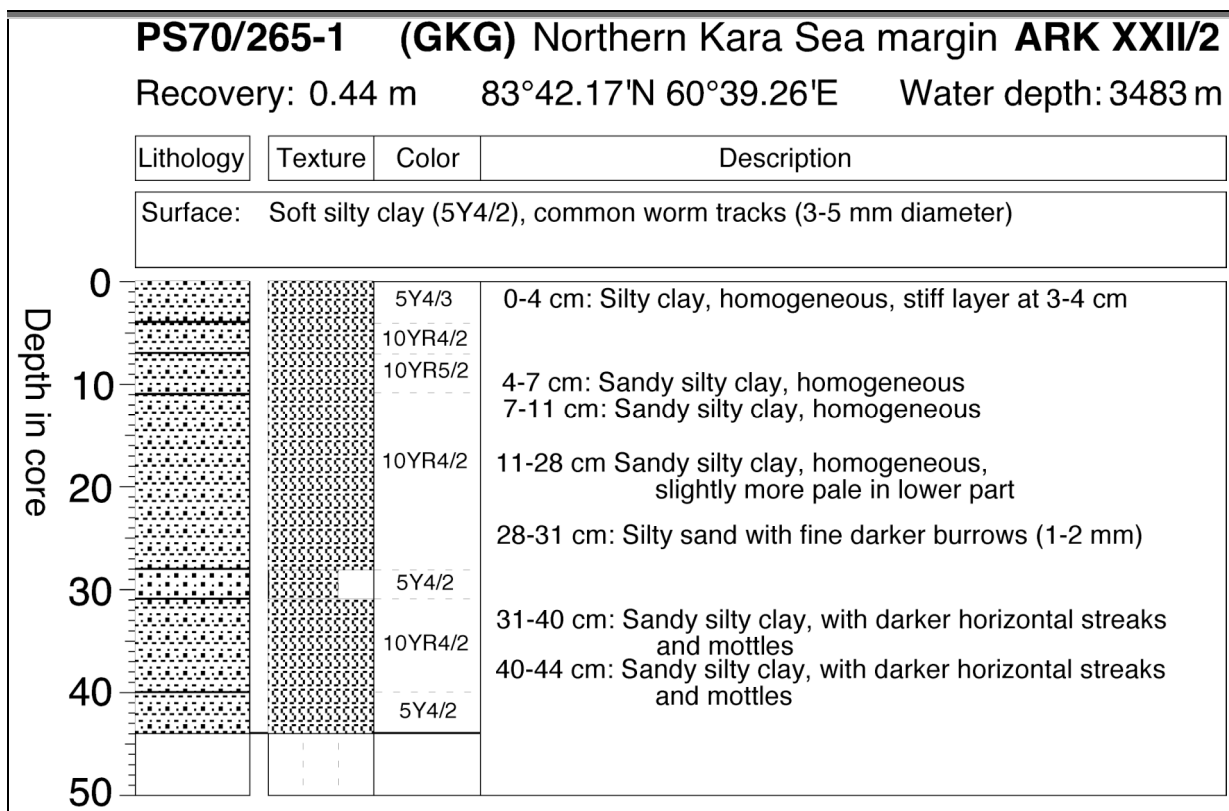
Parasound profile at location PS70/342



Parasound profile at location PS70/358

A.6 SEDIMENT CORE DESCRIPTIONS



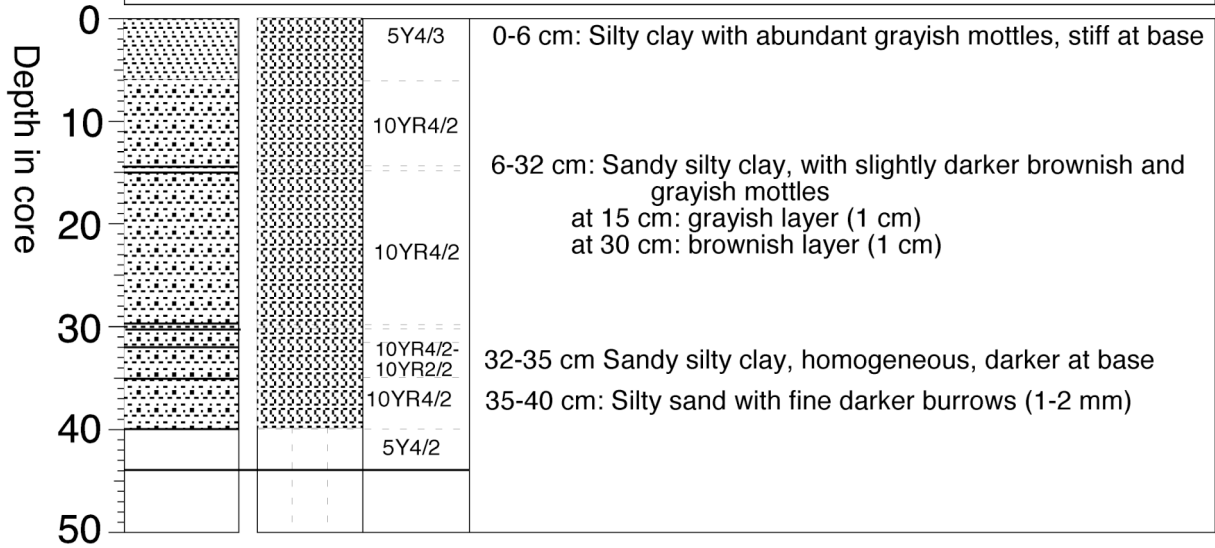


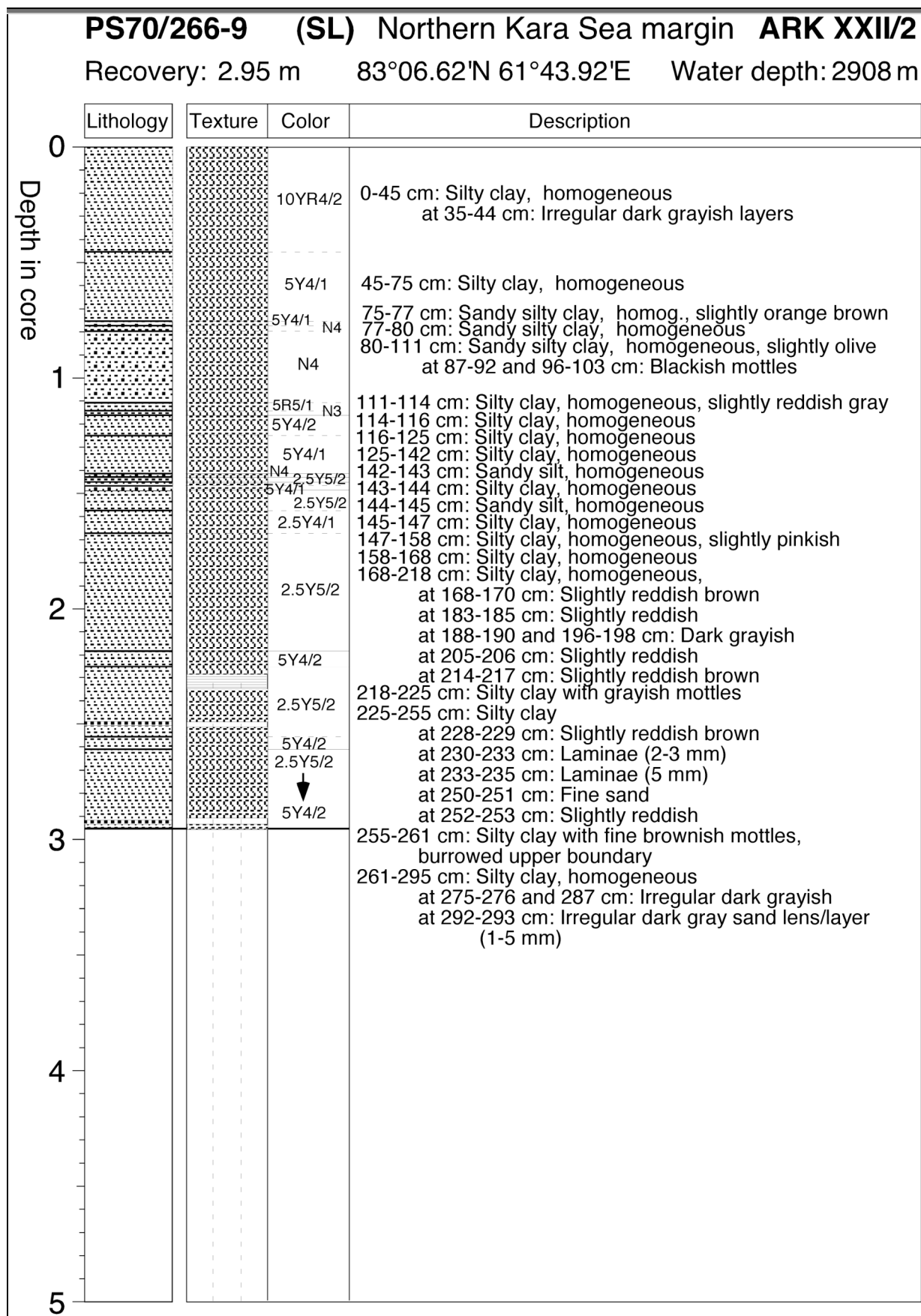
PS70/266-7 (GKG) Northern Kara Sea margin ARK XXII/2

Recovery: 0.40 m 83°06.62'N 61°43.92'E Water depth: 2937 m

Lithology	Texture	Color	Description
-----------	---------	-------	-------------

Surface: Soft silty clay (5Y4/3), common worm tracks (3-5 mm diameter) and benthic foraminifers (Pyrgo)



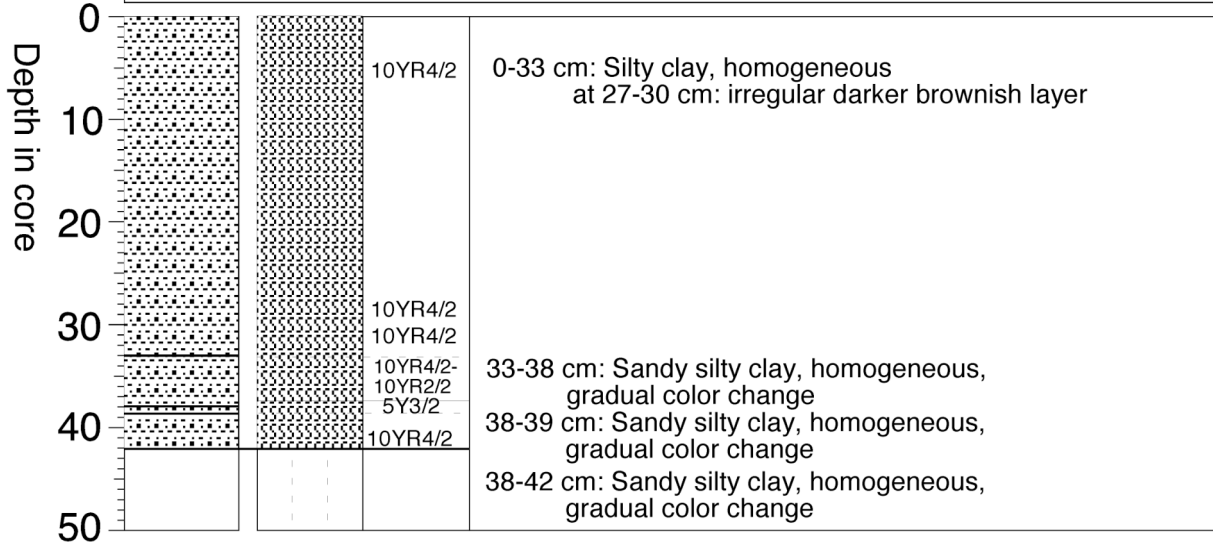


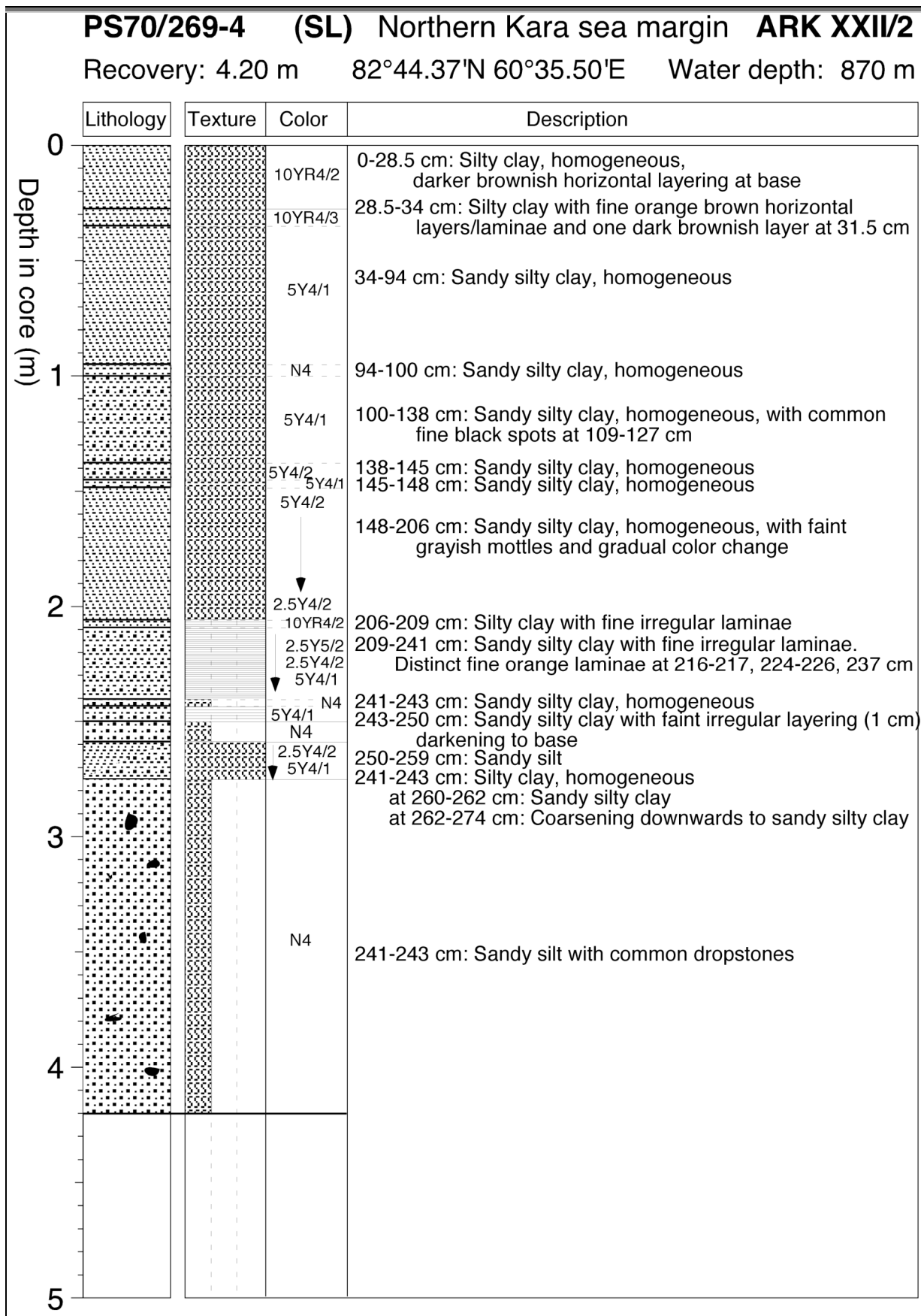
PS70/269-2 (GKG) Northern Kara Sea margin ARK XXII/2

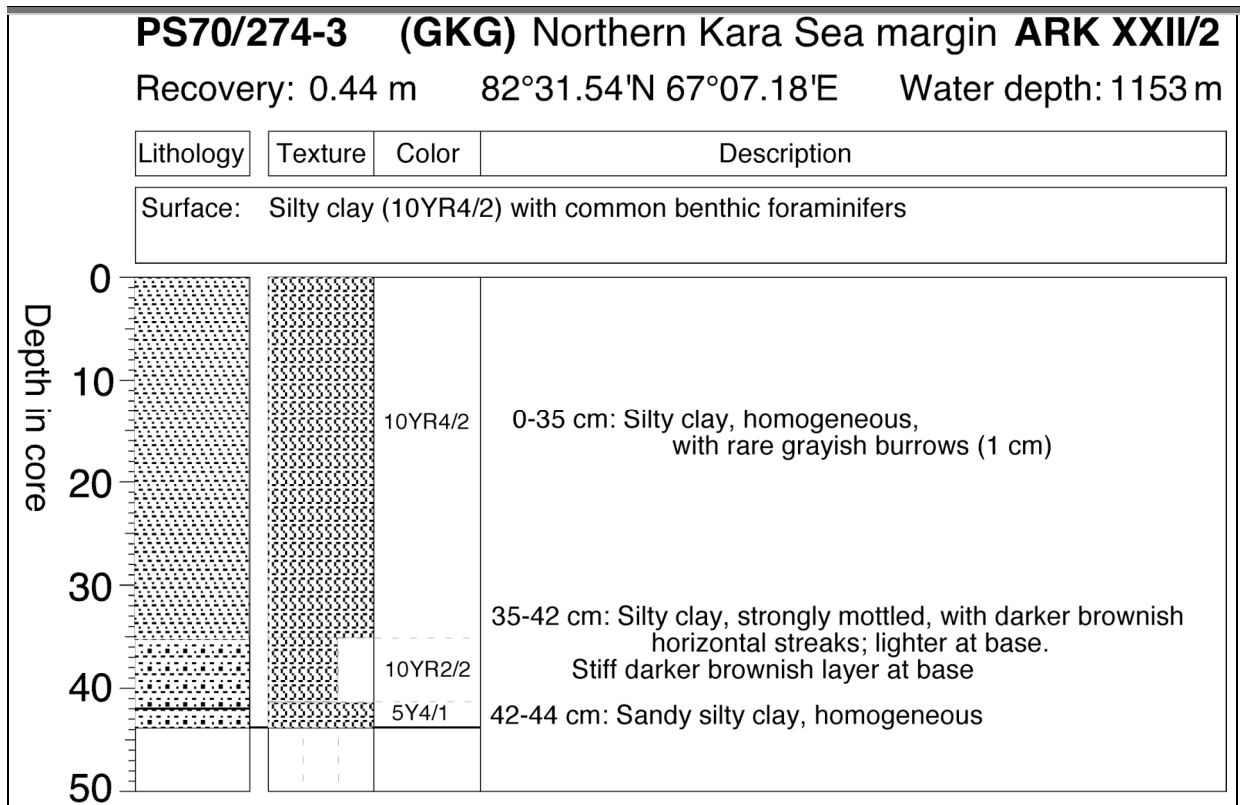
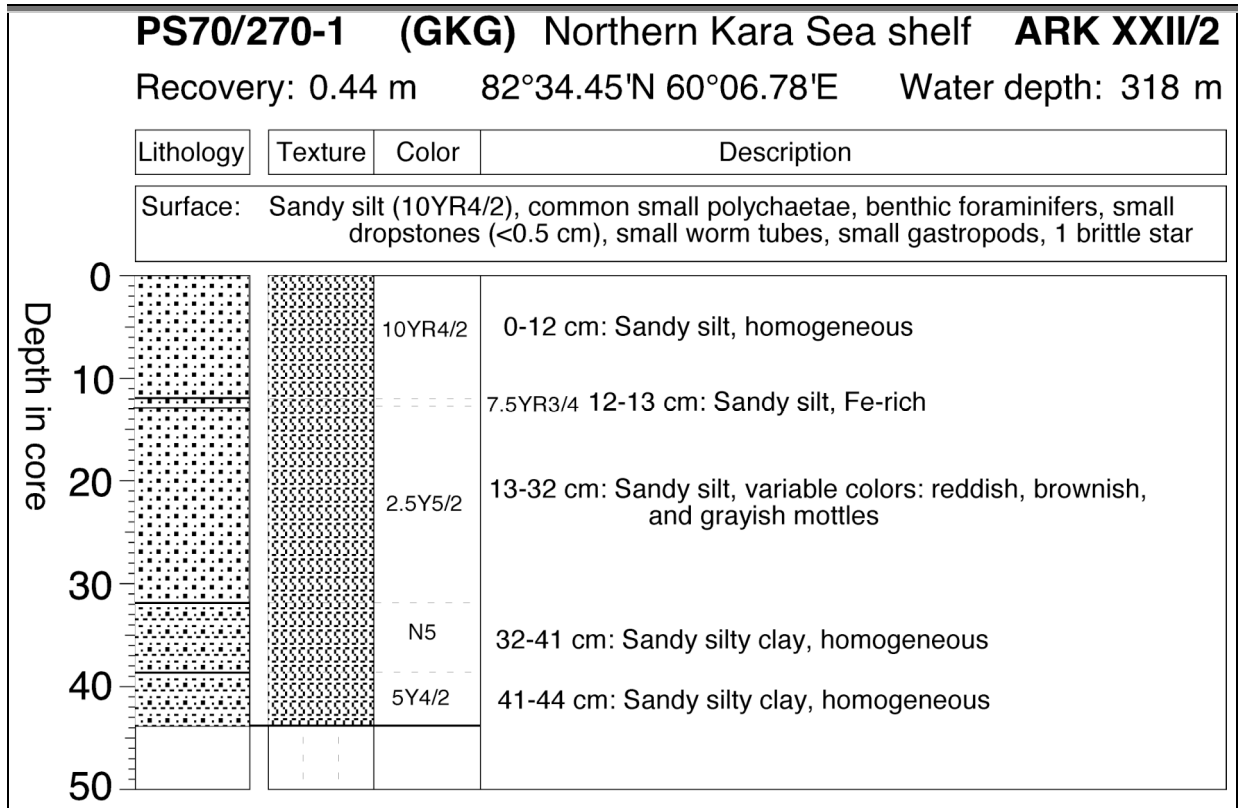
Recovery: 0.42 m 82°44.01'N 60°35.96'E Water depth: 840 m

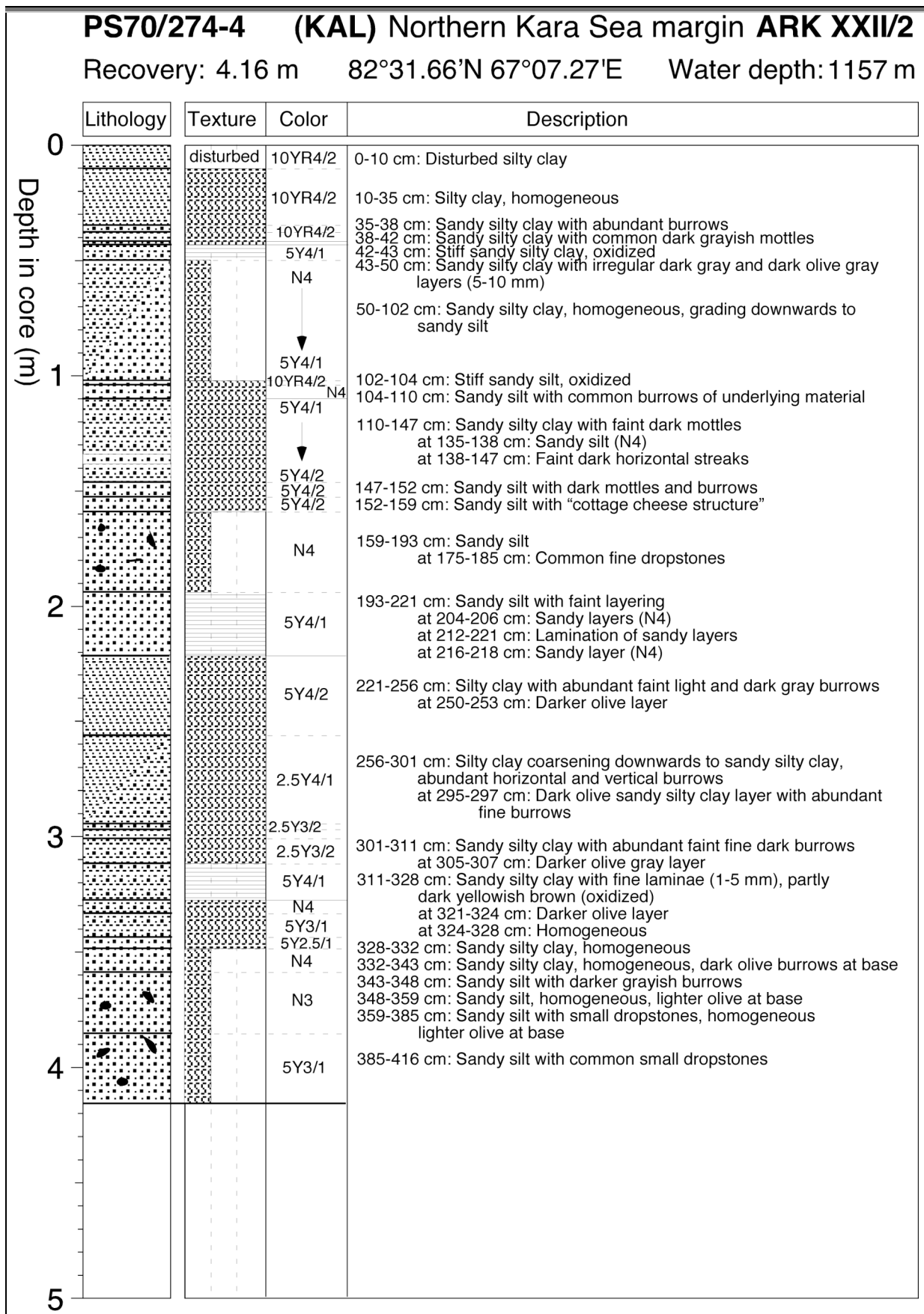
Lithology	Texture	Color	Description
-----------	---------	-------	-------------

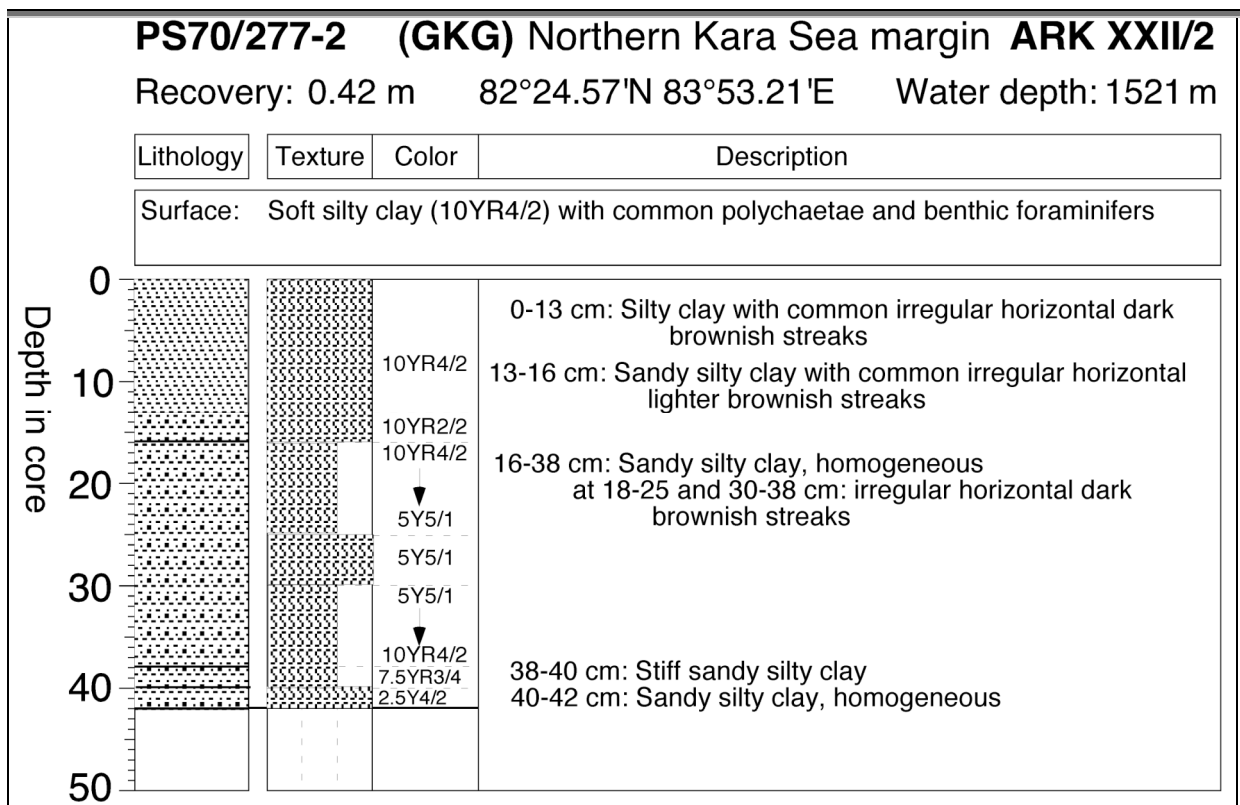
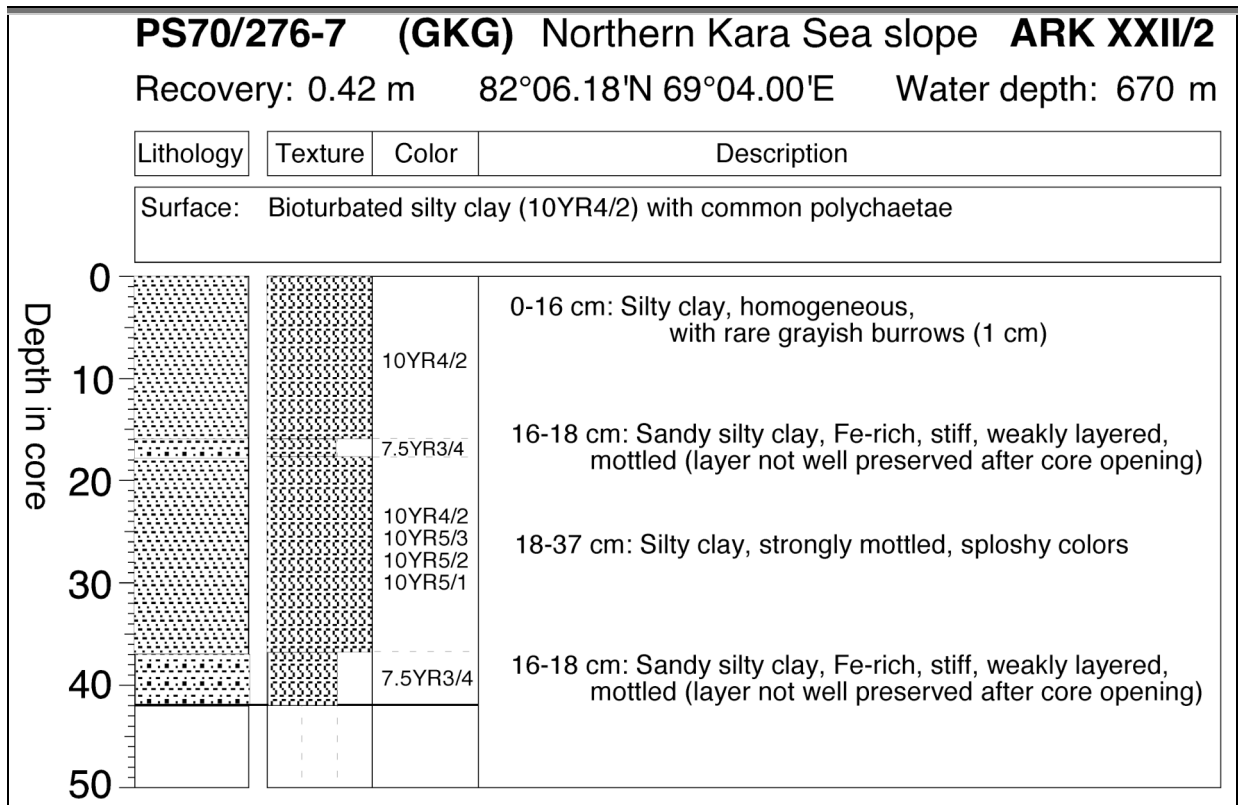
Surface: Soft sandy silty clay (10YR4/2), common polychaetae, 1 dropstone, 1 bivalve fragment

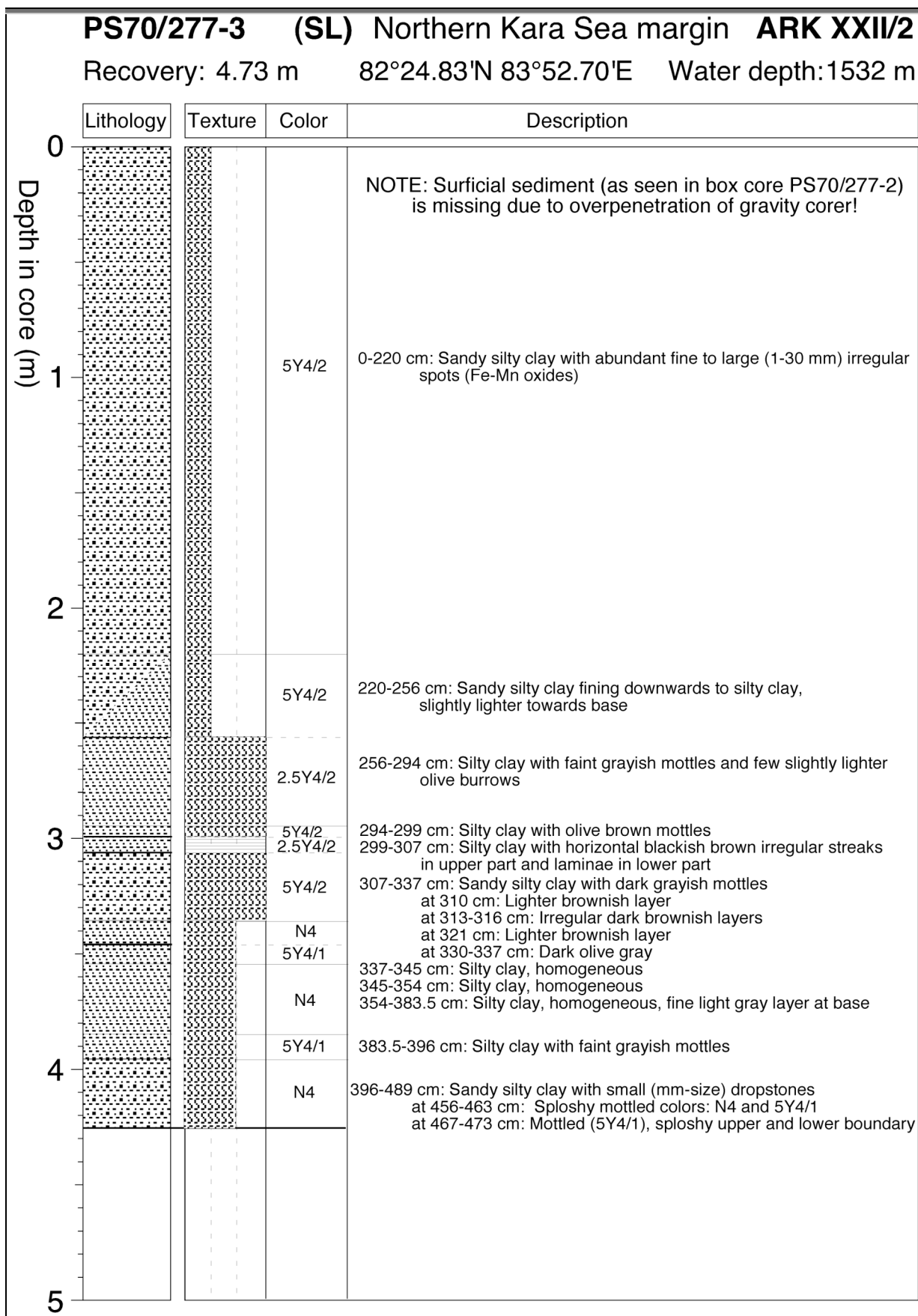


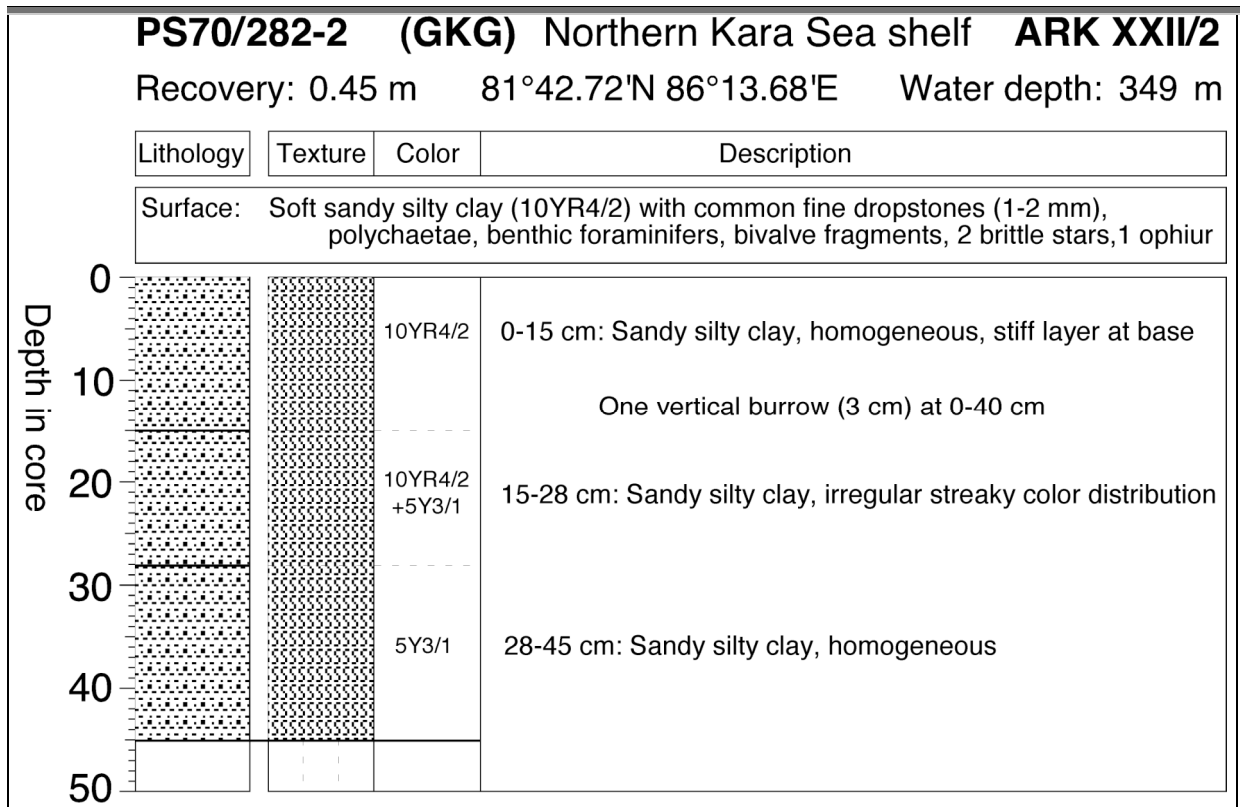
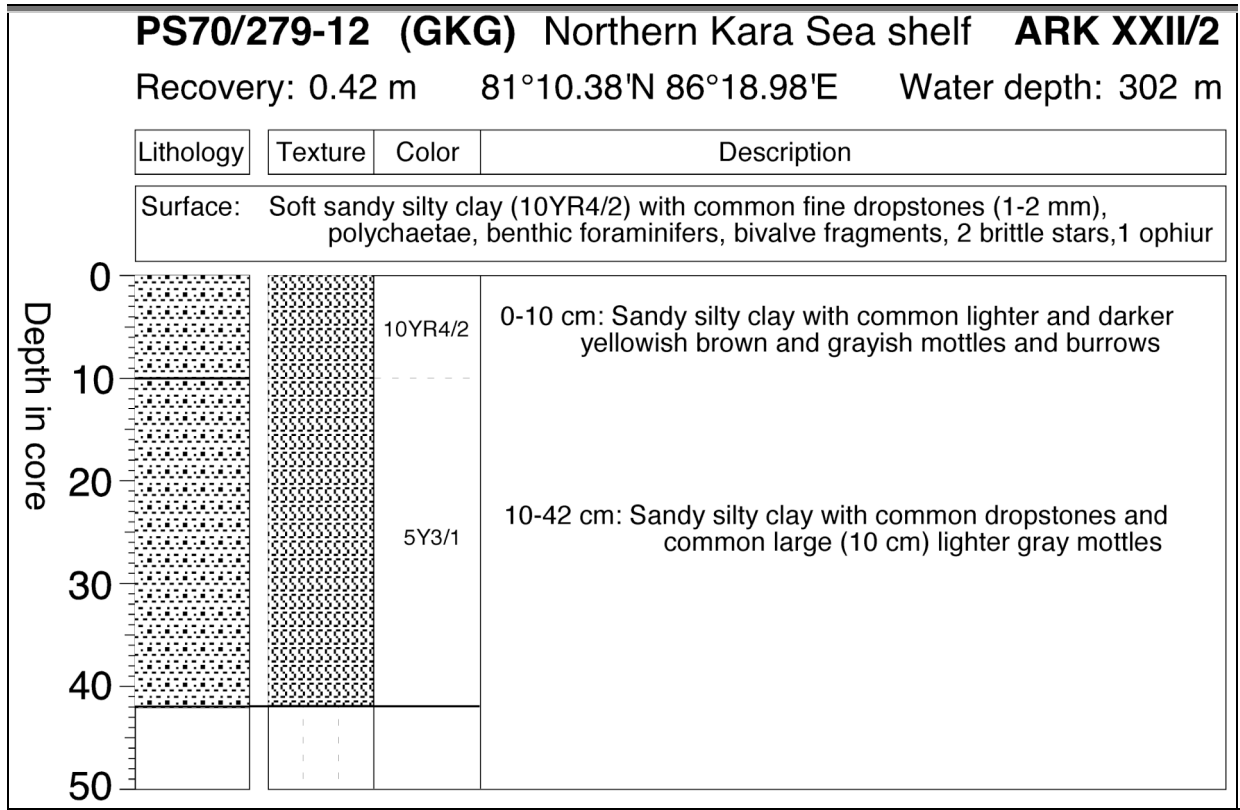






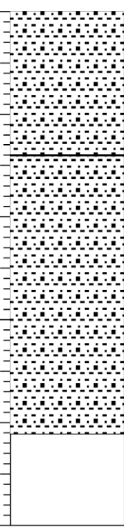
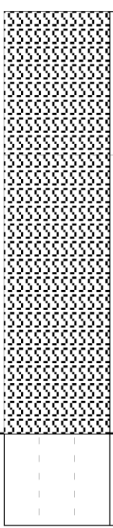


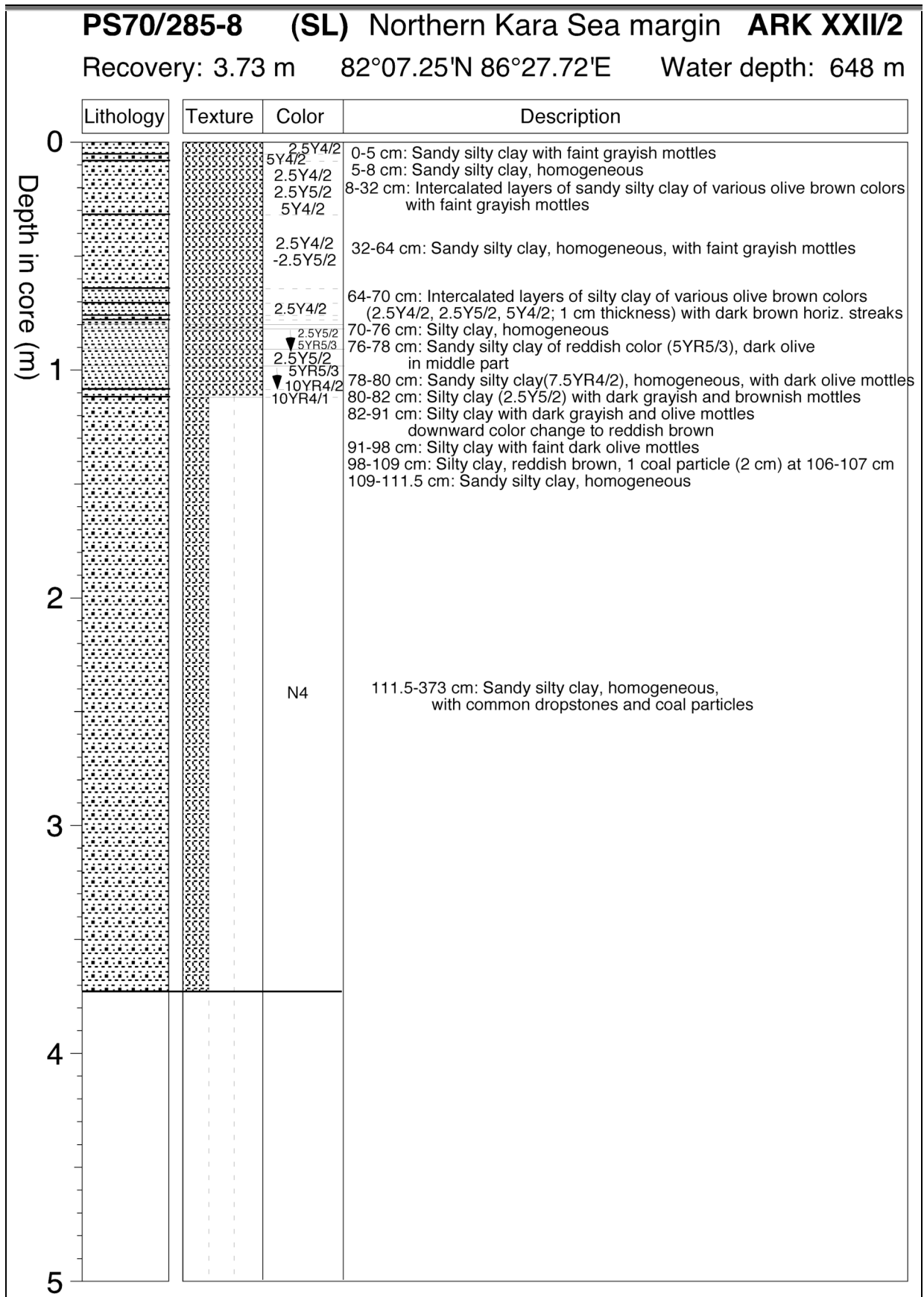


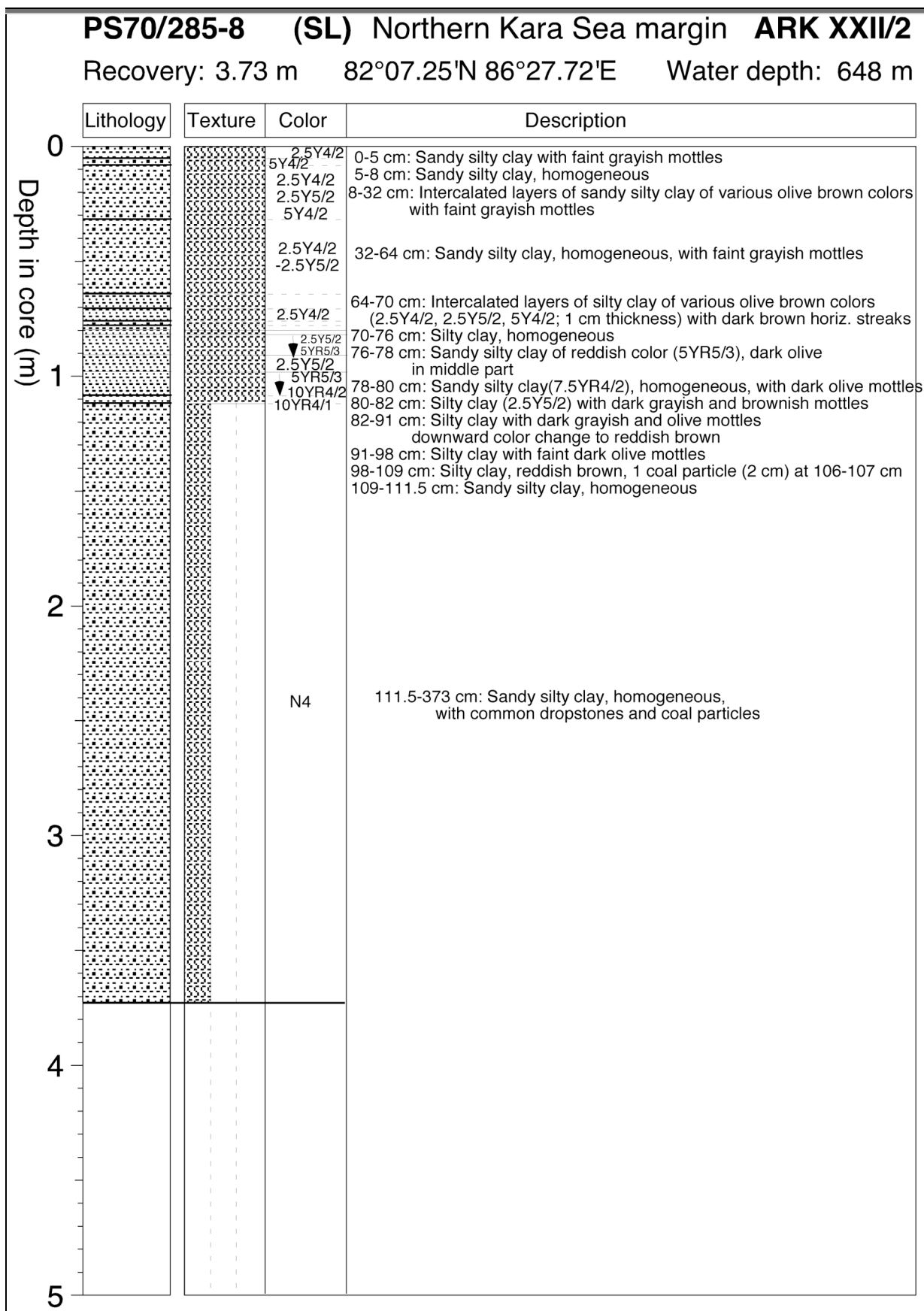


PS70/285-7 (GKG) Northern Kara Sea margin ARK XXII/2

Recovery: 0.41 m 82°07.47'N 86°27.05'E Water depth: 657 m

Lithology	Texture	Color	Description
<p>Surface: Soft sandy silty clay (10YR4/2), undulated surface with large, deep burrow holes (10 cm diam.), abundant fecal pellets, common small worm tubes, 1 polychaet, 1 ugly brittle star</p>			
<p>0</p>  <p>10</p> <p>20</p> <p>30</p> <p>40</p> <p>50</p>		<p>10YR4/2</p> <p>5Y3/1</p>	<p>0-14 cm: Sandy silty clay, homogeneous at top, below 5 cm: mottled horizontal streaks and irregular layers of darker brownish and dark olive gray color</p> <p>14-41 cm: Sandy silty clay, homogeneous, common darker grayish horizontal streaks</p>



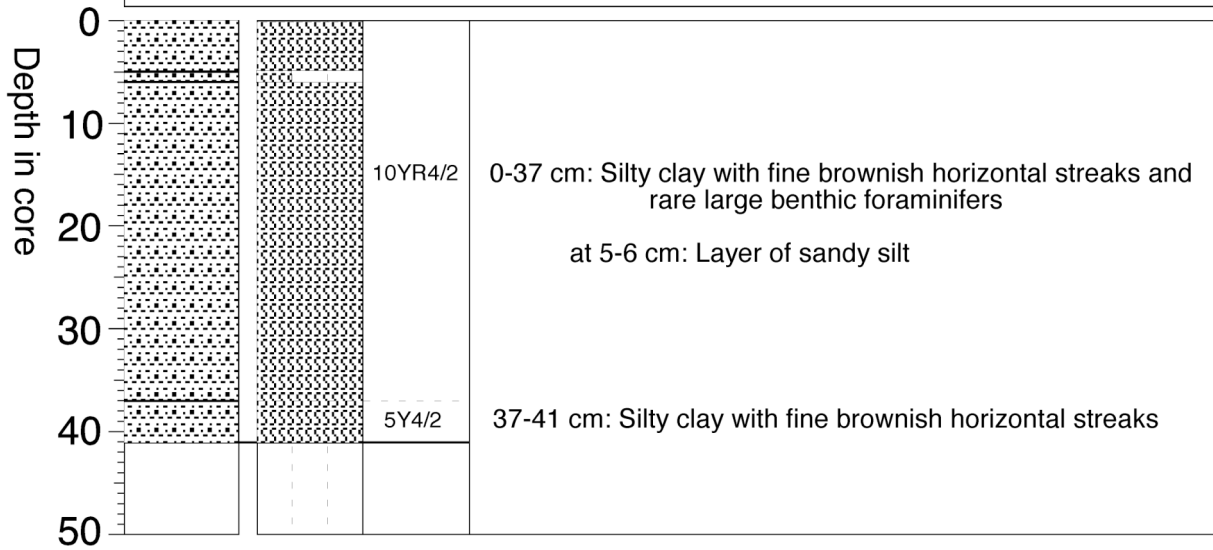


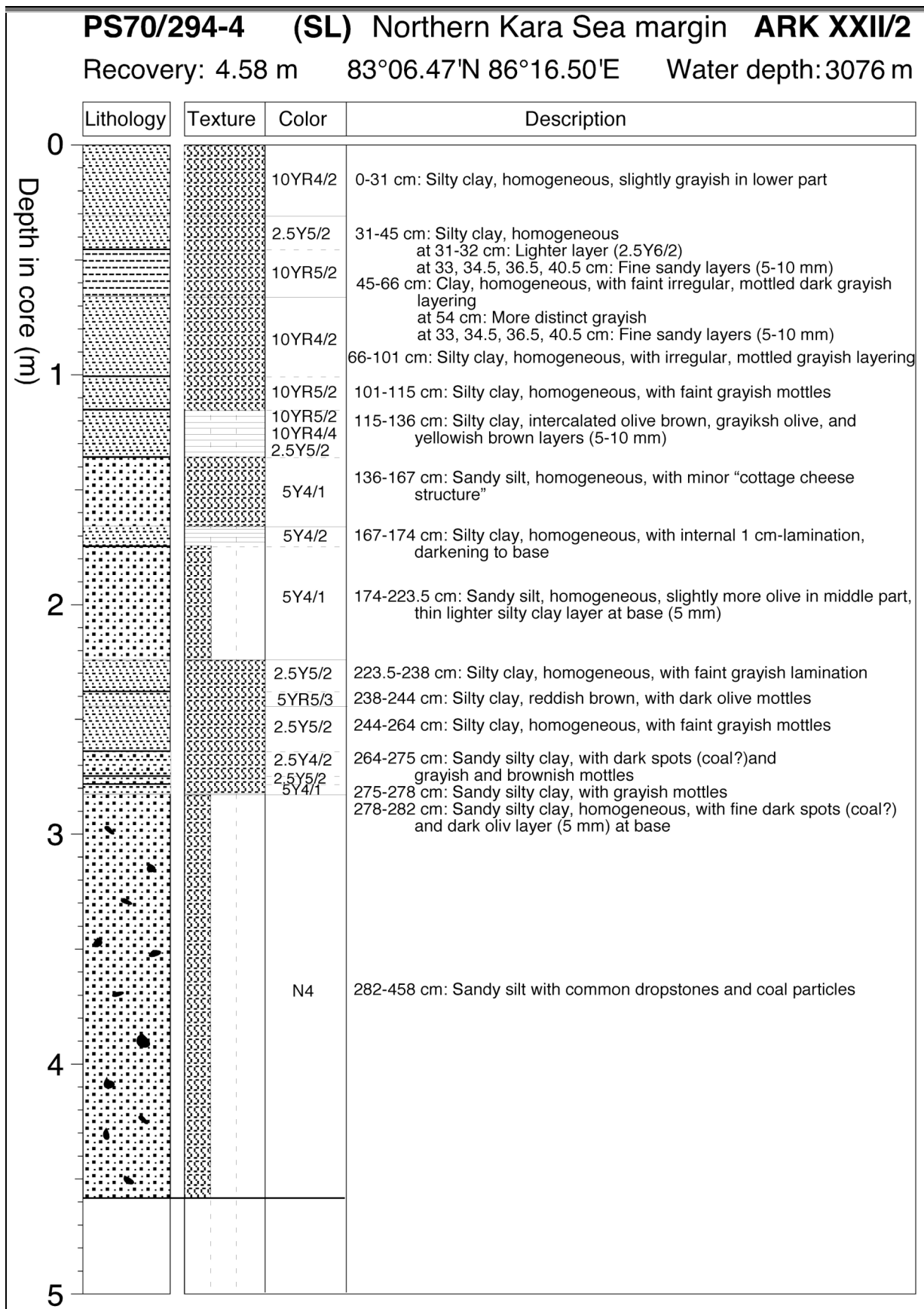
PS70/294-2 (GKG) Northern Kara Sea slope ARK XXII/2

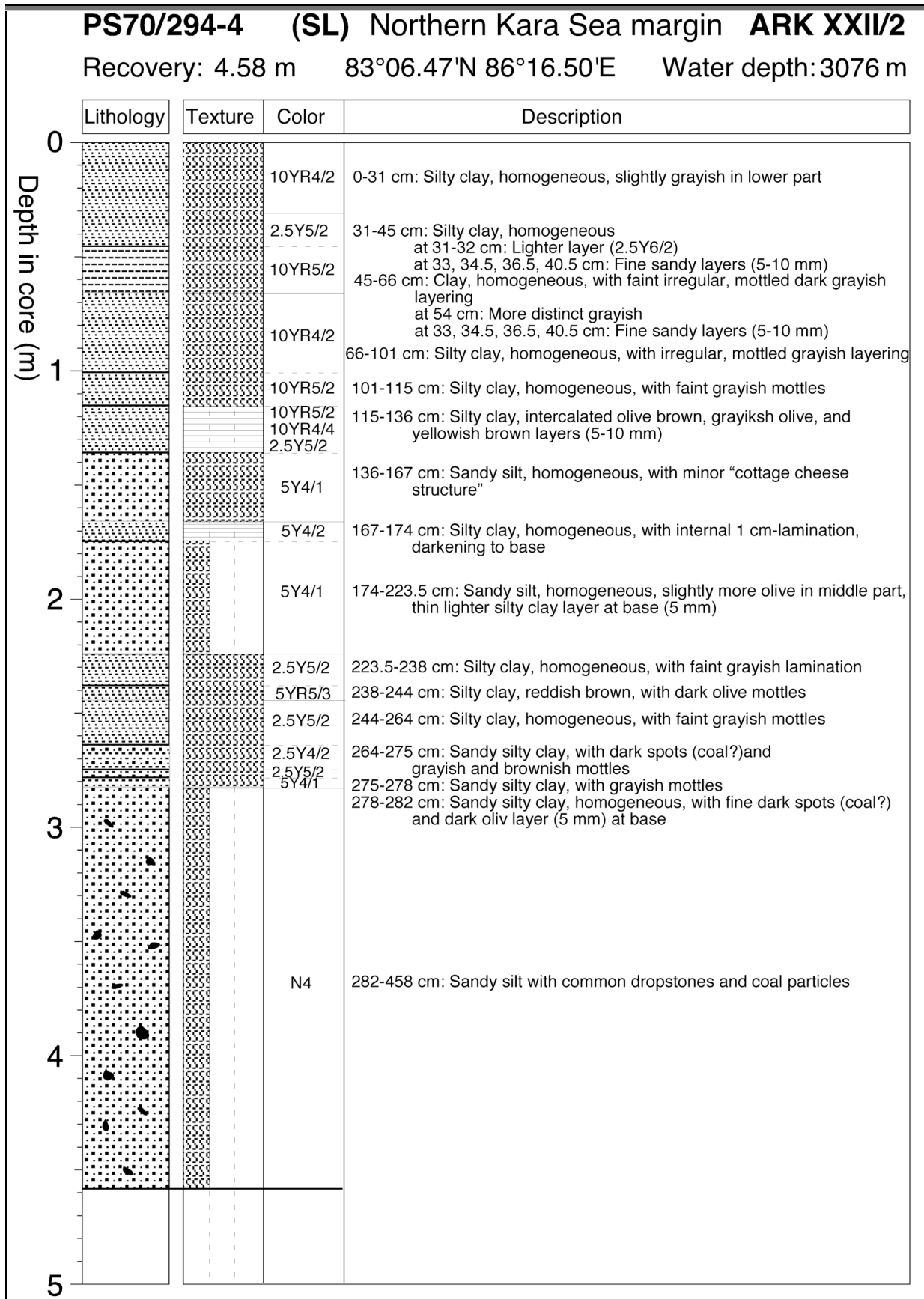
Recovery: 0.41 m 83°06.65'N 86°17.95'E Water depth: 3081 m

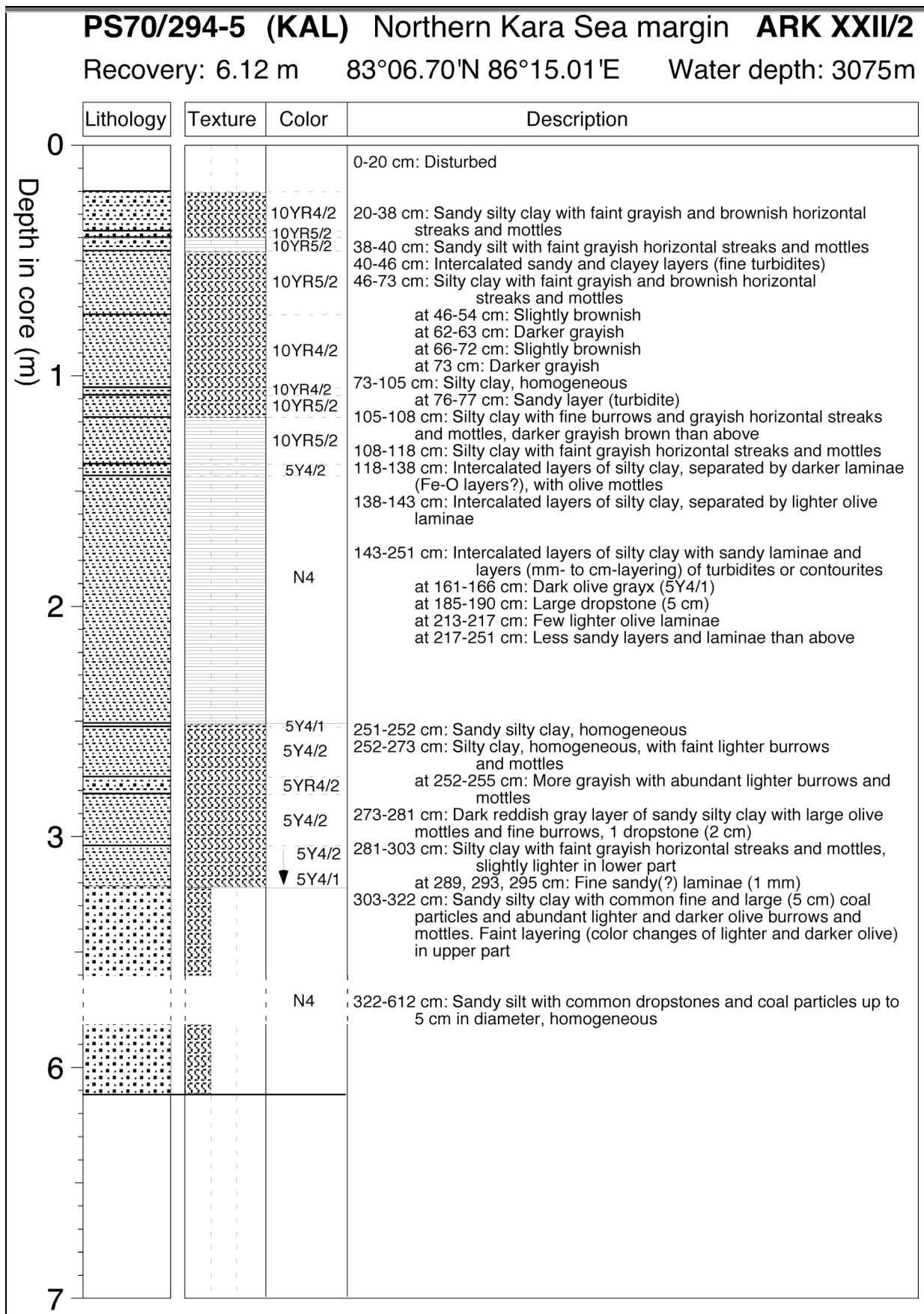
Lithology	Texture	Color	Description
-----------	---------	-------	-------------

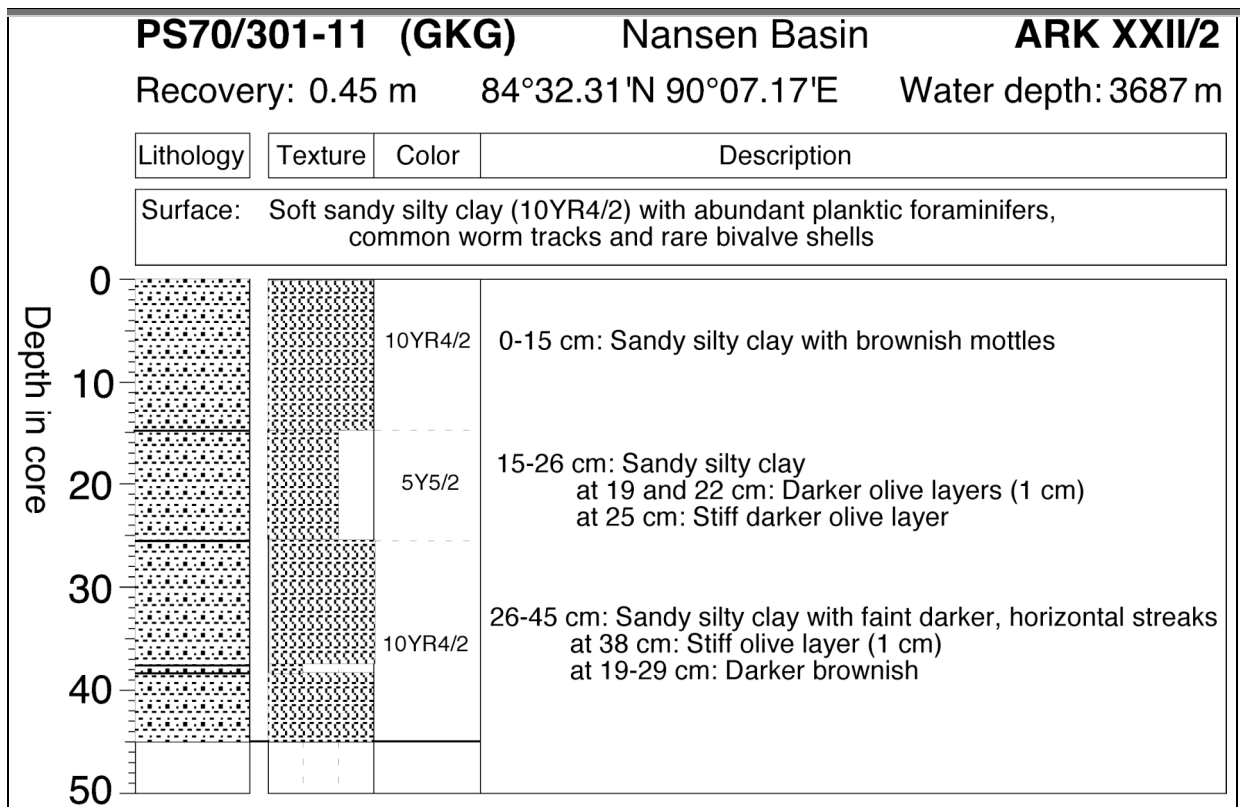
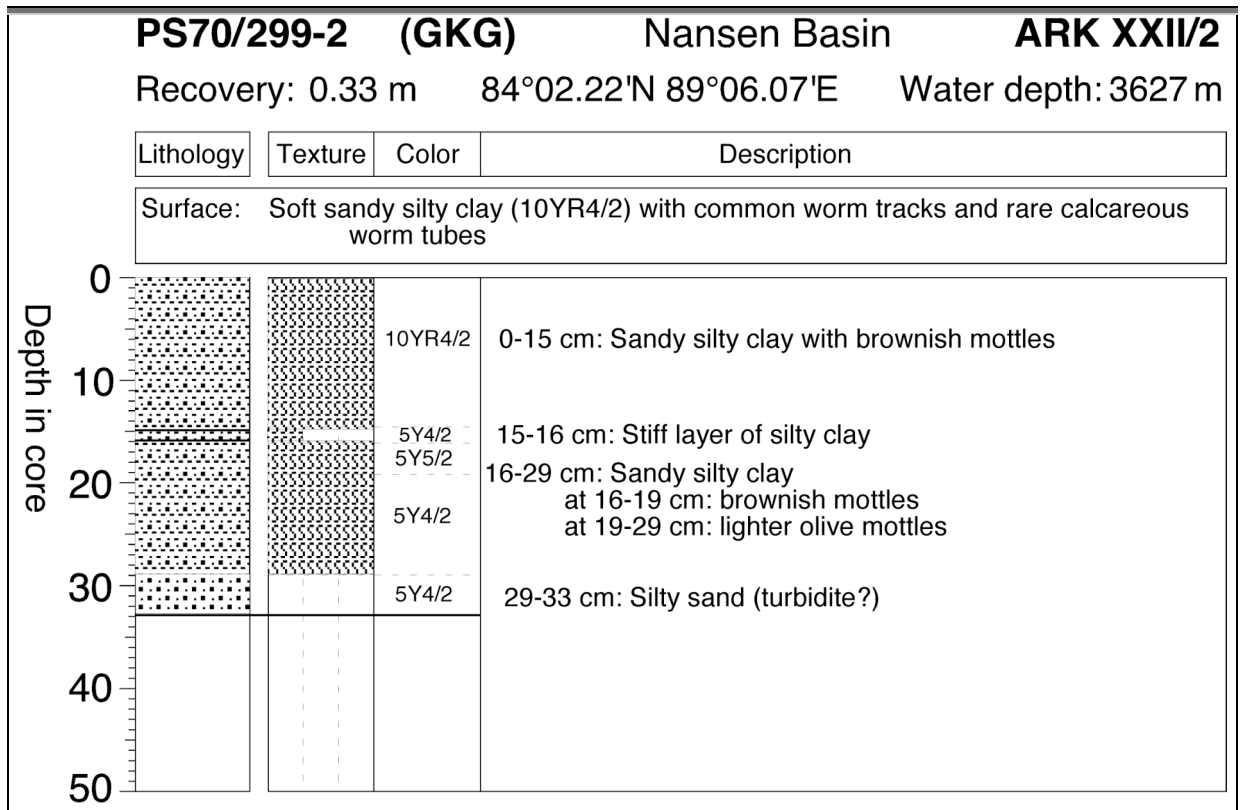
Surface: Soft silty clay (10YR4/2) with common benthic foraminifers (Pyrgo), 1 ophiur,

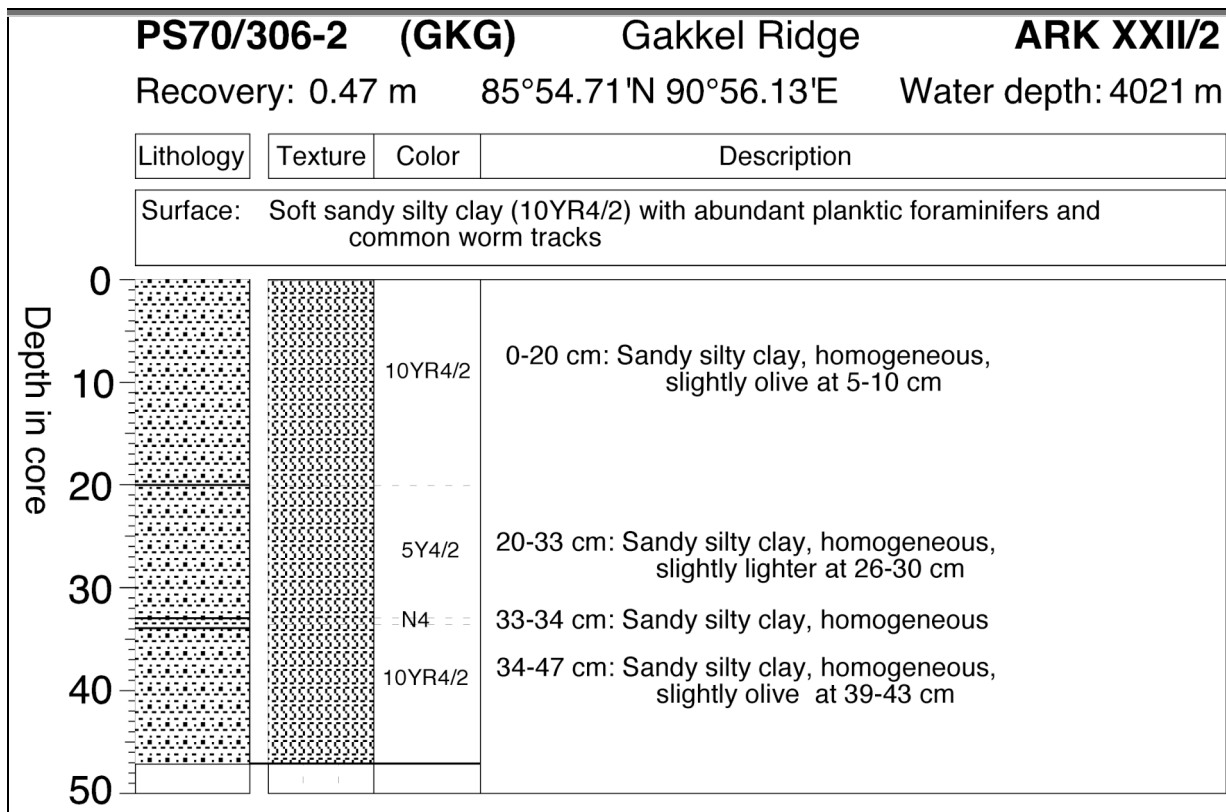


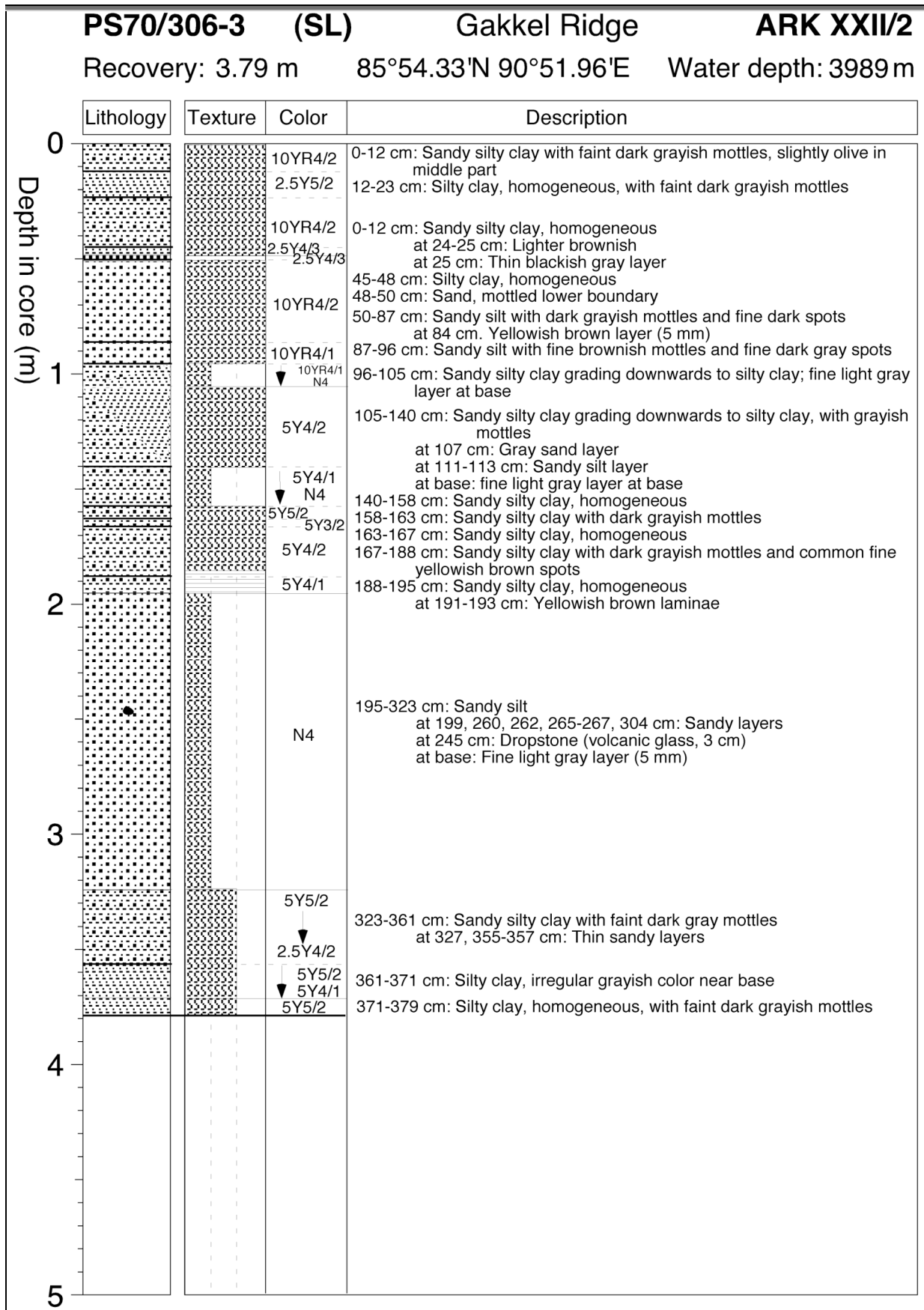


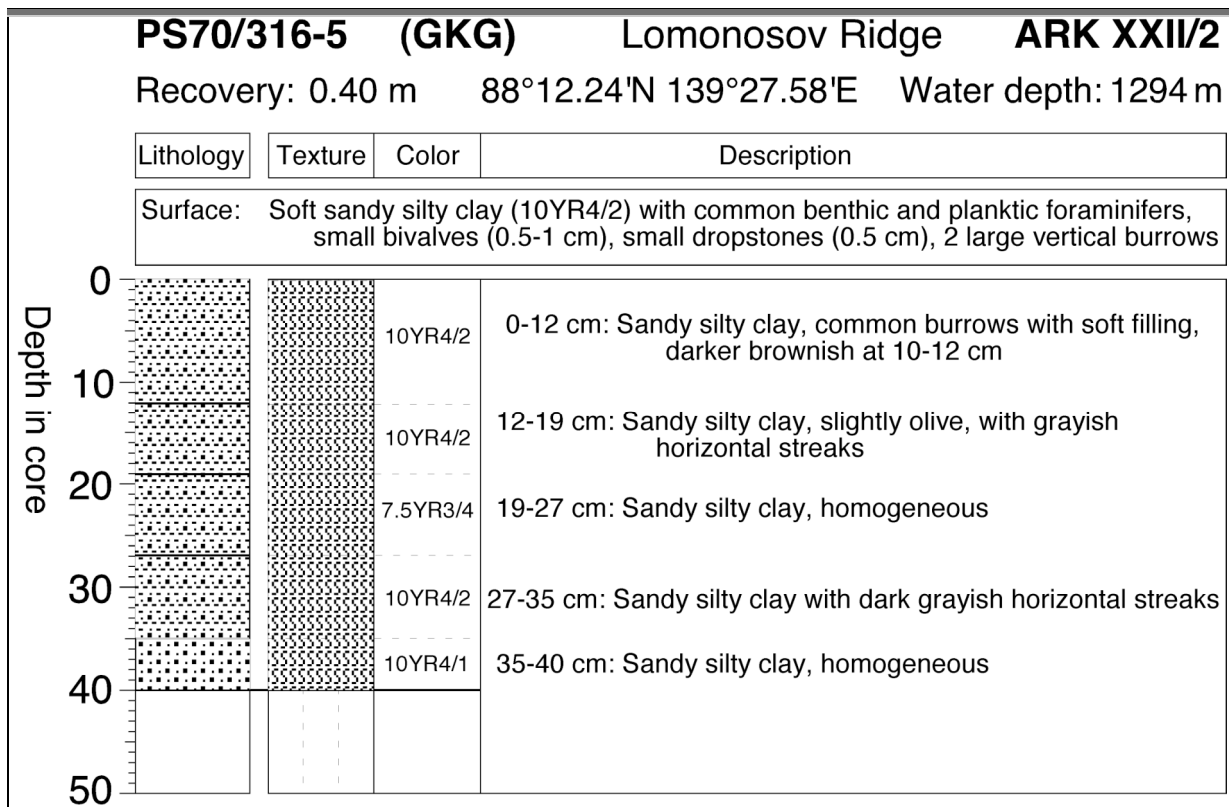
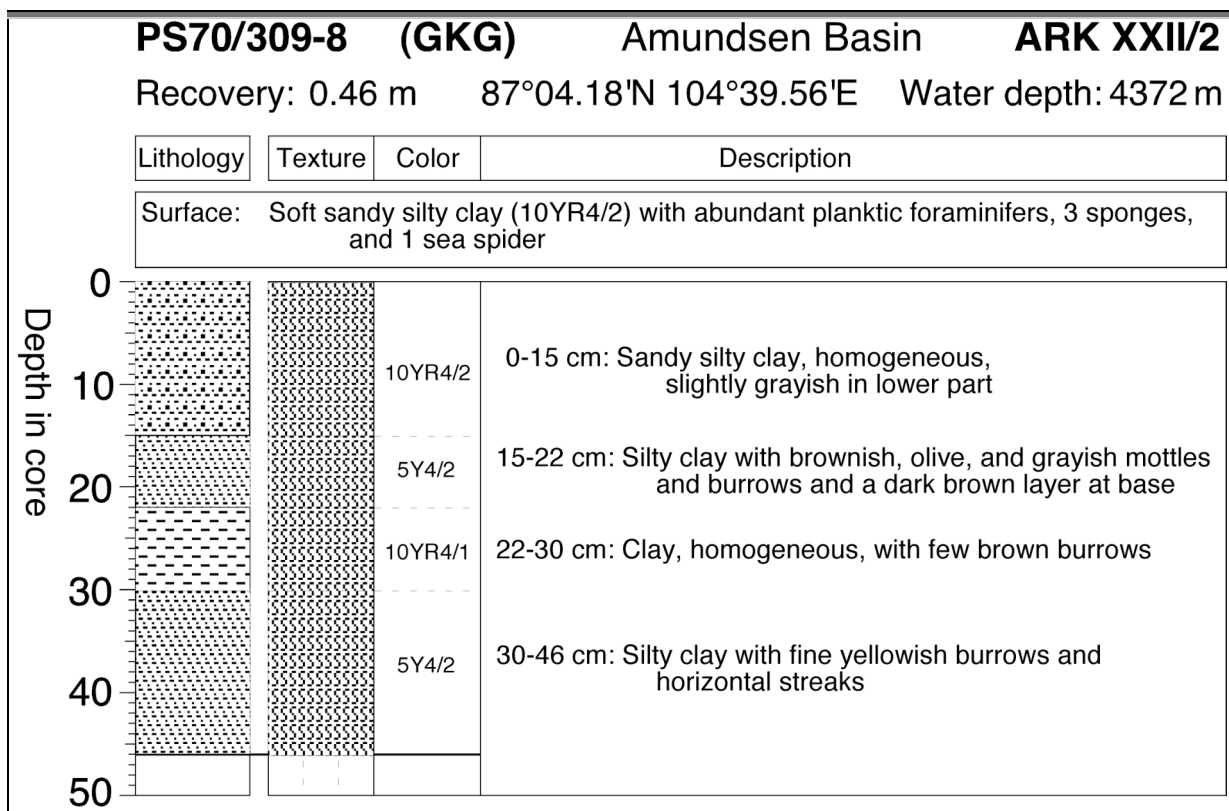




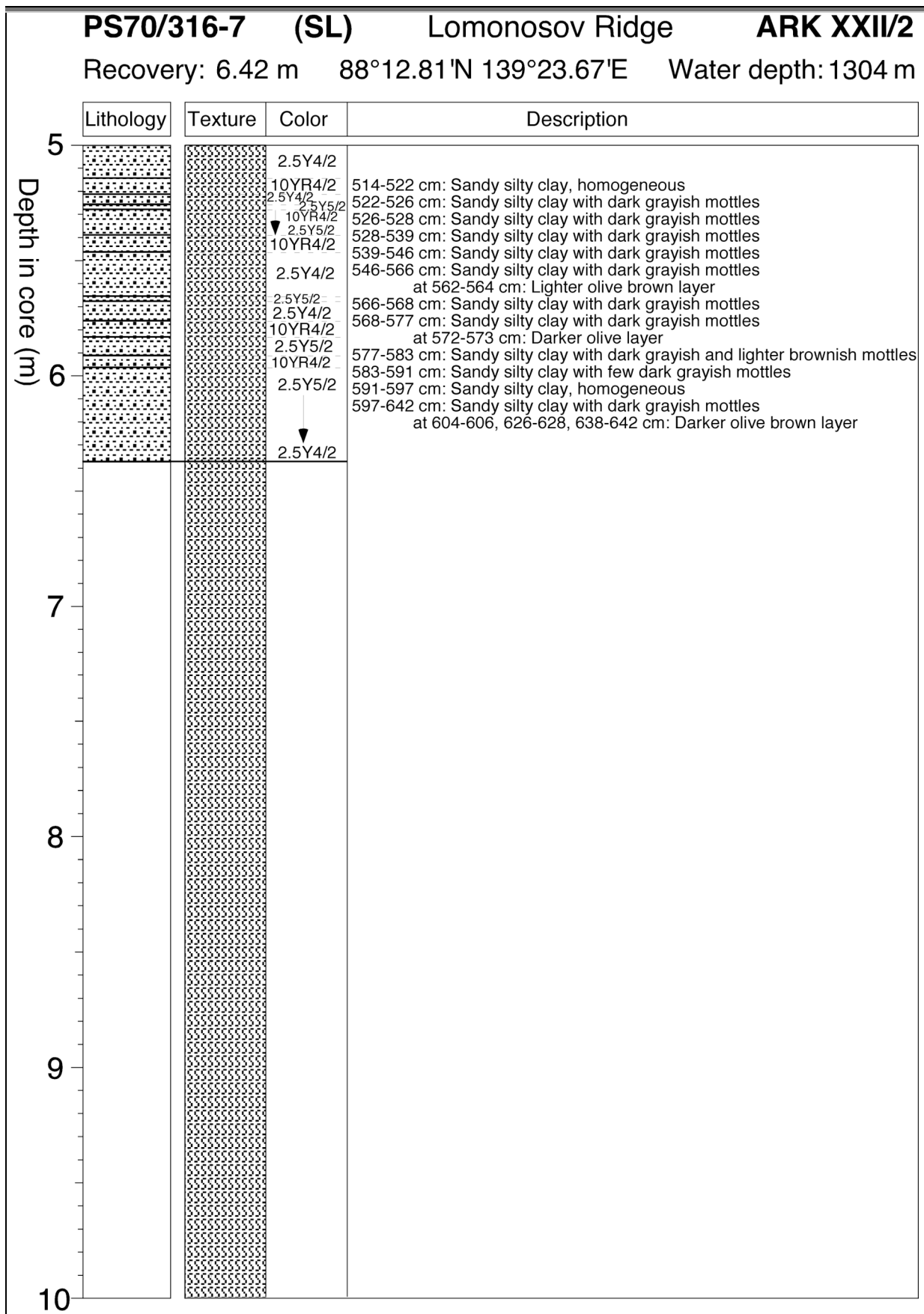


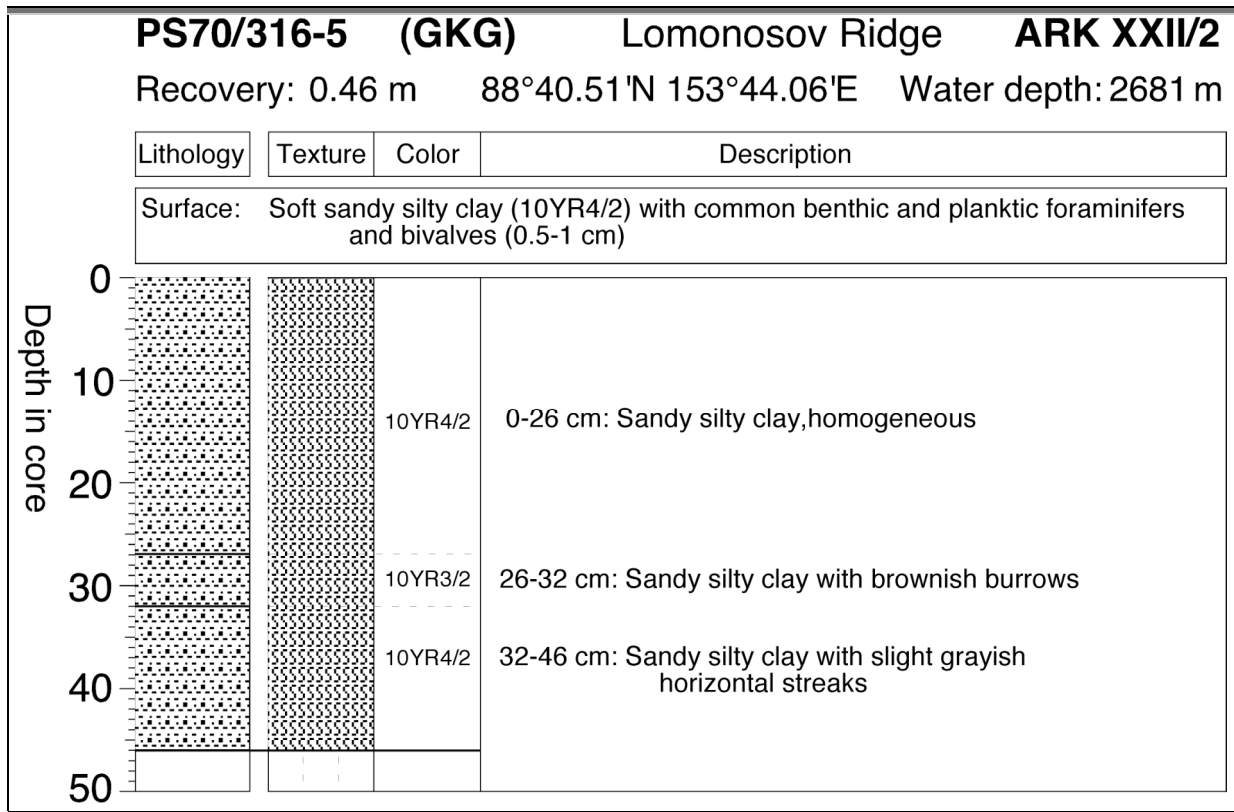


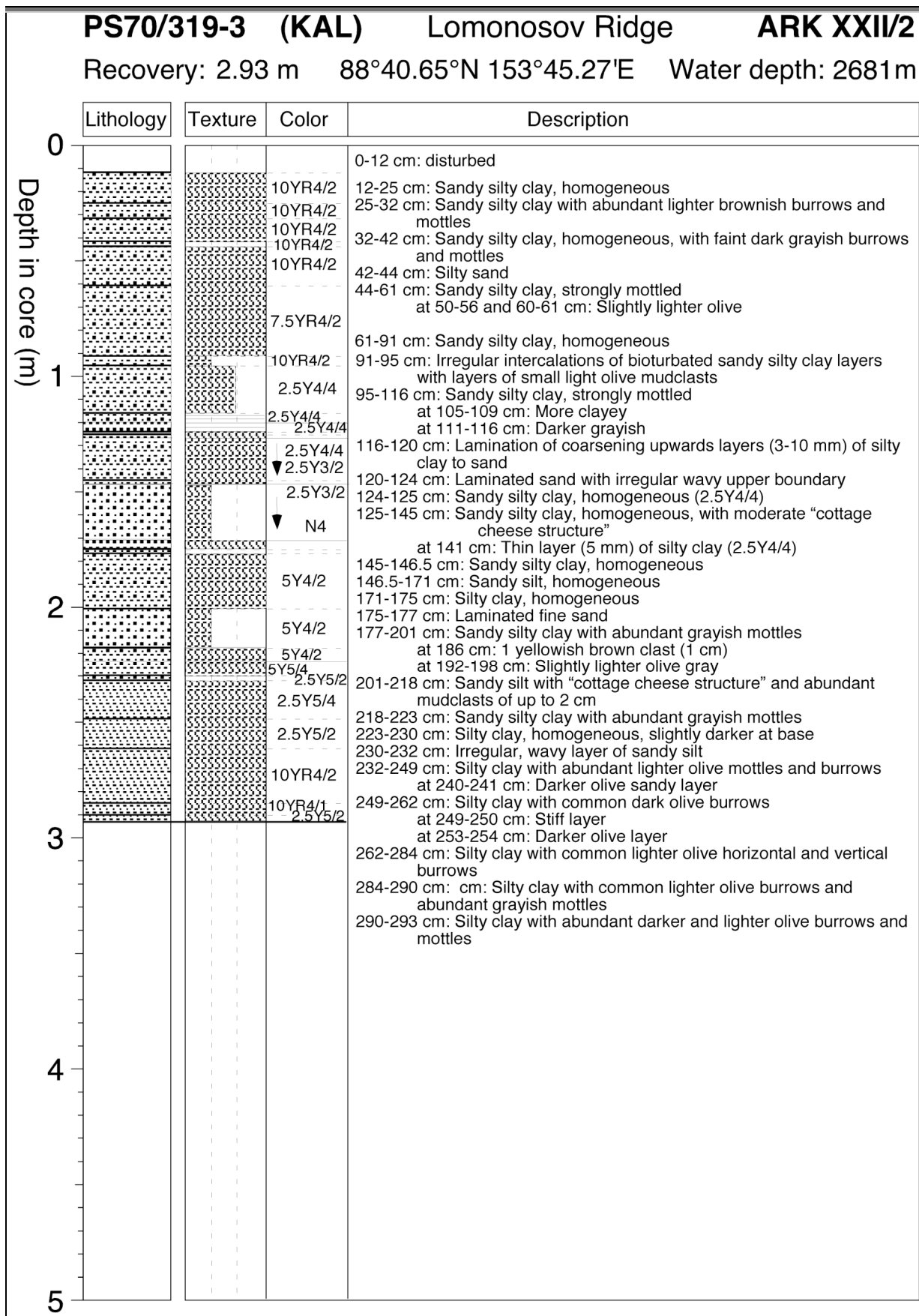


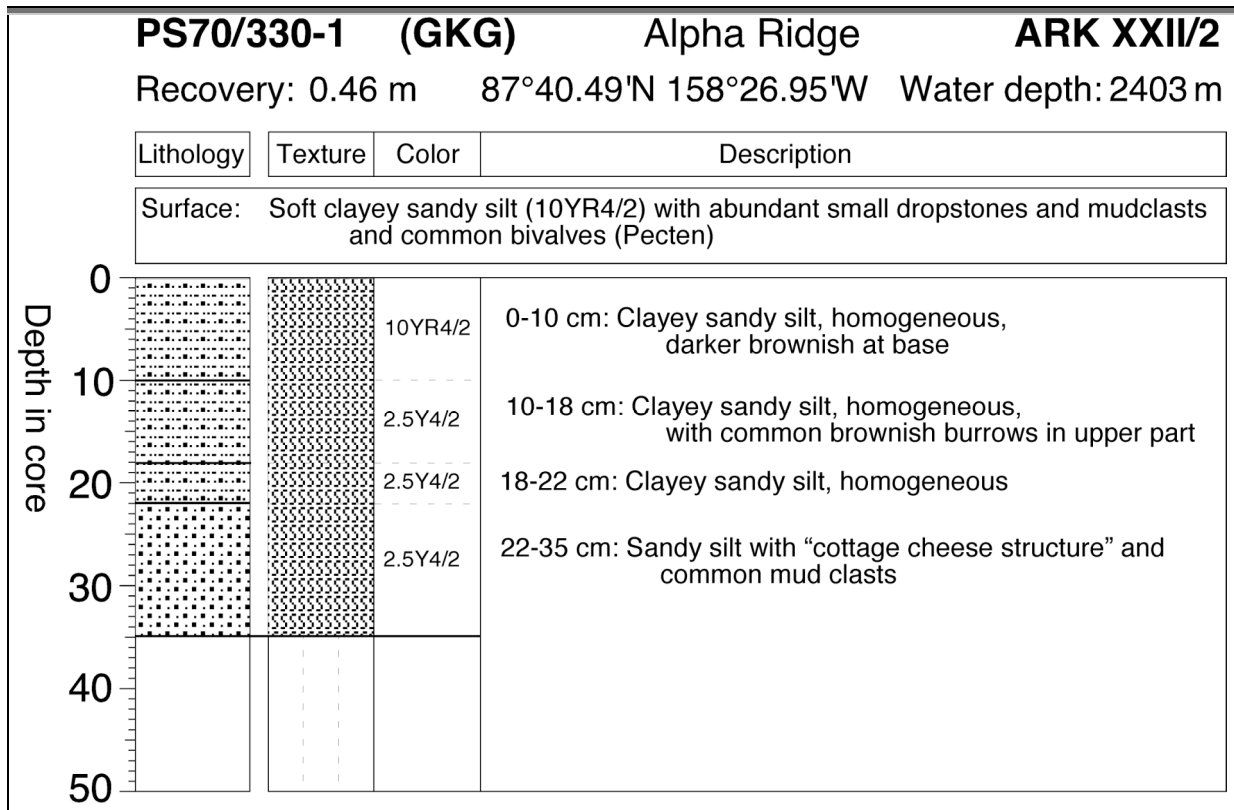


PS70/316-7 (SL)		Lomonosov Ridge		ARK XXII/2
Recovery: 6.42 m		88°12.81'N 139°23.67'E		Water depth: 1304 m
Depth in core (m)	Lithology	Texture	Color	Description
0			10YR4/2	0-17 cm: Sandy silty clay, homogeneous
			2.5Y5/2	17-53 cm: Sandy silty clay Dark brownish mottles at 17-24, 28, 32-34 cm Dark grayish mottles at 42-53 cm
			2.5Y4/2	53-64 cm: Sandy silty clay with faint dark grayish mottles
			2.5Y5/2	64-87 cm: Sandy silty clay with faint dark grayish mottles at 68-69 and 82-84 cm: homogeneous
1			10YR4/2	87-104 cm: Sandy silty clay with lighter brownish mottles
			2.5Y5/2	104-113 cm: Sandy silty clay with faint dark grayish mottles
			10YR4/2	113-125 cm: Sandy silty clay with lighter brownish mottles
			2.5Y4/2	125-135 cm: Sandy silty clay with faint dark grayish mottles
			2.5Y5/2	135-138 cm: Sandy silty clay with lighter brownish mottles
			2.5Y5/4	138-140 cm: Silty clay, homogeneous
			10YR4/2	140-153 cm: Sandy silty clay with lighter brownish mottles
			2.5Y5/4	153-181 cm: Sandy silty clay with faint dark grayish mottles at 163-166 cm: 10YR4/2, strongly mottled at 172 cm: Mottled dark brownish layer (5 mm)
2			10YR4/2	181-197 cm: Sandy silty clay with dark grayish and olive mottles at upper boundary: Irregular blackish lenses and fine light brownish layer with sharp boundaries (2 mm)
			2.5Y5/2	197-207 cm: Sandy silty clay with dark grayish and light brownish mottles
			10YR4/2	207-226 cm: Sandy silty clay with light olive brown mottles
			2.5Y5/2	226-284 cm: Sandy silty clay, homogeneous at 243, 245, 246-247, 249 cm: mottled dark brownish layers at 252-284 cm: Few dark grayish mottles
			2.5Y5/3	
3			2.5Y4/2	284-328 cm: Sandy silty clay with dark grayish mottles at 295-296, 298-300, 301-305, 308-311, 312-318 cm: darker grayish layers at 317-318, 319-328 cm: Silty sand at base: Light gray layer (3 mm)
			2.5Y4/2	328-346 cm: Sandy silty clay with faint dark grayish mottles at 343-346 cm: Dark brownish layers
			2.5Y5/2	346-359 cm: Sandy silty clay with faint dark brownish mottles
			10YR4/2	359-376 cm: Sandy silty clay with light olive brownish mottles in lower and upper part
4			2.5Y5/2	376-399 cm: Sandy silty clay, homogeneous, with few small dark grayish spots
			10YR4/2	399-407 cm: Sandy silty clay with light brownish mottles
			2.5Y4/2	407-421 cm: Sandy silty clay with light and dark brownish mottles
			2.5Y5/2	421-427 cm: Sandy silty clay with dark brownish mottles
			10YR4/2	427-434 cm: Sandy silty clay with light brownish mottles
			2.5Y4/2	434-446 cm: Sandy silty clay, homogeneous
			2.5Y5/2	446-460 cm: Sandy silty clay with dark grayish mottles
			10YR4/2	460-481 cm: Sandy silty clay with dark grayish and light brownish mottles
5			2.5Y4/2	481-514 cm: Sandy silty clay with dark grayish mottles darker grayish in lower part

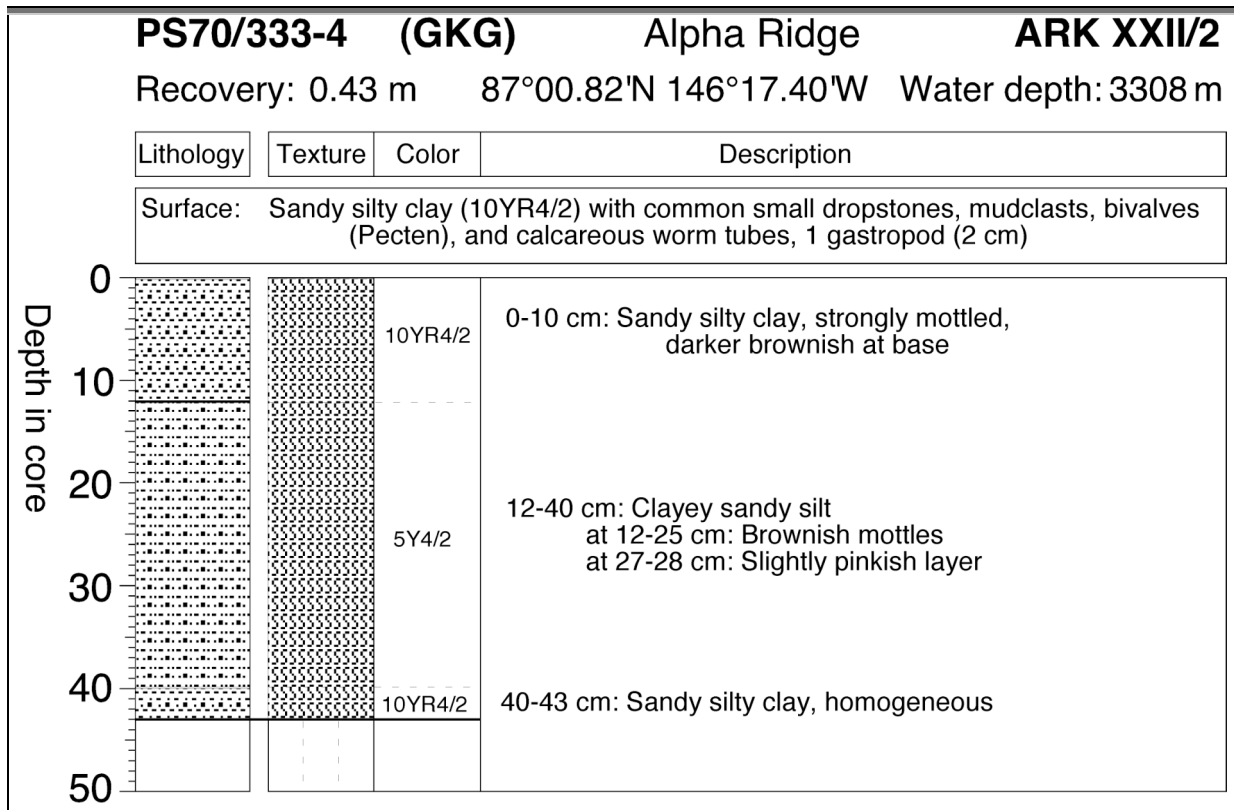




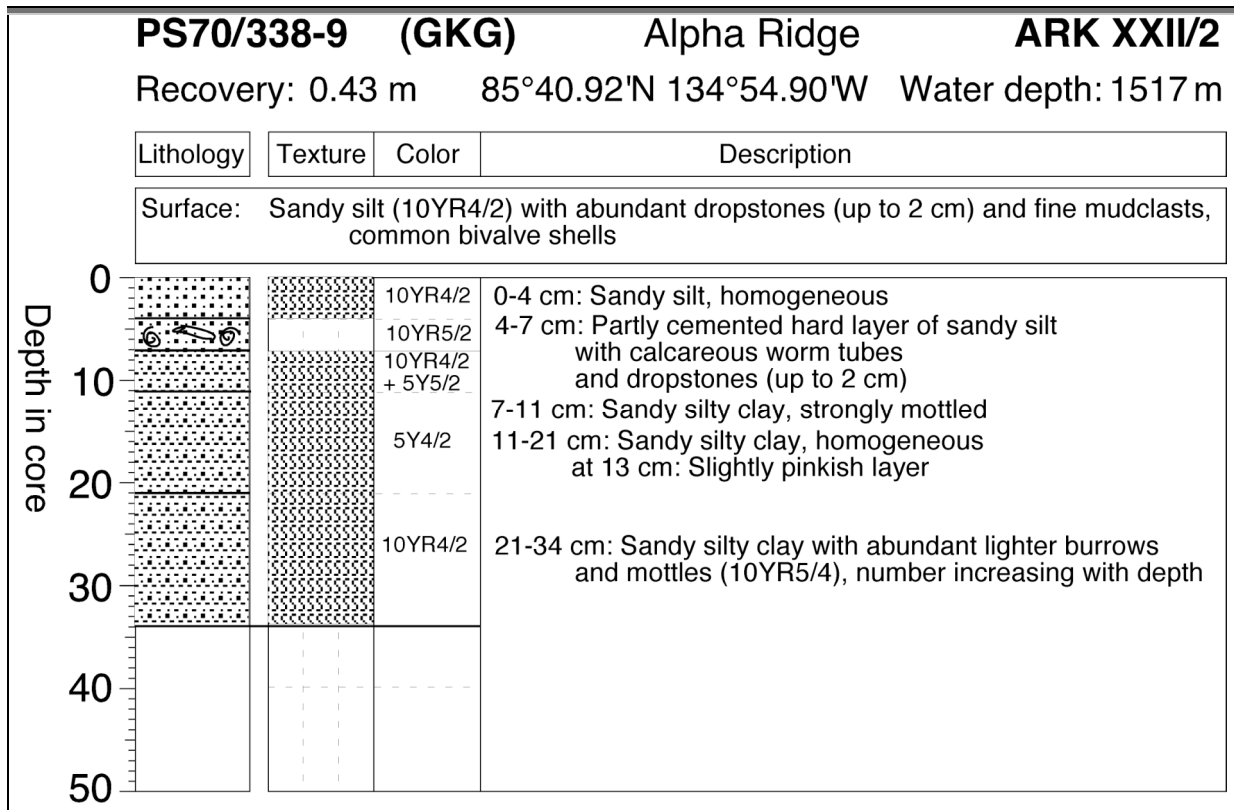




PS70/330-2 (SL)		Alpha Ridge		ARK XXII/2
Recovery: 5.93 m		87°40.55'N 158°29.48'W		Water depth: 2404 m
Depth in core (m)	Lithology	Texture	Color	Description
0			10YR4/2	0-1 cm: Sandy silty clay, homogeneous
			2.5Y4/2	1-24 cm: Sandy silty clay with faint dark grayish mottles at 19-24 cm: Dropstone (6 cm) at 23.5-24 cm: Homogeneous
			10YR5/2	24-39 cm: Sandy silty clay with olive mottles
			2.5Y4/2	at 28-30 cm: Olive brown layer with brownish mottles
			10YR4/2	39-62 cm: Sandy silty clay with abundant dark brownish to olive brownish mottles, 1 dropstone (20 cm) at 45-51 cm
			2.5Y5/2	62-87 cm: Sandy silty clay with faint dark grayish mottles; minor "cottage cheese structure"
1			10YR4/2	87-105 cm: Sandy silty clay with dark and olive brownish mottles
			2.5Y5/2	105-113 cm: Sandy silty clay with dark brownish mottles
			10YR4/2	113-118 cm: Sandy silty clay with olive brownish mottles
			10YR5/2	118-125 cm: Sandy silty clay with dark brownish mottles
			10YR4/2	125-132 cm: Sandy silty clay with olive brownish mottles
			10YR5/2	132-147 cm: Sandy silty clay with faint dark grayish mottles
			10YR4/2	147-157 cm: Sandy silty clay with olive brownish mottles at base: 1 small whitish clast (2 mm)
			10YR5/2	157-180 cm: Sandy silty clay with faint dark grayish mottles, slightly darker near base
2			10YR4/2	180-193 cm: Sandy silty clay with dark brownish and grayish mottles
			2.5Y5/2	193-201 cm: Sandy silty clay with faint dark brownish mottles
			10YR4/2	201-211 cm: Sandy silty clay with olive brownish mottles
			2.5Y5/2	211-226 cm: Sandy silty clay with faint dark grayish mottles and small black spots at 213 cm: Gray clast (1 cm) at lower boundary: Blackish mottles
			10YR5/3	226-256 cm: Sandy silty clay with abundant olive brownish and few dark brownish mottles
			10YR5/3	256-297 cm: Sandy silty clay with faint grayish brown mottles at 260-267 and 275-281 cm: Abundant fine brownish spots/mottles
3			2.5Y5/2	297-437 cm: Sandy silty clay with common dark brownish spots/mottles at 315-316, 353-362, 384-387 cm: Dark olive brown layers
			10YR5/3	437-454 cm: Sandy silty clay with olive brownish and dark brownish mottles
5			2.5Y5/2	454-540 cm: Sandy silty clay with faint grayish mottles and dark spots at 474-475, 478-479, 481-483, 487-489, 493-497, 506-507, 510-511, 516-521, 525-527, 532-534 cm: More brownish layers (10YR5/3)
			10YR5/3	540-568 cm: Sandy silty clay with faint olive brownish mottles at 543-545 and 549-551 cm: Larger olive brownish mottles at 556-560 cm: More olive brownish layer (2.5Y5/2)
			2.5Y5/2	568-585 cm: Sandy silty clay with faint dark mottles at 577-580 cm: Slightly brownish
6			10YR4/2	585-593 cm: Sandy silty clay, homogeneous

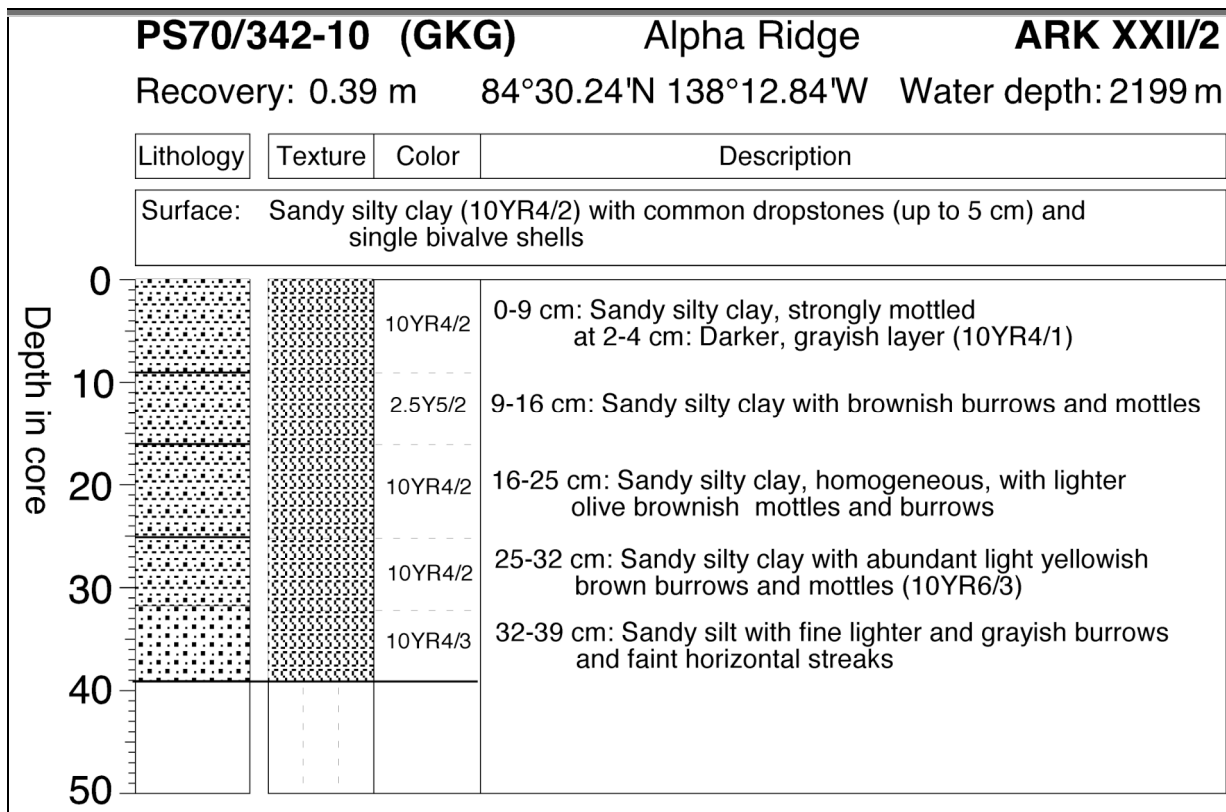


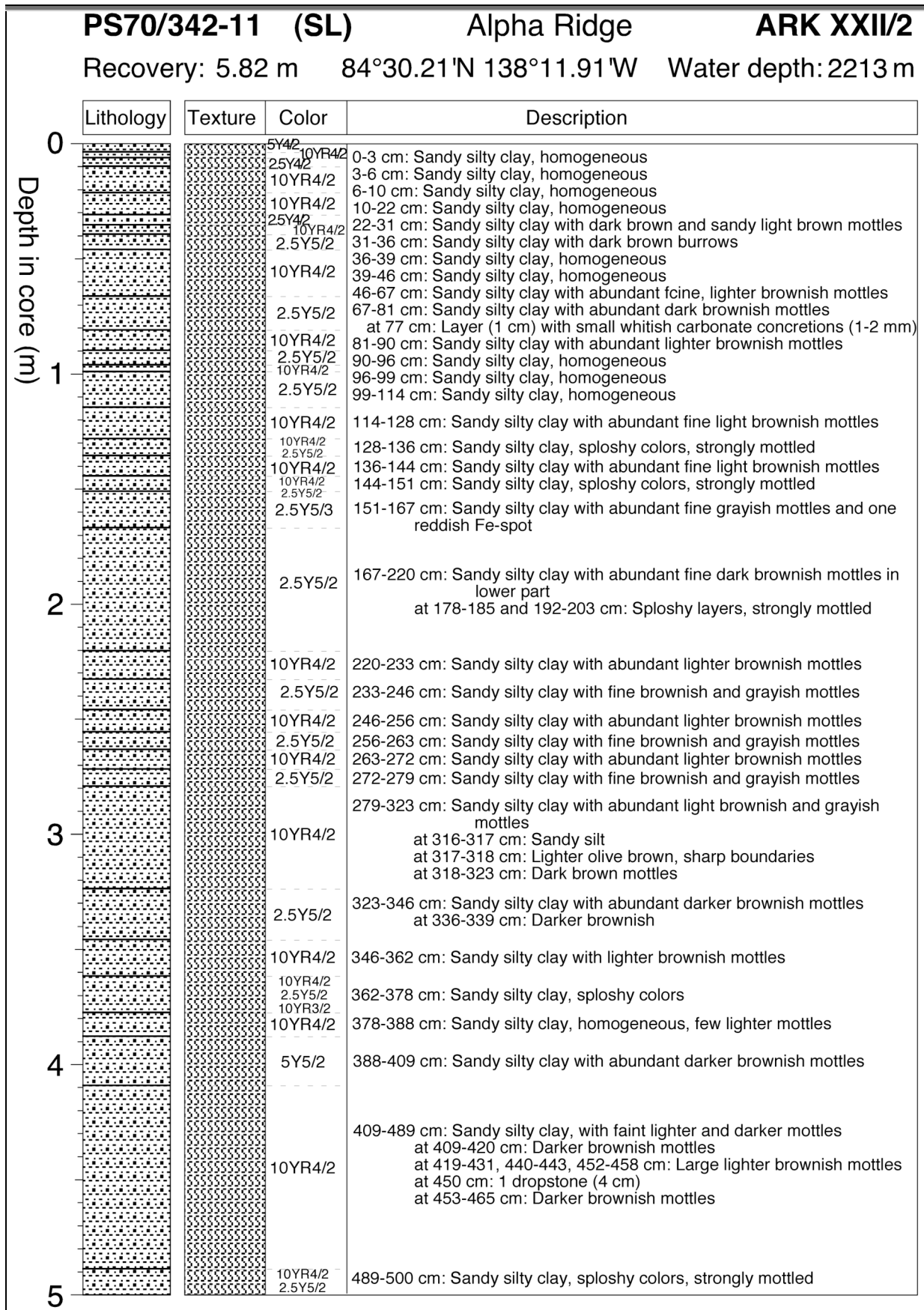
PS70/333-5 (SL)		Alpha Ridge		ARK XXII/2
Recovery: 4.85 m		87°00.71'N 146°15.94'W		Water depth: 3312 m
Depth in core (m)	Lithology	Texture	Color	Description
0			2.5Y4/2	0-16 cm: Sandy silty clay with dark grayish mottles at 8-9, 15-16 cm: Lighter olive layers
			10YR4/2	
			10YR4/3	16-35 cm: Sandy silty clay with lighter brownish mottles
			10YR4/2	35-56 cm: Sandy silty clay with lighter brownish mottles and dark brownish mottles in upper part
			2.5Y4/2	56-79 cm: Sandy silty clay, homogeneous, with faint grayish mottles
1			10YR4/2	79-98 cm: Sandy silty clay, homogeneous at 86-89 cm: Light brownish mottles
			2.5Y4/2	98-106 cm: Sandy silty clay with dark brownish mottles
			10YR4/2	106-122 cm: Sandy silty clay with dark brownish mottles
			2.5Y5/2	122-131 cm: Sandy silty clay, homogeneous
			10YR4/2	131-141 cm: Sandy silty clay with light brownish mottles
			2.5Y5/2	141-152 cm: Sandy silty clay, homogeneous
			10YR4/2	152-169 cm: Sandy silty clay with light brownish mottles
			2.5Y5/2	169-178 cm: Sandy silty clay, homogeneous
			10YR4/2	178-186 cm: Sandy silty clay with light brownish mottles
2			2.5Y5/2	186-200 cm: Sandy silty clay with fine grayish mottles
			10YR4/2	200-222 cm: Sandy silty clay with light brownish and grayish mottles
			10YR5/3	222-236 cm: Sandy silty clay with light brownish mottles
			10YR4/2	236-240 cm: Sandy silty clay, homogeneous
			2.5Y5/2	240-325 cm: Sandy silty clay with abundant dark brownish mottles at 249-254 and 261-265 cm: Sploshy brownish color at 281-284 cm: Brownish layer (10YR5/3) at 300-314 cm: Abundant dark grayish mottles at 314-325 cm: Abundant dark brownish mottles
3			2.5Y5/2	
			2.5Y5/2	325-335 cm: Fine sand, homogeneous
			10YR4/2	335-337 cm: Sandy silty clay with dark brownish mottles
			2.5Y5/2	337-348 cm: Sandy silty clay with light grayish mottles
			2.5Y4/2	348-357 cm: Sandy silty clay with large very dark brownish mottles at base
			10YR4/2	357-363 cm: Sandy silty clay with dark grayish mottles
4			10YR4/2	363-410 cm: Sandy silty clay with dark brownish mottles
			10YR5/3	410-422 cm: Sandy silty clay with dark brownish mottles
			10YR4/2	422-437 cm: Sandy silty clay with dark brownish mottles
			10YR5/3	437-445 cm: Sandy silty clay with dark brownish mottles
			10YR4/2	445-485 cm: Sandy silty clay with dark brownish mottles
5				

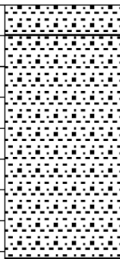



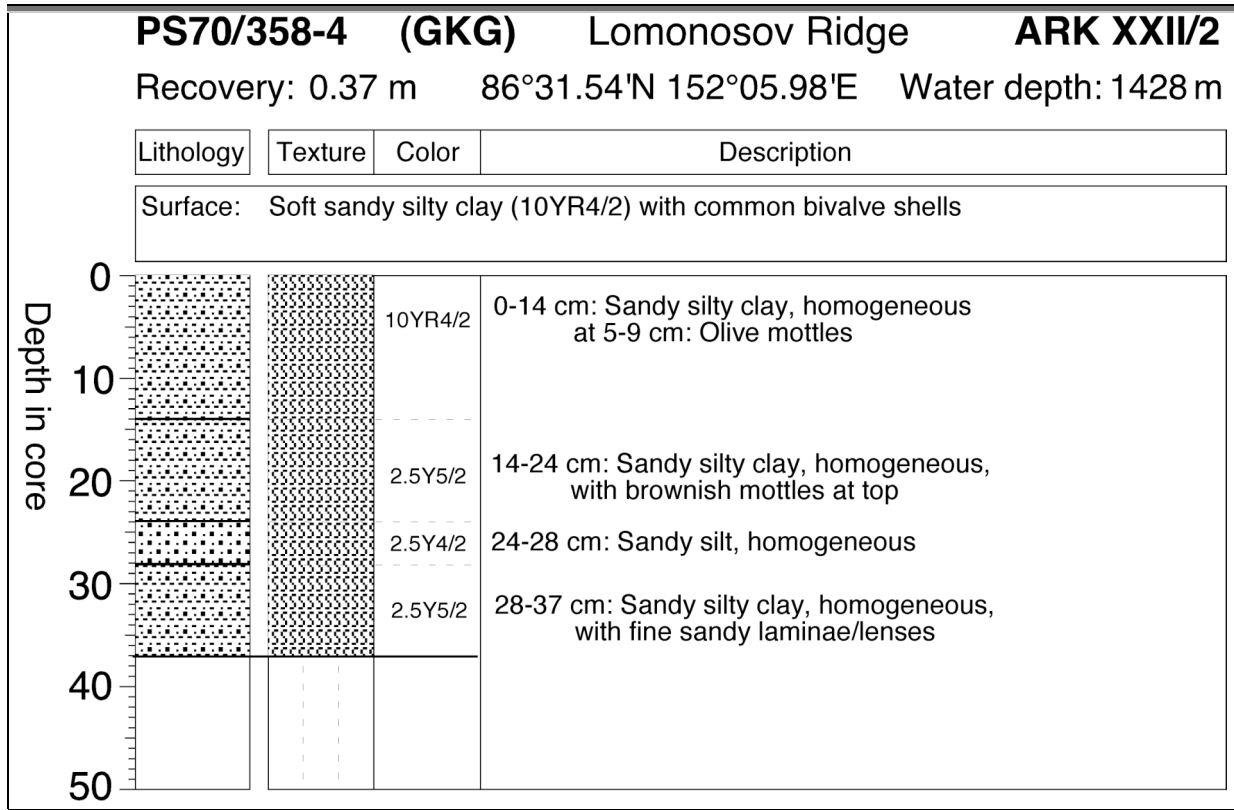
PS70/338-10 (SL)		Alpha Ridge		ARK XXII/2
Recovery: 4.11 m		85°40.84'N 134°54.72'W		Water depth: 1514 m
Depth in core (m)	Lithology	Texture	Color	Description
0			10YR4/2	0-4 cm: Sandy silty clay, homogeneous
			2.5Y4/2	4-7 cm: Cemented layer of calcareous worm tubes with sandy silty clay
1			10YR4/3	7-16 cm: Sandy silty clay
			10YR4/3	at 7-9 cm: Dark brownish mottles
			+ 10YR5/3	at 10 and 16 cm: Irregular light brownish layer
			10YR5/3	16-26 cm: Sandy silty clay, homogeneous, with light brownish mottles in upper part
			10YR4/3	26-[31]-36 cm: Sandy silty clay, splotchy colors
			2.5Y5/2	[31]-[36]-39 cm: Partly carbonate-cemented layer/clasts of sandy silty clay with abundant fine burrows in the cemented clasts
			10YR4/2	39-44 cm: Sandy silty clay with faint light brownish and dark grayish mottles
			10YR5/3	44-53 cm: Sandy silty clay with minor "cottage cheese structure"
			10YR4/2	53-71[-73] cm: Sandy silty clay with fine light brownish mottles
			2.5Y5/2	71[-73]-76[-79] cm: Partly carbonate-cemented layer/clasts of sandy silty clay
2			2.5Y4/2	76[-79]-87 cm: Sandy silty clay with fine light brownish mottles
			2.5Y4/2	87-112 cm: Sandy silty clay with fine dark brownish mottles and burrows
			▼ 2.5Y5/2	at 93 cm: 1 dropstone (1 cm)
			▼ 2.5Y4/2	112-122 cm: Sandy silty clay with fine dark grayish mottles
			▼ 2.5Y5/2	at 115 cm: 1 dropstone (1 cm)
			2.5Y5/2	122-134 cm: Sandy silty clay, splotchy colors, strongly mottled
			2.5Y5/2	134-149 cm: Sandy silty clay, splotchy colors, strongly mottled
			2.5Y5/2	149-154 cm: Sandy silty clay, homogeneous, with few dark grayish mottles
			2.5Y5/2	154-212 cm: Sandy silty clay with fine dark grayish and brownish mottles
			▼ 10YR5/2	212-225 cm: Sandy silty clay with dark brownish mottles; splotchy colors
3			▼ 2.5Y5/2	225-237 cm: Sandy silty clay with fine dark grayish mottles
			2.5Y5/2	237-247 cm: Sandy silty clay with abundant olive mottles
			10YR4/2	247-251 cm: Sandy silty clay with dark brownish mottles
			2.5Y5/2	251-261 cm: Sandy silty clay with abundant olive mottles
			10YR4/2	261-282 cm: Sandy silty clay with dark brownish mottles
			2.5Y5/2	at 269-272 and 275-278 cm: Dark brownish layers
			10YR4/2	282-299 cm: Sandy silty clay with olive and dark brownish mottles
			2.5Y5/2	299-305 cm: Sandy silty clay, homogeneous, with few dark grayish mottles
			2.5Y4/2	305-312 cm: Sandy silty clay, homogeneous, with few dark grayish mottles
			10YR4/2	312-331 cm: Sandy silty clay with faint dark grayish mottles
4			2.5Y5/2	at 318-320 and 324-326 cm: More olive layers
			2.5Y5/2	331-340 cm: Sandy silty clay with faint dark brownish mottles
			10YR4/2	340-411 cm: Sandy silty clay with few dark brownish mottles
			10YR4/2	at 345-347, 377-380, 404-411 cm: Olive mottles
			10YR4/2	at 361-363 and 382-385 cm: Slightly olive layers
			10YR4/2	at 392-403 cm: Darker brownish color (10YR3/2)
			10YR4/2	
			10YR4/2	
			10YR4/2	
			10YR4/2	
5				

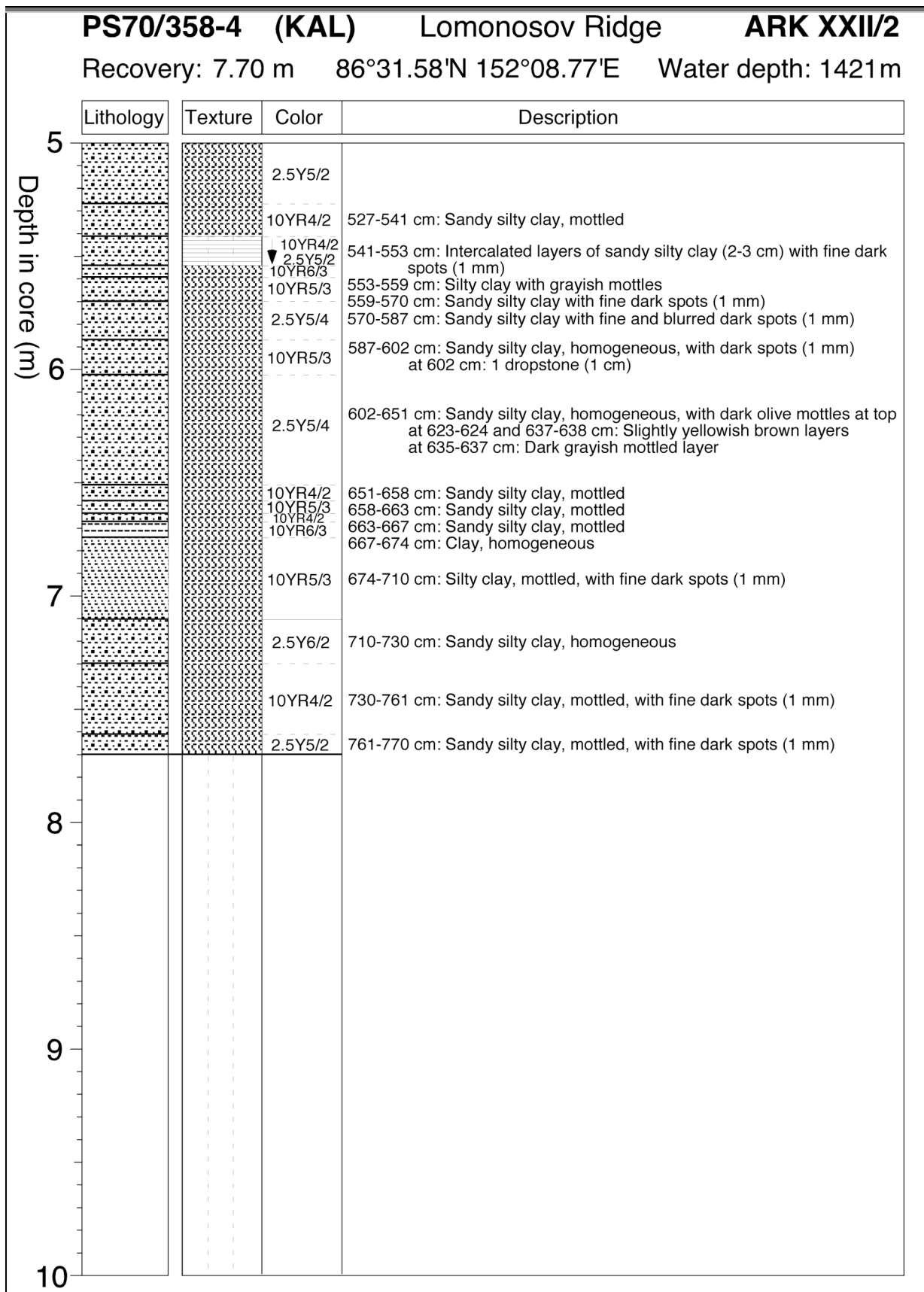
PS70/338-10 (SL)		Alpha Ridge		ARK XXII/2
Recovery: 4.11 m		85°40.84'N 134°54.72'W		Water depth: 1514 m
Depth in core (m)	Lithology	Texture	Color	Description
0			10YR4/2	0-4 cm: Sandy silty clay, homogeneous
			2.5Y4/2	4-7 cm: Cemented layer of calcareous worm tubes with sandy silty clay
1			10YR4/3	7-16 cm: Sandy silty clay
			10YR4/3	at 7-9 cm: Dark brownish mottles
			+ 10YR5/3	at 10 and 16 cm: Irregular light brownish layer
			10YR5/3	16-26 cm: Sandy silty clay, homogeneous, with light brownish mottles in upper part
			10YR4/3	26-[31]-36 cm: Sandy silty clay, splotchy colors
			10YR4/2	[31]-[36]-39 cm: Partly carbonate-cemented layer/clasts of sandy silty clay with abundant fine burrows in the cemented clasts
			10YR5/3	39-44 cm: Sandy silty clay with faint light brownish and dark grayish mottles
			10YR4/2	44-53 cm: Sandy silty clay with minor "cottage cheese structure"
			2.5Y5/2	53-71[-73] cm: Sandy silty clay with fine light brownish mottles
			2.5Y5/2	71[-73]-76[-79] cm: Partly carbonate-cemented layer/clasts of sandy silty clay
2			2.5Y4/2	76[-79]-87 cm: Sandy silty clay with fine light brownish mottles
			2.5Y4/2	87-112 cm: Sandy silty clay with fine dark brownish mottles and burrows
			▼ 2.5Y5/2	at 93 cm: 1 dropstone (1 cm)
			▼ 2.5Y4/2	112-122 cm: Sandy silty clay with fine dark grayish mottles
			▼ 2.5Y5/2	at 115 cm: 1 dropstone (1 cm)
			2.5Y5/2	122-134 cm: Sandy silty clay, splotchy colors, strongly mottled
			2.5Y5/2	134-149 cm: Sandy silty clay, splotchy colors, strongly mottled
			2.5Y5/2	149-154 cm: Sandy silty clay, homogeneous, with few dark grayish mottles
			2.5Y5/2	154-212 cm: Sandy silty clay with fine dark grayish and brownish mottles
			▼ 10YR5/2	212-225 cm: Sandy silty clay with dark brownish mottles; splotchy colors
3			▼ 2.5Y5/2	225-237 cm: Sandy silty clay with fine dark grayish mottles
			2.5Y5/2	237-247 cm: Sandy silty clay with abundant olive mottles
			10YR4/2	247-251 cm: Sandy silty clay with dark brownish mottles
			2.5Y5/2	251-261 cm: Sandy silty clay with abundant olive mottles
			10YR4/2	261-282 cm: Sandy silty clay with dark brownish mottles
			2.5Y5/2	at 269-272 and 275-278 cm: Dark brownish layers
			10YR4/2	282-299 cm: Sandy silty clay with olive and dark brownish mottles
			2.5Y5/2	299-305 cm: Sandy silty clay, homogeneous, with few dark grayish mottles
			2.5Y4/2	305-312 cm: Sandy silty clay, homogeneous, with few dark grayish mottles
			10YR4/2	312-331 cm: Sandy silty clay with faint dark grayish mottles
4			2.5Y5/2	at 318-320 and 324-326 cm: More olive layers
			2.5Y5/2	331-340 cm: Sandy silty clay with faint dark brownish mottles
			10YR4/2	340-411 cm: Sandy silty clay with few dark brownish mottles
			10YR4/2	at 345-347, 377-380, 404-411 cm: Olive mottles
			10YR4/2	at 361-363 and 382-385 cm: Slightly olive layers
			10YR4/2	at 392-403 cm: Darker brownish color (10YR3/2)
			10YR4/2	
			10YR4/2	
			10YR4/2	
			10YR4/2	
5				





		PS70/342-11 (SL)		Alpha Ridge		ARK XXII/2	
		Recovery: 5.82 m		84°30.21'N 138°11.91'W		Water depth: 2213 m	
		Lithology	Texture	Color	Description		
Depth in core (m)	5			10YR4/2	500-510 cm: Sandy silty clay with faint dark grayish and light brownish mottles		
				10YR3/2	510-582 cm: Sandy silty clay, homogeneous, with few light brownish and dark grayish mottles		
	6						
	7						
	8						
	9						
	10						





Die "Berichte zur Polar- und Meeresforschung"

(ISSN 1866-3192) werden beginnend mit dem Heft Nr. 377 (2000) in Fortsetzung der früheren **"Berichte zur Polarforschung"** (Heft 1-376, von 1982 bis 2000; ISSN 0176 - 5027) herausgegeben. Ein Verzeichnis aller Hefte beider Reihen befindet sich im Internet in der Ablage des electronic Information Center des AWI (**ePIC**) unter der Adresse <http://epic.awi.de>. Man wähle auf der rechten Seite des Fensters "Reports on Polar- and Marine Research". Dann kommt eine Liste der Publikationen und ihrer online-Verfügbarkeit in alphabetischer Reihenfolge (nach Autoren) innerhalb der absteigenden chronologischen Reihenfolge der Jahrgänge.

To generate a list of all 'Reports' past issues, use the following URL: <http://epic.awi.de> and select the right frame: Browse. Click on "Reports on Polar and Marine Research". A chronological list in declining order, author names alphabetical, will be produced. If available, pdf files will be shown for open access download.

Verzeichnis der zuletzt erschienenen Hefte:

Heft-Nr. 567/2007 — "Effects of UV Radiation on Antarctic Benthic Algae - With Emphasis on Early Successional Stages and Communities", by Katharina Zacher.

Heft-Nr. 568/2007 — "The Expedition ANTARKTIS-XXIII/2 of the Research Vessel 'Polarstern' in 2005/2006", edited by Volker Strass.

Heft-Nr. 569/2008 — "The Expedition ANTARKTIS-XXIII/8 of the Research Vessel 'Polarstern' in 2006/20067", edited by Julian Gutt.

Heft-Nr. 570/2008 — "The Expedition ARKTIS-XXI/1 a and b of the Research Vessel 'Polarstern' in 2005", edited by Gereon Budéus, Eberhard Fahrback and Peter Lemke.

Heft-Nr. 570/2008 — "The Expedition ARKTIS-XXI/1 a and b of the Research Vessel 'Polarstern' in 2005", edited by Gereon Budéus, Eberhard Fahrback and Peter Lemke.

Heft-Nr. 571/2008 — "The Antarctic ecosystem of Potter Cove, King-George Island (Isla 25 de Mayo). Synopsis of research performed 1999-2006 at the Dallmann Laboratory and Jubany Station", edited by Christian Wiencke, Gustavo A. Ferreyra, Doris Abele and Sergio Marensi.

Heft-Nr. 572/2008 — "Climatic and hydrographic variability in the late Holocene Skagerrak as deduced from benthic foraminiferal proxies", by Sylvia Brückner.

Heft-Nr. 573/2008 — "Reactions on surfaces of frozen water: Importance of surface reactions for the distribution of reactive compounds in the atmosphere", by Hans-Werner Jacobi.

Heft-Nr. 574/2008 — "The South Atlantic Expedition ANT-XXIII/5 of the Research Vessel 'Polarstern' in 2006", edited by Wilfried Jokat.

Heft-Nr. 575/2008 — "The Expedition ANTARKTIS-XXIII/10 of the Research Vessel 'Polarstern' in 2007", edited by Andreas Macke.

Heft-Nr. 576/2008 — "The 6th Annual Arctic Coastal Dynamics (ACD) Workshop, October 22-26, 2006, Groningen, Netherlands", edited by Pier Paul Overduin and Nicole Couture.

Heft-Nr. 577/2008 — "Korrelation von Gravimetrie und Bathymetrie zur geologischen Interpretation der Eltanin-Impaktstruktur im Südpazifik", von Ralf Krockner.

Heft-Nr. 578/2008 — "Benthic organic carbon fluxes in the Southern Ocean: regional differences and links to surface primary production and carbon export", by Oliver Sachs.

Heft-Nr. 579/2008 — "The Expedition ARKTIS-XXII/2 of the Research Vessel 'Polarstern' in 2007", edited by Ursula Schauer.